Novel Fluorescent Sensors for the Detection of Organic Molecules in Extraterrestrial Samples

Thesis

Novel Fluorescent Sensors for the Detection of Organic Molecules in Extraterrestrial Samples

Roy Christopher Adkin

BSc (Hons) Molecular Science (Open)

This thesis is submitted for the degree of
Doctor of Philosophy

The School of Physical Sciences,
The Faculty of Science, Technology, Engineering and Mathematics,
The Open University

Submitted for examination: 29th of December 2017

Abbreviations

ALH88045	Allan Hills 88045
AU	Astronomical Unit
CSE	Circumstellar envelope
D (^{2}H)	Deuterium
DCM	Dichloromethane
DNA	Deoxyribonucleic acids
DO3A	1,4,7,10-tetraazacyclododecane-1,4,7 -triacetic acid
DOTA	1,4,7,10-tetraazacyclododecane-1,4,7,10-tetraacetic acid
EDS	e-XL energy dispersive
EDTA	ethylenediaminetetraacetic acid
ET	energy transfer
Eu	Europium
EWG	Electron withdrawing group
FID	Flame ionisation detection
GC	Gas chromatography
GC-MS	Gas chromatography-mass spectrometry
GC-QMS	*Gas Chromatograph Quadrupole Mass Spectrometry*
GRS	Green River Shale
HCl(aq)	Hydrochloric acid
HPLC	High-performance liquid chromatography
HPLC-UV	High-performance liquid chromatography combined with UV absorption
IC	Internal conversion
IDPs	interplanetary dust particles
IOM	Insoluble organic matter
IPA	Isopropyl alcohol
IR	Infra-Red

ISC	Inter-system crossing
ISM	Interstellar Medium
L1	ethyl 2-[4,10-bis(3-cyano-1-ethoxy-1-oxopropan-2-yl)-1,4,7,10-tetraazacyclododecan-1-yl]-3-cyanopropanoate
L2	1,4-bis(prop-2-en-1-yl) 2-{4,7-bis[1,4-dioxo-1,4-bis(prop-2-en-1-yloxy)butan-2-yl]-1,4,7,10-tetraazacyclododecan-1-yl}butanedioate
L3	Prop-2-en-1-yl 2-[4-(2-{[(tert-butoxy)carbonyl]amino}ethyl)-7,10-bis[2-oxo-2-(prop-2-en-1-yloxy)ethyl]-1,4,7,10-tetraazacyclododecan-1-yl]acetate
L4	Methyl 2-[4,7-bis(2-acetamido-1-methoxy-1-oxopropan-2-yl)-1,4,7,10-tetraazacyclododecan-1-yl]-2-acetamidopropanoate
L5	Ethyl 2-{4,7-bis[1-ethoxy-1-oxo-3-(phenylamino)butan-2-yl]-1,4,7,10-tetraazacyclododecan-1-yl}-3-(phenylamino)butanoate
L6	Ethyl 3-amino-2-[4,10-bis(3-amino-1-ethoxy-1-oxobutan-2-yl)-1,4,7,10-tetraazacyclododecan-1-yl]butanoate
LC-FD	Liquid chromatography fluorescence detection
LC-FT-MS	HPLC coupled with a Fourier Transform mass spectrometer
LC-MS	Liquid chromatography coupled with mass spectrometry
LC-QqQ-MS	HPLC coupled to a triple quadrupole mass spectrometer
Ln	Lanthanide
Ln(III)	Lanthanide tripositive ion
Ma	Million years (mega-annum)
MBTH	*3*-methyl-*2*-benzothiozolonehydrozone hydrochloride
MCAs	Monocarboxylic acids
MeOH	Methanol
MTBSTFA	*N*-methyl-*N*-(*tert*-butyldimethylsilyl)trifluoroacetamide
NAC	*N*-acetyl-(*L*)-cynteine
NaOH	Sodium hydroxide
NR	non-radiative
OPA	*o*-phthalaldehyde
Os	Osmium

OsO_4	Osmium tetroxide
PAHs	Polyaromatic hydrocarbons
PET	Photoinduced electron transfer
q	Inner sphere hydration number (the number of bound water molecules)
QF	Quartz-feldspar
REE	Rare Earth Elements
SEM	Scanning electron microscope
SiC	Silicon carbide
SPE	Solid phase extraction
SPME	Solid phase micro extraction
T_3	Triplet state
TAP	*N*-trifluoroacetyl-(+)-pentyl
Tb	Terbium
t-BDMS	*bis*(*tert*-butyldimethylsilyl)
TFAA	Trifluoroacetic anhydride
TOF-MS	Time of flight mass spectroscopy
Tol	Toluene
TSD	Thermionic selective detector
UV	Ultraviolet

Abstract

The objective of this PhD project was to develop, test and evaluate lanthanide-based fluorescent sensors that could detect organic molecules in extracts taken from carbonaceous chondrite-type meteorites. These contain solvent soluble organic molecules, some of which are potentially prebiotic and are, therefore, of interest in the search for extinct or extant life in extraterrestrial environments.

The sensors are based upon the ligands DOTA and DO3A, the lanthanide complexes of which are well characterised and have been used as contrast agents and sensors in medical and biological sectors. Their application to the extracts of geological samples, and subsequent analysis by fluorescence spectroscopy, is, however, novel.

After testing on individual analytes, it was shown that nucleobases and benzoic acid modified the intensity of the lanthanide emissions and modified the form of the emission spectrum of europium by sensitisation of certain transitions. The presence of these analytes affected the spectra of the DO3A lanthanide complexes more effectively, therefore, novel, structurally similar DO3A-like ligands were synthesised, chelated to lanthanides and tested. Sensors were tested with individual analytes, solution obtained from weathered mineral samples, a terrestrial rock and two carbonaceous chondrites (Murchison and ALH88045).

Tests concluded that the presence of dissolved mineral species or mineral particulates in an extract would be unlikely to interfere with sensor responses. When applied to the extracts of the terrestrial and extraterrestrial rocks, the sensor responses were varied and, by comparing them to responses recorded when in the presence of individual analytes, indicated that the sensors detected the presence of structurally similar molecules. Therefore, it can be concluded that the sensors tested exhibit potential utility for analyte detection in a variety of scenarios. Using fluorescence techniques, perhaps as a 'lab-on-a-chip' device as part of the instrumentation on board a rover on the surface of planetary body, these sensors may be employed in the ongoing quest to detect evidence of alien life and clues as to how life began on Earth.

Acknowledgements

"We are all on the edge of ignorance; none of us *really* know what we're doing".

Dr. James Ironside Bruce (paraphrasing the musings of Terry Pratchett)

The work presented herein would absolutely not have been possible without the support of the wonderful people I have had the immeasurable pleasure of meeting, and supporting me, throughout the duration of my PhD.

I would first and foremost like to thank my supervisors, Dr. Victoria Pearson and Dr. James Bruce. Without Vic's thorough perfectionism in making sure my thesis was as good as it can be, the thesis would not have become as good as it became – not an easy task when having to wade through pages of waffle written by a prolific waffler. Vic, your dedication to the production of this thesis will never be forgotten. Thank you. James' unwavering encouragement and positivity has been consistently timely. Your genuine care and concern in all matters during what has been a tempestuous five years has been appreciated. I consider myself fortunate to have had you as my supervisors. I will conclude my thanks to my supervisors by saying that their support, along with Andrew Norton and Sarah Sherlock, behind the scenes (not related to the actual research) has been magnificent. Completing a PhD has been an ambition since I was very young…your efforts have ensured that that was possible.

I am indebted to the technical support provided by Mabs (whom is singularly wonderful), Matt, Brett, Simona, George, Jill and Michael. Pete Landsburg and Diane Johnson – all my respect and expressions of gratitude and admiration will never suffice to adequately give recognition for your dedication and friendship (not just to me, but all of us PhDers). Thank you.

Apart from a certificate with my name and confirmation of my qualification printed on it, the most valuable thing I will be taking with me after this PhD experience are the friendships I have made. In no particular order: Rachael (a.k.a. 'Minion' – keep swishing that labcoat!), Dan (best flat-mate ever and one of my favourite humans), Phillipa, Samantha, Beth, James, Jessica, Feargus, Jonny, Anton, Andy, Ben, Joe, Bianca, Jean-David, Mohit, Hannah x2, Matt x4, Shannon,

Callum (thank you – your selfless genuine care and support really kept me going and will be treasured), Erika (the wife – I'm going to miss those mid-corridor cuddles!), Professor Monica Grady who has avidly followed my progress, been keenly interested in my work from mini-*viva* right through to the main event – a truly lovely person whom I admire greatly – and Tom (We started together and we, perhaps against the odds, completed the task – thank you for your counsel and cocktails!). The list of people to thank is practically endless; I wish I could mention everyone who has made this process bearable but space does not permit. Suffice it to say I take my memories of you all with me, cherished, forever.

Away from the PhD, I would like to offer special thanks to Dynamic Imaging Analytics Limited (Neil, Sheree, Joe and Anthony) for a fantastic six months working on some amazing space related projects (LUVMI and SμGRE-1). Thanks to my PGCE mentor, Rachael, NQT mentor, Pauline, and Director of Science, Kevin, at Milton Keynes Academy, for your support, patience and understanding. Dr Nigel Russell-Sewell and Dr Corinne Kay (OU Associate Lecturers); thank you for your support during my undergraduate degree, and encouragement to undertake a PhD in the first place. I value the wonderful friendship that has grown over the years. Special mention should also be made for Mr Butler, Dr Moran (the inspiration for wanting to gain a PhD) and Dr Richardson; my brilliant school and college chemistry teachers. They all inspired me to want to teach. Thank you so much; without your influence, I would not be teaching the subject I love today and, hopefully, inspiring the chemists and teachers of tomorrow!

To my family who have been utterly ignored for too many years: for those of you who have, when contact was occasionally made, made sure I know how proud they are of me and all my various achievements, in particular, my wonderful Nan Mary, thank you. Lorraine and Phil – words cannot express the debt I owe you; without your kindness, support and generosity I could not have completed this work. The importance of what you have done for me cannot be overstated.

Dedication

I dedicate this work, in part, to my nieces and nephews: **Jake**, **Kai** and **Imogen**; **Samuel** and **Sophie**; **Zeph** and **Quinn** – never, ever, give up on your dreams…even if it's excruciating and you wonder if the effort you're putting in is worth it…IT IS, ALWAYS! I am so proud of everything you have, and will, achieve. I will always be here for you if, and when, you need me.

And finally…

This thesis would not have been completed if it had not been for the ineffable love and encouragement of my best friend. You have been ever supportive with your caring, and always honest, counsel (especially when I have been an infuriating hysterical mess, which was often). You have understood the enormity of the task at hand, lifting me when I have been crushed by frustration and elevating me to the stratosphere when things have gone well. In fact, I think you may well be more excited about this thesis than anyone else (other than me, of course). My fortitude has been maintained, and amplified, because of all this; your support, unwavering, throughout. I could not have done this without you. I cannot thank you enough. Therefore, Nikolai, this thesis is also dedicated to you, and our friendship.

Table of Contents

List of Figures

List of Tables, Schemes and Equations

1 Introduction

1.1 Aims and description of the project

The aims of this PhD are to develop techniques that utilise fluorescent sensors, and to ascertain their applicability and effectiveness, for the detection of extraterrestrial organic molecules. It is proposed that the sensors will interact with solvent-extracted meteoritic organic species in such a way that it will be possible to identify the presence of specific compound classes or molecules within what are otherwise complex organic mixtures. The intent, therefore, is to lay the foundation for the development of a new analytical technique using fluorescent lanthanide complexes and fluorescence spectroscopy to identify and characterise extraterrestrial organic material in solution and improve on current analytical techniques (see Section 1.3.2). This may eventually lead to the routine use of fluorescent, cyclen-based, lanthanide complex sensors for the detection of organic molecules for any application to samples, *in aquo*, where the identification of organic compounds may be required, e.g. water contamination or science missions to Solar System objects suspected of harbouring organic compounds. With further work, these sensors may be subsequently developed for *in situ* applications that do not require sample manipulation, possibly allowing elucidation of spatial associations between organic species and minerals, and may, in turn, give clues as to the chemical evolution of the building blocks of life.

1.2 Carbonaceous chondrites

The extraterrestrial organic matter targeted in this thesis is present in carbonaceous chondrite-type meteorites. Carbonaceous chondrites are fragments of asteroids (the meteorite 'parent bodies'), which formed at the same time as the Solar System, some 4.56 billion years ago. Their asteroidal origin has been indicated by spectroscopic comparisons and extrapolation of witnessed fall trajectories, for example, the Tagish Lake meteorite has been identified as sourced from a D- or P-type asteroid (Hiroi et al., 2001, Izawa et al., 2015). C-type asteroids are suggested to be the source of most carbonaceous chondrites including Murchison (Cloutis et al., 2011, Matsuoka et al., 2015), a key meteorite used throughout this thesis (Figure 1.1).

Figure 1.1 Murchison CM meteorite: seen to fall in Murchison, Victoria, Australia, in 1969. It is considered to be pristine since it was collected mere hours after it impacted the Earth. Credit: meteorlab.com

The composition of carbonaceous chondrites has remained relatively unchanged since their asteroids accreted, i.e. they have not been subject to differentiation, but have been subject to physical and chemical processing including heat (Tonui et al., 2014), fluid (McSween, 1979) and impacts (Rubin, 2007) on the asteroids from which they originate. As such, they provide an insight into the physical and chemical environment of our local cosmological province, and the component material that coalesced to form the Solar System.

There is compositional heterogeneity between carbonaceous chondrites, indicative of either different parent bodies or conditions that differ on a local (asteroidal) scale. This varying composition, and the mineralogy that is manifest, enables them to be classified into different groups (CI, CM etc.) (McSween, 1999). It is not required to outline the subtle differences between the carbonaceous chondrite groups here, but this thesis has focused on one of the more well-characterised groups, the CM chondrites, and the discussion of carbonaceous chondrite composition is therefore, unless stated, based on studies of CM chondrites.

Carbonaceous chondrites contain products of high- and low-temperature astrophysical processes that vary in abundance between the carbonaceous chondrite groups. For example, they contain condensates, which are believed to be evidence of high temperatures close to the proto-Sun in the accretionary disk from which the Solar System formed (MacPherson et al., 1983, Palme et al.,

1993, Brearley and Jones, 1998, MacPherson, 2003, MacPherson, 2007), as well as secondary minerals, such as clay minerals, that evidence low temperature aqueous alteration in asteroids (Zolensky et al., 1993, Brearley and Jones, 1998, King et al., 2017).

Carbonaceous chondrites are composed of up to more than 95% (by mass) inorganic mineral phases (Hezel and Palme, 2010). These consist of two main fractions: anhydrous components (including calcium-aluminium rich inclusions and chondrules, composed of minerals such as olivine and pyroxene) (Brearley and Jones, 1998) and a fine-grained matrix consisting of clays, oxides, carbonates, sulfates and sulfides (Brearley and Jones, 1998). Chondrules and calcium-aluminium rich inclusions are believed to have been among the earliest condensates to form in the Solar System (MacPherson et al., 1983, Palme et al., 1993, MacPherson, 2003, MacPherson, 2007), however the origin of the matrix is still the subject of debate (e.g. Hezel and Palme, 2010). The prevailing model is that the matrix mineralogy currently identified in carbonaceous chondrites was formed by low-temperature aqueous processing on the asteroidal parent body by the melting of ices shortly after the asteroid accreted (Zolensky et al., 1993, King et al., 2017). Significantly, organic matter in carbonaceous chondrites has been found in intimate relationship with the matrix (Pearson et al., 2002, Pearson et al., 2007, Goodyear et al., 2011), suggesting a co-evolution.

1.3 Organic matter in carbonaceous chondrites

Although organic material has been identified in fluid inclusions in some ordinary chondrite type meteorites (Chan et al., 2012, Kebukawa et al., 2017, Chan et al., 2017), the organic matter in carbonaceous chondrites is well-characterised and provides a baseline for the development of sensors for organic matter detection. Most of the following review is based on the organic component found within the Murchison CM chondrite, one of the most studied carbonaceous chondrites. Importantly, in order to limit the scope of testing needed, Murchison has been selected as the reference meteorite for testing of the sensors in this research.

The proportion of organic matter present in carbonaceous chondrites has not been accurately measured because of difficulties in extracting, analysing and quantifying the different types of organic material present (Goodyear, 2013), but is commonly quoted as up to 5% (by mass). Approximately 30% of this is solvent soluble, i.e. extractable from the meteorite using one or more solvents; the remaining 70% is termed macromolecular material or insoluble organic matter (IOM) which cannot be removed from the meteorite with solvent.

Although the IOM represents the bulk of the organic matter in carbonaceous chondrites, it is not the focus of this thesis, which is on developing a sensor to detect organic molecules in solution, i.e. sourced from the extractable fraction. Hence, details on the IOM are given briefly in Section 1.3.3, for completeness, and the remainder of this chapter will concentrate on the extractable fraction.

1.3.1 Solvent soluble organic compounds

The organic material described below is the most accessible fraction of the total organic component of carbonaceous chondrites because it is solvent soluble. The purpose of this research is to develop a sensor for the detection of organic material contained within the solvent extracts derived from organic-rich extraterrestrial samples, therefore, it is anticipated that the sensor will be applied in solution. For this reason, and in order to develop such a sensor, it is important to understand the type of organic material that a solvent extraction will liberate. Knowledge of these types and classes of organic molecule, and their physical and chemical properties, will enable physical and chemical properties of a suitable sensor to be determined.

The solvent soluble fraction is composed of discrete, functionalised, and therefore reactive, molecules. The chemical groups include hydrocarbons (Levy et al., 1973, Krishnamurthy et al., 1992, Martins et al., 2015, Huang et al., 2015), alcohols (Jungclaus et al., 1976), amines (Pizzarello et al., 1994, Aponte et al., 2014, Martins et al., 2015), sugars (Cooper et al., 2001) and oxygen, sulfur and nitrogen heterocycles (Stoks and Schwartz, 1981, Orthous-Daunay et al., 2010, Callahan et al., 2011). Molecules with carbonyl moieties are in abundance. These include aldehydes,

ketones, amides (Hayatsu et al., 1975, Cronin et al., 1993, McGeoch and McGeoch, 2015), and carboxylic acids (which dominate the solvent soluble fraction) including monocarboxylic acids (Krishnamurthy et al., 1992, Pizzarello et al., 2001), hydroxycarboxylic acids (Peltzer et al., 1984), dicarboxylic acids (Martins et al., 2006), and aromatic carboxylic acids (Martins et al., 2006). Triazines and other biologically important molecules, such as the nucleobase classes of pyrimidines (diazines) and purines are also present (Folsome et al., 1971, Hayatsu et al., 1975, Huang et al., 2005, Martins et al., 2008, Callahan et al., 2011). These are the essential base pair components for the genetic coding part of deoxyribonucleic acids (DNA) (Watson and Crick, 1953).

Amino acids are also present in the extractable fractions (Kvenvolden et al., 1971, Cronin and Pizzarello, 1983, Pizzarello and Cronin, 2000, Meierhenrich et al., 2004, Burton et al., 2012, Burton et al., 2014, Martins et al., 2015). These are particularly important when studying the chemistry and origin of prebiotic molecules and the chemical processes that could lead to the development of self-organising and self-replicating chemical macrostructures, e.g. proteins. The suite of amino acids in carbonaceous chondrites demonstrates a remarkable diversity in isomers, many of which are rare or even unknown on Earth and appear in meteorites as near racemic mixtures of (*L*) and (*D*) enantiomers, e.g. isovaline in the Paris meteorite (Martins, 2015), and enantiomeric excesses of (*L*) isomers in many others (Cronin and Pizzarello, 1997, Pizzarello and Cronin, 2000, Glavin and Dworkin, 2009, Glavin et al., 2012). This mixture of isomers is not known terrestrially in the inventory of biotic amino acids, i.e. those amino acids produced by living organisms. Only the (*L*) enantiomer is essential for maintaining the structure of proteins; thus, it is ubiquitous on Earth, in contrast to the (*D)* enantiomer which is not (except in the case of sugars and other similar abiotic and biotic molecules). The fact that both isomers are found in carbonaceous chondrites is important because it suggests: i) these molecules were synthesised free from constraint in that they can form any branched structure, valence permitting (implying formation in the vacuum of space) and ii) they were formed abiotically.

The extractable organic material is the most accessible fraction of the total organic component of carbonaceous chondrites. As such, and because of the presence of biologically important molecules, it is also the most analysed fraction. The following section outlines the historic methods used for extracting and analysing this organic fraction.

1.3.2 Characterising the solvent soluble organic material

Characterisation of the organic species in carbonaceous chondrites is traditionally undertaken using analytical techniques that requires the destruction of the sample in order to facilitate their extraction, e.g. crushing the sample to a fine dust, or disaggregating the sample using freeze-thaw cycles and sonication (Yuen et al., 1984, Butterworth et al., 2004). Most techniques then require the samples to be refluxed with aqueous and organic solvents to remove the solvent soluble organic species (Lawless et al., 1974, Cronin, 1976, van der Velden and Schwartz, 1977, Lawless and Yuen, 1979, Stoks and Schwartz, 1979, Becker and Epstein, 1982, Stoks and Schwartz, 1982, Yuen et al., 1984, Krishnamurthy et al., 1992, Pizzarello et al., 1994, Cooper and Cronin, 1995, Botta and Bada, 2002, Martins et al., 2008, Smith et al., 2014).

Amino acids can be extracted using only hot water (Cronin *et al.*, 1976, and references therein). The extracts are desalted by cation exchange chromatography (e.g. Burton *et al.*, 2014) and either analysed without pre-treatment (e.g. Cronin *et al.*, 1981, Glavin *et al.*, 2012), or first chemically 'unbound' by acid hydrolysis (e.g. Cronin *et al.*, 1986, Chan *et al.*, 2012, Callahan *et al.*, 2014). The amino acids may also be derivatised prior to analysis by esterification to produce, for example, *2*-pentanyl (e.g. Cronin *et al.*, 1981) and *N*-trifluoroacetyl-(+)-pentyl (TAP) esters (e.g. Cronin *et al.*, 1986), or undergo esterification with propanol and subsequent acylation with trifluoroacetic anhydride (TFAA) (Chan et al., 2012). These 'pre-treatment' techniques facilitate separation for more successful analysis by gas chromatography (GC) (Kvenvolden et al., 1971, Cronin et al., 1981, Meierhenrich et al., 2004, Chan et al., 2012) and gas chromatography-mass spectrometry (GC-MS) (Cronin et al., 1985, Chan et al., 2012, Martins et al., 2015).

Amino acids are not intrinsically fluorescent, but fluorescence spectroscopy has been utilised to identify them once derivatised with the fluorogenic reagent *o*-phthalaldehyde (OPA) and separated by column chromatography (Cronin and Hare, 1977). The relative fluorescence yield (i.e. fluorescence intensity) was then used to distinguish individual amino acids from one another (e.g. Cronin and Hare, 1977, Cronin et al., 1986). Identification of hot-water and acid hydrolysis extracted amino acids using OPA combined with *N*-acetyl-(*L*)-cynteine derivitisation (OPA/NAC), enabled optimised enantiomeric separation and identification of chiral amino acids by liquid chromatography fluorescence detection (LC-FD) combined with time of flight mass spectroscopy (TOF-MS) (e.g. Glavin and Dworkin, 2009, Glavin et al., 2012, Callahan et al., 2014).

Although these techniques ultimately use fluorescence spectroscopy to identify amino acids in meteorite extracts, the amino acids must first undergo extensive processing, even after extraction from the meteorite sample. However, the processing required to achieve amino acid separation and identification is also very cumbersome and multi-stepped, making it an unappealing methodology in a laboratory or in the field. A technique that can use fluorescence spectroscopy that does not require such convoluted procedures would be desirable.

Carboxylic acids are also isolated in hot water (from 80°C to 110°C) extracts and have been found to include straight-chain and branched mono-, di-, hydroxy- and aromatic classes (Huang et al., 2005, Martins et al., 2006, Cooper et al., 2011, Smith et al., 2014), the most abundant of which are the monocarboxylic acids (MCAs) (Lawless and Yuen, 1979, Naraoka et al., 1999). Previous hot-water extractions and analyses undertaken in the 1970's elucidated only 18 MCAs in the Murchison meteorite (Yuen and Kvenvolden, 1973). However, it was suggested that the experimental procedures employed did not reveal the entire carboxylic acid inventory (Huang et al., 2005). Part of the extraction process used dichloromethane (DCM) and water to separate water-miscible low molecular weight carboxylic acid components from the extract; the solvent removal steps may have resulted in the co-volatilisation of low boiling fractions and an underrepresentation of the carboxylic acids present. Cryogenic distillation and ion chromatographic analysis demonstrated retention of ethanoic acid (Yuen et al., 1984) further

suggesting volatile carboxylic acids may be lost when removing solvent by evaporation. This implied that there may be more carboxylic acids present than had been identified. Subsequent analyses addressed the limitations of Yuen and Kvenvolden's (1993) technique by, for example, using fused silica GC columns in preference to stainless steel capillaries (Huang et al., 2005), and the inventory of carboxylic acids increased to 35.

Analysis of the MCA content of Murchison was revisited by Huang et al., (2005), who combined Solid Phase Micro Extraction (SPME), developed for the analysis of water soluble organic molecules (Lord and Pawliszyn, 2000), with GC and GC-MS-FID (Flame Ionisation Detection). This technique negated the use of solvents and so circumvented the volatilisation of low molecular weight components believed to occur during solvent removal (Huang et al., 2005). Using this procedure, the total number of MCAs identified was increased to in excess of 50.

As with amino acids (*vide supra*), carboxylic acids may be derivatised to produce their respective esters to facilitate GCMS analysis. For example, hydroxycarboxylic acids may be separated from dicarboxylic acids using column chromatography and characterised by GCMS, having first been treated with *N*-methyl-*N*-(*tert*-butyldimethylsilyl)trifluoroacetamide (MTBSTFA) to produce *bis*(*tert*-butyldimethylsilyl) (*t*BDMS) derivatives, i.e. silylation (Cronin et al., 1993, Cooper and Cronin, 1995). Aromatic carboxylic acids have also been identified by employing derivatisation prior to GCMS analysis. For example, Pizzarello et al., (2001), identified two isomers of nicotinic acid and twelve of its methyl and dimethyl homologs via their isopropyl derivatives, having been esterified using isopropanol. Martins et al., (2006) identified benzoic acid, phthalic acids and methyl phthalic acids, as their methyl esters, by reaction with tetramethylammonium hydroxide in methanol.

Alcohols and carbonyl compounds such as aldehydes and ketones have been extracted using similar protocols for hot-water extractions, outlined above. Alcohols were identified in Orgueil (CI1) and Murray (CM2) using thermal extraction mass spectrometry (Studier et al., 1965) and in Murchison using colorimetry, GC and GCMS (Jungclaus et al., 1976). Ketones and aldehydes have

been characterised by GC and GCMS, but only after laborious chemical processing to separate them from one another. In order to do this, they must first be converted to their corresponding water-insoluble semicarbazone derivatives, separated and dried. Once dried they must then restored by acidification using phosphoric acid (Jungclaus et al., 1976). However, these techniques cannot provide quantitative information about these compound classes. This has been obtained through the use of other analytical techniques, such as colorimetry (Jungclaus et al., 1976), that require the restored molecules to be pre-treated. For example, aldehydes are reacted with *3*-methyl-*2*-benzothiozolonehydrozone hydrochloride (MBTH) (Weiss, 1970) to produce a greenish-blue complex that can be analysed. Junglaus et al., (1976) used this technique to establish the total aliphatic aldehyde concentration of Murchison. The total molar quantity of primary aliphatic alcohols was elucidated using this reaction, then colorimetry. However, in order to accomplish this, the primary alcohols must first be converted into their respective aldehydes by oxidation using permanganate (Jungclaus et al., 1976).

Aromatic heterocyclic compounds such as purines and pyrimidines, i.e. nucleobases, are less soluble in water than carboxylic acids and amino acids so are not extracted using hot water. They therefore require extraction using other solvents, such as ethyl ethanoate (ethyl acetate) (Stoks and Schwartz, 1982) or, more commonly, methanoic acid (formic acid) (Folsome et al., 1973, Hayatsu et al., 1975, van der Velden and Schwartz, 1977, Stoks and Schwartz, 1982, Callahan et al., 2011, Martins et al., 2008). An activated charcoal wash step, sometimes combined with celite (Folsome et al., 1973), is often included in order to separate the nucleobases from other aromatic or non-polar constituents (Kvenvolden et al., 1970, Folsome et al., 1971, van der Velden and Schwartz, 1977, Martins et al., 2008). Charcoal filtration involves elution of the adsorbed nucleobases with formic acid to yield the heterocyclic extract. This multi-step process for purification may result in contamination and/or loss of analytes, therefore protocols using solid phase extraction (SPE) techniques have been employed (Burton et al., 2012).

Nucleobase extracts have been analysed directly by liquid chromatography coupled with mass spectrometry (LC-MS), high performance liquid chromatography combined with UV absorption

(HPLC-UV) (Stoks and Schwartz, 1979, Shimoyama et al., 1990) and dual-column ion-exclusion chromatography and UV spectroscopy. Further, Hayatsu et al. (1975) directly volatilised nucleobase extracts into the source region of a mass spectrometer from a platinum filament to obtain mass data, while Stoks and Schwartz (1982) employed capillary GC and GCMS-FID and a thermionic selective detector (TSD) (for detection of nitrogen).

These early techniques did not take into account compounds that may co-elute during purification processes or during GC-MS analysis, however, improved techniques for nucleobase analysis have been employed through the use of Gas Chromatograph Quadrupole Mass Spectrometry (GC-QMS) (Martins et al., 2008), HPLC coupled to a triple quadrupole mass spectrometer (LC-QqQ-MS) and HPLC coupled with a Fourier Transform mass spectrometer (LC-FT-MS) (Callahan et al., 2011). QqQ-MS permits more sensitive detection of analytes because characteristic daughter ions are produced when individual parent molecules are fragmented. Furthermore, if the analyte is present in high enough concentrations, verification of analytes may be achieved *via* the collection of fragmentation MS/MS spectra (Burton et al., 2012). FT-MS (Marshall et al., 1998) has also been used to elucidate high resolution mass measurements of analyte and fragment masses, and enables definition of elemental formulae for the amino acids.

Meteoritic hydrocarbon fractions were extracted by Krishnamurthy et al. (1992) by employing the use of freeze-thaw disaggregation of the sample followed by cryogenic transfer of low molecular weight fractions with water through dry sodium hydroxide (NaOH) at liquid nitrogen temperatures. A benzene-methanol solvent was then used to obtain the remainder of the hydrocarbon content and this was separated into fractions using silica gel chromatography. Thereafter, these, and the low molecular weight fractions, were characterised by GCMS. Polyaromatic hydrocarbons (PAHs) have been extracted from crushed samples using successive methanol (MeOH) then dichloromethane (DCM) solvents followed by GC-FID and GC-MS characterisation (Huang et al., 2015), while Martins et al. (2015) employed a MeOH/DCM solvent mixture. Some methods used to determine the hydrocarbon constituent of carbonaceous chondrites have not required the use of a solvent. For example, Butterworth et al. (2004)

detected methane, released by freeze-thaw dissagregation of Murchison and Cold Bokkeveld, using mass spectrometry. Volatile hydrocarbons were also successfully extracted *via* step-wise volatilisation of meteorite samples and analysed by GC (Levy et al., 1973).

As has been made clear, many of the characterisation techniques require the indigenous organic compounds to be derivatised before they can be analysed and this involves complex chemical treatment. Indeed, some organics, such as alcohols and carbonyl compounds, must undergo extensive chemistry in order to even use simple methods (e.g. colorimetry) to determine their concentrations. It is therefore desirable to ascertain the composition of a solvent extract of a carbonaceous chondrite by methods which circumvent the requirement for complicated chemical derivatisation of the analytes of interest. To achieve this, a sensor that can be applied directly to an untreated extract is needed and, moreover, this sensor should be one that does not alter the chemistry of the analyte.

1.3.3 Macromolecular Material (Insoluble organic material, IOM)

The macromolecular fraction of the organic inventory of the carbonaceous chondrites consists of a large network of polyaromatic hydrocarbons linked by aliphatic, hetrocyclic aromatic, aromatic and/or polyfunctionalised bridging structures (Fitch et al., 1962, Hayes, 1967, Kvenvolden et al., 1970, Bandurski and Nagy, 1976, Hayatsu et al., 1977, Botta and Bada, 2002, Pearson et al., 2006, Derenne and Robert, 2010, Schmitt-Kopplin et al., 2010, Remusat, 2014). The size of these polyaromatic groups is generally one to five aromatic rings (such as naphthalene – the predominant aromatic component – benzene, phenylbenzene, anthracene, fluoranthene) and sulfur-, nitrogen- or oxygen-containing aromatic cyclic moieties (such as thiophenes, pyrroles and furans etc.), which are all linked together by aliphatic (alkane and alkene), ester, ether (oxygen atoms), thioether (sulfur atom) and amine (nitrogen atom) bridges (Derenne and Robert, 2010, Remusat, 2014).

These networks are solvent insoluble and are associated with the inorganic component of the matrix (Pearson et al., 2002, Brearley, 2002, Pizzarello et al., 2006, Alexander et al., 2007, Flynn et

al., 2013), which means this fraction is relatively difficult to extract without using degradative techniques. For this reason, the IOM was not studied to the same degree as the solvent soluble fraction. However, as methods were developed to degrade the mineral phase, the IOM became more accessible (for a review, see Pearson, 2010). Although peripheral molecules of the IOM can be liberated without dissolution of the mineral phase (the 'labile' phase; Sephton, 2013), it is only when the inorganic mineral phase is removed or disrupted, using techniques such as carbonate and silicate dissolution via rigorous chemical treatment (Hayes and Biemann, 1968, Amari et al., 1994, Sephton and Gilmour, 2001, Cody et al., 2002), that this insoluble organic phase is fully freed for extraction and characterisation.

Significantly, it was chemical treatment of this kind that revealed for the first time that there may be relationship between organic material and inorganic mineral phases. It was increasingly evident that, as more inorganic mineral matrix was removed using extensive and rigorous techniques, as opposed to simple acid washes, it was possible to liberate even more organic material (Amari et al., 1994). It was therefore possible to infer a correlation between the quantity of organic material extracted and the amount of mineral matrix, and as a result, the idea that relationships between the IOM and mineral phase existed was proposed (Collins et al., 1995, Salmon et al., 2000, Nakamura et al., 2002). This theory was tested by Pearson et al., (2002), who impregnated samples of Murchison, Orgueil, Ivuna and Tagish Lake with osmium tetroxide (OsO_4) vapour. This process labelled carbon-carbon double bond constituents of the IOM with osmium (Os) enabling the use of a scanning electron microscope (SEM) fitted with an e-XL energy dispersive (EDS) x-ray micro-analyser to elucidate spatial associations between IOM and the mineral component of the samples. This work indicated Os labelled IOM was affiliated to hydrous clay minerals but not with any other aqueous mineral phases. These associations were confirmed when ozone impregnation, which also targets carbon-carbon double bonds, to convert them to carbonyl moieties, and molecular tagging was carried out on samples of Murchison (Goodyear et al., 2011). In the long term, a sensor such as the ones presented in this thesis could be developed for application to *in-situ* analysis, however that is beyond the scope of this study.

1.4 Extraterrestrial origins of meteoritic organic compounds

Organic material extracted from carbonaceous chondrites is assumed, by the fact the sample originated from space and fell to Earth, to be of extraterrestrial origin, however, some organic material may be of terrestrial origin, and may be co-extracted with indigenous molecules. The magnitude of terrestrial contamination depends heavily upon the duration that the meteorite sample has been on Earth in the natural environment; therefore, the sooner the sample is collected after its fall, and isolated from the biosphere, the lesser the degree of possible contamination. It has therefore been essential to establish what evidence can be used to be confident of the extraterrestrial origin of chondritic organic material. With this evidence, it is then possible to suggest possible environments of formation in the cosmos.

1.4.1 Evidence for extraterrestrial origins

Chondritic organic matter shows complete structural diversity (Lawless, 1973, Cronin et al., 1981, Cronin and Pizzarello, 1986); every molecular structure is identified for any given molecular formula. This diversity is due to lack of steric restriction, save that of large bulky groups such as tertiary butyl moieties (McMurry, 2000), during their formation process. That is to say, reacting atoms are free to form bonds in whichever orientation is available according to electronic orbital positioning, rather than biologically-controlled or mediated reactions, as in the case of enzymes, where atoms and functional groups are delivered to reactive sites for the sole purpose of controlling structural conformations or reactions (Ringe and Petsko, 2008). Extraterrestrial organic molecules tend to be more commonly branched about a central carbon atom as a consequence of a stabilised carbocation (a positively charged carbon atom) and this stabilisation increases with increasing substitution (McMurry, 2000). The carbocation, therefore, becomes more stable as more bonds form, resulting in the branching observed (Shimoyama et al., 1989, Shimoyama and Shigematsu, 1994, Martins et al., 2006, Smith et al., 2014).

Consequently, there are many organic compounds present within carbonaceous chondrites that are not found on Earth, e.g. α-methylnorvaline, α-methylnorleucine (Engel and Macko, 1997, Pizzarello and Cronin, 2000), or are present in concentrations much greater than those found

naturally occurring on Earth e.g. isovaline, norvaline (Glavin and Dworkin, 2009, Glavin et al., 2012).

Meteoritic organic compounds have also been isotopically analysed and compared with equivalent terrestrial organic species. Terrestrial organic $\delta^{13}C$ values, for example, range from -35 to -25 ‰ whereas meteoritic extracts fall in the range +4.43 to +5.93 ‰ for the solvent extractable organic fraction (Kvenvolden et al., 1970). A study of amines in the Murchison meteorite suggested $\delta\ ^{13}C$ values to be in the +21 ‰ to +129 ‰ range (Aponte et al., 2014), presenting an enrichment of ^{13}C in carbonaceous chondrite organic compounds relative to terrestrial compounds. Similarly, enrichments of ^{15}N are reported for extraterrestrial amino acids, for example, where $\delta^{15}N$ is reported to be +60 to +200 ‰ versus -20 to +30 ‰ for terrestrial organic matter (Engel and Macko, 1997, Sephton and Gilmour, 2001, Pizzarello and Holmes, 2009, Burton et al., 2012, Chan et al., 2016). Enrichments of deuterium, D (^{2}H), have been reported to be up to +2024 ‰ (Huang et al., 2005) and more recently, when studying PAHs in Murchison and the LON94101 meteorite, δD values ranged from +120 to +900 ‰ and +180 to +1200 ‰, respectively (Huang et al., 2015). Other studies have also confirmed enrichment of D in extraterrestrial organic material, the largest ever recorded being that analysed in the GRO95577 (CR) meteorite, which revealed a D enrichment of 19,400 ± 4600 ‰ (Busemann et al., 2006).

Significantly, enrichments differ in magnitude depending upon the class of molecule. For example, values for hydroxyl acids, dicarboxylic acids and hydroxydicarboxylic acids vary, suggesting different source regions and/or different chemical evolution (Cronin et al., 1993, Sandford et al., 2006, Busemann et al., 2006, Alexander et al., 2007, Alexander et al., 2017). These isotopic enrichments may also be a consequence of alteration and modification *via* subsequent chemical reactions in space. Hence, the isotopic composition of organic species in carbonaceous chondrites can be used to infer both their extraterrestrial origin, and, potentially, their environment of formation.

The next section summarises some of the environments in which chondritic organic molecules may have formed, or were modified.

1.4.2 Postulated environments of formation

There have been a number of environments (and therefore processes) proposed to explain the formation of chondritic organic species through the formation and evolutionary processes of our Solar System. These environments include, for example, interstellar space, the Solar Nebula and asteroidal parent bodies, each with distinct chemical and physical environments. Many of these have been tested by laboratory simulations (Brown and Millar, 1989, Hill and Nuth, 2003, Johnson, 2007).

The formation of a planetary system follows a logical stepwise evolution, which includes: 1) circumstellar envelope (CSE); 2) the diffuse interstellar medium (ISM) and molecular cloud; 3) the Solar Nebula and proto-star 4) accretionary, or protoplanetary, disk (including disk edge environments) and 5) parent body (e.g. planetesimals, asteroids and comets). The chemistry that may take place in these varied environments is dictated by the conditions and the atomic and molecular raw materials available. It is impossible to discuss every environment and process proposed, but the most relevant and heavily cited are described here. Each environment will be addressed in turn, and some of the postulated reactions, and their products, will be introduced.

Circumstellar envelope (CSE)

The atoms that comprise the organic material as seen in carbonaceous chondrites were synthesised within stars. Our Sun is a low-mass star; such stars are hot enough to produce carbon, oxygen, nitrogen and other low atomic mass elements in its core. Around 80 gas phase species have been identified around low mass stars. These species include, for example, ethene, methane, methanol, and acetonitrile, has well as carbon-nitrogen chains, small cyclic hydrocarbons, e.g. C_3H_6, and radicals such as HCO^+ (Kwok, 2016). PAHs, polyynes and fullerenes are also likely to form (Helling et al., 1996, Cami et al., 2010, Gielen et al., 2011). These molecules are dispersed into the ISM by stellar winds, which also eventually disperse the CSE.

When the circumstellar environment is exposed, the stellar core is subject to ever more energetic radiation and so the formation of the next wave of molecules may begin (Kwok, 2016). Larger mass stars produce heavier atomic mass elements such as sodium, magnesium, silicon, iron and titanium (Cameron, 1955), but these atoms are dispersed into the interstellar medium (ISM) at the end of the star's life cycle *via* solar winds or supernovae (Heger et al., 2003) and are too hot to allow bond forming processes too occur.

Although polymerisation and subsequent cyclisation of the polyynes to produce PAHs may generate large hydrocarbon networks that bear a close resemblance to the suggested structure of the IOM in carbonaceous chondrites (Section 1.3.4), the IOM is constructed of much smaller aromatic and heterocyclic ring units linked by aliphatic bridges rather than extended two-dimensional (2D) carbon sheets. It is possible, however, that functionalisation of the PAH network may be introduced by the reaction of small molecules or radicals present in the CSE or in prevailing conditions later in the evolution of the Solar System.

The diffuse interstellar medium (ISM) and molecular cloud

Once macromolecular structures and other small molecules synthesised within the CSE are dispersed into the ISM, they are subject to different environmental conditions that determine the mechanism of bond formation.

The ISM consists of gases (mostly H and helium, He), dust grains, and ice particles. The temperature can range from very cold (~10 K) to extremely hot (~10,000 K) and can range in density from diffuse (1 particle cm^{-3}) to dense (>10^4 particles cm^{-3}) (Nuth et al., 2006). Where temperature and density are low, gas phase reactions are less likely to take place since bonds can only form if atoms or molecules are close enough, and attain the activation energy required. Furthermore, gas is mostly transparent to UV radiation and so any molecules that may be formed will be short lived, being rapidly decomposed by this high energy radiation (Nuth et al., 2006). The regions where the density of gas, dust and molecular material is greater are referred to as molecular clouds. In these regions, a mechanism has been proposed that can protect molecules

and reactions from harsh UV radiation. This is termed 'extinction' (Nuth et al., 2006), which invokes the presence of large molecules such as PAHs (Siebenmorgen and Krügel, 2010) and the UV-scattering capabilities of dust, to shield reactions, allowing them to proceed. However, it is also possible that UV bombardment can produce radicals and charged ions in the gas phase, thus facilitating some reactions (Watson, 1976, Herbst and Dishoeck, 2009).

The most likely pathway for the synthesis of simple organic molecules in the ISM is on and within the icy mantles on dust grains in molecular clouds (Allamandola et al., 1999). In this model, atoms and molecules slowly accrete onto the surface of dust grains, often at the rate of one per day (Ehrenfreund and Charnley, 2000). Atoms or molecules may be adsorbed onto the surface and react as a result of proximity rather than acquired activation energy, i.e. the grains act as a catalytic site for reactions to occur; the product molecules will then either desorb or remain locked within the icy mantle.

Further reaction processes are believed to occur in molecular clouds: Strecker synthesis (Shibasaki et al., 2004) (to produce amino acids from simple aldehydes (or ketones) via α-aminonitrile intermediates) and Fischer-Tropsch-type reactions (Anders et al., 1973, Hayatsu et al., 1977) (catalysed reaction processes, producing hydrocarbons from hydrogen, carbon monoxide and other small reduced carbon molecules), are two such processes.

As the molecular clouds become denser, they begin to collapse as a result of increasing gravitational effects. Where this occurs, temperature and density increases, such that the reaction of simple organic molecules to produce more complex compounds becomes favourable. This favourability is exacerbated by the decrease in decomposition of organic molecules by UV radiation, since the dense molecular cloud is less transparent to such wavelengths. This has the effect of increasing the duration that a molecule is stable, thus promoting further reactions and, as a consequence, greater complexity. Such complex organic molecules have been observed by spectroscopic methods and their likely presence confirmed by laboratory simulations (van Dishoeck et al., 1993, Garrod and Herbst, 2006, Belloche et al., 2009, Vastel et al., 2014).

The dense molecular clouds are not uniform and exhibit regions that are denser than others, likely caused by shock events causing compression and promoting contraction under the influence of gravity (Boss and Goswami, 2006). This gravitational contraction elevates the temperature to 50 to 300 K (Andre et al., 2000) causing the icy mantles around dust grains to sublimate, releasing the organic molecules that they contain (Bernstein et al., 1995). Furthermore, the increase in density (10^{16} to 10^{18} particles cm^{-3}) increases the probability of collisions and so increases the rate of reactions and the complexity of likely reaction products (Hasegawa et al., 1992, Langer et al., 2000, Ehrenfreund and Charnley, 2000, Belloche et al., 2009). These regions are called hot molecular cores and are the precursors to solar nebulae, which they eventually form when their increasing density destabilises the region and contraction under gravity takes place (Nichols, 2006, Boss and Goswami, 2006).

Solar Nebula

Before the collapse of molecular clouds, a net angular momentum initiates as a result of the stellar winds and magnetohydrodynamic waves associated with local magnetic fields. This angular momentum results in material collapsing inward to form a proto-star (Andre et al., 2000), and in doing so increases the solar-core temperature to such an extent that nuclear fusion may begin (~10^7 K) (Pashitskii, 2017). The collapsing material rotates around the proto-star, forming an opaque disk that collapses inwards. Hence, conditions close to the proto-star may reach temperatures in excess of 1500 K (Ciesla, 2007), while the outer regions may be as cool as 50 K (Boss, 1998). As matter from the Solar Nebula falls into the developing star, a bipolar outflow of material is also generated, providing locally high temperatures (Boss and Goswami, 2006) that may promote catalytic formation of simple gas molecules such as those produced by the Fischer-Tropsch-type reaction, described above. Kinetic models for such a process have been evaluated and agree that such a process may occur (Kress and Tielens, 2001, Hill and Nuth, 2003).

The production of ammonia gas molecules may take place via the Haber-Bosch reaction, involving iron catalysed reactions of hydrogen and nitrogen (Jennings and Ward, 1989). This reaction would likely take place in regions of the nebula where the temperature is sufficiently high (500K to

900K), and where iron-rich dust grains such as kamacite and taenite (iron/nickel minerals) may be found (Hill and Nuth, 2003). Any organic material that had formed in the ISM would be destroyed by these conditions, however, away from these very hot regions, e.g. at the edges of the nebula, temperatures are cooler (50 to 150 K) (Boss, 1998, Aléon, 2010) organic material may survive.

Urey-Miller type reactions are also hypothesised to occur (Miller, 1953, Stoks and Schwartz, 1981). These reactions of methane, hydrogen, water and traces of ammonia by means of electric discharge synthesis (Ring et al., 1972) or radiation (Kerridge, 1999, Kwok, 2009) produce large inventories of amino acids. Other experimental work has proposed UV-induced synthesis of organic molecules in cooler regions (~40 to 300 K) *via* polymerisation on or in icy mantles in the outer Solar Nebula (Ciesla and Sandford, 2012).

Conversely, research has suggested that, under ionising conditions where reactions are driven by photon- and/or electron-driven processes at 1000 K or greater, organic compounds can be produced with similar chemical and structural features as those found in carbonaceous chondrites (Kuga et al., 2015). This suggests that organic synthesis does not necessarily need to occur in cooler regions of the nebula. As the nebula collapses further, and angular momentum increases, resulting in the inward accretion of more material, the nebula flattens to form a protoplanetary disk; it is the conditions within this region that the following section discusses.

Accretionary, or protoplanetary, disk

An accretionary disk is where the development of a planetary system takes place. At the furthest edges of the accretionary disk, at around 100 AU (1 AU = astronomical unit, or the distance the Earth is from the sun; ~93 million miles) the temperature is similar to that of interstellar space (~10 K), meaning ices and mineral grains with icy mantles containing organic molecules will survive intact. Closer to the Sun, at around 1 AU, the temperature is ~1000 K (Boss, 1998), suggesting ices would vaporise releasing organics which, at these temperatures, may be destroyed. This wide range of temperatures, and associated pressures, throughout the accretionary disk would suggest a similarly wide range of organic syntheses may take place. The

mechanisms of organic synthesis within the cooler regions are likely to follow similar pathways as those of the ISM, and therefore produce similar organic products (Hasegawa et al., 1992, Allamandola et al., 1999, Hill and Nuth, 2003, Remusat, 2014) including nitrogen-containing organic compounds, such as nucleobases (Hill and Nuth, 2003, Cleaves et al., 2012). Nearer the Sun, where it is hotter, reactions akin to those described in hot diffuse clouds, dense molecular clouds and the Solar Nebula may take place (Kress and Tielens, 2001, Hill and Nuth, 2003).

As the temperature of the disk increases, dust grains and similar material coalesces to form larger particles, in doing so incorporating organic material with it. These particles then collide and merge to produce ever larger particulates, and so the process continues. Ices, and grains with icy mantles, which contain organic material, and survived vaporisation in the colder outer regions of the protoplanetary disk (the disk edge and above and below the disk plane), may also be incorporated as the celestial bodies cool. Over time, planetesimals and other celestial bodies, including asteroids, form creating a Solar System (Johansen et al., 2015).

Solar System

There are two main factors which determine whether organic material present in the evolving planetary system survives when it is accreted. These factors are: 1) the proximity to the Sun and 2) the size of the evolving parent body. Logically, if the object is closer to the star, the hotter the body will be. Less obviously, however, is the physical size of the body - the larger the body, the hotter it will be. A larger body will be hotter because of the greater accumulation of radioisotopes with relatively short half-lives, such as ^{26}Al and ^{60}Fe (0.717 and 1.5 million years respectively) which cause radiogenic heating as a result of radioactive decay (Moskovitz and Gaidos, 2011). The hotter a body is, the greater the decomposition of the organic material *via* thermolysis and atomisation processes.

Therefore, a large body close to the sun will not engender an environment where organic material will survive. A large molten, radiogenically-heated body further away from the sun will undergo differentiation (a process where dense material, e.g. metallic elements, migrate to the centre of a

homogenous, fluid planetesimal, under the influence of gravity) and, likewise will not provide ambient conditions that will permit organic molecules to endure (Moskovitz and Gaidos, 2011). Organic material accreted by a smaller body close to the sun will likely undergo volatilisation and thermolysis, also destroying the organics present. Therefore, organic materials will survive in smaller bodies, further away from the Sun, where further organic synthesis may occur. Such bodies include asteroids, comets, and satellites of other planets (Cronin et al., 1988), where organic molecules have been detected by spectroscopy (Biver et al., 2014, Goesmann et al., 2015, De Sanctis et al., 2017, Schmitt et al., 2017, Barucci and Fulchignoni, 2017, Desai et al., 2017). Since carbonaceous chondrites are the main target samples of this study, the following discussion focusses on asteroids, specifically.

There is evidence that the parent bodies of carbonaceous asteroids underwent aqueous (and minor thermal) processing. Under such conditions, any organic molecules incorporated were likely to react further to produce complex molecules (Le Guillou and Brearley, 2014). Volatile organics and organic-rich ices on or near the surface of an asteroid are exposed to the low pressure of the vacuum of space and are prone to sublimation, however, organic material, water and other fluids deep within the interior are not (Brearley, 2006, Le Guillou et al., 2014). As ices melt, minerals such as olivine and pyroxene will hydrolyse resulting in the formation of secondary minerals which provide catalytic sites for reactions, e.g. phyllosilicates such as montmorillonite (Pearson et al., 2002, Cleaves et al., 2012, McAdam et al., 2015).

Alongside catalytically mediated reactions, other synthetic organic pathways have been suggested to explain the meteoritic organic inventory as it is seen today. For example, Strecker synthesis, mentioned previously as a possible route for production of amino acids in the ISM within icy mantles, may also produce amino acids within the parent body (Cronin and Pizzarello, 1997, Botta et al., 2002). Further, aldehydes or ketones may react with cyano compounds and ammonium salts to form α-aminonitriles, which are subsequently hydrolysed to produce amino acids (Lerner and Cooper, 2005). Also, sugars and polyols identified in carbonaceous chondrites may have been

produced by the reaction of formaldehyde and low molecular mass carbonyl compounds *via* the Butlerov reaction (formose reaction) (Cooper et al., 2001).

The movement and flow of fluids within the parent body is dependent upon that body's permeability or porosity such that the organic material is likely to be heterogeneously distributed (Bland et al., 2009, Le Guillou et al., 2014). This heterogeneity will likely be exacerbated by the localised distribution of minerals that allow catalytic chemical processes to take place. These catalytically synthesised organics and minerals are likely be co-located; however, it is also possible that further fluid flow may relocate and redistribute the synthesised organic material to locations throughout the matrix (Vollmer et al., 2014).

1.4.3 Summary of the synthesis of organic molecules in the cosmos

As described in the previous sections, synthesis of organic molecules in space occurs in many different environments under various conditions and *via* several mechanisms. Organic material may be produced in one environment only to be destroyed in another, or may also undergo chemical evolution to create ever more complex molecules. This means the organic material as seen in carbonaceous chondrites may be of pre-Solar System or Solar System origin, or a combination of both.

1.5 The importance of extraterrestrial organic matter

The organic molecules described in the preceding sections are of significance because they are all biologically important to life. Indeed, the organic material found within carbonaceous chondrites may have been delivered to Earth, 'seeding' the planet by acting as precursors or templates for the synthesis of similar organic molecules, or providing the raw materials for the synthesis of more complex organic structures. For this reason, it is important to understand their origin and the processes involved in their chemical evolution. As described *vide supra*, there has been concerted effort by many researchers to establish the identity of the organic components of carbonaceous chondrites with the express intent to offer plausible suggestions as to how they were formed.

At present, the majority of methods used to extract these analytes require the destruction of the extraterrestrial samples and often complicated treatments with several solvents and solvent mixtures to achieve this goal. Moreover, the organic solvent soluble molecules, once extracted, frequently require chemical derivatisation in order to ascertain their identity, which is, in itself, only an inference to the indigenous compounds. Therefore, *ipso facto*, the extracted organic material must also undergo complex processing; this results in convoluted and multi-stage methodologies. It is, therefore, of great interest to develop techniques that may utilise sensors which can directly identify the organic molecules contained within a solvent extract of a carbonaceous chondrite, without the requirement for derivatisation or complicated chemical processing. It is the aim of this research to develop such a sensor.

1.6 Characterisation of organic matter using fluorescence

Fluorescence spectroscopy has been used to identify organic material in terrestrial rocks (Howerton et al., 2002). It has also been used to identify PAHs and aromatic amino acids in extraterrestrial samples (Bramall and Allamandola, 2012, Dartnell et al., 2012), as outlined in Section 1.3.2. The disadvantage of these techniques is twofold: 1) the organic material must be intrinsically fluorescent (Section 1.4.1), thus limiting the scope of possible analytes the techniques may detect, i.e. only those that exhibit intrinsic fluorescence, and 2) any inorganic material in the sample, such as minerals, that also fluoresce, may cause background fluorescence which may interfere with the detection of the organic material of interest.

However, any fluorescent compound with a known fluorescence emission, that may be modified or altered when in the presence of specific organic analytes, may be used as a sensor for particular organic analytes. To be successful, such a sensor must also exhibit properties that differentiate its fluorescence from all other fluorescence emissions produced by the sample constituents. Furthermore, the fluorescent sensor should be one that can be used universally on all samples, for example, on extracts of chondritic organic material or on terrestrial water samples.

The sections that follow explain fluorescence, how it can be used as an analytical tool, and how it is to be harnessed in this study.

1.6.1 Photophysical Concepts

Fluorescence is the spontaneous emission of radiation from an excited molecular entity (Braslavsky, 2007). Essentially, this is the release of energy, often in the form of light, when energetically excited molecules return to their ground state. The wavelength of excitation energy absorbed is less than the wavelength of light emitted, and the emissions are governed by electrons transferring between energy levels for any given permitted transition.

When a substance is observed to emit electromagnetic radiation of a wavelength greater than that which it absorbed, the phenomenon is called luminescence (this is a general term which includes fluorescence and phosphorescence) (Lakowicz, 1983). This occurs because electrons in the ground electronic state of an atom or molecule ($S_0$0 on Figure 1.2) absorb excitation energy (represented by the arrow on the left) and in doing so are promoted to a higher energy electronic singlet state ($S_1$0-6). It is called a singlet state because the promoted electron does not change its spin i.e. it maintains parity.

The higher electronic energy state has a number of vibrational energy levels within it ($S_1$0, $S_1$1, $S_1$2, etc.), into which the excited electron may enter depending on its energy, which in turn is dependent on the energy it absorbs. In this case the electron has been promoted to $S_1$6 and non-radiative transitions occur (represented by small dashed arrows on Figure 1.2). The excited electrons transfer small amounts of energy to their surroundings in the form of heat. This is a very rapid relaxation *via* internal conversion to the lowest vibrational transition state of the first excited electronic state ($S_1$0). What follows is radiative transfer from the lowest vibrational transition state of the first excited electronic state stochastically to any one of the ground electronic state vibrational states ($S_0$0, $S_0$1, $S_0$2, etc.), in this case $S_0$4. It is this radiative transfer that constitutes the fluorescent emission signature (represented by the arrow on the right of Figure 1.2) and will have a slight variation in wavelength depending on which vibrational

transition state the electron enters the ground electronic state. Any electrons entering the ground electronic state at an excited vibrational level within it will undergo the same non-radiative transitions as described above until it reaches the ground state, $S_0 0$.

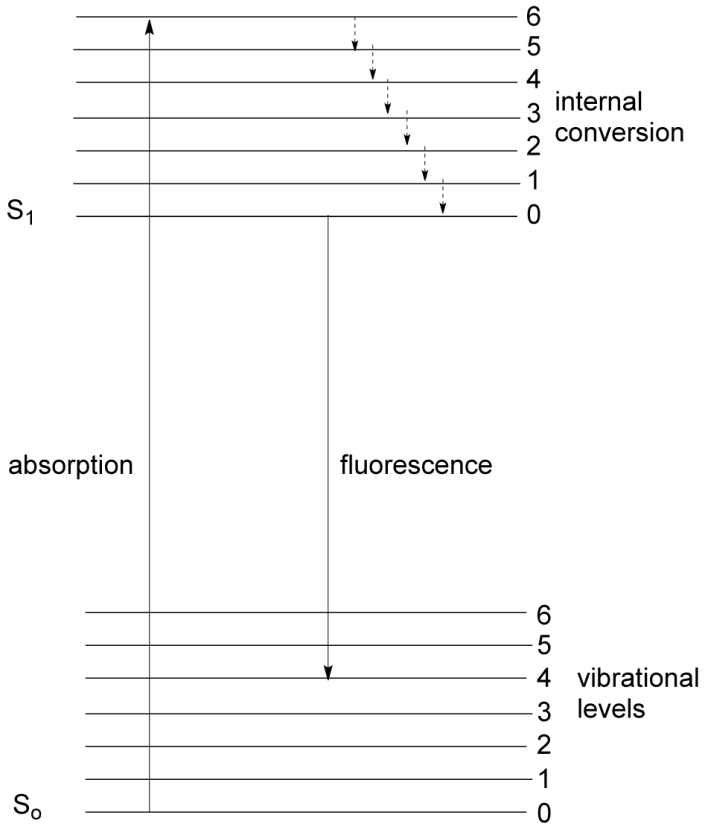

Figure 1.2 A schematic representation of absorption and subsequent fluorescence

1.6.2 Organic characterisation using fluorimetric analytical techniques

Organic molecules with aromatic and conjugated structures (carbon-carbon π (pi) bonded systems), where electrons are not localised to one atom or bond between two or more atoms but are delocalised across the molecular structure, often exhibit intrinsic fluorescence (Birks et al., 1968, Murae, 1999, Clemett et al., 2002, Bramall and Allamandola, 2012, Valeur and Berberan-Santos, 2013). The quantum yield of aromatic and conjugated organic π (pi) bonded systems is very efficient because the rigidity of the molecular structure is such that very little energy is lost to the surroundings due to vibrational, non-radiative, relaxation (Dartnell et al., 2012). Aromatic cyclic systems, such as polyaromatic hydrocarbons (PAHs e.g. naphthalene, pyrene, fluoranthene) have a greater probability of exhibiting fluorescence than straight chained conjugated systems, because the electron density circulates in a uniform fashion, i.e. they are distributed evenly, thus

reducing the probability of radiation-less energy transfer as the electron returns to its ground state. In the case of conjugated chains, the delocalised electrons are found mostly in the centre of the conjugated system and are limited in movement at the ends of the chain meaning that the electrons are less free for radiation-less transitions and therefore less likely to exhibit strong fluorescence (Weiss, 1943).

Electrons are able to make transitions from the filled electronic molecular orbitals to unoccupied, non-bonding, molecular orbitals, while maintaining parity i.e. spin, because the energy required to make the transition between molecular orbital energy levels is so small. If the electron drops back to the original orbital, or one of the same energy, then there will be a fluorescent emission (Weiss, 1943).

The organic material contained within carbonaceous chondrites includes many such intrinsically fluorescent molecules, and as such can be detected using fluorescence microscopy or, when an extract is dissolved in a solvent, spectrofluorimetry (or fluorimetry). The following section details how the fluorescent properties of some organic compounds may be used for their detection or characterisation.

Invoking intrinsic fluorescence

Intrinsic fluorescence can be harnessed by directly irradiating the surface of any sample with electromagnetic radiation of a wavelength sufficient to electronically excite organic molecules. By comparing this to known standard emittance data, it is possible confirm the presence of these compounds (Nadeau et al., 2008, Bramall and Allamandola, 2012). Emission and excitation wavelengths are indicative of certain groups of organic molecules by virtue of their chemical structure and can, therefore, act as a method of identification. The location of light emitted from the sample also provides a direct way to pinpoint the location of the organic material under investigation, if resolution allows.

The fluorescent properties of organic analytes have been used for many decades; fluorimetric techniques to detect intrinsically fluorescent organic molecules originated in the oil industry

(Radke et al., 1982). Other terrestrial uses include evidencing the presence of microbes in harsh environments (Dartnell et al., 2010), pollution monitoring (Howerton et al., 2002) and the detection of microorganisms in food, water and in the environment (Hill and Gray, 1967, Dartnell et al., 2012).

Using intrinsic fluorescence offers an *in-situ* technique that does not require sample preparation, long exposure time, or limited resources or reagents (Dartnell et al., 2012) and has thus been utilised *in situ* to analyse organic nano-globules within meteorites (Messenger et al., 2013). X-ray fluorescence spectrometers on board the Viking missions also utilised the intrinsic fluorescence of the martian soil to ascertain its composition (Klein, 1979) and similar instruments have been payload on board other missions, including NASA's MSL Curiosity rover on Mars. Curiosity's CheMin instrument is an X-ray diffraction and fluorescence spectrometer, designed to obtain data pertaining to the mineralogical composition of the martian regolith (Treiman et al., 2016, Achilles et al., 2017) in order to determine the conditions under which the regolith was formed and whether those infer present or past habitability (Blake et al., 2009, Sobron et al., 2012). Furthermore, the use of intrinsic fluorescence has been proposed for potential instruments on missions to detect bio-signatures and PAHs in the martian regolith (Sims et al., 2004, Nadeau et al., 2008, Storrie-Lombardi et al., 2009, Bramall and Allamandola, 2012, Dartnell et al., 2012).

It has been shown that some of the organic components, in particular PAHs, in solvent extracts of carbonaceous chondrites are fluorescent (Briggs, 1961), having been detected by spectrophotometry. Further, washing the surface of a sample of Murchison with chloroform removes a substantial amount of material with a yellow fluorescence (Murae, 1999). When analysed by spectrofluorimetry, those PAHs that exhibit highly ordered and therefore ridged structures, i.e. they consist of fused six (*hexa*-) membered (benzene) rings (Deamer and Pashley, 1989), show a fine structure. This manifests as well defined peaks in the fluorescence spectra enabling good probability of identification (Howerton et al., 2002). However, those PAHs with less consistent structures, for example those with five (*penta*-) membered rings (Huang et al., 2015),

provide broad spectra with few identifying structural features as a result of a lower rigidity (Howerton et al., 2002).

PAHs, and other simple organic molecules possessing aromatic structures, have been shown to fluoresce over a similar range of wavelengths (Dartnell et al., 2012) (e.g. 320 to 500 nm, Table 1.1) and with a similar 'fluorescent lifetime' (Berezin and Achilefu, 2010). The fluorescent lifetime is the average length of time taken for a population of electronically excited fluorescent molecules to decay from an excited state to the ground state *via* fluorescence; for many organic compounds this is in a nanosecond timeframe (Berezin and Achilefu, 2010). These factors mean that fluorescent emissions can be difficult to resolve for individual polycyclic aromatic compounds and so demonstrates that intrinsic fluorescence is not infallible as a means of facile positive organic compound identification.

Fluorescent molecule	**structure**	**Excitation λ, nm**	**Emission λ, nm**	**References**
benzo[a]anthracene	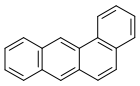	288	387	(Rivera-Figueroa et al., 2004)
benzo[k]fluoranthene	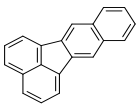	307	403	(Rivera-Figueroa et al., 2004)
benzo[a]pyrene	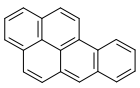	297	405	(Rivera-Figueroa et al., 2004)
chrysene	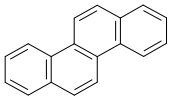	268	382	(Rivera-Figueroa et al., 2004)
phenanthrene	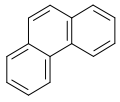	251	366	(Rivera-Figueroa et al., 2004)
anthracene	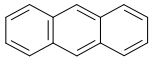	245	380/401	(Wheatley and Sadhra, 1998)
fluoranthene	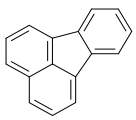	281	465	(Wheatley and Sadhra, 1998)

Fluorescent molecule	structure	Excitation λ, nm	Emission λ, nm	References
pyrene	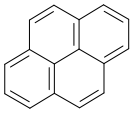	269	378/388	(Wheatley and Sadhra, 1998)
(*L*)-tyrosine	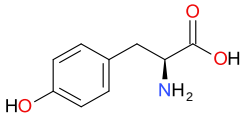	274	304	(Wünsch et al., 2015)
benzoic acid	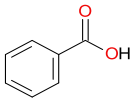	266	315	(Wünsch et al., 2015)

Table 1.1 Examples of emission wavelengths of fluorescent molecules found in carbonaceous chondrites

A further confounding factor on the use of intrinsic fluorescence as an analytical tool is the presence of minerals that also exhibit fluorescence. There are around a thousand fluorescent minerals identified in the literature (Henkel, 1989, Barthelmy, 1996, Ralph, 2001, MacRae and Wilson, 2008, Barmarin, 2009). Some of these minerals are found in carbonaceous chondrites (Fuchs et al., 1973), and, as such, may result in background fluorescence that may mask that associated with organic compounds; many minerals may fluoresce within the same wavelengths as the organic species, making them difficult to differentiate. Moreover, some non-fluorescent minerals exhibit the capability for atoms and ions of elements to 'dope' their ionic lattices by filling holes, or vacancies, within them (MacRae and Wilson, 2008). This can alter the electronic configurations of atoms and ions in the local vicinity and therefore induce fluorescent properties.

For these reasons, analysis of the organic component using direct irradiation to harness intrinsic fluorescence of target analytes is fraught with complications and has very limited analytical utility.

Targeted Fluorescent Labelling

Intrinsic fluorescence does, however, have a utility if it is used indirectly, i.e. molecules with intrinsic fluorescence can be used as markers to label specific analytes (Udenfriend et al., 1972). Some of these markers may bind to the analytes *via* electrostatic attraction or van der Waals type interactions, causing changes in the chosen marker's photophysical properties and indicating location of the analyte in, or on, the sample. Others will react with specific moieties, which are

part of these analytes chemical structure, thus indicating their presence in a sample. Some of these labels will not become fluorescent until a reaction has taken place; the reaction itself alters the electronic properties of the label in some way, thereby activating fluorescence. An example of a label whose fluorescence is activated in this fashion is fluorescamine (Udenfriend et al., 1972).

Fluorescamine is a ridged multi-heterocyclic compound consisting of aromatic benzene-type groups, oxygen containing furan-type groups and some ketone moieties (Figure 1.3).

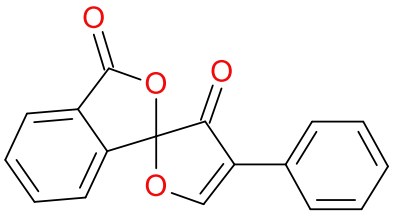

Figure 1.3 Fluorescamine

Fluorescamine and its degradation products are non-fluorescent (Udenfriend et al., 1972), making it an excellent reagent for labelling and detecting organic molecules with primary amine functional groups (Tamaura et al., 1975, Skelley and Mathies, 2003). Upon reaction with primary amine functional groups (Scheme 1.1), fluorescamine will produce fluorescent compounds that are detectable (Clemett et al., 2002, Skelley and Mathies, 2003)(e.g., Figure 1.4, Li *et al.*, 2016).

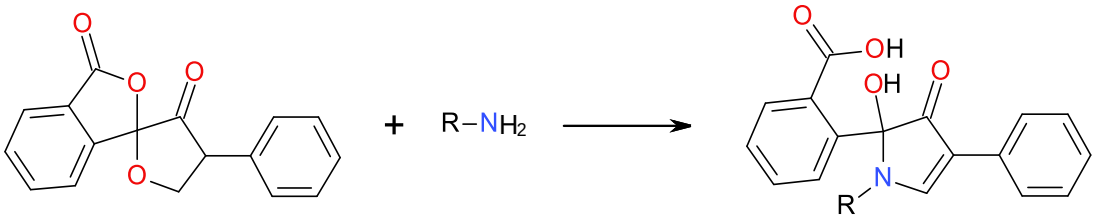

Scheme 1.1 Reaction of non-fluorescent fluorescamine with a primary amine to yield a fluorescent molecule detectable by fluorescence spectroscopy

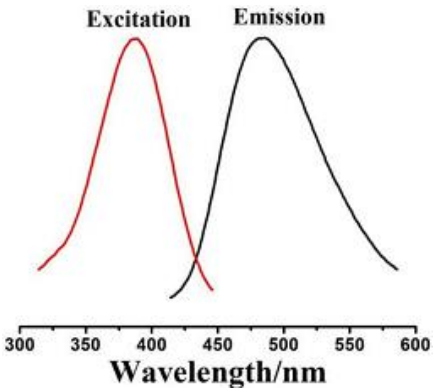

Figure 1.4 Excitation and emission spectra representative of a fluorescent fluorophore derived from the reaction of a primary anime with non-fluorescent fluorescamine (Li *et al.*, 2016)

The reaction occurs rapidly at room temperature and any excess reagent not reacting with primary amines hydrolyses to non-fluorescent products; all fluorescence is therefore directly proportional to amine concentration (Udenfriend et al., 1972).

Fluorescamine has been used in solution in the biological and geochemical sciences to assay amino acids, peptides, proteins and primary amines (Udenfriend et al., 1972, Tamaura et al., 1975) and was trialled for *in situ* use with the Murchison meteorite (Clemett et al., 2002). It was also used to label amino acids in solution to demonstrate the feasibility of chiral separation for the purposes of extraterrestrial exploration (Skelley and Mathies, 2003). Through those studies, it was demonstrated to be an excellent chemical fluorescent label: its reaction time is very fast, and only when it reacts with a primary amine does it become fluorescent. Any unused reagent rapidly hydrolyses. However, its specificity for only primary amines renders it useless for the detection of compounds other than this functional group.

Since fluorescamine relies upon its aromatic structure for its fluorescent properties, it will also have a similar micro- to nanosecond fluorescent lifetime as indigenous organic molecules (Berezin and Achilefu, 2010). Hence, using its fluorescent lifetime as a means of differentiation is also problematic.

Further, if a label such as fluorescamine were to be introduced to a meteorite sample, some knowledge would be needed of other potentially fluorescent components (organic material and minerals); the emission wavelengths associated with fluorescamine (reported as 475 nm; Udenfriend et al., 1972), are similar to those of other native organic components (e.g. Table 1.1) making interpretation of results difficult. Chapter 2 reviews the methodology for identifying and testing the sensor developed in this study with fluorescent minerals analogous to those in carbonaceous chondrites.

1.7 Scientific rationale for this study

As described earlier in this chapter, the elucidation of the carbonaceous chondrite organic inventory has involved destructive and non-destructive techniques and a range of analytical

methods. These include the use of fluorescence spectroscopy, which has relied upon the intrinsic fluorescent properties of some classes of organic matter, limiting the compounds that can be detected. Although intrinsic fluorescence is a useful tool by which to locate these compounds within a sample or sample extract, it cannot be accurately used for specific compound identification. Similarly, fluorescent labelling techniques employed to date has also been limited to specific classes of organic compound (a limitation which this project will attempt to address), and only serves to increase the multitude of fluorescent emission sources already present, making this method problematic for differentiating molecules from background intrinsic fluorescence.

A new fluorescence spectroscopic analytical technique is therefore required which does not rely upon the analyte/s to be intrinsically fluorescent; rather the analyte/s should be required to affect the known fluorescence emissions of an applied marker, or sensor, such that this alteration can be used to detect an analyte/s presence and infer its identity. The overarching objective of this research, therefore, is to lay down the foundation for the development of a new fluorescent sensor that will detect the presence of organic molecules when extracted from extraterrestrial (and terrestrial) samples. This sensor will not rely on intrinsic fluorescence or chemical alteration of the analytes, and will differentiate the target analyte(s) from intrinsic background fluorescent emissions.

Using a sensor that involves lanthanide ions could achieve this by virtue of the fluorescent properties of lanthanides: 1) they do not fluoresce at the same wavelengths as the organic material under investigation; 2) their fluorescent lifetimes are several orders of magnitude longer in duration; 3) their emissions have indicative, sharp, line-like features and; 4) their fluorescence emissions may be altered by the perturbation of their coordination environment by the interaction of external species, such as ligands or organic analytes (Horrocks and Albin, 1984, Parker, 2000, Bruce, 2001).

1.7.1 The Lanthanides

Lanthanides (Ln), sometimes called 'Rare Earth Elements' (REE) are elements 57 to 71 inclusive, examples of which, and salient to this project, are Europium (Eu, n= 63) and Terbium (Tb, n= 65). They are collectively part of the *'f'* block elements because their valence electrons occupy the 4*'f'* orbitals (Armelao et al., 2010), although these electrons are rarely involved in their chemistry or formation of bonds (Horrocks and Albin, 1984). All the elements in this group have a stable oxidation state of 3+, although some are more stable at an oxidation state of 4+ (e.g. Cerium, Ce^{4+}) or 2+ (e.g. Samarium, Sm^{2+}) and are very electropositive (Cotton et al., 1999). They exhibit an unusual property known as the 'lanthanide contraction' whereby the ionic radius decreases as the atomic number increases (Cotton et al., 1999). The reason for this is that the 4*'f'* orbital electrons offer little in the way of effective shielding of the outermost 5*'s'*, 5*'p'* and 6*'s'* electrons from the nucleus, which are, as a result, pulled in ever more tightly by electrostatic attraction (Cotton et al., 1999). Many of the lanthanides have fluorescent properties unlike those of any other element in that they have line-like, fine structure spectral emissions, caused by the efficient shielding of the 4*'f'* electrons by the full 5*'s'* and 5*'p'* shells (Görller-Walrand et al., 1996).

It has been shown that when some lanthanide ions, e.g. europium and terbium, are bound in an organic ligand, e.g. DOTA (1,4,7,10-tetraazacyclododecane-1,4,7,10-tetraacetic acid) (Section 1.7.4), forming a complex, the fluorescent emission spectrum is modified from that of the unbound lanthanide ion's fluorescent emission spectrum (Horrocks and Albin, 1984). Figure 1.5 shows the fluorescence emission of the aqueous Eu^{3+} ion (in black) compared with the modified emission of the same ion when chelated by the DOTA ligand (in red) when both are at a concentration of 3mM and irradiated by an excitation light with a wavelength of 397 nm.

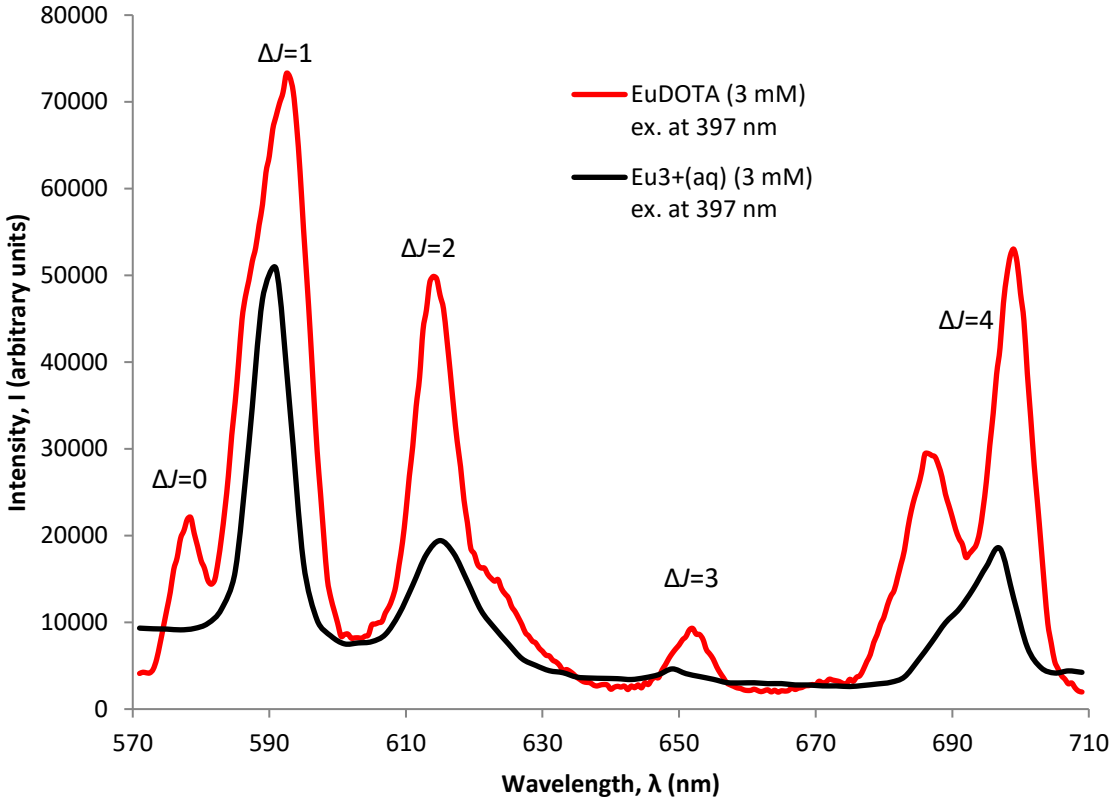

Figure 1.5 Fluorescence spectra for Eu^{3+}(aq) (black) and $[EuDOTA]^-$ (red) (λ_{Ex}=265 nm, acquisition time=0.5 sec, acquisition increment=0.5 nm, excitation and emission slit width=3 nm, pH=5)

This modification is the result of alteration to the environment in which the lanthanide ion sits, called the coordination environment, and is related to the type of ligand used to chelate the metal-centre (Bruce, 2001). It has also been shown that the presence of specific analytes can have a measurable effect on the fluorescent emissions of lanthanide ion complexes because they too influence the coordination environment (Sabbatini et al., 1993, Lowe and Parker, 2000, Parker, 2000, Bruce, 2001, Faulkner et al., 2005, Terai et al., 2006, Ruston et al., 2010, Bünzli and Eliseeva, 2011, Hänninen and Härmä, 2011, Butler and Parker, 2013). The application of such lanthanide complexes to simple aromatic carboxylic acids has revealed that they can increase the intensity of emissions, and sensitise some emissions more than others (Gunnlaugsson et al., 2003); this response may be indicative of this class of compound, and may therefore be used to identify their presence.

Furthermore, the unique electronic structure of the lanthanide ions results in a much greater duration required for absorption and subsequent fluorescence photo-emission of excitation

energy. The result of which is a fluorescent lifetime in the millisecond timeframe (Bruce, 2001) (Section 1.6).

With this information in mind, it may be possible to develop a range of lanthanide-based fluorescent sensors whose fluorescence emissions will be uniquely and measurably affected by the presence of individual analytes, and which may fluoresce for a relatively long period of time. This means, therefore, that they may be capable of detecting organic analytes in complex mixtures of compounds extracted from extraterrestrial samples using solvents and, possibly with much further development, *in situ*.

1.7.2 Fluorescent properties of lanthanides

For this project, it is the fact that the lanthanide's line-like fluorescence emission spectra can be modified (by perturbation of the coordination environment when acted upon by external influences such as coordinating ligands and other molecules) that makes them such good candidates for molecular sensors. Also, they have extremely long fluorescent lifetimes, in the order of milliseconds (10^{-3} s), as opposed to nanoseconds (10^{-9} s), which is the case with most fluorescent organic species (Horrocks and Albin, 1984).

As explained previously (Section 1.3.2), the intrinsically fluorescent organic material found within meteorites all have similar fluorescent lifetimes, such that, when the excitation light is extinguished, all organic material-related fluorescent emissions cease within 1 to 100 nanoseconds (Berezin and Achilefu, 2010). This is true whether *in situ* or in an aqueous solvent extract. Since the lanthanide complex fluorescence does not extinguish so quickly, any fluorescent emissions detected after ~10^{-6} seconds, and up to ~10^{-3} seconds, must emanate from the lanthanide complex. This means that, should the sensor respond to a specific analyte, this response will be detected. Background organic fluorescence can therefore be filtered or 'gated' out (e.g. Figure 1.6, Connally *et al.*, 2004). A short pulse of excitation light excites any organic analytes present (autofluorophores) and the lanthanide complex sensor. When the excitation light is extinguished, the autofluorescence decays rapidly and any fluorescence detected after the

gate delay arises from the lanthanide sensor. In this way, the duration of fluorescent lifetimes can be measured experimentally.

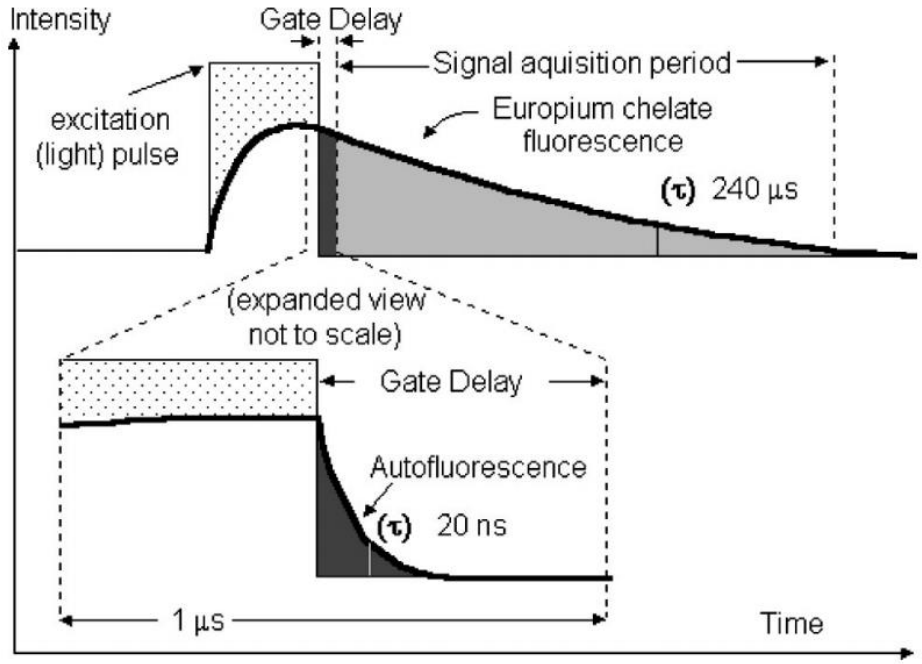

Figure 1.6 Autofluorescence of intrinsically fluorescent organic analytes is resolved by employing a 'gate delay' which relies upon the greater fluorescent lifetime of the lanthanide complex (Connally *et al.*, 2004)

It is the use of this 'time-gating' technique (Thibon and Pierre, 2009) that makes lanthanide sensors such good candidates as analytical sensors for the purpose of detecting organic material in extracts which contain intrinsically fluorescent components.

Fluorescent emissions of lanthanide ions are intense and take a relatively long time to relax from an exited state. Unfortunately though, lanthanides ions are very poor absorbers of energy, i.e. they have a low molar extinction coefficient (Bruce, 2001), resulting from the shielding effects of the full outer 5's' and 5*'p'* orbitals. However, organic complexes can be employed to facilitate excitation energy absorption by what is termed 'The Antenna Effect' (Armelao et al., 2010) (Section 1.8.1).

1.7.3 Rationale for using europium and terbium

Europium (Eu) and terbium (Tb) atoms exhibit fluorescent properties; they produce very well defined and indicative fluorescent spectral emissions. Since the energy levels of their valence orbitals are so similar, their excited states are energetically very close together, resulting in

narrow, line-like and sharp spectra (Bruce, 2001) making them easily identifiable and characteristic. Furthermore, when europium and terbium ions are bound within an organic ligand, their spectra are modified dependent upon the structure of the ligand used, e.g. DOTA (Section 1.7.4) (Figures 1.7 and 1.8 respectively). Any external interactions that may energetically perturb or affect the system can likewise perturb the luminescent emission characteristics. Any organic molecules that interact electronically could alter the known spectra in such a way that the alteration may be indicative of the species causing that change; the europium or terbium, or both, would therefore act as a sensor for that species (Bruce et al., 2000, Dickins et al., 2003).

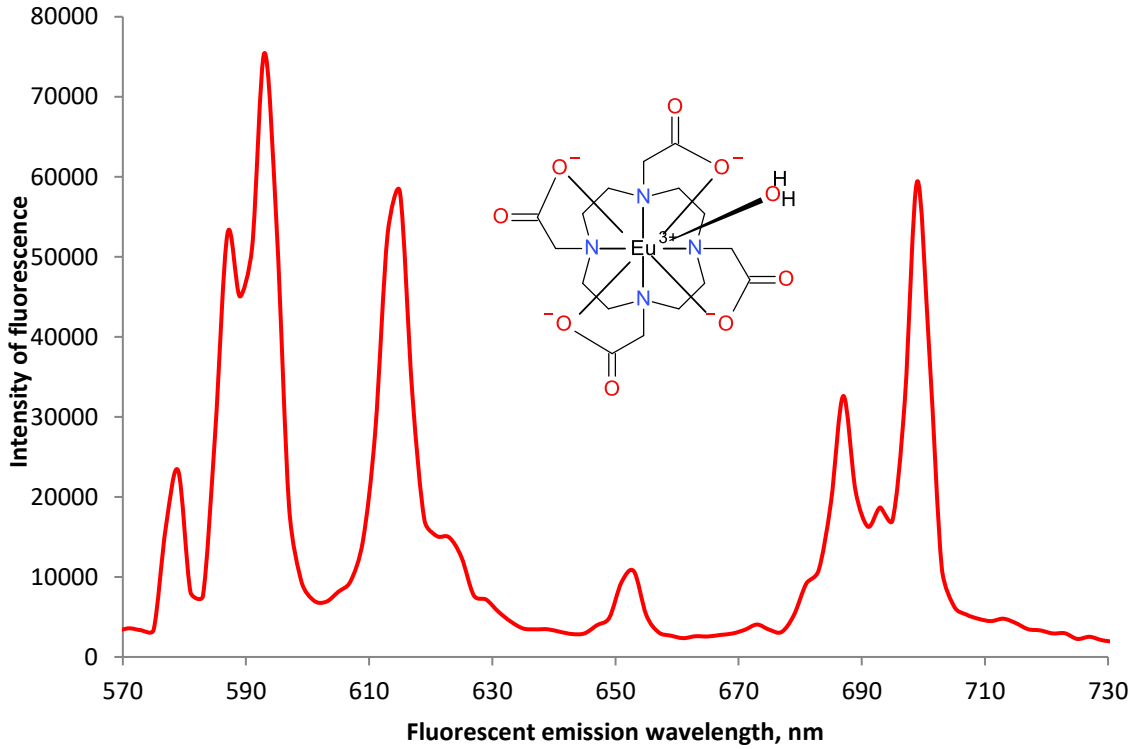

Figure 1.7 Emission spectrum of europium when bound within DOTA, an organic ligand (Section 1.7.4) (λ_{Ex}=265 nm, acquisition time=0.5 sec, acquisition increment=0.5 nm, excitation and emission slit width=3 nm, pH=5)

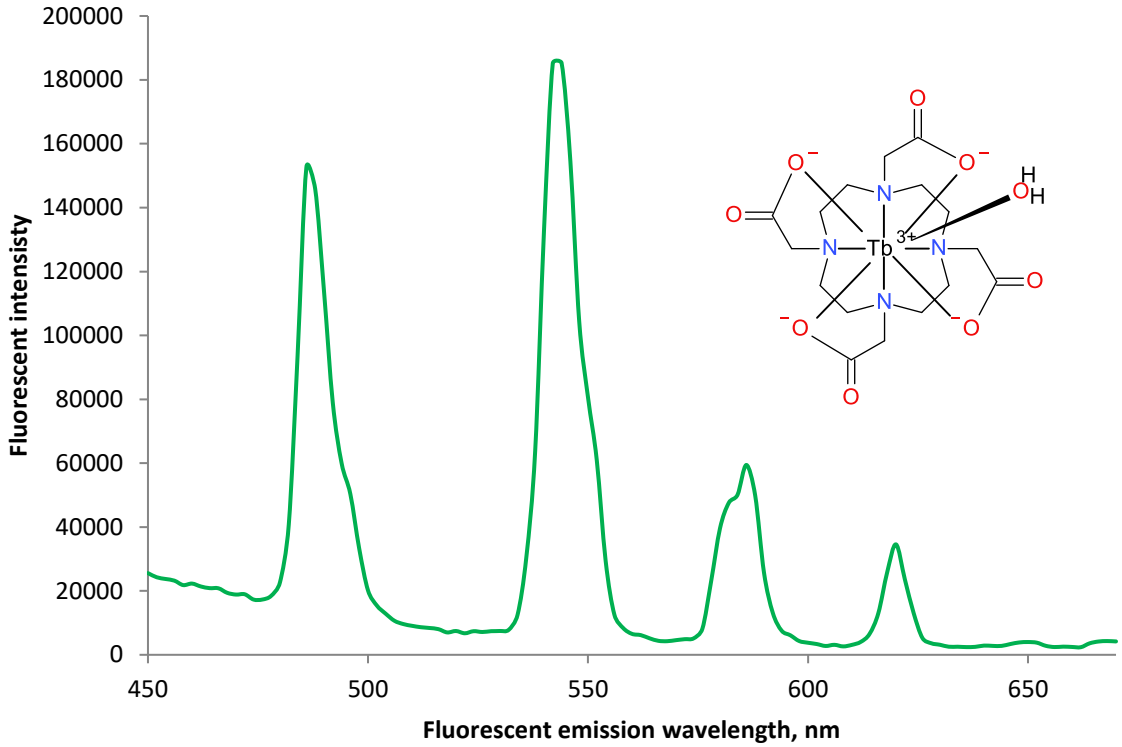

Figure 1.8 Emission spectrum of terbium when bound within DOTA, an organic ligand (Section 1.7.4) (λ_{Ex}=265 nm, acquisition time=0.5 sec, acquisition increment=0.5 nm, excitation and emission slit width=3 nm, pH=5)

The well-documented high intensity, line-like and long lived fluorescent properties (Sabbatini et al., 1993, Bruce, 2001, Bünzli and Eliseeva, 2011), and propensity for modifications to their emissions depending upon their chemical environment (Horrocks and Albin, 1984, Bruce, 2001), make europium and terbium ideal luminescent sources for the sensors in this research; it is expected that the fluorescence emission spectra will be uniquely altered depending upon the interaction afforded by each analyte.

1.7.4 Ligands

Ligands can be neutral molecules (e.g. cyclen), ions (e.g. chloride (Cl^-), cyanide (CN^-), phosphate (PO_4^{3-}), ethanoate (CH_3COO^-)), electrons (e^-), polar molecules with non-bonding or lone pairs of electrons (e.g. water (H_2O), carbon monoxide (CO), ammonia (NH_3), acetonitrile (CH_3CN), pyridine (C_5H_5N)), or organic macromolecules with functional groups (e.g. $[DOTA]^{4-}$ and ethylenediaminetetraacetic acid ($[EDTA]^{4-}$)) (Figure 1.9 (a) and (b), respectively).

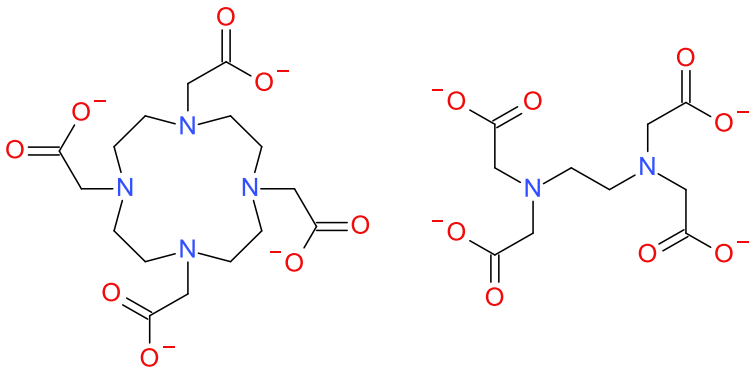

(a) (b)

Figure 1.9 Examples of organic macromolecular ligands: (a) octadentate $[DOTA]^{4-}$ and (b) tetradentate $[EDTA]^{4-}$

Ligands are able to bind to metal atoms or ions and, in doing so, form a coordination complex where the metal atom or ion is usually at the centre with the coordinating atoms arranged around. Ligands with just one atom, lone pair of electrons or moiety that can bind are called monodentate ligands (dentate from the Latin '*dentis*', meaning 'tooth'); having two such sites is termed bidentate, three is tridentate, and so on. Ligands with a denticity of more than one are termed polydentate. In the examples above, DOTA is octadentate, possessing four nitrogen lone pairs and four ethanoate 'pendant arms', and EDTA is hexadentate, possessing two nitrogen lone pairs and four ethanoate 'pendant arms' (Figure 1.9(a) and (b), respectively).

The bonding between the metal centre and ligating species is the result of the formal donation of one or more of the ligand's electron pairs, i.e. the formation of a dative bond. However, this donation can vary in its totality, so the metal to ligand bond can range from mostly ionic (electrostatic) in nature, to mostly covalent. Thus, the ligands that constitute the complex alter the reactivity of the central metal atom and its capacity for redox reactions, while the metal centre dictates the reactivity of any functional groups that constitute the parts of the ligand structure involved in coordination.

As alluded (Section 1.7), it is the ligand that influences the photophysical and chemical properties of the metal ion and, as such, ligands may also be designed to control these properties in order to respond to the presence of specific analytes. So, by ascertaining the effect of individual classes of analytes upon the known fluorescent emissions of a lanthanide complex, it may be possible to

modify the photophysical properties of the lanthanide complex by careful selection of ligand functional groups. It may, therefore, be possible to hone the fluorescent sensor emissions by modifying the coordination environment of the fluorescent lanthanide ion, such that selectivity and/or sensitivity to specific organic analyte classes may be achieved.

1.7.5 Antenna Effect

The Antenna Effect is a mechanism whereby excitation radiation is absorbed by a chromophore (usually an organic molecule which absorbs light of one wavelength and emits light of another; in essence fluorescence), which then transfers that energy to another species that itself becomes excited as a result. In this instance, the ground state electron of the chromophore ('Ligand' on Figure 1.10) absorbs light and is promoted to the first excited S_1 energy level. Instead of non-radiative ('NR') relaxation and subsequent fluorescence ('F') there is inter-system crossing ('ISC'), whereby the electron changes spin and enters the molecule's excited triplet state. Relaxation from the triplet state ('T_3') to the ground state would result in phosphorescence but, in the context of 'The Antenna Effect', there is energy transfer ('ET') from the chromophore triplet state ('T_3') to the lanthanide ion's ('Ln(III)') excited state, ('*f**'). What follows is luminescent decay ('L') from the lanthanide ion's ('Ln(III)') excited state, ('*f**') to its ground state (Sabbatini et al., 1993). Direct ET can occur between the chromophore's ('Ligand') first excited state ('S_1') and one of the lanthanide ion's ('Ln(III)') excited Laporte forbidden transition states, ('*f*'*'). Internal conversion ('IC') between the lanthanide ion ('Ln(III)') electronic structure, via *f-f* transitions, allows the lanthanide ion's ('Ln(III)') excited state, ('*f**') to become populated resulting in further luminescent decay ('L'), to the Lanthanide ion's ('Ln(III)') ground state.

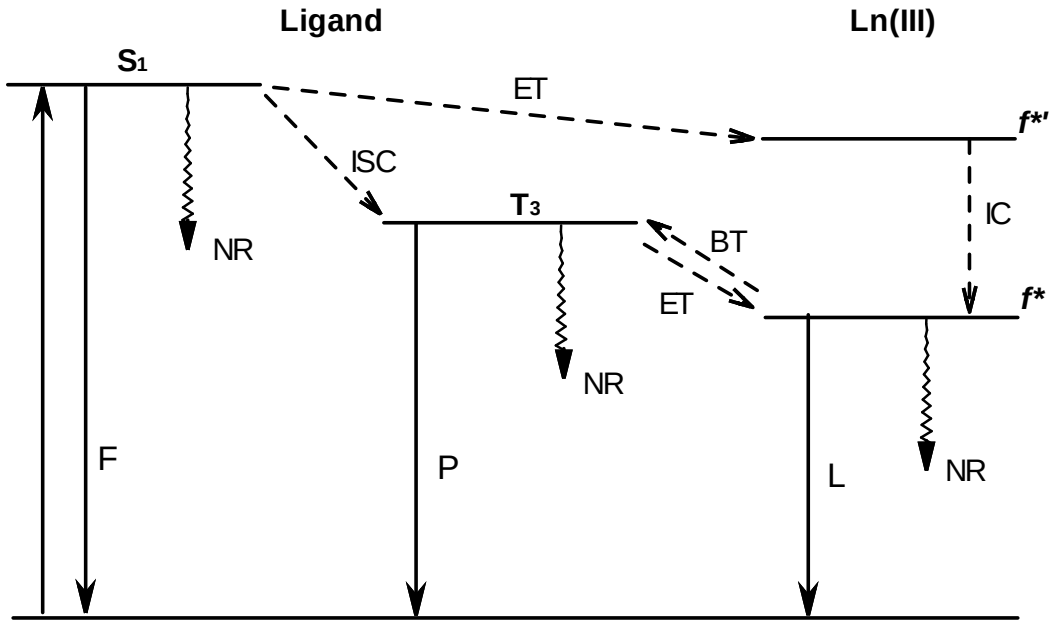

Figure 1.10 A simplified Jablonski diagram showing possible energy absorptions, transfers and emittance for an organic chromophore/lanthanide metal ion (ligand/lanthanide metal ion) complex species

Inter-system crossing ('ISC') occurs because the chromophores ('Ln(III)') triplet state ('T_3') energy level is close to the absorbance frequency of the lanthanide '*f*' orbitals, allowing rapid quenching of the triplet state ('T_3') and subsequent excitation of the lanthanide. This leads to long lived fluorescent emission (Matsuda et al., 1969, Sabbatini et al., 1993, Armelao et al., 2010). Often, the energy difference between the chromophore ('Ligand') triplet state ('T_3') and the lanthanide ('Ln(III)') exited state ('*f**') is so small that there can be some back transfer ('BT') of energy from the lanthanide to chromophore. It has been theorised that chromophore triplet state to lanthanide excited state energy transfer is caused by resonance mechanisms resultant from interactions of the π (pi) electron system of the ligand triplet state with the '*f*' electrons of the lanthanide ion centre (Matsuda et al., 1969).

1.7.6 Proposed methodological approach

As a point from which to begin, the europium and terbium complexes of DOTA, a macrocyclic ligand consisting of four ethanoate pendant arms connected to a cyclen ring, were selected (Chapter 3). The properties of these lanthanide complexes are well-established and understood (Zhang and Jiang, 2010). Uses of lanthanide DOTA-like complexes include bioanalytical applications (Johanna and Tero, 2014) and as molecular probes for biomedical imaging and

sensing (Montgomery et al., 2009). DOTA has been used to chelate other lanthanide ions, such as gadolinium (Gd). The $[GdDOTA]^-$ complex is used as a contrast agent for MRI scanning in the medical sector in the form of the gadoterate meglumine (also, gadoteric acid) salt, trademarked DOTAREM (Aime et al., 1998, Caravan et al., 1999). Although extensively used for biological and biochemical applications, these lanthanide complexes have not, until now, been applied to complex organic mixtures extracted from geochemical samples. This is thus an entirely novel application for these fluorescent compounds.

It has been established that the emissions of such complexes were modified in the presence of analytes such as aromatic carboxylic acids, which sensitised emissions, increasing their intensity (Gunnlaugsson et al., 2003). Hence, it was hypothesised that it may be possible to detect a similar effect upon the addition of molecules with similar structures or moieties. It was this assertion that was the basis for the choices of analogue analytes with which to test this hypothesis (Chapters 3 and 4).

Having decided upon which lanthanide complexes to use, a reference carbonaceous chondrite was chosen in order to limit the scope of the research. This was necessary as each carbonaceous chondrite has differing organic inventories and mineralogical composition. It would not be possible, within the duration of a PhD, to study them all, so the Murchison meteorite was chosen. This became the reference meteorite as it is arguably the most characterised and one of the most pristine, having been recovered only hours after it was seen to fall (Kvenvolden et al., 1970). Choosing this meteorite enabled a finite inventory of organic molecules and minerals to be selected from for testing.

1.8 Project objectives

The overall objective of the project was to develop one or more lanthanide-based sensors that could be used to detect extraterrestrial organic molecules.

The specific objectives were:

- To ascertain if known fluorescent complexes of europium and terbium can be used to determine the presence of organic analytes that are analogues of those molecules known to be present in carbonaceous chondrites, individually and within complex mixtures, in solution.
- Develop new europium and terbium complexes, using structurally similar ligands, in order to determine whether sensitivity and/or selectivity of detection of these analytes may be improved.
- Establish whether those minerals likely to be present in carbonaceous chondrites will interfere with the organic analyte detection.
- To apply the fluorescent lanthanide sensors to solvent-extracted solutions of extraterrestrial and terrestrial organic material.

The initial aim of this research was to demonstrate that selected organic analytes, and complex mixtures thereof, can detectably influence the fluorescence emissions of known fluorescent complexes of europium and terbium, *in aquo* (Chapter 3). Work was then undertaken to develop new, and previously synthesised, structurally similar ligands (based upon those complexes tested in Chapter 3), with which to produce more fluorescent europium and terbium complexes (Chapter 4). These complexes were tested in order to ascertain if these structural modifications may improve selectivity and/or sensitivity to specific analytes. These fluorescent complexes were then tested on solvent extracts of extraterrestrial and terrestrial samples, and the potential for geochemical interference from mineral components intrinsic to the samples was evaluated (Chapter 5).

Chapter 2 presents the rationale and methodological approach employed for the selection of analogue organic analytes and mineral standards for testing (their likelihood to interact with the sensors, and reasons why they might, are also evaluated in detail), the choices of natural organic-rich terrestrial and extraterrestrial samples, and the preparation and manipulation of all samples.

The synthesis of ligands, and their respective complexes, and the development of protocols for their application to the analogue sample solutions are also described.

Chapters 3 and 4 detail the results of sensor responses to the presence, *in aquo*, of the analogue organic molecules, while Chapter 5 describes the results of mineral analysis and the fluorimetric data obtained when the sensors were combined with mineral solutions. Chapter 5 also reports the responses detected when the sensors were applied to the natural organic-rich terrestrial and extraterrestrial extracts, *in aquo*.

Finally, Chapter 6 summarises the results of the fluorimetric analyses and the progress made in achieving the research objectives. Chapter 6 also suggests ways in which future work may develop the sensors further, including a brief overview of potential applications, and how this may better our understanding of the chemical evolution of organic material, specifically prebiotic organic molecules, found within extraterrestrial samples.

2 Methodology

This Chapter outlines the scientific rationale behind, and the details of, the methodological approach used in the remainder of this thesis. It includes the reasoning behind the selection of terrestrial and extraterrestrial geological samples, standard analytes, and minerals selected for testing. Extraction protocols and methodology are described. Analytical techniques, including fluorimetry, used throughout the thesis are also described here. The synthesis of the sensors, and their characterisation, is detailed as well as the development of the protocols used to apply the sensors to the various extracts.

2.1 Cleaning protocols

Extraterrestrial organic compounds are present in extremely low concentrations; in the order of ppm to ppb for total concentration of individual molecules (Sephton, 2002). It is therefore imperative that any traces of terrestrial organic contaminants are entirely eliminated from all stages of sensor and analyte preparation and from any analysis protocols undertaken so as not to interfere with or produce false positive results. To achieve this level of comprehensive cleanliness, all glassware and equipment, including volumetric flasks for making up standard and stock solutions of sensors and organic analytes, micro-syringes, spatulas etc. were cleaned using a rigorous and thorough regime.

2.1.1 General equipment cleaning

Firstly, items were washed thoroughly using hot water and Teepol detergent and a small bottle brush used, where appropriate, to remove traces of grease, oils and dirt. The items were then rinsed in clean hot tap water and drained. Any remaining traces of organic compounds were removed by rinsing with 1 M hydrochloric acid (HCl (aq)). To remove the HCl (aq), the equipment was thoroughly rinsed with copious 18.2 MΩ water and any residual water adhering to the surface of any items was taken up into a methanol (MeOH) rinse. Finally, the MeOH was taken up into a dichloromethane (DCM) rinse, which allows for rapid drying *via* evaporation. All organic solvents used for cleaning were HPLC grade. All items were loosely wrapped in aluminium foil, which had been wiped down with isopropyl alcohol (IPA) using a lint-free cloth, and baked in a

drying oven at ~80°C for a minimum of two hours before cooling to room temperature shortly before use. Once used, all equipment and glassware was treated in the same rigorous manner ready for subsequent use.

2.1.2 Vials for storage of extraterrestrial and terrestrial samples

All vials were cleaned before use. To prepare for this, a 400 ml borosilicate beaker and forceps were cleaned by washing with Decon, then rinsed thoroughly with 18.2 MΩ water, MeOH and DCM and placed in a drying oven at ~80°C for one hour. The beaker was then allowed to cool before being filled with 18.2 MΩ water; the caps and septa were then immersed in the water using the clean forceps. The beaker and contents were sonicated at ~25°C for 30 minutes. The septa and caps were removed using the clean forceps, wrapped in IPA-wiped aluminium foil and placed in a drying oven at ~80°C.

The beaker used for sonicating the caps and septa was emptied and rinsed with MeOH, then DCM, and refilled with a 50:50 MeOH:DCM solvent mixture. 4 ml glass vials were then immersed using the clean forceps and sonicated at ~25°C for 30 minutes, after which time they were removed and wrapped in IPA-wiped aluminium foil and placed in a drying oven at ~80°C. After 24 hours, the aluminium foil packages were removed from the dying oven and placed onto an aluminium IPA-wiped sheet on a laminar flow bench and allowed to cool to ambient temperature. The septa were then placed into the screw-caps using the clean forceps and screwed onto the vials, which were in turn re-wrapped in IPA wiped aluminium foil and stored on the laminar flow bench ready to be used.

2.1.3 Vials for mineral weathering and organic extraction

The vials used for the mineral weathering procedure and for the hot-solvent extraction of organic material from the terrestrial and extraterrestrial samples were cleaned using the following method. 4 ml clear glass vials, plastic screw lids and compatible septa were immersed in 500 ml of 18.2 MΩ water and sonicated for 30 minutes at ~25°C. Using a set of sterile forceps, the vials, lids and septa were removed, drained and placed on an aluminium foil sheet that had been wiped

down with IPA using a lint-free cloth. The vials, lids and septa were then placed in 500 ml of 50:50 DCM:MeOH and sonicated for a further 30 minutes at ~25°C. Using the sterile forceps, the vials, lids and septa were removed, drained and placed on a fresh aluminium foil sheet (again, pre-cleaned with IPA), wrapped loosely and placed in an oven at ~80°C for 24 hours. After cooling to ambient temperature, the aluminium foil package was opened on a laminar flow bench and the septa were carefully inserted into the lids (using sterile forceps). The lids were immediately screwed into place on the vials. The vials were placed in an aluminium rack, which had been cleaned with IPA, and double-wrapped in IPA cleaned aluminium foil ready for use.

2.1.4 Fluorimetry cuvettes

The cuvettes used for fluorimetry are not the same as those used for UV-Vis spectroscopy; the latter cuvettes are frosted on two sides and polished on the other two, whereas the former are polished on all four sides. Prior to use, and between each fluorimetry run, the quartz fluorimetry cuvettes were cleaned using the following procedure: 1) initial wash with 18.2 MΩ water to flush any solution that may be present from previous sample run; 2) wash with 0.1 M hydrochloric acid (HCl (aq)) to remove any traces of residual amino acids or organics from previous sample, not removed by water wash; 3) wash with methanol (MeOH) to remove traces of water and organic impurities; 4) wash with dichloromethane (DCM) to remove traces of methanol and to aid complete dryness *via* evaporation.

2.1.5 Micro-syringes

Prior to use, and between each fluorimetry run, the micro-syringes used to dispense solutions of the sensors, analogue organic analytes, mineral solutions and extracts of the terrestrial and extraterrestrial samples, were cleaned using the following protocol: 1) 18.2 MΩ water was taken up into the full micro-syringe volume and emptied, five times; 2) HCl (aq) was taken up into the full micro-syringe volume and emptied, five times; 3) MeOH was taken up into the full micro-syringe volume and emptied, five times; 4) DCM was taken up into the full micro-syringe volume and emptied, five times and 5) the micro-syringe pump was removed from the micro-syringe barrel and the parts set aside to dry *via* evaporation. When each fluorimetry session was

completed, the cleaning protocol was carried out, and then the syringes were deconstructed, wrapped in aluminium foil and placed in a drying oven at 80°C until required again.

2.1.6 Mineral crushing equipment

An agate pestle and mortar and a crushing mill was used to crush mineral samples. Both the pestle and mortar and mill used to crush minerals were washed thoroughly before and after each sample using the following protocol: i) detergent in 18.2 MΩ water; ii) thorough wash and rinse with 18.2 MΩ water; iii) ground with quartz sand and propanone, iv) wash and rinse with propanone and iv) a final rinse with DCM. Each mineral sample was then transferred to clean, dry vials which were cleaned using the protocol described previously.

2.2 Sample selection

In order to test to response of the sensors developed to the presence of organic compounds in an extract, it was necessary to select suitable samples for testing. The criteria for choosing samples were: 1) they must contain organic material that is solvent extractable; 2) the samples must be available in sufficient quantity for the purposes of extraction and 3) ideally, both the organic and inorganic components of the sample have been previously characterised.

The intended application is specifically for samples of an extraterrestrial origin, and organic material has been identified in carbonaceous chondrites, ordinary chondrites and interplanetary dust particles (IDPs). IDPs are very small (10's to 100's of microns in size) and would therefore not yield sufficient quantities of organic material to which the sensor solutions may be applied. Carbon in ordinary chondrites is present in very low abundance when compared to carbonaceous chondrites (most ordinary chondrites have lower than 0.2 wt% carbon, e.g. Grady *et al.,* 1989, Varela & Metrich, 2000), compared with up to 5% carbon as commonly quoted for carbonaceous chondrites, see Section 1.3) and most of this is believed to be organic. However, only a minor fraction is solvent soluble (Kebukawa et al., 2017) and, as such, does not present such a useful starting point for the development of a sensor as carbonaceous chondrites can. Hence samples of carbonaceous chondrites were selected. Since carbonaceous chondrites are rare specimens and

supply is limited, an analogous terrestrial rock, in plentiful supply was also required for testing. This ensured protocol was established without the loss of meteoritic material.

Further, single mineral analogues were selected that were representative of the types of minerals found in carbonaceous chondrites (Section 2.2.3) because these minerals may be present as particulates, or as dissolved species, in a solvent extract and may interfere with the detection of organic analytes. Commercially available standard compounds were also selected to represent individual organic components found in chondrite extracts so that their sensor responses could be ascertained and compared to the responses of the sensor to the extracts.

2.2.1 Extraterrestrial sample selection

Two samples were selected: Murchison and Allan Hills 88045 (ALH88045).

Murchison

Murchison is one of the most characterised carbonaceous chondrites, both for its organic constituents and for its mineralogy (see Chapter 1). It was seen to fall in 1969 near Victoria, Australia, and is considered to be one of the most pristine meteorites of its kind; it was collected within hours of impact, providing minimal opportunity for terrestrial contamination.

Its solvent extractable fraction is well documented (Chapter 1, Section 1.3), as is its mineralogical component (Fuchs et al., 1973, Brearley and Jones, 1998). A sample was also available *via* The Open University's own meteorite collection. Hence, it was chosen for this study as it fulfilled all the criteria for selection (Section 2.2).

Allan Hills 88045 (ALH88045)

Although Murchison was selected as the main reference meteorite for this study, it was advantageous to select a second carbonaceous chondrite for testing. The ALH88045 CM chondrite is an Antarctic meteorite, which was found in 1988 (Wlotzka et al., 1989); it is not known when the meteorite fell to Earth (i.e. its terrestrial age) and, consequently, there is no information to establish the duration it has been exposed to terrestrial contamination and weathering. For this

reason, it has not been as well studied as the Murchison meteorite, although its mineralogy has been established to be similar to Murchison (Wlotzka et al., 1989, Wlotzka, 1991, Zolensky et al., 1997), only subtle differences classify it as a CM1 chondrite compared to Murchison as a CM2.

Its organic inventory is less well characterised than that of Murchison and only its amino acids have been studied in any detail (Botta et al., 2007). Although the absolute abundances of amino acids in ALH88045 were found to be lower than those in Murchison (suggested to be due to parent body processing), its amino acid fingerprint was the same (e.g. *D*- and *L*-serine, glycine, β-alanine, γ-amino-*n*-butyric acid, *D*- and *L*-alanine; Botta et al., 2007). As is described in Section 2.3, amino acids were anticipated to be suitable analytes for the sensors developed here, since they exhibit moieties that may interact with the metal centre (for example by electrostatic attraction of the negatively charged carboxylate moiety, or the amino lone pair electrons). Hence, it was logical to assume that ALH88045's amino acid inventory could be targeted by the sensors developed.

Although other classes of compound are also targeted (Section 2.3), it was beyond the scope of this PhD to develop protocols that could enable the identification of these; ALH88045 nucleobases, in particular, have been analytically challenging to isolate and unequivocally identify. Hence it was assumed, on the evidence from its amino acids and mineralogy, that ALH88045 is sufficiently similar to Murchison that it should have an analogous solvent extractable organic inventory.

Therefore, as an uncharacterised sample, ALH88045 is analogous to the type of sample that the sensors would be applied to in a real analytical context. It was also readily available in The Open University's meteorite collection.

2.2.2 Terrestrial sample selection

Terrestrial sample for sensor application

Since carbonaceous chondrites are rare and samples are often unavailable in large quantities, it was therefore important to first develop the sensor and application techniques using a suitable

terrestrial analogue. Further, it was anticipated that any fluorescence responses observed to occur in the presence of the terrestrial organic component may be compared to any similar responses when the sensors were applied to extraterrestrial extracts. Hence, it was required to contain a solvent-soluble organic inventory and mineral component comparable to carbonaceous chondrites.

The organic-rich terrestrial analogue rock selected was Green River Shale (GRS). GRS is an oil shale, found in the Green River Formation in Colorado Wyoming and Utah, USA; the sediments were deposited in large lake basins during the Eocene (35.5-48.5 Ma) and are the largest oil shale deposit in the world (Dyni, 2003). GRS was identified as containing solvent-soluble organic material and a mineral composition of mostly carbonates, silicates and clay minerals (Milton, 1971). Studies have identified many organic components including cycloalkanes (Anders and Robinson, 1971), and cholestane, ergostane, sitostane, gammacerane, hopane, lupane, perhydro-b-carotene and steranes (Burlingame et al., 1965, Henderson et al., 2013), all of which are derived from sterols and steroid molecules via diagenetic and catagenetic mechanisms. Analysis of weathered GRS has also suggested a variety of terpenoid hydrocarbons, isoprenoid alkanes and straight chained alkanes are present, and infra-red (IR) analyses indicate the presence of the carboxyl anion and free carboxyl acid groups (Reed, 1977). Other studies have successfully isolated isoprenoid acids and dicarboxylic acids (Haug et al., 1967). GRS therefore contains some solvent extractable organics that are comparable to those found in carbonaceous chondrites, and as such, presents a suitable terrestrial analogue on which to test the sensor. However, a recognisable limitation of its use is that it also contains many organic compounds not found in carbonaceous chondrites, such as those identified by Burlingame et al., (1965), and Henderson et al., (2013). As a geological model for developing the sensor technique, however, this is an acceptable risk (see Chapter 5 for further discussion).

Although the mineral component of GRS differs from that of the Murchison meteorite (it does not contain olivine, for example) it has some similarities, e.g. the presence of clays minerals such as montmorillonite, and carbonates (Milton, 1971). As a consequence of these similarities, if the

organic extraction process on GRS is proven to liberate mineral ions, or produce mineral particulates, it is likely these types of contaminants will also be present in extracts of carbonaceous chondrites. Therefore, if the presence of GRS mineral contaminants is shown to interfere with the fluorescence of the sensor, a method to correct for any interference may be developed in anticipation of application of the sensor to an extract of a carbonaceous chondrite.

Procedural blank – Quartz/feldspar

In addition to a terrestrial organic-rich rock, it was also important to obtain a geological sample that could be used as a procedural blank. The criteria for the selection of a suitable sample were: 1) it is chemically inert to the solvents used for the extraction and 2) it does not contain any organic material that may be extracted.

Previously, serpentine has been used as a procedural blank as it fulfils the criteria outlined above (e.g. Martins et al. (2007), Smith et al. (2014)). In this study, a quartz-feldspar (QF) mixture was selected as the procedural blank as it too fulfils the criteria and was readily available as an in-house laboratory blank (see Section 2.4.2). QF is a mixture of quartz (silicon dioxide, SiO_2) and feldspar (a combination of aluminosilicates of potassium, sodium and calcium ($KAlSi_3O_8$, $NaAlSi_3O_8$ and $CaAl_2Si_3O_8$)). It is entirely organic free and insoluble and inert in the solvents used, meaning any responses observed from this extract would likely be contamination during the extraction process.

2.2.3 Mineral selection

Although the organic component is of primary interest, geological samples contain minerals. It is possible these minerals may dissolve or be present as particulates in any solvent extract obtained, so it was important to establish if any of these could interfere with the fluorescent emissions of the sensors. Such interference may impact on any responses invoked by the target organic analytes. Importantly, it is possible that, if minerals with intrinsic fluorescent properties were present in an extract, they may fluoresce, causing background fluorescence which may obscure

lanthanide fluorescence emissions. For this reason, it was crucial to identify and test minerals found in the Murchison meteorite with intrinsic fluorescence.

An extensive literature review of the mineralogy of Murchison was undertaken. The literature review began by identifying and listing all minerals (Fuchs et al., 1973, MacPherson et al., 1983, Papike, 1998, McSween, 1999, Bland, 2002), including formulae and mineral family. This list was then cross referenced with databases and catalogues (Henkel, 1989, Barthelmy, 1996, Ralph, 2001, MacRae and Wilson, 2008, Barmarin, 2009) to produce a list of those minerals that exhibit fluorescent properties. Data on any possible chemical alterations, or doping, of the crystal structures that can enhance fluorescence and the activators involved were noted, along with emittance wavelengths, colours, intensity and any other notable salient information (see Appendix B).

Samples of minerals in Murchison that were known to fluoresce were sourced (Table 2.1): olivine, calcite, gypsum, and corundum were obtained from The Open University rock store; all other samples (enstatite, nepheline, magnetite, diopside and anorthite) were purchased from Richard Taylor Minerals, U.K. Minerals were supplied as solid fragments ranging from ~1 cm^3 to 5 cm^3; the larger pieces were subsequently broken into smaller pieces ~1 cm^3 (Section 2.4.1).

Mineral	**Formula**	**Family**	**Images of pre-crushed samples used**	**Main emitting colour**
Anorthite	$CaAl_2Si_2O_8$	Silicates		Yellow/white
Diopside	$CaMgSi_2O_6$	Silicates		Blue
Enstatite	$MgSiO_3$ or $Mg_2Si_2O_6$	Silicates		Bluish white

Mineral	Formula	Family	Images of pre-crushed samples used	Main emitting colour
Corundum	Al_2O_3	Oxides		Red
Gypsum	$CaSO_4\ 2H_2O$	Sulfates		Orange/yellow
Olivine	$FeMgSiO_4$	Silicates		Yellowish-white
Calcite	$CaCO_3$	Carbonates		Pink/Red/Blue
Magnetite	Fe_3O_4	Oxides		Blue
Nepheline	$Na_3KAl_4Si_4O_{16}$	Silicates		Orange

Table 2.1 Minerals identified as fluorescent, which are found in the Murchison meteorite. Also included is their chemical composition (formula), mineral; family and colour of emitted fluorescent light. Additional details are given in Appendix B. References: Fuchs et al. (1973), MacPherson et al. (1983), Papike (1998), McSween (1999), Bland (2002), Henkel (1989), Barthelmy (1996), Ralph (2001), MacRae and Wilson (2008), Barmarin (2009)

2.3 Organic standard selection

Commercially available standards were chosen for initial testing and method development, based on the known organic inventory of organic compounds contained within carbonaceous chondrites (Folsome et al., 1971, Kvenvolden et al., 1971, Levy et al., 1973, Hayatsu et al., 1975, Cronin et al., 1981, Stoks and Schwartz, 1982, Cronin and Pizzarello, 1983, Cronin and Pizzarello, 1986, Krishnamurthy et al., 1992, Cronin and Chang, 1993, Pizzarello et al., 1994, Pizzarello and Huang, 2002, Meierhenrich et al., 2004, Huang et al., 2005, Martins et al., 2008).

2.3.1 Selection criteria

One of the key selection criteria for the standard analytes was solubility, to enable them to be used within the planned tests. Solubility of analytes is dependent upon their structure, e.g. their functional groups. Given that, for example, carboxylic acids are ionic and have been shown to invoke a response when added to the lanthanide complexes (Gunnlaugsson et al., 2003), it was concluded that the analytes chosen would also be required to possess ionic functional groups to ensure their solubility in water.

Furthermore, to enable interaction with the positively charged lanthanide ion metal centre, just as carboxylic acids do, they must possess traits that would promote electrostatic attraction, e.g. delocalised electrons - conjugated chains, aromatic molecules and structures with lone pairs of electrons as part of a π (pi) bonded system, and polar molecules with either the capacity for ionisation or a highly localised electron density. It was also important to recognise the steric or spatial considerations; large bulky branched chain molecules may be hindered in approaching the sensor complex, thereby reducing the probability of interaction. Hence, molecules with these structures were omitted. Furthermore, molecules which exhibit conjugated pi bonds and aromatic groups may also act as antennas, sensitising emissions *via* the antenna effect (Lis et al., 2002).

Therefore, the criteria by which to select the standard analytes were as follows:

A. Presence in meteorite extracts. The organic analytes chosen must represent organic molecules likely to be present in the extracts derived from carbonaceous chondrites, or be structurally analogous to those molecules (outlined in Chapter 1).
B. Solubility. The chosen analytes must be soluble in water, since the sensors are to be applied in the form of an aqueous solution and, furthermore, the extracts will be dissolved *in aquo*.
C. Appropriate functionality. The analytes must exhibit ionic or electron-rich moieties to facilitate electrostatic interaction with the lanthanide metal centre.

D. Aromaticity/conjugated pi systems. The analytes must exhibit structures with the potential to act as emission sensitising antennas. These structures include aromatic ring systems or conjugated double bonds.

2.3.2 Choice of standards

Based on the known organic inventory in Murchison, molecules from four chemical classes were chosen (Table 2.2): amino acids; mono- and di- carboxylic acids; nucleobases: purines and pyrimidines, and a highly conjugated nitrogen and oxygen atom containing molecule.

Table 2.2 provides the name, molecular structure of each individual analyte selected and indicates why each analyte was chosen in terms of what its structure provides to suggest analyte/metal-centre interaction may take place and how they might act as sensitisers via the antenna effect.

Analyte name	Analyte Structure	Criterion A – Identified in the solvent extract of Murchison	Criterion B - Solubility	Criterion C – Moieties with potential to interact with the metal centre	Criterion D – Moieties or structure that can act as a sensitising antenna	Absorption and emission wavelengths, λ_{abs} and λ_{Em}, where data available (for aromatic organics only)
(a) Aspartic acid	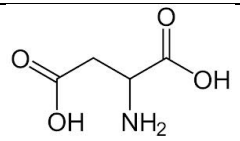	(Kvenvolden et al., 1971)	Water soluble	Two carboxylic acid moieties and an amine group.	Double bond π electrons of the carboxylic acids can absorb UV and act as an antenna.	
(a) Ornithine	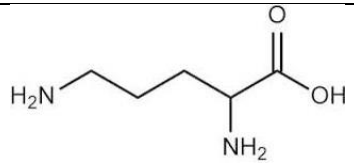	(Meierhenrich et al., 2004)	Water soluble	Carboxylic acid and two amine groups.	Double bond π electrons of the carboxylic acid can absorb UV and act as an antenna.	
(a) Serine	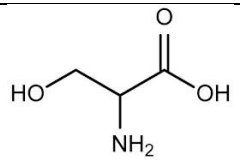	(Cronin and Pizzarello, 1983)	Water soluble	A hydroxyl group, an amine group and a carboxylic acid moiety.	Double bond π electrons of the carboxylic acid can absorb UV and act as an antenna.	
(a) Threonine	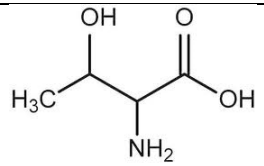	(Cronin and Pizzarello, 1983)	Water soluble	A hydroxyl group, an amine group and a carboxylic acid	Double bond π electrons of the carboxylic acid can absorb UV and act as an antenna.	
(a) Tyrosine	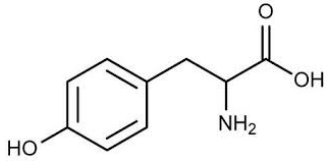	(Engel and Nagy, 1982)	Water soluble	A carboxylic acid and an amine and hydroxyl group.	Double bond π electrons of the carboxylic acid can absorb UV and act as an antenna. Intrinsically fluorescent due to its phenyl group.	λ_{abs}=274 nm λ_{Em}=304 nm (Wünsch et al., 2015)

Analyte name	Analyte Structure	Criterion A – Identified in the solvent extract of Murchison	Criterion B - Solubility	Criterion C – Moieties with potential to interact with the metal centre	Criterion D – Moieties or structure that can act as a sensitising antenna	Absorption and emission wavelengths, λ_{abs} and λ_{Em}, where data available (for aromatic organics only)
(b) Fumaric acid	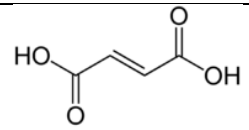	(Lawless et al., 1974)	Water soluble	Two carboxylic acid groups	Double bond π electrons of both carboxylic acids are conjugated via an alkene so are delocalised. Whole molecule can absorb UV and act as an antenna	
(b) Maleic acid	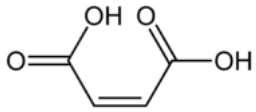	(Lawless et al., 1974)	Water soluble	Two carboxylic acid groups	The double bond π electrons of both carboxylic acids are conjugated with the alkene so are delocalised. Both carboxylic acids can absorb UV and act as an antenna.	
(b) Itaconic acid	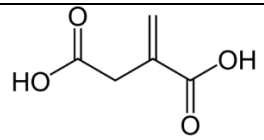	(Shimoyama and Shigematsu, 1994)	Water soluble	Two carboxylic acid moieties	The double bond π electrons of one carboxylic acid are conjugated with the alkene so are delocalised. Both carboxylic acids can absorb UV and act as an antenna.	

Analyte name	Analyte Structure	Criterion A – Identified in the solvent extract of Murchison	Criterion B - Solubility	Criterion C – Moieties with potential to interact with the metal centre	Criterion D – Moieties or structure that can act as a sensitising antenna	Absorption and emission wavelengths, λ_{abs} and λ_{Em}, where data available (for aromatic organics only)
(b) Benzoic acid	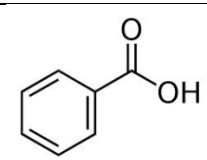	Most abundant aromatic in the Murchison meteorite (Martins et al., 2006)	Water soluble	A carboxylic acid	The double bond π electrons of one carboxylic acid are conjugated with the aromatic benzene ring so are delocalised. Both carboxylic acid and benzene ring can absorb UV and act as an antenna.	λ_{abs}=266 nm λ_{Em}=315 nm (Wünsch et al., 2015)
(c) Purine	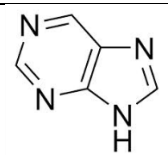	The simplest of the purines identified in the Murchison meteorite i.e. it does not possess any side groups. (Callahan et al., 2011)	Water soluble	Four nitrogen atoms with lone pairs	Whole molecule is aromatic; possessing delocalised π electrons therefore may act as an antenna.	No Data
(c) Guanine	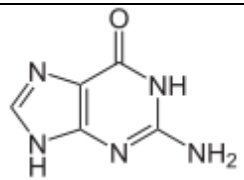	(Callahan et al., 2011)	Water soluble	Carbonyl oxygen, an amine group and four nitrogen atoms with lone pairs.	Whole molecule is aromatic; possessing delocalised π electrons therefore may act as an antenna.	λ_{abs}=265 nm λ_{Em}= 266 nm (Taniguchi & Lindsey, 2018)
(c) Hypoxanthine	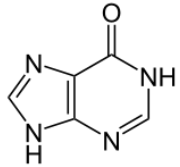	(Callahan et al., 2011)	Water soluble	Carbonyl oxygen, and four nitrogen atoms with lone pairs.	Whole molecule is aromatic; possessing delocalised π electrons therefore may act as an antenna.	λ_{abs}=250 nm (Zhengming & Shaoping, 2016) λ_{Em}= No Data

Analyte name	Analyte Structure	Criterion A – Identified in the solvent extract of Murchison	Criterion B - Solubility	Criterion C – Moieties with potential to interact with the metal centre	Criterion D – Moieties or structure that can act as a sensitising antenna	Absorption and emission wavelengths, λ_{abs} and λ_{Em}, where data available (for aromatic organics only)
(c) Adenine	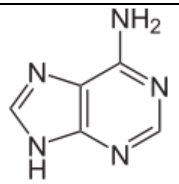	(Callahan et al., 2011)	Water soluble	An amine group and four nitrogen atoms with lone pairs.	Whole molecule is aromatic; possessing delocalised π electrons therefore may act as an antenna.	λ_{abs}=260 nm (Zhengming & Shaoping, 2016) λ_{Em}= 266 nm (Taniguchi & Lindsey, 2018)
(d) Pyrimidine	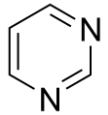	Not reported in Murchison but is the side group-free, simplest form of the pyrimidine class of nucleobases (it is therefore analogous to purine, which is the side group-free, simplest form of the purines).	Water soluble	Two nitrogen atoms with lone pairs.	Whole molecule is aromatic; possessing delocalised π electrons therefore may act as an antenna.	No Data
(d) 2 4-diaminopyrimidine	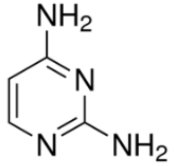	Not identified in Murchison meteorite but is analogous to 2,6- and 6,8 diaminopyrimidine which have (Callahan et al., 2011),	Water soluble	Two amine groups and two nitrogen atoms with lone pairs.	Whole molecule is aromatic; possessing delocalised π electrons therefore may act as an antenna.	No Data

Analyte name	Analyte Structure	Criterion A – Identified in the solvent extract of Murchison	Criterion B - Solubility	Criterion C – Moieties with potential to interact with the metal centre	Criterion D – Moieties or structure that can act as a sensitising antenna	Absorption and emission wavelengths, λ_{abs} and λ_{Em}, where data available (for aromatic organics only)
(d) Cytosine	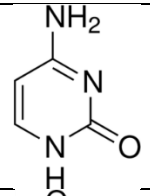	(Stoks and Schwartz, 1979)	Water soluble	A carbonyl oxygen, an amine group and two nitrogen atoms with lone pairs.	Whole molecule is aromatic; possessing delocalised π electrons therefore may act as an antenna.	λ_{abs}= 267 nm λ_{Em}= No Data (Taniguchi & Lindsey, 2018)
(d) Uracil	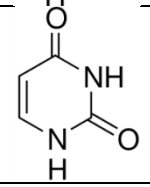	(Stoks and Schwartz, 1979)	Water soluble	Two carbonyl oxygens and two nitrogen atoms with lone pairs.	Whole molecule is aromatic; possessing delocalised π electrons therefore may act as an antenna.	λ_{abs}= 259.5 nm λ_{Em}= No Data (Taniguchi & Lindsey, 2018)
(d) Thymine	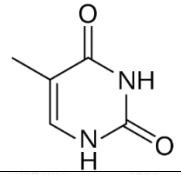	(Stoks and Schwartz, 1979)	Water soluble	Two carbonyl oxygens and two nitrogen atoms with lone pairs.	Whole molecule is aromatic; possessing delocalised π electrons therefore may act as an antenna.	λ_{abs}= 264.5/267 nm λ_{Em}= No Data (Taniguchi & Lindsey, 2018)
(e) Guanylurea	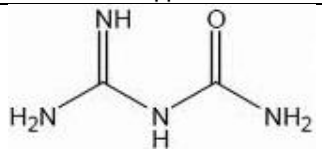	(Folsome et al., 1971, Folsome et al., 1973, Stoks and Schwartz, 1981)	Water soluble	One carbonyl oxygen, 3 amines and an imine.	Double bond π electrons of the carboxylic acid can absorb UV and act as an antenna.	No Data

Table 2.2 Name and molecular structure of the individual analytes selected, indicating how each analyte fulfils the selection criteria

2.4 Sample preparation

2.4.1 Mineral samples

Interior pieces of the minerals were preferred, to minimise surface contamination. Interior samples were obtained by slicing the samples using a diamond saw and polishing the revealed internal surfaces with silicon carbide (SiC) pads using 18.2 MΩ water as a lubricant. The samples were held wearing nitrile gloves to avoid organic contamination from handling, and the procedure was carried out on a laminar flow bench. The fresh mineral surfaces were then rinsed first with propanone, to remove any water, mineral/SiC particulates and organic contamination, and then with DCM, to facilitate drying. Neither of these solvents were likely to dissolve or alter the chemistry of the mineral surface in the timescale of preparation. The samples were then placed in clean, dry glass vials (cleaned as per protocol in Section 2.1.2).

An agate pestle and mortar (hydrated silica, with a Mohs scale hardness of 7) was used to crush those minerals with a hardness of less than 7 to a fine powder. Corundum, which has a hardness of 9, was crushed in a tungsten carbide (Mohs hardness of 9.5, Foote and MacLennan (1984)) mill (Figure 2.1). Mineral grain sizes were no larger than ~0.5 mm which was confirmed using secondary electron imaging (Section 2.6.1). Both the pestle and mortar and mill were cleaned using the previously explained cleaning procedure (Section 2.1.6).

Figure 2.1 Crushed mineral samples, (left to right), anorthite, calcite, corundum, gypsum, enstatite, diopside, nepheline, magnetite and olivine.

2.4.2 Preparation of rock samples

Samples of Murchison, ALH88045, GRS and Q-F were available from The Open University's research collection. The Murchison sample was supplied as a pre-crushed powder kept in a sealed glass vial. A sample of ALH88045 was selected that was free of fusion crust and free of evident secondary weathering products. Preparation was carried out by Dr R. C. Greenwood (The Open University) in a class 100 cleanroom. The sample was crushed in an agate pestle and mortar that had been pre-cleaned using quartz sand, acetone and reverse osmosis (RO) water. All equipment used for sample handling had been cleaned by sonicating in a MeOH:Tol mixture (50:50). Samples of both GRS and Q-F were supplied pre-crushed (Table 2.3).

Crushed Murchison	ALH88045	Crushed GRS	Q-F
			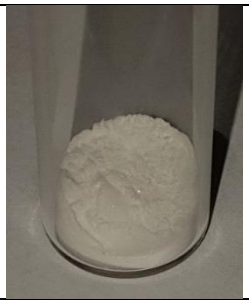

Table 2.3 Geological samples used to provide organic extracts with which to test the sensor responses; Murchison and ALH88045 are carbonaceous chondrite samples, GRS is a terrestrial organic-rich rock and Q-F is the organic-free mineral blank

2.4.3 Preparation of stock solutions

Although analytes may invoke a response to the sensor, the magnitude of that response may differ. In order to determine this, the sensors must be applied to standard solutions of known concentrations.

To prepare the stock solutions, known masses of each standard were weighed using a precision balance (Sartorius BP211D, Max. 210 g, d=0.01 mg (80 g), 0.1 mg (210 g)), which was situated on a laminar flow bench. Standards were weighed onto a ~1x1 cm pieces of aluminium foil that had been washed with propanone, methanol and dichloromethane, baked at 450°C for 24 hours then left to cool to room temperature before use. The measured mass was entered into a spreadsheet to calculate an accurate molarity, for the volume required, of each standard.

The various standards were transferred (on the foil) to clean, dry, volumetric flasks of appropriate volume, and washed into the flask with 18.2 MΩ water (to ensure no contamination could be derived from the water solvent) using a clean, dry Pasteur pipette. The foil was rinsed thoroughly and the flask topped up to the required level. For those standards that did not fully dissolve, the volumetric flasks were placed in a sonicator for 90 minutes at 30°C to facilitate dissolution by breaking up any large particles of solute. The stock solutions were contained in stoppered flasks and were stored at all times in the windowless darkroom that houses the spectrofluorimeter so that the solutions would not be subject to degradation by sunlight or UV radiation. The concentration of the stock solution was 1 mmol.

2.5 Sample extractions

The following sections describe the processes used to produce the extracts for testing the sensor responses.

2.5.1 Minerals

In order to ascertain if the presence of mineral particulates or dissolved mineral ions in a meteorite extract would interact and/or interfere with the fluorescence emissions of the sensor, it was essential to first apply the sensor to an extract of each standard mineral beforehand. This would provide information as to whether the presence of such mineral species would interfere with the sensor fluorescence and, if so, how. This would also allow for the development of contingency as to how this interference may be corrected.

Although the extraction of the extraterrestrial organic material from the samples would involve the use of MeOH and a mixture of MeOH, DCM and toluene, as well as water (see Section 2.5.2), only water was used for the mineral extractions. This is because water dissolves such ionic compounds but MeOH, DCM and toluene are organic solvents, which will not. The presence of water may also result in chemical alteration of the minerals to produce secondary products, or may cause the mineral to disaggregate, forming mineral particulates. The dissolved minerals may also produce reactive species that could further alter the chemistry of the mineral extract, or the

mineral itself, causing interference to the fluorescence emissions. For this reason, the mineral standards were subjected to a simulated 'weathering' process over an extended period (longer than likely during sample extraction), to maximise the possibility of physical breakdown of the mineral or its dissolution.

A previously used protocol was used as a starting point to develop the strategy for the mineral weathering (Hausrath and Brantley, 2010), which subjected minerals to 18.2 MΩ water at an ambient temperature of ~22°C for 8 weeks. The results of that study suggested that maximum dissolution occurs at 4 weeks. Their weathering conditions were adopted (see below); however, to be sure the various selected mineral standards used in this had been allowed to weather sufficiently, a duration of 6 weeks was prescribed. Since this experiment was intended to present a worse-case scenario for sensor use, it was not necessary to monitor dissolution over the 6 week period.

The protocol used was as follows. Approximately 0.5 g of each mineral was placed in a pre-weighed, clean, dry 4 ml vial. 4 ml of 18.2 MΩ water was added using a 5 ml pipette. The samples were then treated using the following procedure: 1) agitated for 30 seconds using a vortex mixer; 2) placed in a centrifuge for 1 hour at 2500 rpm and 3) left to settle under gravity at room temperature for 24 hours. This procedure was repeated four times then left to stand for 48 hours then repeated. The samples were then left at room temperature for three weeks, after which time steps 1 to 3 were repeated for one more week (total process time: 6 weeks). The mineral solution was then carefully decanted into a separate clean dry vial using a Pasteur pipette, so as not to disturb the sediment, ready for fluorimetric experiments. The weathered mineral residues were freeze-dried and retained for further analysis.

2.5.2 Solvent extraction of organic material

In order to test the sensor on a natural, aqueous solution of a complex mixture of organic compounds, a simple extraction procedure was required that could liberate organic material from the natural samples without altering its chemistry (for a review of previous procedures see

Section 1.3.2). Three separate, consecutive organic extractions were carried out using three different solvents: 1) hot-water, at a temperature of 95°C; 2) hot-methanol (hot-MeOH), at a temperature of 95°C and 3) a hot-methanol:dichloromethane:toluene mixture (MeOH:DCM:Tol) (present in the ratio 10:45:45, respectively), and henceforth referred to as 'hot-solvent'.

The hot-water extraction was employed to liberate any highly polar, water soluble, components. The purpose of the hot-MeOH extraction was to dissolve any polar molecules less soluble in pure water. The hot-solvent was chosen based upon an extraction undertaken on samples of GRS (Anders and Robinson, 1971). Although Anders and Robinson (1971) did not stipulate the specific organic molecules liberated, it was anticipated that this polar/non-polar mixture would facilitate the extraction of molecules that exhibit both polar moieties and larger non-polar groups, such as polyaromatic ring structures.

The ratio of solvent volume to sample mass reported in the literature varies greatly; some studies use very low ratios, e.g. 0.4 ml g^{-1} (Martins et al., 2006) and 0.6 ml g^{-1} (Chan et al., 2012); some report a ratio of 1-5 ml g^{-1}, (e.g. (Jungclaus et al., 1976, Pizzarello et al., 1994, Burton et al., 2014, Aponte et al., 2014, Martins et al., 2015). Naraoka et al. (1999) used 10 ml g^{-1}, while Callahan et al. (2014) used 2777 ml g^{-1}. For a study of the purine and pyrimidine content of Murchison, van der Velden and Schwartz (1977) used a solvent to sample ratio of 35 ml g^{-1}. Since the variation in volume of solvent used per gram of sample reported in the literature does not appear to follow a consistent rational, the solvent to sample ratio used for the extraction of organic matter for the study described herein was chosen as 20 ml g^{-1}.

0.2 g aliquots of each crushed sample were weighed into clean, dry vials. Using a 5 ml graduated pipette, 4 ml of 18.2 MΩ water was added. The vials were agitated for 20 seconds using a vortex mixer, sonicated at ~50°C for 20 minutes and then heated at ~95°C in a heating block for 24 hours. The samples were removed from the heating block and left to cool to room temperature. The samples were placed in a centrifuge set at 2500 rpm for 20 minutes and then left to settle for

1 hour. Solvent-only procedural blanks (vials containing just 4 ml of 18.2 MΩ water) were treated in the same way.

The aqueous solutions were decanted into clean, dry vials using clean, dry glass Pasteur pipettes, taking care not to transfer solid material in the process. The remaining solid residues were rinsed with 1 ml portions of 18.2 MΩ water, agitated using a vortex mixer for 20 seconds and placed in a centrifuge set at 2500 rpm for 20 minutes. After centrifuging, the supernatant was combined with the solution already decanted and the process repeated once more. To ensure as full a recovery as possible, this rinsing and centrifuging process was repeated with a further 2 ml portion of 18.2 MΩ water, and the supernatant combined with the extracts already decanted. The aqueous extracts were frozen in the vials, using a liquid nitrogen bath, and freeze-dried. The solid residues were frozen in the vials, using a liquid nitrogen bath, and freeze-dried, to prevent any further chemical reactions taking place.

The solid residues were weighed, 4 ml of MeOH was then added and extraction protocols proceeded as for the hot-water solvent extraction. The heating block temperature for the MeOH extraction was set at ~60°C, since the boiling point of MeOH is ~65°C. Solvent-only procedural blanks were treated in the same way. After 24 hours, and once cooled to room temperature, the vials were centrifuged and the MeOH extracts decanted to clean, dry vials using clean, dry glass Pasteur pipettes, taking care not to transfer any solid material while doing so. The solid residue was rinsed with 1 ml of MeOH, centrifuged, and the MeOH removed and combined with the MeOH extract already decanted. This process was repeated with a further 1 ml of MeOH and as described above, a further 2 ml portion of MeOH. The MeOH was removed from the extract under a flow of nitrogen in a fume hood. The vials containing solid residue (which had undergone separate consecutive extractions with hot-water and then hot-MeOH) were placed in a clean, dry beaker, wrapped in clean aluminium foil, and placed in a drying oven at 50°C where they were heated to dryness to prevent any further chemical reaction. Freeze-drying was not necessary as, unlike water, MeOH may be driven off by this heating.

The dried, solid residues were weighed and 4 ml of MeOH:DCM:Tol (10:45:45) (henceforth, 'the solvent') was added. The samples were agitated using the vortex mixer for 20 seconds, sonicated at ~50°C for 20 minutes and then heated at ~60°C following the same procedure as described previously. Solvent-only procedural blanks were treated in the same way. The solvent solution was decanted to clean, dry 4ml vials using clean, dry glass Pasteur pipettes, taking care not to transfer solid material in the process. The remaining residue was rinsed with a 1 ml portion of the solvent and centrifuged in the same way as previously described, and repeated once more. This rinsing was repeated with a 2 ml portion of the solvent. Those portions were combined with the solvent already decanted. The solvent was removed from the extract under a flow of nitrogen in a fume hood. The vials containing the remaining solid residue had their caps loosely replaced, and were placed in a clean dry beaker, covered in clean aluminium foil and removed to a drying oven at 50°C where they were heated to dryness. The dry solid residues were no longer required for further extractions or work for this study, however, once dry, they were sealed in their vials and stored should they be required for any future purpose.

The vials containing the water extracts, the MeOH extracts and the solvent extracts were rinsed three times with 0.5 ml aliquots of MeOH and the solutions transferred to clean, dry weighed 2 ml vials that were more appropriate to the sample size. The MeOH was removed under a flow of nitrogen in a fume hood; the vials were weighed, capped and stored in a freezer at ~-4°C ready for analysis.

2.6 Analytical techniques

A number of analytical techniques have been used throughout this thesis. These are outlined in the sections that follow.

2.6.1 SEM-EDX analysis

Before subjecting the mineral analogues to any weathering, it was necessary to establish their purity; any contaminants or heterogeneities in their composition may result in a false positive or false negative. To that end, the samples were characterised by scanning electron microscopy-

electron dispersive X-ray spectroscopy (SEM-EDX). SEM-EDX analysis was performed on all un-weathered mineral samples and those weathered samples that affected a change in the observed fluorescent emissions of the sensors.

Crushed minerals (~<1 mg) were loaded onto 12 mm adhesive carbon pads applied to aluminium scanning electron microscope (SEM) sample stubs. The samples were carbon coated using an EMITECH K950X Turbo carbon sputter coater (thickness; ~ <30 nm). The minerals were analysed using a FEI Quanta 200 3-D dual beam scanning electron microscope (SEM), and imaged with secondary and backscattered electron (BSE) detectors to ascertain the topography of the sample i.e. grain size, shape and distribution, and chemical composition, respectively (see Appendix B). The SEM was combined with an Oxford Instruments 80 mm^2 X-MAX energy dispersive X-ray detector in energy dispersive spectroscopy (EDS) mode, using an acceleration voltage of 20 kV and a beam current of 0.6 nA. Point and ID analysis was undertaken to obtain elemental information.

2.6.2 Column and thin layer chromatography

In order to separate the *mono*-, *bis*-, *tris*- and *tetra*-substituted cyclen reaction products from the crude reaction mixture, column chromatography was carried out using silica purchased from Sigma Aldrich; eluents used are as described (Section 2.7). Thin layer chromatography (TLC) was carried out with silica on aluminium foil plates, impregnated with fluorescent indicator (purchased from Fluka). Analyte spots of the individual reagents, a co-spot of all regents and a reaction mixture spot at various times during the reaction, were delivered onto the TLC plates using a glass capillary tube. The eluent used for the TLC mobile phase was 20% ethyl ethanoate in DCM and the TLC spots were visualised with iodine vapour and UV light.

2.6.3 Mass spectroscopy

To obtain mass data for free ligands and lanthanide complexes, approximately 1 mg of each sample to be tested was placed in a clean, dry 2 ml glass vial (taken directly from the packaging; the vials were not required to be pre-cleaned) and dissolved in a 1:1 mixture of 18.2 MΩ (0.5 ml)

water and HPLC grade MeOH (0.5 ml). The samples were loaded into a Finnigan Surveyor auto-sampler Plus, which automatically delivered aliquots of sample, at a flow rate of 500 µl per minute, to a TSQ Quantum GC equipped with an electrospray ionisation (EI) ion source. Electrospray was used either in the positive mode for neutral ligands and complexes, and positively charged complexes, or negative mode for negatively charged complexes, as indicated in Section 2.7.

2.6.4 Nuclear magnetic resonance spectroscopy

^{1}H NMR and ^{13}C NMR data were obtained using a 300 MHz JEOL instrument. Chemical shift values for ^{1}H spectra were recorded in parts per million (ppm) relative to the methyl group in tetramethylsilane (TMS) as the internal standard. For ^{13}C spectra, the chemical shifts were presented as frequencies in ppm relative to the solvent peaks. Solvents used for the samples are indicated in Section 2.7.

2.6.5 Infrared spectroscopy

Infrared spectroscopy was carried out on all lanthanide complexes (with the exception of [TbDO3A] and TbL2, which were analysed using a Thermo Nicolet FT-IR Nexus infrared spectrometer) using a Thermo Scientific Nicolet iS5 infrared spectrometer to obtain infrared transmission spectra of the complexes, enough sample to cover the diamond window (which was cleaned before and after analyses with 18.2 MΩ water and IPA, using a clean, dry tissue) was placed on the sample stage and compressed using the screw clamp. The spectra were produced using Omnic software.

2.6.6 UV-Vis spectroscopy

UV absorption data for the complexes was obtained using a Genesys IOS UV-Vis spectrometer equipped with a pulse xenon lamp. Approximately 3 ml of 1 mM complex solution was decanted into a quartz UV-Vis cuvette (frosted on two sides and polished on the other two). The samples were loaded into the instrument and data collected over the range 190 nm to 720 nm, with an

interval of 0.5 nm. The raw data was saved to a USB memory stick and processed using Microsoft Office Excel to produce spectra.

2.6.7 Fluorimetry

Fluorimetry was carried out using a Fluoromax-P spectrofluorimeter, and the data processed using DataMax version 2.20 software. The light source was a high pressure xenon arc 150 W lamp, which produces a continuous emission from ~250 nm to ~900 nm (the near infrared). Preliminary experimentation was undertaken using different fluorimeter settings in order to determine the optimal fluorimeter settings for the fluorometric assays (See Section 3.2). The final optimised settings are shown in Table 2.4.

Lanthanide	Excitation λ, nm	Excitation Slit, nm	Emission Slit, nm	Acquisition time, s	Acquisition increment, nm	Acquisition range, nm
Europium	280	3	3	0.5	0.5	570-710
Terbium	280	3	3	0.5	0.5	460-640

Table 2.4 Optimised fluorimeter settings used to determine change in sensor fluorescence intensity with increasing concentration of analyte

The cuvettes used for fluorimetry are made of precision quartz, polished on all four sides. This material is non-fluorescent and has a transmission range of 190 nm to 2500 nm, meaning the excitation and emission light will not be absorbed by the cuvette. In order to ensure the cuvettes were free from organic contaminants that may result in unwanted fluorescence emissions, they were thoroughly cleaned using the protocol described (Section 2.1.4). Once samples were added, however, to ensure no additional contaminants had been introduced to the external surfaces of the cuvette, they were wiped with clean, lint-free, optical lens paper and carefully inspected for grease or marks. The cuvette lids were cleaned by the same method.

Once the samples were loaded into the cuvettes, and the cuvettes externally cleaned, the cuvettes were stoppered and upended five times in order to ensure homogeneity of the mixture. When placing the cuvettes into the cuvette holder, it was imperative that the cuvettes were placed in the same orientation so that, should imperfections in the quartz be present, the light

collected would be consistent for each run. Furthermore, extreme care was taken to seat the cuvettes consistently in the cuvette holder, mounted on the sample stage in the fluorimeter, to avoid damage and conserve exact orientation.

Protocols were amended if the availability of stock solution changed, such that the volumes used were reduced but relative concentrations of analyte to sensor were maintained (details are given in Chapters 3, 4 and 5).

Before the sensor was added to any sample, a sensor-only fluorescence spectrum was obtained in order to compare the emissions before and after application of the sensor (Figures 2.2 to 2.7).

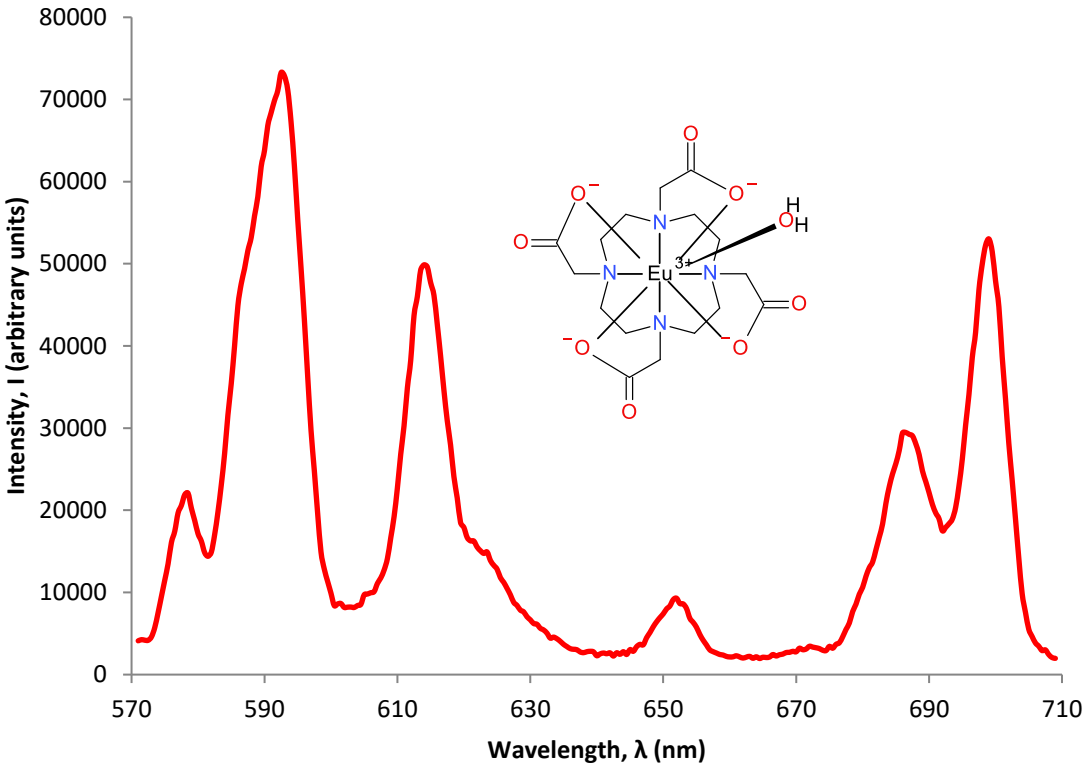

Figure 2.2 Fluorescence emissions of a 0.5 mM solution of $[EuDOTA]^-$ (λ_{Ex}=265 nm, acquisition time=0.5 sec, acquisition increment=0.5 nm, excitation and emission slit width=3 nm, pH=5)

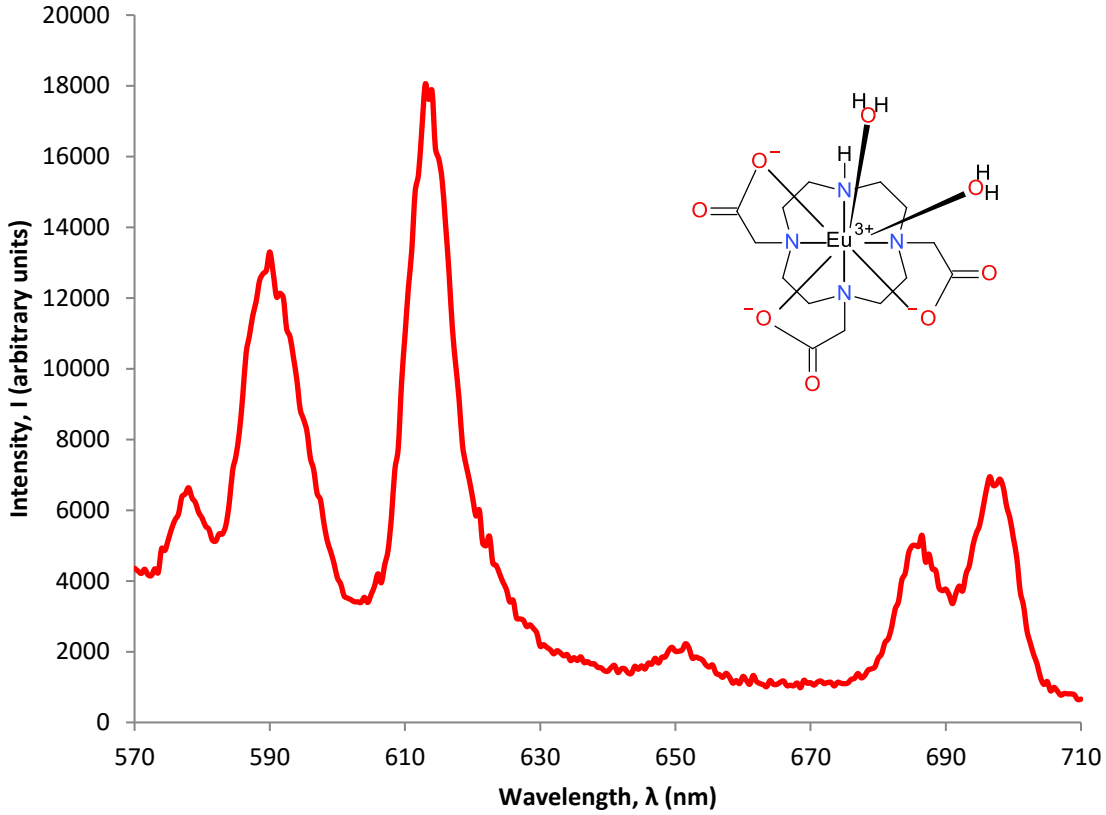

Figure 2.3 Fluorescence emissions of a 0.5 mM solution of [EuDO3A] (λ_{Ex}=265 nm, acquisition time=0.5 sec, acquisition increment=0.5 nm, excitation and emission slit width=3 nm, pH=5)

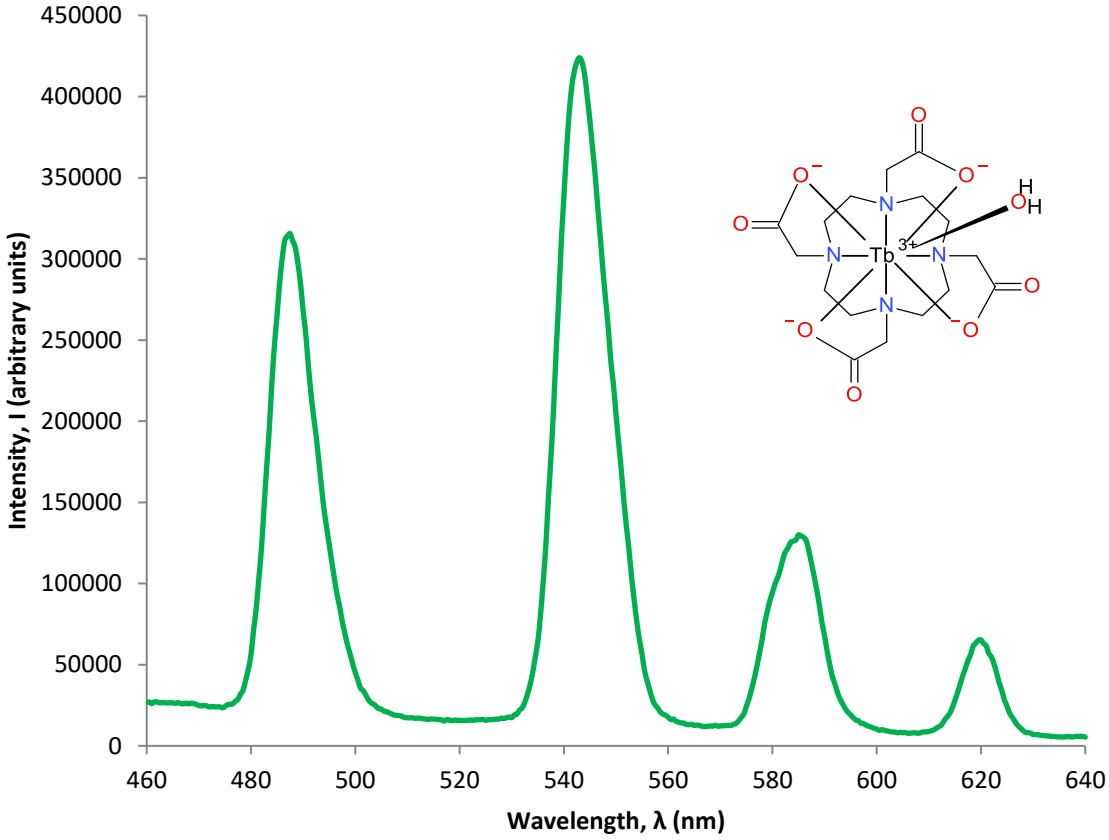

Figure 2.4 Fluorescence emissions of a 0.5 mM solution of $[TbDOTA]^-$ (λ_{Ex}=265 nm, acquisition time=0.5 sec, acquisition increment=0.5 nm, excitation and emission slit width=3 nm, pH=5)

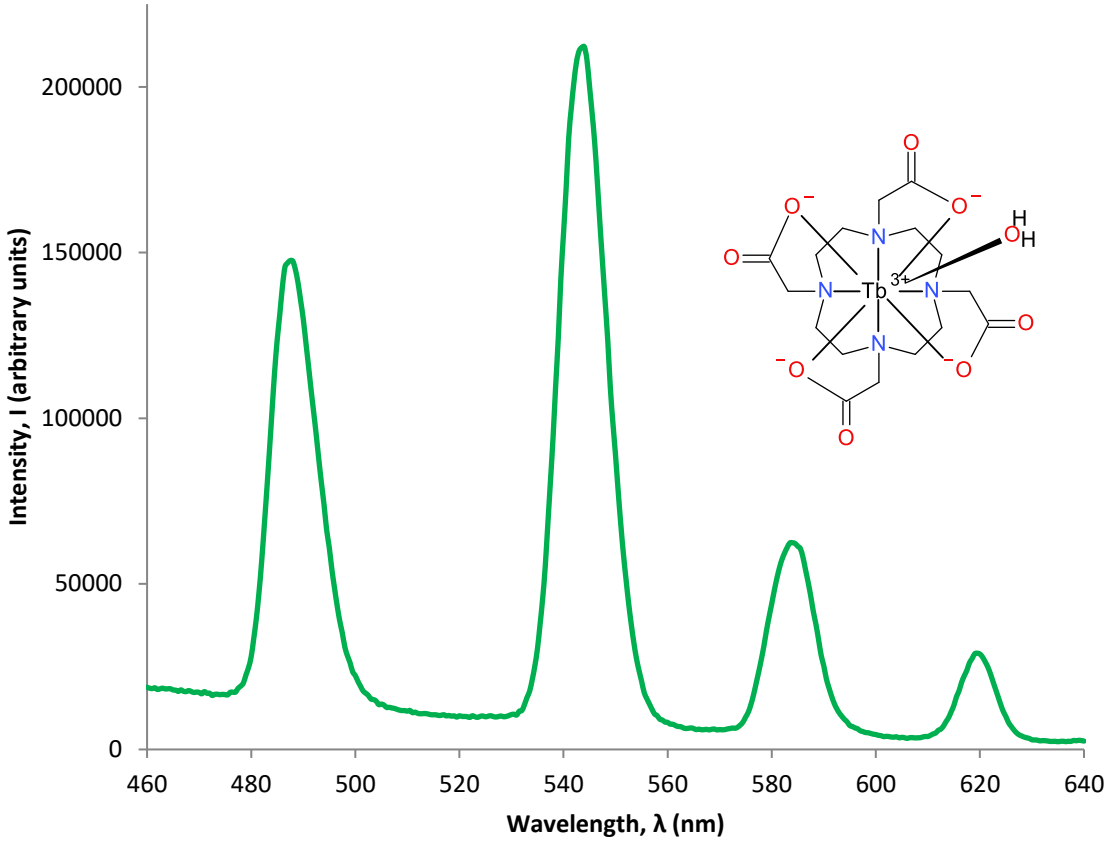

Figure 2.5 Fluorescence emissions of a 0.5 mM solution of [TbDO3A] (λ_{Ex}=265 nm, acquisition time=0.5 sec, acquisition increment=0.5 nm, excitation and emission slit width=3 nm, pH=5)

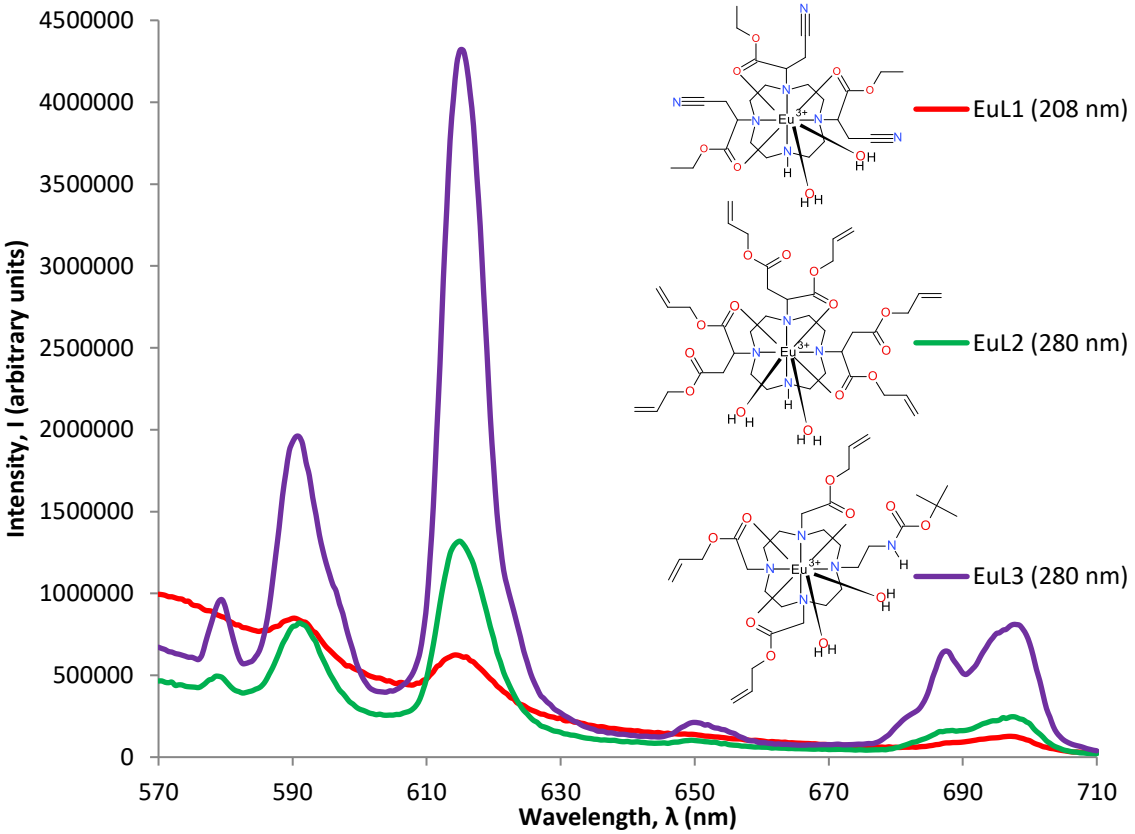

Figure 2.6 Fluorescence emissions of 3 mM solutions of europium complexes of L1, L2 and L3 (λ_{Ex}=280 nm, acquisition time=0.5 sec, acquisition increment=0.5 nm, excitation and emission slit width=3 nm, pH=5)

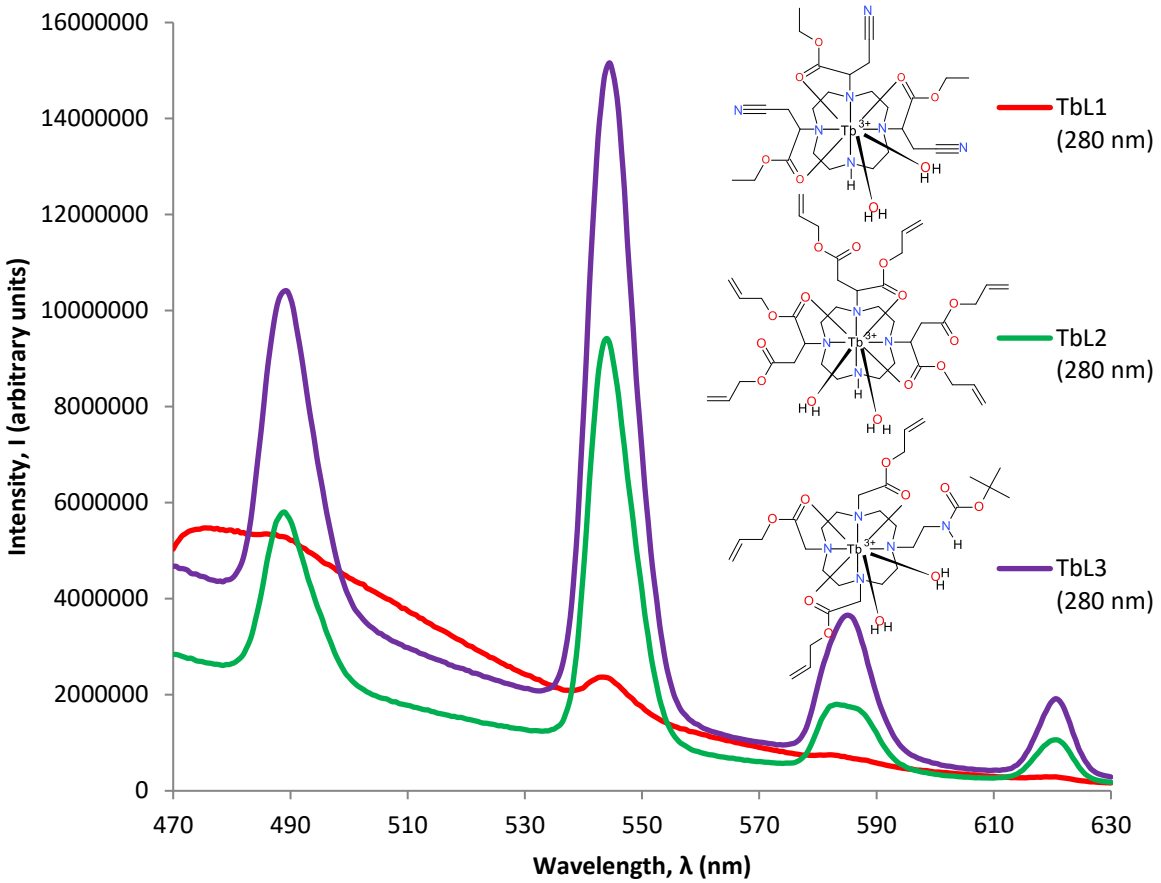

Figure 2.7 Fluorescence emissions of 3 mM solutions of terbium complexes of L1, L2 and L3 (λ_{Ex}=280 nm, acquisition time=0.5 sec, acquisition increment=0.5 nm, excitation and emission slit width=3 nm, pH=5)

2.7 Ligand and complex syntheses

The following section describes the synthesis of the organic ligands used to chelate the europium and terbium ions, and the production of the respective europium and terbium complexes, i.e. the sensors. The information herein includes masses and volumes of reagents, the respective number of moles calculated from these data and relative molecular masses, and relative equivalents (eq.) thereof with respect to cyclen, the reactant used in the syntheses. Information pertaining to the mass and percentage yields of the products obtained is also presented. Carbon-13 and proton nuclear magnetic resonance (^{13}C NMR and ^{1}H NMR, respectively) data and retention factors (R_f) of the ligands, using thin layer chromatography, are presented in the conventionally accepted manner for the characterisation of ligands. The theoretical calculated masses of products are given alongside masses detected by mass spectroscopy, where it was possible to obtain these data. Complexes were characterised by infrared spectroscopy (these data are also presented in the accepted convention). Although not a direct characterisation, chelation of the lanthanide ion

was confirmed qualitatively by fluorescence spectroscopy; solutions of the compounds synthesised produced emissions conducive to excitation of europium and terbium ions and subsequent fluorescent emission by ligand to metal charge transfer when solutions were irradiated at 280 nm. Such emissions could only occur if the lanthanide ions were coordinated to the ligands.

2.7.1 Synthesis of [LnDOTA]$^-$

DOTA (500 mg, 1.24 mmol) (purchased from ABCR, Germany) was combined with europium trichloride hexahydrate ($EuCl_3.6H_2O$) (260 mg, 1.01 mmol, 1 eq.) (Scheme 2.1) in 18.2 MΩ water (10 ml), and heated, while stirring, at 80˚C under a nitrogen atmosphere following a methodology based on protocols developed by Lowe *et al.* (2001) and Nasso *et al.* (2014). Once cooled to room temperature, the reaction mixture was transferred to a 250 ml round bottomed flask. The reaction vessel was rinsed with 18.2 MΩ water (10 ml), followed by a final 18.2 MΩ water rinse (5 ml). All rinsings were added to the 250 ml round bottomed flask. The reaction mixture and rinsings were rapidly frozen using liquid nitrogen and freeze dried overnight. Diethyl ether (10 ml), kept at approximately 0˚C using a crushed ice bath, was added to the residue. The mixture was filtered under vacuum. Two further portions of cold diethyl ether (2x 5 ml) were used to wash the residue. The washed residue was placed in a desiccator for 24 hours. The yield obtained was 600 mg (1.08 mmol), which is 82.2% of the calculated expected yield. IR (ν_{max}/cm^{-1}) 3337 (broad N-H), 2360 (alkane C-H), 1609 (C=O), 1406 (C-H), 1390 (C-H), 1219-1162 (C-O), 1080 (C-N), 998-835 (C-C). The mass spectrometer, in negative mode, detected the target ion at a mass of 553.11 Da; the theoretical mass was calculated to be 553.08 Da. Fluorimetric analysis confirmed chelation of europium by excitation of a 3 mM aqueous solution at 280 nm, indicating sensitisation by ligand to metal charge transfer.

DOTA (280 mg, 1.24 mmol) was combined with terbium trichloride hexahydrate ($TbCl_3.6H_2O$) (280 mg, 1.02 mmol, 1 eq.) (Scheme 2.1) and treated in exactly the same manner, under the same reaction conditions, as described for the production of $[EuDOTA]^-$ above. The residue was stored in a desiccator for 24 hours. The yield obtained was 310 mg (0.55 mmol), which is 79.5% of the

calculated expected yield. IR (ν_{max}/cm^{-1}) 3339 (broad N-H), 2360 (alkane C-H), 1610 (C=O), 1407, 1378-1354 (C-H), 1253 (C-O), 1081 (C-N), 999-835 (C-C). The mass spectrometer, in negative mode, detected the target ion at a mass of 559.11 Da; the theoretical mass was calculated to be 559.09 Da. Fluorimetric analysis confirmed chelation of terbium by excitation of a 3 mM aqueous solution at 280 nm, indicating sensitisation by ligand to metal charge transfer.

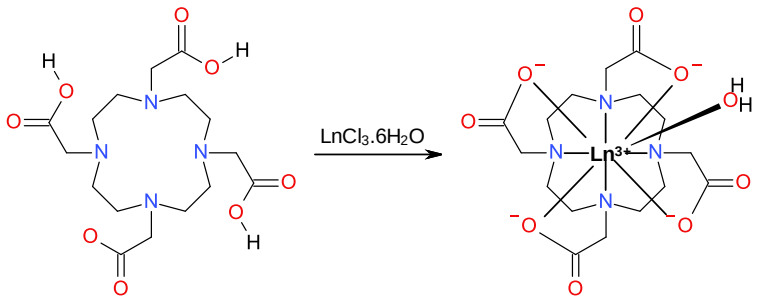

Scheme 2.1 Chelation of Ln^{3+} (Eu^{3+} or Tb^{3+}) by DOTA. One water molecule is also coordinated to the lanthanide ion

2.7.2 Synthesis of DO3A and [LnDO3A]

Following a methodology based on protocols developed by Lowe *et al.* (2001), *tBut*-DO3A (260 mg, 0.51 mmol) (purchased from ABCR, Germany) was dissolved in trifluoroethanoic acid (TFA) (4 ml, 5960 mg, 52.27 mmol) (Scheme 2.2). The reaction mixture was heated at ~40 ˚C for 24 hours after which time the TFA was removed under reduced pressure. The residue was separated using 18.2 MΩ water (10 ml) and DCM (7 ml). The aqueous phase containing the DO3A product was freeze-dried. The yield obtained was 150 mg (0.43 mmol), which is 83.3% of the calculated expected yield. R_f = 0.48 (SiO_2, 50% MeOH in H_2O). ^{1}H NMR (400 MHz, $CDCl_3$); 2.76 (CH_2), 2.91 (CH_2), 2.99 (CH_2), 3.04 (CH_2), 3.18 (CH_2), 3.29 (CH_2), 3.34 (CH_2), 3.49 (CH_2), 3.53 (CH_2), 3.77 (CH_2).^{13}C NMR (75 MHz, D_2O): 28.10 (CH_3), 36.21 (CH_2), 36.63 (CH_2), 42 (CH_2), 45 (CH_2), 48 (CH_2), 49 (CH), 59.16 (ethyl CH_2), 61.68 (ethyl CH_2), 116.69 (CN), 168.80 (C=O), 169.26 (C=O). The mass spectrometer, in positive mode (+ES), detected the target ion at a mass of 347.22 Da ($[M+H]^+$); the theoretical mass was calculated to be 346.19 Da.

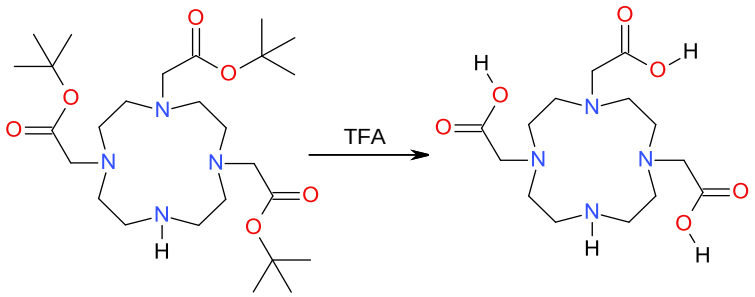

Scheme 2.2 removal (deprotection) of the tertiary butyl (*t*-But) groups from *t*-ButDO3A to yield the free acid ligand DO3A

Following a methodology based on protocols developed by Lowe *et al.* (2001) and Nasso *et al.* (2014), DO3A (75 mg, 0.43 mmol) was combined with $EuCl_3.6H_2O$ (120 mg, 0.33 mmol) (Scheme 2.3) in 18.2 MΩ water (5 ml), and the pH raised to 4.96 using 1 M potassium hydroxide solution (KOH(aq)). This was then heated, and stirred, at reflux of 100˚C under a nitrogen atmosphere for 18 hours. Once cooled to room temperature, the reaction mixture was raised to pH 10.03 using 1 M KOH(aq) and filtered under vacuum through a celite plug. The filtrate pH was lowered to 5.1 using 1 M hydrochloric acid solution (HCl (aq)) and freeze-dried. The residue was washed with 50:50 MeOH in DCM (10 ml), filtered under vacuum and the solvent removed. The residue was dissolved in 18.2 Ω water (5 ml) and freeze dried. The yield obtained was 60 mg (0.12 mmol), which is 56% of the calculated expected yield. IR (ν_{max}/cm^{-1}) 3386 (broad N-H), 2359 (alkane C-H), 1675-1581 (C=O), 1439-1408-1323 (methyl C-H), 1193-1130 (C-O), 1083 (C-N), 1003-798 (C-C). The theoretical mass of [EuDO3A] was calculated to be 497.09 Da. Although mass peaks were detected at 80, 83, 142 and 275 Da, they could not be confidently assigned to products of fragmentation of the parent ion, furthermore, the parent ion mass was not detected. A low intensity peak was detected at 580 Da which may be representative of an adduct of the complex parent ion with the species detected at m/z 83 Da. Fluorimetric analysis, however, confirmed chelation of europium by excitation of a 3 mM aqueous solution at 280 nm, indicating sensitisation by antenna effect afforded by ligand to metal charge transfer.

DO3A (75 mg, 0.43 mmol) was combined with $TbCl_3.6H_2O$ (130 mg, 0.35 mmol) (Scheme 2.3) in 18.2 MΩ water (5 ml). The pH was raised to 5.16. Post reaction, the pH was raised to 10.15 and filtered through celite. The pH was then lowered to 5.17 and freeze-dried. The lyophilised residue

was washed with 50:50 MeOH in DCM (10 ml) and the solvent removed. The yield obtained was 80 mg (0.16 mmol), which was 73% of the calculated expected yield. IR (ν_{max}/cm^{-1}) 3389 (broad N-H), 2359 (alkane C-H), 1673-1592 (C=O), 1434-1405 (methyl C-H), 1179-1121 (C-O), 1084 (C-N), 1003-720 (C-H). The theoretical mass of [EuDO3A] was calculated to be 503.09 Da, however, although mass peaks were detected at 80, 83, 122, 142 and 429 Da, they could not be assigned to the products of fragmentation of the parent ion and, furthermore, the parent ion mass was not detected. A low intensity peak was detected at 586 Da which may be representative of an analogous adduct of the complex parent ion (observed at 580 Da for the [EuDO3A] complex) with the species detected at m/z 83 Da. Fluorimetric analysis, however, confirmed chelation of terbium by excitation of a 3 mM aqueous solution at 280 nm, indicating sensitisation by ligand to metal charge transfer.

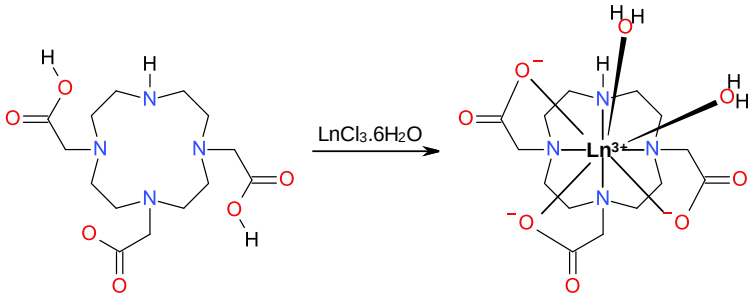

Scheme 2.3 Chelation of Ln^{3+} (Eu^{3+} or Tb^{3+}) by DO3A. Two water molecules are also coordinated to the lanthanide ion

2.7.3 Synthesis of L1 and $[LnL1]^{3+}$

Using protocols developed by O'Connell (2009), to a solution of cyclen (210 mg, 1.19 mmol) in dry MeCN (15 ml), (2Z)-3-cyanoprop-2-enoate (0.48 ml, 460 mg, 3.71 mmol, 3.1 eq.) was added (Scheme 2.4) using an automatic pipette. The reaction was heated to reflux at 80°C for 5 hours, and stirred under an argon atmosphere. Once cooled to room temperature, the solvent was removed *in vacuo* to yield an orange, viscous oil. The organic fraction was isolated, and then purified by silica gel column chromatography using a gradient of 20% to 5% EtOH in DCM. The yield obtained was 200 mg (0.37 mmol), which was 30.6% of the calculated expected yield. R_f = 0.33 (SiO_2, 5% EtOH in DCM).

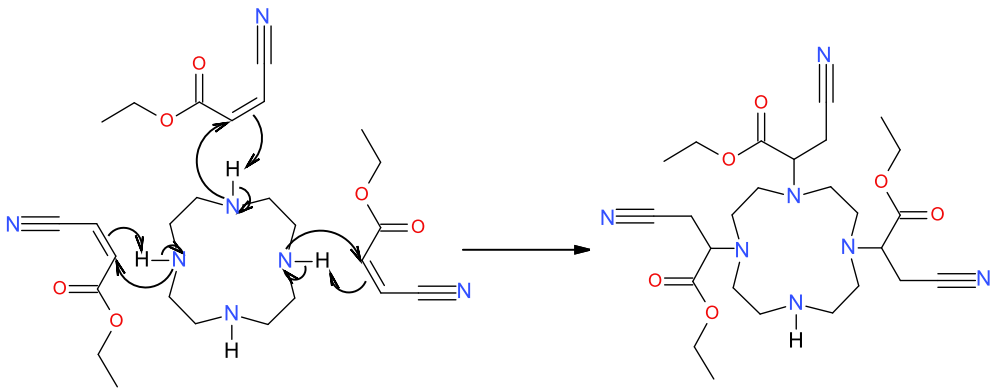

Scheme 2.4 Addition of (2Z)-3-cyanoprop-2-enoate to cyclen

^{1}H NMR (400 MHz, $CDCl_3$); 1.00-1.14 (a), 2.65-2.99 (b-c), 3.33 (d), 3.45-3.53 (e), 3.92-4.08 (f), 4.53-4.71 (g). ^{13}C NMR (75 MHz, $CDCl_3$): 14.08 (A), 14.55 (A), 29.67 (B), 36.21 (C), 36.63 (C), 42 (D), 45 (E), 48 (E), 49 (F), 59.16 (G), 61.68 (G), 116.69 (H), 168.80 (I), 169.26 (I) (letters are designated to atoms responsible for peaks observed, see Figure 2.8). The mass spectrometer, in positive mode (+ES), detected the target ion at a mass of 548.27 Da ($[M+H]^+$); the theoretical mass was calculated to be 547.31 Da.

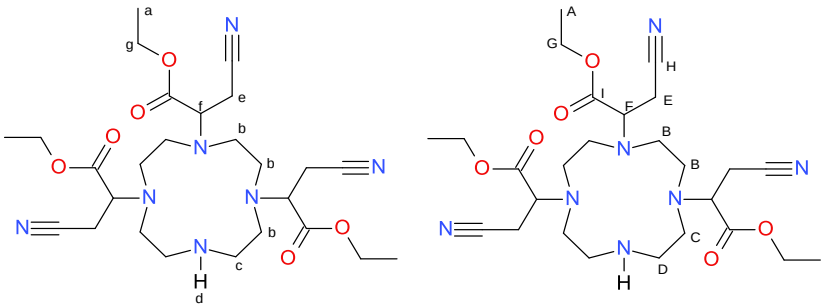

Figure 2.8 Characterisation of L1 by ^{1}H NMR (left), ^{13}C NMR (right)

Following a methodology based on protocols developed by Smith (2008), L1 (140 mg, 0.26 mmol) was combined with $EuCl_3$ (70 mg, 0.26 mmol, 1 eq.) (Scheme 2.5) in dry MeOH (30 ml), and heated and stirred, at 65˚C, under an argon atmosphere for 24 hours. Once cooled to room temperature, addition of cold diethyl ether (10 ml), did not yield a precipitate, so the solvent was removed under vacuum and the residue taken up into 18.2 MΩ water (5 ml) and lyophilised. Cold diethyl ether was added and the resulting precipitate was removed, dissolved in 18.2 MΩ water (5 ml), and freeze-dried. The yield obtained was 60 mg (0.09 mmol), which is 37.2% of the calculated expected yield. IR (ν_{max}/cm^{-1}) 3291 (broad N-H), 2359 (alkane C-H), 2342 (nitrile, weak), 1577

(C=O), 1399 (methyl C-H), 1318 (methyl C-H), 1248 (C-O), 1040 (C-N), 970 (C-H). The theoretical mass was calculated to be 700.23 Da, however, although mass peaks were detected at 83, 128, 159, 201, 221, 229 and 270 Da, they could not be confidently assigned to the products of fragmentation of the parent ion and, furthermore, the parent ion mass was not detected. Fluorimetric analysis, however, confirmed chelation of europium by excitation of a 3 mM aqueous solution at 280 nm, indicating sensitisation by ligand to metal charge transfer.

L1 (70 mg, 0.13 mmol) was combined with $TbCl_3$ (40 mg, 0.13 mmol, 1 eq.) (Scheme 2.5) in dry MeOH (30 ml) and treated in exactly the same manner, under the same reaction conditions, described for the production of EuL1, above. The yield obtained was 86 mg (0.12 mmol), which is 90.6% of the calculated expected yield. IR (ν_{max}/cm^{-1}) 3319 (broad N-H), 2980- (alkane C-H), 2361 (nitrile, weak), 1600 (C=O), 1438-1368 (methyl C-H), 1313 (methyl C-H), 1247-1170 (C-O), 1046 (C-N), 971 (C-H). The theoretical mass was calculated to be 706.24 Da, however, although mass peaks were detected at 128, 173 (possibly cyclen), 201, 229, 271, 299, 355, 369, 396 and 453 Da, they could not be assigned with confidence to the products of fragmentation of the parent ion and, furthermore, the parent ion mass was not detected. Fluorimetric analysis, however, confirmed chelation of terbium by excitation of a 3 mM aqueous solution at 280 nm, indicating sensitisation by ligand to metal charge transfer.

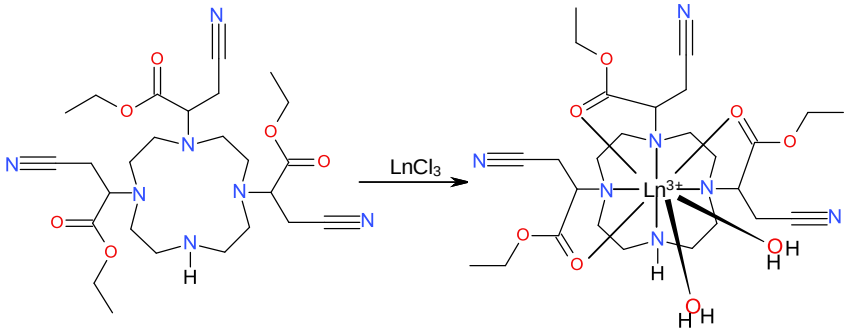

Scheme 2.5 Chelation of Ln^{3+} (Eu^{3+} or Tb^{3+}) by L1. Two water molecules may also coordinate to the lanthanide ion

2.7.4 Synthesis of L2 and $[LnL2]^{3+}$

Using protocols developed by Smith (2008), cyclen (390 mg, 2.27 mmol) was dissolved in dry MeCN (35 ml), to which anhydrous potassium carbonate (K_2CO_3) (1040 mg, 7.51 mmol, 3.3 eq.) was added, heated to 80°C under an argon atmosphere, and stirred. Added to this mixture, over the course of 1 hour, was a solution of diallyl maleate (2.39 ml, 2230 mg, 11.35 mmol, 5 eq.) in dry MeCN (35 ml) (Scheme 2.6). The reaction mixture was heated to reflux at 80°C for 50 hours under an argon atmosphere. The organic phase was separated using silica gel chromatography and eluted with a gradient of 1% to 5% EtOH in DCM eluent. The yield obtained was 580 mg (0.76 mmol), which was 32.6% of the calculated expected yield.

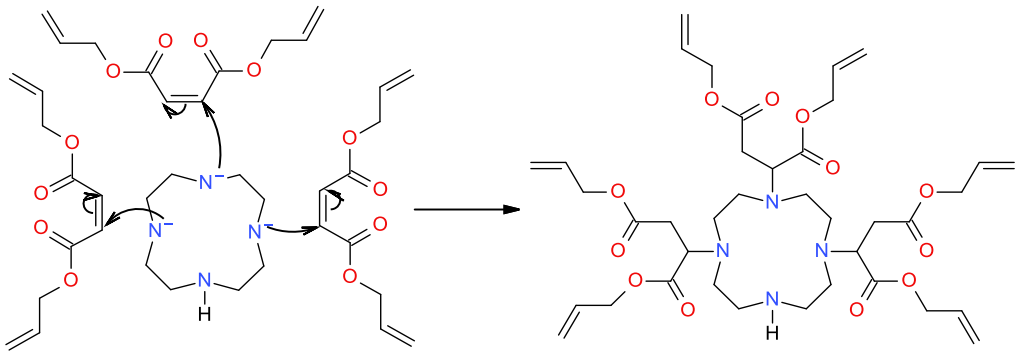

Scheme 2.6 Addition of diallyl maleate to cyclen

More L2 was synthesised, according to the method above, however, the quantities used were as follows: cyclen (430 mg, 2.51 mmol), K_2CO_3 (1170 mg, 8.47 mmol, 3.3 eq.), diallyl maleate (2.64 ml, 2460 mg, 12.50 mmol, 5 eq.), MeCN (35 ml). The yield obtained was 280 mg (0.36 mmol), which was 16.0% of the calculated expected yield. R_f = 0.80 (SiO_2, 10% EtOH in DCM). ^{1}H NMR (400 MHz, $CDCl_3$); 2.57 (CH_2) (a), 2.73 (CH_2) (b), 2.89 (CH_2) (b), 3.09 (CH_2) (c), 3.84 (CH) (d), 4.03 (CH_2) (e), 4.59 (CH_2) (f), 5.19 (CH_2) (h) 5.22 (CH_2) (h), 5.30 (CH) (i) 5.34 (CH) (i), 5.86 (CH) (j). ^{13}C NMR (75 MHz, $CDCl_3$): 34.84 (CH_2) (A), 47.36 (CH) (B), 47.89 (CH) (B), 50.09 (CH_2) (C), 51.80 (CH_2) (D), 57.12 (CH_2) (E), 61.65 (CH_2) (E), 65.79 (CH_2) (F), 66.01 (CH_2) (F), 66.16 (CH_2) (F), 118.80 (CH_2) (G), 119.45 (CH_2) (G), 119.74 (CH_2) (G), 131.53 (CH) (H), 131.77 (CH) (H), 170.72 (C=O) (I), 170.80 (C=O) (I), 170.86 (C=O) (I) (letters are designated to atoms responsible for peaks observed, see Figure 2.9). The mass spectrometer, in positive mode (+ES), detected the target ion at a mass of 761.35 Da ($[M+H]^+$); the theoretical mass was calculated to be 760.19 Da.

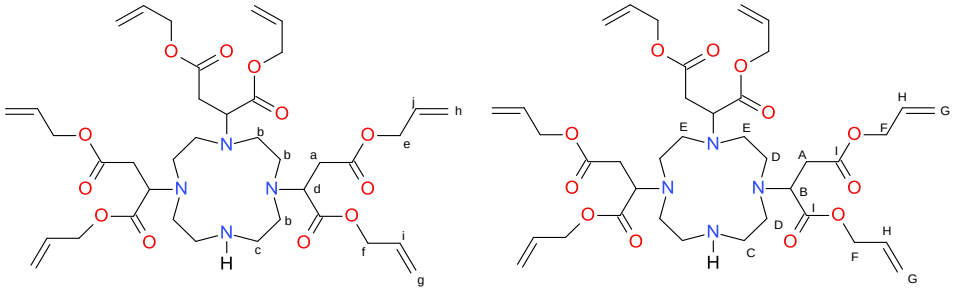

Figure 2.9 Characterisation of L2, ^{1}H NMR (left), ^{13}C NMR (right)

Following a methodology based on protocols developed by Smith (2008), L2 (98 mg, 0.13 mmol) was combined with $EuCl_3$ (34 mg, 0.13 mmole, 1 eq.) in dry MeOH (30 ml) (Scheme 2.7), heated to a rigorous reflux, while stirring, at 65˚C for 24 hours under an argon atmosphere. The reaction mixture was cooled and filtered under vacuum through a celite plug, and the solvent removed. The residue was re-dissolved in dry MeOH (5 ml) and cold diethyl ether (5 ml) added. The resulting precipitate was decanted, the solvent removed and the residue taken up into 18.2 MΩ water (10 ml), and freeze-dried.

The yield obtained was 77 mg (0.08 mmol), which was 65% of the calculated expected yield. The theoretical mass for EuL2 was calculated to be 913.31 Da, however the parent ion was not detected. A peak was detected at 455 Da suggestive of a +2 charged species of the complex parent ion with surrounding peaks indicative of fragmentation of this species, however, when compared to the MS of $[TbL2]^{3+}$, this was discounted (*vide infra*). A cluster of peaks, centred on 683 Da, may be evidence of fragmentation of the free ligand; peaks at 617 and 657 Da, thought to be relating to the free ligand, may be analogues of peaks observed at 257 and 270 Da which may be due to tripositively charged fragments of the europium complex of L2. Fluorimetric analysis, however, confirmed chelation of europium by excitation of a 3 mM aqueous solution at 280 nm, indicating sensitisation by ligand to metal charge transfer.

Synthesis of $[TbL2]^{3+}$ was achieved following the same method as described above using L2 (99 mg, 0.13 mmol) and $TbCl_3$ (35 mg, 0.13 mmol, 1 eq.) (Scheme 2.7). The yield obtained was 20 mg (0.02 mmol), which was 17% of the calculated expected yield. IR (ν_{max}/cm^{-1}) 3340 (broad N-H), 2953 (N-H), 2250 (alkane C-H), 1727-1650 (C=O), 1437 (methylene C-H), 1367 (methyl C-H), 1166

(C-O), 1083 (C-O), 986 (C=C), 818-764 (C-H). The theoretical mass was calculated to be 919.31 Da, however the parent ion was not detected, although a peak at 761 Da was, representing the mass of the unfragmented free ligand. Peaks of comparable m/z relating to the free ligand fragments in the $[EuL2]^{3+}$ sample were observed for the $[TbL2]^{3+}$ sample, as was the peak at 455 Da, indicating this peak could not be related to the dipositively charged species as suggested above (if an equivalent peak was observed in the $[TbL2]^{3+}$ MS, then this would be indicated by a relative increase in m/z due to the difference in mass of the chelated lanthanide ions). Peaks at 260 and 272 Da may be the terbium analogues of peaks observed at 257 and 270 Da for the MS of the EuL2, and may also be due to tripositively charged fragments of the terbium complex of L2. Fluorimetric analysis, however, confirmed chelation of terbium by excitation of a 3 mM aqueous solution at 280 nm, indicating sensitisation by antenna effect afforded by ligand to metal charge transfer.

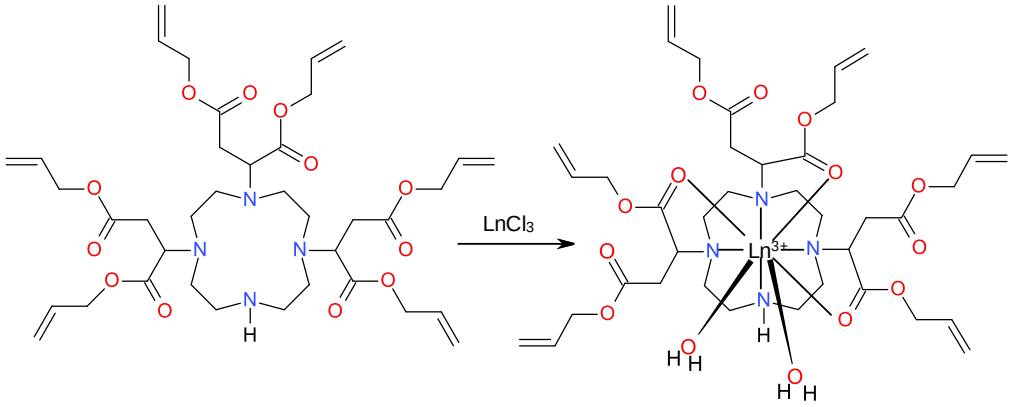

Scheme 2.7 Chelation of Ln^{3+} (Eu^{3+} or Tb^{3+}) by L1. Two water molecules may also coordinate to the lanthanide ion

2.7.5 Synthesis of $[LnL3]^{3+}$

Following a methodology based on protocols developed by Smith (2008), to synthesise $[EuL3]^{3+}$, L3 (275 mg, 0.45 mmol) was dissolved in dry MeCN (50 ml), added to which was anhydrous $EuCl_3$ (117 mg, 0.45 mmol, 1 eq.) (Scheme 2.8); the reaction mixture was refluxed rigorously at 65˚C under an argon atmosphere for 24 hours. The reaction mixture was cooled and filtered through celite and the solvent removed, the residue was dissolved in 18.2 MΩ water (10 ml) and lyophilised for 24 hours. The yield obtained was 371 mg (0.41 mmol), which was 95% of the calculated expected yield.

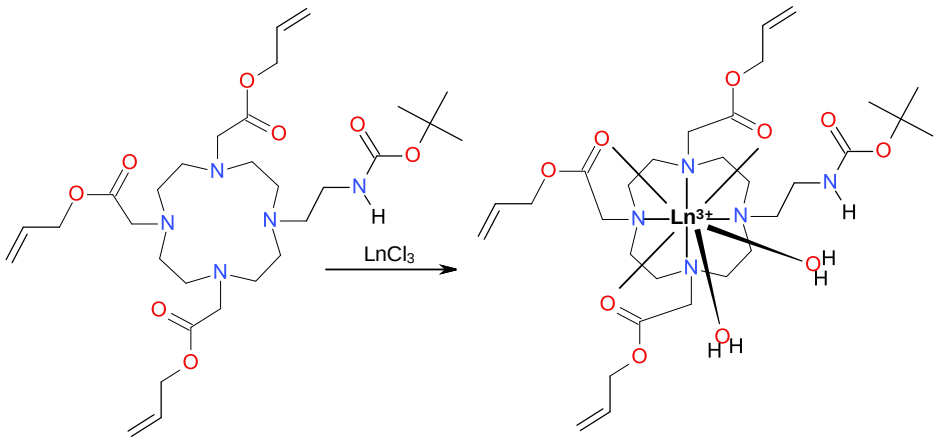

Scheme 2.8 Chelation of Ln^{3+} (Eu^{3+} or Tb^{3+}) by L3. Two water molecules may also be coordinated to the lanthanide ion

IR (ν_{max}/cm^{-1}) 3211 (broad N-H), 2359-2343 (alkane C-H), 1733 (C=C, weak), 1577 (C=O), 1441-1403 (methyl C-H), 1319 (methyl C-H), 1247-1161 (C-O), 1084 (C-N), 979 (C-C). The theoretical mass was calculated to be 762.29 Da. Although mass peaks were detected at 208, 221, 228, 255, and 313 Da, they could not be confidently assigned to specific products of fragmentation of the parent ion. The peak at 160 Da may be a tripositively charged complex fragmentation species of $[EuL3]^{3+}$, e.g. Figure 2.4 (a), however, the parent ion mass was not detected. Fluorimetric analysis, however, confirmed chelation of europium by excitation of a 3 mM aqueous solution at 280 nm, indicating sensitisation by antenna effect afforded by ligand to metal charge transfer.

Synthesis of $[TbL3]^{3+}$ was achieved following the same method as described above using L3 (309 mg, 0.51 mmol) and $EuCl_3$ (135 mg, 0.51 mmol, 1 eq.) (Scheme 2.8). The yield obtained was 391 mg (0.51 mmol), which was 88% of the calculated expected yield. IR (ν_{max}/cm^{-1}) 3270 (broad N-H), 2997, 2361-2343 (alkane C-H), 1734 (C=C, weak), 1581 (C=O), 1366-1319 (methyl C-H), 1274-1164 (C-O), 1085 (C-N), 982-946 (C-C). The theoretical mass was calculated to be 768.30 Da. Although mass peaks were detected at 204, 224, 292, 584 Da, they also could not be confidently assigned to specific products of fragmentation of the parent ion. However, the peaks at 610 and 305 Da may be the free ligand as mono and dipositively charged species, possibly by protonation, respectively. The species detected at 162 Da may be a species similar to that detected in the mass spectrum of $[EuL3]^{3+}$ at 160 Da, where the change in m/z correlates with the replacement of the europium ion with the terbium ion (Figure 2.10 (a)). There may also be an analogous singly

positive species detected at 486 Da (Figure 2.10 (b)), however a comparable peak was not observed in the mass spectrum of $[EuL3]^{3+}$. The parent ion mass was not detected. Fluorimetric analysis, however, confirmed chelation of terbium by excitation of a 3 mM aqueous solution at 280 nm, indicating sensitisation by antenna effect afforded by ligand to metal charge transfer.

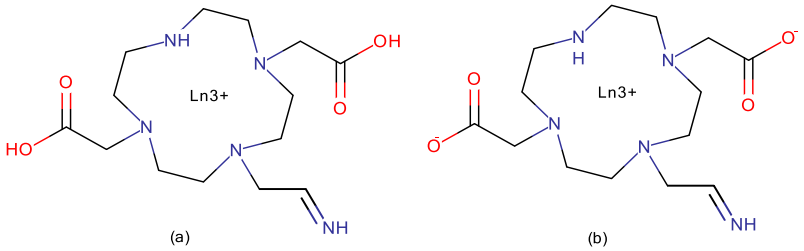

Figure 2.10 Possible fragmentation of L3 parent ion to account for peaks at (a) 160 and 162 Da and (b) 486 Da ($[TbL3]^{3+}$ only)

2.8 Summary of methodological approach

This methodology chapter has outlined the general preparation and synthesis protocols used in the subsequent chapters, along with the analytical techniques used to monitor and confirm the production of the lanthanide sensors. This methodology chapter has also outlined the selection and preparation of commercial standards used to test these sensors (Chapters 3 and 4), and the selection, preparation and treatment of the geological samples used in Chapter 5. Any variation from the regimes described here is described, where appropriate. The following chapters describe the methodological approaches used in the development of fluorimetric analytical protocols using the lanthanide complexes. The results of the application of these commercial standards and geological extracts to the lanthanide complexes, in order to determine their applicability as sensors and to ascertain their validity as probes for organic molecules, is reported.

3 [LnDOTA]$^-$ and [LnDO3A] and their application to analogue analytes

3.1 Introduction

As described in Chapter 1, ligands can be used to chelate metal ions, rendering them inert to chemical reaction but susceptible to physical interaction with external species (for a review of metal-ligand complex properties, and uses, see Hass and Franz, 2009). 1,4,7,10-tetraazacyclododecane-1,4,7,10-tetraethanoic acid (DOTA) and 1,4,7,10-tetraazacyclododecane-1,4,7-triethanoic acid (DO3A) (Figure 3.1 (a) and (b) respectively) are examples of such ligands.

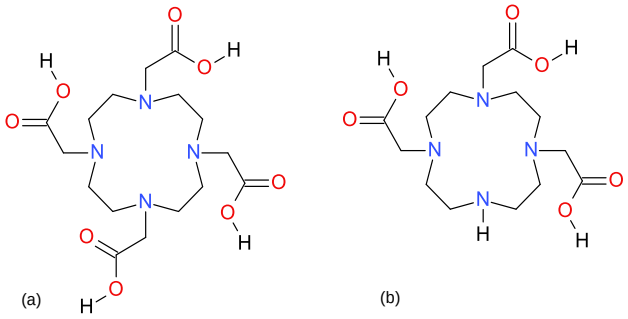

Figure 3.1 (a) DOTA and (b) DO3A

DOTA and DO3A are organic molecules featuring a heterocyclic central framework of a twelve membered, *tetra*-aza (four nitrogen atom) ring, with each nitrogen bonded to adjacent methylene (-CH_2-) groups. The nitrogen atoms of the central ring of the molecule are bonded to 'pendant arms', which are ethanoic acid moieties. In DOTA, the pendant arms are bound at all four amine nitrogen atoms, making them tertiary amines. In DO3A, only three nitrogen atoms are bound to the pendant arms, leaving one nitrogen atom bound to a proton, making this nitrogen a secondary amine. DOTA and DO3A are 'free acids' because all pendant arm moieties are carboxylic acid functional groups.

DOTA and DO3A, and derivatives thereof, have been used to chelate lanthanide metal atoms such as europium (Eu) and terbium (Tb) to produce complexes that are known to have fluorescent properties (Horrocks and Albin, 1984, Delgado et al., 2007, Armelao et al., 2010, Stasiuk and Long, 2013, Nasso et al., 2014). These molecules can act as antennae, which sensitise fluorescence emissions (see Chapter 1, Section 1.7.5). The complexes formed by the chelation of lanthanide ions are, therefore, themselves fluorescent, and have been used extensively in fluorescent

analytical and biological assays and as MRI contrast agents (Faulkner et al., 2005, Raghunand et al., 2010, Schäferling, 2012). As a result of their extensive use, data regarding their structure, stability, coordination, electronic structure and fluorescence have been elucidated (Armelao et al., 2010, Stasiuk and Long, 2013), and therefore they were considered as novel sensors for meteoritic, or other geochemical, organic material.

DOTA is an octadentate ligand, meaning it has eight coordination points on its molecular structure to which an ion may be bound; in this thesis, the ion of interest is the tripositive lanthanide ions (Ln^{3+}) of europium and terbium. These coordination points are lone pairs of electrons associated with the four nitrogen atoms that make up the cyclen ring framework of the molecule, and four negatively charged carboxylate groups comprising the four pendant arms. Since the lanthanide ion is tripositive and DOTA possesses four singly negatively charged ethanoate arms, the complex possesses an overall single negative charge and is written thus: $[LnDOTA]^-$. When fully chelated, the lanthanide ion will be positioned such that it sits centrally above the cyclen ring, held in place by the nitrogen lone pairs, while the pendant ethanoate arms will swing into position and bind the lanthanide ion, locking it in place (Figure 3.2) (Delgado et al., 2007). When in aqueous solution, a water molecule occupies a ninth coordination point directly above the metal centre, as depicted in Figure 3.2, and the pendant arms are free to move unhindered such that, when the lanthanide ion is added, they will be electrostatically attracted into position to form the complex structure. The resulting ion-ligand complex exhibits very strong binding because of the high positive charge of the lanthanide ion and the eight highly electron rich coordination points.

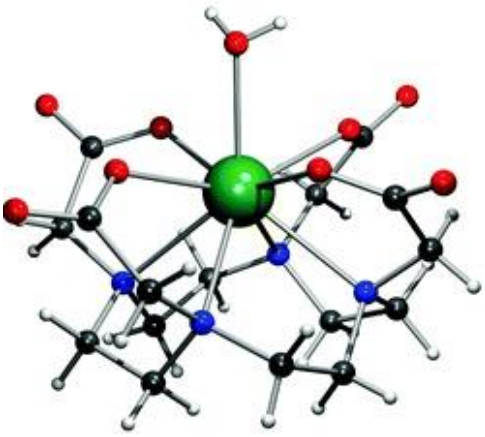

Figure 3.2 $[LnDOTA]^-$. Black balls: carbon atoms; blue: nitrogen. Red are oxygen atoms of the ethanoate pendant arms; green represents either Eu^{3+} or Tb^{3+} (Delgado et al., 2007)

In order to prove the viability of such lanthanide complexes as fluorescent sensors for organic molecules, it was necessary to ascertain whether, in the presence of relevant analytes, their fluorescent emission spectra would be changed. A change in intensity or shape of the emission spectra would suggest a response and, therefore, suggest the complex could be used as a sensor. To that end, the respective $[LnDOTA]^-$ and [LnDO3A] complexes would first need to be synthesised in the laboratory. This chapter describes this synthesis and the results of the complexes' application to relevant analytes.

3.2 Complexes based on DOTA

As outlined in Chapter 2 (Section 2.7.1), $[LnDOTA]^{3+}$ complexes were synthesised using commercially available DOTA combined with either europium trichloride hexahydrate ($EuCl_3.6H_2O$) or terbium trichloride hexahydrate ($TbCl_3.6H_2O$). Chelation was confirmed by mass spectrometry and fluorimetry. The fluorescence emissions of these complexes were then characterised in the presence and absence of analogue analytes (see Chapter 2, Section 2.3.2 for details on the analytes chosen). The results of these tests are presented here.

3.2.1 Direct excitation of $[LnDOTA]^-$

When europium or terbium are irradiated with light at a wavelength of 397 nm (Bruce, 2001) or 378 nm (Chang, 2007), respectively, the energy provided is sufficient to promote the inner-shell electrons in the *'f'* orbitals directly to higher energy states such that, upon returning to the ground state, fluorescent emissions occur (Horrocks and Albin, 1984, Bruce, 2001, Aneesh and Jayaraj, 2010). However, this direct excitation is inefficient (they have a low molar extinction coefficient, ε) as it is difficult to excite the *'f'* orbital electrons as they are shielded by the *'s'* and *'p'* orbitals of the next electron shell, resulting in relatively weak emissions (Valeur and Berberan-Santos, 2013).

Figure 3.3 (black line, and also Table 3.1) shows the fluorescence spectrum generated by aqueous Eu^{3+} when directly excited at 397 nm. Figure 3.4 is the energy level diagram showing the same electronic transitions described in graphical form. The $[EuDOTA]^-$ emissions, when directly excited at the same wavelength (red line on Figure 3.3 and also Table 3.1), were comparable and

indicative of an eight coordinated Eu^{3+} ion (Bruce, 2001). However, in the $[EuDOTA]^-$ spectrum, the transition at $\Delta J=0$ is sensitised, resulting in an emission at 578 nm, and the $\Delta J=4$ transition is split into two maxima – features not seen for the aqueous europium ion.

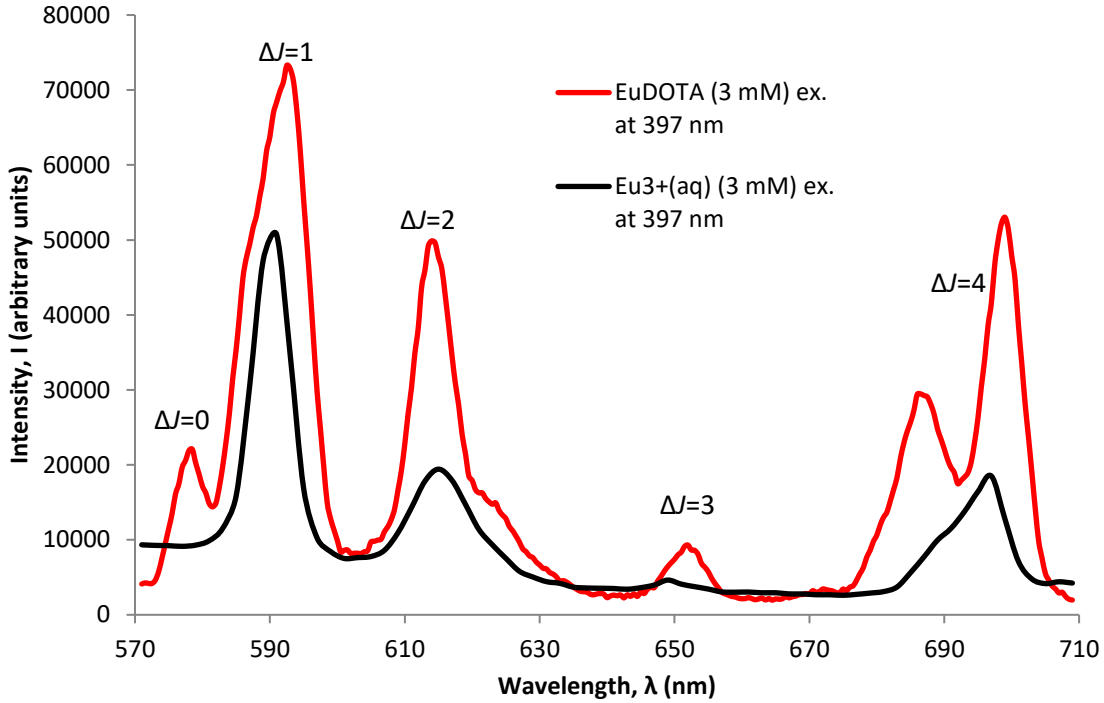

Figure 3.3 (Figure 1.5 repeated) Fluorescence spectra for Eu^{3+} (aq) (black) and $[EuDOTA]^-$ (red) (λ_{Ex}=397 nm, acquisition time=0.5 sec, acquisition increment=0.5 nm, excitation and emission slit width=3 nm, pH=5)

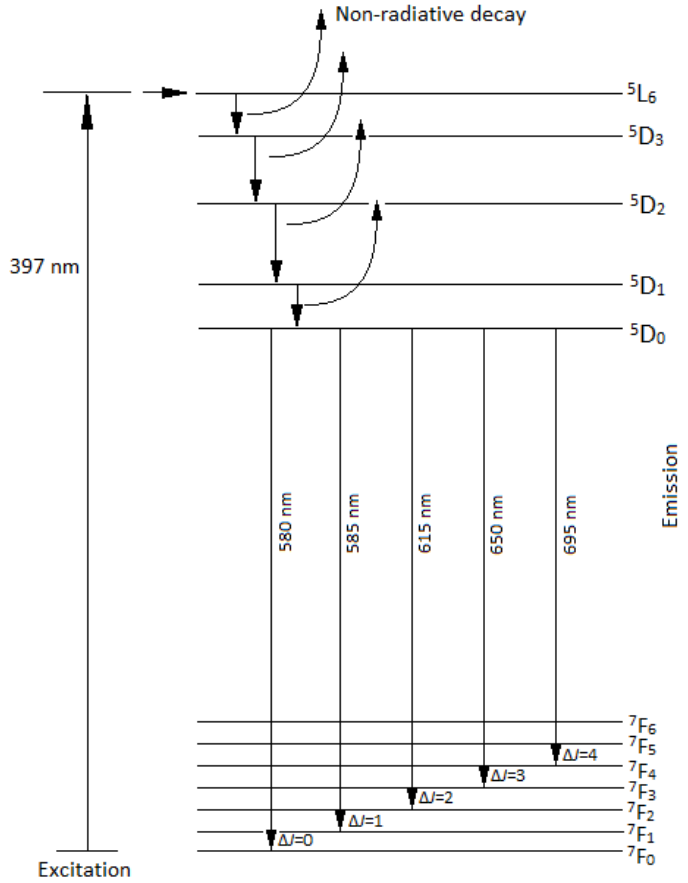

Figure 3.4 An energy level diagram showing the electronic transitions when excited europium '*f*' electrons decay to their ground state *via* fluorescence emissions

ΔJ=	0	1	2	3	4	4
Transition responsible	$^5D_0 \rightarrow {}^7F_0$	$^5D_0 \rightarrow {}^7F_1$	$^5D_0 \rightarrow {}^7F_2$	$^5D_0 \rightarrow {}^7F_3$	$^5D_0 \rightarrow {}^7F_4$	$^5D_0 \rightarrow {}^7F_4$
$Eu^{3+}(aq)$	_	~591 nm	~615 nm	~648 nm	_	~696 nm
$[EuDOTA]^-$	~578 nm	~592 nm	~613 nm	~651 nm	~686 nm	~698 nm

Table 3.1 Emissions, and transitions responsible, of aqueous and DOTA-chelated europium

Water molecules quench europium fluorescence because of non-radiative decay by oscillation of the water O-H bonds (Bruce, 2001). When chelated by DOTA, an increase in europium fluorescence intensity is observed because water molecules are displaced; the coordination of water molecules quench the ΔJ=0 in particular, so displacement of water molecules by chelation of DOTA gives rise to the sensitisation of this transition. The ΔJ=4 transition is hypersensitive (Peacock, 1975) meaning it is particularly affected by variations in coordination environment of the europium ion (Bruce *et al*., 2000); the water molecules coordinated about the europium ion in the aquo complex are symmetrically distributed, however the distribution of the coordination points of DOTA are not. This displacement of water and uneven perturbation of energy levels caused by the coordination of DOTA therefore give rise to the splitting of the ΔJ=4 emission.

A published spectrum for $[EuDOTA]^-$ (Figure 3.5, Bruce 2001) shows greater splitting of peaks at ΔJ=1, ΔJ=2 and ΔJ=4; however, 'shoulders' in the peaks on the $[EuDOTA]^-$ spectrum on Figure 3.3 suggest their presence. Further, the peaks in Figure 3.3 are not as well resolved as those in Figure 3.5 (from Bruce, 2011), but this can be explained by the use of different spectrometer conditions in their study that affect the range and/or intensity of emission wavelengths detected.

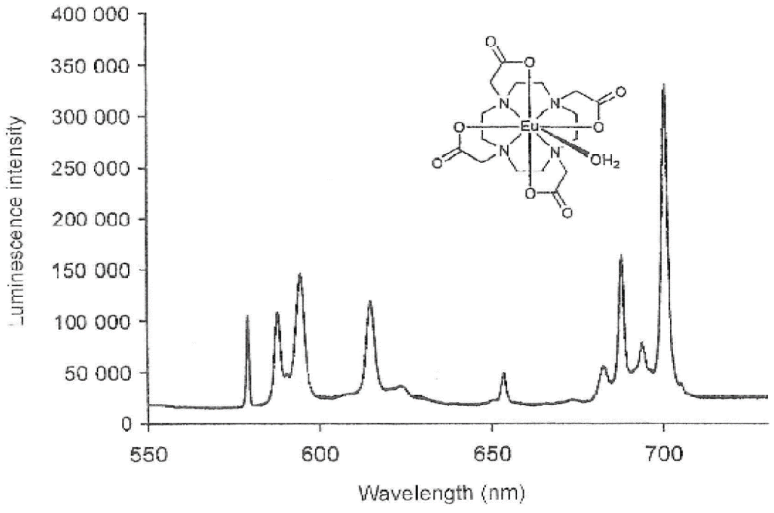

Figure 3.5 $[EuDOTA]^-$ fluorescence spectrum (Bruce, 2001)

Fluorimetric analysis of the $[TbDOTA]^-$ residue, when directly excited at 378 nm (Chang et al., 2007), produced fluorescent emissions at wavelengths indicative of Tb^{3+} ions (Figure 3.6 and Table 3.2) with no differences observed between the emission wavelengths of free or DOTA-chelated terbium. Figure 3.7 is the energy level diagram showing the same electronic transitions described in graphical form. However, when chelated, an increase in fluorescence intensity is also observed since the DOTA ligand displaces water molecules. Since it is water molecules that quench terbium fluorescence by oscillation of water O-H bonds, in the same way as observed when the europium fluorescence intensity is quenched (see above), the chelation of the lanthanide by DOTA reduces such quenching resulting in the increase in intensity observed. The emission wavelengths obtained for $[TbDOTA]^-$ were comparable with terbium emission wavelengths reported in the literature (Richardson, 1982, Bruce, 2001, Podhorodecki et al., 2010).

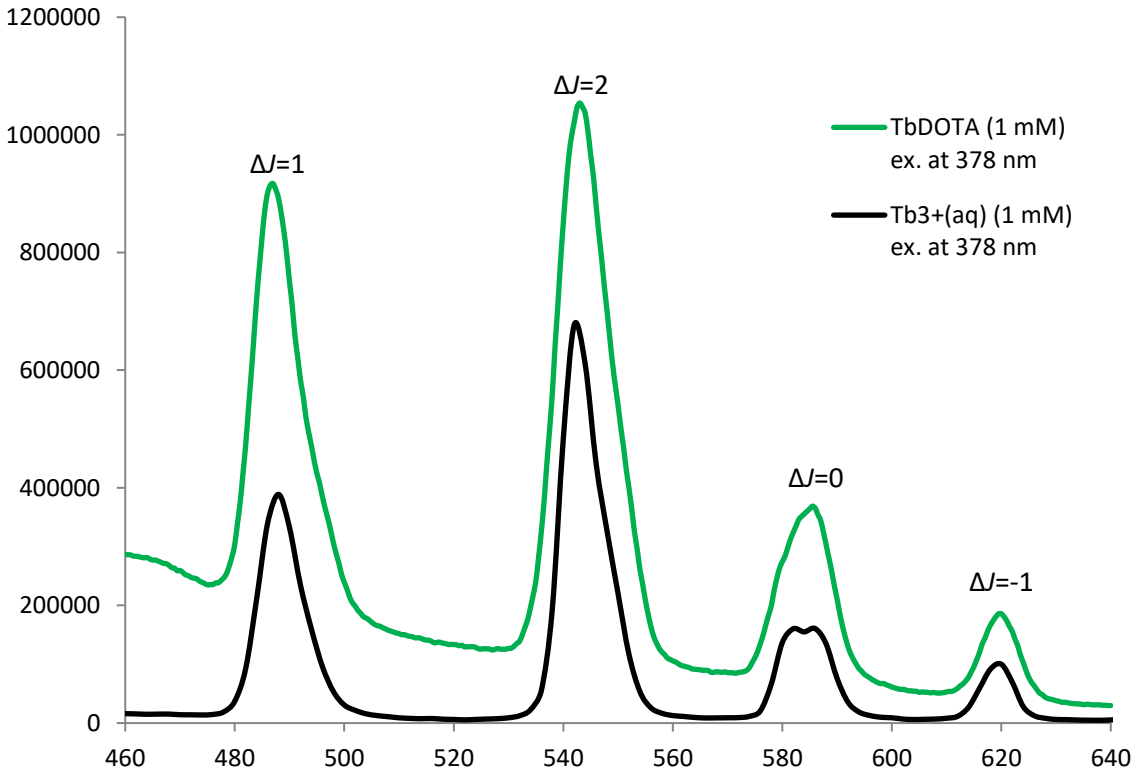

Figure 3.6 Fluorescence spectra for Tb^{3+}(aq) (black) and $[TbDOTA]^-$ (green) (λ_{Ex}=378 nm, acquisition time=0.5 sec, acquisition increment=0.5 nm, excitation and emission slit width=3 nm, pH=5)

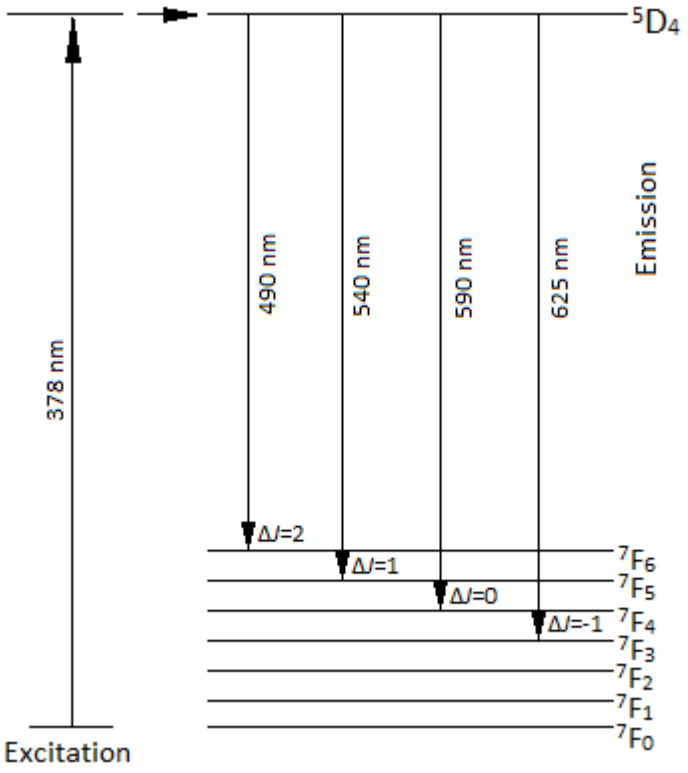

Figure 3.7 An energy level diagram showing the electronic transitions when excited terbium '*f*' electrons decay to their ground state *via* fluorescence emissions

ΔJ=	2	1	0	-1
Transition responsible	$^5D_4 \rightarrow {}^7F_6$	$^5D_4 \rightarrow {}^7F_5$	$^5D_4 \rightarrow {}^7F_4$	$^5D_4 \rightarrow {}^7F_3$
Tb^{3+} emissions	~493 nm	~543 nm	~584 nm	~620 nm

Table 3.2 The four distinct transitions for Tb^{3+}

3.2.2 Direct excitation of [EuDOTA]$^-$ at 397 nm and response to analytes

In order to test the responses of [EuDOTA]$^-$ to analogue analytes (see Chapter 2, Table 2.2), 1 mM [EuDOTA]$^-$ stock solutions were prepared and a sensor-only spectrum was obtained (Figure 3.8, black line). 1 mM analyte stock solutions were also prepared (see Section 2.4.3). Equal volumes (0.75 ml) of analyte and [EuDOTA]$^-$ were combined, resulting in a solution containing an equimolar mixture of analyte and [EuDOTA]$^-$ at 0.5 mM each. It was, therefore, possible to compare the sensor-only spectrum for a 1 mM solution of [EuDOTA]$^-$ with that of the [EuDOTA]$^-$ /analyte mixture (Figure 3.8).

The perceived decrease in emission intensity when [EuDOTA]$^-$ was in the presence of analytes was approximately 50% (Figure 3.8), which was not unexpected since the concentration of [EuDOTA]$^-$ was half that observed for the sensor-only intensity. These results also suggested that there was

little deviation from sensor-only europium emission intensity when in the presence of analytes and that, in all likelihood, there was no useful analyte/sensor interaction detected when the [EuDOTA]$^-$/analyte mixture was directly excited at 397 nm (Figure 3.8).

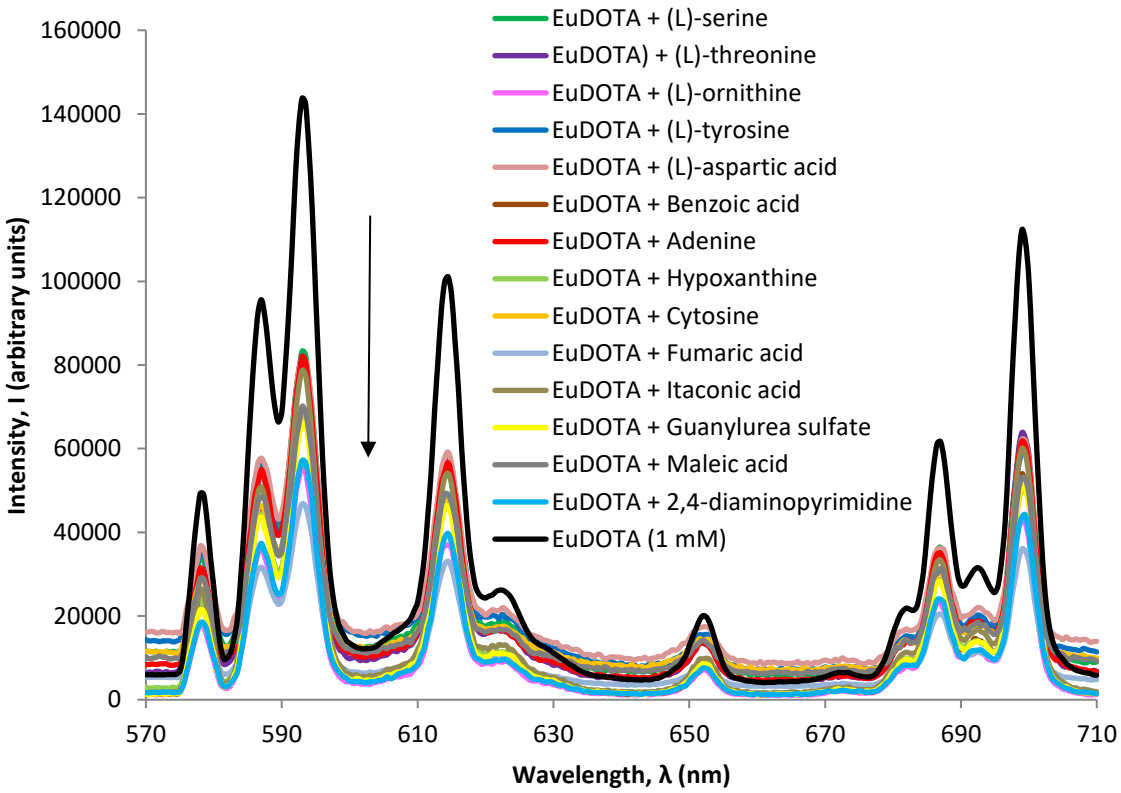

Figure 3.8 [EuDOTA]$^-$ fluorescence, at 1mM (black line), compared with an [EuDOTA]$^-$/analyte mixture, where both sensor and analyte are present at a concentration of 0.5 mM, respectively (coloured lines) (λ_{Ex}=397 nm, acquisition time=0.5 sec, acquisition increment=0.5 nm, excitation and emission slit width=3 nm, pH=5)

It is possible that analyte/sensor interaction may not be detected when directly excited at 397 nm because only the europium is affected by this wavelength; this excitation wavelength would not be expected to interact with organic molecules and as such could not facilitate antenna effect even if organic analytes were bound to, or coordinated with, the complex. Further, the range of europium emission wavelengths of interest in this study (570 nm to 710 nm) are not sufficiently energetic to excite organic molecules either, thus, europium emission intensities will also be unaffected by the presence of organic analytes, which cannot absorb them.

3.2.3 Excitation of [EuDOTA]$^-$ at 265 nm

Since direct excitation of the [EuDOTA]$^-$/analyte mixtures at 397 nm did not elucidate any responses in the presence of analytes, an alternative method of lanthanide excitation was required. Excitation at 265 nm was chosen because previous work had shown this wavelength

successfully sensitises europium emissions when chelated to DOTA (Bruce et al., 2000). Also, since analyte selection was based upon the requirement that they all had delocalised electrons (conjugated pi bonds etc., see Section 2.3.1), excitation at a wavelength that may directly excite the organic analytes may enhance sensitisation if interactions do take place.

Despite 265 nm being considerably below the necessary energy to promote electrons to energy levels required for Eu^{3+} fluorescence directly, a $[EuDOTA]^-$ spectrum indicated Eu^{3+} fluorescence, furthermore, excitation at 265 nm greatly increased fluorescent yield, i.e. intensity (Figure 3.9).

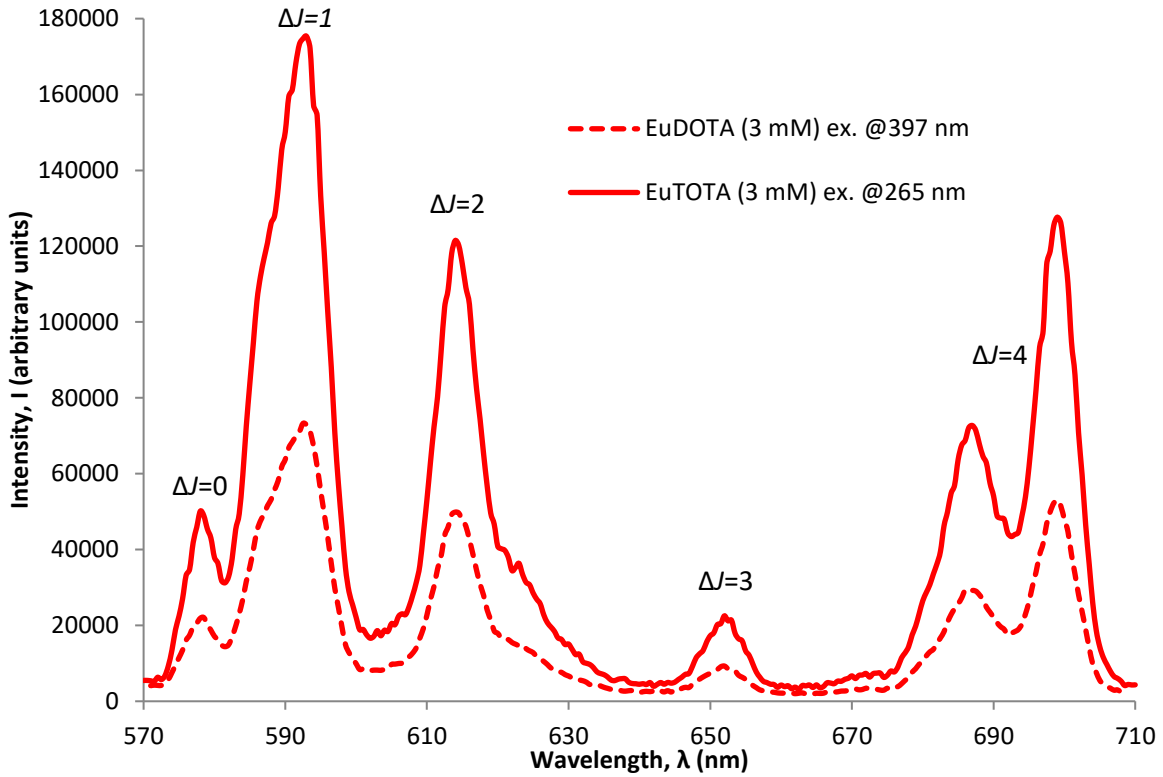

Figure 3.9 $[EuDOTA]^-$ fluorescence, at a concentration of 3mM, when excited at 397 nm (dashed red line), compared with $[EuDOTA]^-$ fluorescence, at a concentration of 3mM, when excited at 265 nm (solid red line) (acquisition time=0.5 sec, acquisition increment=0.5 nm, excitation and emission slit width=3 nm, pH=5)

It is probable that the carboxylate moieties of the ligand pendant arms had absorbed the excitation energy and transferred the energy, *via* an intersystem energy transfer, directly to the europium electrons (Horrocks and Albin, 1984). This energy transfer enabled promotion of these electrons to a higher energy level, thus permitting fluorescent emission as they returned to their ground state. This describes precisely the antenna effect (Section 1.7.5); in this case, the carboxylate C=O moieties may have acted as the antennas in the absence of a specific

chromophore via a ligand-metal charge transfer mechanism (Horrocks and Albin, 1984, Parker and Williams, 1996, Bruce, 2001).

3.2.4 Excitation of [TbDOTA]$^-$ at 265 nm

In light of the success of excitation of [EuDOTA]$^-$ at 265 nm, a 1 mM solution the [TbDOTA]$^-$ complex was also excited at that wavelength. Excitation of terbium was observed, probably *via* the same ligand-metal charge transfer mechanism as attributed to the sensitisation of europium, described above (3.2.3) (Horrocks and Albin, 1984, Parker and Williams, 1996, Bruce, 2001). Again, excitation at 265 nm increased fluorescent yield (Figure 3.10).

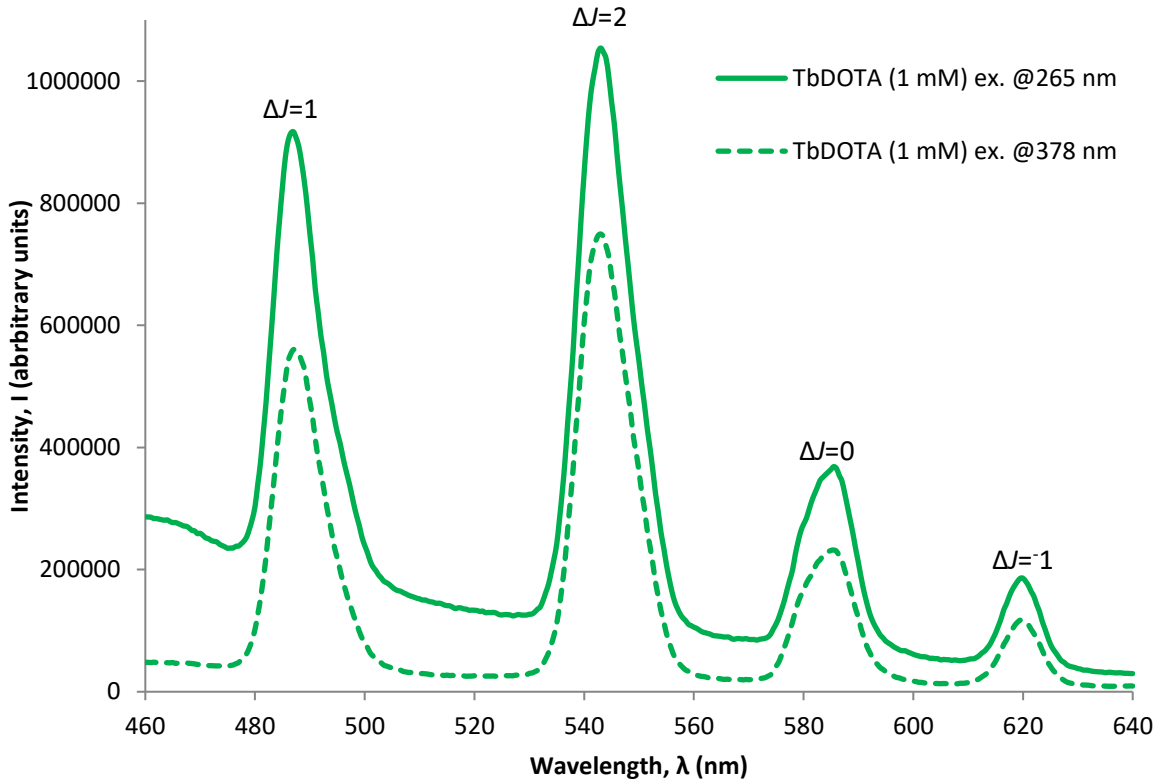

Figure 3.10 [TbDOTA]$^-$ fluorescence, at a concentration of 1 mM, when excited at 378 nm (dashed green line), compared with [TbDOTA]$^-$ fluorescence, at a concentration of 1 mM, when excited at 265 nm (solid green line) (acquisition time=0.5 sec, acquisition increment=0.5 nm, excitation and emission slit width=3 nm, pH=5)

3.2.5 [LnDOTA]$^-$ and non-nucleobase analytes

A spectrum of 1.5 ml of 0.5 mM [LnDOTA]$^-$ sensor solution was obtained with which to compare sensor/analyte mixture fluorescence emissions. 0.75 ml of 1 mM lanthanide DOTA complex solutions were applied to 0.75 ml of 1 mM individual non-nucleobase and nucleobase analytes solutions to give 1.5 ml of solution, where sensor and analyte were present at equimolar concentrations of 0.5 mM, and fluorescence emission spectra obtained (Figures 3.11 and 3.13,

black lines). Analyte solutions were mixed with the sensor solutions in clean quartz fluorimetric cuvettes as described previously (see Section 2.6.7).

A modest increase in fluorescent intensity was seen when $[EuDOTA]^-$ was in the presence of all non-nucleobase analytes, with the exception of fumaric acid, which showed a small decrease in intensity, and (*L*)-serine, which showed no change (Figure 3.11). The presence of benzoic acid resulted in a large increase in europium emission intensity, and resulted in sensitisation of the ΔJ=2 transition at ~615 nm; this emission became more intense than the ΔJ=1 emission at ~590 nm (Figure 3.11). (*L*)-tyrosine is anomalous in that the 'tail end' of its own broad intrinsic fluorescence (Figure 3.12) was detected, resulting in some overlap or 'swamping' of europium emissions.

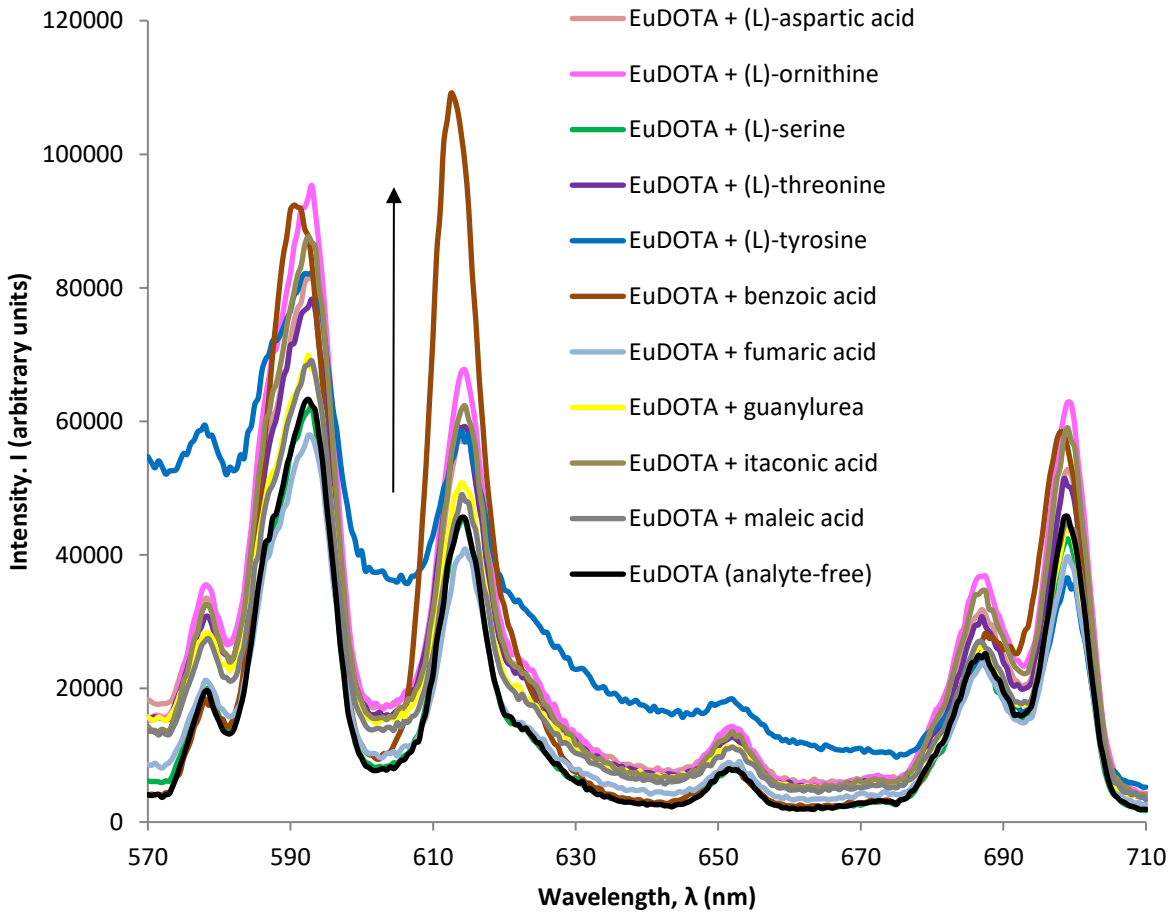

Figure 3.11 Fluorescence spectrum for 0.5 mM $[EuDOTA]^-$ (black) compared with emissions when 0.5 mM $[EuDOTA]^-$ was in the presence of 0.5 mM non-nucleobase analytes (λ_{Ex}=265 nm, acquisition time=0.5 sec, acquisition increment=0.5 nm, excitation and emission slit width=3 nm, pH=5)

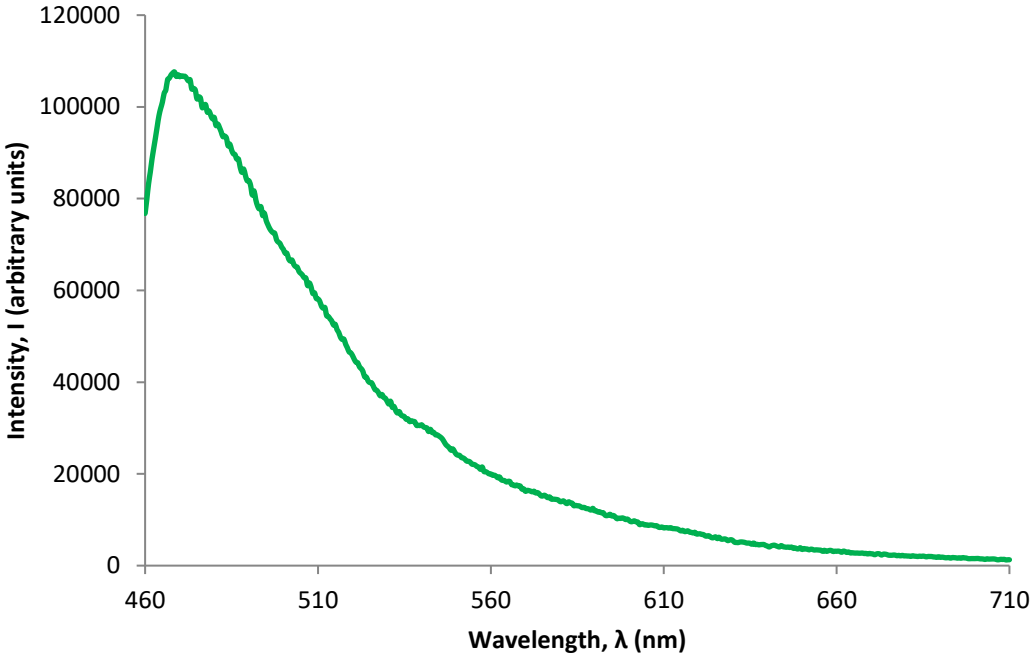

Figure 3.12 Fluorescence emission spectrum of (*L*)-tyrosine (saturated solution, ~2.50x10^{-3} M), indicating its emission maxima is at ~466 nm (λ_{Ex}=265 nm, acquisition time=0.5 sec, acquisition increment=0.5 nm, excitation and emission slit width=3 nm, pH=5)

In contrast, all fluorescence spectra of [TbDOTA]$^-$, when combined with non-nucleobase analytes, showed either no change in fluorescent intensity or a small decrease (Figure 3.13). Addition of benzoic acid, as previously observed when mixed with [EuDOTA]$^-$, increased the intensity, suggesting same mechanism may operate to cause the response in both cases (Figure 3.13).

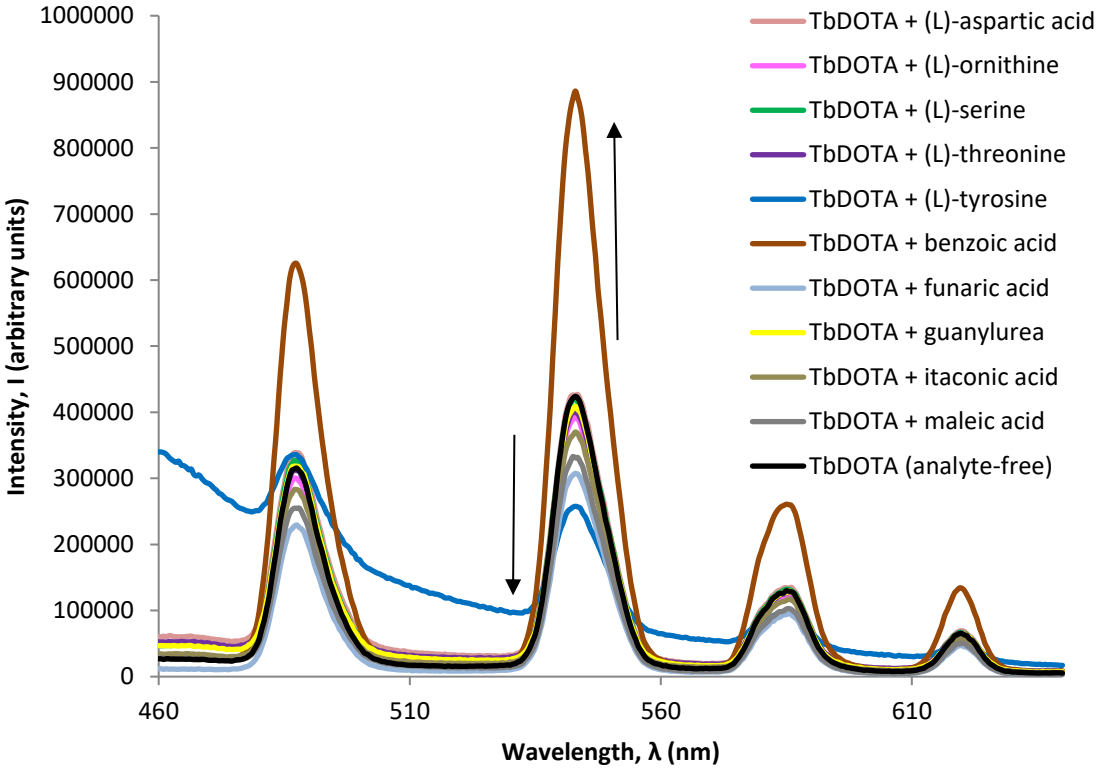

Figure 3.13 Fluorescence spectrum for 0.5 mM [TbDOTA]$^-$ (in black) and spectra obtained when [TbDOTA]$^-$ was mixed with non-nucleobase analytes, at equimolar concentrations (λ_{Ex}=265 nm, acquisition time=0.5 sec, acquisition increment=0.5 nm, excitation and emission slit width=3 nm, pH=5)

The sensitisation of europium and terbium upon addition of benzoic acid, and derivatives thereof, has been reported previously (Pikramenou et al., 1994, Gunnlaugsson et al., 2003) and explained by the coordination of the carboxylate moiety of the benzoic acid with the lanthanide complex metal-centre (in the same manner as the carboxylate groups of the ligand). The benzene group then acts as an antenna absorbing excitation photons which are transferred to the lanthanide *via* the coordinating carboxylate (Section 3.5).

Since these experiments established that non-nucleobase analytes had little detectable effect on lanthanide fluorescence at equimolar concentrations (Figures 3.11 and 3.13), decreasing concentration sequentially to that more reminiscent of meteoritic abundance was not considered a worthy course of investigation.

3.2.6 $[LnDOTA]^-$ and nucleobase analytes

Nine nucleobases were chosen for testing: four purines and five pyrimidines (Section 2.3.2, Table 2.2). When these nucleobases were added to the $[LnDOTA]^-$ sensors (at equimolar concentrations) and their emissions compared to those of the $[LnDOTA]^-$ sensors alone, in most cases, europium and terbium fluorescence intensity was almost entirely quenched (Figure 3.14 and 3.15, respectively). The exception to this was adenine; the spectrum obtained for $[LnDOTA]^-$ in the presence of adenine indicated the lanthanides were still sensitised enough to emit fluorescence. The most intense emission obtained was that of the adenine/$[TbDOTA]^-$ mixture. This was approximately 25% of the intensity of the emissions of $[TbDOTA]^-$ alone (Figure 3.15, black and red lines, respectively) and suggested that the quenching effect of adenine on terbium fluorescence was not as efficient, or effective, as the other nucleobases.

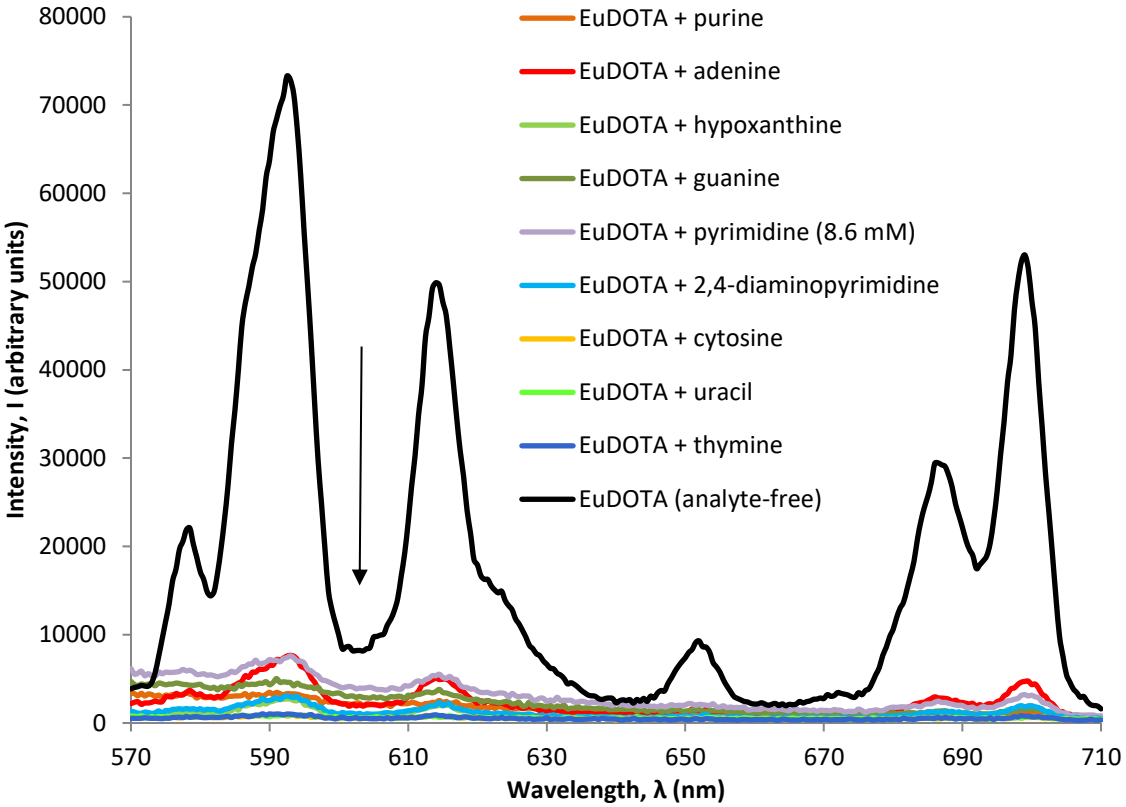

Figure 3.14 Fluorescence emission spectrum of 0.5 mM $[EuDOTA]^-$ (black) compared to the spectra of 0.5 mM $[EuDOTA]^-$ with 0.5 mM nucleobase analytes(λ_{Ex}=265 nm, acquisition time=0.5 sec, acquisition increment=0.5 nm, excitation and emission slit width=3 nm, pH=5)

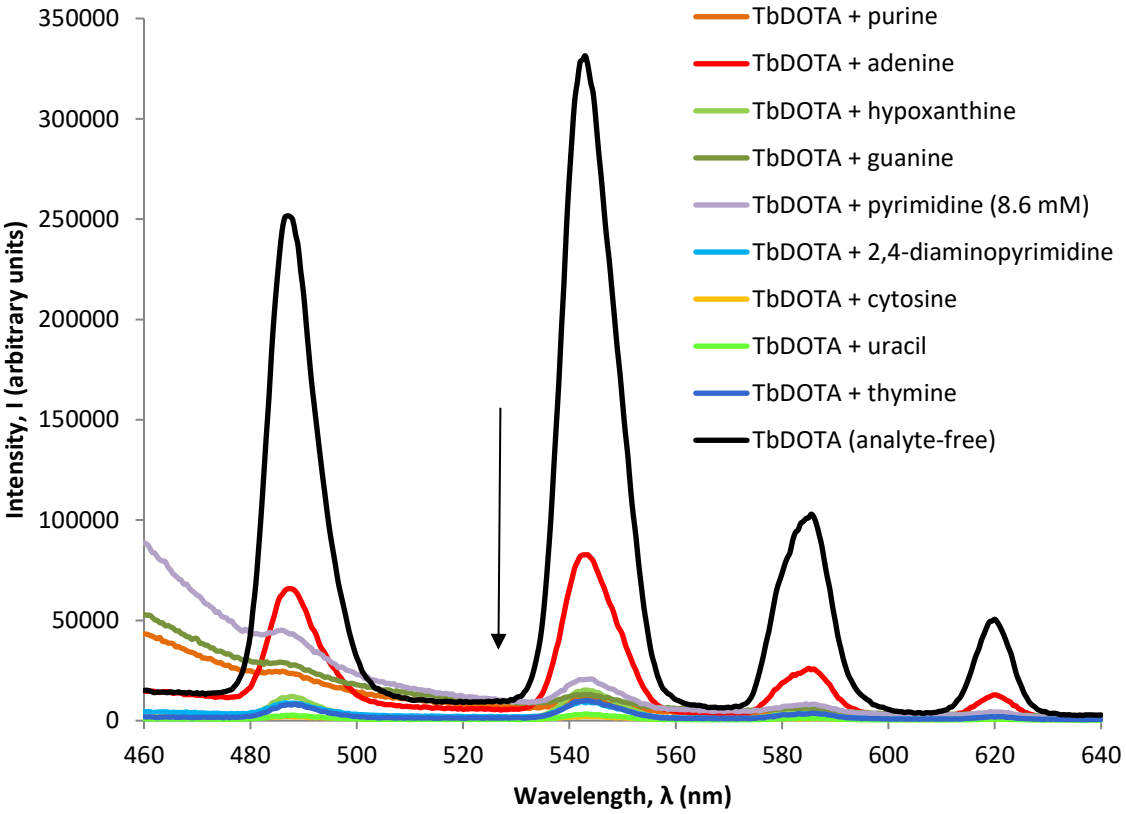

Figure 3.15 Fluorescence spectrum of 0.5 mM $[TbDOTA]^-$ (black) compared with when in the presence of 0.5 mM nucleobase analytes(λ_{Ex}=265 nm, acquisition time=0.5 sec, acquisition increment=0.5 nm, excitation and emission slit width=3 nm, pH=5)

Since nucleobases cause lanthanide fluorescence to quench, a limit of detection could be ascertained that would be useful in the development of the technique as a sensor. Sequentially decreasing the concentration of the nucleobase analytes, while maintaining constant sensor concentration, could reveal at what concentration the nucleobase no longer causes a reduction in intensity. To that end, the equimolar mixtures of nucleobase/$[LnDOTA]^-$ were altered successively so that the analyte concentration was halved, while the $[LnDOTA]^-$ concentration remained the same. To do this, 1 ml of 1 mM $[LnDOTA]^-$ sensor solution was applied to 1 ml of 1 mM nucleobase, so that both species were present at a concentration of 0.5 mM in 2 ml. Consecutive dilutions were achieved by removing 1 ml of the mixture and adding 1 ml of 1 mM $[LnDOTA]^-$ sensor solution, thus the concentration of the analyte would halve with each dilution while maintaining the $[LnDOTA]^-$ solution at a constant 0.5 mM. A fluorescence emission spectrum was obtained for each dilution and the process repeated until the spectrum intensity remained unchanged upon further dilution.

As expected, with each reduction in concentration of the nucleobase analyte, the lanthanide fluorescence intensity increased (e.g., thymine, Figures 3.16 and 3.17). The results of these analyses suggest that the limit of detection of nucleobases for these sensors is approximately $1x10^{-8}$ M since, at this concentration, no change in sensor-only fluorescence intensity is observed.

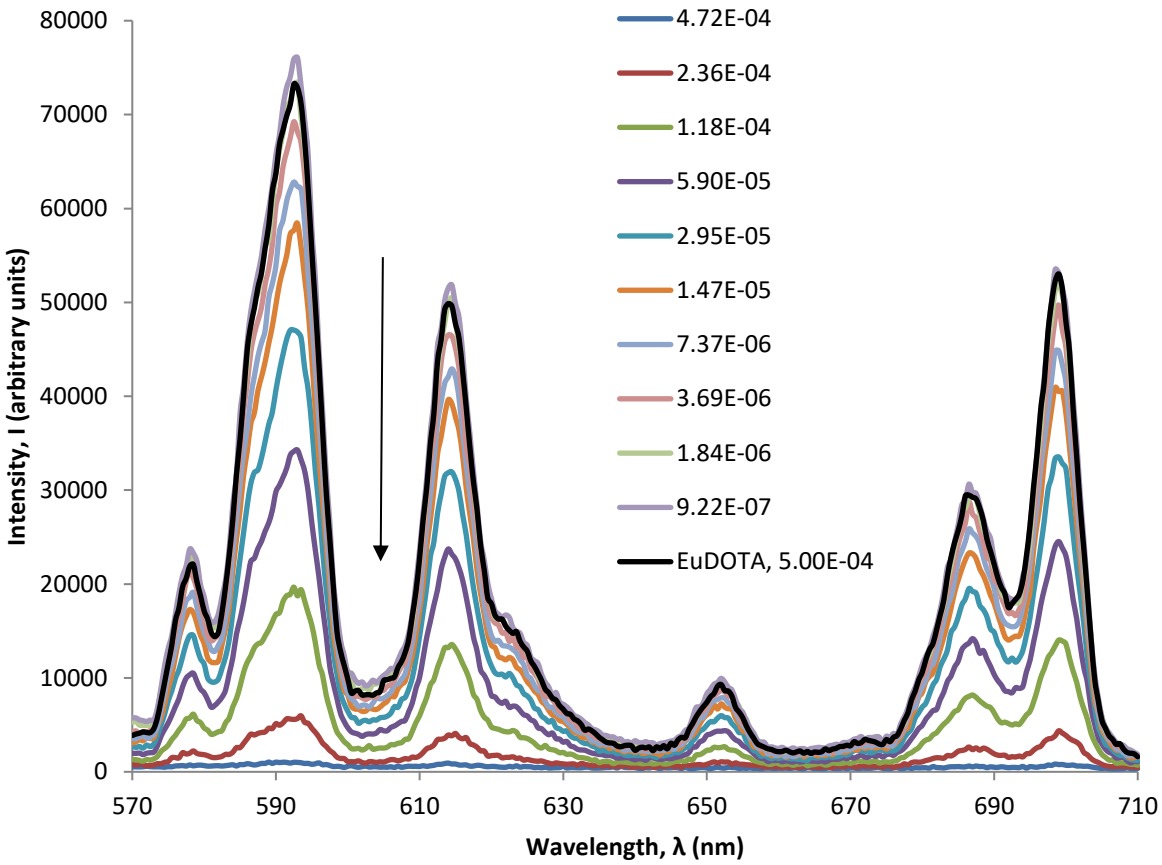

Figure 3.16 $[EuDOTA]^-$ at 0.5 mM (black) compared to equimolar thymine/$[EuDOTA]^-$ mixture (blue) and subsequent half dilutions of thymine with $[EuDOTA]^-$ maintained at 0.5 mM (Key – mol dm^{-3} (M)) (λ_{Ex}=265 nm, acquisition time=0.5 sec, acquisition increment=0.5 nm, excitation and emission slit width=3 nm, pH=5)

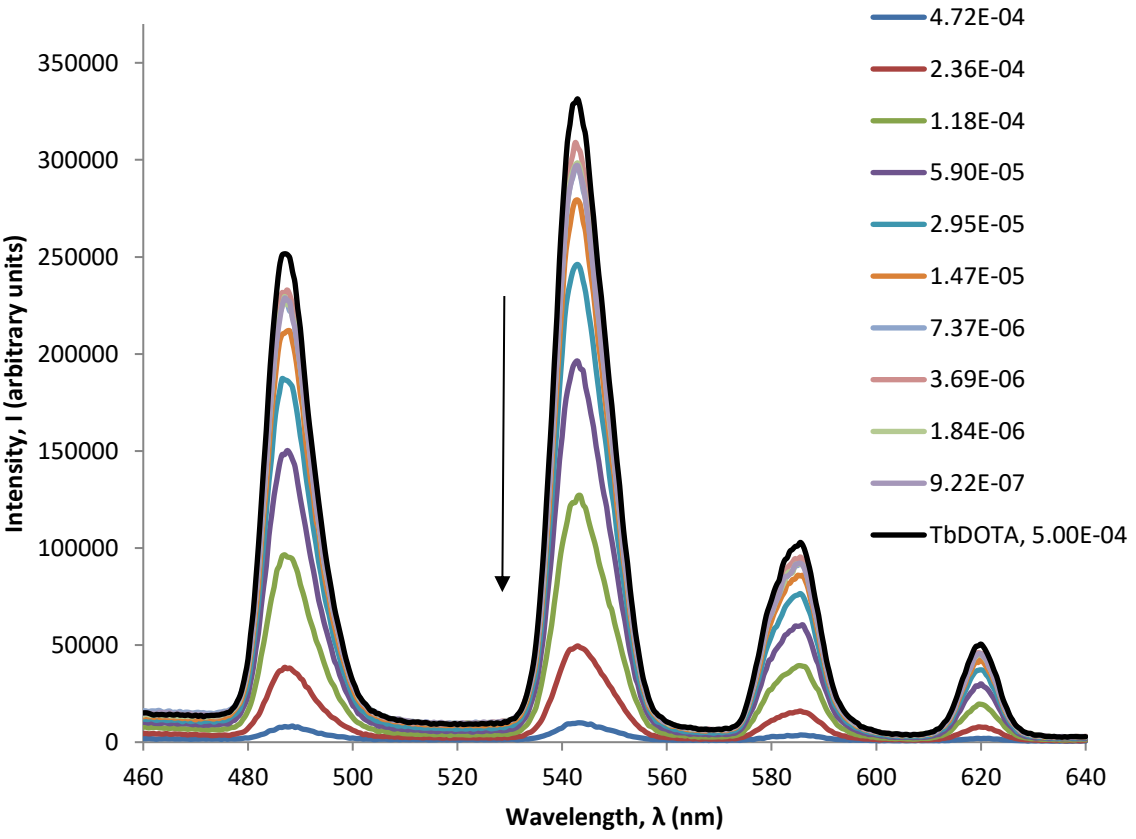

Figure 3.17 $[TbDOTA]^-$ at 0.5 mM (black) compared to equimolar thymine/[TbDOTA]- mixture (blue) and subsequent half dilutions of thymine with $[TbDOTA]^-$ maintained at 0.5 mM (Key – mol dm^{-3} (M)) (λ_{Ex}=265 nm, acquisition time=0.5 sec, acquisition increment=0.5 nm, excitation and emission slit width=3 nm, pH=5)

3.2.7 [LnDOTA]$^-$ and complex mixtures of analytes

Having established the effects of individual analytes upon [LnDOTA]$^-$ fluorescence, it was necessary to investigate complex mixtures of analytes in order to provide an indication of the fluorescence spectra expected when the sensors were applied to the extracts of meteorites and GRS. Therefore, it was necessary to apply the [LnDOTA]$^-$ solutions to complex mixtures of the selected analogue organic analytes.

As demonstrated in Section 3.2.5, the presence of most individual non-nucleobase analytes caused a small, but ultimately analytically insignificant, increase or decrease in intensity (depending on the lanthanide) in the [LnDOTA]$^-$ emission spectrum. These observations may be an effect of dilution (decrease in intensity) or small increases or decreases in relative volumes of sensor aliquots i.e. aliquot volumes were not identical for each experiment run. Conversely, there was total quenching of emissions in the presence of most individual nucleobases. Hence, the experiments were performed using 0.25 mM of sensor and 0.05 mM of the following complex mixtures: i) all non-nucleobases; ii) all non-nucleobases excluding benzoic acid; iii) all nucleobases; iv) purines-only; v) pyrimidine-only; and vi) all nucleobases and non-nucleobases, i.e. all analytes (see Section 2.4.3 for a description of the preparation of the analyte mixture).

The purpose of mixtures i) and ii) were to discover if the presence of benzoic acid, shown in this study and others (Gunnlaugsson et al., 2003) to sensitise lanthanide emissions, could be detected in a mixture of analytes. Mixtures iii), iv) and v) were selected in order to ascertain if the effect upon sensor fluorescence may be differentiated between purines and pyrimidines. The final mixture was chosen as it contained all the analytes and, although not representative of the full complexity of a natural sample extract may elucidate whether any one of the selected analogue analytes may be identified in the mixture.

All non-nucleobases

When a mixture of all non-nucleobase molecules (Table 2.2, Chapter 2) were mixed with the [LnDOTA]$^-$ solutions, the previously observed trends held true; there was a small increase in

intensity compared to the $[EuDOTA]^-$ emission intensity (Figure 3.18, purple and black lines, respectively), and a decrease in intensity compared to the $[TbDOTA]^-$ emission intensity (Figure 3.19, purple and black lines, respectively).

Considering the marked increase in intensity afforded by the addition of benzoic acid, as observed when mixed individually (Section 3.3.5, Figures 3.11 and 3.13), it was of interest to repeat the non-nucleobase mixture experiment excluding benzoic acid (Figures 3.18 and 3.19, orange lines) in order to determine its influence on the magnitude of the increase in intensity when present in the mixture. For both the europium and the terbium complexes of DOTA, a small detectable decrease in intensity was observed from that recorded for the mixture of all non-nucleobase analytes including benzoic acid. It is possible that in a complex mixture of analytes, benzoic acid may have to compete with other analytes in order to coordinate and thus affect a sensitisation of emissions. Should other components of the mixture coordinate or interact with the lanthanide to the preclusion of successful benzoic acid coordination, then sensitisation by antenna effect may not take place.

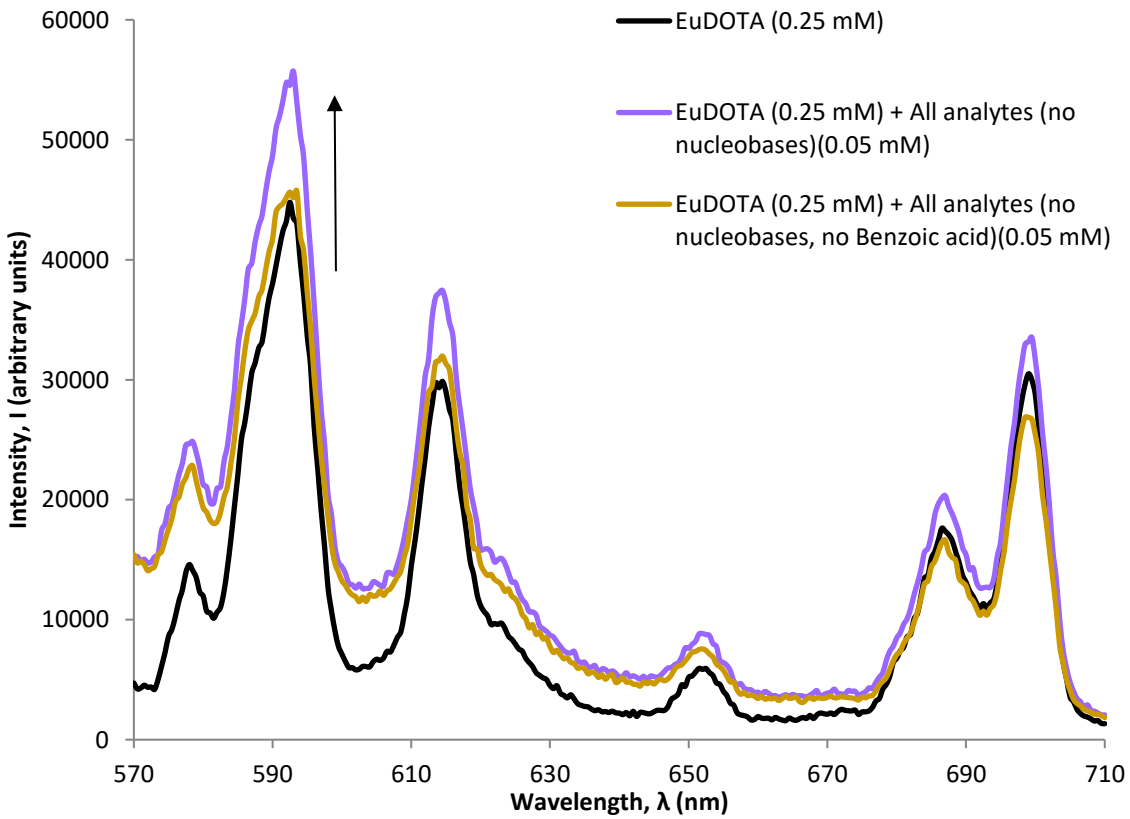

Figure 3.18 Fluorescence spectrum of 0.25 mM $[EuDOTA]^-$ compared with the fluorescence spectra in the presence of 0.05 mM of all analytes except nucleobases and 0.05 mM of all analytes except nucleobases and benzoic acid (λ_{Ex}=265 nm, acquisition time=0.5 sec, acquisition increment=0.5 nm, excitation and emission slit width=3 nm, pH=5)

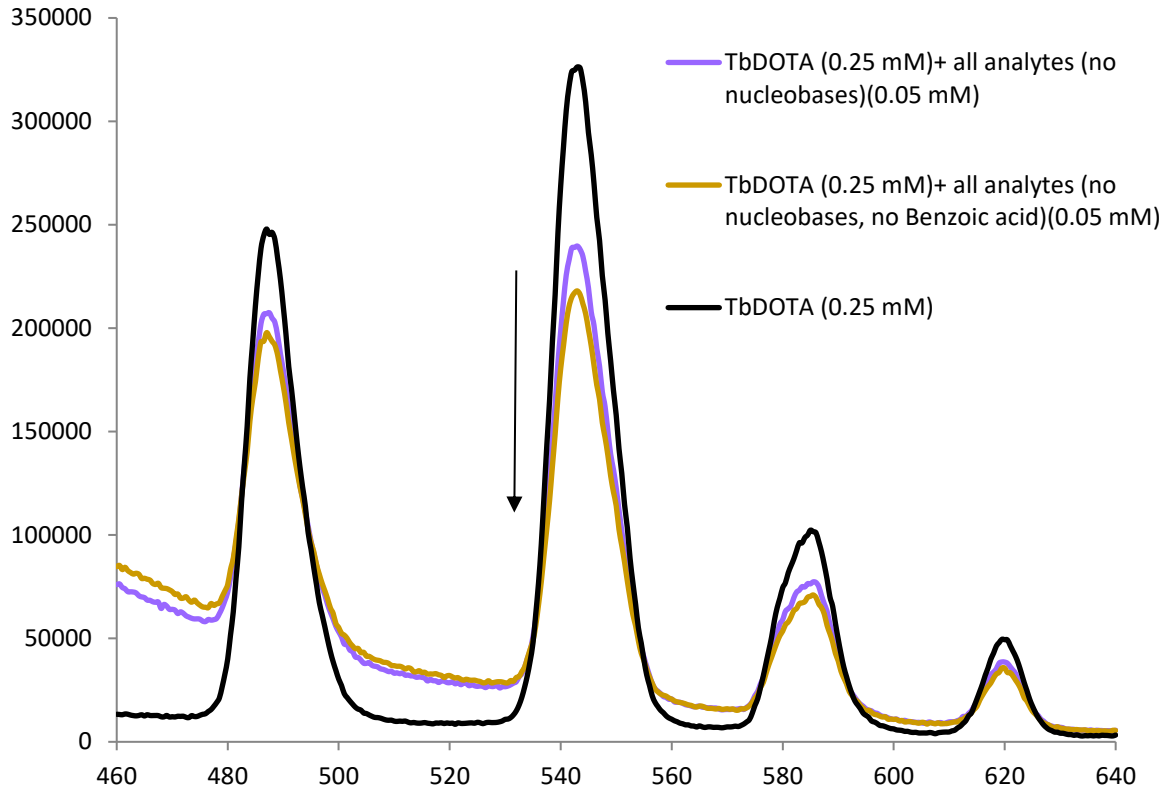

Figure 3.19 Fluorescence spectrum of 0.25 mM $[TbDOTA]^-$ compared with the fluorescence spectra in the presence of 0.05 mM of all analytes except nucleobases and 0.05 mM of all analytes except nucleobases and benzoic acid (λ_{Ex}=265 nm, acquisition time=0.5 sec, acquisition increment=0.5 nm, excitation and emission slit width=3 nm, pH=5)

Nucleobases

The nucleobases consist of two groups; purines and pyrimidines. It had been shown, both in experimental results (Section 3.2.6) and in work previously reported (Seidel et al., 1996), that nucleobases, as individual analytes, quenched fluorescence. When the individual nucleobases were diluted sequentially, while maintaining $[LnDOTA]^-$ at a constant concentration, fluorescence intensity was observed to increase accordingly (Section 3.2.6). It was logical, therefore, to run experiments for: i) all nucleobases together; ii) purine-only; and iii) pyrimidine-only, in order to ascertain if one class of nucleobase invokes quenching more or less than the other. Although spectra of individual nucleobases may provide this information, it was also not known if application of the sensors to mixtures of nucleobases would result in a comparable change in intensity. Therefore, this line of inquiry would elucidate whether the sensor could differentiate between nucleobase classes when mixed. Further, in all tests, concentration was sequentially decreased in order to ascertain if mixtures of nucleobases would similarly reduce quenching.

At equimolar concentrations of all nucleobases (where analytes and sensor were 0.5 mM), total quenching of fluorescent emission was recorded. The limit of resolution of fluorescent emissions was observed at dilution 4, where the analytes were present at a concentration of ~3.13×10^{-5} M for both $[LnDOTA]^-$ sensors (Figures 3.20 and 3.21).

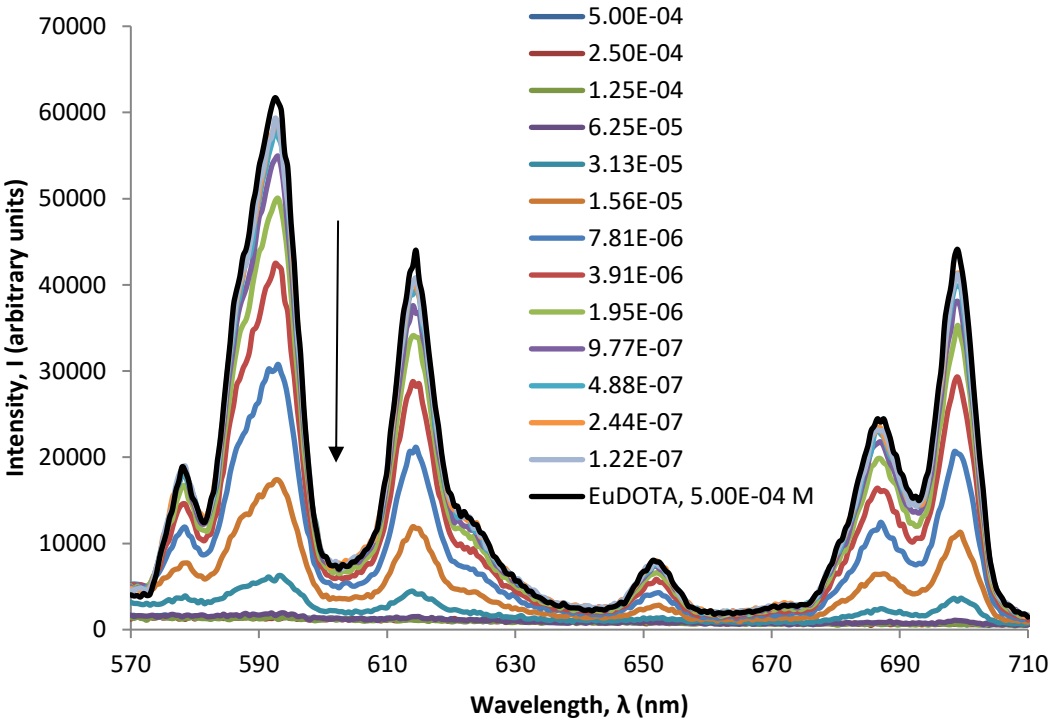

Figure 3.20 Fluorescence spectrum of 0.5 mM $[EuDOTA]^-$ compared with fluorescence spectra in the presence of a mixture of all nucleobases at an initial concentration of 0.5 mM, and then subsequent dilutions (Key – mol dm^{-3} (M)) (λ_{Ex}=265 nm, acquisition time=0.5 sec, acquisition increment=0.5 nm, excitation and emission slit width=3 nm, pH=5)

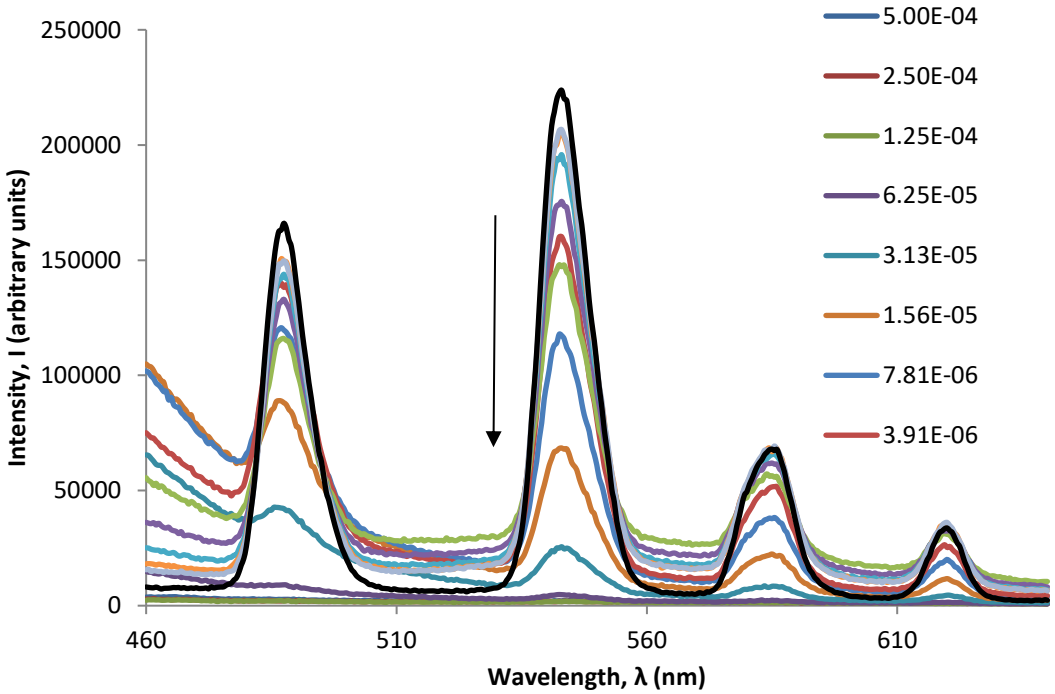

Figure 3.21 Fluorescence spectrum of 0.5 mM $[TbDOTA]^-$ compared with fluorescence spectra in the presence of a mixture of all nucleobases at an initial concentration of 0.5 mM, and then subsequent dilutions (Key – mol dm^{-3} (M)) (λ_{Ex}=265 nm, acquisition time=0.5 sec, acquisition increment=0.5 nm, excitation and emission slit width=3 nm, pH=5)

The purine-only mixture exhibited the same quenching of fluorescence at equimolar

concentrations, with lanthanide emissions detected at the third dilution, ~6.25×10^{-5} M (Figures 3.22 and 3.23), suggesting the limit of detection is slightly higher for purine-only mixtures since they have to be diluted less for the fluorescence to be detected. The mixture of pyrimidines gave comparable results to the purine mixture in that equimolar analyte/sensor mixtures quenched emissions, and the limit of detection was the same, i.e. Eu^{3+} peaks were detected at the third dilution, ~6.25×10^{-5} M (Figures 3.24 and 3.25).

Furthermore, it was clear that, whether the sensors were applied to complex mixtures of all nucleobases, mixtures of separate nucleobase classes or individual nucleobases, the quenching effect was common in all cases, i.e. the fluorescence emissions were quenched entirely when sensor and analyte were present in the mixture at equimolar concentrations, and that the limit of detection was approximately the same.

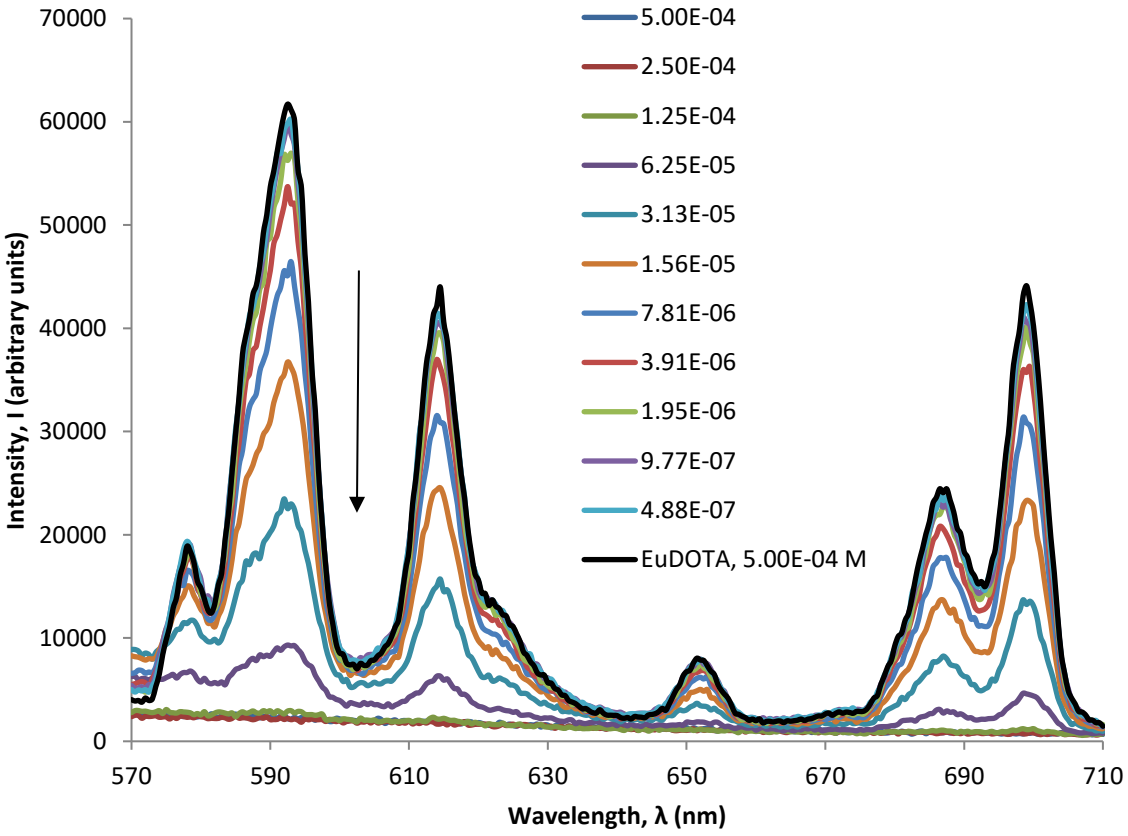

Figure 3.22 Fluorescence spectrum of 0.5 mM $[EuDOTA]^-$ compared with fluorescence spectra in the presence of a mixture of purines-only at an initial concentration of 0.5 mM, and then subsequent dilutions (Key – mol dm^{-3} (M)) (λ_{Ex}=265 nm, acquisition time=0.5 sec, acquisition increment=0.5 nm, excitation and emission slit width=3 nm, pH=5)

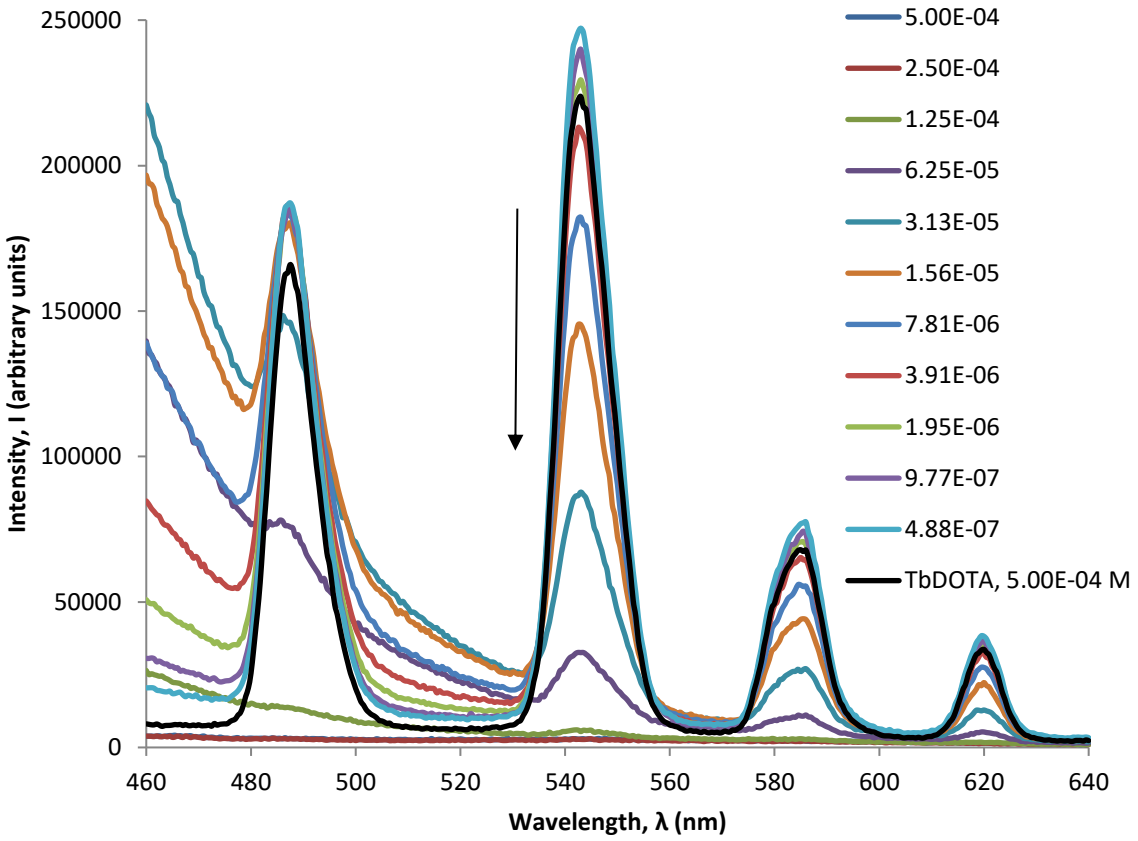

Figure 3.23 Fluorescence spectrum of 0.5 mM $[TbDOTA]^-$ compared with fluorescence spectra in the presence of a mixture of purines-only at an initial concentration of 0.5 mM, and then subsequent dilutions (Key – mol dm^{-3} (M)) (λ_{Ex}=265 nm, acquisition time=0.5 sec, acquisition increment=0.5 nm, excitation and emission slit width=3 nm, pH=5)

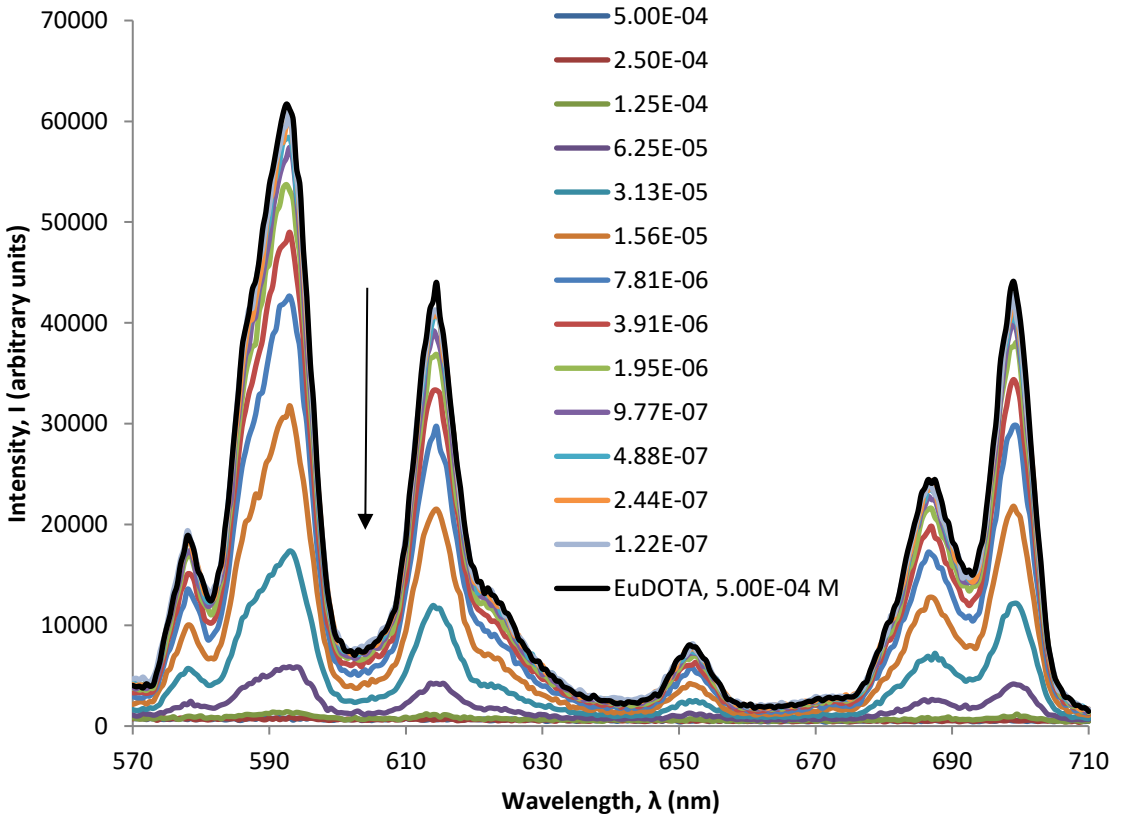

Figure 3.24 Fluorescence spectrum of 0.5 mM $[EuDOTA]^-$ compared with fluorescence spectra in the presence of a mixture of pyrimidines-only at an initial concentration of 0.5 mM, and then subsequent dilutions (Key – mol dm^{-3} (M)) (λ_{Ex}=265 nm, acquisition time=0.5 sec, acquisition increment=0.5 nm, excitation and emission slit width=3 nm, pH=5)

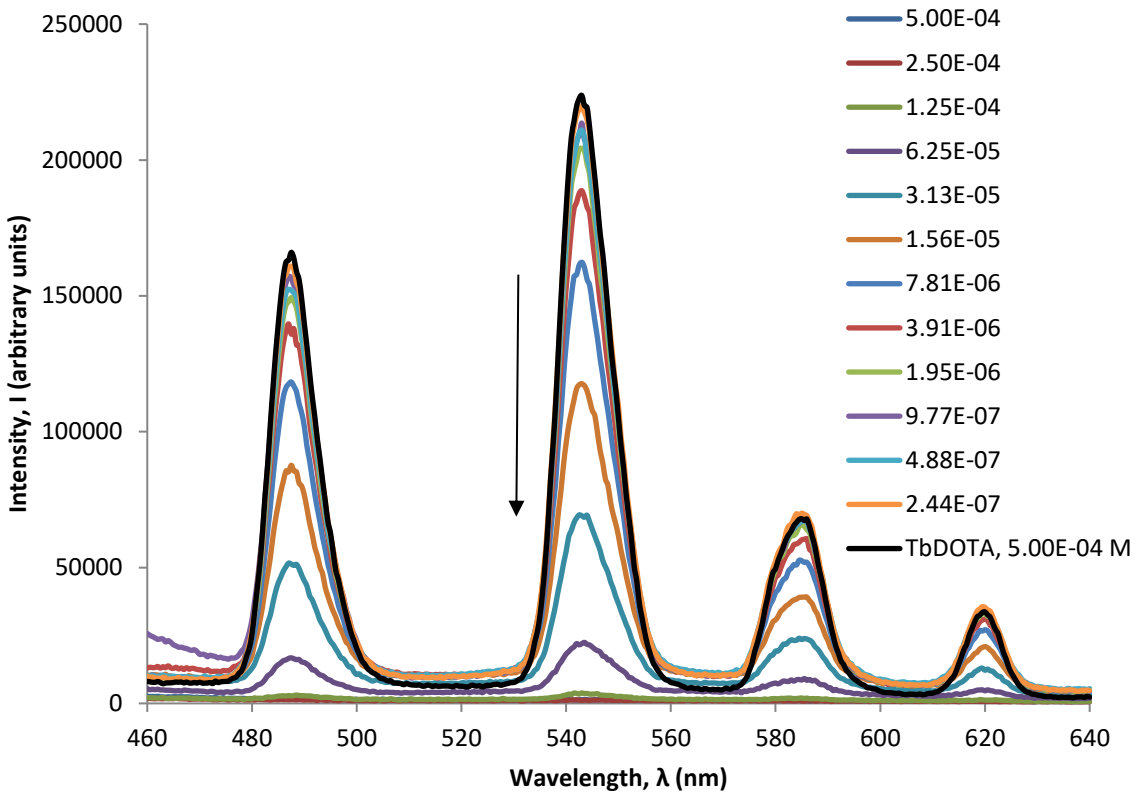

Figure 3.25 Fluorescence spectrum of 0.5 mM $[TbDOTA]^-$ compared with fluorescence spectra in the presence of a mixture of pyrimidines-only at an initial concentration of 0.5 mM, and then subsequent dilutions (Key – mol dm^{-3} (M)) (λ_{Ex}=265 nm, acquisition time=0.5 sec, acquisition increment=0.5 nm, excitation and emission slit width=3 nm, pH=5)

All analytes

Having established the effects of complex mixtures of non-nucleobase analytes (with, and without benzoic acid), and mixtures of nucleobase analytes, on the analyte-free $[LnDOTA]^-$ complex fluorescence emissions, it was necessary to combine the sensor with a mixture of all selected analytes. The purpose of this was to emulate an aqueous meteorite extract and provide an insight into what the $[LnDOTA]^-$ fluorescence response might be when the sensors were applied to a real sample.

The stock solution contained all analytes at equal concentrations (1 mM). 0.75 ml of this mixture was combined with 0.75 ml of 2 mM sensor solution such that the final concentration of sensor was 1 mM in 1.5 ml and each analyte was present at a concentration of 0.5 mM. Upon excitation at 265 nm, a spectrum was obtained for this mixture, which showed that fluorescence was quenched (Figures 3.26 and 3.27).

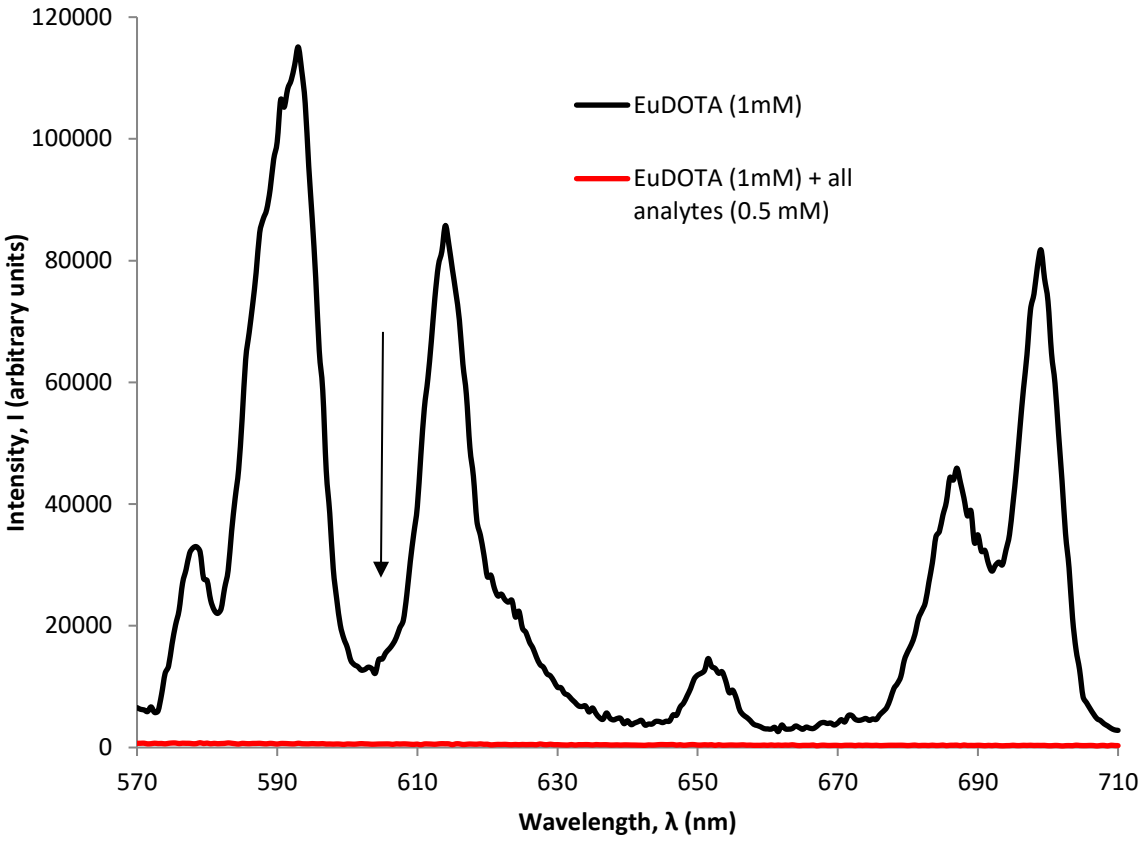

Figure 3.26 Fluorescence spectrum of 1 mM $[EuDOTA]^-$ compared with fluorescence spectra in the presence of a mixture of all analytes at a concentration of 0.5 mM (λ_{Ex}=265 nm, acquisition time=0.5 sec, acquisition increment=0.5 nm, excitation and emission slit width=3 nm, pH=5)

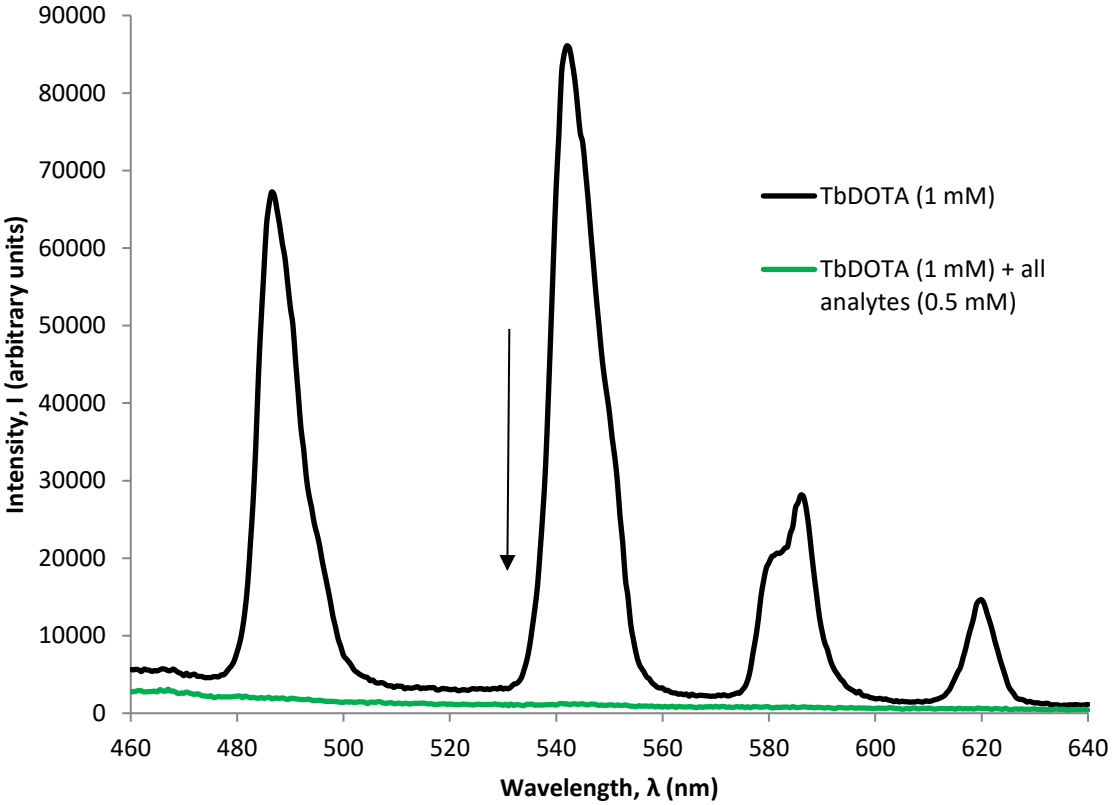

Figure 3.27 Fluorescence spectrum of 1 mM $[TbDOTA]^-$ compared with fluorescence spectra in the presence of a mixture of all analytes at a concentration of 0.5 mM (λ_{Ex}=265 nm, acquisition time=0.5 sec, acquisition increment=0.5 nm, excitation and emission slit width=3 nm, pH=5)

Since non-nucleobase analytes, when mixed individually (Figures 3.11 and 3.13) and as a complex mixture (with and without benzoic acid) (Figures 3.18 and 3.19) had little effect on the analyte-free $[LnDOTA]^-$ emission intensity, it is likely that the loss of intensity observed in the presence of the all-analyte complex mixture was a direct consequence of the presence of nucleobases. Based upon the observations recorded in this study, if nucleobases were present in a mixture at the limit of detection (in this study, established to be ~$1x10^{-8}$ M) and all other analytes present in excess, no effect on the sensor-only fluorescence intensity would be expected.

Having developed the methodology outlined above, europium and terbium complexes of DO3A were produced and applied to the organic analyte solutions in the same manner (Section 3.4.3 to 3.4.6, inclusive).

3.3 Complexes based on DO3A

DO3A is the tris-substituted cyclen analogue of the tetra-substituted cyclen DOTA molecule discussed previously (Sections 3.1 and 3.2). Unlike DOTA, DO3A cannot be purchased as the 'free-acid'; however it is available as the protected tertiary butyl ester, t-BuDO3A (Figure 3.28 a). In order to remove these protecting groups, an acid catalysed hydrolysis reaction was required in which the esters are converted into carboxylic acids. The reaction occurs at all three ester groups so that the target tricarboxylic acid molecule DO3A is produced (Figure 3.28 b).

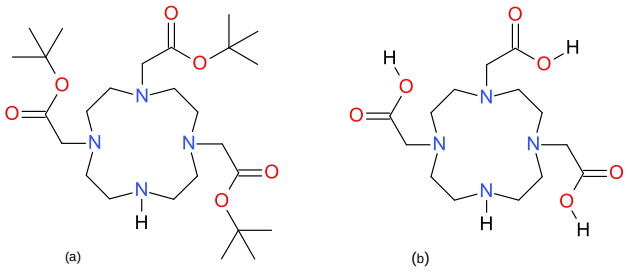

Figure 3.28 t-BuDO3A (a) and DO3A (b)

As outlined in Chapter 2 (Section 2.7.2), [LnDO3A] complexes were synthesised, first by synthesising DO3A from *tBut*-DO3A, and them combining DO3A with $EuCl_3.6H_2O$ or $TbCl_3.6H_2O$. Chelation was confirmed by mass spectrometry and fluorimetry. The fluorescence

emissions of these complexes were then characterised in the presence and absence of analogue analytes (see Chapter 2, Section 2.3.2 for details on the analytes chosen).

While $[LnDOTA]^-$ bears a single overall negative charge, [LnDO3A] is a neutral complex; the tripositive lanthanide ion charge is cancelled by the three negatively charged ethanoate pendant arms. Moreover, DO3A possesses one fewer pendant arm than DOTA, thus increasing access to the lanthanide metal-centre for external species. As a result of these structural and electronic differences, it is therefore possible that the responses observed when $[LnDOTA]^-$ was applied to the analytes, and mixtures of analytes, may not be comparable to those observed when the same analytes are combined with [LnDO3A]. The results of these tests are presented here.

3.3.1 Excitation of [LnDO3A] at 265 nm

As previously explained (Sections 3.2.3 and 3.2.4), direct excitation of the europium complex at 397 nm did not yield spectra that provided evidence of analyte interaction with the sensor. However, indirect excitation of the europium and terbium *via* the antenna effect afforded by excitation of the carboxylate moieties of the DOTA ligand at 265 nm did. Therefore, the [LnDO3A] complexes were also irradiated at 265 nm in order to obtain the sensor-only fluorescence spectra (Figures 3.29 and 3.30).

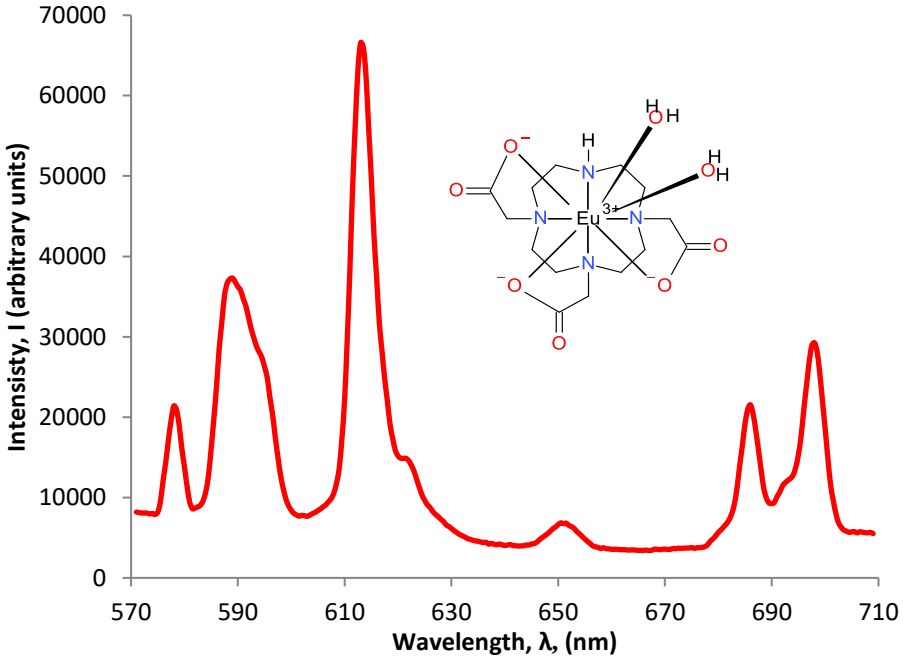

Figure 3.29 Fluorescent emission spectrum of 2 mM [EuDO3A]. This spectrum is as expected for hepta-coordinated Eu^{3+} emissions, where sensitisation of $\Delta J=2 > \Delta J=1$ (λ_{Ex}=265 nm, acquisition time=0.5 sec, acquisition increment=0.5 nm, excitation and emission slit width=3 nm, pH=5)

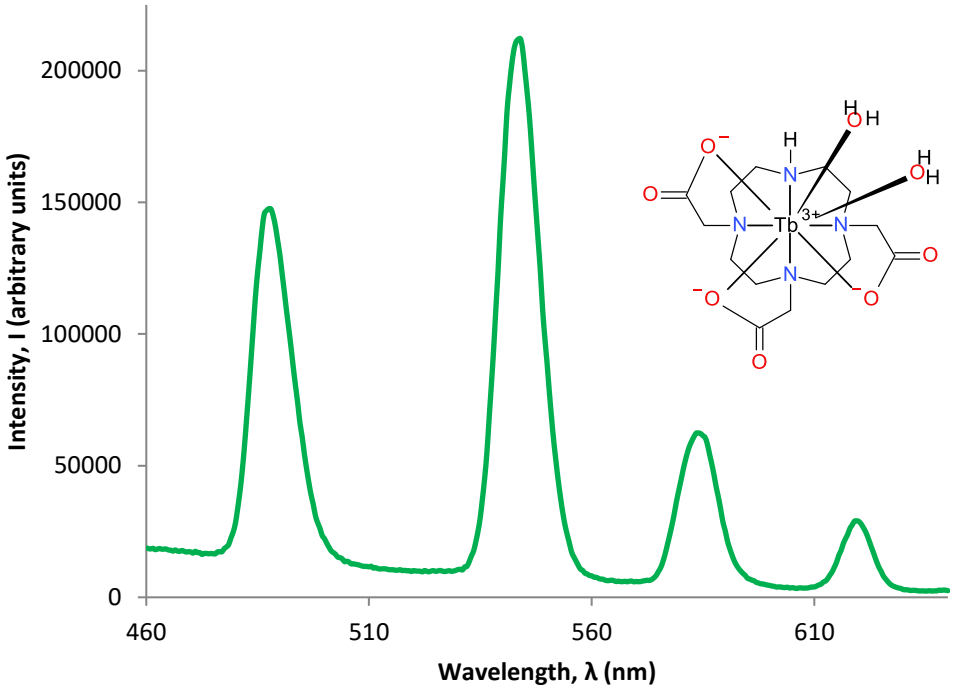

Figure 3.30 Fluorescent emission spectrum of 2 mM [TbDO3A] (λ_{Ex}=265 nm, acquisition time=0.5 sec, acquisition increment=0.5 nm, excitation and emission slit width=3 nm, pH=5)

3.3.2 [LnDO3A] and non-nucleobase analytes

The tests using the non-nucleobase analytes and [LnDO3A] followed the same procedures and protocols as previously described (Section 3.2.5).

The responses observed for [EuDO3A] and [TbDO3A] were mostly comparable to those seen for the assays using $[EuDOTA]^-$. There was little deviation from the [EuDO3A] fluorescence emission intensity (Figure 3.31; compare with Figure 3.11), but fluorescence emissions observed when [TbDO3A] was applied to the non-nucleobase analytes suggested no interaction had taken place, contrary to the results for $[TbDOTA]^-$ (Figure 3.32; compare with Figure 3.13). The fluorescent emissions recorded upon addition of (*L*)-tyrosine for both [LnDO3A] sensors (Figures 3.31 and 3.32) resulted in the same overlap seen previously for $[LnDOTA]^-$ (Section 3.2.5) and is similarly likely to be due to the 'tail end' of its broad intrinsic fluorescent emission rather than a sensor/analyte interaction. However, when (*L*)-aspartic acid was combined with [TbDO3A], sensitisation was observed, manifesting as an increase in intensity of all emissions (Figure 3.33).

When the sensors were combined with benzoic acid, a substantial increase in emission intensity was observed (Figures 3.31 and 3.32), comparable to that previously recorded when benzoic acid was combined with $[LnDOTA]^-$. The shape of the europium spectrum recorded was reminiscent of $[EuDOTA]^-$ (Figure 3.11) *not* the shape of the spectrum of [EuDO3A] (Figure 3.29). Specifically, the ΔJ=1 emission, for which the $^5D_0 \rightarrow {}^7F_1$ transition is responsible, became more intense than that of the ΔJ=2 emission (see Section 3.4).

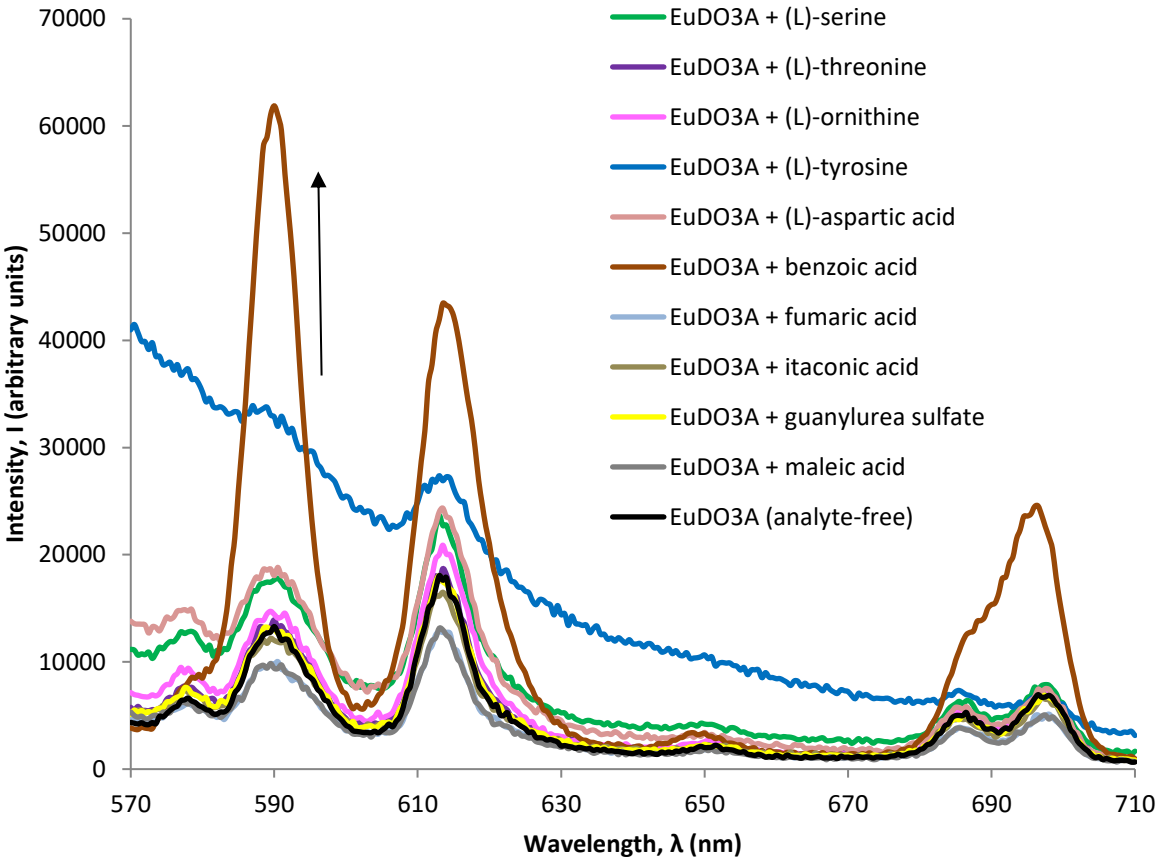

Figure 3.31 [EuDO3A] fluorescence, at 0.5 mM (black line), compared with an [EuDO3A]/analyte mixture, where both sensor and analyte are present at a concentration of 0.5 mM, respectively (coloured lines) (λ_{Ex}=265 nm, acquisition time=0.5 sec, acquisition increment=0.5 nm, excitation and emission slit width=3 nm, pH=5)

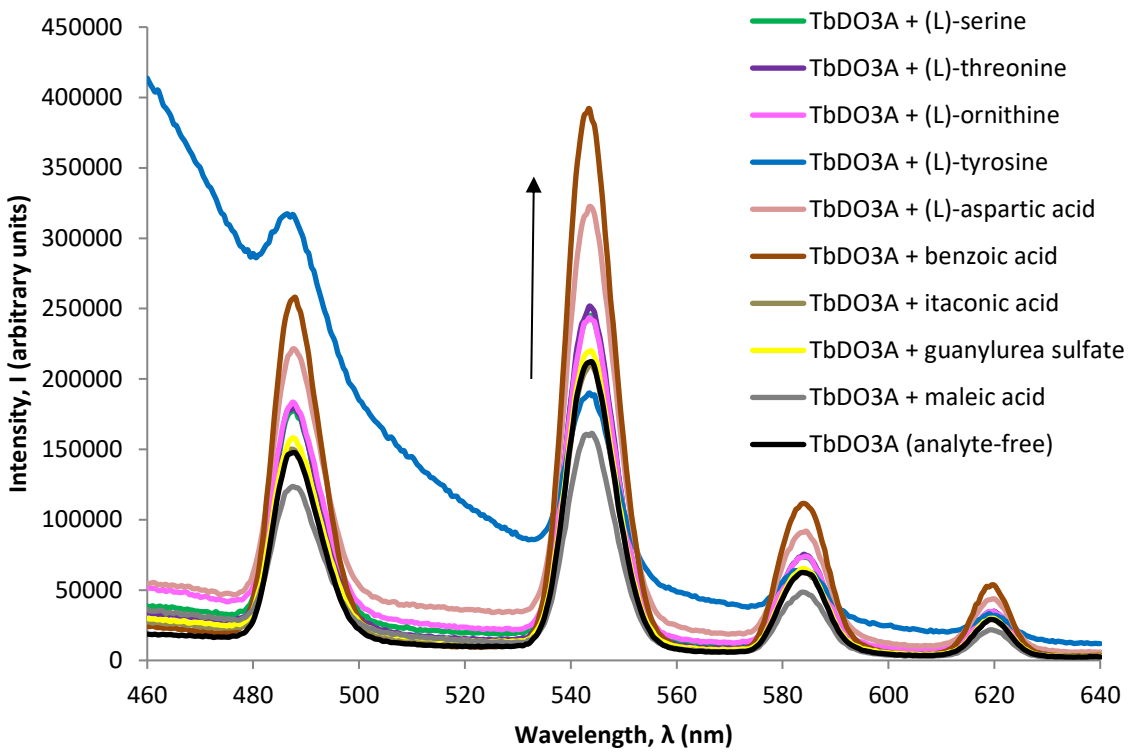

Figure 3.32 [TbDO3A] fluorescence, at 0.5 mM (black line), compared with an [TbDO3A]/individual non-nucleobase analyte mixture, where both sensor and analyte are present at a concentration of 0.5 mM, respectively (coloured lines) (λ_{Ex}=265 nm, acquisition time=0.5 sec, acquisition increment=0.5 nm, excitation and emission slit width=3 nm, pH=5)

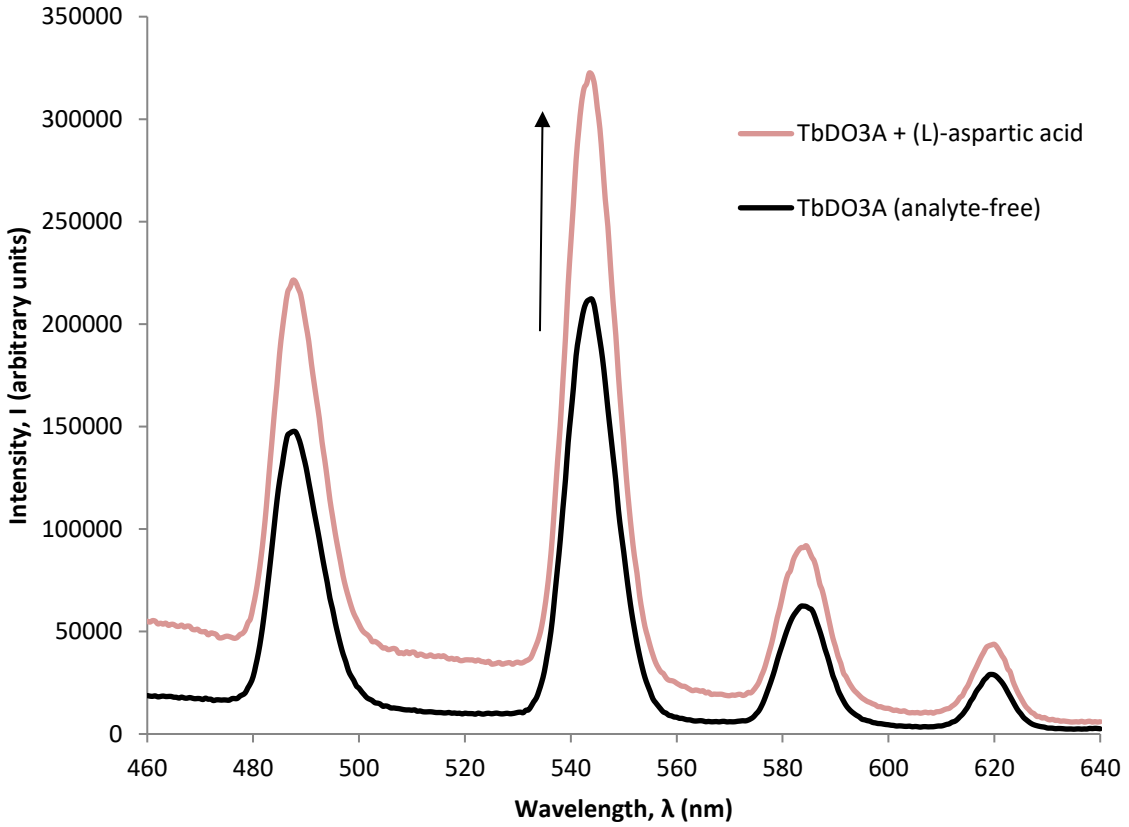

Figure 3.33 Fluorescence spectrum for 0.5 mM [TbDO3A] (in black) and spectra obtained when [TbDO3A] was mixed with (*L*)-aspartic acid, at equimolar concentration, i.e. 0.5 mM (λ_{Ex}=265 nm, acquisition time=0.5 sec, acquisition increment=0.5 nm, excitation and emission slit width=3 nm, pH=5)

3.3.3 [LnDO3A] and nucleobase analytes

Individual nucleobase analytes were combined with the [LnDO3A] sensors in the same manner as in the $[LnDOTA]^-$ analyses (Section 3.2.6).

All nucleobases, with the exception of adenine, quenched lanthanide fluorescence when combined at equimolar concentrations with [LnDO3A] (Figures 3.34 and 3.35), just as they had when mixed with the $[LnDOTA]^-$ complexes (see Figures 3.14 and 3.15). These observations suggest a similar quenching mechanism must be responsible for all complexes when mixed with these analytes (see Section 3.4). Addition of adenine, however, resulted in a marked sensitisation of lanthanide fluorescence (red line, Figures 3.34 and 3.35); in this case, there must be a different interaction taking place.

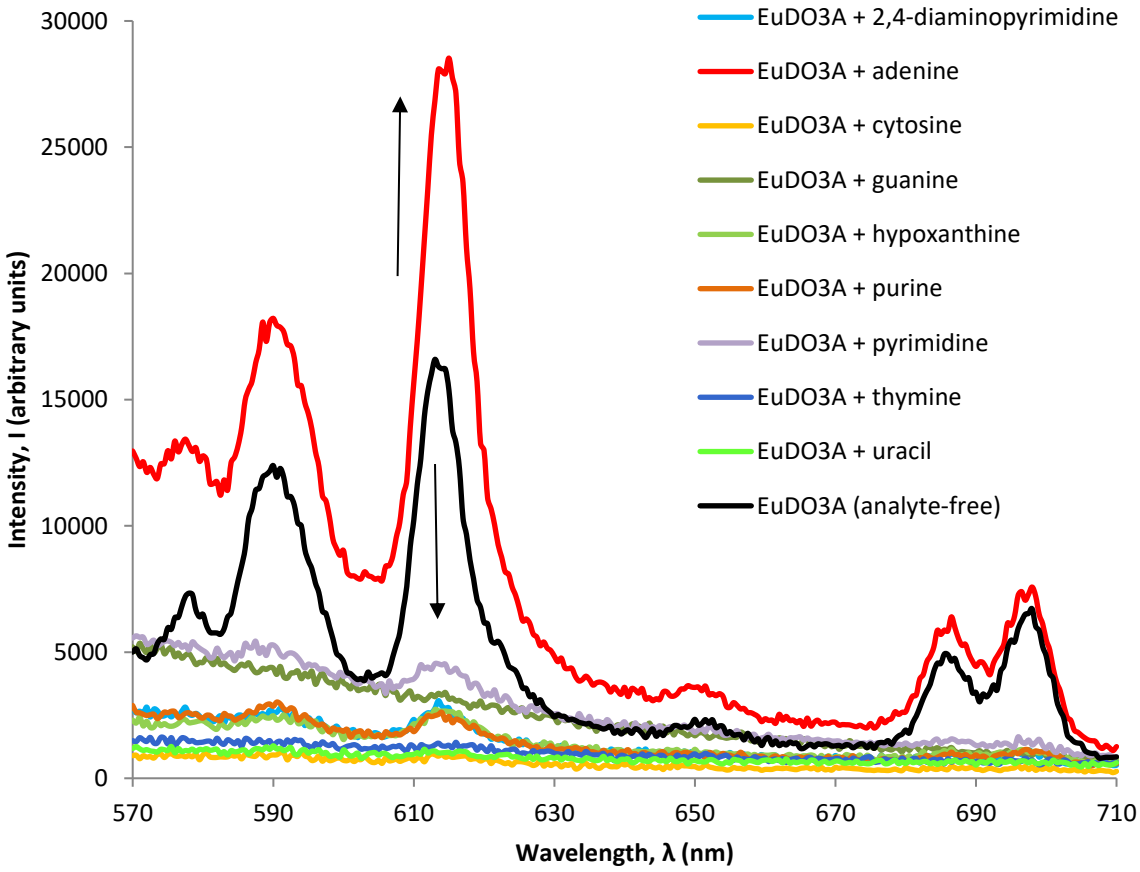

Figure 3.34 [EuDO3A] fluorescence, at 0.5 mM (black line), compared with an [EuDO3A]/individual nucleobase analyte mixture, where both sensor and analyte are present at a concentration of 0.5 mM, respectively (coloured lines) (λ_{Ex}=265 nm, acquisition time=0.5 sec, acquisition increment=0.5 nm, excitation and emission slit width=3 nm, pH=5)

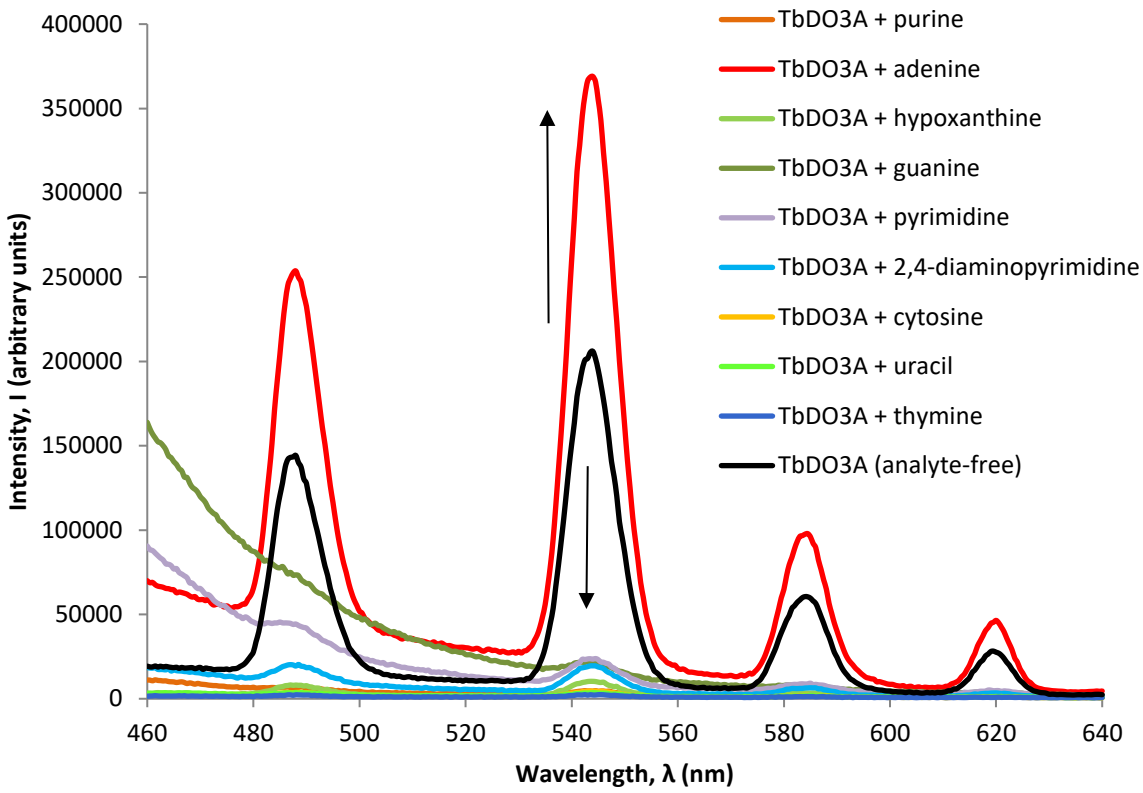

Figure 3.35 [TbDO3A] fluorescence, at 0.5 mM (black line), compared with an [TbDO3A]/individual nucleobase analyte mixture, where both sensor and analyte are present at a concentration of 0.5 mM, respectively (coloured lines) (λ_{Ex}=265 nm, acquisition time=0.5 sec, acquisition increment=0.5 nm, excitation and emission slit width=3 nm, pH=5)

There have not been any published instances of the sensitisation of lanthanide fluorescence in the presence of adenine. It is possible that adenine can displace water molecules coordinated to the lanthanide complex thereby removing the O-H oscillator quenching effect of the water molecule (Chapter 1), facilitating an increase in emission intensity. It is equally possible that adenine can interact directly with the metal centre and act as an antenna by absorbing excitation energy and directly transferring it to the lanthanide ion, thereby sensitising emissions. These hypotheses are not mutually exclusive and could work together to incur the intensity increase: the adenine could interact directly, acting as an antenna, *and* displace water at the same time.

Confirmation of inner sphere hydration, q, (the number of bound water molecules) could be achieved by measuring the fluorescent lifetimes of the complexes in water (H_2O), then in deuterated water (or deuterium oxide) (D_2O) (Borbas & Bruce, 2007). The coupling between the emissive europium energy levels and the O-D oscillation, which leads to non-radiative decay, is less efficient with the heavier isotope than the lighter O-H oscillation. Thus, the fluorescent lifetime of the complex in D_2O will be greater (Beeby & Faulkner, 1997). By measuring the two

fluorescent lifetimes, and using Equation 3.1 (where k is the reciprocal of the measured lifetime in the given solvent and A is an experimental value in units of ms^{-1}), it is possible to calculate the number of bound water molecules.

$$q = A(k_{H_2O} - k_{D_2O}) \qquad \text{Equation 3.1}$$

In the same way, if the presence of an analyte was shown to alter the analyte-free spectrum, then the fluorescent lifetime of the complex in the presence of that analyte could be measured in D_2O and H_2O solvents, compared to the analyte-free lifetime and the q value calculated to determine if water molecules have been displaced. If it was shown that water molecules had not been displaced, but a change in intensity recorded none-the-less, then this would confirm the antenna effect – the increase in intensity cannot be the result of displaced water. These experiments were, however, not attempted within this thesis.

Nucleobases are all similar in their structure, so it would be expected that other nucleobase analytes could have the ability to displace water in the same way as adenine may. That being the case, a similar increase in intensity would be observed. Since an increase in intensity has not been observed, water displacement may not be the cause of the increase in intensity recorded here and, thus, it is more likely that a sensor/adenine interaction may be the cause.

[LnDO3A]/nucleobase dilution experiments were carried out in the same manner described previously (Section 3.2.6), i.e. the sensors were applied to nucleobases so that sensor and nucleobase were initially present at equimolar concentrations, then the nucleobase concentration reduced while maintaining initial sensor concentration. This was undertaken in order to ascertain whether the DO3A lanthanide complex sensors respond to a decrease in nucleobase analyte concentration in the same way as that previously recorded for $[LnDOTA]^-$. It may be possible to elucidate whether [LnDO3A] complexes are more, or less, sensitive to nucleobase interactions than $[LnDOTA]^-$ complexes by observing and comparing the extent by which their emission intensities change upon each nucleobase mixture dilution.

With each analyte dilution, emission intensity increased toward the [LnDO3A] fluorescence intensity (e.g. Figure 3.36). In the case of adenine, which showed an increase in intensity when mixed at equimolar concentration, upon dilution, the intensity decreased toward the analyte-free [LnDO3A] emission intensity, as would be expected (Figure 3.37).

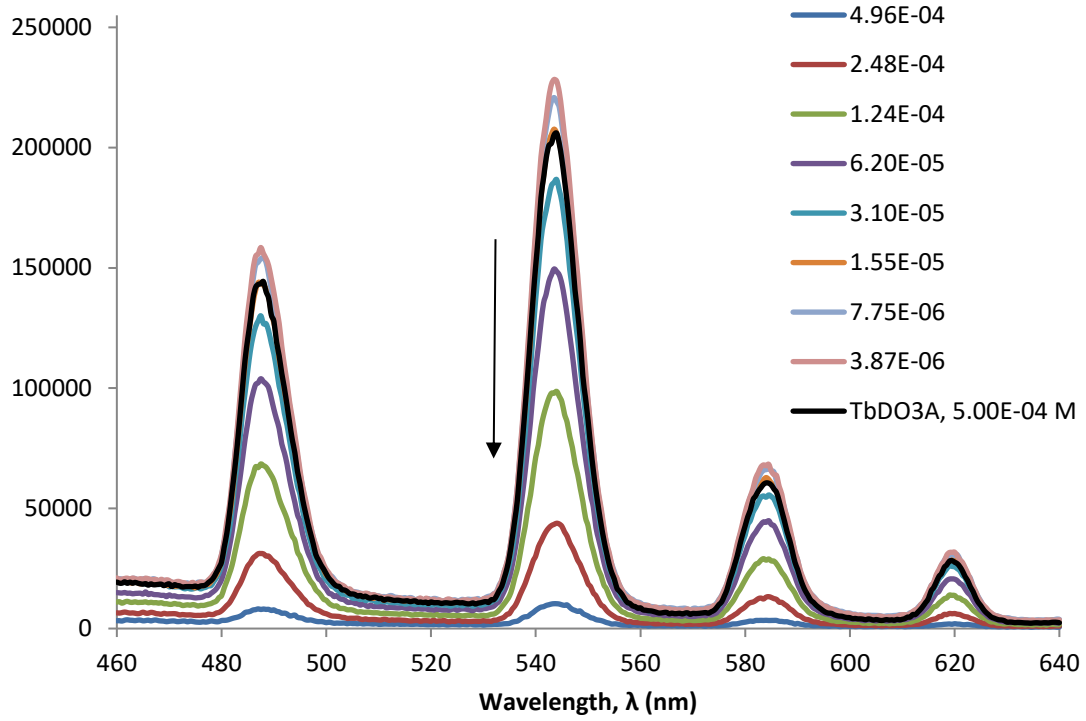

Figure 3.36 [TbDO3A] at 0.5 mM (black) compared to equimolar hypoxanthine/[TbDO3A] mixture (dark blue) and subsequent half dilutions of hypoxanthine with [TbDO3A] maintained at 0.5 mM (Key – mol dm^{-3} (M)) (λ_{Ex}=265 nm, acquisition time=0.5 sec, acquisition increment=0.5 nm, excitation and emission slit width=3 nm, pH=5)

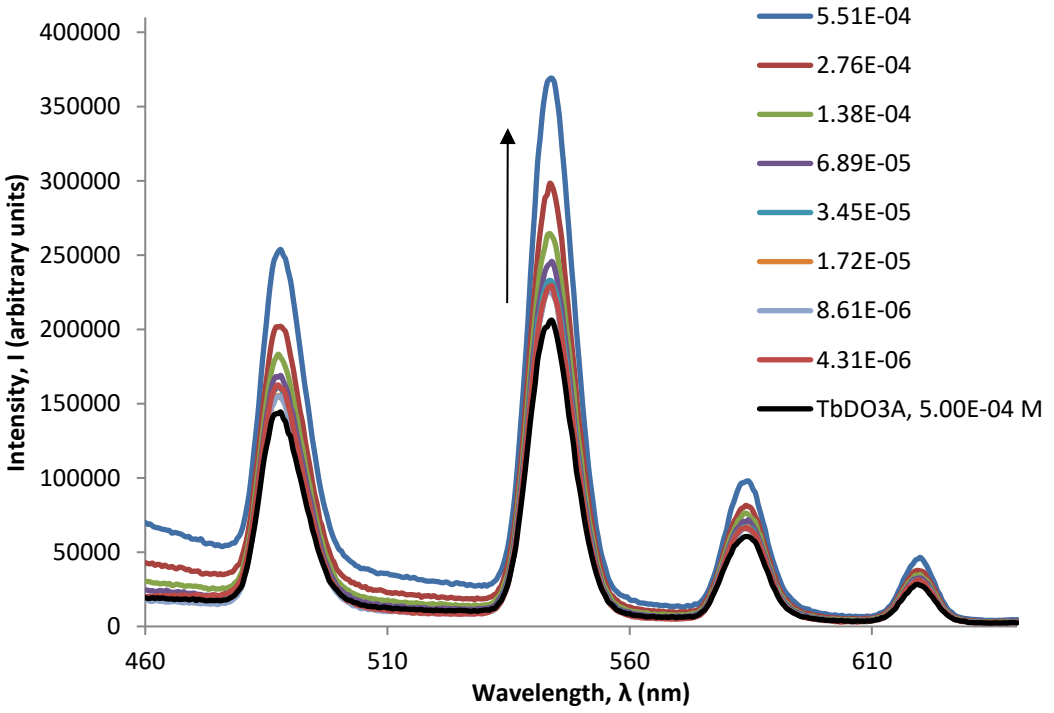

Figure 3.37 [TbDO3A] at 0.5 mM (black) compared to equimolar adenine/[TbDO3A] mixture (dark blue) and subsequent half dilutions of adenine with [TbDO3A] maintained at 0.5 mM (Key – mol dm^{-3} (M)) (λ_{Ex}=265 nm, acquisition time=0.5 sec, acquisition increment=0.5 nm, excitation and emission slit width=3 nm, pH=5)

3.3.4 [LnDO3A] and complex mixtures of analytes

As with $[LnDOTA]^-$, it was necessary to run [LnDO3A] fluorimetric analyses with complex mixtures of the analytes, following the same procedures and using the same analyte mixture combinations as described in Section 3.2.7.

When all non-nucleobase analytes were combined with [EuDO3A], the intensity detected at ΔJ=0 and ΔJ=1 (~580 nm and 590 nm, respectively) were greater than the sensor emissions alone; however, there was a decrease in intensity at ΔJ=4 (~690 nm) and no deviation at ΔJ=2 (~ 615 nm) (Figure 3.38, purple line). The overall shape of the spectrum is reminiscent of that observed for the (*L*)-tyrosine/[EuDO3A] mixture (Figure 3.31, blue line, Section 3.3.2), which suggests the intrinsic fluorescence of (*L*)-tyrosine may be dominating the response rather than a sensitisation of europium emissions. The intensity increase recorded was the same whether benzoic acid was present in the mixture or not (Figure 3.38, orange line).

When all non-nucleobase analytes were mixed with [TbDO3A], a marked increase in fluorescence was seen at all transitions; however, there was very little difference in intensity between the spectra recorded for the mixture with or without benzoic acid (Figure 3.39, purple and orange lines, respectively). These results, common to both [LnDO3A] complexes, suggest the increase in intensity is not as a result of interaction between benzoic acid and the lanthanide metal-centre but instead may be attributable to swamping of the fluorescent signal by the broad intrinsic fluorescence of (*L*)-tyrosine (Figure 3.12) (see Section 3.2.5).

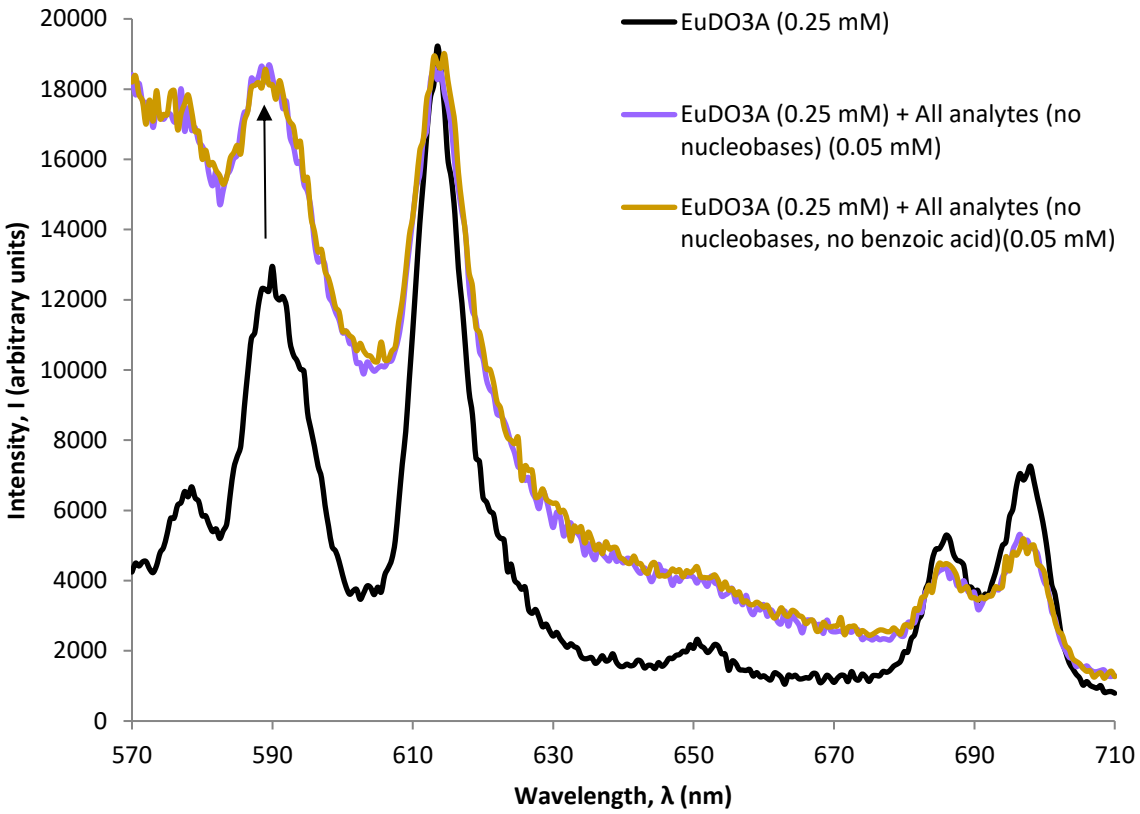

Figure 3.38 Fluorescence spectrum of 0.25 mM [EuDO3A] compared with the fluorescence spectra in the presence of 0.05 mM of all analytes except nucleobases and 0.05 mM of all analytes except nucleobases and benzoic acid (λ_{Ex}=265 nm, acquisition time=0.5 sec, acquisition increment=0.5 nm, excitation and emission slit width=3 nm, pH=5)

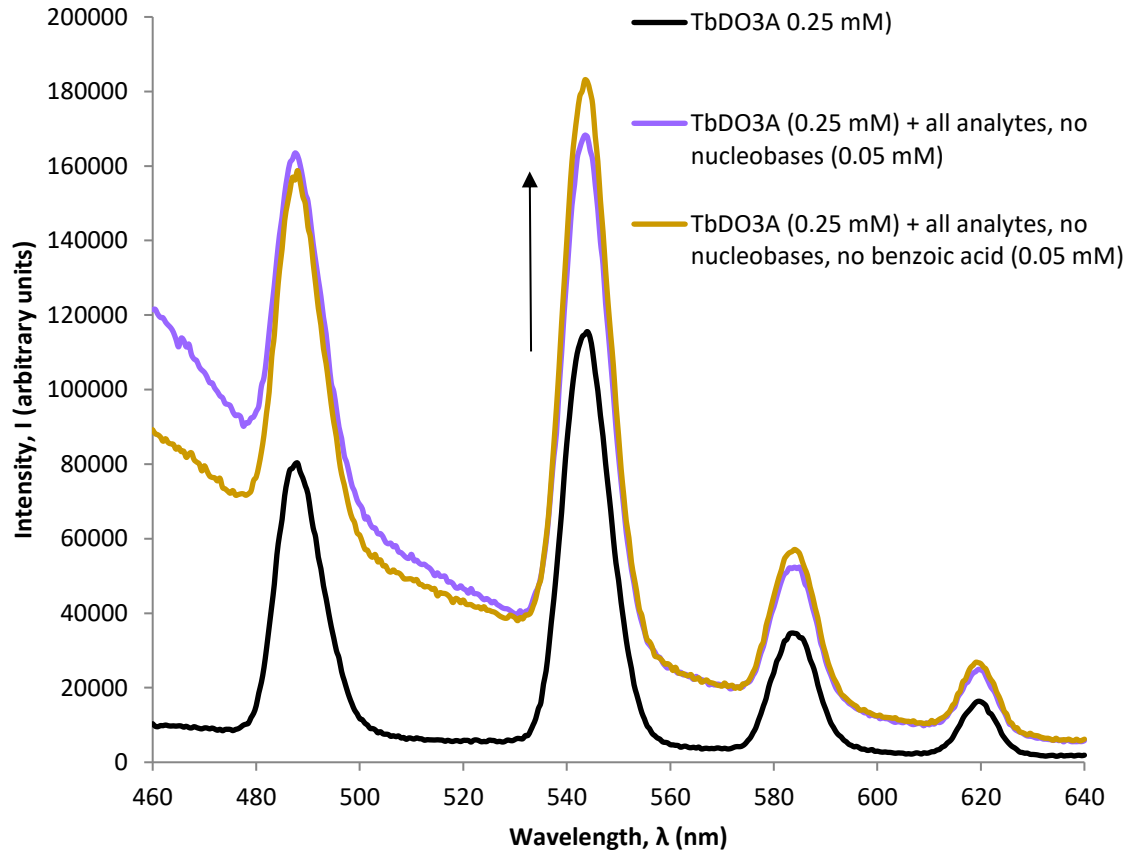

Figure 3.39 Fluorescence spectrum of 0.25 mM [TbDO3A] compared with the fluorescence spectra in the presence of 0.05 mM of all analytes except nucleobases and 0.05 mM of all analytes except nucleobases and benzoic acid(λ_{Ex}=265 nm, acquisition time=0.5 sec, acquisition increment=0.5 nm, excitation and emission slit width=3 nm, pH=5)

Equimolar purine-only and pyrimidine-only mixtures quenched [LnDO3A] fluorescence at equimolar concentrations. [EuDO3A] fluorescent emissions were not well resolved until after dilution 3 (~$6.25x10^{-5}$ M), when either the purine-only or pyrimidine-only mixtures were present (e.g. Figure 3.40). When all nucleobases were combined, europium emissions were detected after the fourth dilution (~$3.13x10^{-5}$ M, Figure 3.41). The resolution of terbium fluorescent emission was tentatively evident after the third dilution of the pyrimidine-only mixtures (~$6.25x10^{-5}$ M, Figure 3.42), and more obviously after the third for the purine-only mixture (~$6.25x10^{-5}$ M, Figure 3.43). When all nucleobases were combined, terbium emissions were only significantly detected after the fourth dilution (~$3.13x10^{-5}$ M, Figure 3.44).

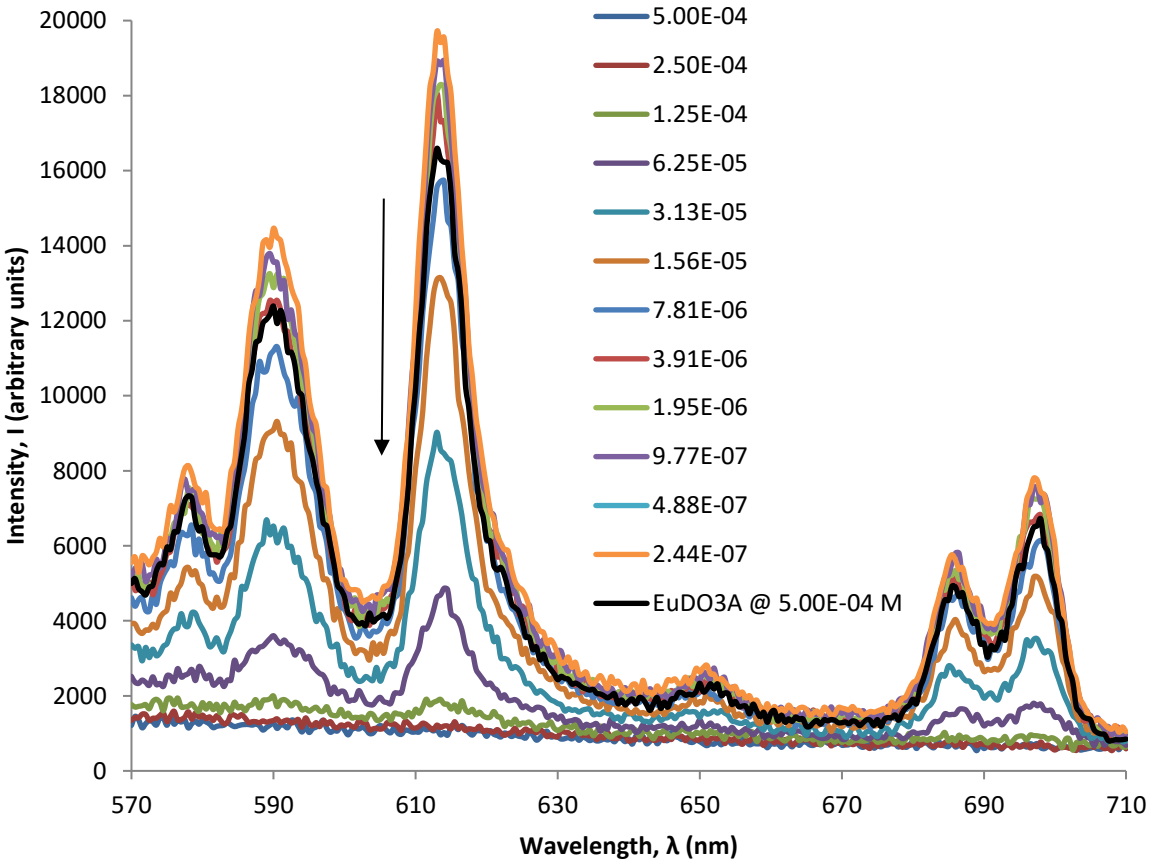

Figure 3.40 Fluorescence spectrum of 0.5 mM [EuDO3A] compared with fluorescence spectra in the presence of a mixture of pyrimidines-only at an initial concentration of 0.5 mM, and then subsequent dilutions (Key – mol dm^{-3} (M)) (λ_{Ex}=265 nm, acquisition time=0.5 sec, acquisition increment=0.5 nm, excitation and emission slit width=3 nm, pH=5)

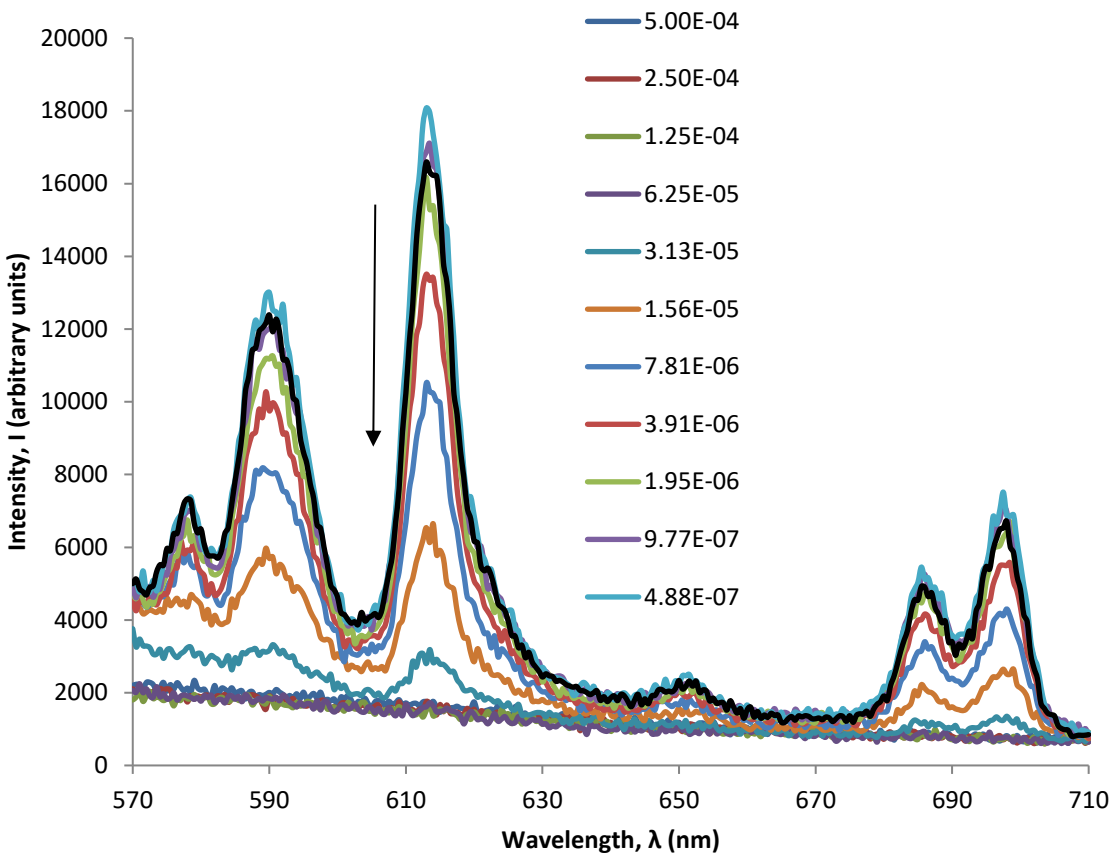

Figure 3.41 Fluorescence spectrum of 0.5 mM [EuDO3A] compared with fluorescence spectra in the presence of a mixture of all nucleobases at an initial concentration of 0.5 mM, and then subsequent dilutions (Key – mol dm^{-3} (M)) (λ_{Ex}=265 nm, acquisition time=0.5 sec, acquisition increment=0.5 nm, excitation and emission slit width=3 nm, pH=5)

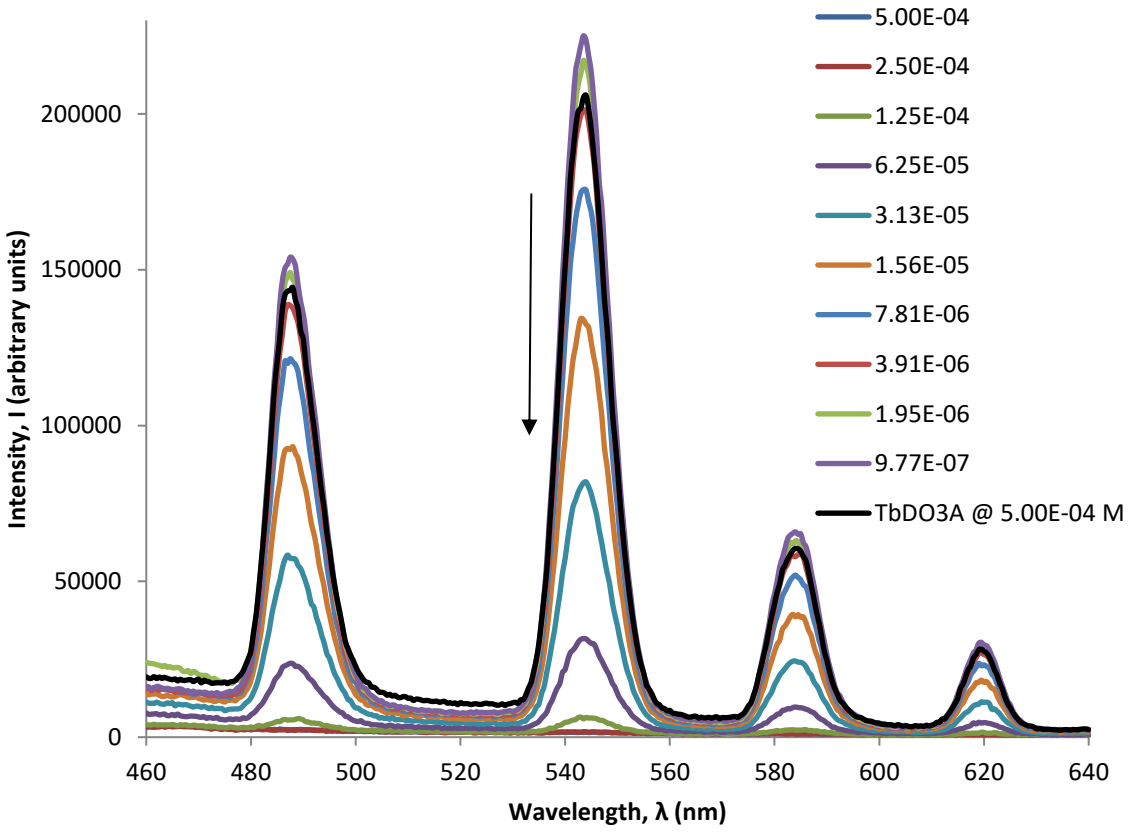

Figure 3.42 Fluorescence spectrum of 0.5 mM [TbDO3A] compared with fluorescence spectra in the presence of a mixture of pyrimidines-only at an initial concentration of 0.5 mM, and then subsequent dilutions (Key – mol dm^{-3} (M)) (λ_{Ex}=265 nm, acquisition time=0.5 sec, acquisition increment=0.5 nm, excitation and emission slit width=3 nm, pH=5)

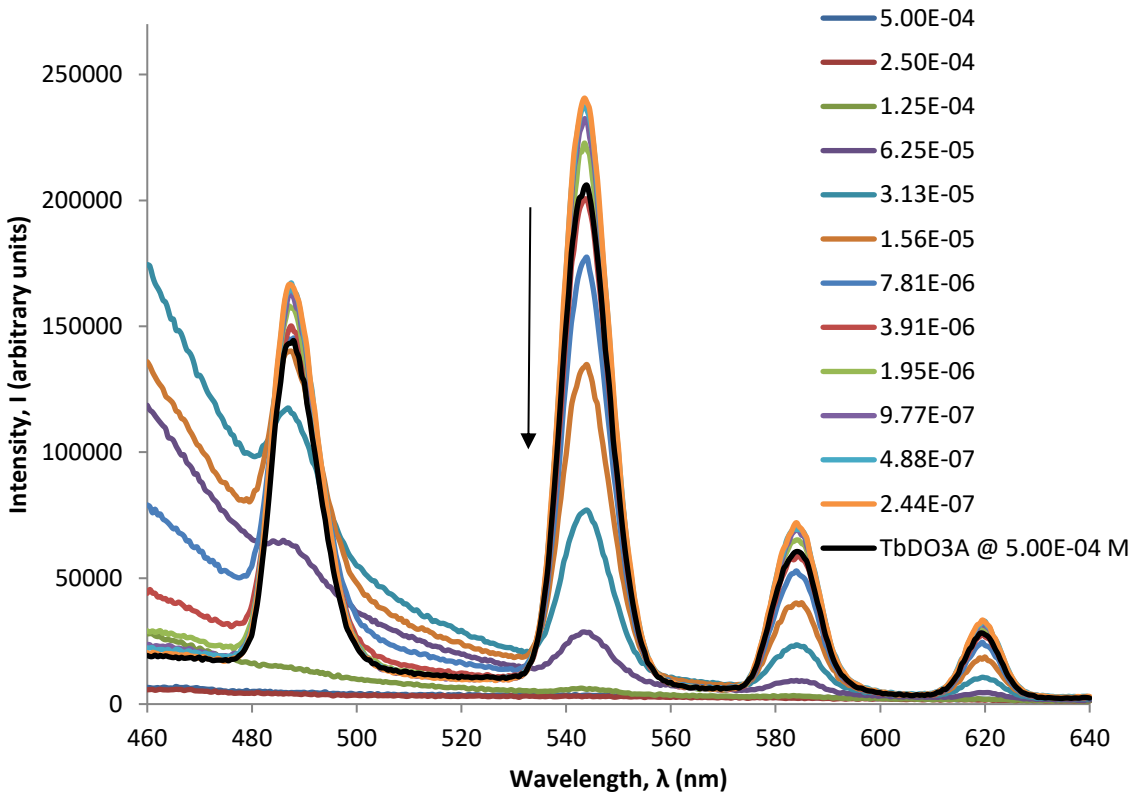

Figure 3.43 Fluorescence spectrum of 0.5 mM [TbDO3A] compared with fluorescence spectra in the presence of a mixture of purines-only at an initial concentration of 0.5 mM, and then subsequent dilutions (Key – mol dm^{-3} (M)) (λ_{Ex}=265 nm, acquisition time=0.5 sec, acquisition increment=0.5 nm, excitation and emission slit width=3 nm, pH=5)

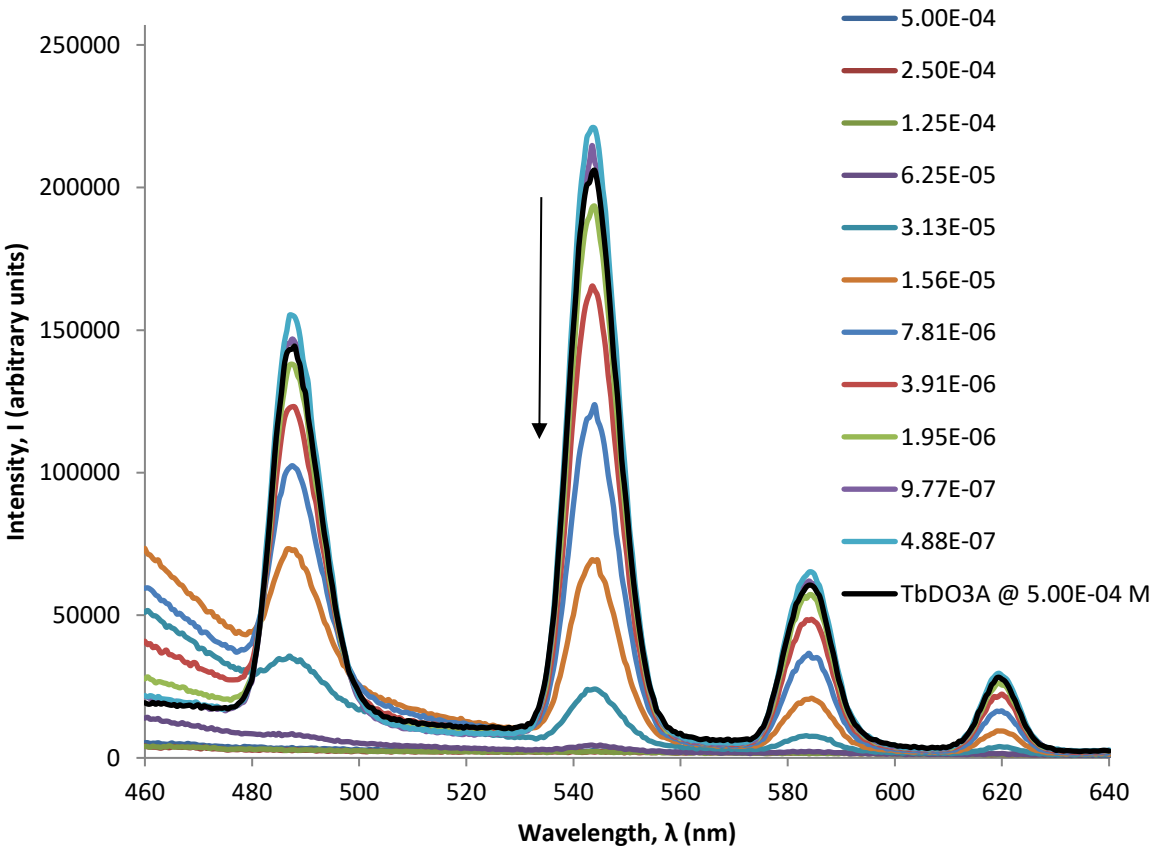

Figure 3.44 Fluorescence spectrum of 0.5 mM [TbDO3A] compared with fluorescence spectra in the presence of a mixture of all nucleobases at an initial concentration of 0.5 mM, and then subsequent dilutions (Key – mol dm^{-3} (M)) (λ_{Ex}=265 nm, acquisition time=0.5 sec, acquisition increment=0.5 nm, excitation and emission slit width=3 nm, pH=5)

When mixtures of purines and pyrimidines (separately) were added to [EuDO3A], lanthanide fluorescence emissions were detected at dilution 3. The same was true for [TbDO3A] in the case of the purine mixture. Resolution of lanthanide fluorescence emissions was only achieved at dilution 4 for [TbDO3A] with the pyrimidine mixture. This suggests that [TbDO3A] is more sensitive to the presence of a mixture of pyrimidines than other nucleobase mixtures. However, when either sensor is applied to mixtures of all nucleobases, resolution of emissions is not achieved until dilution 4. This suggests that the quenching effect of the purines in an equimolar mixture of all nucleobases is dominant.

When the all-analyte mixture was combined with the [LnDO3A] sensor solutions, the lanthanide emission was entirely quenched, with no lanthanide fluorescence detected (Figures 3.45 and 3.46). This response is comparable to the responses recorded for the $[LnDOTA]^-$ assays when they were also combined with the all-analyte mixture, and was proposed to be because of the presence of nucleobases (see Section 3.4).

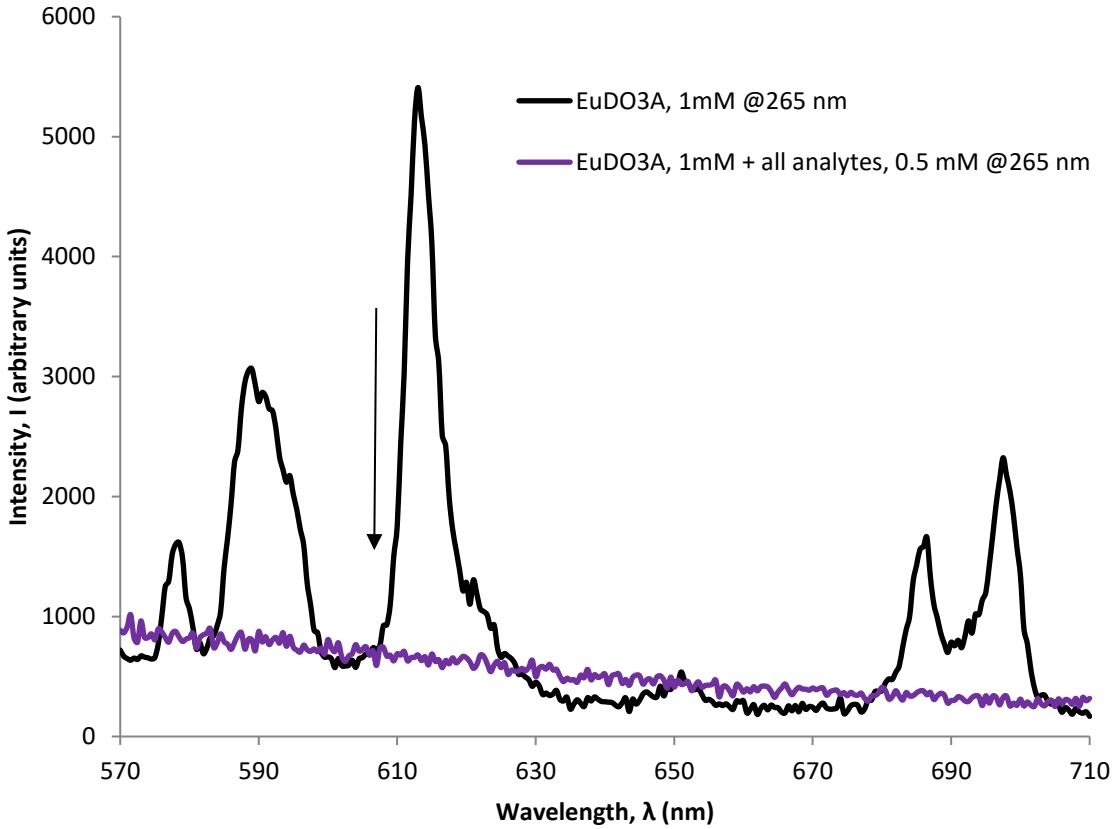

Figure 3.45 Fluorescence spectrum of 1 mM [EuDO3A] compared with fluorescence spectra in the presence of a mixture of all analytes at a concentration of 0.5 mM (λ_{Ex}=265 nm, acquisition time=0.5 sec, acquisition increment=0.5 nm, excitation and emission slit width=3 nm, pH=5)

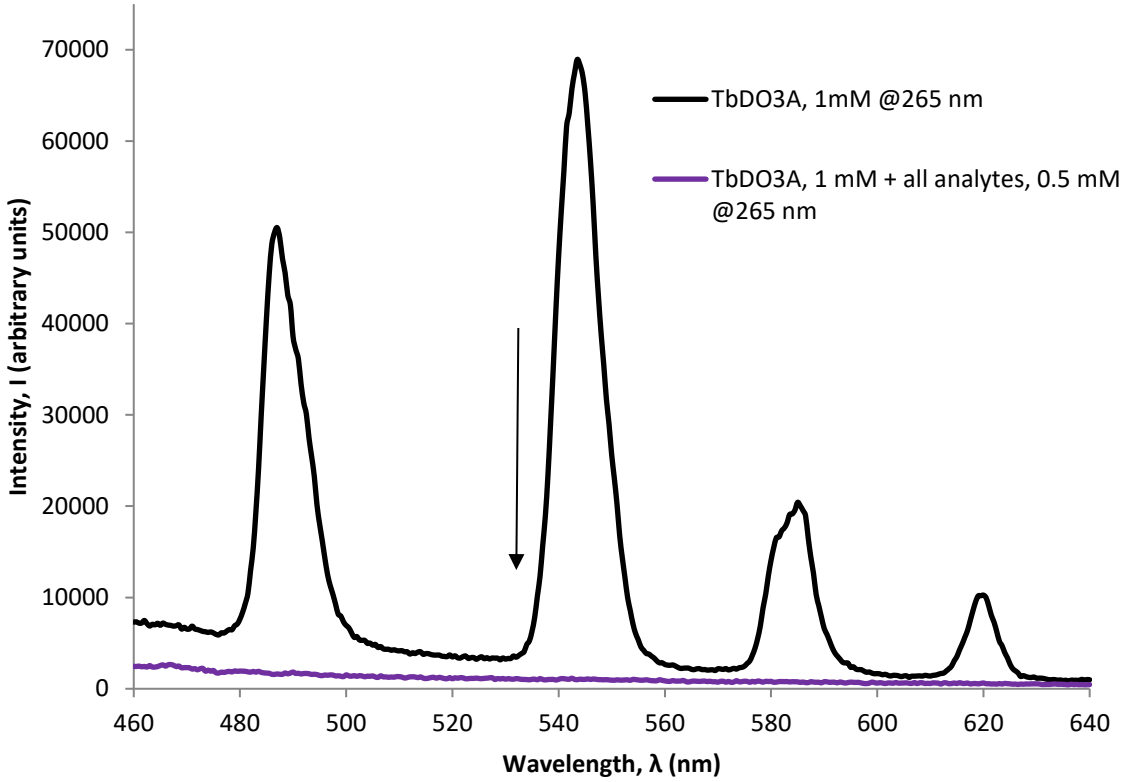

Figure 3.46 Fluorescence spectrum of 1 mM [TbDO3A] compared with fluorescence spectra in the presence of a mixture of all analytes at a concentration of 0.5 mM (λ_{Ex}=265 nm, acquisition time=0.5 sec, acquisition increment=0.5 nm, excitation and emission slit width=3 nm, pH=5)

3.4 Discussion

3.4.1 Sensor-only fluorescence

When chelated to DOTA, lanthanide fluorescent emissions were detected when europium and terbium were directly excited at 397 nm and 378 nm. Indirect excitation of europium and terbium when chelated by of DOTA and DO3A at 265 nm resulted in emissions (Figures 3.9, 3.10, 3.29 and 3.30, respectively) whereby excitation of the carboxylate C=O groups of the ligand takes place, followed by a ligand-metal energy transfer mechanism A comparison of the spectra for europium and terbium when excited at 397 nm and 378 nm, respectively, and then both at 265 nm, when chelated to DOTA, can also be seen in Figures 3.9 and 3.10.

When in aqueous solution, europium spectra indeed exhibit four distinct emissions at ΔJ=1, 2, 3 and 4, where ΔJ=1 has a greater intensity than ΔJ=2, and the transition responsible for ΔJ=4 emission has just one peak, or intensity maximum (Figure 3.3). When chelated to DOTA and DO3A, the transition responsible for europium emissions at ΔJ=0 is sensitised, resulting in better

resolution, and the Δ*J*=4 emission is split into two peaks. When europium is chelated to DO3A, the emission at Δ*J*=2 become more intense than Δ*J*=1, but this was not observed for DOTA-chelated europium; this observation has been reported previously when europium is chelated by other heptadentate ligands (Bruce et al., 2000, Lowe et al., 2001, Rizzo et al., 2009). These modifications to the spectra form are related to the coordination environment of the europium metal centre and can, therefore, be used to give an indication as to how the europium ion is chelated.

However, the form, or shape, of the terbium spectrum remained unchanged; there were four emissions attributed to the Δ*J*=2*,* 1, 0 and -1 transitions and the relative intensities remained the same ($^5D_4 \rightarrow {}^7F_5 > {}^7F_6 > {}^7F_4 > {}^7F_3$) when chelated to either ligand (Figure 3.6). The reason for this is that, unlike the europium ion, terbium is not hypersensitive and as such its electronic energy levels are not perturbed by changes to its coordination environment. This means that coordination about the terbium ion cannot be ascertained by scrutinising changes in the relative intensities of each transition, and would not be expected; only europium is expected to show this (Richardson, 1982).

3.4.2 Sensor response to non-nucleobase analytes

Upon addition to the sensors of non-nucleobase analytes at equimolar concentrations, and excitation at 265 nm, some changes in intensity were observed (Figures 3.11 and 3.13). However, no discernible trend relating to compound class was evident. Intensity changes were most likely caused by small changes in ligand environment, such as slight displacement of water molecules (resulting in a small increase in intensity), minor deformation of ligand shape (which can sensitise or weaken emissions) (Bruce, 2001) or by intrinsic low intensity analyte fluorescence adding to Ln^{3+} fluorescence (resulting in a perceived increase in intensity).

(L)-tyrosine

(*L*)-tyrosine, when added to any of the four lanthanide complexes, resulted in an increase in fluorescence (Figures 3.11, 3.13, 3.31 and 3.32). It is possible that *some* increase in intensity could be attributable to ligand environment perturbances (as described in Section 1.7.1), or by

displacement of coordinated water molecules, thereby reducing their quenching effect (as described in Section 3.3.3). However, in this instance, the increase in intensity may only be perceived and likely to be the result of analyte fluorescence overlapping lanthanide fluorescence. (*L*)-tyrosine is itself intrinsically fluorescent, exhibiting a broad emission spectrum with a maximum intensity at ~466 nm (Figure 3.12, Section 3.2.5). The 'tail end' of this broad emission overlaps with the lanthanide emissions, resulting in these emissions being swamped and, therefore, less well resolved.

This is a particular problem for complexes using terbium, since terbium's most intense emissions are at Δ*J*=2 (~493 nm) and Δ*J*=1 (543 nm) (e.g. Figure 3.10). Likewise, europium emissions at Δ*J*=0 (~578 nm), Δ*J*=1 (~590 nm) and Δ*J*=2 (~614 nm) (e.g. Figure 3.9) are overlapped. So, the increase in intensity observed here may be an artefact of the intrinsic fluorescence of (*L*)-tyrosine, rather than a Ln^{3+} fluorescence response affected by its interaction with the sensor. Thus, if (*L*)-tyrosine, or any other highly fluorescent analyte that strongly fluoresces in the range in which the sensor fluoresces, is present, its intrinsic fluorescence could swamp the emissions originating from the sensor, negating the sensor's utility. The broad (*L*)-tyrosine intrinsic fluorescence spectrum does not overlap all lanthanide emissions, however, meaning those emissions not swamped could still be useful to detect organic analytes.

It is known that meteorite solvent extracts contain intrinsically fluorescent molecules (Section 1.6.2) in addition to those tested here, and those molecules also fluoresce over a broad range of wavelengths (see Table 1.1, Section 1.6.2). Like (*L*)-tyrosine, these molecules may similarly obscure the sensor emissions, rendering the sensor useless. However, the fluorescent lifetime of the intrinsically fluorescent organic components is orders of magnitude shorter than that of the lanthanide fluorescent lifetime, and as such, would not affect the effectiveness of the sensor if time-gating were used (see Section 1.7.2).

Benzoic acid

As described previously, the coordination and ligand environment of Eu^{3+} may be determined by the relative emission intensities for given transitions; when eight coordinate (e.g. chelated to DOTA) the Δ*J*=1 emission is more intense than the Δ*J*=2 (Figure 3.9), and when seven coordinated (e.g. chelated to DO3A), the emission intensity of the Δ*J*=2 is greater than that of the Δ*J*=1 emission (Figure 3.29). Furthermore, the intensity of the emissions may be increased by displacement of fluorescence-quenching water molecules from the lanthanide coordination sphere. However, it is the fact that changes in the coordination environment of the lanthanide ion can determine the sensitisation and, therefore, relative intensity, of given transitions that is important for the interpretation of the results for the application of the sensors to benzoic acid.

The addition of benzoic acid to $[LnDOTA]^-$ and [LnDO3A] resulted in a marked increase in Ln^{3+} fluorescence emission and it is likely that the mechanism causing this is twofold. First, the carboxylate moiety of the benzoic acid coordinates with the metal centre, and the benzene ring, or benzyl moiety, absorbs excitation energy, acting as a light harvesting antenna. The energy collected by the benzyl group is delivered to the Ln^{3+} via the carbonyl group (Butler and Parker, 2013) thereby increasing total energy input and subsequently increasing emission intensity. Secondly, coordination of the carboxylate moiety of benzoic acid displaces water molecules which, when coordinated to the lanthanide metal-centre, quench fluorescent emissions via absorption of photons by O-H bond stretching, as described above. Displacement of these water molecules, as a result of the coordination of benzoic acid, from the lanthanide coordination sphere thus increases lanthanide fluorescence (Beeby et al., 1999).

Sensitisation of emissions by displacement of water molecules alone would be unlikely to result in the magnitude of fluorescent yield seen here. Indeed, coordination of benzoic acid, acting as an antenna, is likely to be the most significant factor influencing the increase in intensity.

Furthermore, when the complexes are mixed with an equimolar concentration of benzoic acid, the relative intensity of the octadentate europium emissions, where Δ*J*=1>Δ*J*=2, (Figure 3.47,

black line) is reversed, such that the Δ*J*=2 emission is more intense than the Δ*J*=1 emission (Figure 3.47, orange line). Likewise, when an equimolar concentration of benzoic acid is mixed with the heptadentate [EuDO3A] complex, where the Δ*J*=1 transition is less intense than the Δ*J*=2 (Figure 3.48, black line), the Δ*J*=1 is now more intense than the Δ*J*=2 (Figure 3.48, orange line).

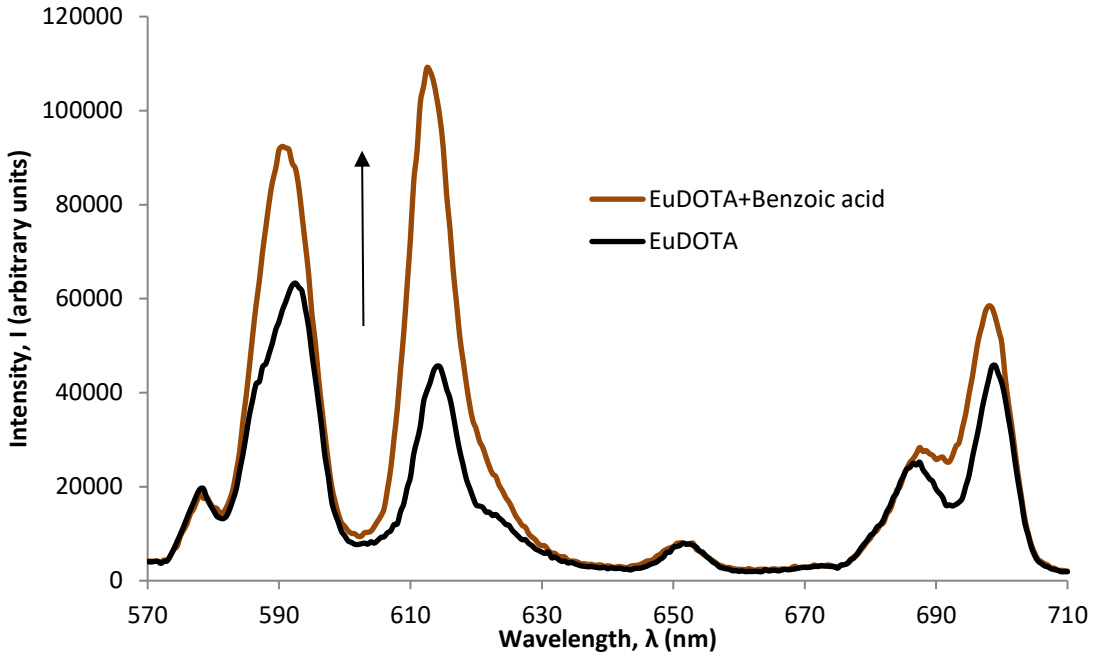

Figure 3.47 Fluorescence emissions of 0.5 mM $[EuDOTA]^-$ compared with emissions when 0.5 mM $[EuDOTA]^-$ was in the presence of 0.5 mM of benzoic acid (λ_{Ex}=265 nm, acquisition time=0.5 sec, acquisition increment=0.5 nm, excitation and emission slit width=3 nm, pH=5)

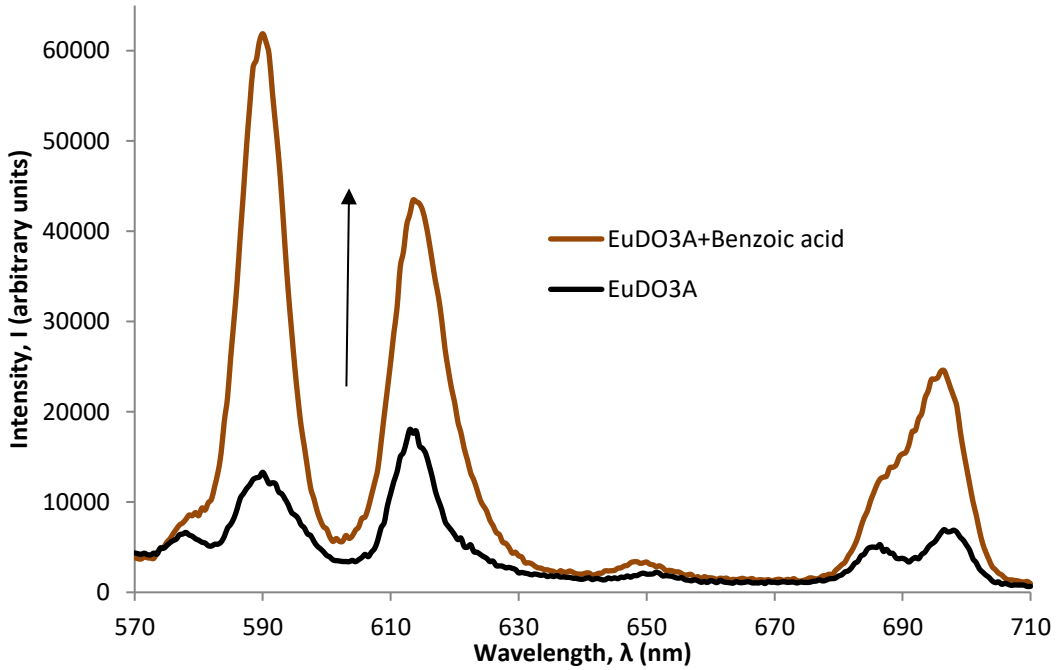

Figure 3.48 Fluorescence emissions of 0.5 mM [EuDO3A] compared with emissions when 0.5 mM [EuDO3A] was in the presence of 0.5 mM benzoic acid (λ_{Ex}=265 nm, acquisition time=0.5 sec, acquisition increment=0.5 nm, excitation and emission slit width=3 nm, pH=5)

It may be that the similarities in relative emission intensities observed for $[EuDOTA]^-$ without benzoic acid, and those recorded for [EuDO3A] with benzoic acid, arise because they have very similar coordination environments; $[EuDOTA]^-$ is eight coordinate about Eu^{3+} with one water molecule coordinated to the metal centre, while [EuDO3A] is seven coordinate with two water molecules coordinated. In the presence of benzoic acid, the carboxylate moiety of benzoic acid coordinates and, in doing so, displaces one water molecule, effectively forming an eight coordinate ligand environment with one water molecule and producing the same spectral shape as $[EuDOTA]^-$.

It is also possible that the chelation of benzoic acid can alter the shape of the ligand in such a way that certain transitions are more favourable and the intensity of those emissions therefore increases. These observations imply that the europium and terbium complexes of DOTA and DO3A can detect benzoic acid by virtue of an increase in fluorescent intensity. However, the implications for the europium complexes with DOTA and DO3A, alone, suggest that identification of benzoic acid is unambiguous. Not only does the fluorescent intensity of europium increase, but also the shape of the spectrum changes such that coordination about the metal centre can be determined and assigned to the presence of benzoic acid, *in aquo*.

In order to determine or distinguish which mechanism(s) are in effect, the number of bound water molecules, q, can be calculated (see Section 3.3.3) before and after the addition of benzoic acid. If the value of q changes then water molecules must be being displaced by coordination of benzoic acid, however if the q value remains unaltered then the increase in intensity can only be caused by a change in coordination environment and antenna effect without displacement of water molecules.

Since this work has shown that the sensors used can detect the presence of benzoic acid *via* the mechanism described, i.e. coordination by the carboxylate resulting in displacement of water molecules in combination with the sensitisation of transitions *via* the antenna effect, it is probable that the sensors may also be able to detect any molecule with aromatic carboxylic acid structure

in a sample. Detection of these species in carbonaceous chondrites has been achieved by liberation by thermochemolysis then Py-GC-MS, however this is not a straightforward analysis; they become defunctionalised during pyrolysis, or are simply not GC-amenable (Watson et al., 2005). Free aromatic carboxylic acids have also been identified in solvent extracts of carbonaceous chondrites by GC-MS analysis (Naraoka et al., 1999, Martins et al., 2006, Hilts et al., 2014) and GC-IR-MS and FTIR (Hilts et al., 2014). These characterisation techniques generally require chemical work-up, i.e. derivatisation of the analytes, before analysis, and therefore are cumbersome and unusable in a potential field setting. In light of the limitations of these previous studies, the application of sensors tested herein could, therefore, provide an unambiguous, rapid and facile method for their detection.

Importantly, it has been suggested that benzoic acid may be a potential prebiotic molecule, involved in the synthesis of complex organic molecules *via* 'on-water' reaction (as opposed to 'in-water' reactions) (Kolb, 2012). This means that DOTA- and DO3A-based lanthanide sensors, such as those tested in this thesis, could be further developed for use on future life-detection missions targeting benzoic acid, and its derivatives.

3.4.3 Sensor response to nucleobases

All individual nucleobases quenched lanthanide fluorescence when mixed with the complexes at equimolar concentrations. Adenine was shown to increase fluorescent intensity but only when mixed with lanthanide complexes of DO3A, not those of DOTA. However, the form of the europium spectrum did not alter, i.e. the relative intensities of the ΔJ=1 and the ΔJ=2 emissions remained unchanged (Figure 3.49). As expected, the form of the terbium spectrum also remained unchanged.

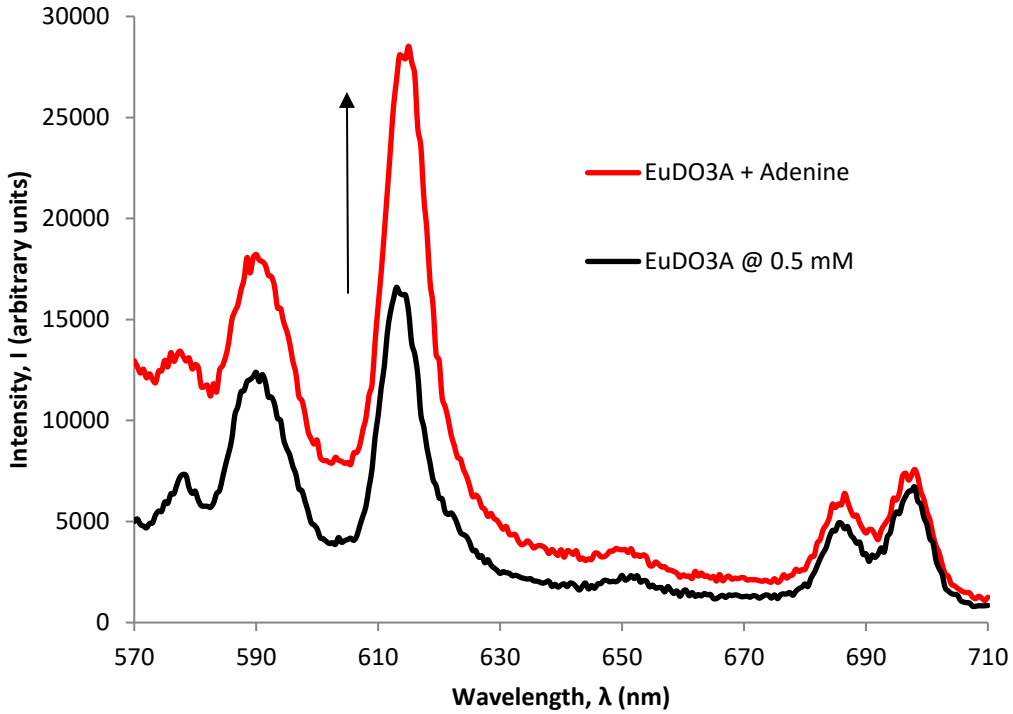

Figure 3.49 Fluorescence emissions of 0.5 mM [EuDO3A] compared with emissions when 0.5 mM $[EuDOTA]^-$ was in the presence of 0.5 mM of adenine (λ_{Ex}=265 nm, acquisition time=0.5 sec, acquisition increment=0.5 nm, excitation and emission slit width=3 nm, pH=5)

Since the presence of nucleobases, both individually and within a complex mixture, quench the fluorescence of the $[LnDOTA]^-$ complexes, the utility of the [LnDOTA] sensors tested is compromised because they become undetectable. Likewise, other than in the presence of adenine, utility of [LnDO3A] complexes as sensors is also rendered moot, for the same reason.

Although the magnitude of the increase in intensity observed when [EuDO3A] is applied to adenine is not as great as that with benzoic acid, the fact that the relative intensities of the ΔJ=1 and the ΔJ=2 emissions remains the same in the presence of adenine permits distinction between these two analytes. Therefore, if [EuDO3A], for example, were applied to an extract from a carbonaceous chondrite, an observed increase in intensity may indicate the presence of either adenine or benzoic acid, or both molecules; scrutiny of the relative intensity of the ΔJ=1 and the ΔJ=2 emissions may be used to distinguish which is present.

It has been reported that nucleosides and nucleotides can quench fluorescence of fluorescent dyes by photo-induced electron transfer (PET) (Seidel et al., 1996, Torimura et al., 2001, Marquez et al., 2003). The likelihood of this is dependent upon relative oxidation and reduction potentials

of the fluorophore and the analyte (Doose et al., 2009), in this case the Ln^{3+} complex and the nucleobase, respectively, either of which could be the electron donor or acceptor. There are two possible mechanisms for this to occur: i) static quenching - charge/electron transfer quenching of the Ln^{3+} by an electron rich donor (e.g. a nucleobase) (Poole et al., 2005) and ii) dynamic quenching. In the latter case, when an excited Ln^{3+} complex transfers its energy to ground state nucleobase via a physical collision, the excited nucleobase loses energy via non-radiative, vibrational, relaxation to the solvent molecules, in this case water, returning to its ground state (Poole et al., 2005).

An explanation to account for the quenching by other nucleobases is that of energy transfer. It is possible that the lanthanide complexes act as an energy donor and the nucleobase molecules act as an energy acceptor, thus quenching the fluorescence (Horrocks and Albin, 1984). The lanthanide complex solution then exhibits sensitised emissions by virtue of ligand-metal energy transfer, where the ligand acts as the energy donor and the lanthanide acts as the energy acceptor; resulting in the lanthanide fluorescence emissions observed. When the nucleobases are added, they become the energy acceptor instead and thus absorb the energy released by the ligand-sensitised lanthanide. For this to occur, the energy required to promote nucleobase electrons to an excited energy level must be in close proximity to the excited state energy levels of the lanthanide. Thus, when excited lanthanide electrons release energy as they return to their ground state, the nucleobases absorb that energy, themselves becoming electronically excited and quenching lanthanide fluorescence in the process. As the excited nucleobase molecules return to their ground state, the energy they had absorbed is released non-radiatively via the solvent molecules, in this case, water.

An alternative, more complex, explanation to account for the quenching of fluorescence observed is that of static quenching, whereby the nucleobases are firstly electronically excited by the irradiating energy, *hv* (Equation 3.2). In order to return to their ground state, an electron is transferred to, and subsequently reduces, the Eu^{3+}, which is fluorescent, to Eu^{2+}. When chelated in this system and *in aquo*, Eu^{2+} is not fluorescent (Equation 3.3).

$$NB + hv \rightarrow NB^* \quad \text{Equation 3.2}$$

$$NB^* + 1e^- + Ln^{3+} \rightarrow NB + Ln^{2+} \quad \text{Equation 3.3}$$

However, previous work has shown that under some conditions, when directly excited, Eu^{2+} does exhibit fluorescence but only when Eu^{2+} is incorporated into materials and crystal structures ('doped') in order to stabilise it and protect it from oxidation (Tsuboi et al., 1998, Saradhi and Varadaraju, 2006). Under the highly oxidising aqueous conditions described in experiments conducted in this thesis, Eu^{2+} cannot exist and so an absence of Eu^{2+} fluorescence is not unexpected. Furthermore, in this thesis, Eu^{3+} was indirectly excited, rather than directly excited (Tsuboi et al., 1998, Saradhi and Varadaraju, 2006), so cannot fluoresce via the same mechanism.

Data presented in this chapter have shown that fluorescence returns as nucleobase concentration decreases, likely to be because, *ipso facto*, the quantity of available electrons for transference is functionally reduced. This suggests the europium oxidation state reduction must be reversible, i.e. Eu^{2+} is oxidised back to Eu^{3+}. This is to be expected since Eu^{2+} is highly oxidisable, *in aquo*.

The free energy of the system, $\Delta G°$ (Equation 3.4) (calculated using the number of moles of electrons transferred in the reaction, n, the Faraday constant, F, given as 96485 C mol^{-1}, and the standard cell potential of the reaction, *E°*), provides information regarding the likelihood of a reaction taking place. $\Delta G°$ can therefore be calculated for the processes that may be occurring here by using the one-electron redox potential for the nucleobases (one half of the reaction, or half-cell, Equation 3.5) and the redox potential for the Ln^{3+}/Ln^{2+} half-cell (the other half of the reaction, or half-cell, Equation 3.6).

$$\Delta G° = -nFE^o \quad \text{Equation 3.4}$$

$$NB^* \rightarrow NB + 1e^- \quad \text{Equation 3.5}$$

$$Ln^{3+} + 1e^- \rightarrow Ln^{2+} \quad \text{Equation 3.6}$$

In order to calculate *E°*, the half cells must be added together (Equation 3.7).

$$E^o = E_{red} + E_{ox} \quad \text{Equation 3.7}$$

In order to validate the suggestion that PET is the mechanism responsible for the observations recorded, one-electron redox potential data was obtained from the literature (Jovanovic and

Simic, 1986) for a selection of nucleobases used in this study, in order to calculate the free energy and, therefore, the theoretical probability of PET in each case. Table 3.3 provides data for the Eu^{3+}/Eu^{2+}||nucleobase and Tb^{3+}/Tb^{2+}||nucleobase systems. The redox potential for Eu^{3+}/Eu^{2+} is -0.36 V (Ferro and De Battisti, 2002) and -3.47 V for Tb^{3+}/Tb^{2+} (Morss, 1976). For a reaction to be favourable, the calculated value of ΔG should be negative.

Nucleobase	**1 electron redox potential (V)**	**Calculated E° (Eu system) (V)**	**Calculated E° (Tb system) (V)**	**ΔG (For PET Eu^{3+}/Eu^{2+} reaction) (kJ mol^{-1})**	**ΔG (For PET Tb^{3+}/Tb^{2+} reaction) (kJ mol^{-1})**
Uracil	0.88	0.52	-2.59	-50.1722	249.8962
Cytosine	0.81	0.45	-2.66	-43.4183	256.6501
Thymine	0.78	0.42	-2.69	-40.5237	259.5447
Adenine	0.75	0.39	-2.72	-37.6292	262.4392
Hypoxanthine	0.74	0.38	-2.73	-36.6643	263.4041
Guanine	0.63	0.27	-2.84	-26.0510	274.0174

Table 3.3 ΔG is calculated for the Eu^{3+}/Eu^{2+}||nucleobase and the Tb^{3+}/Tb^{2+}||nucleobase systems. The redox potential for Eu^{3+}/Eu^{2+} and Tb^{3+}/Tb^{2+} is -0.36 V (Ferro and De Battisti, 2002) and -3.47 V (Morss, 1976) respectively.

According to Table 3.3, PET is a viable mechanism to explain observations made with the Eu^{3+}/Eu^{2+}||nucleobase system, since calculated ΔG is negative. However, Tb^{3+}/Tb^{2+}||nucleobase data suggests the reaction is not favourable, with ΔG values between ~250 and ~275 kJ mol^{-1}. However, in all cases, observations, made when comparing effects of individual and complex mixtures of nucleobases on fluorescence of both Ln^{3+} complexes, are identical, implying the mechanisms responsible are the same and cannot be down to PET. Hence, the mechanism causing the quenching of fluorescence in the presence of nucleobases may be that first described, i.e. the nucleobases are electronically excited by the sensitised lanthanides which quench fluorescence in the process. To elucidate the possible mechanism further, lifetime measurements and q values could be found to determine if water molecules are displaced and the nature of the complex-analyte interactions (see Section 3.3.3), but this was not attempted here.

Nucleobase analytes reduced Ln^{3+} fluorescence to almost zero when mixed at equimolar concentrations, with the exception of adenine. Adenine quenching is not as efficient when the Ln^{3+} is chelated to DOTA (some fluorescence is detectable) compared to when chelated to DO3A (florescent intensity is markedly increased). Why adenine should increase [LnDO3A] fluorescence so markedly when the other nucleobases cause complete quenching, especially considering it has

virtually the same redox potential as all the other nucleobases (see above, and Table 3.3) (Jovanovic and Simic, 1986), is not clear. There is nothing remarkable about its structure that would make it more likely to coordinate than the other nucleobases. When present in a mixture of all-nucleobases, and in a purine-only mixture, the increase in intensity afforded by adenine is no longer detectable meaning that [LnDO3A] may be a sensor for adenine but only when adenine is the only nucleobase present in a sample. This is unfortunate, since it is known that extracts from carbonaceous chondrites contain a vast array of compounds (Section 1.3.1) and, therefore, it is certain that adenine would not be the only compound present.

Importantly, adenine is seen as a prebiotic molecule; a potentially important target for life detection missions since it is one of the base pairs present in DNA and RNA and is therefore present in all living organisms. Its detection could imply the possibility of the development of life, as well as a biomarker, where its detection could indicate the possibility of the past or present existence of life (Aerts et al., 2014). Facile detection of adenine is of great importance, specifically in the context of planetary exploration (Aerts et al., 2014), and may help elucidate how complex molecules such as RNA may be formed on planetary surfaces in the presence of water (Cafferty et al., 2016). Although unlikely to be useable in an organic-rich environment, the sensors tested here may present opportunities for detection of adenine in environments where organic matter is low, e.g. on Mars. The implication that [LnDO3A] may be able to identify the presence of adenine by a simple process of isolation and fluorimetry suggests that it could be used as a sensor as part of an extinct or extant life-detection experiment incorporated (similar to the 'lab-on-a-chip' methodology) on board a planetary lander or rover (e.g. Sims et al. 2004).

Although this study has shown that adenine alone cannot be detected when in a complex mixture of standard organic compounds (just-purines, all-nucleobases or all-analytes) using [LnDO3A], [LnDO3A] may still be employed to identify the presence of adenine if nucleobases are separated from a solvent extract within a laboratory environment. Techniques to separate nucleobases from extracts have been employed using activated charcoal and the individual nucleobases isolated by ion-exchange techniques (e.g. Martins et al., 2008). Nucleobases have been characterised using

convoluted analytical methodologies that often require complex chemical work-up in order to make them amenable to detection by complicated instrumentation, e.g. GC-QMS (Martins et al. 2008), or by techniques that do not directly identify the analytes, only infer, e.g. LC-MS (Callahan et al., 2011). [LnDO3A] may then be applied to each fraction; the isolated nucleobase fraction that does not quench fluorescence may then be identified as adenine. However, this makes the assumption that the range of nucleobases present in such a sample are as limited as those used here, since others may also sensitise fluorescence (see Chapter 6).

3.4.4 Sensor response to complex mixtures of analytes

The addition of the mixture of all non-nucleobase analytes did not have an appreciable effect on fluorescence intensity for any sensor when compared to the lanthanide complex emission spectra, regardless of whether benzoic acid was present or not. From these results, a number of hypotheses can be drawn to explain these observations.

It is possible that the ligand pendant arms preclude sufficient proximity between analyte and metal-centre, preventing direct interactions. It has been shown that steric hindrance caused by bulky ligands can obstruct the path of molecules such as water (Rodríguez-Rodríguez et al., 2012). Electrostatic repulsion can also influence certain interactions (Snowden and Anslyn, 1999), such as those between ligand and analyte, e.g. the high localised electron density of the analytes' structures, and the full negative charges of the carboxylate groups, could be sufficiently repulsive. A further possible explanation for the lack of a detectable change in fluorescence is that there may be a minimum analyte concentration that can affect the sensor, i.e. a limit of detection with an analyte concentration insufficient to effectively alter fluorescent emission intensity of the lanthanide. When a mixture of all analytes was mixed with the sensors, such that the sensors were present at 1 mM and all analytes present at a concentration of 0.5 mM, the lanthanide emission intensity was completely quenched, with no indicative lanthanide emissions detected.

Complex mixtures of all nucleobases, however, quenched fluorescent emissions in the same way as when tested individually. Since the sensor is intended to be deployed to identify analytes in

meteorite samples, if the sensor cannot detect analyte concentrations considerably below 0.5 mM, as is indicated by the analyses carried out upon application of the sensors to nucleobases in this work (see Section 3.3.5), then the sensor would certainly not be suitable for this application.

Concentrations of individual organic classes identified in the solvent extractable fraction of carbonaceous chondrites are often in the ppm to ppb range (Pearson, 2010). Concentrations (in mM) of some classes of these compounds identified in the Murchison meteorite, relevant to the organic analytes selected to test the sensors in this study, are given in Table 3.4.

Class of organic molecules	**Abundance (mM)**	**Reference**
Amino acids	60	(Cronin et al., 1988)
Monocarboxylic acids	332	(Yuen et al., 1984, Lawless and Yuen, 1979)
Dicarboxylic acids	25.7	(Lawless et al., 1974)
Hydroxycarboxylic acids	14.6	(Peltzer et al., 1984)
Purines	1.2	(Stoks and Schwartz, 1982)
Pyrimidines	0.06	(Stoks and Schwartz, 1979)

Table 3.4 Abundances of classes of organic compounds identified in Murchison, from which representatives were selected as standard analytes to test the sensor responses

With the exception of the nucleobases that quenched fluorescence, and adenine which sensitised emissions, the presence of organic analytes representative of compounds shown in Table 3.4 did not illicit a sensor response. However, that does not mean that they do not play a role; they may prevent the interaction of molecules that could result in a response. Therefore, if an extract contains a high relative concentration of components that may hinder the interactions of an analyte that would otherwise be detected by the sensor, then those molecules may not be identified.

The unequivocal response to the presence of benzoic acid, and the likely mechanism by which that response is achieved, suggest that structurally similar molecules may also invoke a comparable response. Several benzoic acid molecules have been identified in the Murchison meteorite by Martins et al., (2006), the abundances of which are given in Table 3.5.

Class and individual aromatic acids	Abundance (mM)
Benzoic acid	$4.7x10^{-2}$
2-methylbenzoic acid (+phenylacetic acid)	$1.4x10^{-3}$
3-methylbenzoic acid	$8x10^{-4}$
4-methylbenzoic acid	$8x10^{-4}$
2-hydroxybenzoic acid + 3-hydroxybenzoic acid	$4.4x10^{-2}$
4-hydroxybenzoic acid	$2.4x10^{-2}$
Methylhydroxybenzoic acids	$4.0x10^{-2}$
1,2-phthalic acid	$3.2x10^{-1}$
1,3-phthalic acid	$4.6x10^{-2}$
1,4-phthalic acid	$5.4x10^{-1}$
Methylphthalic acid	$33x10^{-2}$

Table 3.5 Abundances of aromatic carboxylic acids identified in Murchison (Martins et al., 2006).

Therefore, the implication, based upon sensor responses observed when the sensors were applied to the all-analyte mixture, is that for the sensor to detect benzoic acid (or its derivatives) it may be required to be in excess, or that other analytes should be absent. These are unlikely scenarios based upon the compound class data presented in Tables 3.2 and 3.3 for carbonaceous chondrites. Thus, to detect benzoic acids, the extract must undergo a process of separation, e.g. chromatography, in order to use the sensor effectively.

When irradiated at wavelengths known to be in the range that excites the delocalised pi electrons, Ln^{3+} fluorescence was observed. These wavelengths are of insufficient energy to promote Ln^{3+} electrons to higher electronic energy levels within the Ln atom directly, so a different mechanism of energy transfer, leading to promotion and subsequent fluorescence emission, must be taking place. It is thought that delocalised π electrons, in this case associated with the carbonyl functionality of the ligand ethanoate moieties (and possibly to a lesser extent the lone pair electrons residing on the nitrogen atoms of the cyclen ring), absorb UV wavelengths (Sabbatini et al., 1993, Bünzli and Eliseeva, 2011). The electronically promoted ligand rapidly decays to the lowest triplet state at which point intersystem energy transfer takes place, where the energy stored by excited ligand electrons 'siphon' across to a resonant energy state of the

Ln^{3+}. This then returns to its ground state via emission of photons and, in doing so, produces indicative Ln^{3+} fluorescence (de Mesquita et al., 1997). This is a ligand-to-metal energy transfer and is described as the antenna effect (Section 1.7.5).

When analytes were added to the lanthanide complex solutions, and irradiated at lanthanide direct excitation wavelengths (Eu – 397 nm, Tb – 378 nm), there were no determinable alterations to the emissions of the lanthanide complexes. Changes to the lanthanide fluorescence emissions were detected when some sensor/analytes mixtures (e.g. nucleobases and carboxylic acids), were instead irradiated at 265 nm. It is therefore likely that sensor responses are reliant upon analytes themselves absorbing excitation energy in order to invoke quenching or sensitisation of the lanthanide emission, and the extent of this is dependent on the analyte. It is therefore the response of the analyte to excitation and the form of interaction with the lanthanide metal-centre that determines whether a response will be observed in the sensor.

3.4.5 Utility of $[LnDOTA]^-$ and [LnDO3A] as sensors

All the experiments in this chapter have been undertaken to ascertain the suitability of lanthanide complexes of DOTA and DO3A for use as sensors for a selection of analogue organic analytes chosen from molecules identified in a solvent soluble extract of the Murchison meteorite. Results suggest all four complexes used in this study can be used as sensors for the nucleobases chosen, by virtue of the quenching effect they have on fluorescent intensity. However, a sensor which 'turns off' is not as useful as one which 'turns on'. Moreover, the quenching is comparable for all the chosen nucleobases and so cannot differentiate between them. Only europium and terbium DO3A complexes 'switch on' in the presence of adenine. Unfortunately, when in a complex mixture of nucleobases, the sensitising effect that adenine invokes is no longer detectable. This indicates that lanthanide DO3A complexes are not suitable for sensing adenine within complex mixtures.

The results of this work also indicate that none of the lanthanide complexes tested can be used to unambiguously identify the non-nucleobase molecules selected for these assays. Any changes in

intensity observed could not be confidently attributed to analyte/sensor interaction; the observed alterations to sensor fluorescence were comparable for each analyte used. The exception to this was the effect the presence of benzoic acid had on emissions. However, benzoic acid sensitises fluorescent emissions when only benzoic acid is present, not when within a complex mixture (when all analytes are present at equimolar concentrations).

In a solvent extract of a carbonaceous chondrite, the relative abundance of each analyte, or class of analytes, will not be equimolar. It has been shown that lanthanide sensitisation may be achieved by coordination of a carboxylate moiety combined with a light harvesting mechanism afforded by a phenyl group. It is therefore reasonable to suggest that any molecule with a carboxylate moiety, and a group capable of acting as an antenna, may similarly invoke a sensitisation of the lanthanide fluorescence. It is known that carbonaceous chondrites contain functionalised polyaromatic hydrocarbons in high abundance (Messenger et al., 1998, Martins et al., 2006, Le Guillou et al., 2014, Huang et al., 2015). It is therefore possible that these sensors may be used to ascertain if a solvent extract contains these analytes.

Furthermore, by submitting a total extract to procedures that can separate classes of compound, and then further isolate individual components from within those classes, the sensors may be able to identify the presence of specific analytes e.g. benzoic acid (or other aromatic acids) and adenine. This process can be achieved not just in the laboratory but could also be carried out 'in the field' as part of a 'lab-on-a-chip'-type experiment on board a life detection mission. Also, should methodology be developed for the application of these sensors for *in situ* sample analysis, it could be possible to locate and identify adenine and benzoic acid, or any aromatic-carboxylate molecule, using $[LnDOTA]^-$ and [LnDO3A] because they may result in localised sensitised lanthanide fluorescence.

3.5 Conclusion

Before the utility of a fluorescent sensor can determined, consideration must be given to what the sensor is required to do. The purpose of this research was to develop sensors which can identify organic molecules extracted from a meteorite sample.

So, in order for the sensor to be effective, there must be a response invoked in the sensor by the analyte. The sensors developed and used in this study have fluorescent properties which emit light with known emission wavelengths, with a measurable intensity for a given concentration of the sensor. The response of the sensor when in the presence of analytes should therefore be one that modifies the intensity, or wavelength, of emissions of the sensor-only fluorescence. The response should also be one that is unambiguous: it should be distinguishable from any deviation/variation from the sensor-only emission. The response should also be accurate and reproducible: the same sensor response should be observed every time the sensor is in the presence of the given analyte.

Direct excitation of Eu^{3+} or Tb^{3+} when chelated to DOTA or DO3A produces insufficient alteration of baseline lanthanide fluorescence when mixed with any individual analyte, or any mix of non-nucleobase or nucleobase analytes, to provide utility as a sensor for the intended. When the complexes were irradiated at a wavelength that excited the carboxylate component of the ligands, Ln^{3+} fluorescence was observed, presumably facilitated by intersystem energy transfer from the excited organic moieties directly to the Ln^{3+} electrons. The electronically promoted electrons return to the ground state producing the indicative lanthanide fluorescence. Although not undertaken in this research, the excitation of ligand carboxylate moieties could be demonstrated by obtaining UV-Vis and excitation spectra of the complexes, which would reveal the wavelengths of light absorbed and thus indicate which moieties were experiencing the excitation and were facilitating the lanthanide sensitisation via ligand to metal charge transfer (Horrocks and Albin, 1984, Bruce, 2001, Valeur and Berberan-Santos, 2013).

When chelated to DOTA, and upon addition of equimolar concentration of nucleobases as individual analytes or as complex mixtures, Ln^{3+} fluorescence was quenched. Likewise, when chelated to DO3A, Ln^{3+} fluorescence was similarly 'turned off' by all nucleobases (with the exception of adenine, which increases intensity by some margin). In all cases, when concentration of nucleobase analytes was decreased, intensity increased until approximate baseline Ln^{3+} fluorescence was observed (again, with the exception of adenine).

Clearly, when the fluorescence is quenched, the sensor can no longer be observed and no information can be gleaned. If the sensor increases in intensity, and there is a change in form of the spectra, then this can be detected and will afford information about the interactions taking place, enabling analyte identification. That being the case, the following conclusions can be made regarding the utility of europium and terbium complexes of DOTA and DO3A as sensors:

1. All complexes can be used to detect benzoic acid when benzoic acid is the only analyte present by virtue of an increase in fluorescence;
2. Europium complexes of DOTA and DO3A can be used to identify benzoic acid specifically because the form of the spectrum changes to reflect coordination about the Eu metal centre;
3. [EuDO3A] and [TbDO3A] can be used to detect adenine, specifically, because *only* adenine causes an increase in fluorescent intensity when the Ln is chelated to DO3A;
4. These changes in fluorescence cannot be detected when adenine or benzoic acid are combined with other analytes in complex mixtures, *in aquo*.

The sensors used in the work contained within Chapter 3 have been lanthanide complexes of DOTA and DO3A. As explained, $[LnDOTA]^-$ complexes, although sensitised by the presence of benzoic acid, were not as versatile as the [LnDO3A] complexes, in that they did not respond to the presence of adenine. Furthermore, the DOTA ligand consists of four pendant ethanoate arms, which increase steric hindrance around the lanthanide ion. This may inhibit the approach of analytes and reduce the likelihood of analyte/metal-centre interactions. Also, the charge on the

DOTA ligand is four minus so that the overall charge on the complex when the tripositive lanthanide ion is chelated is one minus. This overall negative charge may further impede analyte interaction as a result of electrostatic repulsion between carboxylate moieties or molecules with dipoles.

Therefore, on the basis of the limitations of DOTA and the versatility of DO3A, Chapter 4 details the development of ligands which are structurally similar to DO3A, and are electronically neutral, in order to produce other complexes that are less sterically hindered and, when chelated to tripositive lanthanide ions, are also electronically tripositive overall. It is anticipated this will promote electrostatic attraction of organic molecules with negatively charged ionic moieties, such as carboxylates, or moieties with delocalised, and therefore polarisable, electron density, such as aromatic groups. These were developed to test if analyte/metal-centre interaction might be improved. These new complexes may afford improved sensitivity and/or selectivity for the detection and identification of the same standard organic analytes already selected and tested in this chapter, so that comparisons may be made and recommendations given for utility of such sensors to geological samples.

4 Synthesis of DO3A-like Lanthanide Complexes and their application to analogue analytes

4.1 Introduction

The purpose of this research is to ascertain whether lanthanide complexes, based on the *tetra*-substituted cyclen ligand DOTA, can be used as fluorescent sensors for the detection of individual organic analytes in an extract of a carbonaceous chondrite. In Chapter 3, it was established that the presence of certain analytes when mixed with lanthanide complexes of DOTA, and its *tris*-substituted cyclen ligand analogue DO3A, did invoke a response, e.g. sensitisation of fluorescence when in the presence of benzoic acid. Also, quenching of fluorescence was observed upon the addition of nucleobases to both lanthanide complexes of DOTA and DO3A. The extent of fluorescent lanthanide emission quenching was comparable for every nucleobase and, therefore, could not differentiate between the individual nucleobase molecules. However, only [LnDO3A] could detect adenine. It was, therefore, demonstrated that DO3A lanthanide complexes are more susceptible to sensitisation than $[LnDOTA]^-$ complexes.

With this information in mind, it was logical to investigate what effect, if any, those analytes might have on europium and terbium fluorescence when chelated to other, structurally similar DO3A-like ligands. Moreover, it was advantageous to discover whether selectivity or improved sensitivity could be introduced by modifying the structure of the pendant arms (Section 4.1.2), while maintaining the structure of the ethanoate coordinating moieties.

Development and use of *tris*-substituted cyclen products have three further benefits. First, metal-centres bound to *tris*-substituted cyclen ligands are less sterically hindered than when bound to their *tetra*-substituted counterparts by virtue of one less pendant arm, thus promoting the possibility of direct metal-centre to analyte interaction; this is more likely if there is space to do so. Secondly, the fourth cyclen secondary amine is labile, providing a potential reaction site for the addition of, for example, a light harvesting antenna molecule to exploit the antenna effect (Chapter 1) should this be desired at a later stage. Finally, it is a more attractive proposal to synthesise the *tris*-substituted cyclen ligands, since they are easier to produce and isolate; *tetra*-

substituted cyclen ligands require the addition of a fourth pendant arm, which is often sterically hindered by the other three, thus reducing the expected yield, e.g. Figure 4.1 (a) and (b), respectively. This reduction in yield is also compounded by the difficulty in separating *tris*-substituted cyclen ligands from the other substituted cyclen by-products.

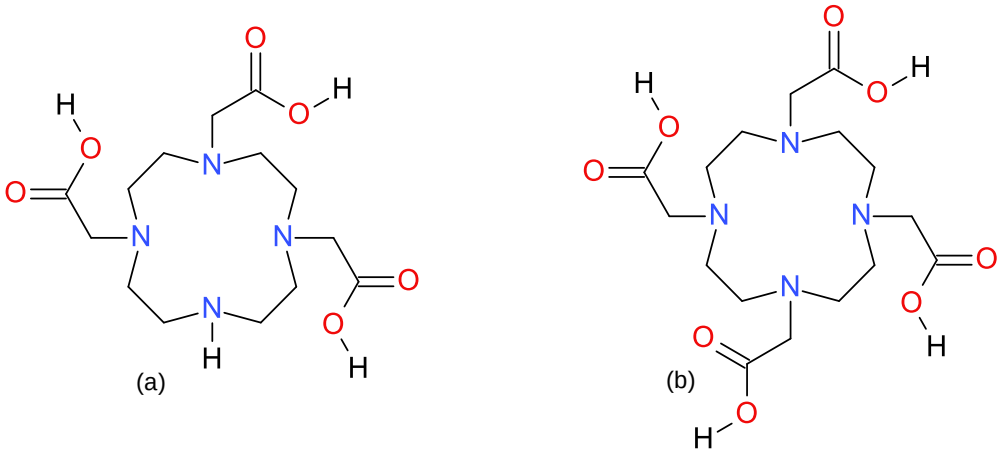

Figure 4.1 *tris*-substituted cyclen, DO3A, is less sterically hindered than the *tetra*-substituted cyclen, DOTA

Heptadentate chelation of lanthanide ions in DO3A is partially achieved through electronic attraction of the cyclen secondary amine nitrogen lone pair electrons, which provide four of the seven coordination points. The other three coordination points are provided by the lone pair electrons of the carbonyl oxygen atoms of the pendant arms. Since this chelation is well characterised and known to be very stable (Chapter 3), it is prudent to maintain the position of the carbonyl carbon of the free carboxylic acid at the β-position to the α-carbon of the pendant arm (that is to say, the carbon bonded directly to the secondary amine nitrogen of the of the cyclen ring). This structure should therefore be a requisite of any new ligand.

The syntheses are required to be simple 'one-pot' direct additions of readily available pendant arm reagents to cyclen so that the reactions can be achieved with as few steps, using as little materials, as possible. In order to provide a scope in which to work and begin the development of the DO3A-like ligands, in addition to the structure outlined above, a set of prerequisites were put in place for the syntheses:

1. The reaction must not require catalysts. If reactions required catalysts, then they would need to be isolated and removed from the reaction mixture post-synthesis adding extra

steps, and therefore additional time, to the work-up. Also, exotic catalysts are often expensive.

2. Reactions should not require extreme conditions, e.g. high temperatures or pressures. Reactions requiring extreme conditions are often costly, time consuming and would likely incur increased risk.
3. Reactions must be fast and facile with a minimum of work-up, i.e. separation and purification. Fast, easy to achieve reactions with good yields and uncomplicated isolation will reduce cost, wastage and time needed to produce the target compound.

Upon synthesis and isolation, it is a requirement that the ligand should easily chelate lanthanide ions without complicated conditions or isolation procedures, for the same reasons as outlined above.

4.1.1 The aza-Michael Reaction

Synthesis of DOTA and DO3A (and their derivatives) from cyclen starting material can be achieved using various methodologies, including alkylation under basic or acidic conditions using *tert*-Butyl bromoacetate as the pendant arm reagent (Li and Wong, 2002). However, to synthesise the ligands described in this chapter, a variation of the Michael Reaction (McMurry, 2000) was employed, namely the aza-Micheal reaction. The Michael Reaction itself involves the formation of a C-C bond between a nucleophilic enolate ion (a Michael donor) and a β-carbon of an α,β-unsaturated carbonyl compound (a Michael acceptor). To produce the ligands in this chapter using the aza-Michael reaction, a C-N bond is formed instead (Kumar et al., 2006, O'Connell, 2009), when nucleophilic attack of a cyclen secondary amine (the Michael donor) takes place upon an 'activated' carbon of a conjugated alkene (the Michael acceptor). Which alkene carbon is activated depends upon the combined electron-withdrawing strength of the electron withdrawing groups (EWG) adjacent to each alkene carbon (Scheme 4.1). Since the bond formed is between a nitrogen and carbon atom, the reaction is given the 'aza-' prefix.

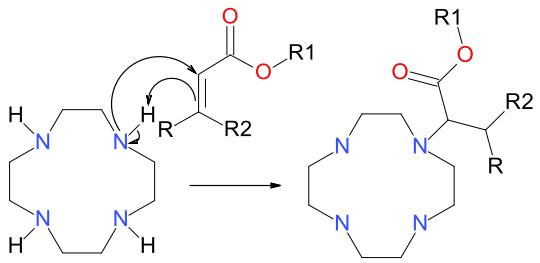

Scheme 4.1 aza-Michael Reaction mechanism. R1 = methyl or ethyl group, R = a proton or small alkyl group and R2 = any suitable electron withdrawing group (EWG)

In order to maintain the DO3A-like ethanoate pendant arm structure of the ligand, the alkene must be conjugated to at least one ethanoate ester (Scheme 4.1, R1). R2 is an EWG chosen to increase the draw of electron density from the carbon-carbon double bond (C=C) which, in conjunction with the adjacent ester carbonyl group, introduces regioselectivity to the molecule. This selectively activates the alkene carbon nearest the ester – henceforth denoted as the alkene α-carbon (Figure 4.2). This increases its electropositivity, thereby increasing the likelihood of attack by a nucleophile.

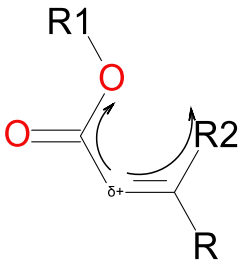

Figure 4.2 Regioselective alkene α-carbon activation

4.1.2 Criteria for choosing pendant arm reagents

In light of the discussion above, the successful synthesis of a DO3A-like ligand using the aza-Michael reaction depends upon a pendant arm possessing three features. These are:

A. The pendant arm reagent must be commercially available, inexpensive and high purity.

B. An alkene functional group. This is the reactive moiety necessary for the reaction to take place; the carbon atom adjacent to the ester moiety (the α-carbon atom) must be sufficiently activated, however.

C. An electron withdrawing group (EWG). This must be directly adjacent to the alkene β-carbon to facilitate the selective activation of the α-carbon.

D. An ester moiety adjacent to the alkene α-carbon atom. This functional group must be directly adjacent to the activated alkene α-carbon atom in order to maintain the DO3A-like ester structure (that also selectively activates the α-carbon in conjunction with the EWG, which is positioned adjacent to the β-carbon).

As long as the alkene carbon atom adjacent to the ester is activated, it does not matter which alkene conformation is used. So, when considering options for suitable pendant arm reagents, it was the chemical and physical properties of the EWG, and the structure of the ester, that had to be carefully scrutinized, since these determine how selectivity and sensitivity could be introduced to the sensor.

The criteria for the choice of the terminal moieties of the ester groups was based on the requirement that they should be easily hydrolysed to yield the free acid, should this be desired, and/or provide further synthetic utility. Methyl and ethyl groups are easily hydrolysed, as are allyl groups; however hydrolysis is not strictly necessary as chelation of the lanthanide ions will occur as effectively both in the free acid form, and as the ester. In both cases, the carbonyl oxygen is the coordinating atom. Allyl moieties, however, can undergo addition reactions, which provide the potential for the addition of chromophores to exploit the antenna effect, thus improving lanthanide fluorescence intensity.

To determine the criteria for the choice of EWG, consideration must be given not only to what properties the EWG provides to ensure facile reaction with cyclen, but also what properties the EWG will afford the final ligand. A highly EWG could successfully activate the α-carbon but if it occupies a large space, i.e. it is 'bulky', then there could potentially be steric hindrance. Although the addition reaction itself may, in theory, be achievable because the α-carbon is strongly activated, steric hindrance may prevent facile addition of the third pendant arm resulting in a predominance of *bis*-substituted cyclen. Likewise, a less electron-withdrawing but smaller, less sterically hindering group may not sufficiently activate the α-carbon, precluding the reaction from occurring at all. EWGs containing alkenes, carbonyl, sulfonate, cyano, nitro groups etc. can undergo chemical reactions allowing for the addition of chromophores to make use of the

antenna effect. Weakly electron-donating groups such as amines can also be used in such a manner too, e.g. the addition of fluorescamine (Udenfriend et al., 1972).

EWGs that possess structures such as aromatic rings are also advantageous as they would not need to undergo addition of chromophores; they would already possess the potential to act as antennas. Choice of suitable EWGs needs to be based, therefore, on selection criteria, with a 'trade-off' to find the most efficacious combination of: i) electron-withdrawing strength; ii) size of the group so as not to hinder reactivity, and iii) ability to facilitate the antenna effect (either by synthetic addition of a chromophore or by possessing an antenna already, e.g. an aromatic group) to sensitise the europium and terbium when they are chelated.

4.1.3 Pendant arm reagents considered

To identify suitable pendant arm reagents, molecular structures were drawn that satisfied the criteria for pendant arm selection (outlined above, Section 4.1.2), and that contained suitable EWGs attached to the β-carbon of the alkene (Table 4.1). Those structures were then entered into chemical structure search engines (Sigma Aldrich and ABCR) to identify if they were commercially available. Other structurally similar 'best match' reagents were suggested by the chemical structure search engines and, where they satisfied the criteria, were also considered (Table 4.1).

As Table 4.1 indicates, nineteen molecules were considered; thirteen reagents were not commercially available (mono- and di-nitro analogues of molecule 2, molecules 4 and 6, seven of the eight stated analogues of molecule 8, and the fluoro- and chloro-analogues of molecule 10). Of the six remaining reagents that were identified as commercially available, the purity of one (molecule 7) could not be assured. As previously explained (Section 4.1), criteria for selection were also dependent upon the purity of the reagent (the reagent should be 'off the shelf' without requiring preparatory purification) meaning only five of the considered reagents were ultimately chosen (see Section 4.1.4, Table 4.2)

		Selection criteria				
Molecule	**Potential pendant arm structure and name**	**A) Commercial availablity, cost and purity**	**B) Alkene**	**C) EWG**	**D) Ester moiety**	**Outcome/comments**
1	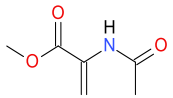 Methyl 2-acetamidoprop-2-enoate/*methyl 2-acetamidoacrylate*	The reagent is commercially available at a cost of ~£33/g with 98% purity.	Yes.	The amidocarbonyl is a good EWG – the carbonyl is conjugated to the alkene via the amine lone pair. Both EWG are attached to the α-carbon and is expected to be activated.	The methyl ester maintains the DO3A-like structure.	All structural and chemical criteria are met as well as high purity and low cost, making (1) a good pendant arm reagent candidate.
2	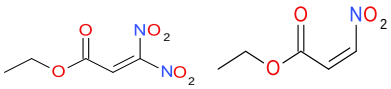 Ethyl 3,3-dinitroprop-2-enoate	No dinitro or mononitro molecules were found to be comercially available.	Yes.	NO_2 groups are strong EWGs.	The ethyl ester maintains the DO3A-like structure.	The NO_2 groups have synthetic utility; they can be reduced to amines using $LiAlH_4$. The resulting NH_2 groups can be reacted with fluorescamine to utilise the antenna effect to sensitise lanthanide fluorescent emissions. However (2) was not comercially available, so was not considered further.
3	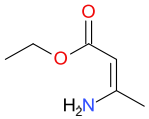 Ethyl (2*Z*)-3-aminobut-2-enoate/*ethyl 3-aminocrotonate*	The reagent is commercially available at a cost of ~£0.23/g with 98% purity.	Yes.	Amines are not good EWGs, however, the ester may sufficiently activate the α-carbon.	The ethyl ester maintains the DO3A-like structure.	The primary amine can be used to attach a fluorescamine chromophore to exploit the antenna effect. The EWG of (3) is not strong but may still be a suitable candidate for use to produce a DO3A-like ligand.

		Selection criteria				
Molecule	**Potential pendant arm structure and name**	**A) Commercial availablity, cost and purity**	**B) Alkene**	**C) EWG**	**D) Ester moiety**	**Outcome/comments**
4	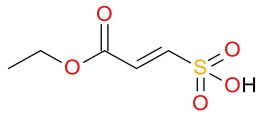 (1E)-3-ethoxy-3-oxoprop-1-ene-1-sulfonic acid	Not comercially available.	Yes.	SO_2OH (sulphonic acid) is a highly EWG and is small and distant from the activated α-carbon.	The ethyl ester maintains the DO3A-like structure..	(4) meets all the criteria chemically and physically, but is not comercially available. This molecule was not considered further but should be investigated as a potential pendant arm reagent if future work was undertaken.
5	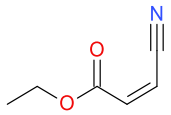 Ethyl (2*Z*)-3-cyanoprop-2-enoate/*ethyl cis-(β-cyano)acrylate)*	Commercially at a cost of ~£40/g with 97% purity.	Yes.	Nitrile (CN) is a strong EWG activating the α-carbon.	The ethyl ester maintains the DO3A-like structure.	(5) is an excellent candidate, fulfilling all the prerequisite criteria. Successful DO3A-like ligand synthesis has been previously reported (O'Connell, 2009).
6	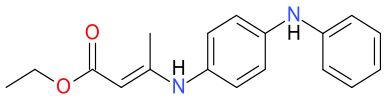 Ethyl 3-(4-anilinoanilino)-2-butenoate	'Not commercially available at this time'.	Yes.	Assuming the α-carbon is suitably activated, reaction was expected to occur.	The ethyl ester maintains the DO3A-like structure.	(6) was considered because 3-(4-anilinoanilino) should act as an excellent antenna, sensitising lanthanide emissions. The molecule is found in the structure library of Sigma-Aldrich but was not available. Should (6) become available for future work, it should be considered as a good pendant arm and synthesis of a DO3A-like ligand should be attempted.

		Selection criteria				
Molecule	**Potential pendant arm structure and name**	**A) Commercial availablity, cost and purity**	**B) Alkene**	**C) EWG**	**D) Ester moiety**	**Outcome/comments**
7	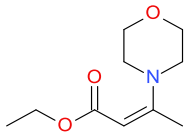 Ethyl β-morpholinocrotonate	Commercially available but purity was stated as 'not guaranteed'.	Yes.	The morpholino moiety may introduce regioselectivity to activate the α-carbon.	The ethyl ester maintains the DO3A-like structure.	The morphilino group is not a strong EWG and its size proximity to the α-carbon is likely to cause some steric hindrance. The purity of the reagent is not known accurately. (7) does not meet the criteria of a good reagent so this molecules was no longer considered.
8	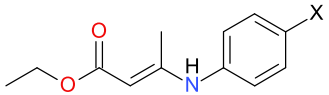 ethyl (2E)-3-(phenyl amino)but-2-enoate	Phenyl-only reagent was commercially available at a cost of £180/g with a purity of 97%.	Yes.	Although amines are not strong EWGs, the phenyl group was expected to acatívate the α-carbon *via* conjugation with the amine lone pairs. X represents other possible EWGs.	The ethyl ester maintains the DO3A-like structure.	EWGs (X) considered were NO_2, SO_2OH, F, aldehyde, ketone, carboxylic acid and acid chloride because they are very strong EWGs. The molecules considered with EWG at 'X' were not commercially available.
9	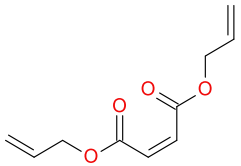 1,4-bis-(prop-2-en-1-yl)-(2*Z*)-but-2-enedioate/*diallyl maleate*	Commercially at a cost of ~£0.46/g with a purity of 98%.	Yes.	Esters are strong EWG	The allyl ester maintains DO3A-like structure.	Successful synthesis using a structurally similar pendant arm has been previously reported (Smith, 2008). (9) maintains DO3A-like structure regardless of the alkene carbon nucleophilically attacked. Allyl groups are reactive providing opportunity for further synthetic utility, e.g. addition of chromophores to exploit the antenna effect.

		Selection criteria				
Molecule	**Potential pendant arm structure and name**	**A) Commercial availablity, cost and purity**	**B) Alkene**	**C) EWG**	**D) Ester moiety**	**Outcome/comments**
10	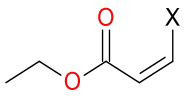 Ethyl *cis*-3-fluoroacrylate and ethyl *cis*-3-chloroacrylate	Not commecially available.	Yes.	The EWG here are F or Cl. These candidates are the most simple molecules considered, exhibiting the requisite structure (an alkene and ester adjacent to the α-carbon) and a single atom as the EWG	The ethyl ester maintains the DO3A-like structure.	They both meet the chemical and physical criteria with expected α-carbon activation; however, as these reagents were not commercially available, they were not potential pendant arm candidates. They should be considered to produce ligands if future work was to be undertaken.

Table 4.1 Molecule structures considered as potential pendant arm reagents

4.1.4 Pendant arm reagents and new ligands

Table 4.2 indicates the structures of the five molecules chosen as potential candidates for pendant arm reagents in accordance with the criteria outlined heretofore (Section 4.1.1), along with their IUPAC and colloquial names (where appropriate) and any drawbacks or issues surrounding their use. The IUPAC names of the *tris*-substituted cyclen ligands they would potentially produce are consequently complex, so in order to minimise confusion, each ligand has been designated an 'L' number. Henceforth, all ligand molecules will only be referred to by their 'L' designations (L1, L2 etc.).

Chelation of the lanthanide ions with these new ligands was expected to take place using the same methodology as described for the production of the [LnDO3A] complexes (Chapter 3, Section 3.4.2), since the coordinating structures of the new ligands are DO3A-like. Although the denticity of the ligands, and the coordinating ethanoate structure about the lanthanide ion, is the same, it was hoped that pendant arm structural modifications not involved in chelation would invoke an improved selective and/or sensitised sensor response.

L3, a *tetra*-substituted ligand by-product (designated 'triallyl BOC cyclen') (Table 4.2) had been synthesised (using an alkylation reaction, not an aza-Michael reaction) and isolated as part of a different but related PhD research project (Vitiello, 2017). Fortuitously, as described on Table 4.2, this was considered to be suitable for development along with the other ligands here, and L3 was provided for use in this thesis. Although *tetra*-substituted, L3 still maintains the DO3A-like structure with three carbonyl groups; the fourth pendant arm is not involved in the chelation of the lanthanide ion. This ligand maintains the three ethanoate ester arms in the DO3A-like conformation, with allyl groups attached to the ester oxygen, and a tertiary butyl *N*-ethylcarbamate arm attached at the fourth cyclen nitrogen. It was anticipated that the lanthanide ions would be chelated in the same manner as DO3A; it is unlikely that the carbonyl oxygen of the fourth pendant arm will chelate, forming an *octa*-coordinated metal centre, but this would be confirmed when the spectrum of the europium complex is obtained (the ΔJ=1 transition is more intense than the ΔJ=2 transition for an *octa*-coordinated europium ion). The *N*-ethylcarbamate *t*-

But ester arm and allyl groups have synthetic utility by offering the potential to introduce chromophores to act as light harvesting molecules enabling the sensitisation of the lanthanide emissions via the antenna effect (Chapter 1).

The fluorescent assays undertaken using the new DO3A-like lanthanide complexes followed the same, and modified, protocols developed and described in Chapter 3. However, the complexes were combined with a reduced selection of organic analytes (Section 4.2.2) consisting of molecules that invoked a response to the fluorescent emissions of [LnDO3A].

Ligand	Ligand structure	Ligand: IUPAC/*colloquial*	Pendant arm structure	Pendant arm: IUPAC/*colloquial*	Possible drawbacks
L1	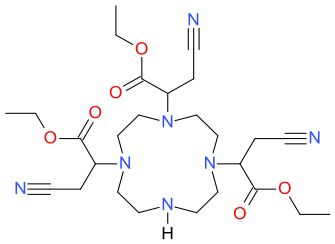	Ethyl 2-[4,10-bis(3-cyano-1-ethoxy-1-oxopropan-2-yl)-1,4,7,10-tetraazacyclododecan-1-yl]-3-cyanopropanoate	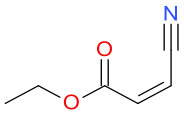 (5)	Ethyl (2*Z*)-3-cyanoprop-2-enoate/*ethyl cis-(β-cyano)acrylate)*	The reaction has been previously reported (O'Connell, 2009). The CN group is a powerful EWG ensuring activation of the α-carbon and its small size is unlikely to cause steric hindrance to the reaction.
L2	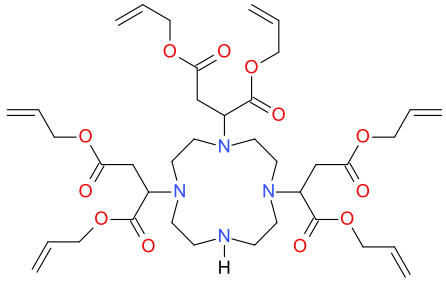	1,4-bis(prop-2-en-1-yl) 2-{4,7-bis[1,4-dioxo-1,4-bis(prop-2-en-1-yloxy)butan-2-yl]-1,4,7,10-tetraazacyclododecan-1-yl}butanedioate	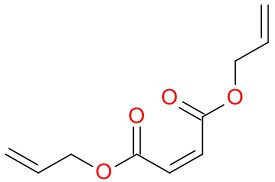 (9)	1,4-bis-(prop-2-en-1-yl)-(2*Z*)-but-2-enedioate/*diallyl maleate*	The previously reported reaction using a similar pendant arm reagent (Smith, 2008) suggests the reaction should proceed without issue. Increased steric hindrance may, however, result in slightly lower yield due to the larger size of the terminal allyl ester groups (the previously used reagent possessed simple, smaller ethyl groups). The presence of the larger allyl groups may also hinder facile isolation by silica column separation.
L3	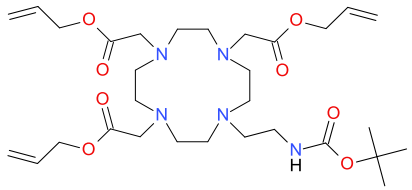	Prop-2-en-1-yl 2-[4-(2-{[(tert-butoxy)carbonyl]amino}ethyl)-7,10-bis[2-oxo-2-(prop-2-en-1-yloxy)ethyl]-1,4,7,10-tetraazacyclododecan-1-yl]acetate/*triallyl BOC cyclen*	N/A (ligand was provided already synthesised)	N/A	L3 was synthesised previously and provided for use, as is (Vitiello, 2017) (Section 4.1.4). No further reactions were performed on the ligand. L3 arms provide the same coordination as L2 but the arms are less bulky having only one branch. The fourth arm is unlikely to coordinate to the lanthanide as a result of its length (an extra CH_2 group) but may hinder direct analyte/metal-centre interactions because of the large, non-polar ester terminal tertiary butyl group.

Ligand	Ligand structure	Ligand: IUPAC/*colloquial*	Pendant arm structure	Pendant arm: IUPAC/*colloquial*	Possible drawbacks
L4	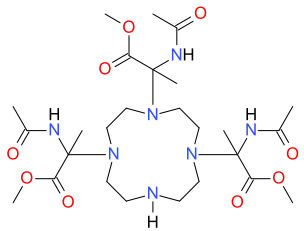	Methyl 2-[4,7-bis(2-acetamido-1-methoxy-1-oxopropan-2-yl)-1,4,7,10-tetraazacyclododecan-1-yl]-2-acetamidopropanoate	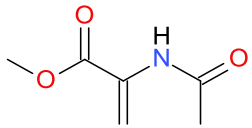 (1)	Methyl 2-acetamidoprop-2-enoate/*methyl 2-acetamidoacrylate*	The β-carbon is conjugated to the carbonyl EWG via the nitrogen lone pair, so may be activated and, therefore, as reactive as the α-carbon. Also, the β-carbon is not sterically hindered so may react, possibly preferentially. The resulting ligand may not maintain a DO3A-like ethanoate structure (the arms would lengthen by one CH_2 group). Also, if both alkene carbons are equally reactive, several isomers may result (see Section 4.1.6).
L5	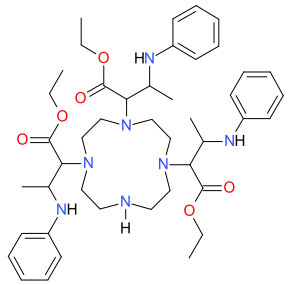	Ethyl 2-{4,7-bis[1-ethoxy-1-oxo-3-(phenyl amino)butan-2-yl]-1,4,7,10-tetraazacyclododecan-1-yl}-3-(phenyl amino)butanoate	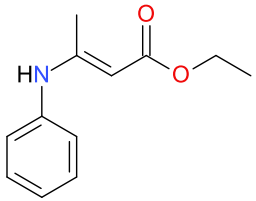 (8)	Ethyl (2*E*)-3-(phenyl amino)but-2-enoate/*ethyl 3-aniliocrotonate*	Although the phenyl and methyl groups are weakly electron-donating, it is hoped the ester is sufficiently electron-withdrawing to activate the α-carbon. The phenyl should introduce the potential to exploit the antenna effect, thus sensitising the lanthanide emissions. The large phenyl amino group may sterically hinder the reaction, however.
L6	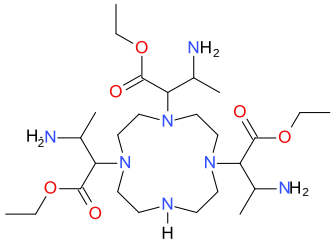	Ethyl 3-amino-2-[4,10-bis(3-amino-1-ethoxy-1-oxobutan-2-yl)-1,4,7,10-tetraazacyclododecan-1-yl]butanoate	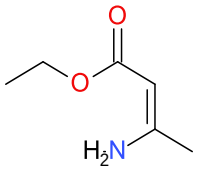 (3)	Ethyl (2*Z*)-3-aminobut-2-enoate/ *ethyl 3-aminocrotonate*	The ester group should be electron-withdrawing enough to sufficiently activate the α-carbon while the small size of amine and methyl groups are not expected to sterically hinder the reaction even though they are electron donating. The free amine moieties could then be used to introduce a light harvesting chromophore to sensitise lanthanide emissions.

Table 4.2 Pendant arm reagents chosen and the expected ligand structure

It was anticipated that each of these new complexes would be sensitised by different, individual, analytes in a similar way to that observed when adenine was combined with [LnDO3A]. If a specific DO3A-like lanthanide complex were to be combined with a specific analyte, and an unambiguous fluorescence response observed, then that complex may be used as a sensor to detect that specific analyte. If the same response is detected when that specific DO3A-like lanthanide complex is combined with a carbonaceous chondrite extract, then the implication is that that specific analyte may be present in the extract.

4.2 Synthesis of the DO3A-like ligands and their lanthanide complexes

4.2.1 Synthesis of DO3A-like ligands

A procedure for the successful synthesis of L1 had been previously reported (O'Connell, 2009) whereby 3.1 equivalents of the pendant arm reagent (used to minimise the synthesis of unwanted tetra-substituted cyclen) was combined with cyclen at room temperature in dry acetonitrile (MeCN). This methodology was used as a starting point for all the ligand syntheses because it had been shown to be effective for the aza-Michael reaction (O'Connell, 2009). However, since each pendant arm reagent is slightly different, adjustments to reaction conditions were required to optimise yield.

All reactions were monitored using thin layer chromatography (TLC) and electrospray mass spectroscopy (MS). The crude reaction mixture was separated using column chromatography and the fractions analysed by TLC and electrospray MS. Synthesis of the target ligands were confirmed by ^{1}H NMR and ^{13}C NMR spectroscopy. Full methodology for synthesising and characterising individual ligands can be found in Chapter 2, Sections 2.7.3 to 2.7.5.

4.2.2 Reaction mechanism for the synthesis of L1

Using the synthesis method of (O'Connell, 2009), ethyl 2-[4,10-bis(3-cyano-1-ethoxy-1-oxopropan-2-yl)-1,4,7,10-tetraazacyclododecan-1-yl]-3-cyanopropanoate, L1, was synthesised with a yield of 30.6%, using (2*Z*)-3-cyanoprop-2-enoate as the Michaels acceptor. Since the nitrile adjacent to the β-carbon has a stronger electron-withdrawing effect (and the ester less so), the α-carbon of the alkene adjacent to the ester is activated. As a result, the cyclen secondary amine Michael

donor will nucleophilically attack the Michael acceptor alkene and the N-C bond will form. The remaining cyclen protons (removed by the base used in the reaction) will then protonate the alkene β-carbon adjacent to the nitrile group (Scheme 4.2). Full methodology for the synthesis and characterisation of L1 can be found in Chapter 2, Sections 2.7.3.

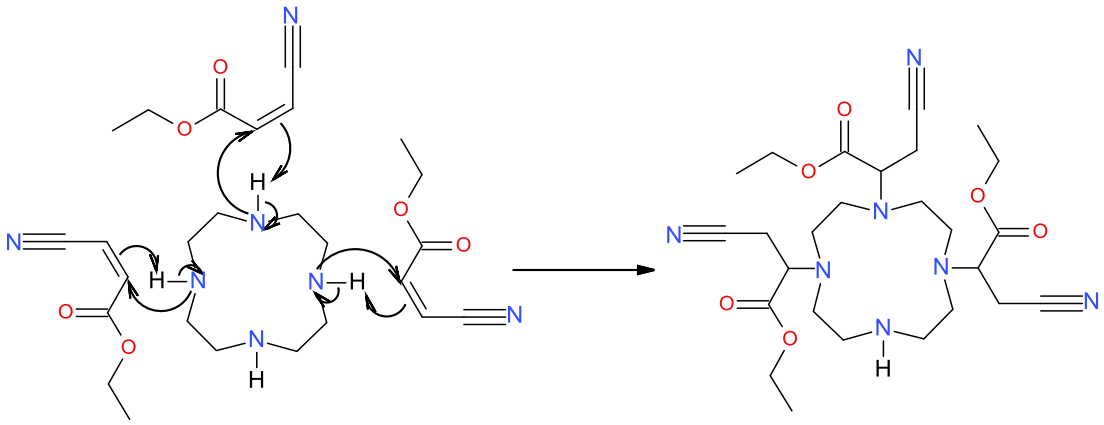

Scheme 4.2 Addition of (2Z)-3-cyanoprop-2-enoate to cyclen to produce L1

4.2.3 Reaction mechanism and rationale for the synthesis of L2

The synthesis of 1,4-bis(prop-2-en-1-yl) 2-{4,7-bis[1,4-dioxo-1,4-bis(prop-2-en-1-yloxy)butan-2-yl]-1,4,7,10-tetraazacyclododecan-1-yl}butanedioate, L2, has not been reported previously. A similar ligand, however, has been synthesised (Smith, 2008), whose architecture is almost identical to L2. The only difference is that the L2 pendant arm reagent has terminal alkene moieties; the pendant arms used by Smith (2008) are ethyl esters, not allyl esters (Figure 4.3 (a) and (b), respectively).

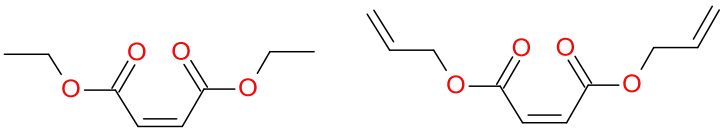

(a) (b)

Figure 4.3 (a) 1,4-bis(ethyl)(2Z)-but-2-enedioate (diethyl maleate), used in the synthesis reported by Smith (2008) and (b) 1,4-bis(prop-2-en-1-yl) (2Z)-but-2-enedioate (diallyl maleate)

The benefit of the allyl group is that it offers greater synthetic utility than the simpler alkyl groups; the allyl groups could be used to attach chromophores, for example, to exploit the antenna effect (Section 1.7.5). They could also be cleaved by hydrolysis, just as the alkyl groups can, to yield the free acids instead, two on each pendant arm: ethanoic acid and propanoic acid groups,

respectively. Leaving them *in situ* would not affect the ability of the ligand to chelate the lanthanide ions, however.

Diallyl maleate (the pendant arm reagent used to synthesise L2) is a symmetrical molecule meaning that both alkene carbon atoms are equally activated. This means the reaction will yield the same product regardless of which carbon atom the cyclen secondary amine's nitrogen nucleophilically attacks. By using the diallyl maleate, the DO3A-like ethanoate ester moiety is retained. The second, propanoate, ester moiety is adjacent to the carbon atom bonded to the nitrogen atom of the cyclen frame and may have some involvement in coordination. The nucleophilic deprotonated cyclen amine nitrogen acts as a Michael donor and attacks at either alkene carbon atom (the Michael acceptor) on the arm reagent, forming the C-N bond (Scheme 4.3).

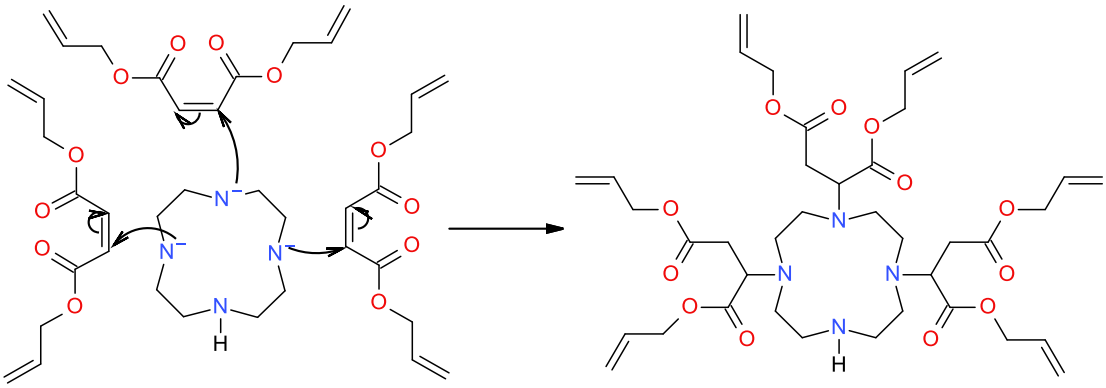

Scheme 4.3 Addition of diallyl maleate to cyclen to produce L2

Using the synthesis methodology of Smith (2008), which resulted in a yield of 35.58%, it was expected that a mixture of L2 substituted cyclen analogue products would be produced during the synthesis. A yield of 32.6% was achieved, and a full methodology for the synthesis and characterisation of L2 can be found in Chapter 2, Section 2.7.4.

4.2.4 Rationale for the use of L3 (triallyl BOC cyclen)

A concurrent project being undertaken within the research group at the Open University had developed a *tetra*-substituted DO3A-like ligand, designated 'triallyl BOC cyclen', L3 (Figure 4.4) as a by-product of a related novel ligand total synthesis. This by-product was identified as being advantageous to this project because, although a *tetra*-substituted cyclen (all four cyclen

secondary amine nitrogens are bonded to pendant arms) three pendant arms are allyl ethanoate esters which maintain the DO3A-like structure.

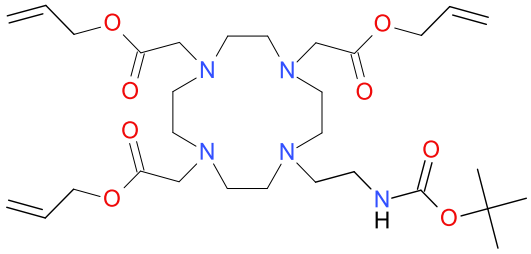

Figure 4.4 triallyl BOC cyclen, L3

Three of the L3 pendant arms have similarities with the pendant arms of L2 (Section 4.3); the esters all consist of terminal allyl groups. The fourth arm does not, however, exhibit the same ethanoate carbonyl structure of the other pendant arms; rather, it is an arm consisting of a tertiary butyl ester connected to the cyclen secondary amine via a secondary ethyl amine. It is unlikely that the ester carbonyl will coordinate to the lanthanide centre since the *t*-Butyl group is large and bulky (resulting in steric effects). The fourth arm would, however, offer synthetic utility since the *t*-Butyl group can be removed, via hydrolysis, such that it could potentially offer an eighth coordination as a free acid. As explained above, since three of the L3 pendant arms are ethanoate esters, and as such L3 is a DO3A-like ligand, the chelation of europium and terbium ions was attempted.

L3 was provided for this work by Bianca Vitiello and details of its synthesis can be found in her PhD thesis (Vitiello, 2018).

4.2.5 Other ligand syntheses attempted

The syntheses of L4, L5 and L6 ligands (Table 4.2, Section 4.1.4) were previously unreported so it was not known whether the Michaels type addition would take place between cyclen (the Michael donor) and the alkene moiety of the chosen pendant arm reagents (the Michael acceptors) but it was hoped the alkene α-carbon would be sufficiently activated to allow this. The pendant arm reagents were chosen because they each exhibited an alkene functional group adjacent to an ester, such that, should the expected reaction take place at the alkene α-carbon, a ligand should be produced with a DO3A-like ester conformation. The factor that would ensure the

reaction takes place at the required alkene carbon atom is the correct choice of electron-withdrawing moiety to introduce this regioselectivity.

The syntheses of L4, L5 and L6 were attempted and the reactions monitored by TLC and electrospray MS. Although MS revealed that the aza-Michael reaction does take place between the L4 pendant arm reagent and cyclen, the abundance of the L4 target ligand was very low. It is possible this was as a result of steric hindrance when the addition of the second pendant arm, probably *trans* to the first, took place. The abundance of *mono*- and *bis*- analogues would suggest this is likely. It was also revealed that separation of the reaction mixture to yield the target ligand was problematic, for two reasons. Firstly, it was not possible to separate the products; both aqueous and organic phases contained all reaction products, indicating they are more-or-less equally soluble in water and organic solvents. Secondly, the analysis of fractions eluted during the attempt at separation of products by column chromatography suggested the compounds remained adhered to the column. For these reasons, contrary to the theoretical likelihood that the requirement for fast and facile synthesis could be met, the overall synthesis of L4 was unsuccessful. L4, as a potential ligand with DO3A-like structure, should be considered further if future work were to be carried out on its synthesis, with particular attention needed to establish a methodology which successfully increases the yield and isolates the pure compound. Methodology, results and analysis of characterisation, discussion and conclusions for the attempted synthesis of L4 can be found in Appendix A, Section A.1.

The anticipated reactions to produce L5 and L6 did not occur. No evidence for any substituted cyclen products were observed at any time during the attempted syntheses. As a result, and adhering to the criteria set out before the reagents were chosen, the synthesis of L5 and L6 were retired. Methodology, results and analysis of characterisation, discussion and conclusions for the attempted synthesis of L5 and L6 can be found in Appendix A, Sections A.2 and A.3, respectively.

4.2.6 Synthesis of DO3A-like lanthanide complexes

To produce the lanthanide complexes, anhydrous chloride salts of europium or terbium were combined with the ligands in dry methanol (MeOH) with a 1:1 stoichiometry, and heated to rigorous reflux (~65°C) for 24 hours. The reaction mixture was filtered under vacuum through a celite plug to remove unreacted lanthanide salts. Characterisation of the complexes was undertaken using infrared spectroscopy, and chelation of the lanthanide ions was confirmed by fluorimetry. Full details for individual complex syntheses, and their characterisation, are given in Chapter 2, Sections 2.7.3 to 2.7.5.

4.3 Results

4.3.1 Fluorimetry of the synthesised lanthanide complexes

$[LnDOTA]^-$ and [LnDO3A], and organic analyte mixtures thereof, had been irradiated at 265 nm in order to obtain fluorescence emission spectra. The required excitation wavelength for lanthanide complexes of the DO3A-like ligands was not known, so in order to ascertain a suitable wavelength at which to excite these complexes, it was necessary to obtain an ultra-violet/visible (UV-Vis) light absorption spectrum. 1 ml of a 3 mM solution of each complex was decanted into a clean, dry quartz UV-Vis cuvette (cleaned using the indicated protocol, Section 2.1.4) and the absorption spectra obtained using a JASCO V-530 UV-Vis spectrometer set to collect photons at increments of 0.5 nm in the range 190 nm to 720 nm. The data were processed using GENESYS 10S UV-Vis v4.006 software (Section 4.6).

In order to ascertain a suitable wavelength at which to excite the lanthanide complexes, it was necessary to obtain a ultra-violet/visible (UV-Vis) light absorbance spectrum (Figure 4.5), using the method described in Section 2.6.6. The resultant peaks are broad; however it is the peak maximum that is used as the reference absorbance.

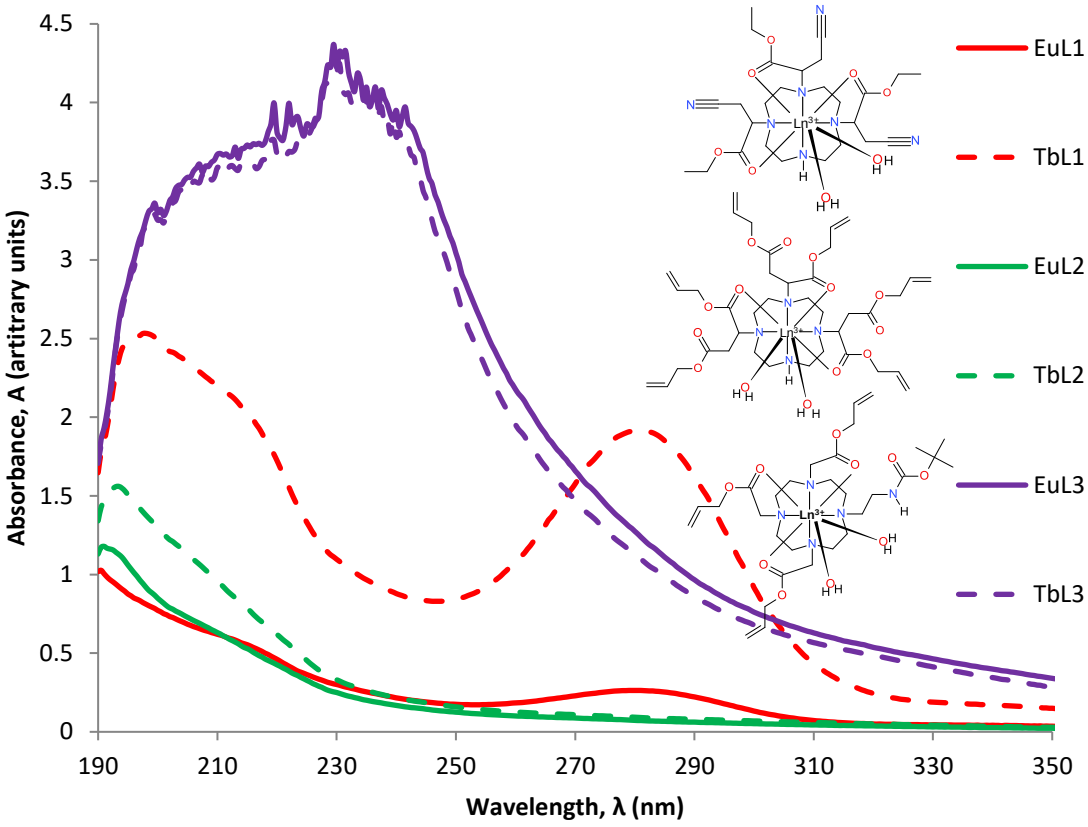

Figure 4.5 UV-Vis absorbance spectra of all lanthanide DO3A-like complexes

The spectra obtained suggested europium and terbium complexes of L1 absorb at ~280 nm, which is the excitation of the ester carbonyl groups ($[TbL1]^{3+}$ also absorbs at ~ 197nm). The lanthanide complexes of L2 absorb at ~ 192 nm and L3 complexes at ~230 nm (Section 4.6). If ligand/metal energy transfer takes place, thus sensitising fluorescent emissions, then it was anticipated that excitation of the complexes at these wavelengths would facilitate this.

In order to test this, excitation acquisitions for each complex were obtained using the most intense lanthanide emission as the acquisition reference, i.e. the fluorimeter excites the complex sample solution using a range of wavelengths while the detector measures the emission intensity of the acquisition reference wavelength. For europium this was ΔJ=2 at 614 nm; for terbium it was ΔJ=1 at 543 nm. The most intense excitation peak for each complex indicated the wavelength at which the reference emission was at its greatest intensity, and was interpreted as the wavelength at which the most effective lanthanide sensitisation takes place (Section 4.6).

Excitation acquisition revealed broad absorbance with maxima at ~275 to 285 nm for all europium complexes, and comparable absorbance for terbium complexes of L2 and L3. However, $[TbL1]^{3+}$ exhibited a very large, broad absorbance with a maximum absorbance at ~368 nm.

Excitation of the carbonyl moieties at 280 nm is already known to sensitise effectively lanthanide fluorescence via a ligand to metal-centre energy transfer mechanism (Chapter 3). Emission acquisition experiments, therefore, were carried out at the excitation wavelengths determined by excitation acquisition (absorbance), described *vida supra*, and at 280 nm, to determine which excitation yields the greatest fluorescent intensity. Lanthanide complexes of L3 were also excited at 230 nm as UV-Vis indicated a high absorbance at this wavelength (Section 4.6). For $[TbL1]^{3+}$, excitation was carried out at 368 nm, but fluorescence was not detected. This suggested that the absorbance recorded at 368 nm may be due to direct absorbance by the terbium ion (Fu et al., 2010).

Excitation acquisitions of the DO3A-like complexes revealed lanthanide emissions were most sensitised, and therefore most intense, when excited using light at a wavelength of 280 nm; this is most likely due to excitation of ligand carbonyl groups, described above. Chapter 3 outlined that the emission intensity of direct lanthanide excitation is low and, therefore, all sensors and sensor/analyte mixtures were tested using an excitation wavelength of 280 nm.

Having confirmed, by fluorimetry, the successful synthesis of all DO3A-like lanthanide complexes, and ascertained that excitation at a wavelength of 280 nm was most effective to sensitise fluorescent europium and terbium emissions, 3 mM stock solutions were prepared in order to undertake fluorimetric assays using the selected organic molecules (Sections 4.6.1 and 4.6.2).

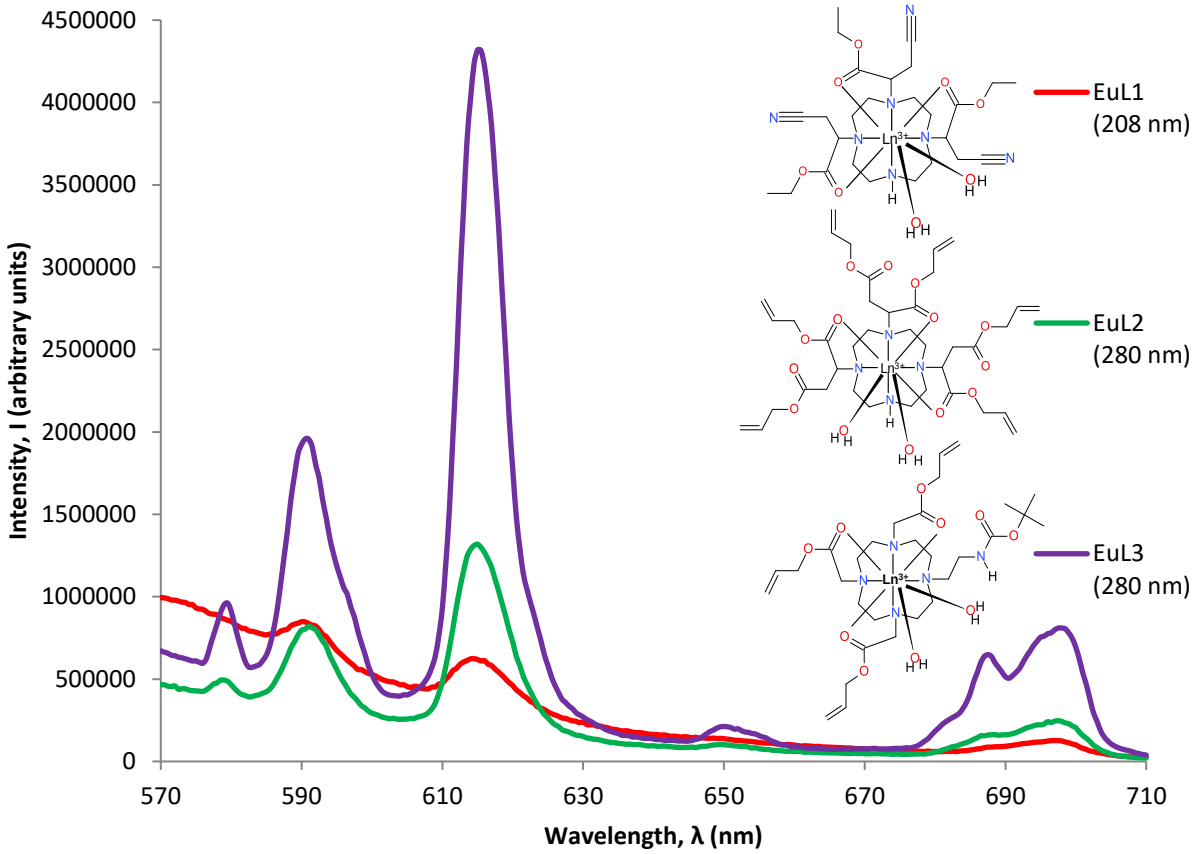

Figure 4.6 Comparison of 1 mM solutions of $[EuL1]^{3+}$, $[EuL2]^{3+}$ and $[EuL3]^{3+}$ fluorescent emission intensities (λ_{Ex}=280 nm, acquisition time=0.5 sec, acquisition increment=0.5 nm, excitation and emission slit width=3 nm, pH=5)

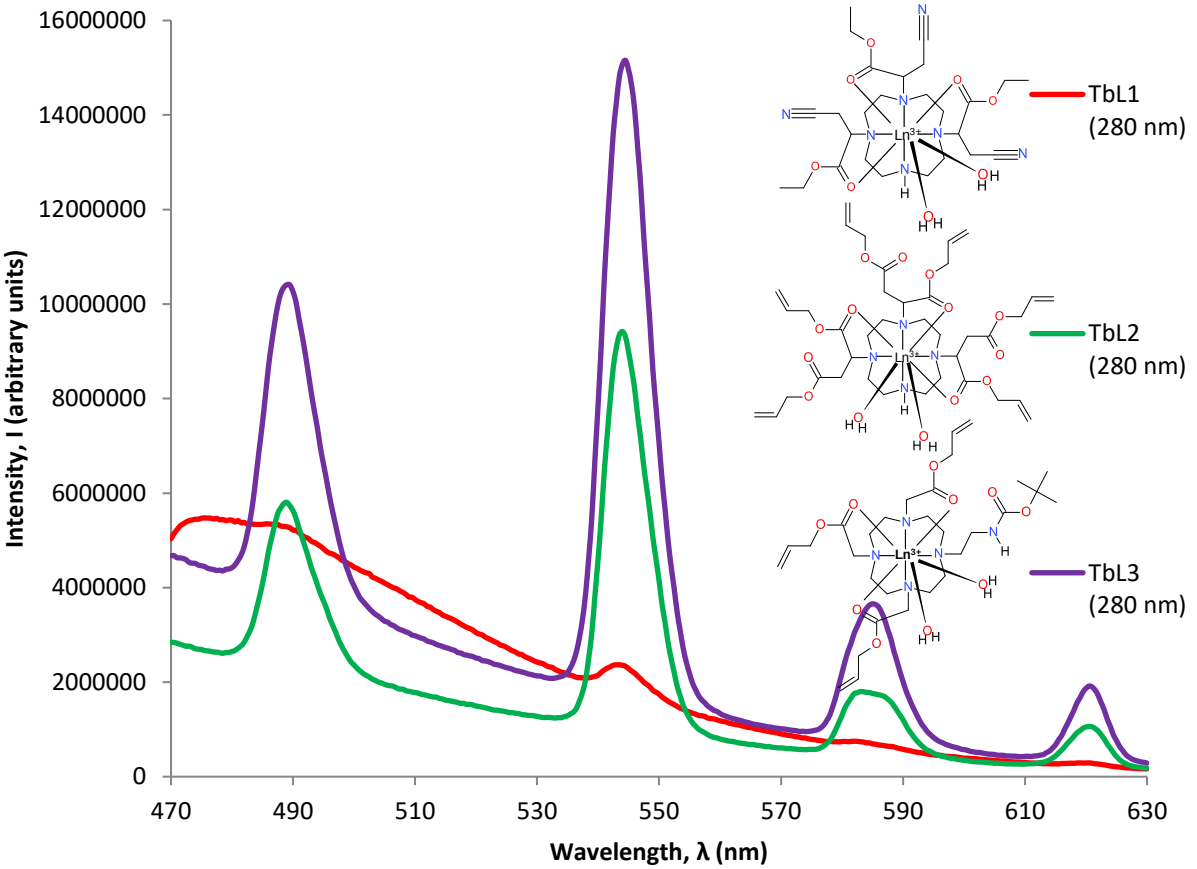

Figure 4.7 Comparison of 1 mM solutions of $[TbL1]^{3+}$, $[TbL2]^{3+}$ and $[TbL3]^{3+}$ fluorescent emission intensities (λ_{Ex}=280 nm, acquisition time=0.5 sec, acquisition increment=0.5 nm, excitation and emission slit width=3 nm, pH=5)

Lanthanide complexes of L3 were excited at 230 nm, since UV-Vis indicated a high absorbance at this wavelength; however lanthanide fluorescence was not detected, suggesting lanthanide excitation did not occur.

Fluorescence analysis of the $[LnL1]^{3+}$ complexes revealed that lanthanide fluorescence was heavily obscured by a broad fluorescence response (~470 nm to ~530 nm) not observed previously with $[LnDOTA]^-$ or [LnDO3A], or with the other lanthanide complexes studied (Figures 4.6 and 4.7). It is possible that the excitation energy absorbed by the ligand is not transferred as efficiently to the lanthanide; rather some energy is re-emitted by the ligand resulting in the broad emission. This broad emission obscures the line-like peaks of europium, when it is chelated by L1, at 578 nm, 590 nm and 514 nm.

For all DO3A-like ligand europium complexes, the ΔJ=2 transition (responsible for the emission at 614 nm) was more intense than the ΔJ=1 transition (responsible for the emission at 591 nm), suggesting that the complexes are indeed hepta-coordinated. This is important because this indicates the three DO3A-like pendant arms of L3 were coordinating the lanthanide ion, and the fourth *t*-But *N*-ethylcarbamate arm was not, i.e. the *N*-ethylcarbamate arm is not involved in the chelation of the lanthanide.

Having confirmed by fluorimetry the successful synthesis of all DO3A-like lanthanide complexes, and having ascertained that excitation at a wavelength of 280 nm was most effective to sensitise fluorescence europium and terbium emissions, 3 mM stock solutions were prepared in order to undertake fluorimetric assays using the selected organic analytes (Section 4.3.2).

Development of sensor application methodology

Methodology for the application of $[LnDOTA]^-$ and [LnDO3A] sensors involved the sequential decrease in concentration of organic analytes while maintaining a constant sensor concentration (Section 2.7.1). In order to do this, an initial equimolar sensor/analyte mixture was produced with dilution of analyte achieved by removing half the mixture and topping up with sensor solution. This methodology was not economical and consumed too much of the supply of the sensor

complexes, so it was important to develop a new methodology that would conserve supplies but provide the information necessary for valid comparison between the various sensor responses to be made. It was essential to maintain a constant sensor concentration so that the effect upon sensor-only fluorescence emission intensity, as a consequence of varying the concentration of analytes present, may be ascertained.

In order to do this, much smaller volumes of saturated analyte solutions, of known concentrations were added to the sensor solutions, with the sensors present at much higher concentrations. This meant that the concentration of the organic analyte would increase while the effective volume of solvent remained constant as, *ipso facto*, does the concentration of the sensor.

Therefore, the protocol to determine change in sensor fluorescence intensity with increasing concentration of analyte was as follows: i) 0.5 ml of 3 mM sensor solution was decanted into a 0.5 ml capacity cuvette using a 500 µl micro syringe; ii) a sensor-only fluorescence spectrum was obtained using 280 nm excitation wavelength and, iii) using a 100 µl micro syringe, the analyte solution was added in 20 µl aliquots until the total volume added was 200 µl, or when no further change in detected fluorescence emission was observed (Sections 4.6.1 and 4.6.2). In cases where lanthanide fluorescence emissions were quenched or sensitised when the first 20 µl aliquot of analyte was added, the protocol was amended so that these responses were gradual. To achieve this, 2 µl aliquots of analyte was added sequentially until no further change in detected fluorescence emission was observed (Sections 4.6.1 and 4.6.2). The fluorimeter settings for these assays are shown on Table 4.3 (Table 2.4, repeated).

Lanthanide	**Excitation λ, nm**	**Excitation Slit, nm**	**Emission Slit, nm**	**Acquisition time, s**	**Acquisition increment, nm**	**Acquisition range, nm**
Europium	280	3	3	0.5	0.5	570-710
Terbium	280	3	3	0.5	0.5	460-640

Table 4.3 (Table 2.4 repeated) Optimised fluorimeter settings used to determine change in sensor fluorescence intensity with increasing concentration of analyte

4.3.2 Application of lanthanide complexes of L1, L2 and L3 to analogue analytes

Initial experiments using europium and terbium complexes of DOTA and DO3A suggested some of the selected analytes may not affect the fluorescence emissions of these complexes, or, at the very least, were not detected. However, the presence of some classes of analyte caused lanthanide sensitisation or fluorescence quenching (Section 3.5). Upon considering the analytes which affected sensor fluorescence emissions, it was likely that their structure and, consequently, their photophysical properties, are the factors that govern their interaction with the complexes resulting in the sensor responses observed.

Further, experiments using europium and terbium complexes of DOTA and DO3A had elucidated that where individual analytes did not invoke a response, all analytes of the same class also presented no response when tested, e.g. there was no response detected when the sensor was applied to any aliphatic carboxylic acid. This suggested that these classes of molecule would invoke a similar response regardless of the number of individual molecules of each class, therefore, the suite of analytes of each class could be reduced to just one representative analyte of each class.

Likewise, where an unequivocal response was detected, e.g. application of the sensor to a nucleobase, the same response was detected for all nucleobases. Since this was a positive response, i.e. intensity was observed to increase; the suite of analytes was reduced to two representative analytes of each class.

The reduction in the selection of analytes used to test the DO3A-like lanthanide sensors, therefore, served two purposes. The first was to reduce the significant amount of time it took to perform the experiments and the second was in order to conserve the depleting supply of sensor solutions available for testing.

Reduced selection of organic analytes

It was established that all nucleobases quenched fluorescence, with the exception of adenine (Section 3.4.5), therefore the suite of nucleobases was reduced to four (two purines, including

adenine, and two pyrimidines). The amino acid selection was reduced to two and included tyrosine, since this amino acid is intrinsically fluorescent and may act as an antenna when combined with the LnDO3A-like complexes. Two carboxylic acids were selected: benzoic acid (since the presence of this is known to sensitise emissions), and fumaric acid (a conjugated dicarboxylic acid). One other analyte was selected (guanyl urea) because this molecule is also highly conjugated and exhibits several moieties that could potentially interact with the lanthanide metal centre. The reduced suite of organic analytes chosen is tabulated (Table 4.4).

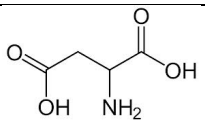 Aspartic acid (Amino acid)	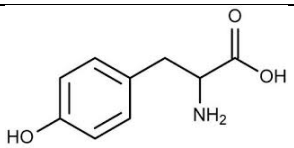 Tyrosine (Amino acid)	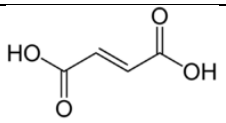 Fumaric acid (carboxylic acid)
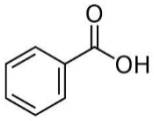 Benzoic acid (carboxylic acid)	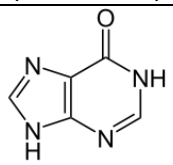 Hypoxanthine (Nucleobases – Purines)	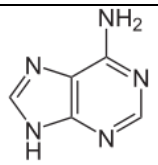 Adenine (Nucleobases – Purines)
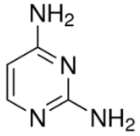 2 4-diaminopyrimidine (Nucleobases – Pyrimidines)	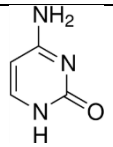 Cytosine (Nucleobases – Pyrimidines)	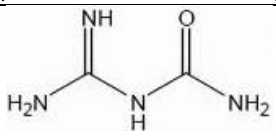 Guanyl urea (Other organic)

Table 4.4 Organic analytes used in fluorimetry assays

Sensor concentrations used with $[LnDOTA]^-$ and [LnDO3A] were low (0.25 to 0.5 mM) and so fluorescent emission intensity was consequently also low. If intensity of fluorescent emissions is low then changes to the intensity of sensor fluorescence emissions upon application of the sensors to the analytes are less easy to detect. In order to address this issue, it was resolved to increase the working concentration of the DO3A-like complex sensors to 3 mM, with the expectation that sensor responses would be more sensitive to the presence of analytes, and thus easier to discern.

The results presented in Chapter 3 indicated that the concentration of analytes had to be similar to the sensor for lanthanide fluorescence responses to be detected. However, producing 3mM solutions of the chosen organic analytes proved to be problematic, since most have very low solubility. In order to address this issue, saturated solutions of each compound were prepared, and their concentrations calculated using their individual solubility in pure water in the range 20-25°C (Table 4.5).

Analyte	RMM (g mol^{-1})	Solubility in H_2O (g l^{-1})	Temp. (°C)	Number of moles in 1 l at saturation	Concentration (mol dm^{-3})
Adenine	135.13	1.03E+00	25	7.62E-03	7.62E-06
Hypoxanthine	136.11	7.00E-01	23	5.14E-03	5.14E-06
Cytosine	111.1	9.66E+01	25	8.69E-01	8.69E-04
2,4-diaminopyrimidine	110.12	8.36E+02	25	7.59E+00	7.59E-03
(*L*)-aspartic acid	133.100	5.39E+00	25	4.05E-02	4.05E-05
(*L*)-tyrosine	181.189	4.53E-01	25	2.50E-03	2.50E-06
Benzoic acid	122.120	3.40E+00	25	2.78E-02	2.78E-05
Fumaric acid	116.072	4.41E+02	25	3.80E+00	3.80E-03
Guanylurea sulfate	302.26	5.00E+01	No data	1.65E-01	1.65E-04

Table 4.5 Concentration of saturated analyte solutions (mol dm-3)

The organic analytes were combined in aliquots of varying volume (2 µl to 20 µl) because the responses obtained varied from analyte to analyte. Therefore, smaller volume aliquots were added, where necessary, to best determine the effect of analyte concentration on emission intensity. Upon each addition, the cuvette and contents were inverted ten times to ensure homogeneity.

4.3.3 Addition of non-nucleobase analytes

No significant changes in fluorescence intensity were observed when (*L*)-aspartic acid, (*L*)-tyrosine, fumaric acid or guanylurea sulfate were added to $[EuL1]^{3+}$ (e.g. Figure 4.8). Addition of benzoic acid, however, did invoke a response (Figure 4.9).

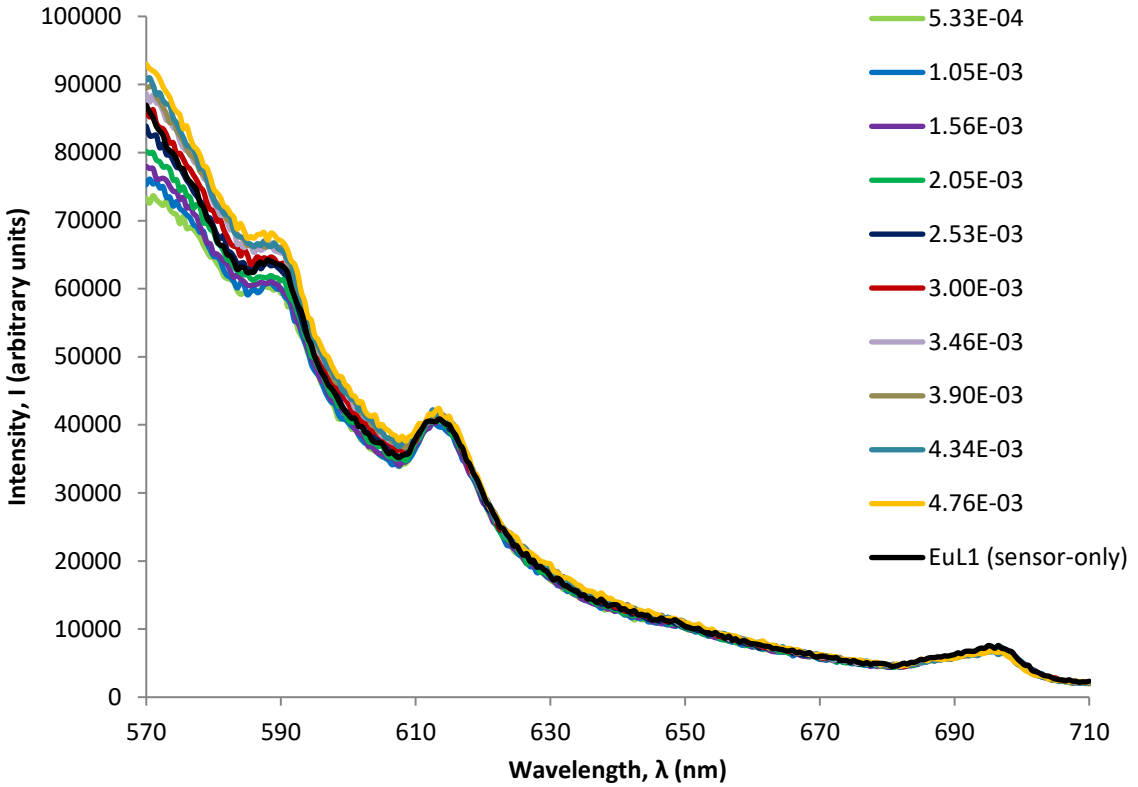

Figure 4.8 Spectra obtained for $[EuL1]^{3+}$ (3 mM) and subsequent additions of (L)-aspartic acid (concentration after each addition, mol dm^{-3}) (λ_{Ex}=280 nm, acquisition time=0.5 sec, acquisition increment=0.5 nm, excitation and emission slit width=3 nm, pH=5)

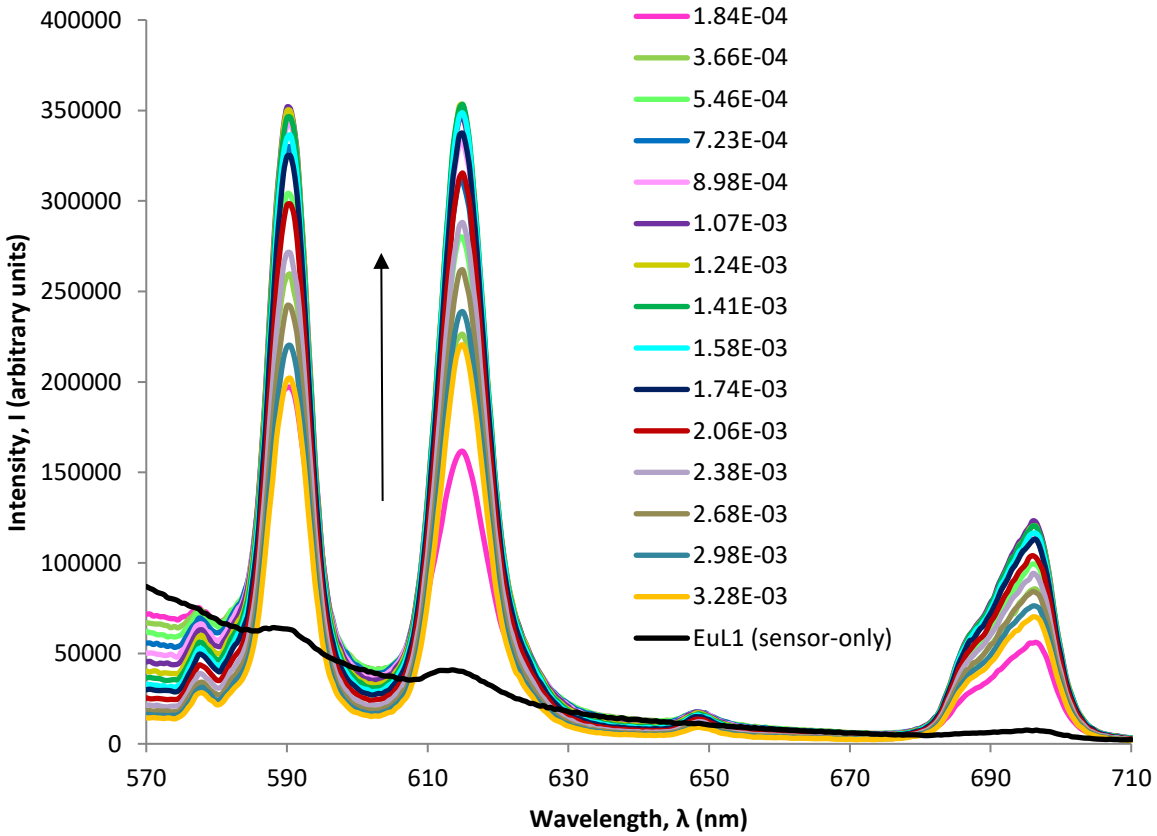

Figure 4.9 Spectra obtained for $[EuL1]^{3+}$ (3 mM) and subsequent additions of benzoic acid (concentration after each addition, mol dm^{-3}) (λ_{Ex}=280 nm, acquisition time=0.5 sec, acquisition increment=0.5 nm, excitation and emission slit width=3 nm, pH=5)

The fluorescence spectra obtained for the non-nucleobase analytes suggests there is no detectable interaction, since intensity and shape of the europium fluorescence emission does not alter appreciably from the $[EuL1]^{3+}$ spectrum. Benzoic acid affords a significant increase in intensity at the ΔJ=1, 2 and 4 transitions, in particular, and causes the emission at 591 nm (ΔJ=1) to become as intense as that at 614 nm (ΔJ=2). This suggests these transitions are sensitised by the presence of benzoic acid and, furthermore, this interaction increases efficiency of energy transfer to electrons. This populates the energy levels responsible for the ΔJ=1 transition emission, in particular. It is likely, then, that the carboxylic acid moiety coordinates the europium ion in the same way as the carbonyl groups of the ligand. The form of the spectrum is comparable to that observed for $[EuDOTA]^-$, where the complex is eight-coordinate, and to that obtained when benzoic acid was combined with [EuDO3A] (Chapter 3). It is therefore probable that benzoic acid interacts with $[EuL1]^{3+}$ in a similar manner to that when combined with [EuDO3A].

Unlike $[EuL1]^{3+}$, when (*L*)-aspartic acid, (*L*)-tyrosine, fumaric acid and guanylurea were added to $[TbL1]^{3+}$, an increase in fluorescence intensity was observed (e.g. Figure 4.10). This increase in detected fluorescence, upon each addition, produced a spectrum which maintained the shape of that of the $[TbL1]^{3+}$ solution. There was modest sensitisation of the terbium ΔJ=1 emission but it was not possible to observe the ΔJ=2 emission as this was obscured by the broad unassigned emission in this region. The transitions at ΔJ=2 (~488 nm), ΔJ=1 (~543 nm), ΔJ=0 (~590 nm) and ΔJ=-1 (~620 nm) all experienced significant sensitisation when in the presence of benzoic acid, however (Figure 4.11). This result is comparable to observations made when benzoic acid was combined with solutions of $[TbDOTA]^-$ and [TbDO3A].

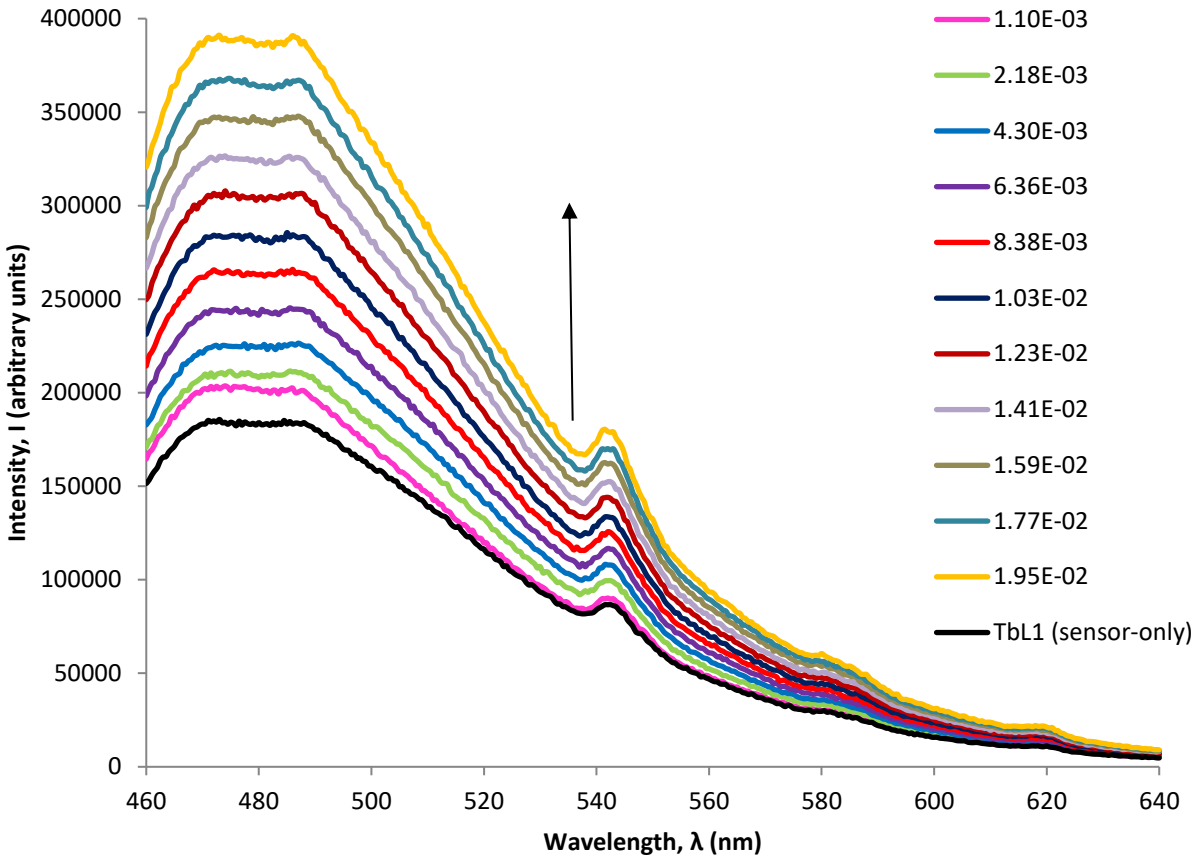

Figure 4.10 Spectra obtained for $[TbL1]^{3+}$ (3 mM) and subsequent additions of non-nucleobase, guanylurea sulfate (concentration after each addition, mol dm^{-3}) (λ_{Ex}=280 nm, acquisition time=0.5 sec, acquisition increment=0.5 nm, excitation and emission slit width=3 nm, pH=5)

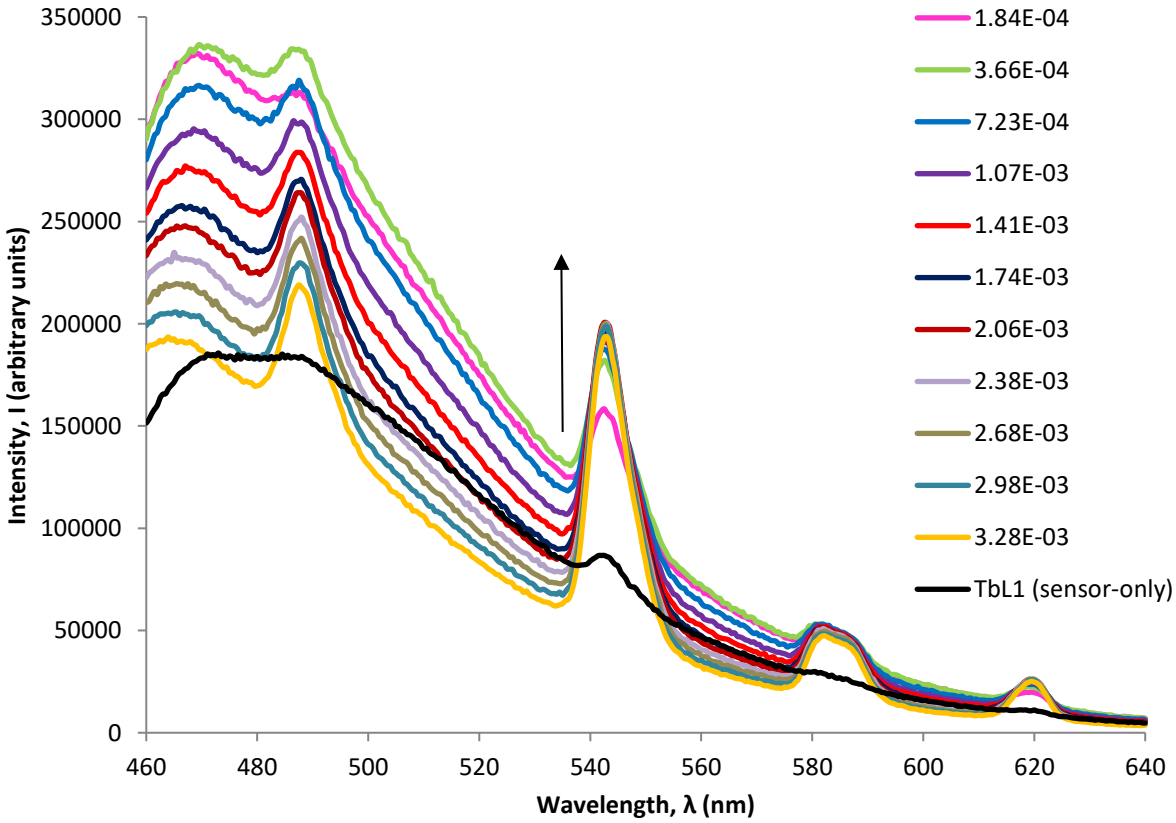

Figure 4.11 Spectra obtained for $[TbL1]^{3+}$ (3 mM) and subsequent additions of non-nucleobase, benzoic acid (concentration after each addition, mol dm^{-3}) (λ_{Ex}=280 nm, acquisition time=0.5 sec, acquisition increment=0.5 nm, excitation and emission slit width=3 nm, pH=5)

No significant change in fluorescent intensity was observed when guanylurea sulfate was added to $[EuL2]^{3+}$, other than that expected with dilution (Figure 4.12), however, upon addition of (*L*)-aspartic acid and (*L*)-tyrosine, a decrease in intensity was detected (e.g. Figure 4.13). The decrease was not significant enough to confidently ascribe to analyte interaction; however, the observations could also be an effect of dilution. The reduction in fluorescent intensity detected when fumaric acid was added was more marked suggesting a response to analyte presence is more likely (Figure 4.14). Addition of benzoic acid, however, invoked the same substantial response seen previously when this analyte was combined with other lanthanide complexes (Figure 4.15).

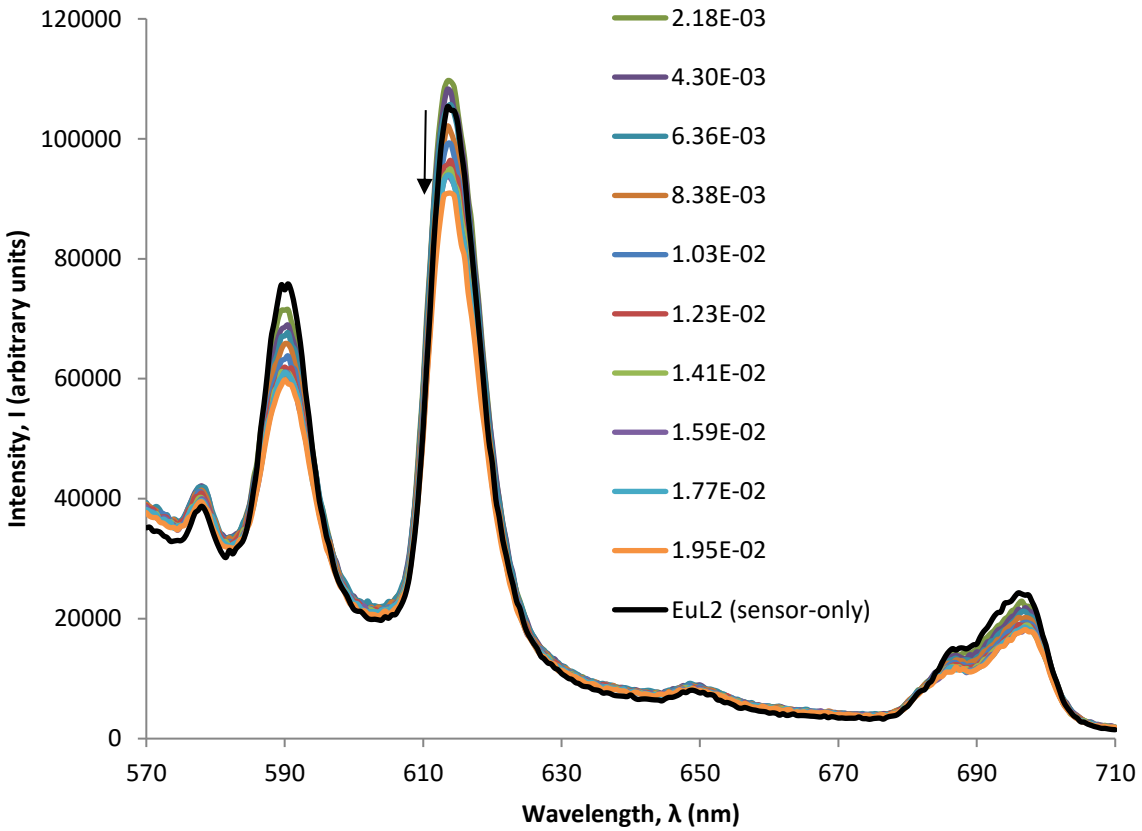

Figure 4.12 Spectra obtained for $[EuL2]^{3+}$ (3 mM) and subsequent additions of guanylurea sulfate (concentration after each addition, mol dm^{-3}) (λ_{Ex}=280 nm, acquisition time=0.5 sec, acquisition increment=0.5 nm, excitation and emission slit width=3 nm, pH=5)

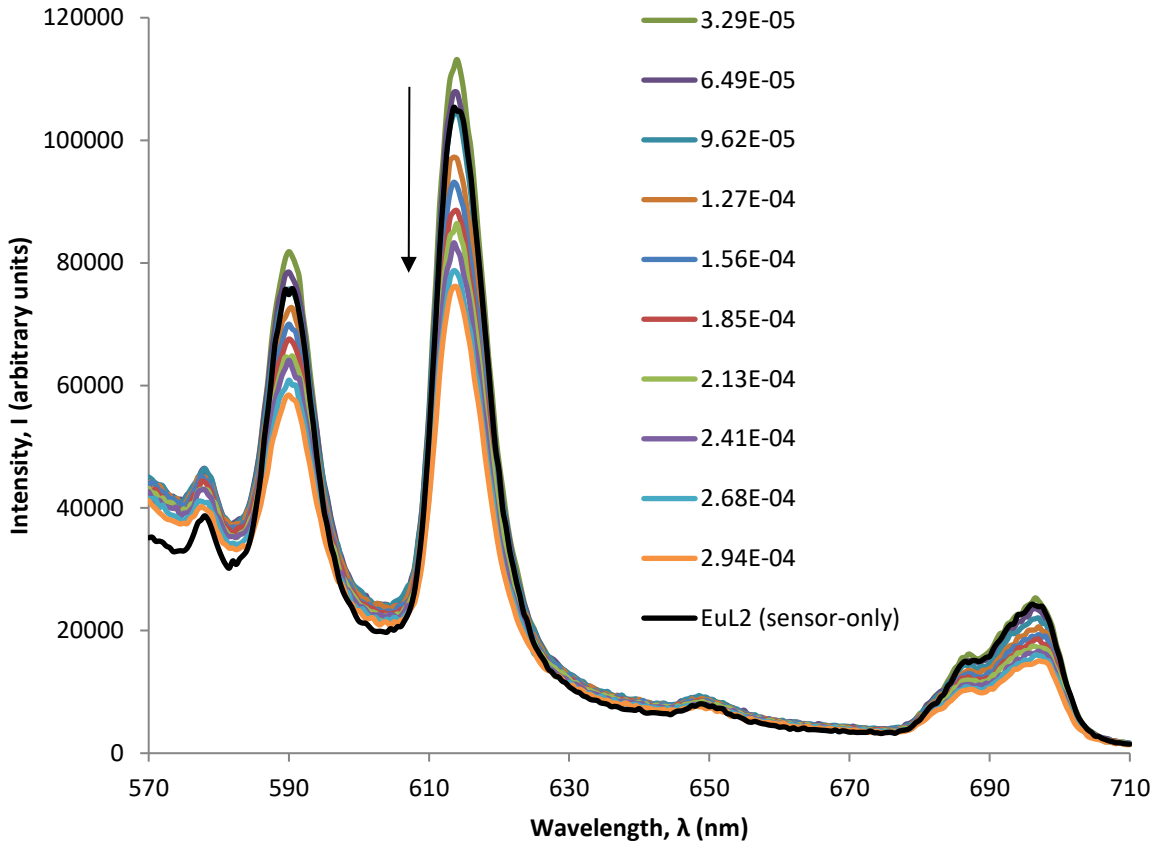

Figure 4.13 Spectra obtained for $[EuL2]^{3+}$ (3 mM) and subsequent additions of (L)-aspartic acid (concentration after each addition, mol dm^{-3}) (λ_{Ex}=280 nm, acquisition time=0.5 sec, acquisition increment=0.5 nm, excitation and emission slit width=3 nm, pH=5)

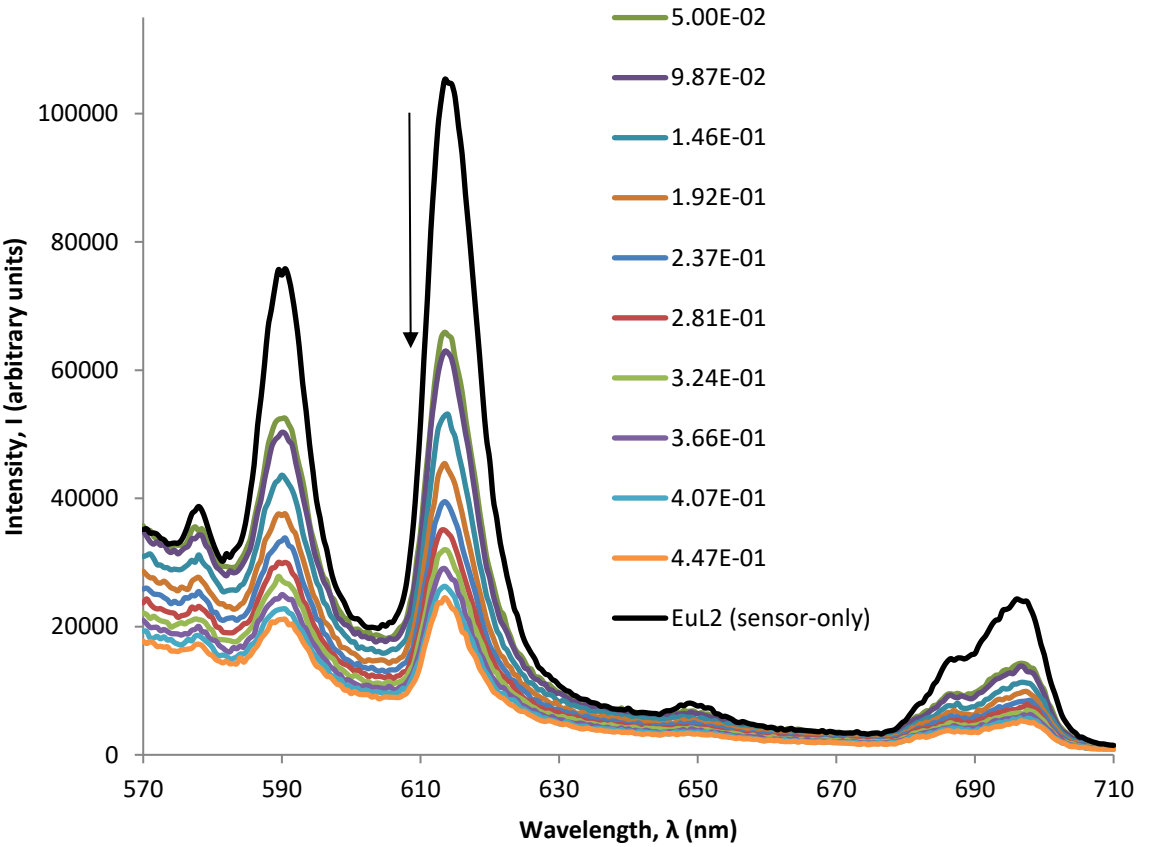

Figure 4.14 Spectra obtained for $[EuL2]^{3+}$ (3 mM) and subsequent additions of fumaric acid (concentration after each addition, mol dm^{-3}) (λ_{Ex}=280 nm, acquisition time=0.5 sec, acquisition increment=0.5 nm, excitation and emission slit width=3 nm, pH=5)

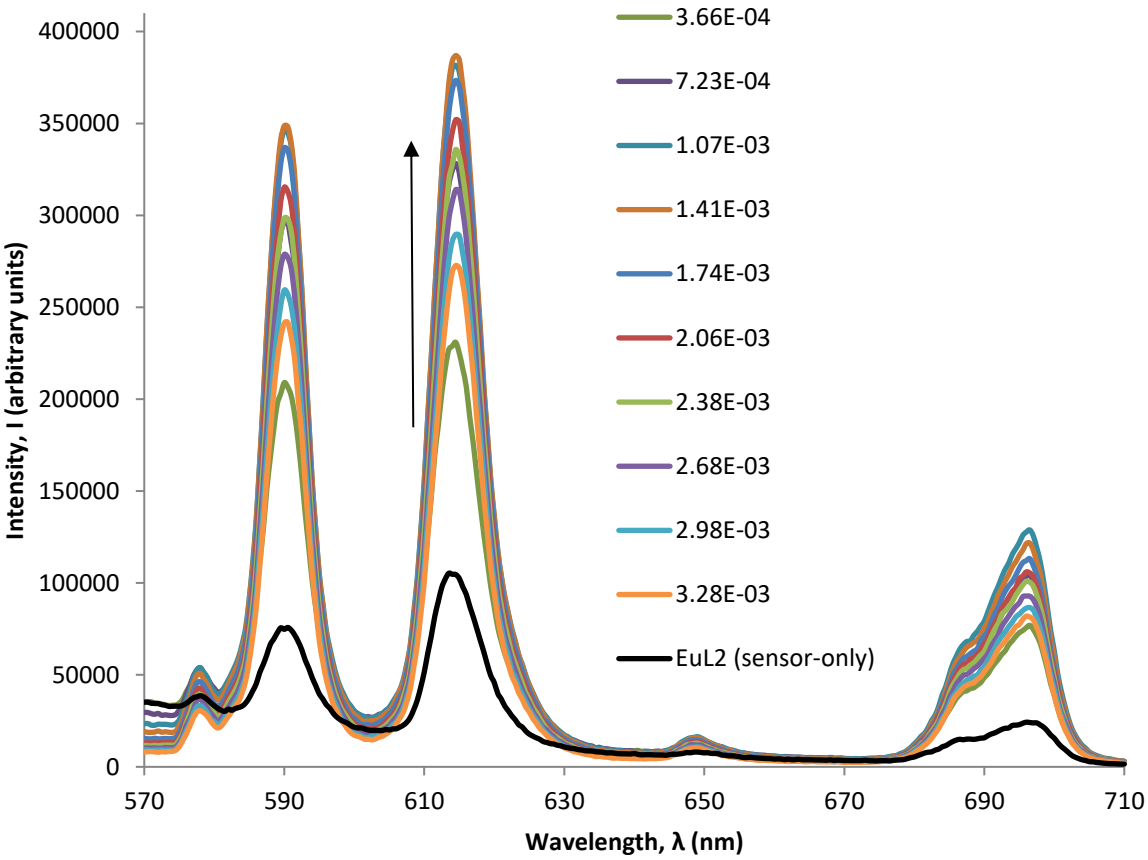

Figure 4.15 Spectra obtained for $[EuL2]^{3+}$ (3 mM) and subsequent additions of benzoic acid (concentration after each addition, mol dm^{-3}) (λ_{Ex}=280 nm, acquisition time=0.5 sec, acquisition increment=0.5 nm, excitation and emission slit width=3 nm, pH=5)

The effect on terbium fluorescence of the presence of non-nucleobase analytes was comparable to the observations made by their presence with $[EuL2]^{3+}$; guanylurea sulfate had no effect on intensity other than that expected of dilution (Figure 4.16) and (*L*)-aspartic acid and (*L*)-tyrosine resulted in a decrease in intensity that could not be confidently explained by a dilution effect alone (e.g. Figure 4.17). When fumaric acid was combined with $[TbL2]^{3+}$, the reduction in fluorescent intensity was more obvious than that afforded by (*L*)-aspartic acid and (*L*)-tyrosine with $[EuL2]^{3+}$. This suggests $[TbL2]^{3+}$ could be more sensitive to the presence of fumaric acid than $[EuL2]^{3+}$ (Figure 4.18).

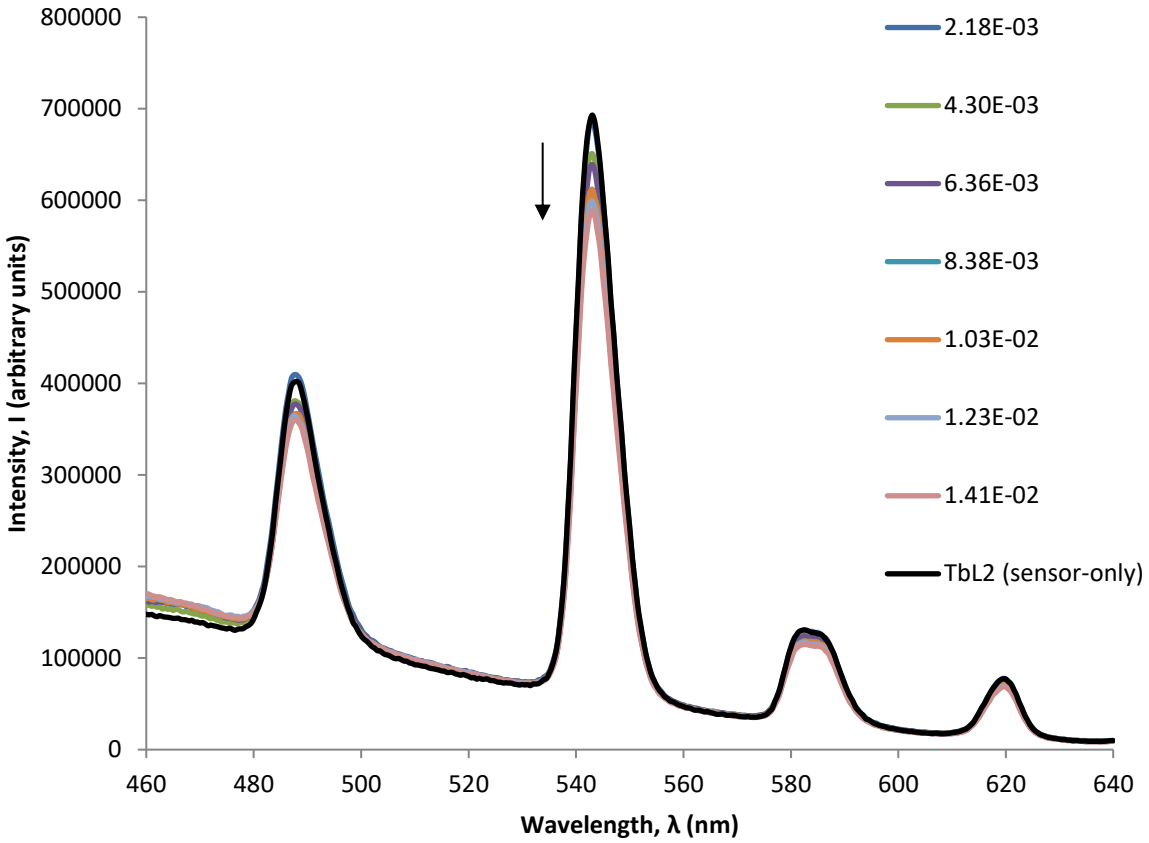

Figure 4.16 Spectra obtained for $[TbL2]^{3+}$ (3 mM) and subsequent additions of guanylurea sulfate (concentration after each addition, mol dm^{-3}) (λ_{Ex}=280 nm, acquisition time=0.5 sec, acquisition increment=0.5 nm, excitation and emission slit width=3 nm, pH=5)

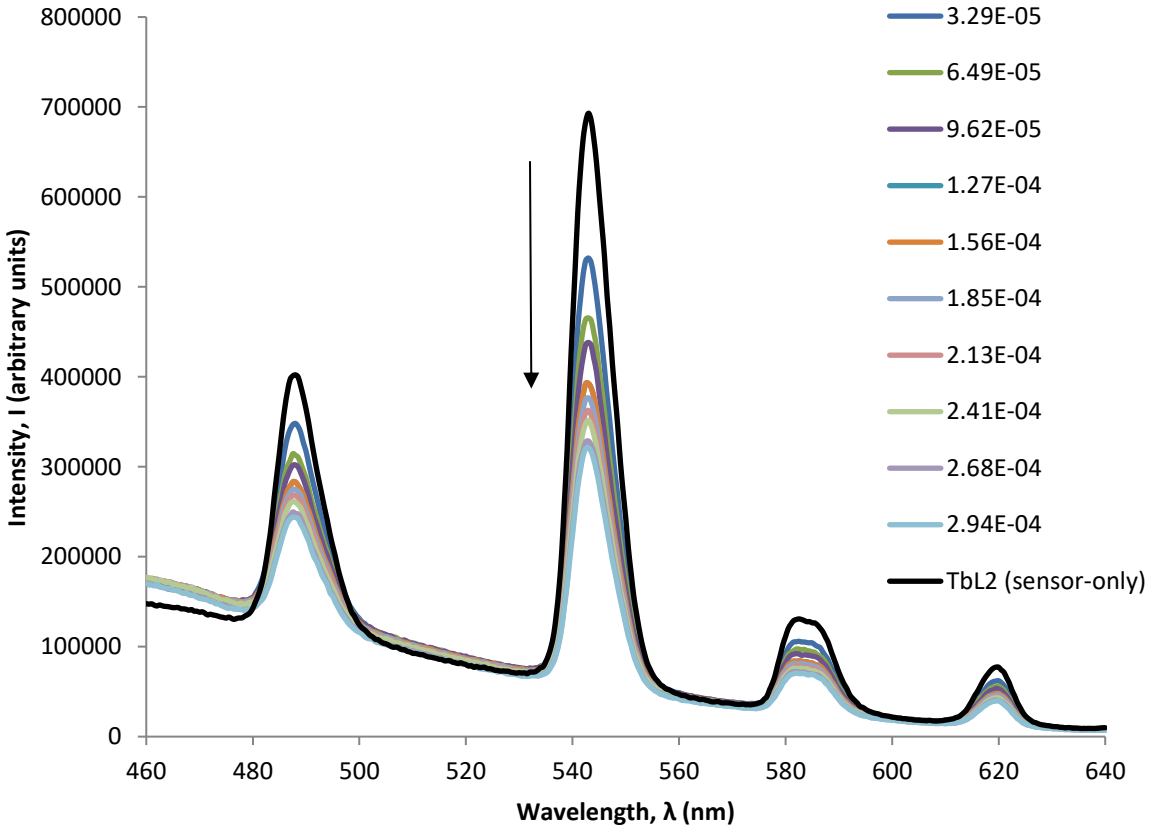

Figure 4.17 Spectra obtained for $[TbL2]^{3+}$ (3 mM) and subsequent additions of (L)-aspartic acid (concentration after each addition, mol dm^{-3}) (λ_{Ex}=280 nm, acquisition time=0.5 sec, acquisition increment=0.5 nm, excitation and emission slit width=3 nm, pH=5)

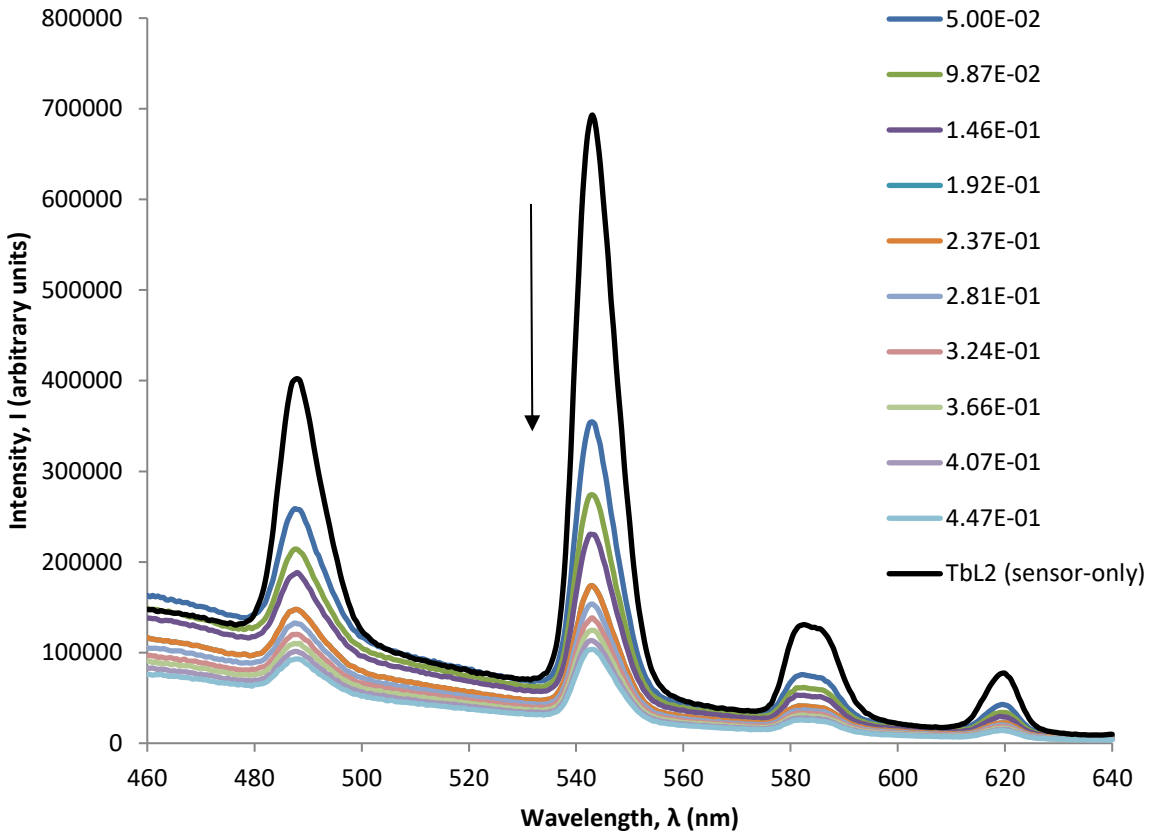

Figure 4.18 Spectra obtained for $[TbL2]^{3+}$ (3 mM) and subsequent additions of fumaric acid (concentration after each addition, mol dm^{-3}) (λ_{Ex}=280 nm, acquisition time=0.5 sec, acquisition increment=0.5 nm, excitation and emission slit width=3 nm, pH=5)

When $[TbL2]^{3+}$ was in the presence of benzoic acid, an increase in the intensity of the terbium fluorescent transition emissions occurred, as has been previously observed (Figure 4.19). Using lower volume aliquots of benzoic acid in order to better resolve the effect of its concentration, it was found that maximum sensitisation occurs at a concentration of ~$3.3x10^{-4}$ mol dm^{-3} (addition of 18 µl of saturated benzoic acid solution). The addition of further aliquots, therefore increasing the concentration of benzoic acid present in the mixture, resulted in a decrease in fluorescence intensity. This result is comparable to that observed when benzoic acid was combined with $[EuL1]^{3+}$. It is probable, then, that the decrease in sensitisation seen in both cases has a common mechanism. It is not clear what may cause this, however it may be that as concentration of benzoic acid increases, the pH of the solution decreases, thus altering the photophysical properties of the complexes fluorescence emissions (Parker, 2000).

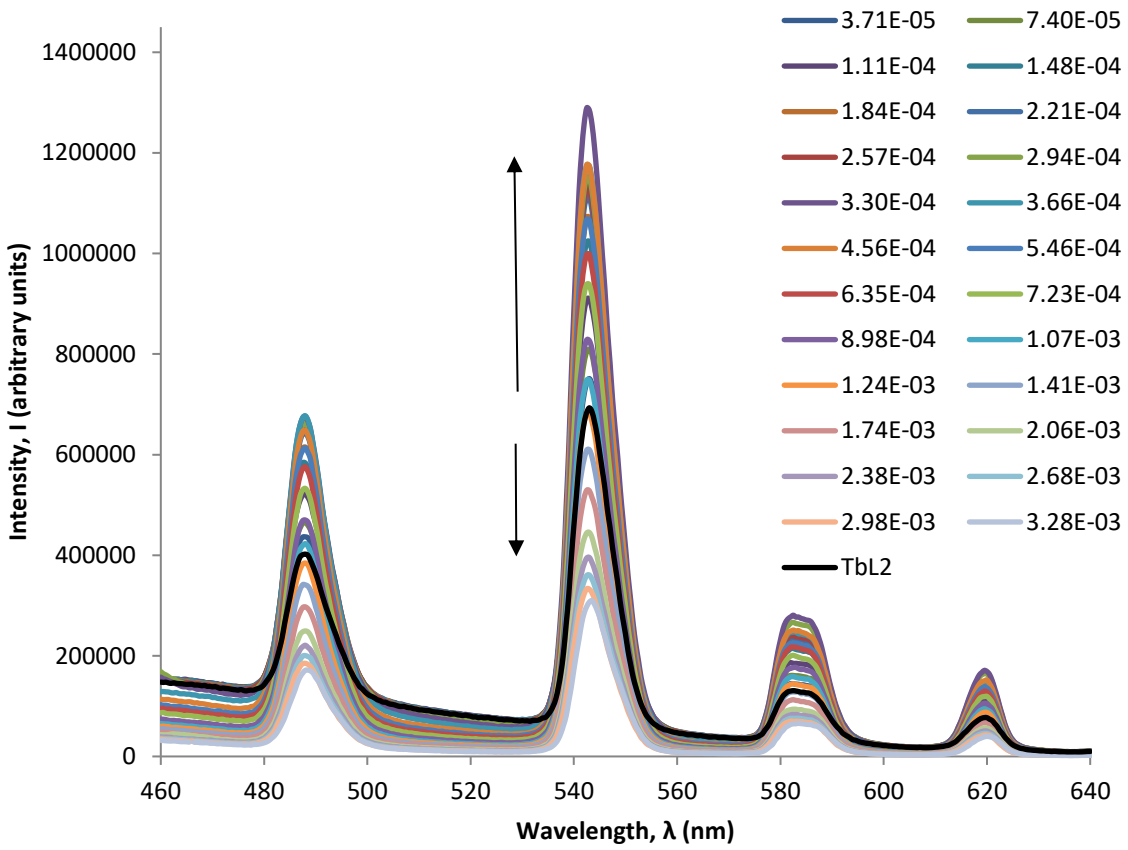

Figure 4.19 Spectra obtained for $[TbL2]^{3+}$ (3 mM) (sensor-only, black line) and subsequent additions of benzoic acid (concentration after each addition, mol dm^{-3}) (λ_{Ex}=280 nm, acquisition time=0.5 sec, acquisition increment=0.5 nm, excitation and emission slit width=3 nm, pH=5)

Addition of (*L*)-aspartic acid (*L*)-tyrosine, guanylurea sulfate and fumaric acid resulted in a reasonably modest decrease in europium fluorescence intensity with each aliquot addition i.e. increase in analyte concentration (e.g. Figure 4.20). The addition of benzoic acid resulted in sensitisation of europium fluorescence comparable to all other europium complexes. All Δ*J* transitions emitted intensely and the emission at ~590 nm (Δ*J*=1) became comparably intense to that of the Δ*J*=2 transition at ~614 nm (e.g. Figure 4.21).

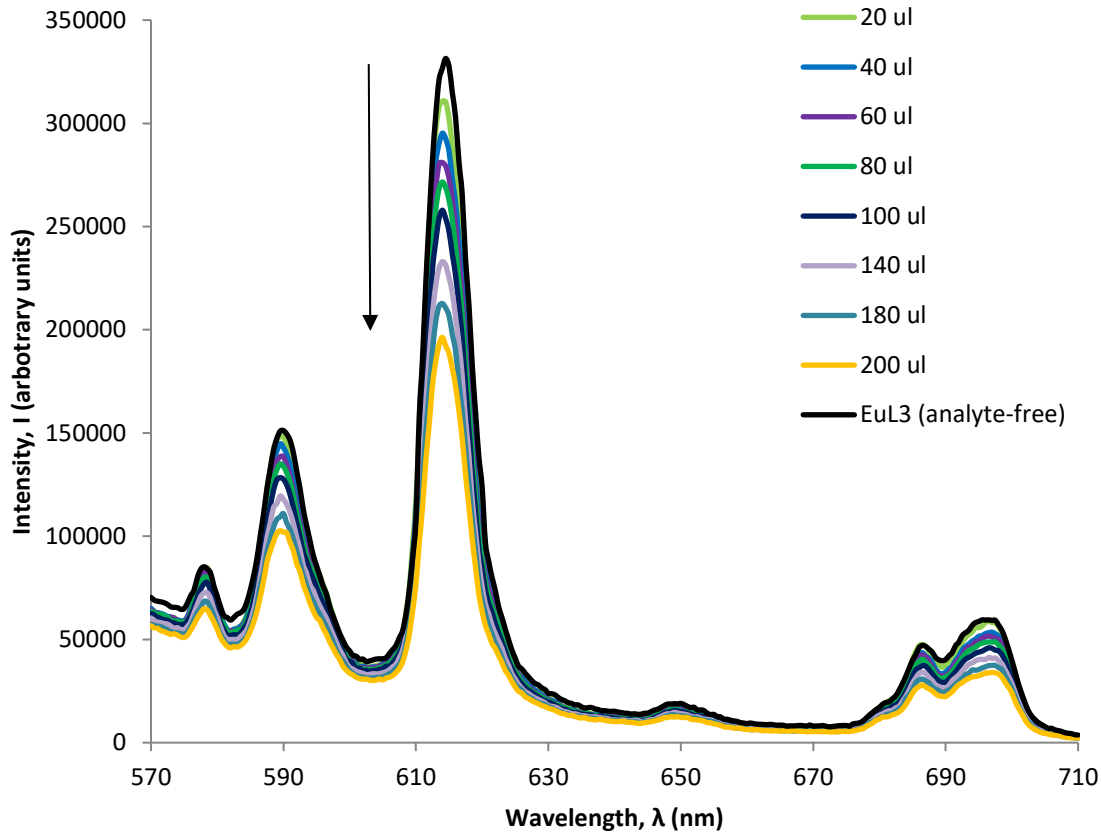

Figure 4.20 Spectra obtained for $[EuL3]^{3+}$ (3 mM) and subsequent additions of (L)-aspartic acid (concentration after each addition, mol dm^{-3}) (λ_{Ex}=280 nm, acquisition time=0.5 sec, acquisition increment=0.5 nm, excitation and emission slit width=3 nm, pH=5)

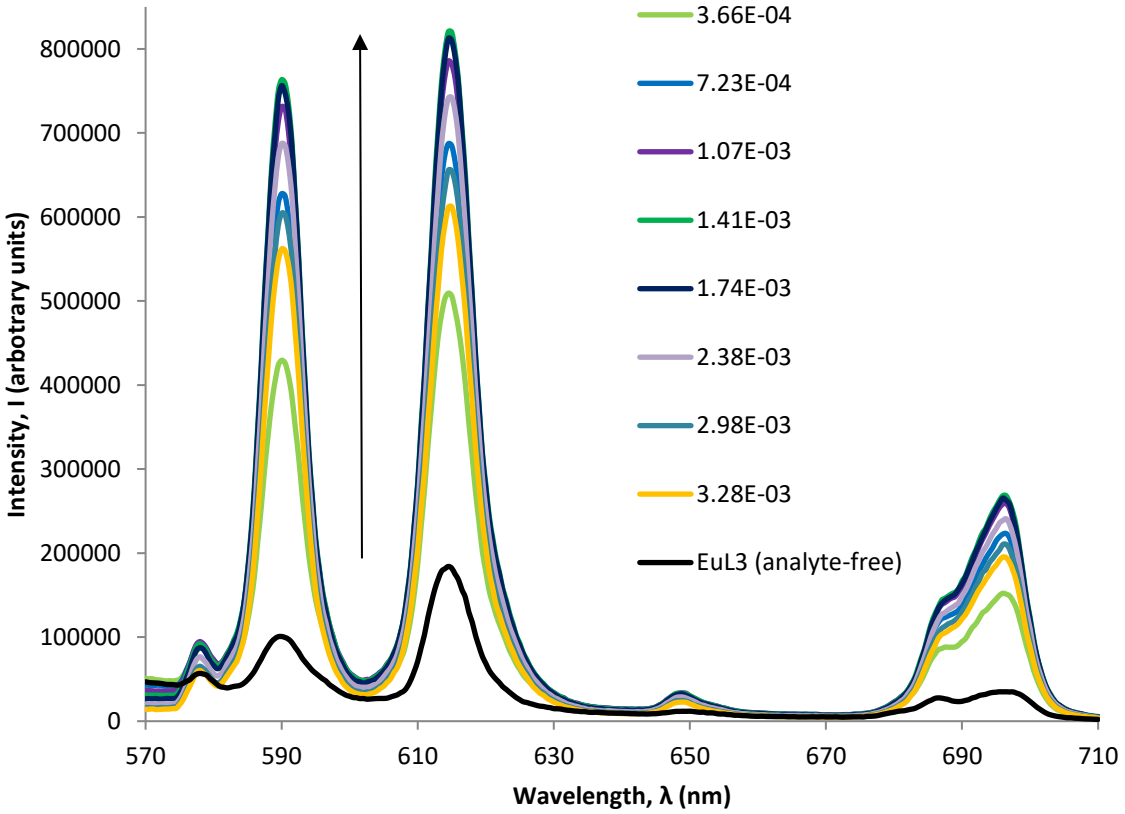

Figure 4.21 Spectra obtained for $[EuL3]^{3+}$ (3 mM) and subsequent additions of benzoic acid (concentration after each addition, mol dm^{-3}) (λ_{Ex}=280 nm, acquisition time=0.5 sec, acquisition increment=0.5 nm, excitation and emission slit width=3 nm, pH=5)

(*L*)-aspartic acid, (*L*)-tyrosine, guanylurea sulfate and fumaric acid appeared to invoke quenching of europium fluorescence. In all these cases, the degree of quenching suggested this response may be due to the presence of the analyte rather than a dilution effect. In the case of benzoic acid, as has been for all lanthanide complexes used in this study, the response was unambiguous; there was a substantial increase of all the europium emissions, particularly at the Δ*J*=2 transition.

When guanylurea was added to the terbium complex of L3 there was no effect on the fluorescence emissions (Figure 4.22). However, the response to (*L*)-tyrosine, (*L*)-aspartic acid and fumaric acid showed comparable decreases in terbium fluorescence emissions, relative to the first addition of each analyte (e.g. Figure 4.23).

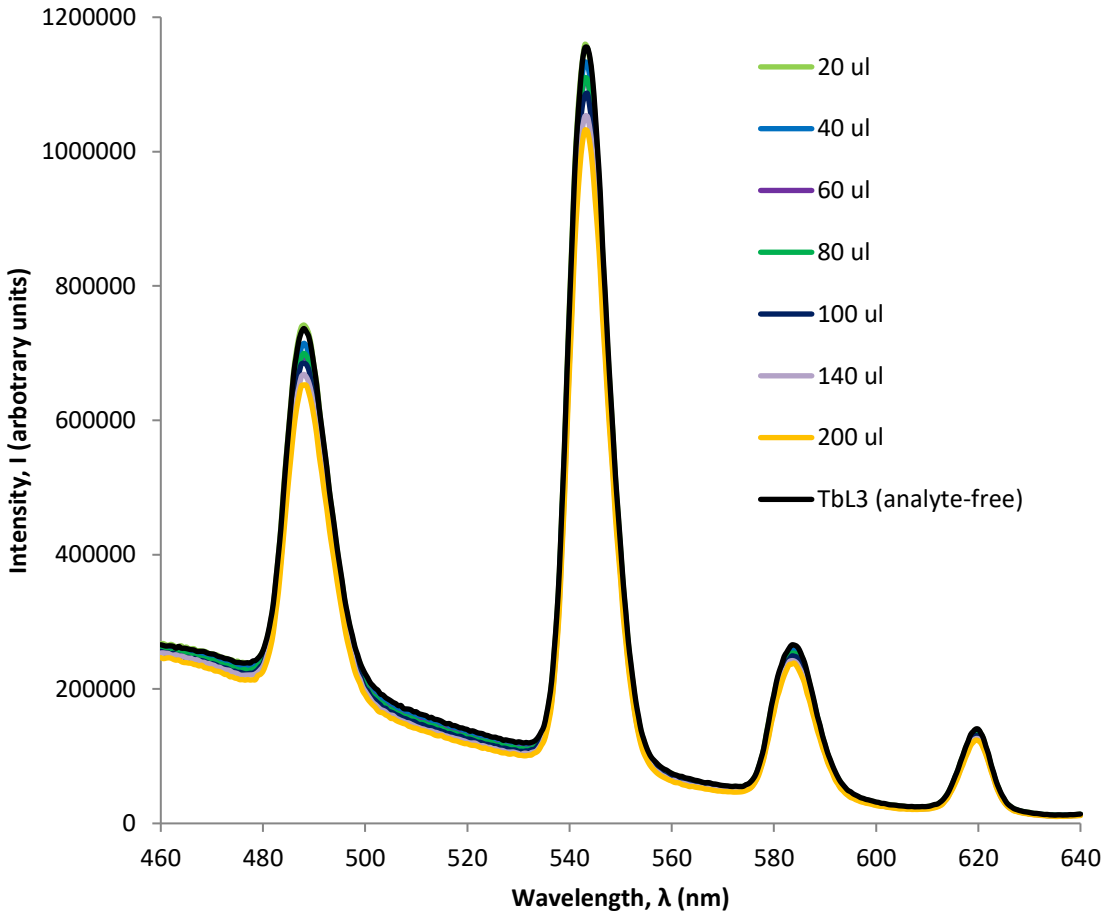

Figure 4.22 Spectra obtained for $[TbL3]^{3+}$ (3 mM) and subsequent additions of guanylurea sulfate (concentration after each addition, mol dm^{-3}) (λ_{Ex}=280 nm, acquisition time=0.5 sec, acquisition increment=0.5 nm, excitation and emission slit width=3 nm, pH=5)

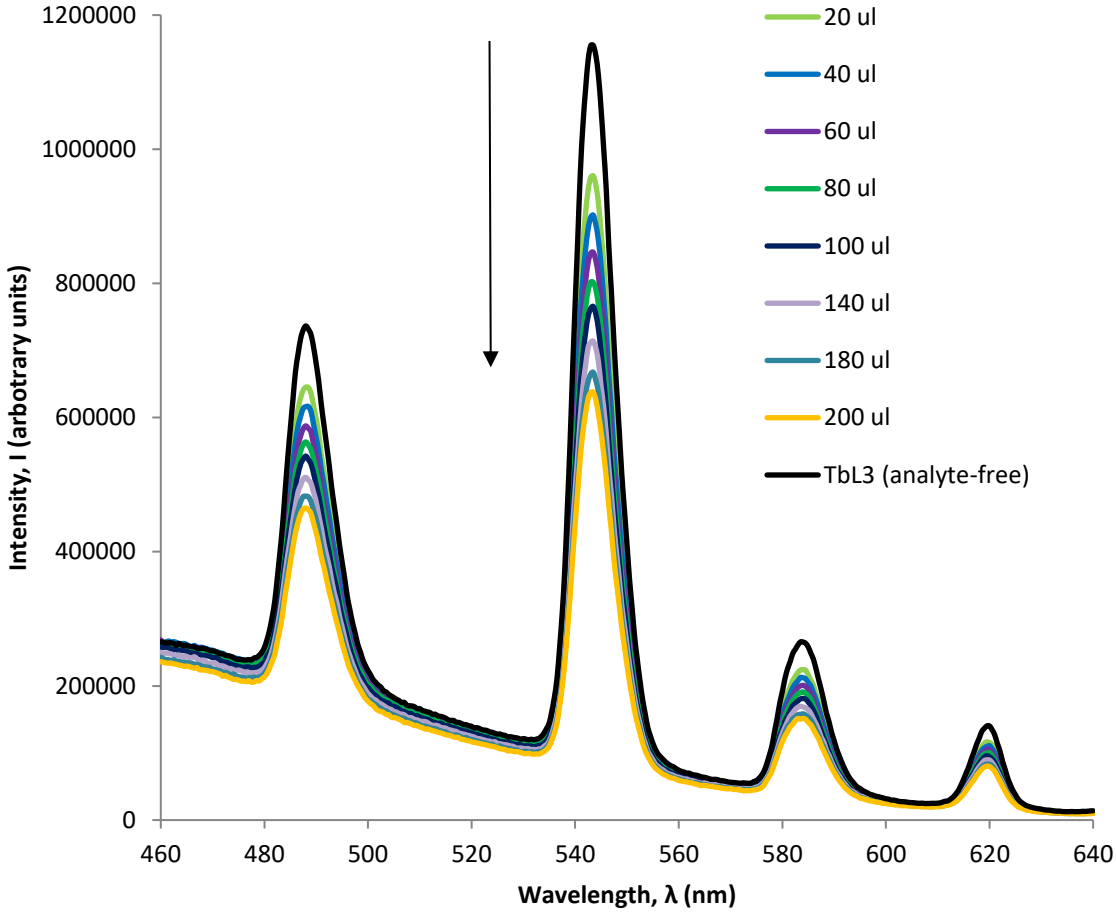

Figure 4.23 Spectra obtained for $[TbL3]^{3+}$ (3 mM) and subsequent additions of (L)-aspartic acid (concentration after each addition, mol dm^{-3}) (λ_{Ex}=280 nm, acquisition time=0.5 sec, acquisition increment=0.5 nm, excitation and emission slit width=3 nm, pH=5)

The responses for $[TbL3]^{3+}$ when mixed with benzoic acid were as previously observed; all emissions representative of terbium were sensitised, as evidenced by a large increase in intensity relative to the first addition of benzoic acid (Figure 4.24). With the exception of guanylurea sulfate, which did not invoke a sensor response, and benzoic acid, which caused terbium sensitisation, all other non-nucleobase analytes quenched the fluorescence. The response was likely to be due to the presence of the analyte rather than a dilution effect.

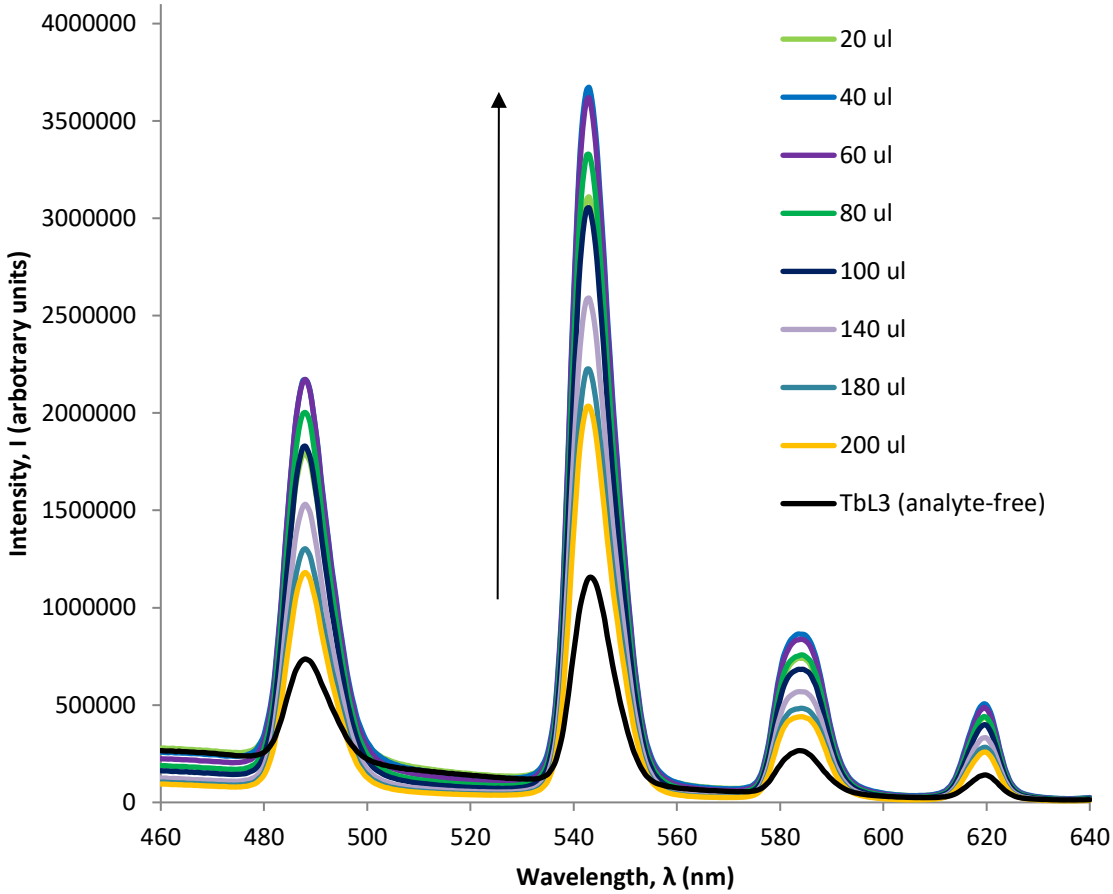

Figure 4.24 Spectra obtained for $[TbL3]^{3+}$ (3 mM) and subsequent additions of benzoic acid (concentration after each addition, mol dm^{-3}) (λ_{Ex}=280 nm, acquisition time=0.5 sec, acquisition increment=0.5 nm, excitation and emission slit width=3 nm, pH=5)

4.3.4 Addition of nucleobase analytes

Of the four nucleobases used as analytes in these assays, two were purines: hypoxanthine and adenine; and two were pyrimidines: cytosine and 2,4-diaminopyrimidine (2,4-DAP). Upon addition of the purine or pyrimidine nucleobases to $[EuL1]^{3+}$, the fluorescent intensity diminished (e.g. Figures 4.25 and 4.26). The intensity of each spectrum decreased with increasing concentrations of analyte; the presence of the analyte quenches the fluorescent emissions.

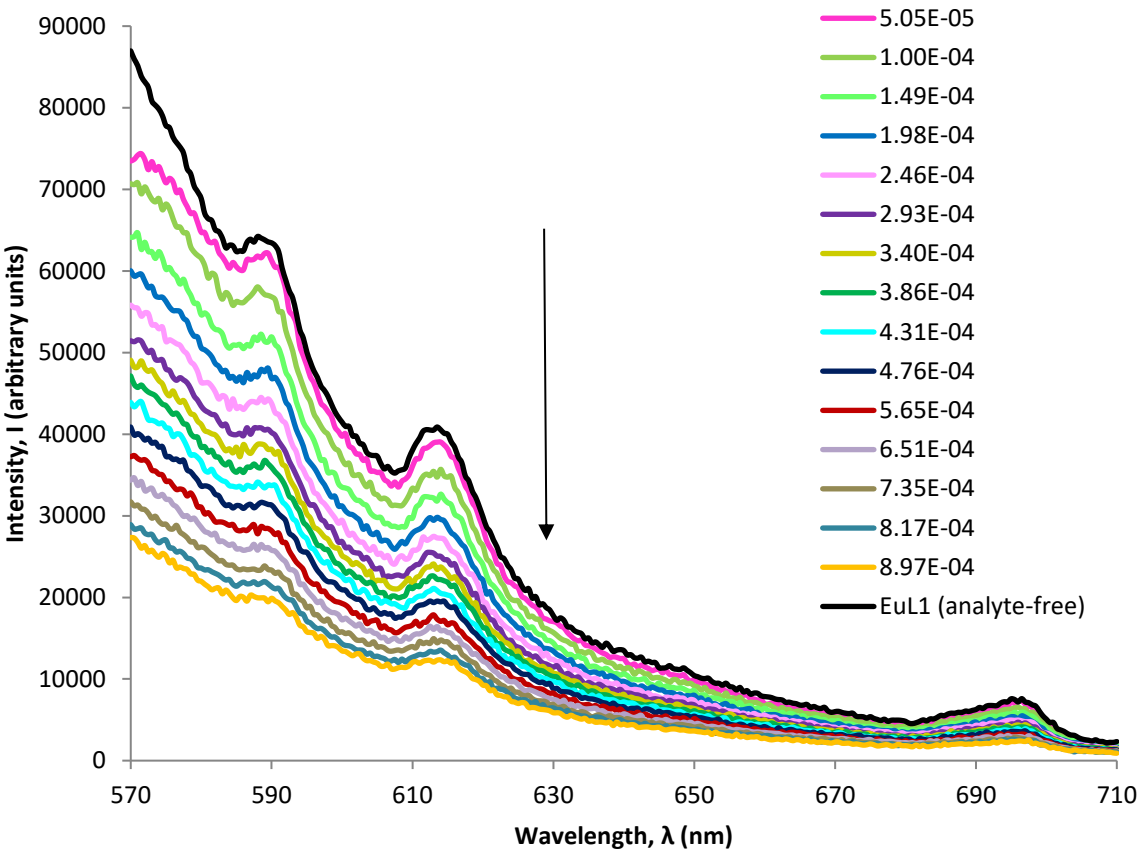

Figure 4.25 Spectra obtained for $[EuL1]^{3+}$ (3 mM) and subsequent additions of the purine, adenine (concentration after each addition, mol dm^{-3}) (λ_{Ex}=280 nm, acquisition time=0.5 sec, acquisition increment=0.5 nm, excitation and emission slit width=3 nm, pH=5)

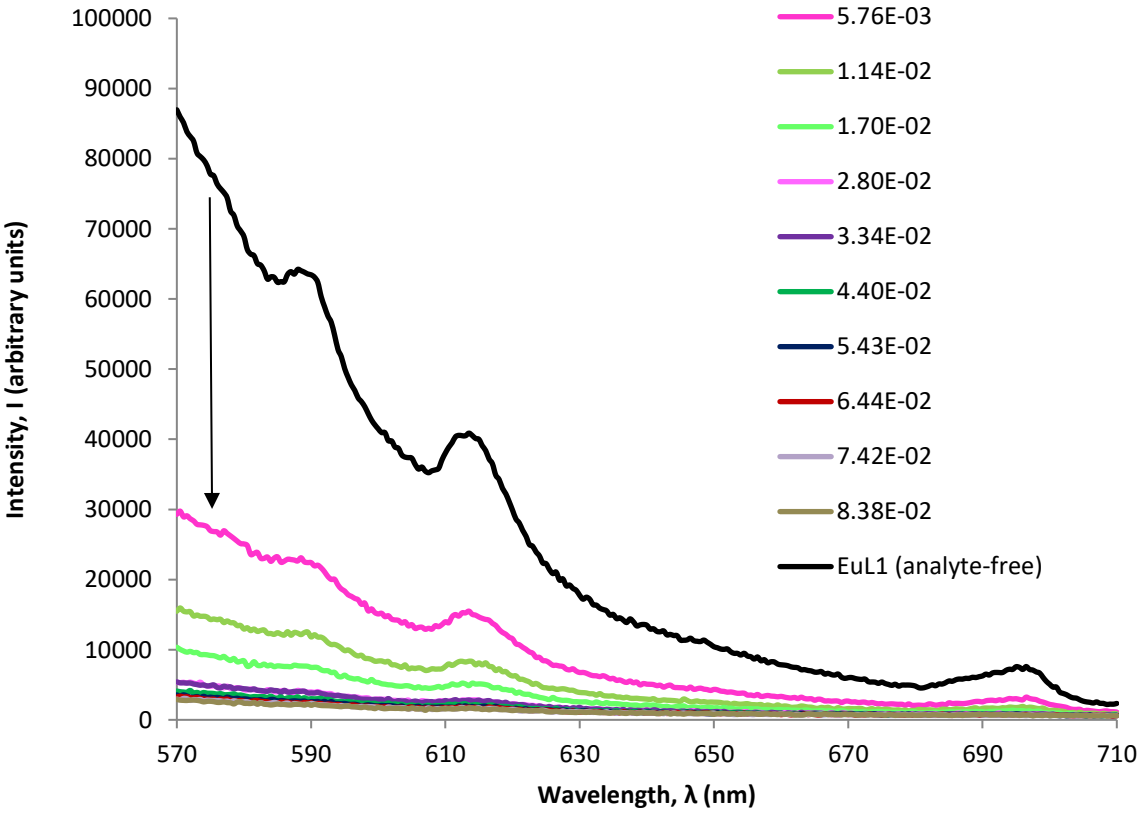

Figure 4.26 Spectra obtained for EuL1 (3 mM) and subsequent additions of the pyrimidine, cytosine (concentration after each addition, mol dm^{-3}) (λ_{Ex}=280 nm, acquisition time=0.5 sec, acquisition increment=0.5 nm, excitation and emission slit width=3 nm, pH=5)

At first glance it would appear that the pyrimidines are more efficient quenchers than the purines, however, 200 µl of saturated adenine solution ($7.62x10^{-6}$ mol dm^{-3}) and 10 µl of saturated cytosine solution ($8.69x10^{-4}$ mol dm^{-3}), when combined in 0.5 ml of the lanthanide complex solution, are both present at similar concentrations (see Table 4.5, Section 4.3.2). This suggests all the nucleobase analytes have a similar quenching effect on the fluorescence emissions; the magnitude of quenching, regardless of nucleobase analyte, at a given concentration, is comparable for all nucleobases used in these assays. This is also comparable to the results in Chapter 3 for interactions of nucleobases with $[EuDOTA]^-$ and [EuDO3A], and suggests similar mechanisms may be responsible.

In contrast, the addition of saturated solutions of the purines to the $[TbL1]^{3+}$ solution did not appear to result in a detectable change in the observed fluorescence, when compared to the $[TbL1]^{3+}$ fluorescence spectra (e.g. Figure 4.27). The effect of combining $[TbL1]^{3+}$ with pyrimidines, however, is comparable to that observed when these analytes are mixed with $[EuL1]^{3+}$, in that fluorescent emissions are quenched (e.g. Figure 4.28) and the extent of quenching is approximately the same.

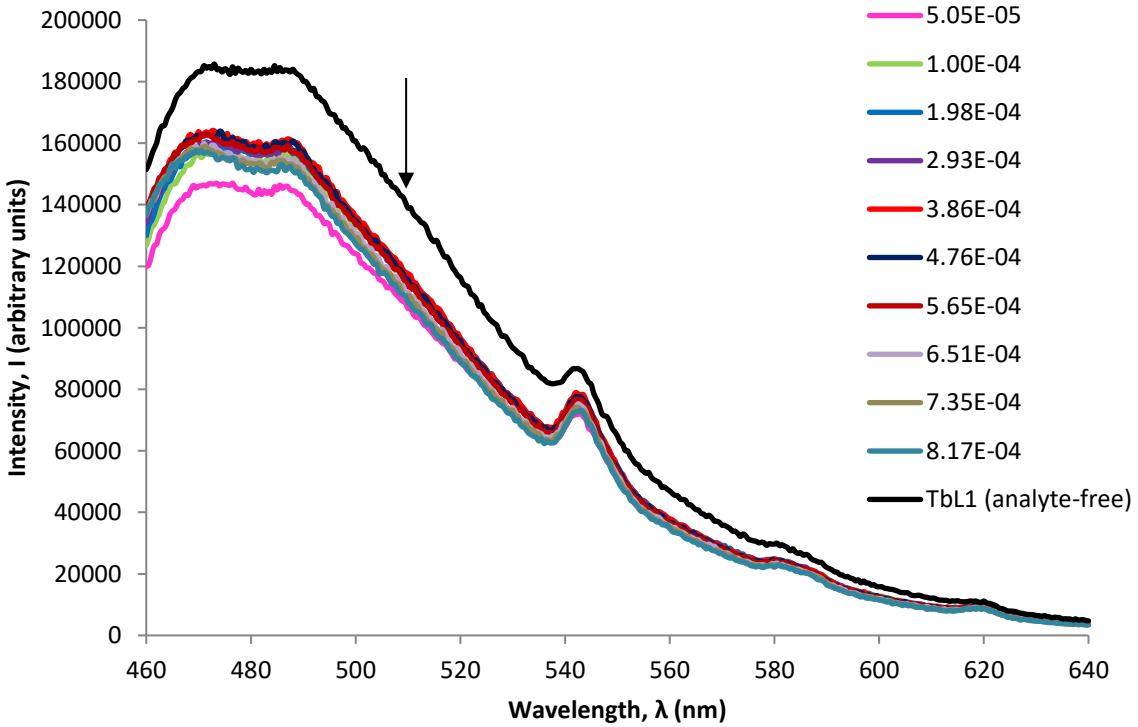

Figure 4.27 Spectra obtained for $[TbL1]^{3+}$ (3 mM) and subsequent additions of nucleobases, adenine (concentration after each addition, mol dm^{-3}) (λ_{Ex}=280 nm, acquisition time=0.5 sec, acquisition increment=0.5 nm, excitation and emission slit width=3 nm, pH=5)

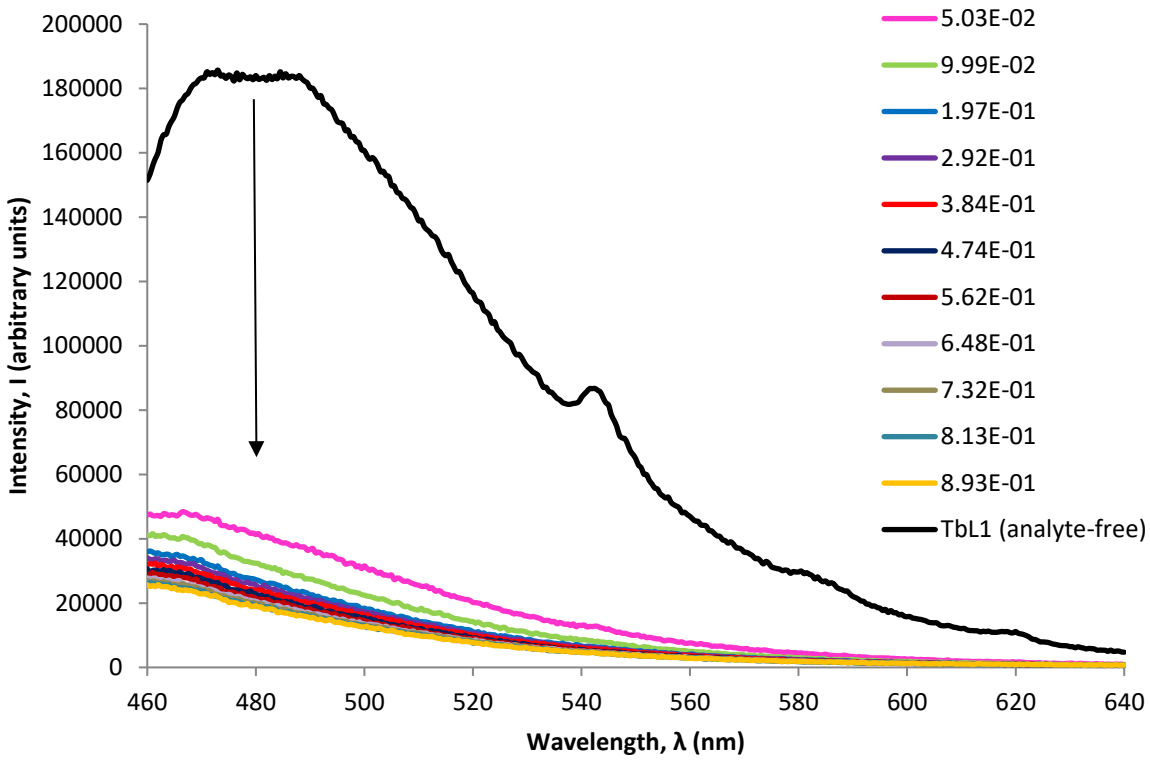

Figure 4.28 Spectra obtained for $[TbL1]^{3+}$ (3 mM) and subsequent additions of nucleobase, 2,4-diaminopyrimidine (concentration after each addition, mol dm^{-3}) (λ_{Ex}=280 nm, acquisition time=0.5 sec, acquisition increment=0.5 nm, excitation and emission slit width=3 nm, pH=5)

All nucleobases, when added to $[EuL2]^{3+}$, affected quenching of europium fluorescence. Moreover, the extent of quenching was comparable regardless of the nucleobase (purine or pyrimidine) present in the mixture. This observation was confirmed using smaller aliquots (2 µl) of the higher concentration 2,4-diaminopyrimidine (Figure 4.29) and comparing the fluorescence intensity detected for addition of larger volumes (20 µl) of the less concentrated adenine solution (Figure 4.30) (See Table 4.5, Section 4.3.2). The effect that nucleobases had on fluorescence emissions of europium in $[EuL2]^{3+}$ is comparable to that observed when nucleobases were added to $[EuL1]^{3+}$, and to [EuDO3A].

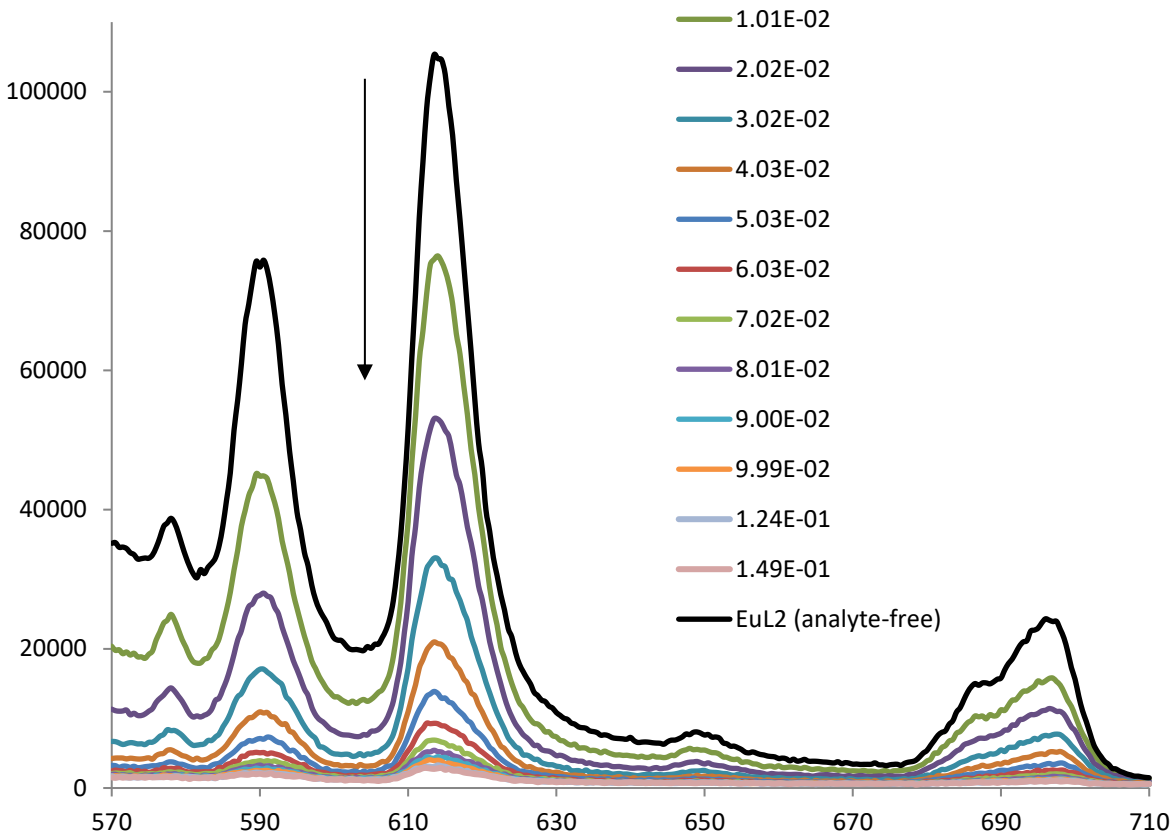

Figure 4.29 Spectra obtained for $[EuL2]^{3+}$ (3 mM) and subsequent additions of 2,4-diaminopyrimidine (concentration after each addition, mol dm^{-3}) (λ_{Ex}=280 nm, acquisition time=0.5 sec, acquisition increment=0.5 nm, excitation and emission slit width=3 nm, pH=5)

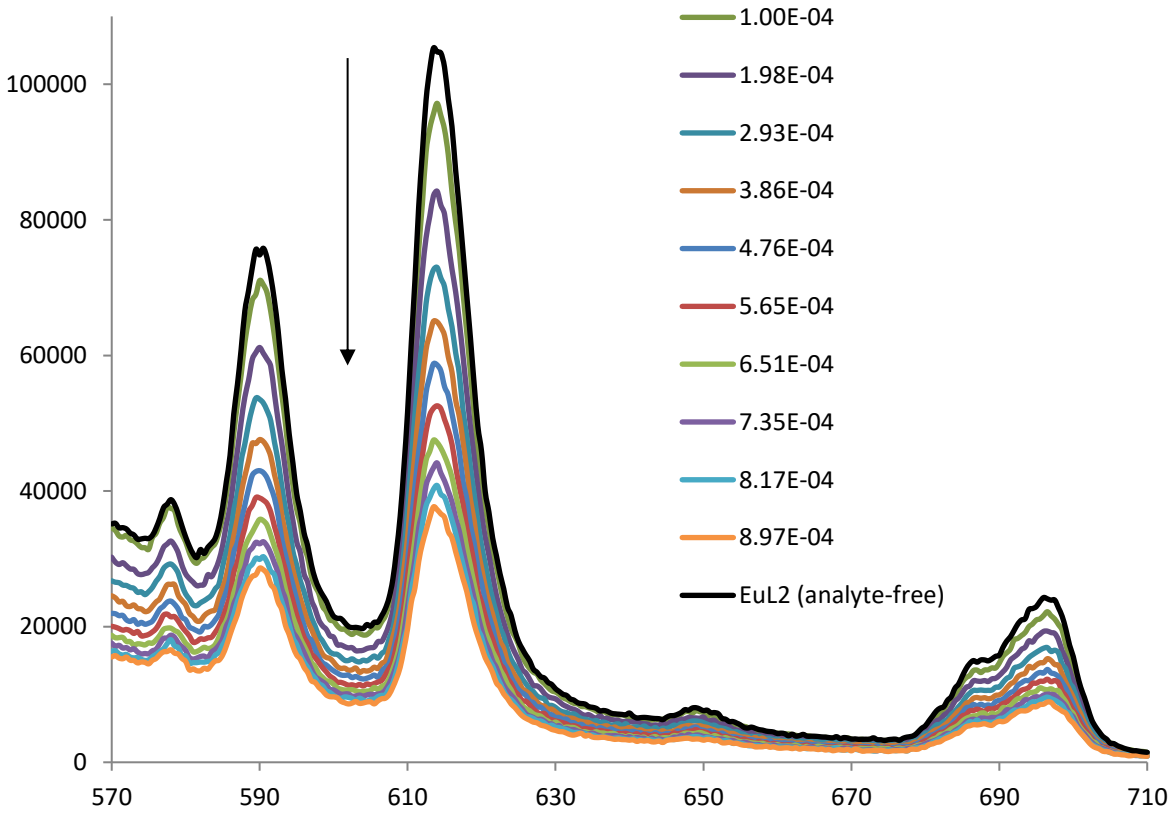

Figure 4.30 Spectra obtained for $[EuL2]^{3+}$ (3 mM) and subsequent additions of adenine (concentration after each addition, mol dm^{-3}) (λ_{Ex}=280 nm, acquisition time=0.5 sec, acquisition increment=0.5 nm, excitation and emission slit width=3 nm, pH=5)

All nucleobases, when added to $[TbL2]^{3+}$, caused quenching of terbium fluorescence. As has been seen previously, the observed intensity decrease versus increasing concentration was similar in each case. The observation that the purines are comparable to the pyrimidines at reducing europium fluorescence intensity was further suggested by repeating the experiment with smaller aliquots (2 µl) of the higher concentration cytosine (Figure 4.31) and comparing the results to those obtained with larger volumes (20 µl) of the less concentrated hypoxanthine solution (Figure 4.32) (See Table 4.5, Section 4.3.2). The effect nucleobases had on fluorescent emissions of europium in $[TbL2]^{3+}$ was comparable to that observed when nucleobases were added to $[EuL1]^{3+}$, $[TbL1]^{3+}$, and to $[EuDO3A]^{-}$ and [TbDO3A].

When the nucleobase analytes were combined with $[EuL3]^{3+}$, the response was the same as that seen with other complexes; the europium fluorescence was quenched by both the purines and the pyrimidines (e.g. Figure 4.33 and Figure 4.34, respectively). In fact, as observed previously for L2, all nucleobases had approximately the same quenching effect for a given concentration.

Terbium fluorescence was quenched by both purines and pyrimidines when combined with $[TbL3]^{3+}$ (e.g. Figure 4.35 and Figure 4.36, respectively), in accordance with previous results for other europium and terbium complexes tested.

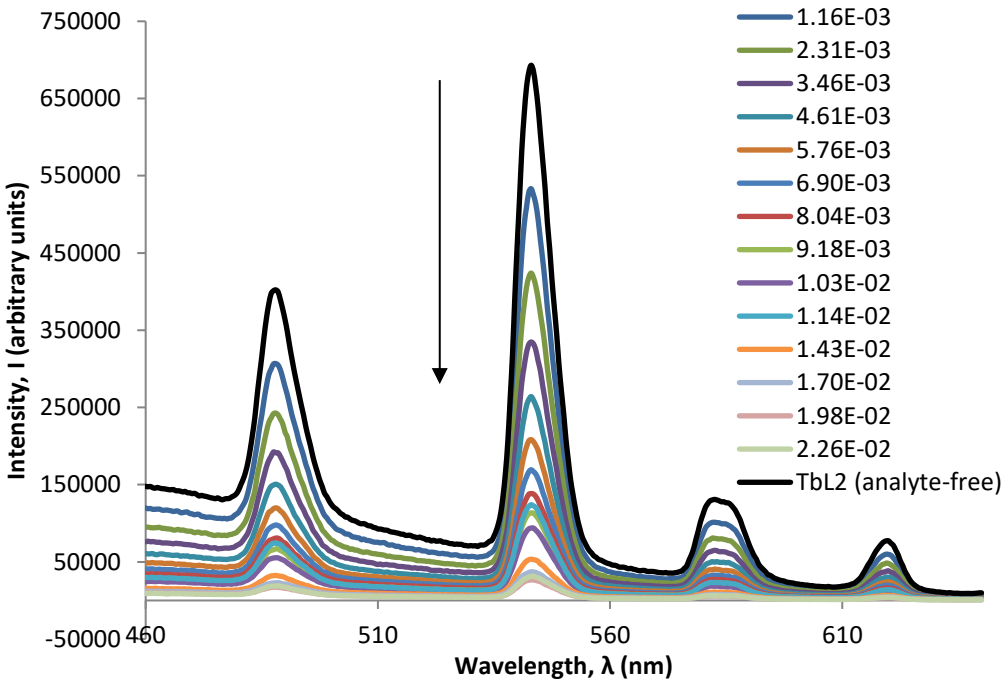

Figure 4.31 Spectra obtained for $[TbL2]^{3+}$ (3 mM) and subsequent additions of cytosine (concentration after each addition, mol dm^{-3}) (λ_{Ex}=280 nm, acquisition time=0.5 sec, acquisition increment=0.5 nm, excitation and emission slit width=3 nm, pH=5)

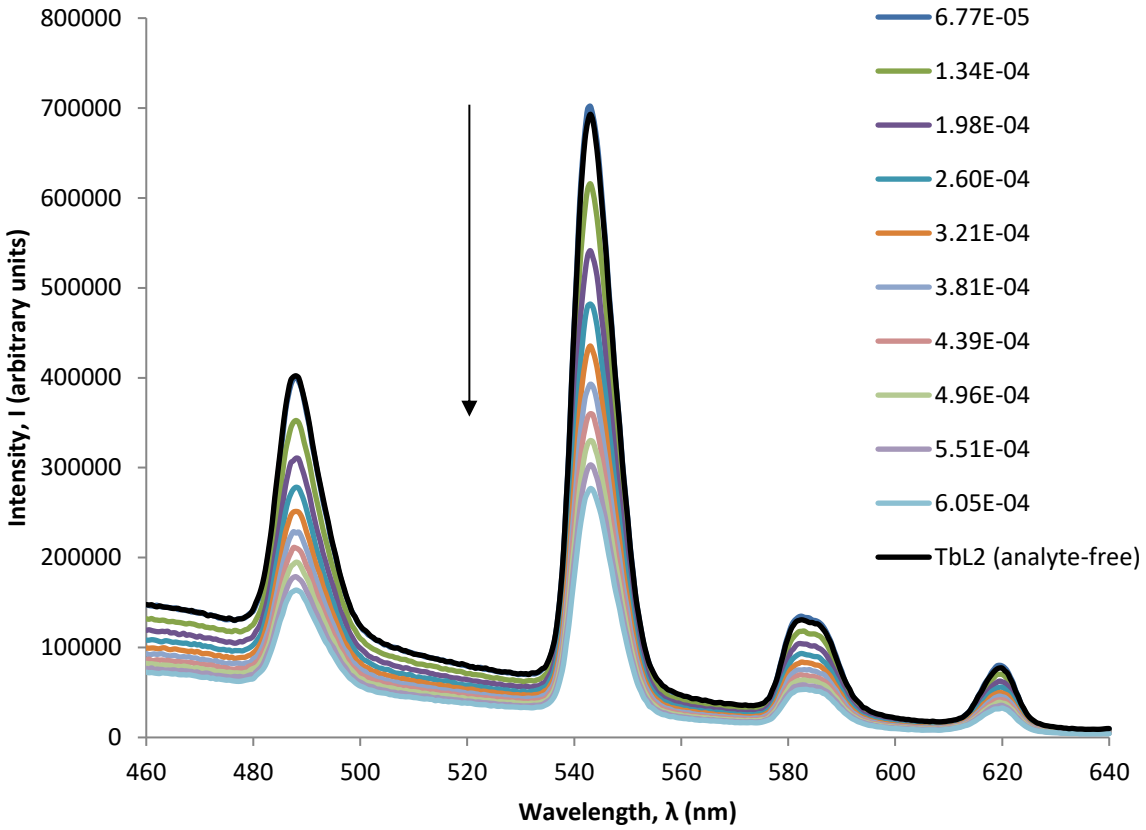

Figure 4.32 Spectra obtained for $[TbL2]^{3+}$ (3 mM) and subsequent additions of hypoxanthine (concentration after each addition, mol dm^{-3}) (λ_{Ex}=280 nm, acquisition time=0.5 sec, acquisition increment=0.5 nm, excitation and emission slit width=3 nm, pH=5)

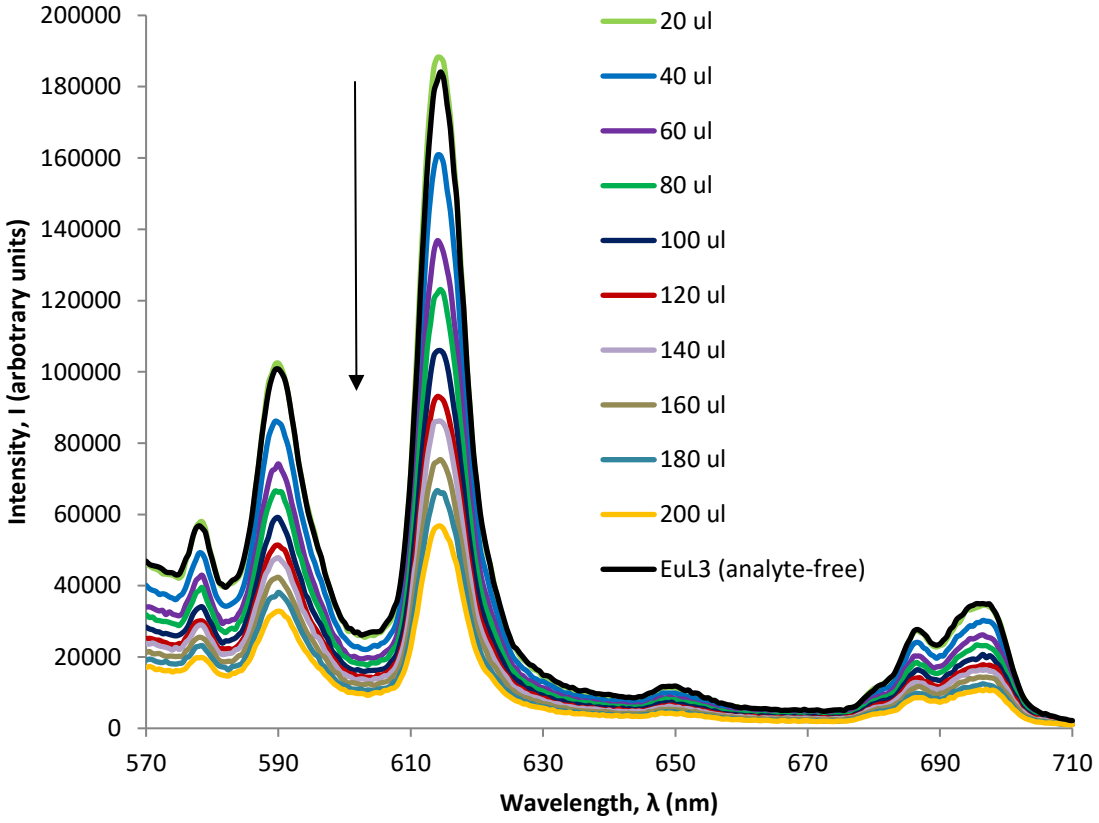

Figure 4.33 Spectra obtained for $[EuL3]^{3+}$ (3 mM) and subsequent additions of adenine (concentration after each addition, mol dm^{-3}) (λ_{Ex}=280 nm, acquisition time=0.5 sec, acquisition increment=0.5 nm, excitation and emission slit width=3 nm, pH=5)

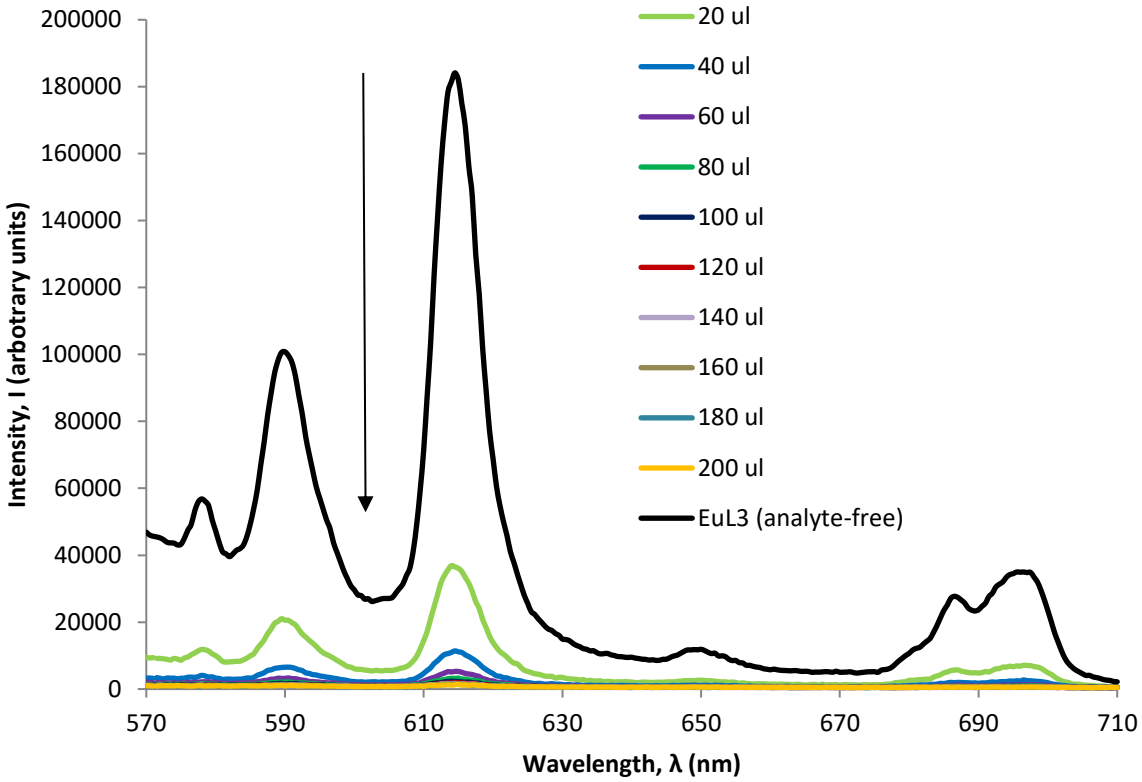

Figure 4.34 Spectra obtained for $[EuL3]^{3+}$ (3 mM) and subsequent additions of cytosine (concentration after each addition, mol dm^{-3}) (λ_{Ex}=280 nm, acquisition time=0.5 sec, acquisition increment=0.5 nm, excitation and emission slit width=3 nm, pH=5)

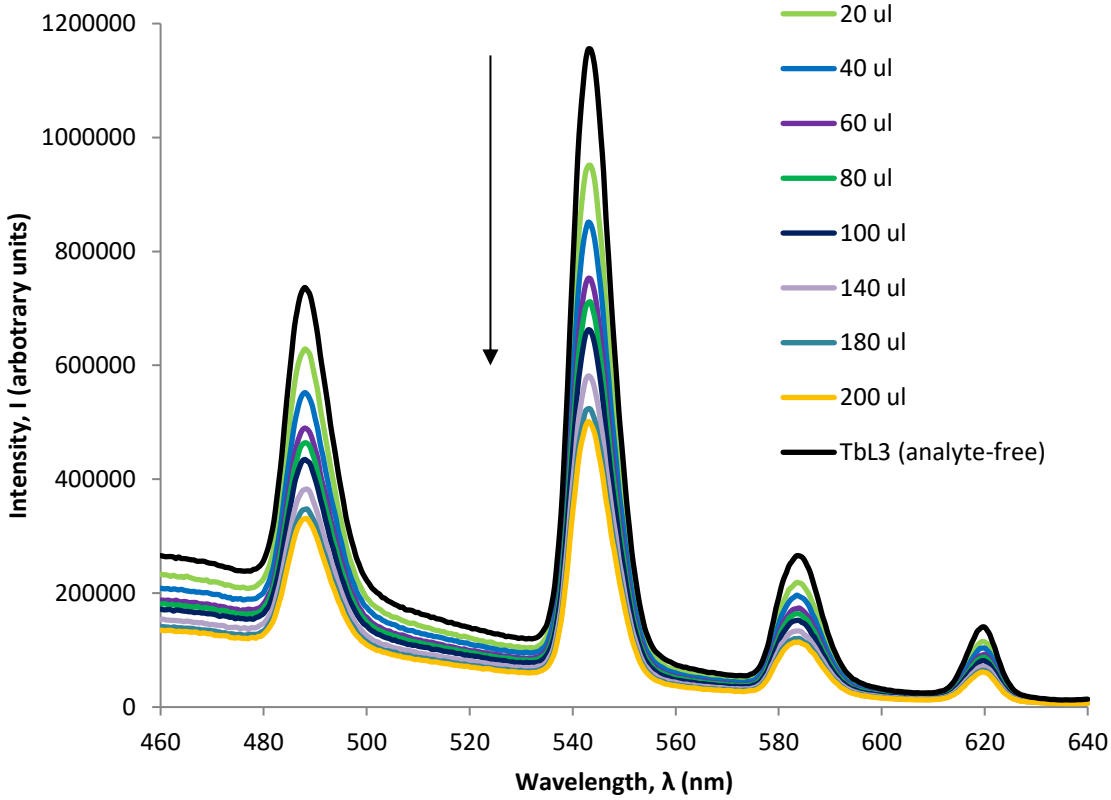

Figure 4.35 Spectra obtained for $[TbL3]^{3+}$ (3 mM) and subsequent additions of hypoxanthine (concentration after each addition, mol dm^{-3}) (λ_{Ex}=280 nm, acquisition time=0.5 sec, acquisition increment=0.5 nm, excitation and emission slit width=3 nm, pH=5)

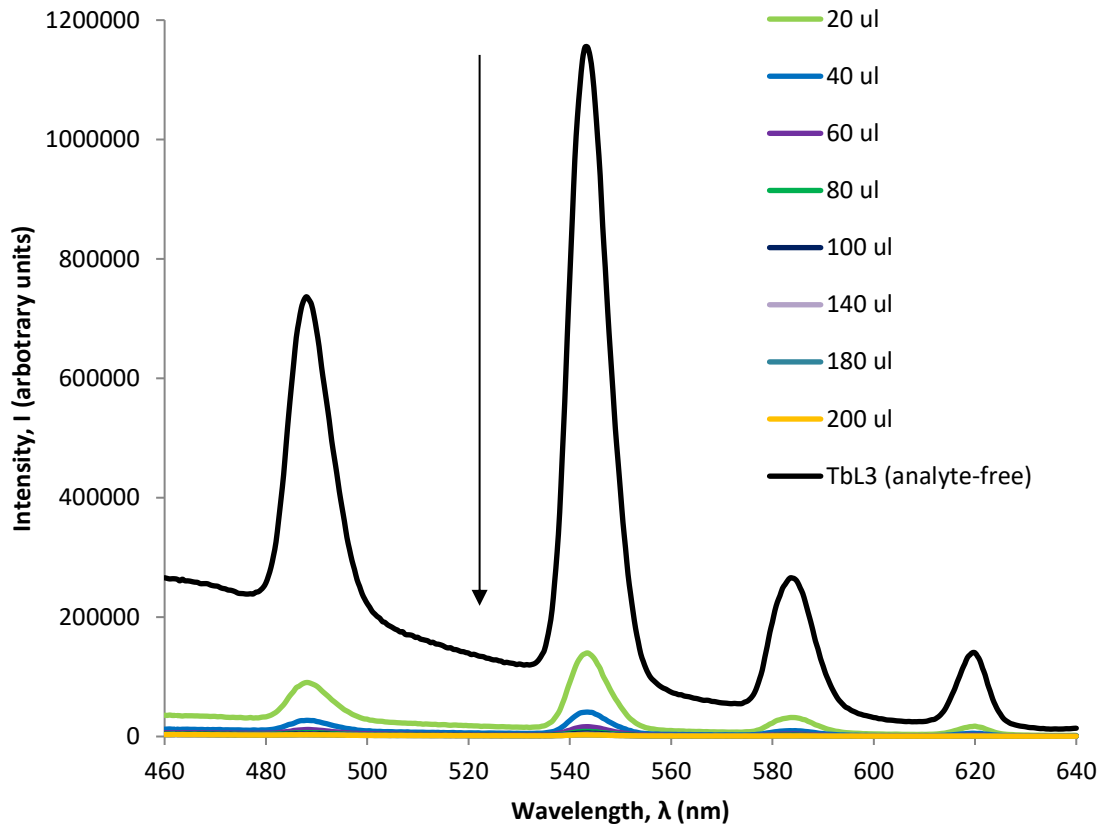

Figure 4.36 Spectra obtained for $[TbL3]^{3+}$ (3 mM) and subsequent additions of cytosine (concentration after each addition, mol dm^{-3}) (λ_{Ex}=280 nm, acquisition time=0.5 sec, acquisition increment=0.5 nm, excitation and emission slit width=3 nm, pH=5)

4.4 Discussion

Both lanthanide complexes of all the DO3A-like ligands used in this study exhibit fluorescence quenching when combined with nucleobase analytes (e.g. Figures 4.25 to 4.36), as was seen when these molecules were combined with $[LnDOTA]^-$ and [LnDO3A] (Chapter 3). Since the DO3A-like ligand lanthanide complexes described in this Chapter do not exhibit the same sensitisation that the presence of adenine invoked, they cannot be used as a sensor for adenine, specifically. Furthermore, although an unequivocal response was observed, i.e. fluorescent quenching, the complexes cannot be used to differentiate between individual nucleobases. Also, a more useful sensor is one whose response to an analyte is to be 'turned on' rather than 'turned off', i.e. fluorescence emissions are sensitised rather than quenched, which is not the case for the complexes presented here.

When $[EuL1]^{3+}$ was applied to non-nucleobase analytes, no change in sensor-only fluorescence was observed (e.g. Figure 4.8), however when $[TbL1]^{3+}$ was applied to the same analytes, an

increase in intensity was detected (e.g. Figure 4.10). Unfortunately, the increase in intensity was comparable for each analyte and, therefore, could not discriminate between them. Furthermore, although modest sensitisation of the terbium Δ*J*=1 emission was recorded, it was not possible to observe the Δ*J*=2 emission. For these reasons, $[LnL1]^{3+}$ complexes would not be useful as sensors for the non-nucleobase analytes used to test the sensors in this study.

The fluorescence emissions of the lanthanide complexes of L2 and L3 were not affected by the presence of guanyl urea, except for that which would be anticipated for the effect of dilution (e.g. Figures 4.12, 4.16 and 4.22). The application of both lanthanide complexes of both ligands to all other analytes produced a decrease in intensity but these could not be confidently ascribed to analyte interaction (e.g. Figures 4.13, 4.14, 4.17, 4.18, 4.20 and 4.23). It is possible, however, that where a decrease in intensity is less likely to be dilution effect only, it may be that the presence of the analyte perturbs the coordination environment of the lanthanide ion, thus reducing the efficiency of ligand to metal charge transfer. Therefore, based upon the observations recorded when the lanthanide complexes of L1, L2 and L3 are applied to non-nucleobase analytes in this study, it is likely that these complexes are not viable sensors for these analytes.

The transitions responsible for fluorescent emissions of the europium and terbium complexes of all DO3A-like ligands described in this chapter, however, were unambiguously sensitised by the addition of benzoic acid (Figures 4.9, 4.11, 4.15, 4.19, 4.21 and 4.24). This was also observed when benzoic acid was mixed with europium and terbium complexes of DOTA and DO3A (Chapter 3). This suggests that the mechanism responsible for this sensitisation is likely to be the same; the benzene ring absorbs and transfers excitation energy to the lanthanide *via* ligand to metal-centre charge transfer (antenna effect). This response makes all the lanthanide complexes of DO3A-like ligands ideal sensors for benzoic acid; the increase in intensity of the fluorescence detected is unambiguous and only occurs in the presence of benzoic acid. These responses confirm that the sensitisation seen when $[LnDOTA]^-$ and [LnDO3A] were applied to benzoic acid were a consequence of the presence of this analyte. The increase in intensity detected when L1, L2 and

L3 were applied to benzoic acid supports the suggestion that sensors based upon these complexes may be used as sensors for the detection of aromatic carboxylic acids.

Similar work has been reported in the literature (Gunnlaugsson et al., 2003) but this has concentrated on simple carboxylic-acid-based antenna-possessing analytes *in aquo*, not carboxylic-acid-based PAHs. Carbonaceous chondrites are known to contain solvent soluble PAHs, (e.g. Messenger et al., 1998) and complex carboxylic acid-functionalised aromatic-containing organic material (e.g. Remusat et al., 2014). It may be possible, therefore, that the use of DO3A-like lanthanide complexes, such as those tested herein, could be used to sense the presence of solvent soluble carboxylic acid-based aromatic molecules extracted from meteorite samples.

4.5 Summary and conclusions

The purpose of work presented in this chapter was: i) to generate new DO3A-like ligands that could be used to chelate lanthanide ions; ii) for those lanthanide complexes to be tested in the presence of organic analytes, and iii) for interactions to be monitored using fluorescence spectroscopy.

4.5.1 DO3A-like ligand syntheses

It was intended that the reactions should use a simple 'one-pot' direct addition of readily available pendant arm reagents to cyclen. The pendant arm reagents and the rationale for their selection is summarised in Table 4.6. Upon synthesis and isolation, it was a requirement that the ligands should easily chelate lanthanide ions without complicated conditions or isolation procedures, and produce good yields.

Pendant arm structure and name	Rationale for selection
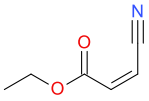 Ethyl cis-(β-cyano)acrylate	Nitrile (CN) is a strong EWG - activates the α-carbon – can be converted to an amine to attach chromophore - ester maintains DO3A-like structure – commercially available, inexpensive and high purity. Successful DO3A-like ligand synthesis has been previously reported (O'Connell, 2009).
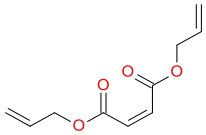 Diallyl maleate	Esters are strong EWGs - both alkene carbons activated as molecule is symmetrical - maintain DO3A-like structure. Allyl groups are reactive - opportunity for addition of chromophore. Commercially available, inexpensive and high purity. Successful synthesis using a similar pendant arm previously reported (Smith, 2008).

Pendant arm structure and name	Rationale for selection
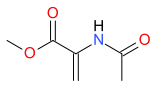 Methyl 2-acetamidoacrylate	Amidocarbonyl is a good EWG – carbonyl is conjugated to the alkene via the amine lone pair. Ester and EWG attached to the α-carbon. Ester maintains DO3A-like structure. Commercially available, inexpensive and high purity.
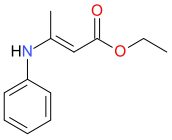 Ethyl 3-aniliocrotonate	Ester maintains DO3A-like structure - expected to activate α-carbon. Phenyl should sensitise lanthanide emissions via antenna effect. Commercially available, inexpensive and high purity. Phenyl may sterically hinder reaction.
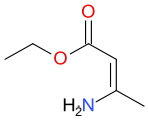 Ethyl (2Z)-3-aminobut-2-enoate	Ester expected to activate α-carbon and maintain the DO3A-like ligand structure. Amine and methyl groups are electron donating but are small so are not expected to sterically hinder the reaction. Commercially available, inexpensive and high purity

Table 4.6 Summary of pendant arms selected

The synthesis of L1 was not novel (O'Connell, 2009), however, the published reaction conditions (room temperature) did not successfully produce the target compound. L1 was produced when the reaction was carried out at reflux (80°C) for five hours. The yield attained (30.6%) was better than that in the literature (20%) (O'Connell, 2009). The yield of TbL1 was 90.6%, while the yield of EuL1 was 37.2%. The syntheses of these lanthanide complexes are not known to have been undertaken previously, but the yield of an analogous gadolinium L1 complex was produced with a yield of 70% (O'Connell, 2009).

L2 had not (knowingly) been synthesised before, although a very similar ligand had (Smith, 2008). The pendant arm reagent chosen to produce L2 was almost identical to the reagent used in the previously reported synthesis. It was therefore reasonable to assume reaction conditions described in the literature should yield similar results. The first synthesis produced a yield of 32.58% which was comparable to that reported, however a second synthesis under the same conditions, although successful, produced only 16% yield. It is not known why this decrease in yield occurred. Europium chelation of the published ligand afforded a yield of 75%, which was similar to that for $[EuL2]^{3+}$ (65%). $[TbL2]^{3+}$ only produced a yield of 17%.

L3 was a ligand by-product of a synthesis undertaken for a different research project within the research group (Vitiello, 2017). It was donated to this study because it is a *tetra*-substituted

DO3A-like ligand, i.e. it exhibits three ethanoate pendant arms affording the same structure and coordination as DO3A, yet possesses a fourth arm that is not involved in chelation of the lanthanide ion. The lanthanide complexes were synthesised using L3 as is, with no further modifications to its structure required.

Although L4 was not isolated, mass spectrometry has proven the reaction does take place since the ligand parent mass peak was identified. Ligands L5 and L6 were not produced at all. By comparing the structures of each pendant arm reagent, it is possible to identify the common factors that may have hindered the success of the aza-Michael addition. The EWGs of the reagents chosen for L5 and L6 syntheses were not sufficiently alkene α-carbon activating and this may have been compounded by the electron-donating methyl groups also present. Furthermore, the bulky phenyl group of the L5 reagent may have also hindered the reaction due to steric factors. In the case of the reagent used for L4 (and also L1 and L2), the electron-withdrawing nature was suitable for α-carbon activation, and therefore successful synthesis of the target ligand.

If future work were to be carried out to produce more DO3A-like cyclen ligands using the aza-Michael reaction to achieve the addition of pendant arms, the moieties most likely to achieve the required regioselectivity are esters or other carbonyl-containing groups, or nitriles directly adjacent to the alkene carbon next to the alkene carbon that requires activation.

4.5.2 Sensor-only fluorescence

Sensitisation of all lanthanide complexes was achieved by excitation of the ligand carbonyl moieties at a wavelength of 280 nm and *via* an antenna effect and a ligand-to-metal energy transfer mechanism.

Both lanthanide complexes of L1 exhibited fluorescence emissions. Those emissions were at wavelengths expected for the associated transitions of the respective lanthanide ions. The emissions that were most intense for europium, when chelated to L1, were the ΔJ=1, 2 and 4 transitions, where the intensity is greatest at ~590 nm, ~615 nm and ~696 nm, respectively. The

emissions at ~590 nm and ~615 nm were obscured by a broad fluorescence emission which was not europium centred, and all emissions were of low intensity for the 3 mM sensor-only solution. Terbium L1 chelated fluorescence was of comparable quality, where all emissions were of low intensity for the sensor-only 3 mM solution. The most intense peaks at Δ*J*=2 (~488 nm) and Δ*J*=1 (~543 nm) were obscured by the broad non-terbium centred fluorescence. The emissions associated with the Δ*J*=0 (~582 nm) and Δ*J*=-1 (~620 nm) were very weak. The source of the broad fluorescence is undetermined.

When europium and terbium complexes of L2 and L3 were irradiated with 280 nm wavelength excitation energy, they exhibited fluorescence emissions commensurate with europium and terbium transitions. All emissions associated with the europium Δ*J*=0, 1, 2 3 and 4 transitions were clearly observed. Δ*J*=1 transition was less intense than the Δ*J*=2 transitions, which is suggestive of a heptacoordinated europium metal centre (Bruce *et al.*, 2001). All emissions for the terbium L2 and L3 chelated complexes were observed and all transmissions responsible for the fluorescence were sensitised.

4.5.3 Fluorimetric analysis of lanthanide complexes with organic analytes

Addition of non-nucleobase analytes to $[EuL1]^{3+}$ had no detectable effect on europium fluorescence intensity that could not be ascribed to dilution effect. $[TbL1]^{3+}$ was sensitised by the addition of non- nucleobase analytes but cannot differentiate between individual analytes. Also, the strongest transition terbium emissions were obscured by the broad non-terbium-centred fluorescence, meaning $[TbL1]^{3+}$ cannot be effectively used as a sensor for these molecules. Both $[LnL1]^{3+}$ complexes were unequivocally sensitised by the addition of benzoic acid. Benzoic acid invoked an increase in fluorescence emissions associated with all transitions. Nucleobase analytes had the opposite effect, maybe causing fluorescence quenching, but it was not possible to differentiate between the individual nucleobases since the quenching effect was comparable regardless of the nucleobase present in the mixture.

$[EuL2]^{3+}$ and $[TbL2]^{3+}$ responded in a variety of ways to the presence of the non-nucleobase analytes. Guanylurea sulfate had no detectable effect on either europium or terbium fluorescence

intensity. A small decrease in intensity was detected when (*L*)-aspartic acid or (*L*)-tyrosine was added to $[EuL2]^{3+}$, but the deviation was not enough to rule out a dilution effect being responsible. The decrease was more obvious when these analytes were combined with $[TbL2]^{3+}$, however. This made the possibility of dilution effect as the sole cause less likely. This observation suggests there could have been interaction between these analytes and the europium complex of L2, but the terbium may be more sensitive to this interaction, resulting in its greater desensitisation. As with all lanthanide complex sensors thus far investigated, benzoic acid invoked an increase in lanthanide fluorescence emissions of the L2 complexes, suggesting the mechanism resulting in sensitisation is the same for all complexes (Figure 4.37).

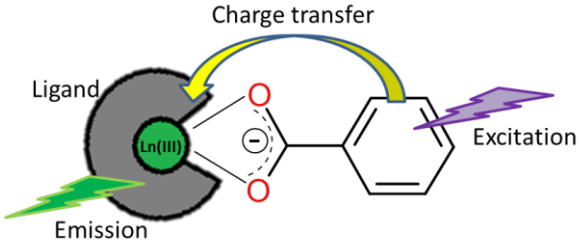

Figure 4.37 Indirect excitation of a lanthanide *via* antenna effect facilitated by excitation of bound benzoic acid which transfers charge to the chelated Ln(III) ion

Addition of the non-nucleobase analytes to the $[EuL3]^{3+}$ and $[TbL3]^{3+}$ complexes resulted in a range of responses in fluorescence intensity. Guanylurea sulfate had no detectable effect on terbium fluorescence intensity; however, some decrease in intensity was detected when it was mixed with the europium complex. This was so subtle, however, that the effect of analyte interaction cannot be confidently attributed. A modest decrease in intensity was detected when (*L*)-aspartic acid was combined with $[TbL3]^{3+}$, but the decrease in intensity seen when combined with $EuL3]^{3+}$ was less ambiguous; the same responses were observed upon addition of (*L*)-tyrosine. The decrease in intensity was enough to suggest the response may not be an effect of dilution but be due to analyte interaction. The quenching effect observed upon addition of fumaric acid was very clear and was unequivocally a sensor response to the presence of this analyte. As in the cases of the other analytes above, the decrease in intensity was more obvious when fumaric acid was combined with $[TbL3]^{3+}$. This would indicate the terbium L3 complex is also

more sensitive to interactions with the non- nucleobases than the europium L3 complex. Benzoic acid invoked an increase in lanthanide fluorescence emissions of both L3 complexes.

The addition of nucleobase analytes to all europium and terbium complexes (L1, L2 and L3) resulted in quenching of fluorescence. This response is the result of the presence of nucleobases. The amount of quenching, in relation to nucleobase concentration, was approximately the same for all nucleobases used. However, none of the lanthanide complexes can differentiate between individual nucleobases. Moreover, the response to nucleobases was a desensitisation rather than a sensitisation and so, for those reasons, none of the lanthanide complexes L1, L2 or L3 would be considered a suitable sensor for the detection of individual nucleobases.

When non-nucleobase analytes were combined with the sensors, the responses were varied. $[EuL1]^{3+}$ gave no response to any analyte and $TbL1]^{3+}$ gave a moderate sensitisation, but with no differentiation between analytes. Therefore, $[LnL1]^{3+}$ complexes are not considered suitable sensors for non-nucleobase analytes. Addition of guanylurea to $[LnL2]^{3+}$ garnered no response, but all other non-nucleobases caused moderate quenching. However, this cannot be confidently attributed to either the presence of analytes or a dilution effect. Fumaric acid did, however, affect the greatest quenching and could be as a result of analyte interaction. The ambiguity of responses, however, suggests $[LnL2]^{3+}$ is not suitable for sensing the presence of non-nucleobase analytes. $[LnL3]^{3+}$ responses mirrored those observed when non-nucleobases were added to $[LnL2]^{3+}$, so it can be similarly concluded that $[LnL3]^{3+}$ is also not a suitable sensor. Experiments suggest however, that terbium complexes are more sensitive to non-nucleobases than the europium analogues.

4.5.4 Implications for use as sensors

In order for a sensor to be effective, it must respond to the presence of the analyte. The lanthanide complexes produced, tested and discussed in this Chapter have varying responses to the addition of non-nucleobase analytes. In most cases this cannot be confidently attributed to the presence of the analytes, and is more likely to be a dilution effect. However, it appears that terbium complexes are more sensitive to both dilution effects and the presence of non-

nucleobase analytes than europium complexes. Although $[TbL1]^{3+}$ terbium emissions were sensitised by the presence of the non-nucleobase analytes, the sensitisation was comparable for each and subsequently could not differentiate between them. Hence, the sensors tested in this Chapter may be unable to unambiguously identify the presence of the selected non-nucleobase analytes.

The presence of adenine did not invoke a sensitisation of lanthanide DO3A-like fluorescence emissions, contrary to the effect its presence had on [LnDO3A] (Chapter 3). All lanthanide DO3A-like complexes, therefore, experience desensitisation in the presence of nucleobases.

As was reasoned for $[LnDOTA]^-$ (Chapter 3), the lanthanide complexes of the DO3A-like ligands may not be suitable sensors for the detection of nucleobases in extraterrestrial extracts, since the presence of these analytes affected a quenching of lanthanide fluorescence.

When benzoic acid was combined with the lanthanide complexes of the DO3A-like ligands, a marked increase in fluorescence intensity was observed, indicating benzoic acid sensitises fluorescent emissions. All complexes of europium responded with a sensitisation of all emissions, but the wavelengths caused by the ΔJ=1 transition become as intense as the emission caused by the ΔJ=2 transition. This is a comparable response to that observed when benzoic acid was combined with $[EuDOTA]^-$ and [EuDO3A] (Chapter 3), though, in the case of the latter, the ΔJ=1 transition became substantially more sensitised than the ΔJ=2 transition. It can therefore be concluded that DO3A-like lanthanide complexes, like DO3A lanthanide complexes, are excellent sensors for the detection of benzoic acid. As discussed in Chapter 3, since sensitisation of transitions, in the case of benzoic acid, relies upon: i) a carboxylate moiety to coordinate to the metal centre and, ii) an aromatic phenyl antenna to harvest and transfer energy to the lanthanide, it is reasonable to hypothesise that lanthanide DO3A-like complexes may be able to sense any organic analyte which possesses a carboxylic acid bound to any polyaromatic structure (or any structure that can act as an antenna).

It is known that carbonaceous chondrites contain functionalised polyaromatic hydrocarbons in high abundance (Messenger et al., 1998, Martins et al., 2006, Le Guillou et al., 2014, Huang et al., 2015). It is therefore possible that the DO3A-like lanthanide sensors may be used to ascertain if a solvent extract contains these analytes. Should this be the case, DO3A-like lanthanide complexes may also be considered for use on life detection missions, 'in the field', as part of 'lab-on-a-chip'-type experiments as was proposed for [LnDO3A] sensors (Chapter 3).

To test this hypothesis, Chapter 5 describes the application of the DO3A-like lanthanide sensors (this Chapter) and the [LnDO3A] sensors (Chapter 3), to the extracts of a terrestrial rock (Green River Shale, 'GRS'), known to contain organic molecules, specifically PAHs, and two carbonaceous chondrites (Murchison and ALH88045). Furthermore, Chapter 5 describes the application of all sensors described in Chapters 3 and 4 to mineral extracts in order to ascertain if dissolved mineral species, or mineral particulates, liberated by aqueous weathering, may interact with the lanthanide fluorescence emissions.

5 Application of sensors to geological samples

5.1 Introduction

It has been shown that the fluorescence emissions of europium and terbium complexes may be modified by the presence of certain organic and inorganic analytes in aqueous solution (Gunnlaugsson et al., 2003, Bruce et al., 2000).

To test this, the lanthanide complex sensors were applied to extracts of minerals, GRS, Murchison and ALH88045, and then analysed by fluorimetry. To evaluate the cause of any modification to the emissions observed for the sensor alone, they were compared to the emissions recorded when the sensors were applied to extracts.

Having established in Chapters 3 and 4 the utility of the complexes as sensors for detecting the presence of nucleobases and benzoic acid, it was necessary to test them with extracts of terrestrial and extraterrestrial geological samples. The purpose of the work presented in this chapter, therefore, was threefold.

Firstly, those minerals from the Murchison meteorite (the reference meteorite used in this study, Chapter 2) that are known to exhibit fluorescent properties, were purchased and subjected to aqueous weathering to produce solutions that could be tested with the sensors. This would ascertain whether, when dissolved, those minerals may interact with the sensors, and determine whether suspended mineral particulates would generate fluorescent emissions that may interfere with emissions from the sensors. To that end, solutions of both europium and terbium complexes of DO3A, L2 and L3 (there was insufficient supply of L1 complexes) were applied to the mineral solutions produced.

Secondly, a terrestrial organic-rich rock (Green River Shale, GRS), was selected as a model for testing the sensors on complex geological samples. The Green River Shale was selected because its organic material is well characterised (e.g. Haug et al., 1967) and it contains minerals similar to those found in Murchison, e.g. clays (Milton, 1971) (Section 2.2.2). From this, a solvent extract was obtained and tested with some of the lanthanide complexes (Table 5.1) to determine

whether a response could be detected. It was anticipated that these responses could be compared with those observed when the sensors were applied to the analogue organic analytes (Chapters 3 and 4) and mineral extracts (this chapter) in order to attribute the GRS responses to the presence of particular organic or mineral species.

Finally, the fluorescent lanthanide complexes were applied to carbonaceous chondrite extracts. Murchison and ALH88045 meteorites were selected (see Section 2.2.1) and solvent extracts obtained from them. These were then tested with the lanthanide complexes (Table 5.1) in the same way as for GRS. If similar responses were detected, it may be possible to suggest the type of components present in an extract, e.g., carboxylic aromatic compounds with the capacity to facilitate antenna effect. This is a utility required for potential future application of the sensors to unknown analyte mixtures.

5.2 Methodological approach

5.2.1 Mineral standards

The fluorescent mineral standards, selected from the known mineral inventory of the Murchison reference meteorite, were subjected to aqueous weathering in order to produce a sample that contained the same inorganic mineral particulate or dissolved species that might be present in a natural sample extract, without the organic component. It was intended that this would indicate what effect the mineral component may have on the responses of the lanthanide complexes.

The preparation of these mineral standards for weathering is described in Section 2.4.1. Before weathering, the minerals were analysed by SEM-EDX (Section 2.6.1) in order to establish their chemical composition and confirm homogeneity so that likely ionic species liberated by the aqueous weathering could be identified; if sensor responses were observed it would be possible to suggest which dissolved species may be responsible. Once SEM-EDX analysis had been completed, the crushed mineral samples were subjected to an aqueous weathering regime, the rationale and details of which are described in Section 2.5.1. The sensors were then applied to the mineral solutions obtained from this procedure and tested using fluorimetry (Section 2.8.3).

A crushed sample of GRS was subjected to a three-step extraction protocol in which the sample was extracted first with hot 18.2 MΩ water, followed by a hot MeOH extraction and finally a hot mixture of organic solvents. This procedure was also carried out on crushed samples of Murchison and ALH88045; the details of these processes are given in Section 2.5.2. Sensor-only fluorescence spectra were obtained, then the solvent extracts were combined with the sensor solutions in order to determine the sensor fluorescence response when in the presence of these extracts; details of the methodology used are given in Section 2.4.8.

5.2.2 Organic extraction and characterisation

Methodology

In order to provide an explanation for fluorescence emissions observed when the fluorescent lanthanide sensors were applied to the organic extracts of the natural samples, it was necessary to ascertain what compounds were present in the extracts. Those responses could be compared with the responses detected when sensors were applied to the analogue analytes and, in doing so, suggest which components may be responsible for the emission responses observed. Fluorimetric analysis (see Chapters 3 and 4) had suggested that application of the fluorescent sensors to solutions of compounds with both an ionic carboxylate group and a non-polar aromatic hydrocarbon moiety invoke a fluorescence emission response, so these compounds were of particular interest. To identify these components (and others), gas chromatograph mass spectrometry (GCMS) was selected as the most appropriate method.

The extracts were prepared by adding 500 µl of MeOH to the procedural blank (solvent-only and quartz-feldspar), Murchison and ALH88045 extracts, and 500 µl of DCM to the MeOH:DCM:Tol extracts, contained within the 2 ml vials. The vials, extracts and solvents were agitated using a vortex mixer for 10 seconds and left to stand for five minutes. This process was repeated a further three times, and then the vials were placed in a centrifuge at 2500 rpm for 5 minutes. The supernatant was transferred, avoiding any solid particles, to clean, dry, 2 ml vials and the solvents reduced, but not to dryness, under a stream of nitrogen in a fume hood to avoid potential contamination during the drying process. Using a 100 µl syringe, 50 µl of MeOH was introduced

taking care to rinse any extract that was adhered to the walls of the vials while doing so. In order to ensure all the extract was dissolved into the solvent expediently, the solvent was agitated by pumping the syringe a few times taking care not to splash any of the solution onto the walls of the vials. Between each treatment, the full volume of the syringe was washed ten times with clean MeOH to avoid cross-contamination between samples. A 1 µl aliquot of each sample was introduced to the GC column manually using a syringe through a septum.

The chromatographic analysis was performed on a gas chromatography mass spectrometry (GCMS) system from Agilent, consisting of a gas chromatograph model 6890 and an Agilent 5973 mass selective detector (MSD).

The column used was a S.G.E. BPX5 (5% phenyl polysilphenylenesiloxane stationary phase), 30m in length, 0.25 mm internal diameter and a 0.25 µm film thickness. The column required had to be neither too polar nor too non-polar. Using a non-polar stationary phase separates analytes by boiling point; the greater the abundance of phenyl in the stationary phase would result in separation based upon charge distribution and dipole moment of the analyte components (Trajan, 2016). As such, this column was expected to facilitate the separation of molecules that exhibit both polar and non-polar characteristics. A small internal diameter and thin stationary phase film thickness were required as a small diameter improves efficiency by providing a relatively large surface area for solute to adsorb and increases resolution making it ideal for mass spectrometry (a larger diameter would also provide good resolution but requires a larger sample volume) and a thin stationary phase film means less solute will be retained so a lower elution temperature is required (Trajan, 2016).

The inlet was held at 270°C to prevent organic components from condensing after injection, and the sample split 10:1 in order to avoid detector saturation. The GC oven was held at 50°C, to volatilise the sample solvent, for two minutes then the temperature increased to 300°C at a ramp rate of 20°C min^{-1}, with a GC run time of 23.5 minutes. Helium (He) was used as the carrier gas, with a head pressure of 7.3 psi at 50°C (oven temperature), providing a He flow rate of 1 ml min^{-1}, maintained constant throughout the GC run.

The oven conditions were selected to achieve good separation between analytes and provide good sensitivity. A lower ramp rate would provide better separation between peaks but this would result in a much longer run time. A higher ramp rate would reduce run time but make the peaks too narrow; this would decrease the number of data points and reduce MS detection time for sample component fragment ions.

The transfer line to the Agilent 5973 mass selective detector (MSD) was held at 280°C, again, to prevent condensation of molecules. The mass spectrum was run in the full scan mode, within the range m/z= 40 to 500, ensuring 5.92 scans per second, thus resulting in 14-15 data points per peak. The average base peak width was 2.4 seconds.

Peaks were identified manually by comparing spectra with reference spectra taken from the NIST database, which was embedded within the Agilent system software. Mass peaks were tentatively identified using mass fragmentation data from the National Institute of Standards and Technology (NIST) library.

Results - GRS

The organic components of the hot-water and hot-MeOH extract of GRS suggested by GCMS analysis are tabulated below (Tables 5.1 and 5.2, respectively).

GRS hot-water extract		
<u>Ketones</u>	<u>Furanones</u>	<u>Others (cont…)</u>
Cyclopentanone	5-methyl dihydro-2(3H)-furanone	4,8,12-trimethyl tridecane-4-olide
Cyclohexanone	5-propyl dihydro-2(3H)-furanone	4-ethoxy benzonitrile
6-methyl heptan-2-one	5-ethyl dihydro-2(3H)-furanone	Napthalene
2,6,6-cyclohexanone	5-hexyl dihydro-2(3H)-furanone	2,6,10,10-tetramethyl-1-oxa spiro[4,5]dec-6-ene
6,10-dimethyl undecan-2-one		2,3,5-trimethyl 1,3,-hexadiene
4-(3;4-dimethoxybenzylidine-1,4-nitrophenyl-3-phenyl-2-pyrazolin-5-one	<u>Others</u>	1-methyl-4-(1-methyl *E*-ethenyl) cyclohexane
3,4,5-trimethyl 2-cyclopenten-1-one	8-ethyl 4,5,6,7-tetrahydro-10-isopropyl azepino[3,2,1-hi]indole	2-*o*-tolyl benzothiazole
1-(3-cyclopentane-1,3-dienyl-bicyclo[2,1,1]hept-5-ene-2-yl) ethanone	2,4,5,6,7,7-hexahydro-4,7,-methano-iH-indene	Heptamethyl-3-phenyl 1,4-cyclohexadiene
	Bicycle(2,2,1)heptane-2-methanol	
<u>Carboxylic acids</u>	Undecane	
4-methyl pentan-3-oic acid	Octadecanamine	
2,3-dazabicyclo(2,2,1)hept-5-ene-2,3-dicarboxylic acid	2-methoxy-5-methyl benzamine	
	N-3-butenyl-*N*-methyl cyclohexamine	
	Non-7-ynamide	

Table 5.1 Organic components suggested by GCMS as present in the hot-water extract of GRS

GRS hot-MeOH extract		
Ketones	Alkanes/Alkenes	Carboxylic acids (cont…)
4-amino-5-methyl-2-1H-pyrimidinone	Nonadecane	Tridecanoic acid
4-*N*-ethyl cytosine	Cyclopentene	Tetradecanoic acid
6,10-dimethyl undecan-2-one	2,6,10,14-tetramethyl pentadecane	Pentadecanoic acid
Pentadecanone	2,6,10,14-tetrahexadecane	Propyl propandioic acid
Pentadecan-2-one	Squalane	Butylcyclohexyl benzenedioic acid
Tridecanone	Eicosane	
6,10,14-trimethyl Pentadecanone	Heneicosane	Others
2,3-dihydro-3,3,5,7-tetramethyl-1H-inden-1-one	Carboxylic acids	Pyrene
	Butanoic acid	2,6-dimethyl naphthalene
	Heptanoic acid	Anthraceneamine
Alkanes/Alkenes	Octanoic acid	1,1-(dimethyl ethyl)-2,5-*bis*-phenol
Undecane	Nonanoic acid	1,2-dimethoxy cycloheptane
Tridecane	Decanoic acid	2,4-dimethoxyanthracene
Heptadecane	Undecanoic acid	7-ethyl benz[a]anthracene
Octadecane	Dodecanoic acid	3,7,11-trimethyl dodecan-3-ol

Table 5.2 Organic components suggested by GCMS as present in the hot-MeOH extract of GRS

GRS is an organic-rich oil shale, the components of which are discussed in Section 2.2.2, and therefore the components of the hot-water and hot-MeOH extracts of GRS were complex and contained many oxygen and nitrogen moieties. These oxygen-rich molecules, such as ketones and furanones, were confined to the GRS hot-water extract. The hot-MeOH extract, however contained a higher proportion of monocarboxylic acids and alkenes than the hot-water extracts, in which only two carboxylic acid components were suggested by the GCMS.

Results - ALH88045

The components of the hot-water, hot-MeOH and hot-solvent extract of ALH88045 suggested by the GCMS analysis are tabulated below (Table 5.3, 5.4 and 5.5, respectively).

ALH88045 hot-water extract		
Phthalates	Organic sulphides	Aliphatic monocarboxylic acids (methyl esters)
Phthalic anhydride	Methyl ethyl disulphide	Nonanoic acid
Diethyl phthalate	Diethyl disulphide	Hexadecanioic acid
Bis-(2-ethylhexyl)phthalate	Dimethyl trisulfide	
	Diethyl trisulfide	
	Dimethyl tetrasulfide	Others
		Undecane

Table 5.3 Organic components suggested by GCMS as present in the hot-water extract of ALH88045

ALH88045 hot-MeOH extract		
Aliphatic monocarboxylic acids (methyl esters)	Branched carboxylic acids (methyl and ethyl esters)	PAHs
Pentanoic acid	4-methyl pentanoic acid	Phenanthrene
Hexanioic acid	14-methyl pentadecandioic acid	Pyrene
Nonanoic acid		Diisopropyl napthaline

Decanoic acid		Others
Dodecanoic acid	Alkanes	Dimethyl trisulfide
Octadecanoic acid	Hexadecane	Dimethyl tetrasulfide
	Octadecane	Dimethyl ester of sulphuric acid
Aliphatic dicarboxylic acids	Nonadecane	2,4-*bis*(1,1-dimetyl ethyl)
(dimethyl esters)	Eicosane	phenol
Pentandioic acid	2-methyl eicosane	Diheptyl-1,2-dicarboxylate
Hexandioic acid	Docosane	9-Octadecanamide
Heptandioic acid		Tetradecanamide
Octandioic acid	Phthalates	
Nonandioic acid	Phthalic anhydride	
Decandioic acid	Dimethyl phthalate	
Pentadecandioic acid	Diethyl phthalate	
	Dibutyl phthalate	
Carboxylic acid	*Bis*-(2-ethylhexyl)phthalate	
2,5-dimethyl benzoic acid		
1,2-benzene dicarboxylic acid		

Table 5.4 Organic components suggested by GCMS as present in the hot-MeOH extract of ALH88045

ALH88045 hot-solvent extract		
Aliphatic monocarboxylic acids	Phthalates	PAHs
(methyl esters)	*Bis*-(2-ethylhexyl)phthalate	Napthacene
Hexadecanioic acid	Diethyl phthalate	Anthracene
		Chrysene
Aliphatic alkanes	Others	Pyrene
Undecane	2,4-*bis*(1,1-dimetyl ethyl)	Fluoranthene
	phenol	Triphenylene
	Methyl 3(3,5-ditert-butyl 4-	Benzo[a or e]pyrene
	hydroxyphenyl)propanoate	Perylene

Table 5.5 Organic components suggested by GCMS as present in the hot-solvent extract of ALH88045

The GCMS analysis of both hot-water extracts of ALH88045 suggested they contained organic sulfides and monocarboxylic acids. The components with the highest abundance detected were, in order of increasing abundance, the ethyl methyl ester of 1,2-benzenedicarboxylic acid, phthalic anhydride, diethyl phthalate and *bis*-(2-ethylhexyl)phthalate. As was recorded with the Murchison hot-methanol extract, the range of organic molecules detected in the hot-methanol extraction of ALH88045 were more numerous and varied than the hot-water extract. Six $C_{5\text{-}18}$ monocarboxylic acids, seven $C_{5\text{-}15}$ dicarboxylic acids and two branched chain carboxylic acids were identified, as well as eight aromatic carboxylic acids, which include five phthalates. Six alkanes, three PAHs, organic sulfides and two esters were also detected.

Results - Murchison

The components for the hot-water, hot-MeOH and hot-solvent extract of Murchison indicated by the GCMS analysis are tabulated below (Table 5.6, 5.7 and 5.8, respectively).

Murchison hot-water extract		
Branched monocarboxylic acids (methyl and ethyl esters)	Others	Others
2-ethyl butanoic acid	pyridine acetaldehyde (could also be [2,(2-pyridinyl)ethylidine]hydrazone)	1,2-phenylene diisothiocyanate
3-methyl pentanoic acid	Undecane	Dimethyl trisulfide
2-methyl hexanoic acid	Bicyclopentyl-1,1-diene	Dimethyl tetrasulfide

Table 5.6 Organic components indicated by GCMS as present in the hot-water extract of Murchison

Murchison hot-MeOH extract		
Aliphatic monocarboxylic acids (methyl esters)	Aliphatic alkanes	PAHs
Pentanoic acid	Undecane	Phenanthrene
Hexanioic acid	Hexadecane	Pyrene
Octanoic acid	Octadecane	Fluoranthene
Nonanoic acid	Nonadecane	
Decanoic acid	Tricosane	Others
Undecanoic acid	Tetracosane	Dimethyl ester of sulphuric acid
Dodecanoic acid	Eicosane	2,4-*bis*(1,1-dimetyl ethyl) phenol
	Docosane	Fluoren-9-one
Aliphatic dicarboxylic acids (dimethyl esters)	Phthalates	Dimethyl trisulfide
Butandioic acid	Dimethyl phthalate	Dimethyl tetrasulfide
Octandioic acid	Diethyl phthalate	4-methyl dibenzothiophene
Nonandioic acid	Dibutyl phthalate	2,8-dimethyl dibenzothiophene
Decandioic acid	*Bis*-(2-ethylhexyl)phthalate	1,3-diphenyl 2-propen-1-one
Undecandioic acid		
Pentadecandioic acid		

Table 5.7 Organic components indicated by GCMS as present in the hot-MeOH extract of Murchison

Murchison hot-solvent extract		
Aliphatic monocarboxylic acids (methyl esters)	Phthalates	PAHs
Hexadecanioic acid	*Bis*-(2-ethylhexyl)phthalate	Phenanthrene
		Pyrene
	Others	Fluoranthene
Aliphatic alkanes	Dimethyl trisulfide	Triphenylene
Undecane	2,4-*bis*(1,1-dimetyl ethyl) phenol	Benzo[a]anthracene
		Benzo[c]anthracene
		Benzo[e]pyrene
		Benzo[a]pyrene
		Perylene
		Benzo[ghi]perylene
		Benzo[e]acephenanthrylene

Table 5.8 Organic components indicated by GCMS as present in the hot-solvent extract of Murchison

The GCMS of the hot-water Murchison extract did not elucidate many components; the compounds it did suggest were present were branched monocarboxylic acids and organic sulfides. The hot-methanol extract indicated a suite of aliphatic mono- and dicarboxylic acids ranging from chains of four to fifteen carbon atoms. There was also a suite of aliphatic alkanes, polyaromatic hydrocarbons, aromatic carboxylic acids (phthalates), organic sulfides, and organic molecules containing aromatic structures such as benzene and thiophene. The MeOH:DCM:Tol extract was shown to contain a number of PAHs.

Discussion and conclusion

All GCMS data, including the procedural blanks, displayed evidence of substantial column bleed such that peaks related to the siloxane stationary phase obscured low intensity peaks relating to the organic components of the extracts (see Appendix D for examples of GCMS spectra, clearly showing column bleed peaks). Because of this, only the most abundant components of the extracts were discernible. Moreover, the results obtained when fragment ion analysis using the NIST database was undertaken do not conform to the published data for these samples/extracts. This indicated that the problem was not only bleed from the column stationary phase, but also contamination from organic material still adsorbed in the column. A further confounding factor was the identification of phthalates, which are likely to be contaminants from plastics, possibly originating from the septa used in the caps of the vials or the inlet. As a result, it was concluded that the data obtained from GCMS analysis was not robust enough to be used to indicate the full and expected organic inventory of the extracts and could not provide a reliable indication of the molecules present.

Unfortunately, there were insufficient extracts available, and no time in which to extract more from the samples, to repeat the GCMS analysis and optimise the procedure, therefore, the inventory established from the review of relevant literature (see Sections 1.3 and 2.2) was used to inform the results obtained when applying the sensors.

5.2.3 Summary of sensors applied

Limited supplies of sensor solutions and/or natural sample extracts meant that not all sensors could be tested with all natural sample extracts, therefore sensors were strategically selected for testing in order to conserve supplies while providing as much information as possible with regards to sensor responses to extracts. Table 5.9, therefore, summarises which sensors were applied to which sample extracts.

Natural sample extract	Sensors tested
Anorthite ($CaAl_2Si_2O_8$)	[LnDO3A]; $LnL3]^{3+}$
Diopside ($CaMgSi_2O_6$)	[LnDO3A]; $[LnL3]^{3+}$
Enstatite ($Mg_2Si_2O_6$)	[LnDO3A]; $[LnL3]^{3+}$

Natural sample extract	Sensors tested
Corundum (Al_2O_3)	[LnDO3A]; $[LnL2]^{3+}$; $[LnL3]^{3+}$
Gypsum ($CaSO_4$ $2H_2O$)	[LnDO3A]; $[LnL2]^{3+}$; $[LnL3]^{3+}$
Olivine (Forsterite) (Mg_2SiO_4)	[LnDO3A]; $[LnL2]^{3+}$; $[LnL3]^{3+}$
Calcite ($CaCO_3$)	[LnDO3A]; $[LnL2]^{3+}$; $[LnL3]^{3+}$
Magnetite (Fe_3O_4)	[LnDO3A]; $[LnL2]^{3+}$; $[LnL3]^{3+}$
Nepheline ($Na_3KAl_4Si_4O_{16}$)	[LnDO3A]; $[LnL2]^{3+}$; $[LnL3]^{3+}$
GRS (Hot-water)	[EuDO3A]; $[EuL1]^{3+}$; $[EuL2]^{3+}$; $[EuL3]^{3+}$
GRS (Hot-MeOH)	[EuDO3A]; $[EuL2]^{3+}$; $[EuL3]^{3+}$
GRS (Hot-solvent)	[EuDO3A]; $[EuL3]^{3+}$
Murchison (Hot-water)	[EuDO3A]; $[EuL3]^{3+}$
Murchison (Hot-MeOH)	[EuDO3A]; $[EuL3]^{3+}$
Murchison (Hot-solvent)	$[EuL3]^{3+}$
ALH88045 (Hot-water)	[EuDO3A]; $[EuL3]^{3+}$
ALH88045 (Hot-MeOH)	[EuDO3A]; $[EuL3]^{3+}$
ALH88045 (Hot-solvent)	[EuDO3A]; $[EuL3]^{3+}$

Table 5.9 Sensors tested in the presence of individual geological sample extracts ('solvent' is a mixture of MeOH:DCM:Toluene in a ratio of 10:45:45). Ln represents both europium and terbium complexes

5.3 Analogue minerals

5.3.1 SEM characterisation

In order to establish the homogeneity of the mineral samples and to confirm their chemical composition, electron backscatter detection (EBSD) and secondary electron (SE) detection combined with EDX was used to obtain images and elemental analysis of the minerals, which confirmed the bulk chemistry and, therefore, identity of each.

Most samples were free of chemical anomalies, however, there some notable exceptions. A single iron/titanium-enriched feature was identified in anorthite ($CaAl_2Si_2O_8$), possibly a natural inclusion, vein or growth on the mineral grain (Figure 5.1). However, this appeared to be an isolated occurrence and it was considered that the anorthite sample was otherwise homogenous. Bright (high atomic number in backscatter) grains were identified in the corundum (Al_2O_3) sample (e.g. Figure 5.2, left) and were revealed to be metal flakes rich in iron, chromium, nickel, and manganese (Figure 5.2, spectrum, right). These grains were few in number and are likely to be extraneous contaminants rather than intrinsic to the mineral; however, during the weathering process they may liberate ionic species into the extract, affecting the sensor responses. This contamination may, however, be advantageous since, although in extremely low abundance, native metal grains have been identified in carbonaceous chondrites such as Murchison (Fuchs et

al., 1973) and, hence, this contaminated sample may produce a more realistic extract with which to test the sensors.

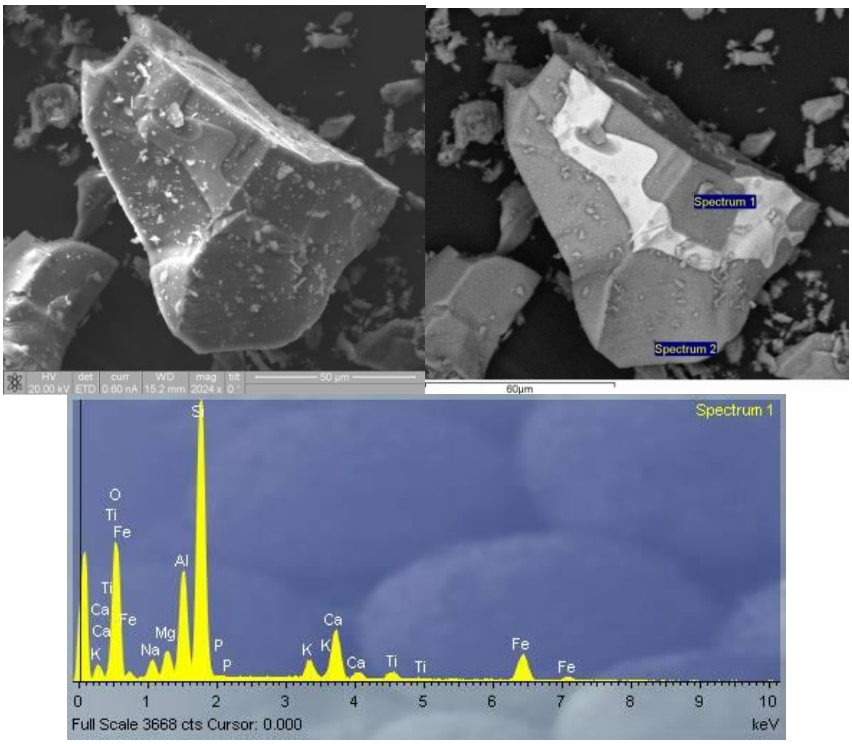

Figure 5.1 Isolated anomalous anorthite grain (SE image, top left and EBSD image, top right) was analysed. The spectrum generated revealed a higher concentration of iron and titanium (bottom)

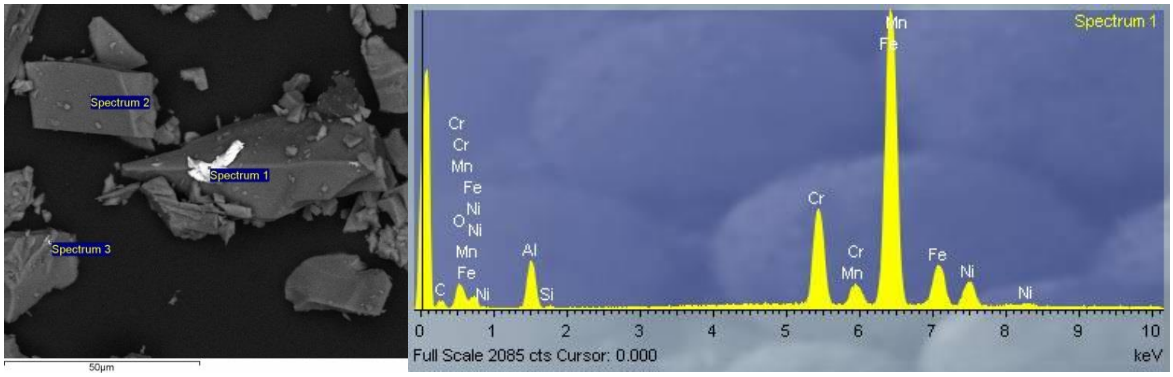

Figure 5.2 An EBSD image of corundum, revealing an anomalous, bright single grain (left). Analysis of the elemental composition revealed the grain to be an iron-rich metal flake (spectrum, right)

Bright anomalies were also observed throughout the enstatite ($Mg_2Si_2O_6$) sample. Analysis of a typical selection of grains (Figure 5.3, top left) indicated that the cause of the anomalies was titanium- and iron-enriched particles or areas within grains (Figure 5.3). These are homogenously distributed throughout the crushed sample but are not unexpected since enstatite is known to contain iron enrichments (Minerals.net, n. d.). This is a factor that needs to be considered in the interpretation of any subsequent results if a sensor response is observed.

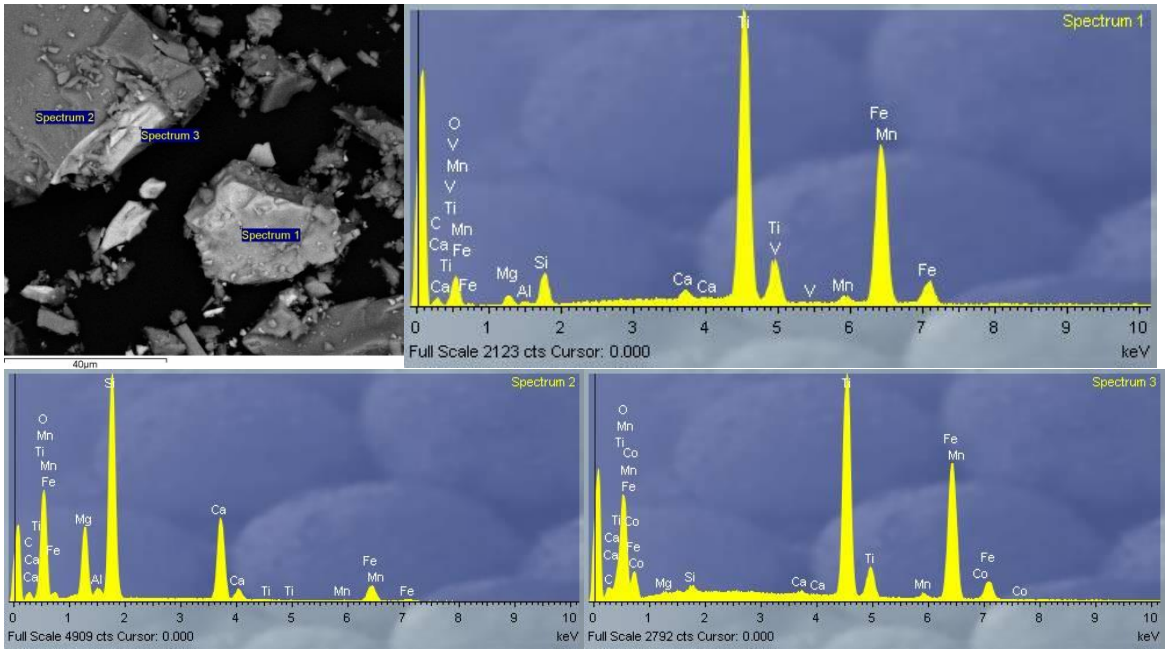

Figure 5.3 Enstatite sample composition EBSD image with individual grain point analyses (top left) and associated spectra of chemical composition (top right, and bottom left and right)

5.3.2 Fluorimetry of sensor application to mineral extracts

The protocol for analysis of weathered mineral solution effect, with increasing concentration of weathered mineral solution, upon sensor lanthanide complex fluorescence was the same as that used for the application of lanthanide DO3A-like complex sensors to analogue analytes (Section 2.7.2). However, in order to conserve supplies of sensor solutions, and maintain continuity of sensor concentrations (to enable valid comparison of results), varied volumes of sensor (and subsequently volumes of mineral solutions) were used depending upon the sensor being applied (Section 5.3.1).

Therefore, the protocol to determine change in sensor fluorescence intensity with increasing concentration of mineral solution was as follows: 0.5 ml of 3 mM of both lanthanide complexes of DO3A and L3 (triallyl Boc cyclen) solutions were combined with 20 µl aliquots of weathered mineral solution, up to a total of 200 µl or, where experiments required repetition. 0.25 ml of these sensor solutions were combined with 10 µl aliquots of mineral solution, up to a total of 100 µl. Lanthanide complex solutions of L2 were depleted so reduced volumes were utilised such that 0.25 ml of LnL2 solutions were combined with 10 µl aliquots of mineral solution, up to a total of 100 µl. Because of a limited supply of L1, it was not tested on mineral solutions. In the case of

LnDOTA, 1.5 ml of 3 mM sensor solution was combined directly with 100 µl of weathered mineral solution in order to ascertain and confirm the effect of dilution upon fluorescent emission intensity (Section 5.3.1).

These volumes would ensure that, in all cases, the concentration of the sensor would remain constant at 3 mM, regardless of the volume used, and that the relative volume increases caused by addition of the mineral solutions would be comparable for every mixture. This protocol was essential in order to conserve limited sensor supplies and so that direct comparisons could be made between all lanthanide complex sensors and concentration of the mineral solution.

The fluorimeter settings for these assays were the same as those used for the assays involving the application of lanthanide DO3A-like complex sensors to the analogue organic analytes (Section 2.7.2).

In order to test the sensor responses in the presence of dissolved ions or mineral particulates, the sensors were applied to extracts obtained from the weathering of standard analogue minerals (see Section 2.5.1). All sensors based on DO3A, with the exception of $[LnL1]^{3+}$, were applied to the mineral extracts (using protocols described, *vide supra*) and the results are presented in the following sections.

[LnDO3A]

When [EuDO3A] was in the presence of mineral solutions of anorthite, diopside, enstatite, corundum, gypsum, magnetite, or nepheline, no responses in the sensor-only fluorescence intensity were observed (e.g. Figure 5.4) that could be attributable to anything other than a dilution effect. However, a response was detected when [EuDO3A] was applied to the olivine solution (where 20 µl aliquots of olivine solution were incrementally added to 0.5 ml of 3 mM sensor); sensitisation of the ΔJ=1 transition was observed (Figure 5.5).

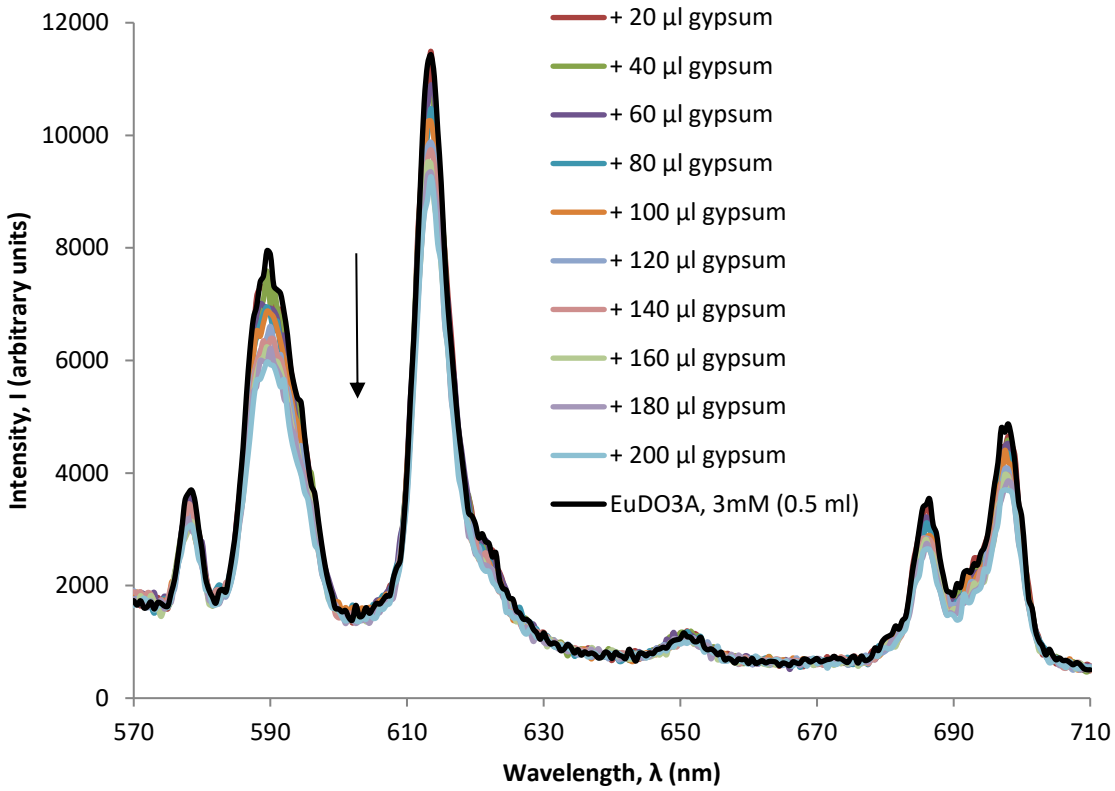

Figure 5.4 Fluorescence spectrum of 0.5 ml (3 mM) [EuDO3A] compared with the spectra obtained when 20 µl aliquots of gypsum solution were incrementally added presenting decreases in intensity commensurate with an effect of dilution (λ_{Ex}=280 nm, acquisition time=0.5 sec, acquisition increment=0.5 nm, excitation and emission slit width=3 nm, pH=5)

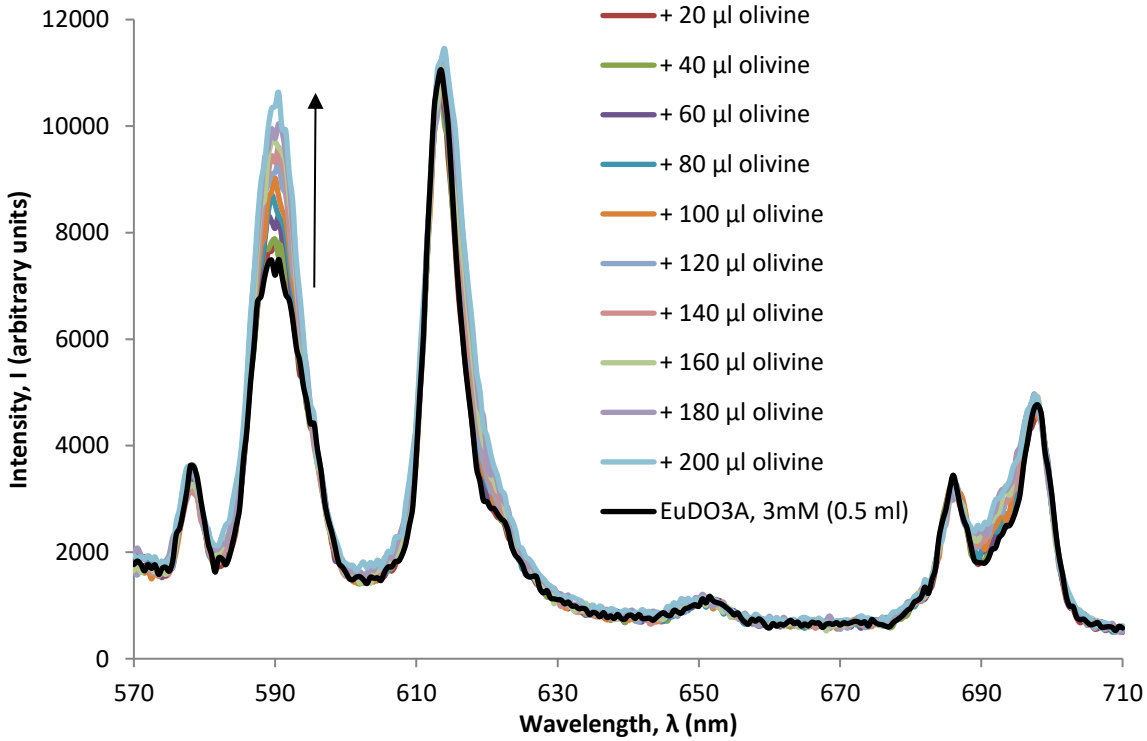

Figure 5.5 Fluorescence spectrum of 0.5 ml (3 mM) [EuDO3A] compared with the spectra obtained when 20 µl aliquots of olivine extract were incrementally added. The emission at ΔJ=1 is increasingly sensitised upon each aliquot addition (λ_{Ex}=280 nm, acquisition time=0.5 sec, acquisition increment=0.5 nm, excitation and emission slit width=3 nm, pH=5)

Olivine is an iron-magnesium silicate and, although limited by slow dissolution kinetics, its dissolution may liberate iron ions (Fe^{3+}). Studies have shown that fluorescence responses from

europium complexes are quenched by the presence of Fe^{3+} (Wen et al., 2016), however that study did not use DO3A or DO3A-like ligands. Furthermore, the Wen *et al*., (2016) study suggested that quenching of fluorescence response was the result of cation exchange between the europium and iron ions (Wen *et al*., 2016). This ion exchange, or 'transmetalation' resulting in quenching of fluorescence, has also been shown to occur in a study of complexes of gadolinium used as MRI contrast agents (Telgmann *et al*., 2012). Since the presence of the olivine extract caused an increase in intensity of the Δ*J*=1 transition rather than a decrease, cation exchange cannot have taken place. Indeed, if Eu^{3+} was displaced, indicative heptadentate [EuDO3A] emissions would not have been observed, not only because the complex would no longer be present in the solution, but also because europium would not be sensitised at all by excitation at 280 nm. Thus, the responses recorded when [EuDO3A] was in the presence of the olivine extract may not be the result of dissolved Fe^{3+} species.

Olivine is also readily aqueously altered to the mineral iddingsite ($MgFe_2Si_3O_{10}.4H_2O$), a psuedomorphic mineral consisting of iron oxides, ferrihydrites and clay minerals (e.g. smectite and goethite) (Katherine, 1987, Ralph, n. d.). It may be possible that the presence of such clay minerals, which carry potential electrostatic sites on their structure, might interact with, and perturb, the shape of the complex such that Δ*J*=1 transitions are sensitised, causing the recorded increase in this emission (Bruce, 2001). However, neither iddingsite, nor its components, are fluorescent so even if it were present, it is unlikely to result in the increase in intensity observed. Hence, it is difficult to explain the responses seen for olivine with [EuDO3A] using the data available.

When the calcite solution was incrementally added to 0.25 ml of 3 mM [EuDO3A], only 10 µl aliquots were used (this was in order to conserve sensor supplies, while maintaining the relative concentration of sensor to mineral solution; 20 µl were used for other mineral solutions, see Section 2.8.3 for rationale) an increase in intensity of all emissions was recorded (Figure 5.6). This may be due to the liberation of carbonate ions (CO_3^{2-}) during weathering, the latter of which could be responsible for these results since carbonate ions readily displace bound water, removing their

O-H oscillation quenching effect, and binding in their place (Figure 5.7) (see 5.4.2 for a discussion of the role of carbonate ions).

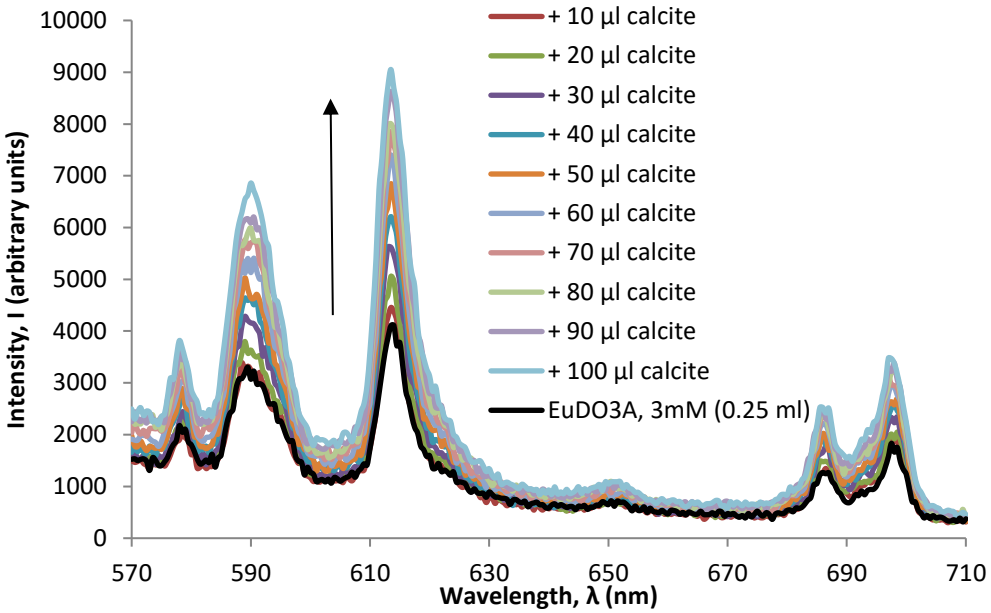

Figure 5.6 Fluorescence spectrum of 0.25 ml (3 mM) [EuDO3A] compared with the spectra obtained when 10 µl aliquots of calcite extract were incrementally added. The intensity of all emissions increased upon each aliquot addition (λ_{Ex}=280 nm, acquisition time=0.5 sec, acquisition increment=0.5 nm, excitation and emission slit width=3 nm, pH=5)

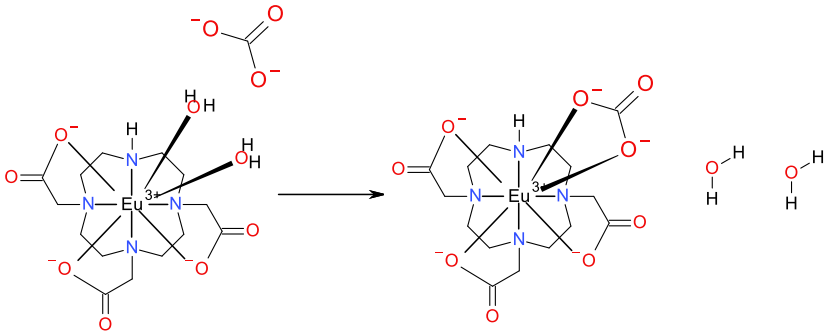

Figure 5.7 Carbonate ions displace fluorescence quenching water molecules thus removing the O-H oscillator resulting in an increase in fluorescence intensity

In order to confirm that the [EuDO3A] response to the olivine and calcite solutions were attributable only to the presence of dissolved ions or disaggregated mineral particulates, it was necessary to test using a volume of sensor sufficiently large that its concentration would be unaffected by the addition of a relatively small volume aliquot of extract. To that end, 100 µl of olivine and calcite solutions were each combined directly with 1.5 ml of 3 mM [EuDO3A] solution. No change in sensor-only emission intensity was observed (e.g. Figure 5.8) for either mineral solution. Since an increase in intensity of the ΔJ=1 transition had been observed in the presence of olivine solution (when added incrementally), and an increase in intensity of all emissions

observed in the presence of calcite solution (when added incrementally), this result indicated that the results were probably not down to the presence of the mineral solutions. One possible explanation is that contamination may have been introduced to the cuvette, and its effect on the sensor response would be exacerbated by the very small sensor volumes used, causing the responses seen here. However, this could not be proven from the results obtained, and there was insufficient sensor available to repeat the tests.

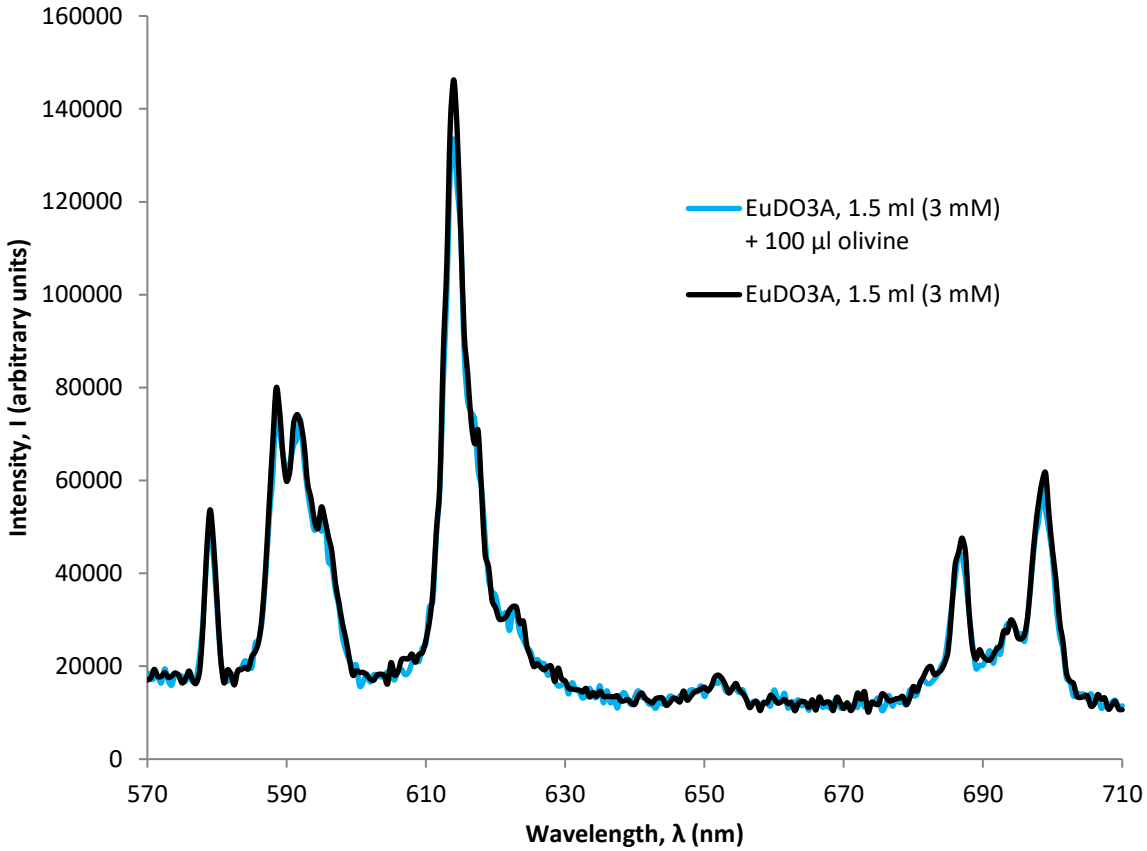

Figure 5.8 Fluorescence spectrum of 1.5 ml (3 mM) [EuDO3A] compared with the spectrum obtained when 100 µl of olivine extract was added, showing no change in sensor-only fluorescence intensity (λ_{Ex}=280 nm, acquisition time=0.5 sec, acquisition increment=0.5 nm, excitation and emission slit width=3 nm, pH=5)

A response in the sensor-only fluorescence intensity of [TbDO3A] was detected when it was applied to anorthite, diopside, and enstatite extracts (where 20 µl aliquots of these extracts were incrementally added to 0.5 ml of 3 mM sensor). A decrease in the sensor-only fluorescent emission intensity was observed, commensurate with what could be an effect of dilution (e.g. Figure 5.9) rather than an effect caused by the presence of dissolved ions or mineral particulates. However, calcite, corundum, gypsum, olivine, magnetite and nepheline extracts invoked a

decrease in intensity, which could not be confidently ruled out as an effect of dilution alone (e.g. Figure 5.10).

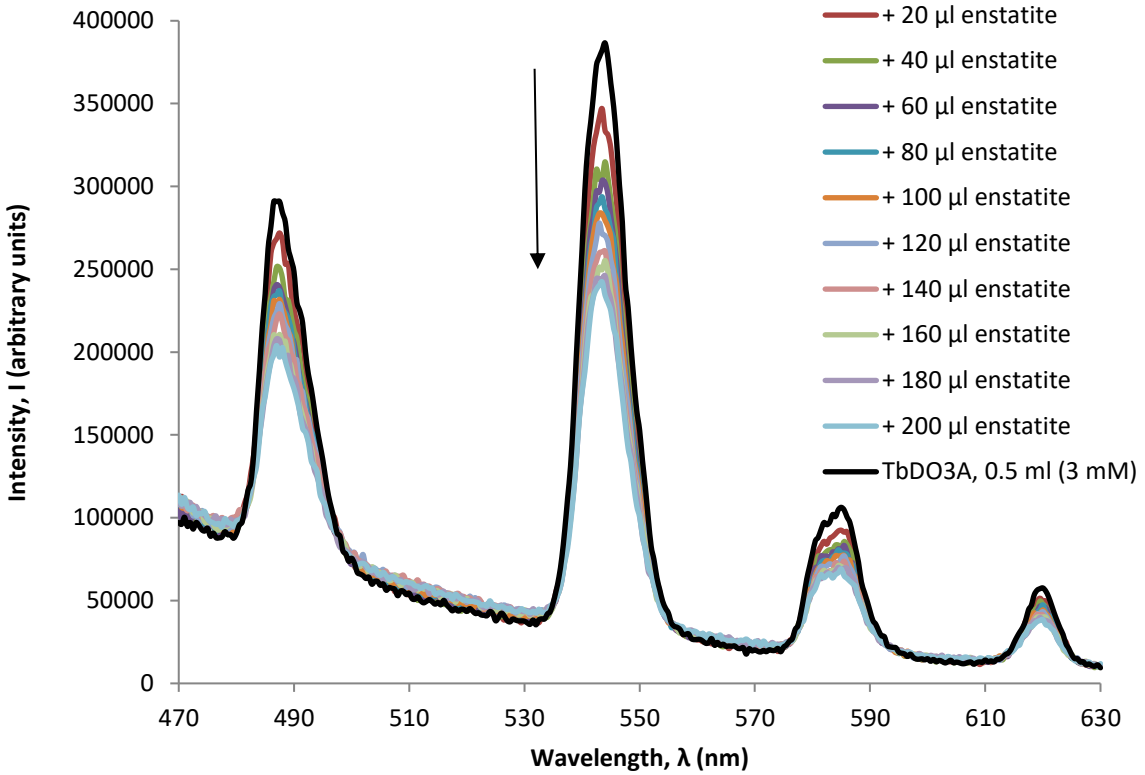

Figure 5.9 Fluorescence spectrum of 0.5 ml (3 mM) [TbDO3A] compared with the spectra obtained when 20 µl aliquots of enstatite extract were incrementally added (λ_{Ex}=280 nm, acquisition time=0.5 sec, acquisition increment=0.5 nm, excitation and emission slit width=3 nm, pH=5)

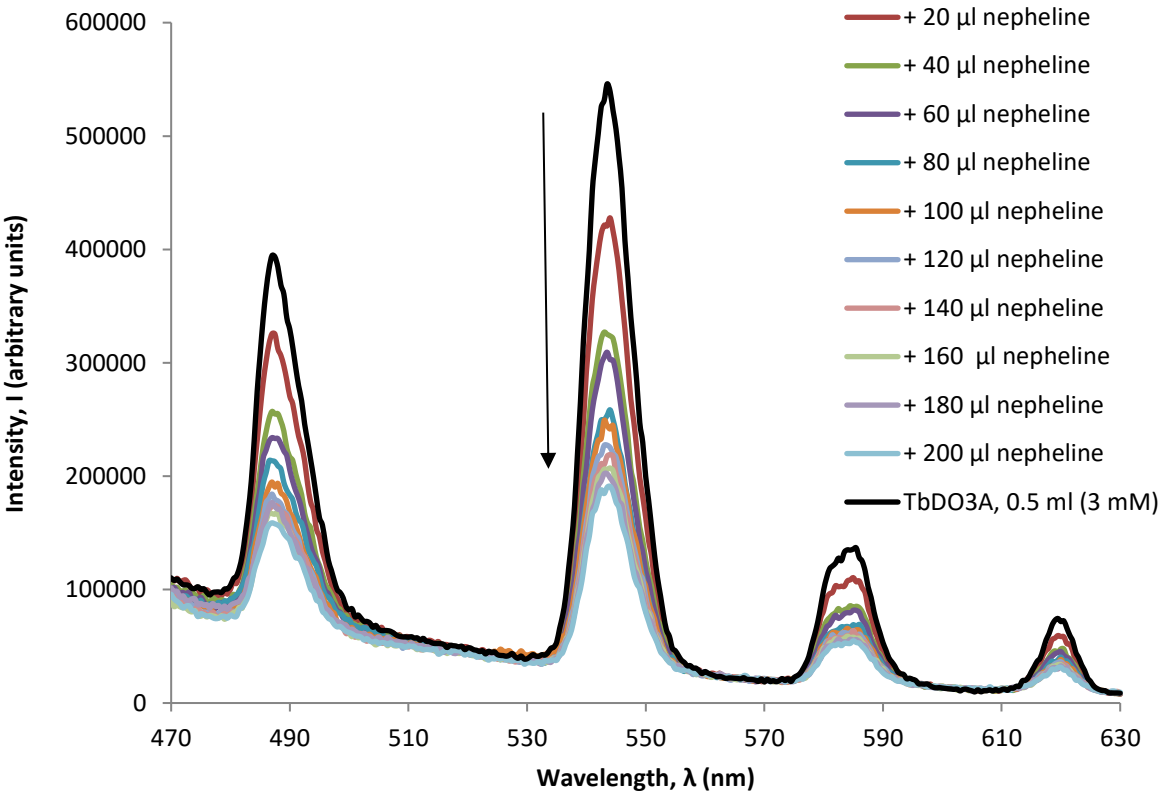

Figure 5.10 Fluorescence spectrum of 0.5 ml (3 mM) [TbDO3A] compared with the spectra obtained when 20 µl aliquots of nepheline extract were incrementally added (λ_{Ex}=280 nm, acquisition time=0.5 sec, acquisition increment=0.5 nm, excitation and emission slit width=3 nm, pH=5)

The likely products liberated by weathering of olivine and calcite, and the effects of their presence may have upon sensor-only [EuDO3A] fluorescence, are given above, but these cannot explain the changes to sensor-only fluorescence when [TbDO3A] was applied. The presence of CO_3^{2-}, for example, should cause an increase in intensity *via* displacement of water molecules, not cause a decrease in intensity, as observed here. The responses to olivine and calcite cannot be explained with the data available but, since a decrease in intensity was recorded and not one that could be attributable to the effect of dilution.

Weathering of corundum is unlikely to occur in the conditions invoked in the weathering procedure, since it is insoluble in water; the liberation of dissolved species from corundum is not anticipated. However, the iron-rich contaminants identified by SEM-EDX may be oxidised in water to produce hydrated oxides that could contribute to the sensor responses seen. Quenching has been reported when terbium was complexed with ligands that coordinate *via* monodentate carboxylate moieties, although those ligand were not DO3A or DO3A-like (Wang et al., 2014). Wang and Tan (2011) proposed that the presence of Fe^{3+} may change the original coordination sphere of the complex, thereby reducing the efficiency of ligand to metal-centre energy transfer and reducing terbium emission intensity. It is possible that, if an extract of olivine or magnetite (or a sample that contains native iron grains), did liberate dissolved Fe^{3+}, its presence in solution may cause a decrease in fluorescence intensity *via* the same mechanism. However, the ligands used by Wang and Tan (2011) in their study were likely to be more susceptible to this coordination sphere perturbation than DO3A (their ligands were individual monodentate rather than heptadentate DO3A) so their explanation for the fluorescence quenching of terbium may not be applicable here.

Further, as discussed for olivine, the low solubility and, therefore, liberation of iron ions (Fe^{3+}) from these iron oxides is limited by slow dissolution kinetics (Kraemer, 2004). Moreover, the high positive charge of the Fe^{3+} species would hinder interaction with the lanthanide because of electrostatic repulsion. These limitations are also, by extension, applicable to magnetite, and an explanation for the quenching observed remains elusive.

A decrease in fluorescence intensity was also seen for gypsum. Aqueous weathering of gypsum may liberate Ca^{2+} ions and sulfate ions (SO_4^{2-}) but gypsum is only moderately soluble (~2.0-2.5 g l^{-1} at 25°C (Bock, 1961). It has also been shown that the presence of SO_4^{2-} does not affect the intensity of lanthanide emissions when it is present (Bruce et al., 2000). Therefore, any dissolved mineral species in a solution of gypsum are unlikely to cause a sensor response. The decrease in intensity seen was larger than that expected from a dilution effect, and loss of sensor solution, as suggested previously, may be responsible for the results seen.

Quenching of sensor response was also seen for nepheline. Weathering of nepheline may generate hydrated aluminium (Al^{3+}) ionic species (e.g. $AlOH^{2+}$, $Al(OH)_2^{+}$, $Al_2(OH)_2^{4+}$ and $Al(OH)_4^{-}$), as well as Na^{+}, K^{+} and H_4SiO_4, and may also precipitate kaolinite ($Al_2Si_2O_5(OH)_4$) and halloysite ($Al_2Si_2O_5(OH)_4$) clay minerals (Huang, 1974). However this occurs over geological timescales (Huang, 1974), and so these species are unlikely to have been generated in the mineral solutions tested. However, if they were present, it is equally unlikely their presence will be responsible for the decreases in intensity observed, since the tripositive aluminium metal-centre/tripositive lanthanide ion electrostatic repulsion would preclude interaction. It is plausible, however, that Wang and Tan's (2011) theory of perturbation of the coordination sphere by interaction with the negatively charged ligand carboxylate moieties may be applicable here, but as explained previously, it is more likely to be the loss of sensor solution during the addition of aliquots of nepheline solution.

In light of the possible theories for the responses seen, to check whether the responses recorded were caused by the presence of dissolved mineral species in the mineral solutions or a consequence of dilution, 100 µl of all mineral extracts were combined with 1.5 ml of 3 mM [TbDO3A]. The spectrum obtained for corundum presented a small decrease in intensity (Figure 5.11), but small increases in intensity were observed for all the other mineral solutions tested (e.g. Figure 5.12). The small decrease in intensity with corundum is expected for a dilution effect, however the increases in intensity for all other minerals cannot be confidently attributed to the dissolved mineral species or mineral particulates. However, given the low probability of dissolved

species being present in solution, any increase in intensity may be attributable to inadvertent contamination during the addition of aliquots of mineral solutions.

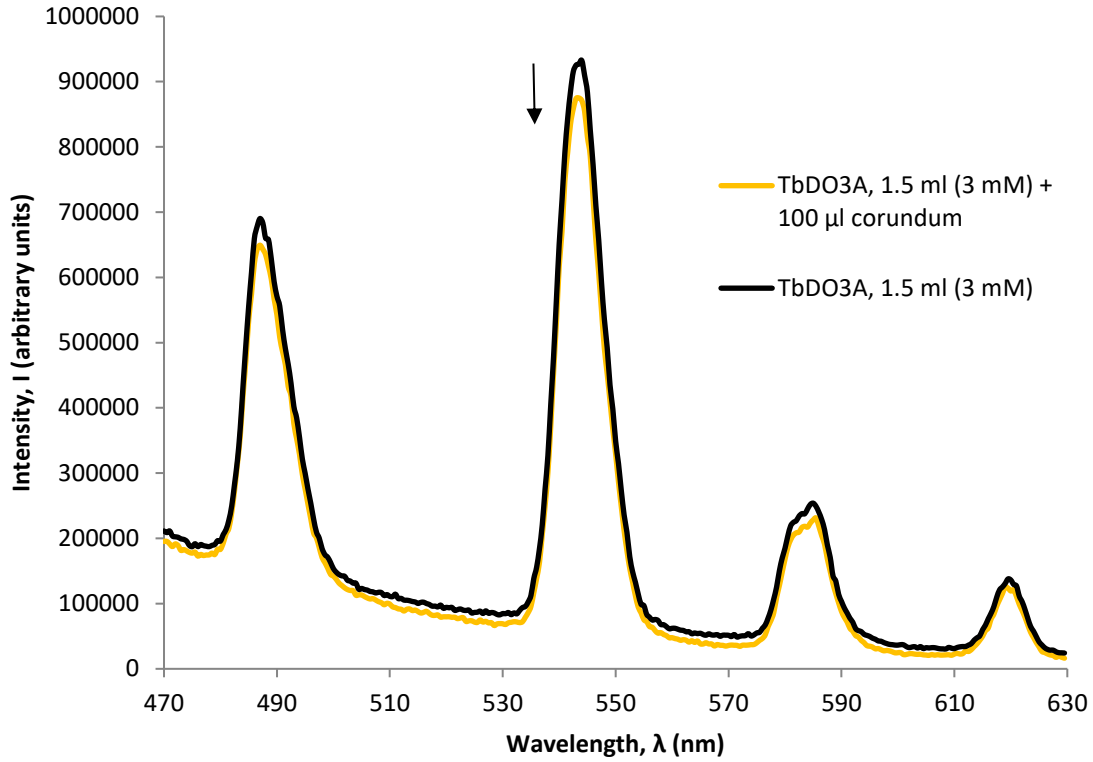

Figure 5.11 Fluorescence spectrum of 1.5 ml (3 mM) [TbDO3A] compared with the spectrum obtained when 100 µl of corundum extract was added, showing a small decrease in sensor-only fluorescence intensity (λ_{Ex}=280 nm, acquisition time=0.5 sec, acquisition increment=0.5 nm, excitation and emission slit width=3 nm, pH=5)

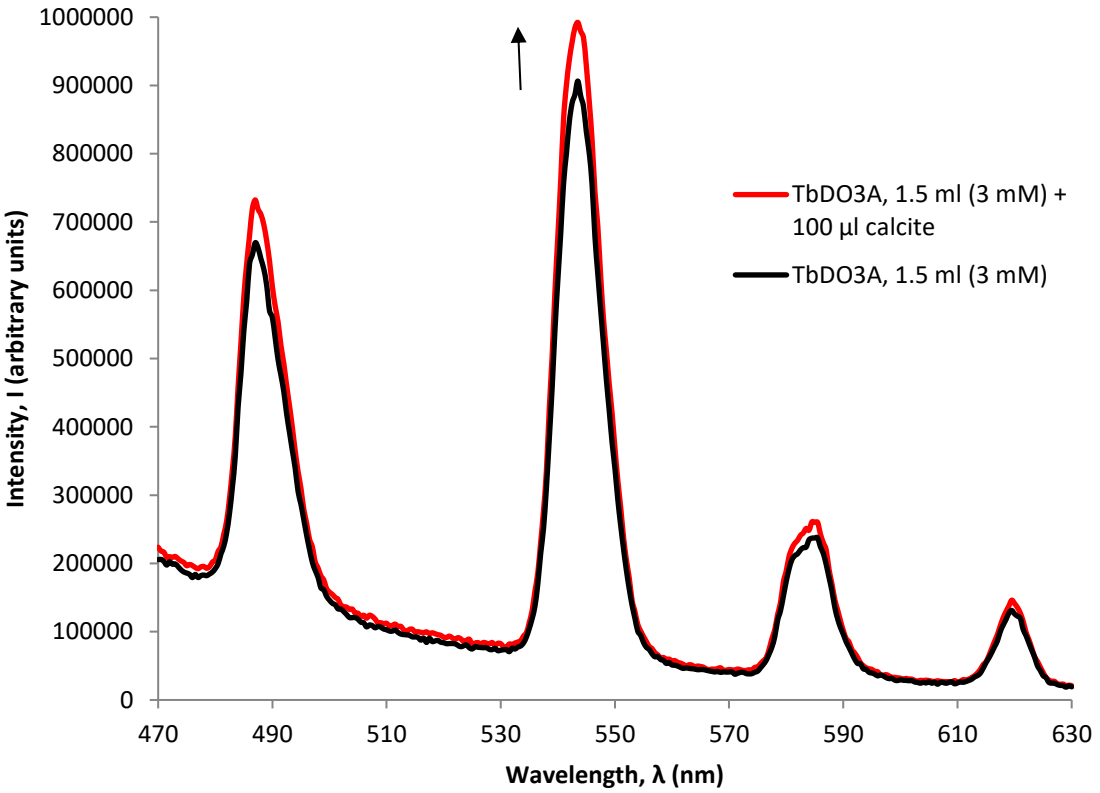

Figure 5.12 Fluorescence spectrum of 1.5 ml (3 mM) [TbDO3A] compared with the spectrum obtained when 100 µl of calcite extract was added, showing a small increase in sensor-only fluorescence intensity (λ_{Ex}=280 nm, acquisition time=0.5 sec, acquisition increment=0.5 nm, excitation and emission slit width=3 nm, pH=5)

Given the relative magnitude of the unambiguous changes in intensity observed when the [LnDO3A] sensors were applied to nucleobases and benzoic acid (Chapters 3 and 4), regardless of their inconsistencies, it is unlikely that the very small increases or decreases observed upon addition of the mineral solutions tested herein would have a marked influence on the overall sensor response if present in extracts of geological samples. This is particularly true since the GRS and meteorite extracts presented later in this chapter were produced over only 24 hours, as opposed to 6 weeks for the mineral weathering, insufficient time for dissolved ionic species or mineral particulates to be liberated that could influence the sensor responses. This suggests that the presence of dissolved mineral species or mineral particulates (if present within an extract) may not impact the utility of [LnDO3A] as a sensor for detecting organic species liberated during the extraction of an organic-rich geological sample. A caveat to this, however, may be applied if the sensor was to be used on water samples taken from the natural environment, which may contain dissolved species and particulates to much higher abundance because of longer-term weathering and erosion processes.

$[LnL2]^{3+}$

Before mineral solutions were applied to $[LnL2]^{3+}$ sensors, in light of the results for [LnDO3A] that suggested a dilution effect may be at play, 10 µl aliquots of water were added to 0.25 ml of 3 mM EuL2 sensor solution. The expected incremental decrease with dilution that had been recorded with [LnDO3A] was not observed, rather, a decrease in intensity was recorded upon addition of the first aliquot, followed by an increase with the second, then a sudden drop in intensity with little further incremental decrease for the remainder of the dilutions (Figure 5.13). Comparable, inconsistent, results were obtained for the incremental addition of corundum solution (e.g. Figure 5.14), however, the addition of calcite solution resulted in an initial decrease in intensity followed by incremental increases until there was an overall sensitisation of emissions from 60 to 100 µl aliquot additions (Figure 5.15). There were no observable responses when $[EuL2]^{3+}$ was in the presence of any other mineral solutions.

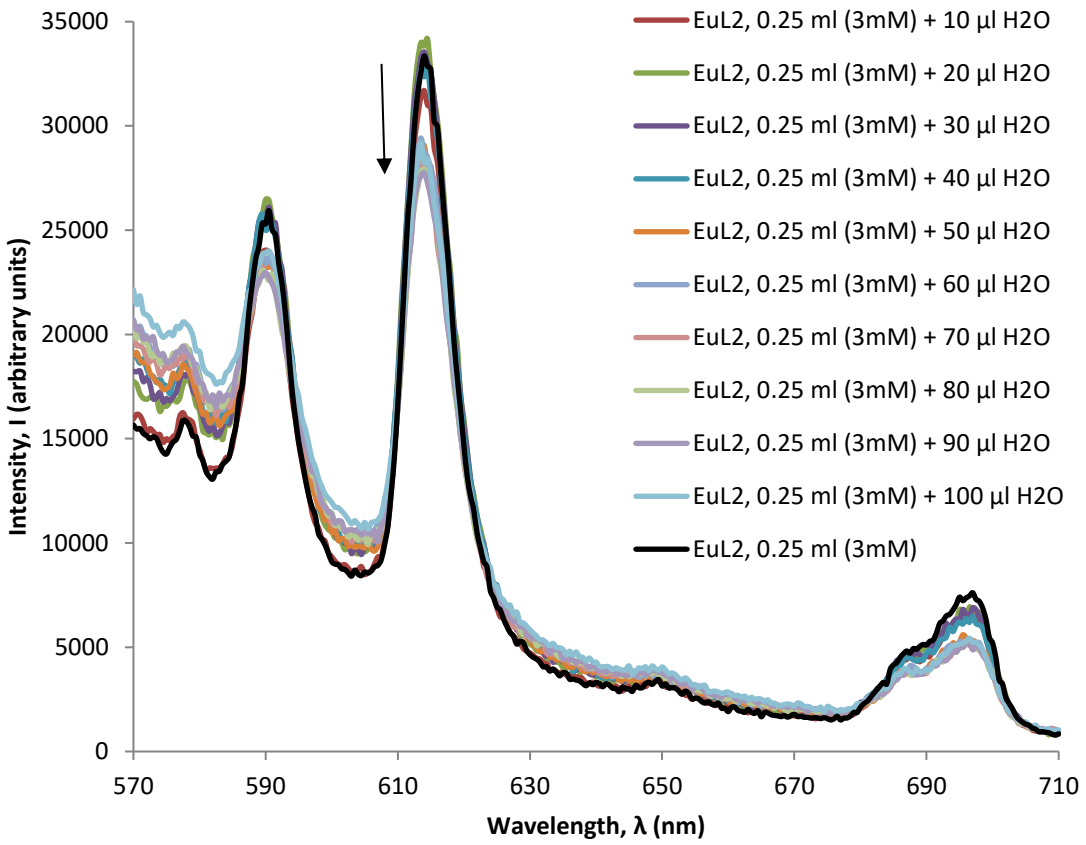

Figure 5.13 Fluorescence spectrum of 0.25 ml (3 mM) $[EuL2]^{3+}$ compared with the spectra obtained when 10 µl aliquots of water were incrementally added (λ_{Ex}=280 nm, acquisition time=0.5 sec, acquisition increment=0.5 nm, excitation and emission slit width=3 nm, pH=5)

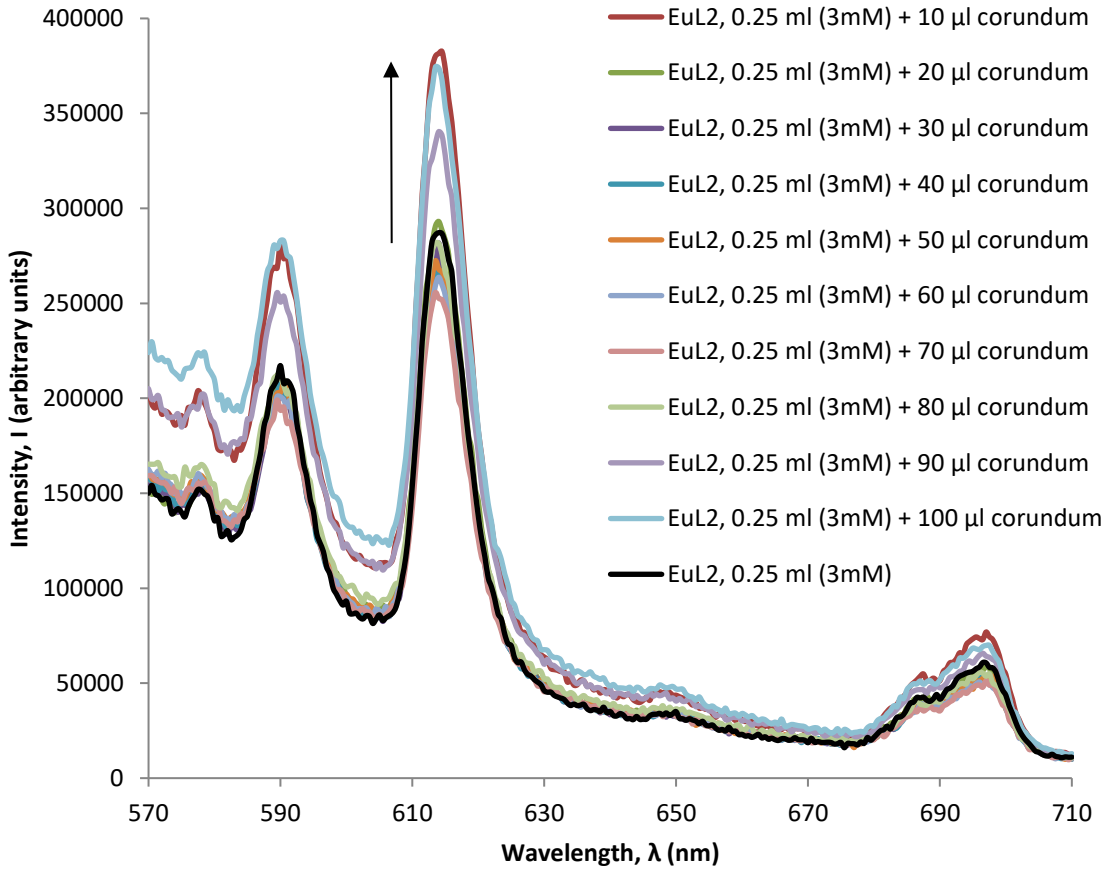

Figure 5.14 Fluorescence spectrum of 0.25 ml (3 mM) $[EuL2]^{3+}$ compared with the spectra obtained when 10 µl aliquots of corundum extract were incrementally added (λ_{Ex}=280 nm, acquisition time=0.5 sec, acquisition increment=0.5 nm, excitation and emission slit width=3 nm, pH=5)

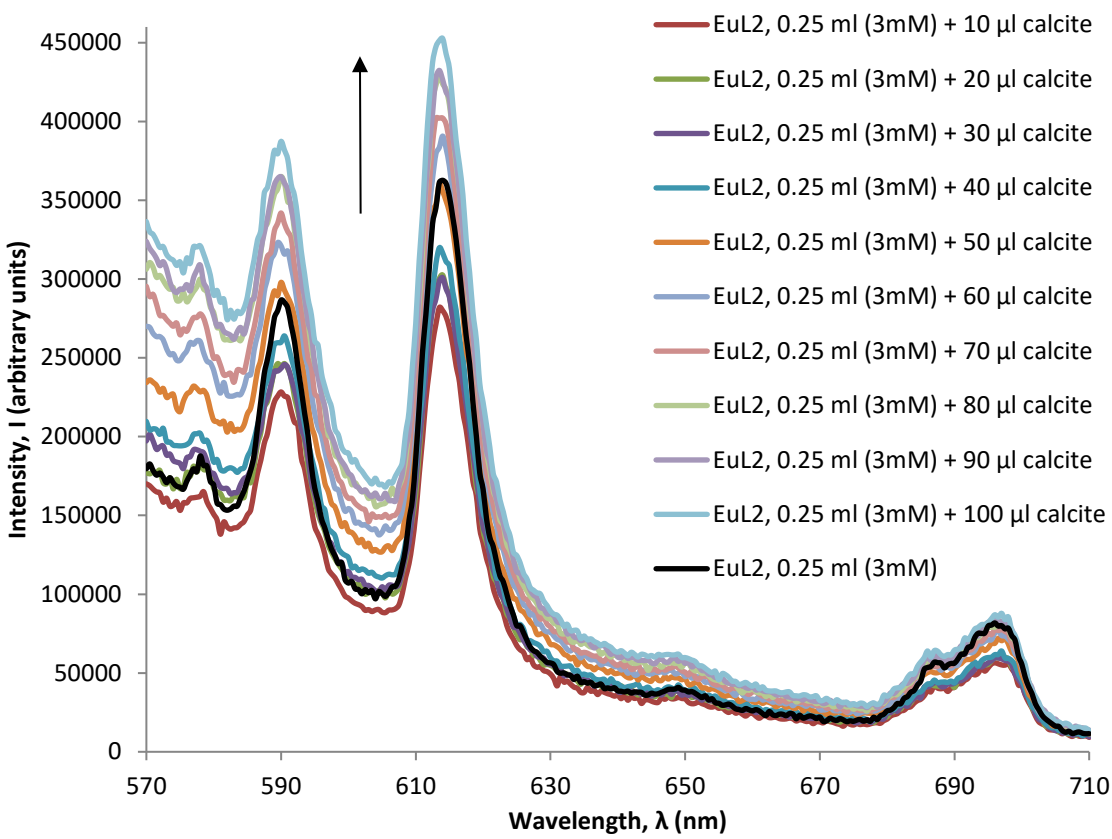

Figure 5.15 Fluorescence spectrum of 0.25 ml (3 mM) $[EuL2]^{3+}$ compared with the spectra obtained when 10 µl aliquots of calcite extract were incrementally added (λ_{Ex}=280 nm, acquisition time=0.5 sec, acquisition increment=0.5 nm, excitation and emission slit width=3 nm, pH=5)

These inconsistencies are difficult to explain. It is possible that, during the addition of aliquots, some sensor solution may have been lost from the fluorimetry cuvette, adhered to the stopper as it was removed. Since a very small volume of sensor solution was being used, even a small loss could explain the results obtained. However, the responses were inconsistent so it is not possible to pinpoint exactly when and how much of the sensor may have been lost during this process.

In order to test whether loss of sensor solution could be the cause of these observations, the experiments were re-run with aliquots of water (Figure 5.16), corundum solution (Figure 5.17), and calcite solution (Figure 5.18), since these were the solutions that appeared to cause a sensor response. The results for the calcite solution were inconsistent, displaying no trend with incremental additions of aliquots (e.g. Figure 5.18), possibly confirming sensor solution loss as the cause. The additions of aliquots of water and of corundum solution caused an increase in intensity with each aliquot added (Figures 5.16 and 5.17, respectively). The likelihood of dissolved mineral species being liberated by weathering of corundum is low (see above), and the effect of

Fe^{3+} in solution (if present at all) is likely to cause a reduction in intensity, rather than an increase (see [LnDO3A] section above). Furthermore, the addition of aliquots of pure water will only produce incremental decreases in intensity since this is a straightforward dilution effect. Therefore, as hypothesised previously (when [EuDO3A] was applied to calcite), the cause of the increase in intensity observed when aliquots of water or corundum solution were added to $[EuL2]^{3+}$, is probably the introduction of contamination and not the result of the presence of water or the corundum solution.

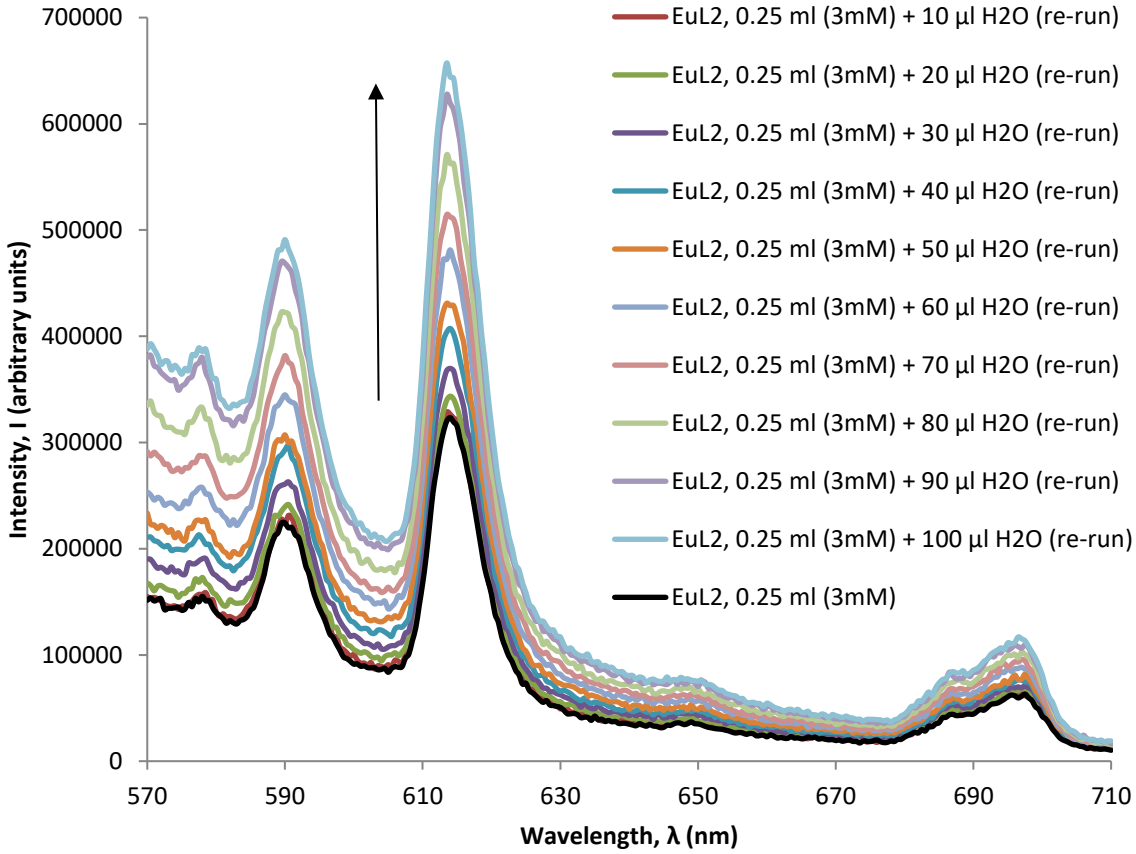

Figure 5.16 Fluorescence spectrum of 0.25 ml (3 mM) $[EuL2]^{3+}$ compared with the spectra obtained when 10 µl aliquots of water were incrementally added (re-run) (λ_{Ex}=280 nm, acquisition time=0.5 sec, acquisition increment=0.5 nm, excitation and emission slit width=3 nm, pH=5)

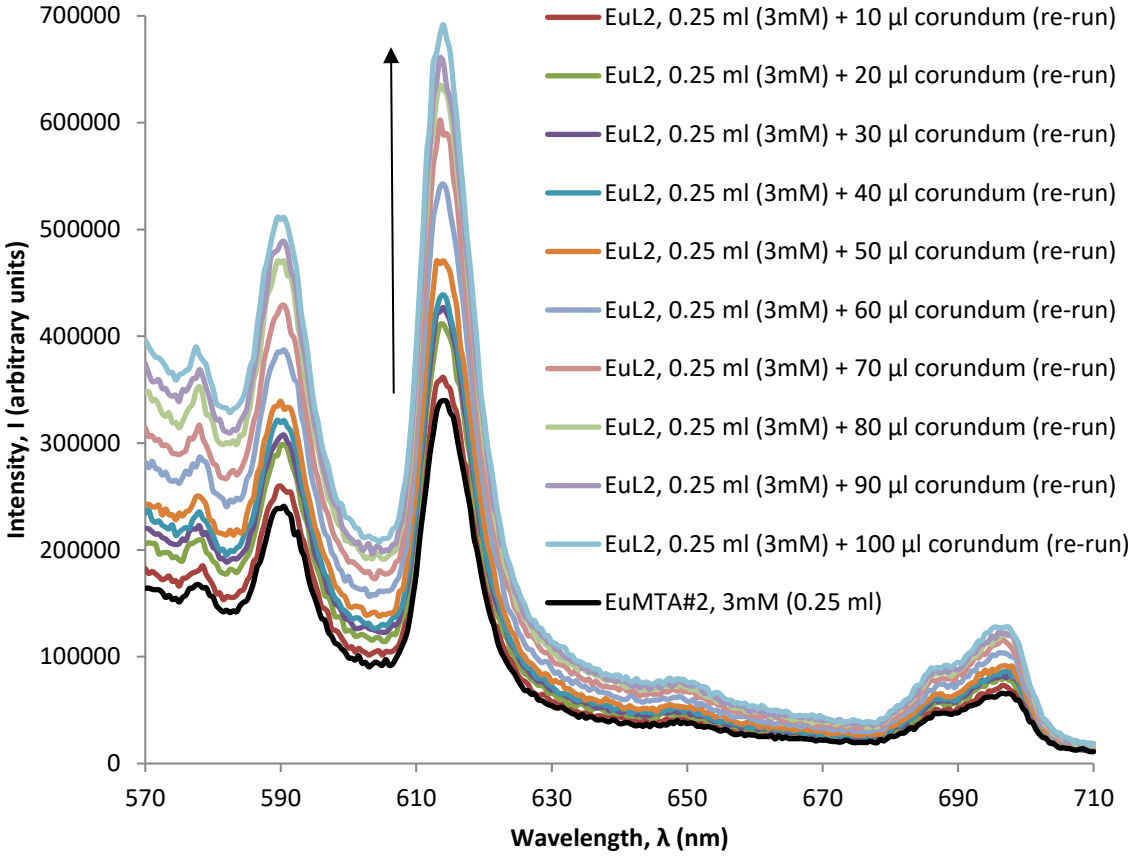

Figure 5.17 Fluorescence spectrum of 0.25 ml (3 mM) $[EuL2]^{3+}$ compared with the spectra obtained when 10 µl aliquots of corundum were incrementally added (re-run) (λ_{Ex}=280 nm, acquisition time=0.5 sec, acquisition increment=0.5 nm, excitation and emission slit width=3 nm, pH=5)

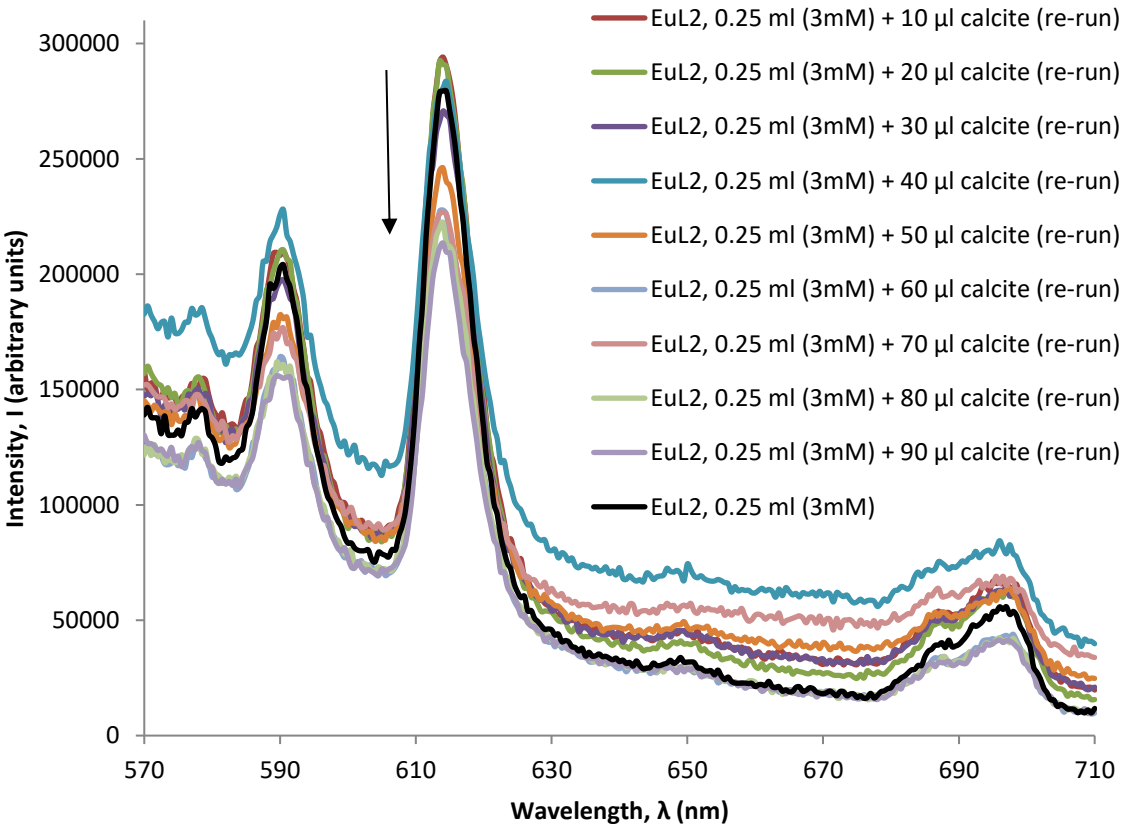

Figure 5.18 Fluorescence spectrum of 0.25 ml (3 mM) $[EuL2]^{3+}$ compared with the spectra obtained when 10 µl aliquots of calcite extract were incrementally added (re-run) (λ_{Ex}=280 nm, acquisition time=0.5 sec, acquisition increment=0.5 nm, excitation and emission slit width=3 nm, pH=5)

There was little deviation in the observed emission intensity of $[EuL2]^{3+}$ upon addition of aliquots of gypsum solution when compared to the sensor-only solution (Figure 5.19). This is difficult to explain since, at the very least, a dilution effect would be expected. It is possible that incremental introduction of contamination (which would be manifest as an increase in intensity) may be cancelled out by procedural loss of sensor (manifested as a decrease in intensity) to result in the unchanging sensor-only intensity recorded here. However, this is impossible to prove from the results here, and there were insufficient supplies of $[EuL2]^{3+}$ available to establish the true cause.

A decrease commensurate only with dilution effect was recorded for the addition of olivine aliquots to $[EuL2]^{3+}$; however, incremental increases were observed upon addition of magnetite and nepheline solutions (e.g. Figure 5.20). As previously suggested, these mineral solutions are unlikely to contain dissolved ionic species, and even if present, are unlikely to invoke any sensor response, the only plausible conclusion to account for the results obtained is one involving the introduction of contaminants to the very low volume of sensor solution.

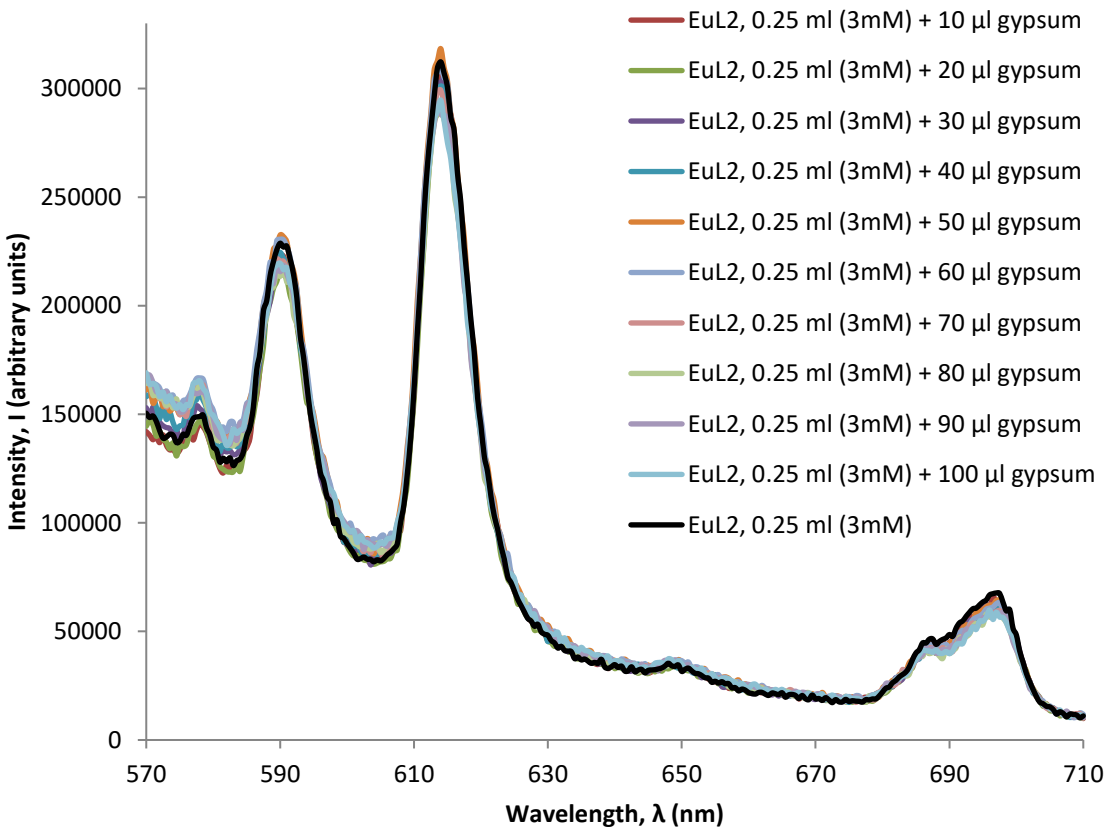

Figure 5.19 Fluorescence spectrum of 0.25 ml (3 mM) $[EuL2]^{3+}$ compared with the spectra obtained when 10 µl aliquots of gypsum extracts were incrementally added (λ_{Ex}=280 nm, acquisition time=0.5 sec, acquisition increment=0.5 nm, excitation and emission slit width=3 nm, pH=5)

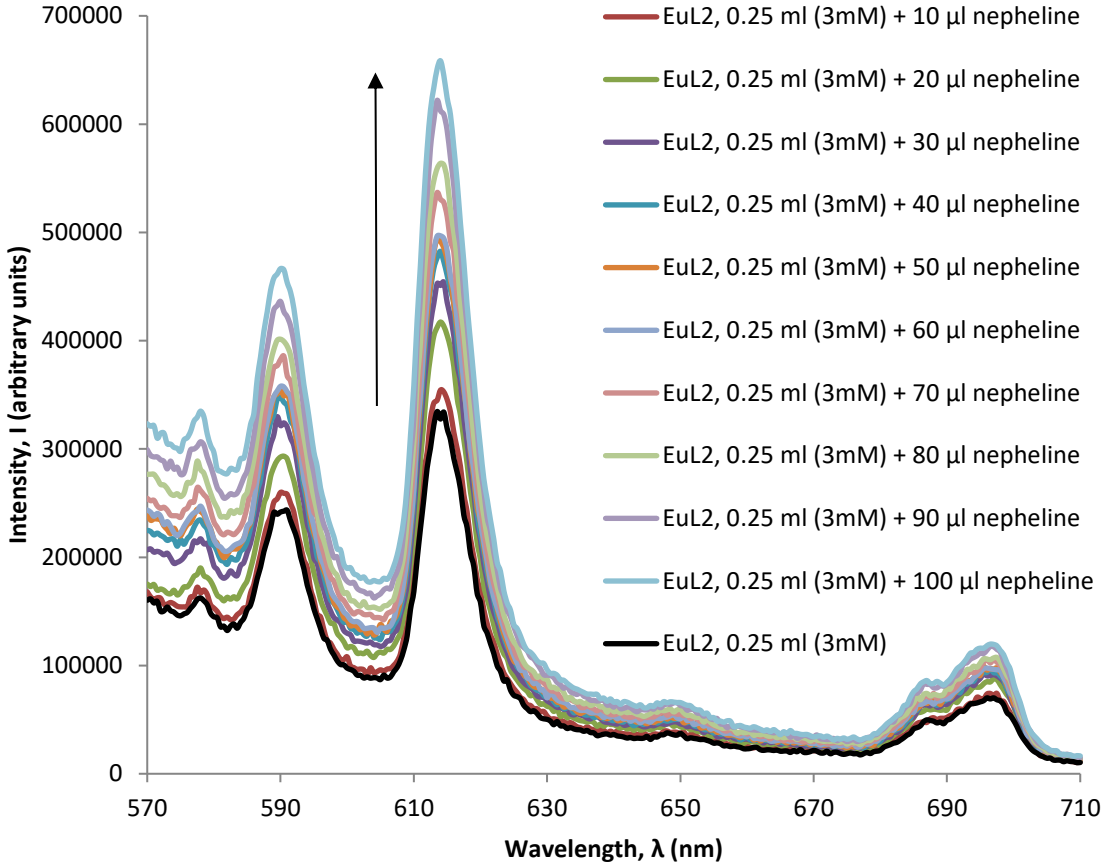

Figure 5.20 Fluorescence spectrum of 0.25 ml (3 mM) $[EuL2]^{3+}$ compared with the spectra obtained when 10 µl aliquots of nepheline extracts were incrementally added (λ_{Ex}=280 nm, acquisition time=0.5 sec, acquisition increment=0.5 nm, excitation and emission slit width=3 nm, pH=5)

To positively ascertain if responses were the result of the presence of the mineral solution, 100 µl of all mineral solutions were combined with 1.5 ml of 3 mM $[EuL2]^{3+}$ and compared with the response obtained from the addition of a 100 µl aliquot of water to $[EuL2]^{3+}$. In all cases, a small increase in intensity was recorded for the addition of the mineral solutions (e.g. Figure 5.21) and the addition of water (Figure 5.22). The comparable results suggest that the mineral solutions do not contain species that cause a change in intensity of the sensor-only fluorescence emissions.

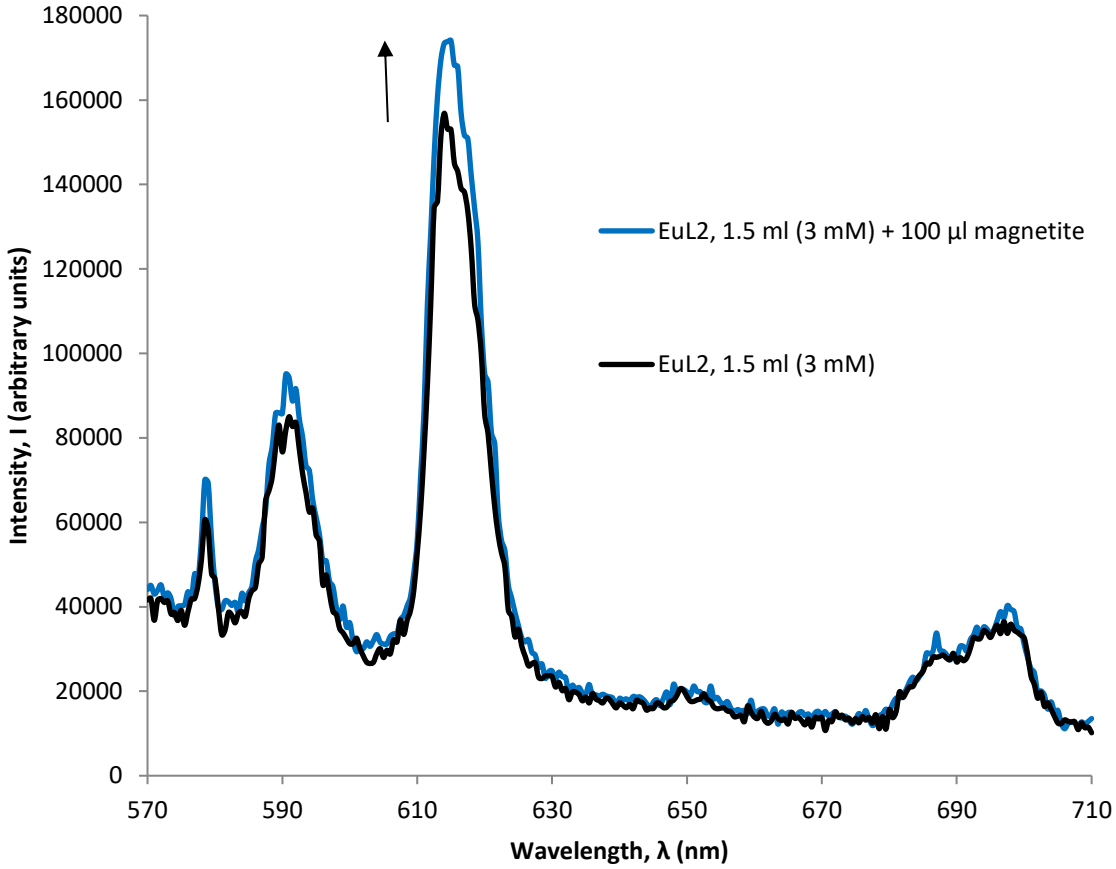

Figure 5.21 Fluorescence spectrum of 1.5 ml (3 mM) $[EuL2]^{3+}$ compared with the spectrum obtained when 100 µl of magnetite extract was added, showing a small increase in sensor-only fluorescence intensity (λ_{Ex}=280 nm, acquisition time=0.5 sec, acquisition increment=0.5 nm, excitation and emission slit width=3 nm, pH=5)

As for $[EuL2]^{3+}$, to first establish the dilution effect on sensor response, 10 µl aliquots of water were added incrementally to $[TbL2]^{3+}$; incremental decreases in intensity were observed, as expected (Figure 5.23). Addition of aliquots of corundum solution (Figure 5.24) also resulted in incremental decreases in intensity of sensor-only fluorescence; all other mineral solutions caused an incremental increase in intensity (e.g. Figure 5.25). Again, the only likely conclusion to account for these results is the introduction of contamination, the effect of which may be enhanced by the very low sensor solution volume. Hence, the mineral solutions appeared to have no effect on the sensor response. In order to ensure there was some $[TbL2]^{3+}$ available to test on the geological samples, this was not used in further tests with mineral solutions.

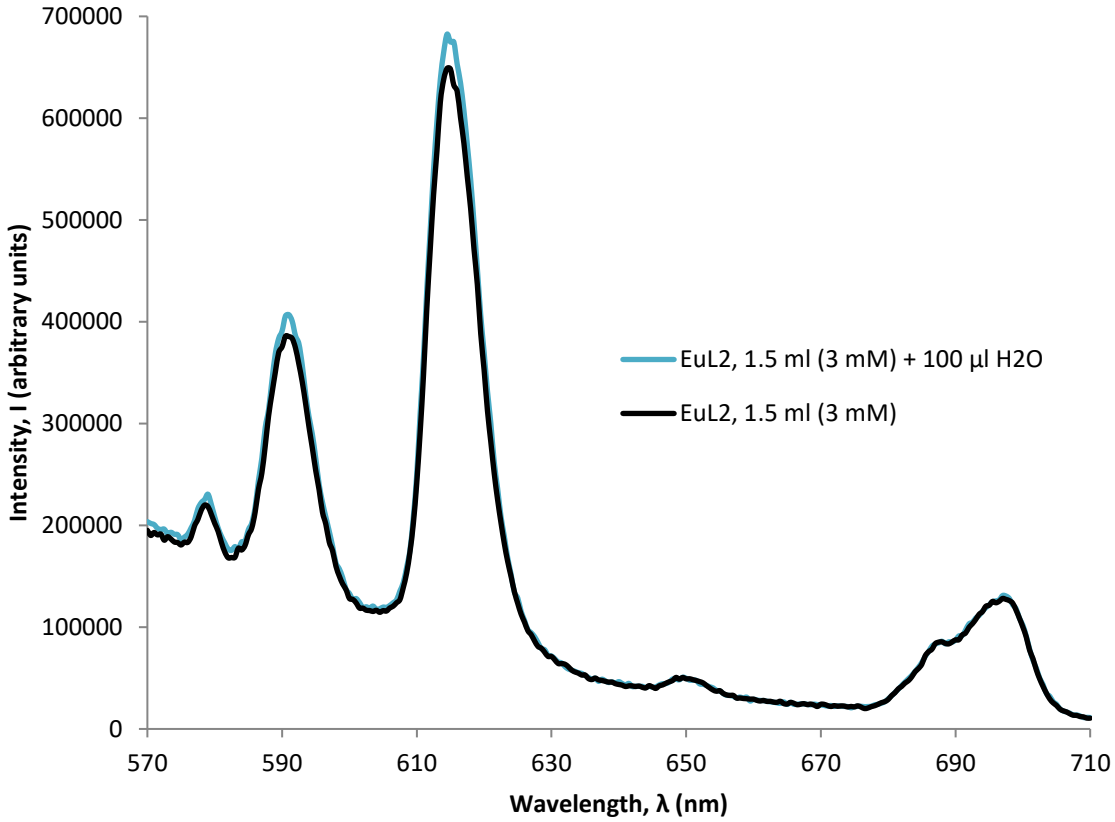

Figure 5.22 Fluorescence spectrum of 1.5 ml (3 mM) $[EuL2]^{3+}$ compared with the spectrum obtained when 100 µl of water was added, showing a small increase in sensor-only fluorescence intensity(λ_{Ex}=280 nm, acquisition time=0.5 sec, acquisition increment=0.5 nm, excitation and emission slit width=3 nm, pH=5)

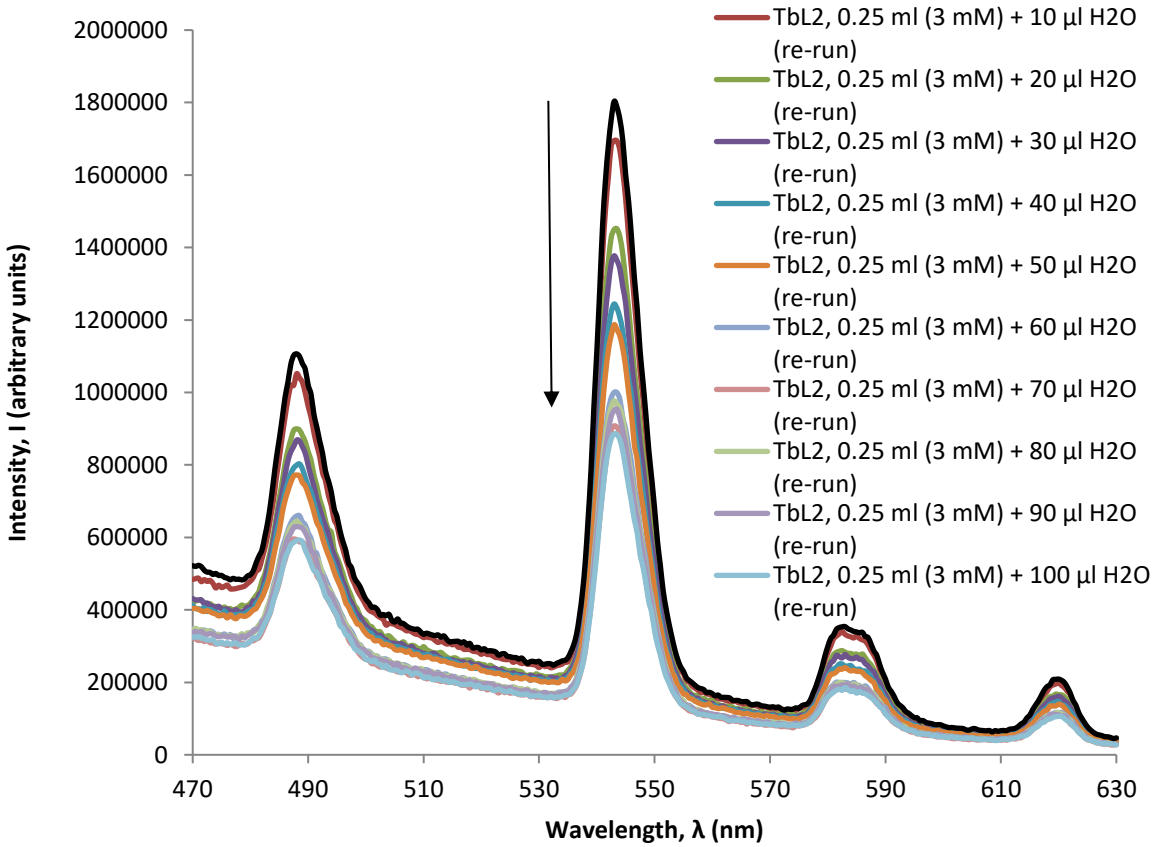

Figure 5.23 Fluorescence spectrum of 0.25 ml (3 mM) $[TbL2]^{3+}$ compared with the spectra obtained when 10 µl aliquots of water were incrementally added (re-run) (λ_{Ex}=280 nm, acquisition time=0.5 sec, acquisition increment=0.5 nm, excitation and emission slit width=3 nm, pH=5)

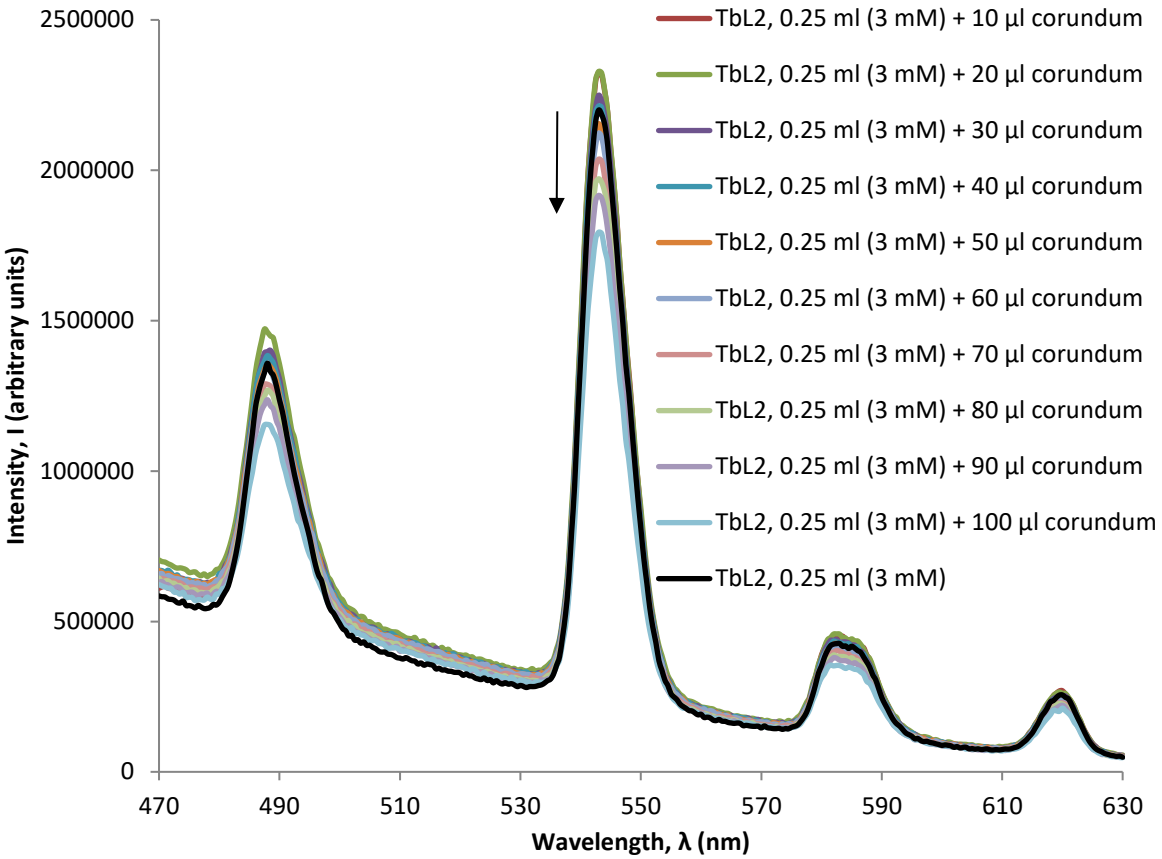

Figure 5.24 Fluorescence spectrum of 0.25 ml (3 mM) $[TbL2]^{3+}$ compared with the spectra obtained when 10 µl aliquots of corundum extracts were incrementally added (λ_{Ex}=280 nm, acquisition time=0.5 sec, acquisition increment=0.5 nm, excitation and emission slit width=3 nm, pH=5)

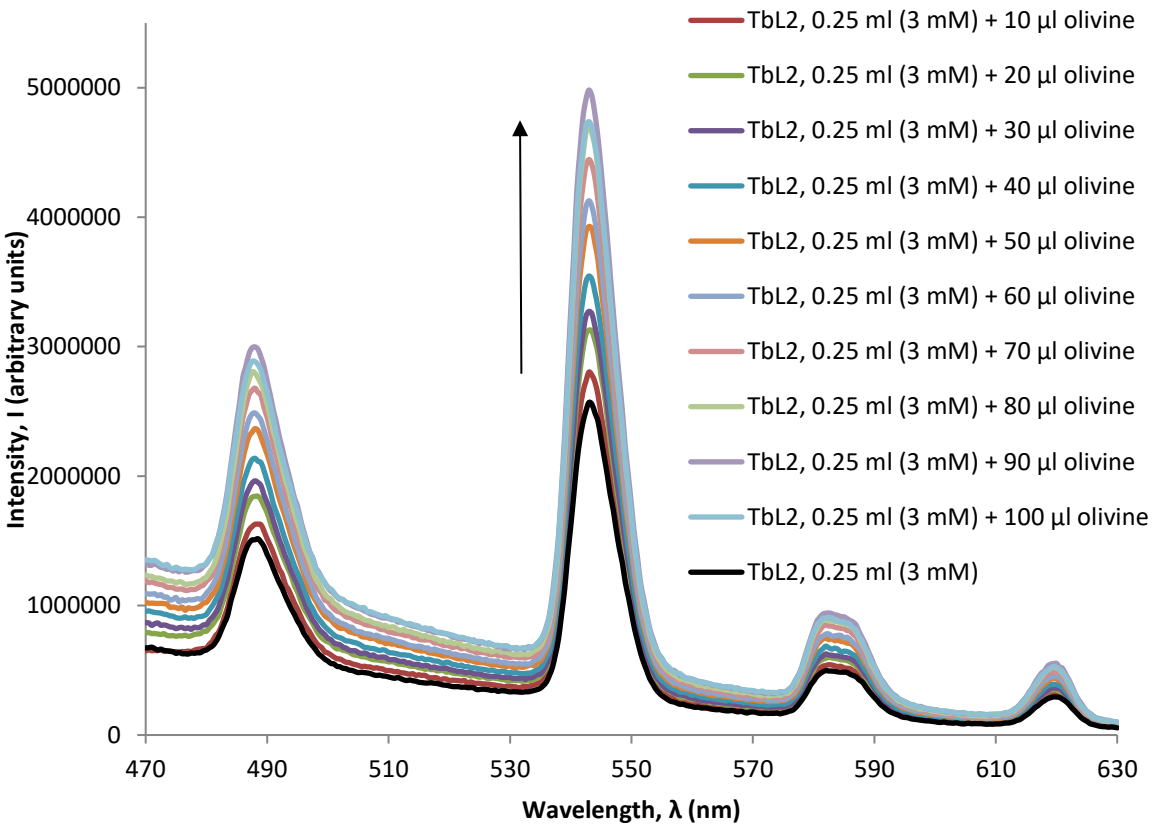

Figure 5.25 Fluorescence spectrum of 0.25 ml (3 mM) $[TbL2]^{3+}$ compared with the spectra obtained when 10 µl aliquots of olivine extracts were incrementally added(λ_{Ex}=280 nm, acquisition time=0.5 sec, acquisition increment=0.5 nm, excitation and emission slit width=3 nm, pH=5)

[LnL3]$^{3+}$

The methodology used to test [LnDO3A] and [LnL2]$^{3+}$ was also applied to the addition of aliquots of mineral solutions to the [LnL3]$^{3+}$ sensor solutions. First, in order to establish the effect of dilution on the fluorescence intensity of the [LnL3]$^{3+}$ complexes, 20 µl aliquots of water were added incrementally to 0.5 ml of 3 mM of [EuL3]$^{3+}$ and [TbL3]$^{3+}$ (Figures 5.26 and 5.27). The spectra obtained indicated expected decreases in intensity attributable to the effect of dilution, thereby providing a basis for comparison for when mineral solutions were applied in the same manner.

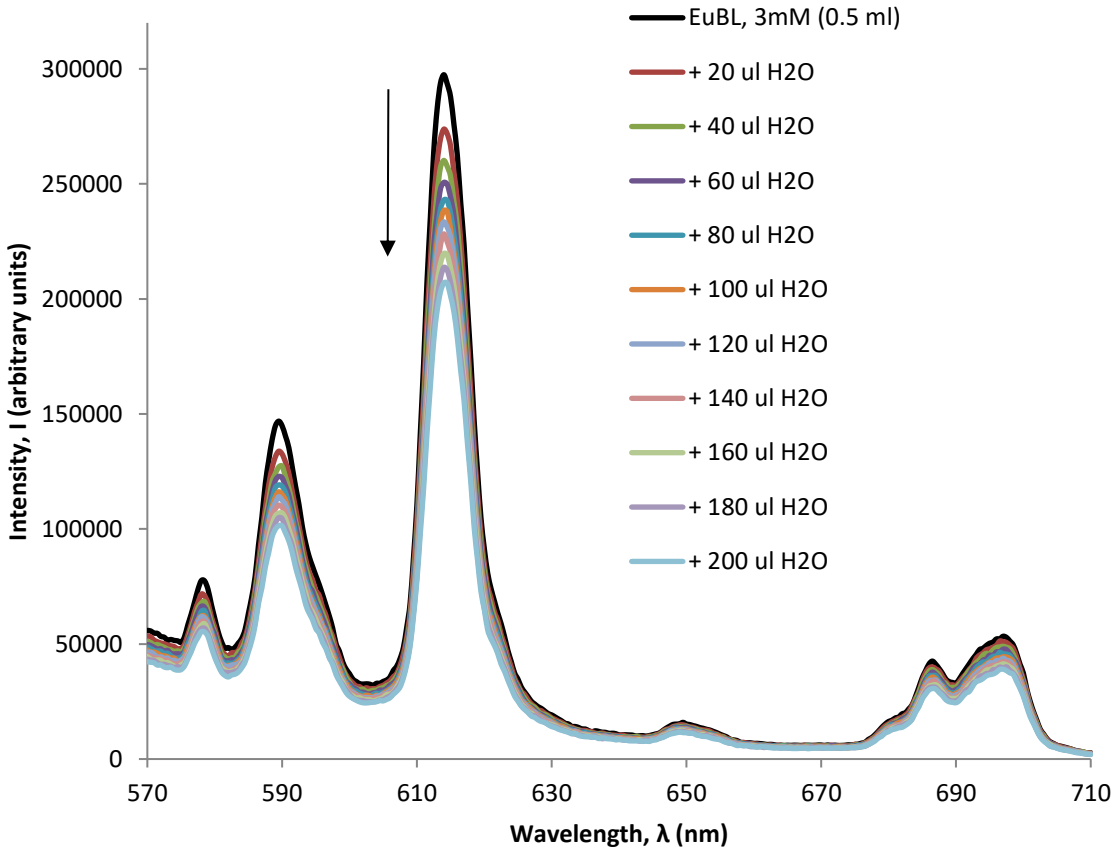

Figure 5.26 Fluorescence spectrum of 0.5 ml (3mM) [EuL3]$^{3+}$ compared with the spectra obtained when 20 µl aliquots of water were added incrementally to show the effect of sensor dilution (λ_{Ex}=280 nm, acquisition time=0.5 sec, acquisition increment=0.5 nm, excitation and emission slit width=3 nm, pH=5)

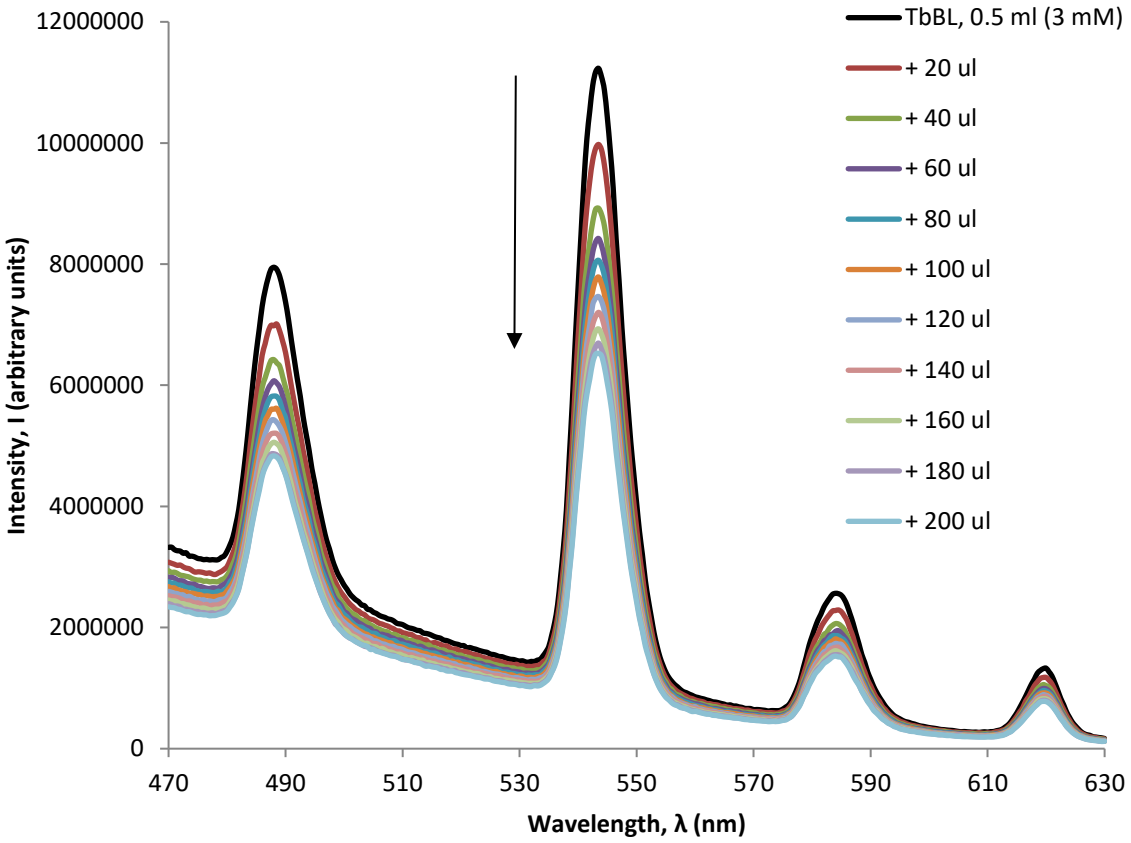

Figure 5.27 Fluorescence spectrum of 0.5 ml (3mM) $[TbL3]^{3+}$ compared with the spectra obtained when 20 µl aliquots of water were added incrementally to show the effect of sensor dilution (λ_{Ex}=280 nm, acquisition time=0.5 sec, acquisition increment=0.5 nm, excitation and emission slit width=3 nm, pH=5)

When 20 µl aliquots of each mineral solution were added incrementally to 0.5 ml of 3 mM of $[EuL3]^{3+}$ and $[TbL3]^{3+}$, the spectra obtained for all these mineral solutions indicated sequential decreases in fluorescence intensity (e.g. Figures 5.28 and 5.29, respectively) commensurate with those obtained for the serial dilution test using water (outlined above). This suggests that the decreases in intensity recorded, when the mineral solutions were added to $[LnL3]^{3+}$, were an effect of dilution and not the result of the presence of dissolved species or mineral particulates within the mineral solutions. Therefore, the $[LnL3]^{3+}$ sensor showed no response to the presence of any dissolved mineral species or mineral particulates.

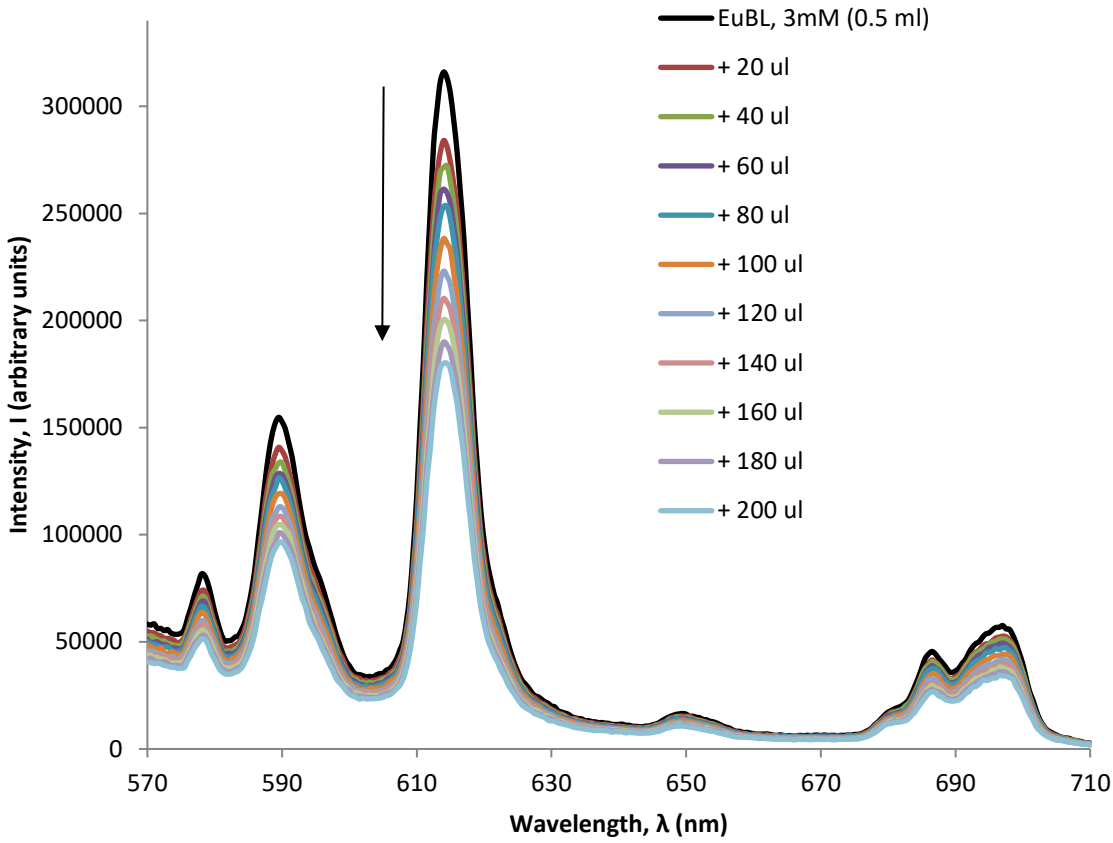

Figure 5.28 Fluorescence spectrum of 0.5 ml (3mM) $[EuL3]^{3+}$ compared with the spectra obtained when 20 µl aliquots of calcite extract were added incrementally (λ_{Ex}=280 nm, acquisition time=0.5 sec, acquisition increment=0.5 nm, excitation and emission slit width=3 nm, pH=5)

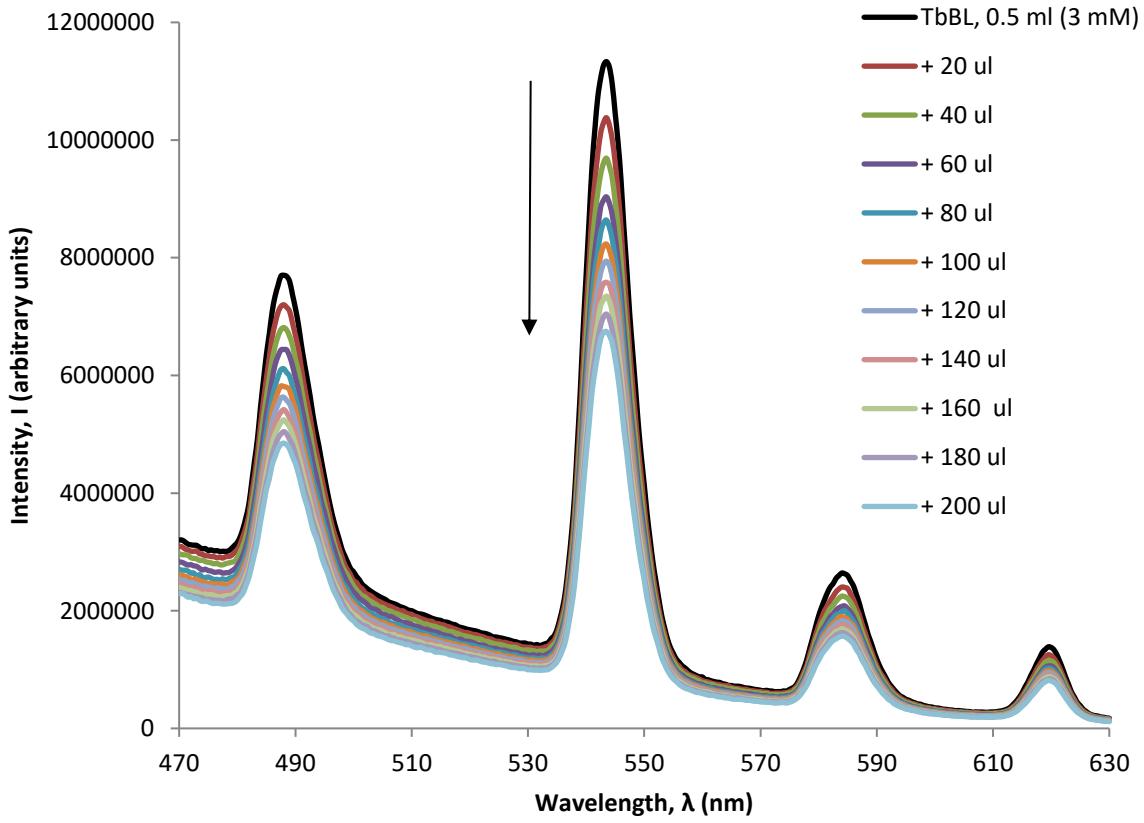

Figure 5.29 Fluorescence spectrum of 0.5 ml (3mM) $[TbL3]^{3+}$ compared with the spectra obtained when 20 µl aliquots of calcite extract were added incrementally(λ_{Ex}=280 nm, acquisition time=0.5 sec, acquisition increment=0.5 nm, excitation and emission slit width=3 nm, pH=5)

5.3.3 Summary and Discussion of sensor response to mineral solutions

Mineral identification

Prior to weathering, the mineral samples were analysed using SEM-EDX, which established bulk chemistry and mineral identity while confirming homogeneity; most minerals were free of chemical anomalies with the exception of anorthite and corundum. A single iron/titanium-enriched feature was identified in anorthite, possibly a natural inclusion, vein or growth on the mineral grain (Figure 5.1) and corundum was shown to contain some extraneous metal grain contamination (Figure 5.2). These features, however, appeared to be isolated occurrences and, therefore, it was considered that the minerals were otherwise homogenous.

Sensor responses to mineral extracts

In order to ascertain the effect of dilution on sensor-only fluorescence, aliquots of water were added to the [EuDO3A] solution; the fluorescence intensity decreased upon each aliquot addition, as would be expected. The incremental addition of mineral solutions to [EuDO3A] resulted in intensity decreases that may also be the result of sensor dilution, and not likely to be caused by the presence of dissolved mineral species or mineral particulates. The exception to this was the incremental addition of olivine solution (where an increase in intensity of the ΔJ=1 transition only was observed) and the incremental addition of calcite solution (which caused increases in intensity of all emissions and would be expected if dissolved CO_3^{2-} is present in the solution). In order to corroborate these results, 100 µl of olivine solution was combined with 1.5 ml of [EuDO3A], however, the observed sensitisation of the ΔJ=1 transition was not evident, rather, a decrease that may be a dilution effect was recorded. When 100 µl of calcite extract was added to [EuDO3A], no increase in intensity of any europium emission was observed; a decrease in intensity was seen that may also be a dilution effect.

Having recorded the effect of dilution of [TbDO3A] by incremental additions of water, incremental additions of solutions from anorthite, diopside and enstatite to [TbDO3A] also resulted in decreases in intensity commensurate with that expected for an effect of dilution. However, the incremental decreases in intensity recorded for the addition of all other mineral solutions

indicated they may not be attributable to dilution alone, but may be a consequence of the presence of dissolved mineral species or mineral particulates in these solutions. To test this, 100 µl of each of the mineral solutions were combined with 1.5 ml of [TbDO3A]. The spectra obtained presented a small decrease in intensity from the sensor-only [TbDO3A] fluorescence spectrum when combined with the corundum extract, but a small increase in intensity for all the other mineral extracts tested. As previously surmised, this is likely to be a result of inadvertent contamination during the addition of aliquots of mineral solutions, rather than the presence of mineral species.

The results obtained for the addition of mineral solutions to the [LnDO3A] sensors were largely inconsistent and could be the result of sensor dilution effects, contamination (exacerbated by the very small sensor volumes use, or loss of sensor solution from the cuvette during aliquots additions. It is, therefore, not clear if the presence of dissolved mineral species or mineral particulates (should they be present at all) have an effect upon sensor fluorescence emissions. The effect of incremental aliquot additions of mineral extracts on $[EuL2]^{3+}$ were similarly inconsistent, with apparently random increases and decreases in intensity, including when incremental additions of aliquots of water were made. Again this may be the result of sensor loss or contamination. Thus, the results were rendered too inaccurate to be attributed to the presence of dissolved minerals with any confidence, and so any effect the mineral solutions may have had on the fluorescent emissions of the sensor could not be determined with any certainty.

All results obtained for the application of $[LnL3]^{3+}$ sensors to incrementally increasing concentrations of mineral solution indicated only decreases in sensor fluorescence intensity commensurate with that recorded for an effect of dilution. The implication is that, if dissolved mineral species or mineral particulates are present in these mineral extracts, $[LnL3]^{3+}$ sensors are unaffected by their presence. Hence, if a response is observed when these sensors are applied to extracts obtained from organic-rich geological samples, it could be considered with some certainty that the response is due only to the presence of organic analytes. However, the extracts

are likely to contain many more dissolved inorganic species than the single mineral extracts applied in this set of tests.

Recommendations to resolve inconsistencies in results obtained

In this study, the dissolved mineral species expected to be present in the mineral solutions were ascertained only by understanding the chemical composition of the minerals and the likely products that their weathering may liberate. Much of this was based on literature, which described ionic species or aqueous alteration products (i.e. secondary minerals) liberated under conditions or timescales different to those used in this work. Nevertheless, the suggested dissolved species that may be expected to be in the solutions with which the sensors were tested were valid, but the likelihood of their presence would be negligible given the short time period of the weathering and the mild condition under which it took place (6 weeks at room temperature in aqueous medium).

It would, therefore, have been advantageous to identify any dissolved species, mineral particulates or secondary minerals contained within the solutions before testing with the sensors. This would allow predictions to be made as to what type of interactions might occur given the properties of the species identified, and how the sensor may respond as a result. Moreover, should any unexpected fluorescence responses be observed, caused by the presence of a particular mineral solution, an alternative interpretation may be suggested. This would avoid the inability to confidently attribute sensor responses. Moreover, it may enable interpretation of results when inconsistencies occur due to sensor losses or contamination.

Much of the work in this section has suffered from inconsistences in sensor responses which have been attributed to probable loss of sensor, and possible introduction of contamination, during the addition of aliquots of mineral solution. An effective way to avoid these issues, or at the very least minimise the impact this may cause, is to use larger sensor solution volumes. All of the sensor tests began with the addition of very small volume aliquots of mineral solutions (either 10 or 20 µl) to very small volumes of sensor solution (0.25 or 0.5 ml). Removal of even a few

nanolitres (nl) of 3 mM sensor solution from a cuvette containing 0.25 ml, when the stopper is removed, may impede the detection of an increase in intensity when 10 µl of mineral solution is added. If a few nl of sensor solution is removed from 1.5 ml, the effect on fluorescence intensity recorded would be considerably less. Moreover, given that the purpose of the sensors developed and tested in this work is to detect the presence of organic molecules, should any contamination derived from organic material take place, the relative concentration of the contaminant to the sensor complex would be large, and so the response to its presence would be observed. Again, a larger volume of sensor would mean the relative concentration of contaminant to sensor would be greatly reduced, thereby reducing the sensors response to its presence.

All of the mineral solution work presented in Section 5.3.2 (and indeed all fluorimetry work) has been undertaken in open laboratories. As such, the risk of contamination from airborne or other organic material cannot be ruled out, even given the meticulous cleaning protocols rigorously maintained for all cuvettes, glassware and syringes (see Section 2.1).
All aliquots of sensor solutions, analogue organic analytes, mineral solutions and water blanks for dilution-effect determination, were all measured using precision micro-syringes and pipettes. However, this still does not rule-out the possibility of user-error during the measuring and/or delivery of aliquots of these solutions.

All of these possible sources of contamination and error cannot be entirely controlled and so the only way to minimise or assure against them is for the various mechanical handling procedures, required for testing the application of sensors to analytes, to be automated. An automated system would ensure that accurate and consistent aliquot volumes of sensor or analyte solution could be measured for every test and, to remove any chance of contamination, this process would need to be carried out under sterile or clean conditions. The removal of human error and sources of contamination would result in accurate and reliable spectra which would enable sensor responses to be ascertained, even if very small volumes were used, possibly with very low concentrations of analytes.

Should the sensors developed in this study be required for the detection of organic material contained within extracts obtained from the regolith of a planetary surface, as part of a 'life detection' mission or analyses to find biomarkers, for example, it is likely that the concentration of organic analytes would be extremely low. Furthermore, it is likely that only small volumes of sensor could be accommodated on board a planetary surface instrumentation vehicle, the sterilisation and contamination levels of which would be controlled. Therefore, to accurately test the utility of the sensors, it would be advantageous to test them in a setting likely to be similar to one in which their deployment would be undertaken in a field setting and to develop an automated system to minimise the sample handing problems encountered here.

However, the applicability and responses to extracts obtained from an organic-rich terrestrial rock must be carried out in the absence of an automated system, or an entirely contamination-free environment in which to do it, in order to ascertain if the sensors may be used to detect organic analytes in real sample complex mixtures. The sensors must then be applied to extracts obtained from extraterrestrial samples. It is the work in the following section that will determine if the sensors could be used for planetary exploration, and it is the application and results of this work that is presented next.

5.4 Green River Shale terrestrial analogue

In order to develop an extraction protocol and test the validity of sensors before application to the extraterrestrial samples, a terrestrial analogue was chosen. Green River Shale is known to contain extractable organic material (e.g. Haug et al., 1967, Reed, 1975, McKay et al., 1983, Henderson et al., 2013) and a similar mineralogy to that of carbonaceous chondrites, e.g. carbonates, silicates, clays (Milton, 1971). A description of this terrestrial rock and the rationale for its selection is given in Section 2.2.2.

The crushed sample was subjected to a three-step extraction protocol using hot 18.2 MΩ water, followed by a hot MeOH and finally a hot mixture of organic solvents; the details of the process are given in Section 2.5.2. The extract masses obtained are presented in Table 5.10 to show the

disparity between each fraction and, moreover, the abundance of organic material obtainable from each geological sample. The extracts were dissolved in 200 µl of 18.2 MΩ water and the sensors (europium only, since there were insufficient terbium sensors available) were then applied to the extracts for fluorimetric analyses (see Section 2.8.4 for the procedure).

Sensors applied to the GRS extracts	Hot-water extract mass obtained (mg)	Hot-MeOH extract mass obtained (mg)	Hot-solvent extract mass obtained (mg)
[EuDO3A]	2.17	2.93	0.07
$[EuL1]^{3+}$	2.16	-	-
$[EuL2]^{3+}$	1.81	2.85	-
$[EuL3]^{3+}$	2.25	2.45	0.03

Table 5.10 Mass of GRS extract obtained by each solvent extraction (in milligrams) and the sensors that were applied for fluorimetric analysis

5.4.1 Fluorimetry of sensor application to GRS extracts

The purpose of all the preceding work (Chapters 3 and 4, and Section 5.3.2) was to produce spectra of the responses of lanthanide complexes to selected analytes likely to make up the content of extracts derived from extraterrestrial and terrestrial samples. This was in order that, when the lanthanide fluorescent complex sensors were applied to extracts derived from organic-rich extraterrestrial and terrestrial natural samples, some foreknowledge of responses to expect could be anticipated and compared to those obtained when the sensors were mixed with analogue analytes. Comparable responses, therefore, may indicate the presence of similar molecules contained within the organic-rich extraterrestrial and terrestrial natural sample extracts.

Chapters 3 and 4 show that, where fluorescence emission responses to the presence of analogue analytes were recorded, terbium sensors respond in the same way as europium sensors. Where analytes were applied to terbium complexes causing a response, all transitions were sensitised or quenched such that the relative intensity of the emissions remained constant. Europium transitions, however, had shown selective sensitisation such that some transitions were more sensitised by the presence of certain analytes than others. For this reason, and because of the

limited volumes of extracts from meteorites and GRS, only complexes of europium were used to ascertain sensor responses with these samples.

In order to ascertain the concentration of total organic material to which the fluorescent sensors were to be applied, it was necessary to record the mass of the 2 ml vial containing the extract before dissolution, and the mass of the 2 ml vial after the extract was dissolved, decanted and dried. 200 µl of 18.2 MΩ water was added directly to the various organic extracts isolated from the selected solid natural samples using a 250 µl micro-syringe. The caps were replaced and the extracts and aqueous solvent were agitated using a vortex mixer for 30 seconds. 3 ml of 3 mM sensor solution was decanted into a fluorimetry quartz cuvette using a 500 µl micro-syringe, to which the 200 µl aqueous extract solution was directly added, using the same 250 µl micro-syringe. The cuvette and contents were inverted 10 times in order to ensure complete mixing. The micro-syringes were washed between samples using the cleaning method described (Section 2.1.5).

The fluorimeter settings for these assays were the same as those used for previous assays involving the application of lanthanide DO3A-like complex sensors to the analogue organic analytes extracts (Section 2.7.2) and weathered mineral extracts (Section 2.7.3).

Sensor responses to GRS hot-water extracts

When [EuDO3A] was applied to the hot-water extract of GRS, there was a clear increase in intensity recorded for all transitions, with the relative peak intensities remaining approximately the same as the sensor-only spectrum, i.e. the intensities of the transitions were in the order ΔJ=2>ΔJ=1>ΔJ=4>ΔJ=0>ΔJ=3, however there appeared to be some preferential sensitisation of the ΔJ=2 transition (Figure 5.30). Although the sensor-only spectrum of $[EuL1]^{3+}$ was poorly resolved, upon application to the hot-water extract, sensitisation of all transitions was recorded, with the exception of ΔJ=0 (which may be as a result of poor resolution), suggesting a component of the extract may bind as a sensitiser (Figure 5.31). Conversely, when $[EuL2]^{3+}$ was applied to the hot-water extract, there was a desensitisation of all transitions, with the exception of ΔJ=2, which did not alter from the sensor-only emission intensity (Figure 5.32). The $[EuL3]^{3+}$ sensor-only

fluorescence intensity was reduced by approximately 35% when in the presence of the hot-water extract of GRS (Figure 5.33).

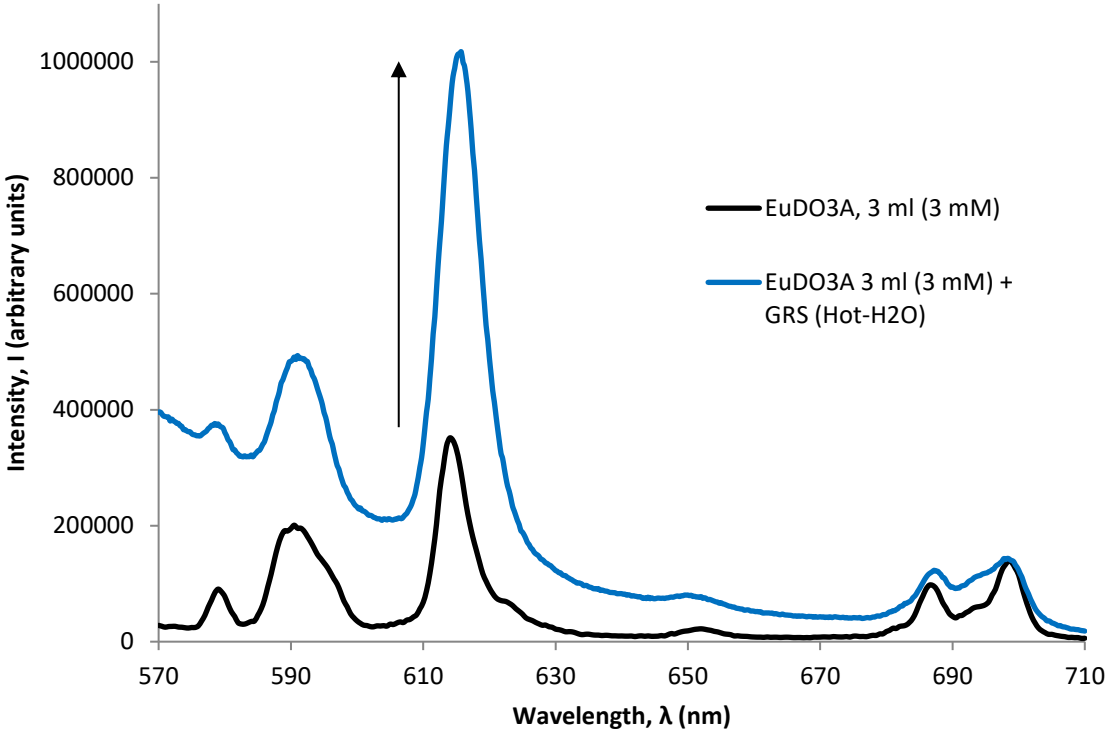

Figure 5.30 Sensor-only [EuDO3A] (3 ml, 3mM) fluorescence spectrum (black) compared with the [EuDO3A] (3 ml, 3mM) fluorescence spectrum in the presence of the GRS hot-water extract (blue) (λ_{Ex}=280 nm, acquisition time=0.5 sec, acquisition increment=0.5 nm, excitation and emission slit width=3 nm, pH=5)

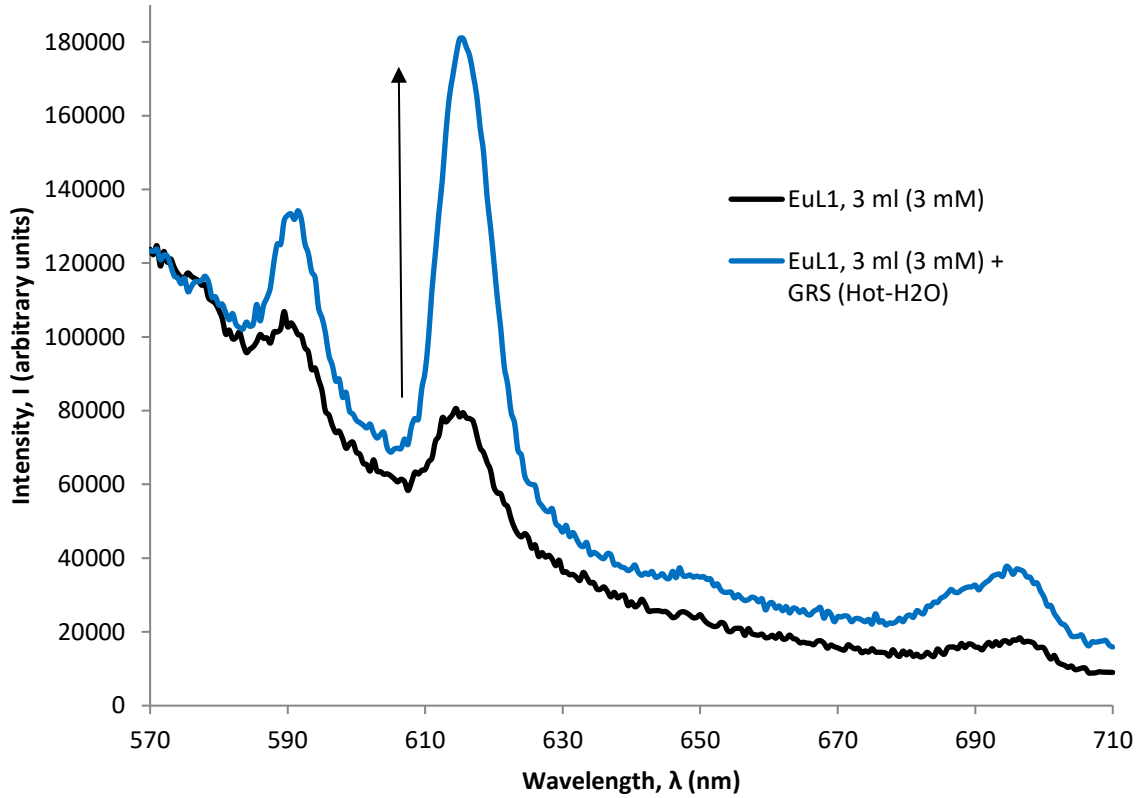

Figure 5.31 Sensor-only $[EuL1]^{3+}$ (3 ml, 3mM) fluorescence spectrum (black) compared with the $[EuL1]^{3+}$ (3 ml, 3mM) fluorescence spectrum in the presence of the GRS hot-water extract (blue) (λ_{Ex}=280 nm, acquisition time=0.5 sec, acquisition increment=0.5 nm, excitation and emission slit width=3 nm, pH=5)

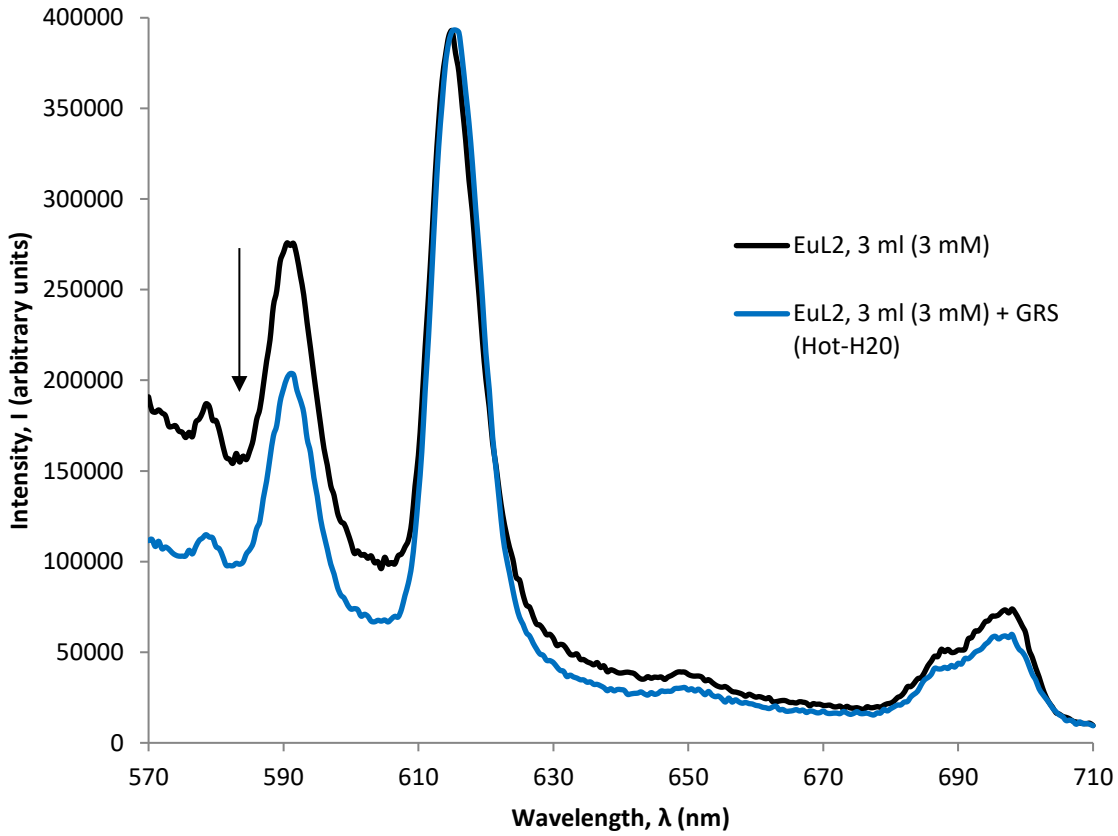

Figure 5.32 Sensor-only $[EuL2]^{3+}$ (3 ml, 3mM) fluorescence spectrum (black) compared with the $[EuL2]^{3+}$ (3 ml, 3mM) fluorescence spectrum in the presence of the GRS hot-water extract (blue) (λ_{Ex}=280 nm, acquisition time=0.5 sec, acquisition increment=0.5 nm, excitation and emission slit width=3 nm, pH=5)

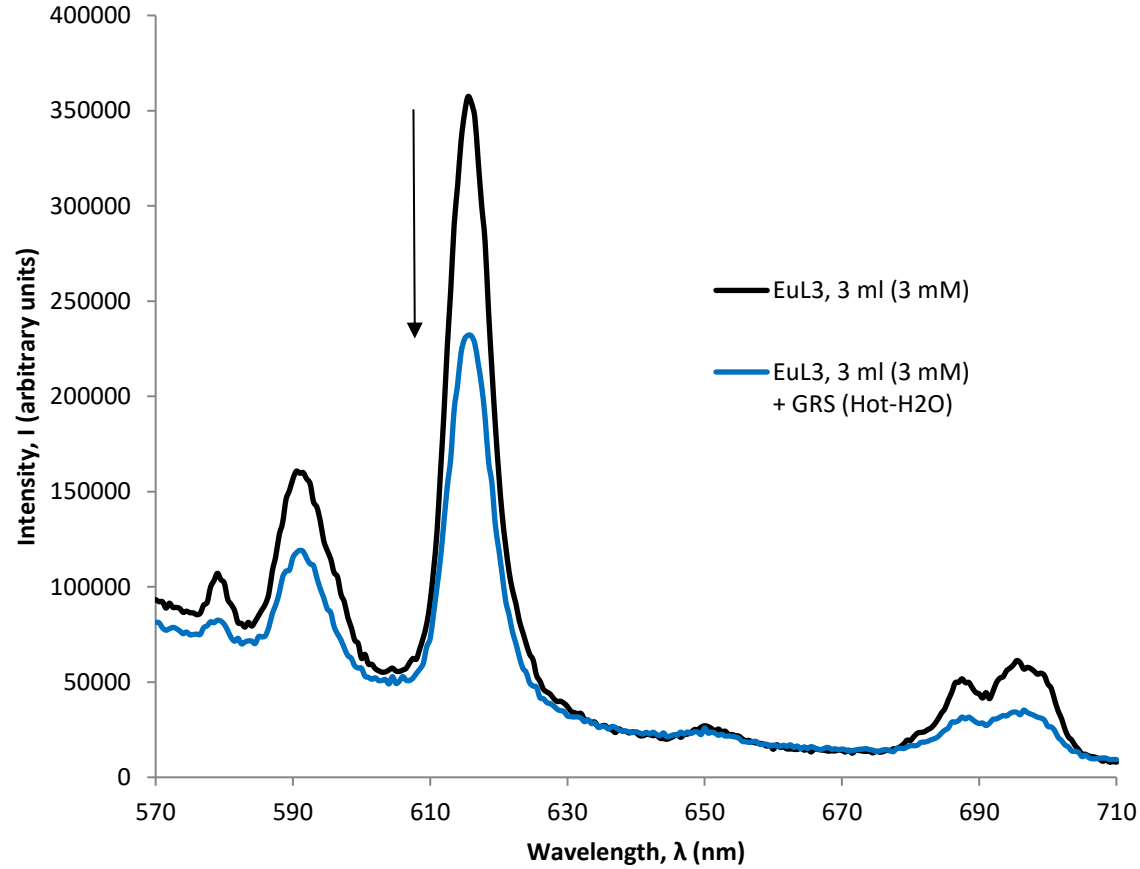

Figure 5.33 Sensor-only $[EuL3]^{3+}$ (3 ml, 3mM) fluorescence spectrum (black) compared with the $[EuL3]^{3+}$ (3 ml, 3mM) fluorescence spectrum in the presence of the GRS hot-water extract (blue) (λ_{Ex}=280 nm, acquisition time=0.5 sec, acquisition increment=0.5 nm, excitation and emission slit width=3 nm, pH=5)

Sensor responses to GRS hot-MeOH extracts

A sensitisation of all transitions was observed when [EuDO3A] was applied to the hot-MeOH GRS extract, particularly at Δ*J*=1 and Δ*J*=2 (intensity increased 5 fold and 8 fold, respectively) (Figure 5.34). This increase was larger in magnitude than that seen when [EuDO3A] was applied to the hot-water extract. The GRS hot-MeOH extract also caused the $[EuL2]^{3+}$ europium emissions to respond with a sensitisation of all transitions, particularly at Δ*J*=1 and Δ*J*=2 (Figure 5.35) and also caused a sensitisation of the $[EuL3]^{3+}$ europium emissions (Figure 5.36). The $[EuL2]^{3+}$ and $[EuL3]^{3+}$ senstitisations were comparable with those seen with the hot-water extract. These observations suggest there is an organic component in the GRS hot-MeOH extract that binds and facilitates indirect excitation by antenna effect.

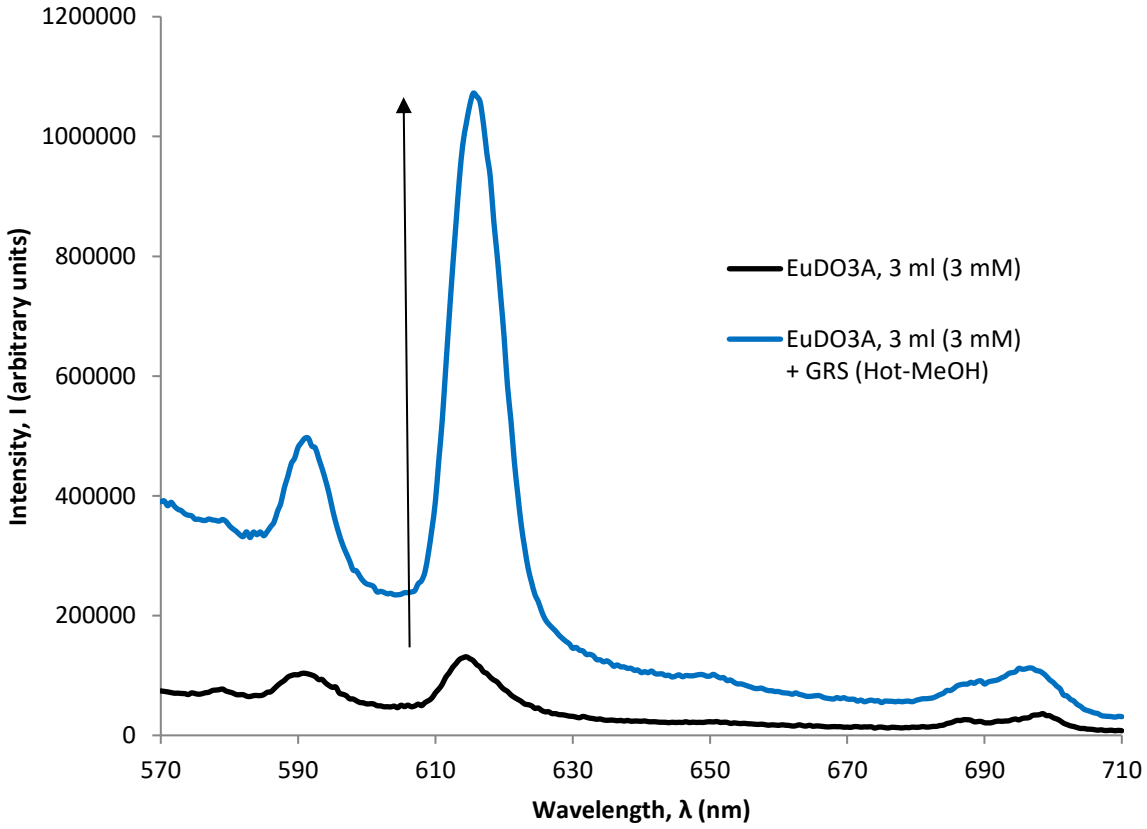

Figure 5.34 Sensor-only [EuDO3A] (3 ml, 3mM) fluorescence spectrum (black) compared with the [EuDO3A] (3 ml, 3mM) fluorescence spectrum in the presence of the GRS hot-MeOH extract (blue) (λ_{Ex}=280 nm, acquisition time=0.5 sec, acquisition increment=0.5 nm, excitation and emission slit width=3 nm, pH=5)

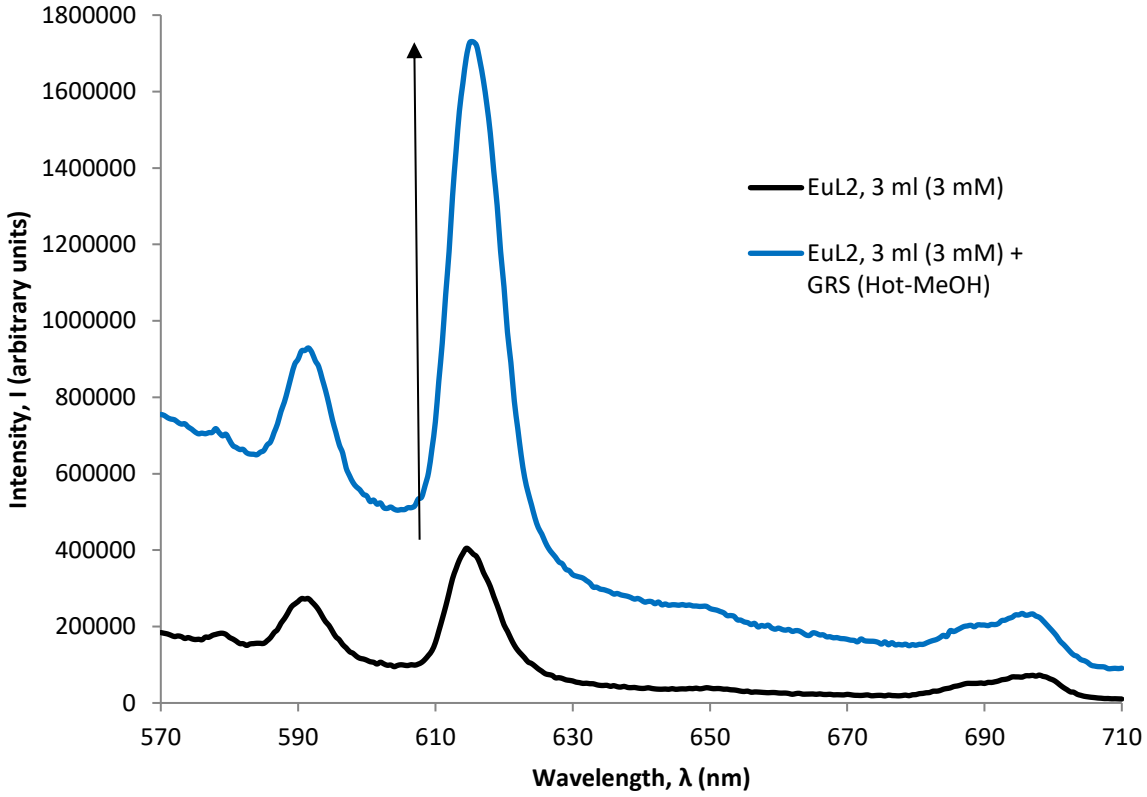

Figure 5.35 Sensor-only $[EuL2]^{3+}$ (3 ml, 3mM) fluorescence spectrum (black) compared with the $[EuL2]^{3+}$ (3 ml, 3mM) fluorescence spectrum in the presence of the GRS hot-MeOH extract (blue) (λ_{Ex}=280 nm, acquisition time=0.5 sec, acquisition increment=0.5 nm, excitation and emission slit width=3 nm, pH=5)

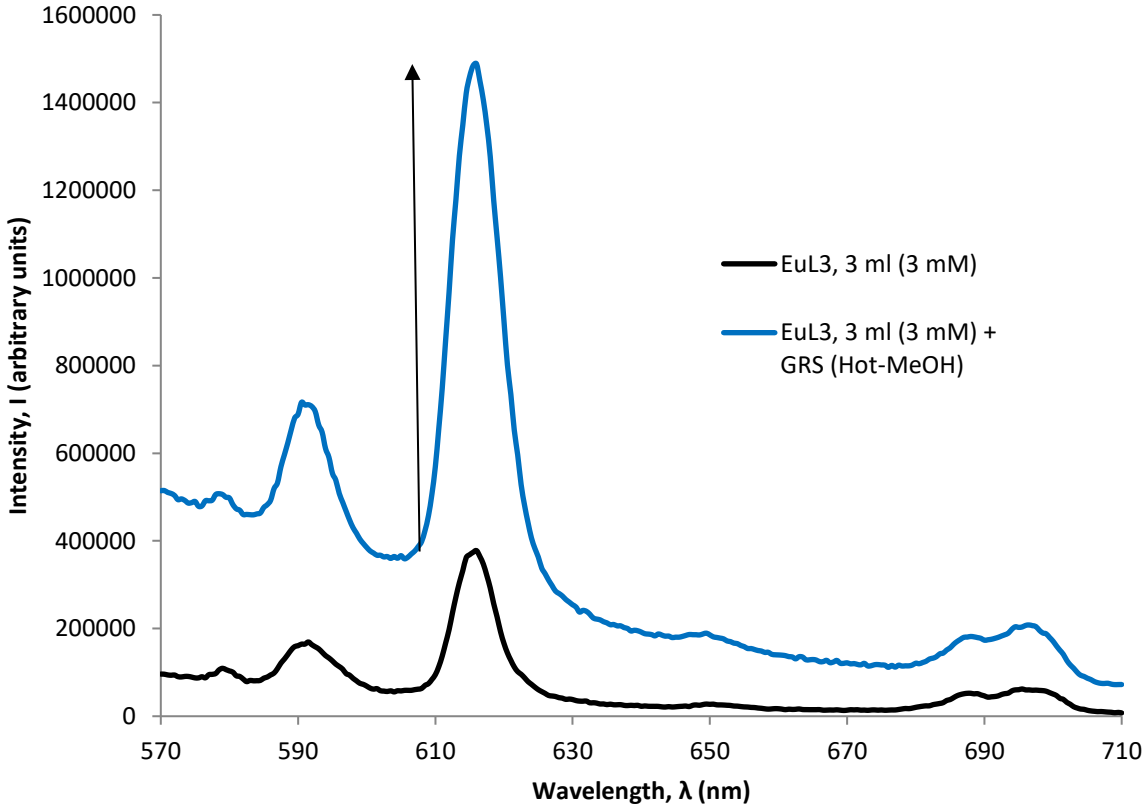

Figure 5.36 Sensor-only $[EuL3]^{3+}$ (3 ml, 3mM) fluorescence spectrum (black) compared with the $[EuL3]^{3+}$ (3 ml, 3mM) fluorescence spectrum in the presence of the GRS hot-MeOH extract (blue) (λ_{Ex}=280 nm, acquisition time=0.5 sec, acquisition increment=0.5 nm, excitation and emission slit width=3 nm, pH=5)

Sensor responses to GRS hot-MeOH:DCM:Toluene (hot-solvent) extracts

When the GRS hot-solvent extract was combined with the [EuDO3A] sensor solution, a broad fluorescence emission was observed below 630 nm (Figure 5.37) that overlays and obscures indicative lanthanide emissions rendering them difficult to resolve. However, the increases in intensity of the europium emissions within this region of the spectrum (~592 nm and ~613 nm, in particular) suggest that the ΔJ=1 and ΔJ=2 transitions may have been sensitised. Application of $[EuL3]^{3+}$ to the GRS hot-solvent extract did not invoke a sensor response (Figure 5.38).

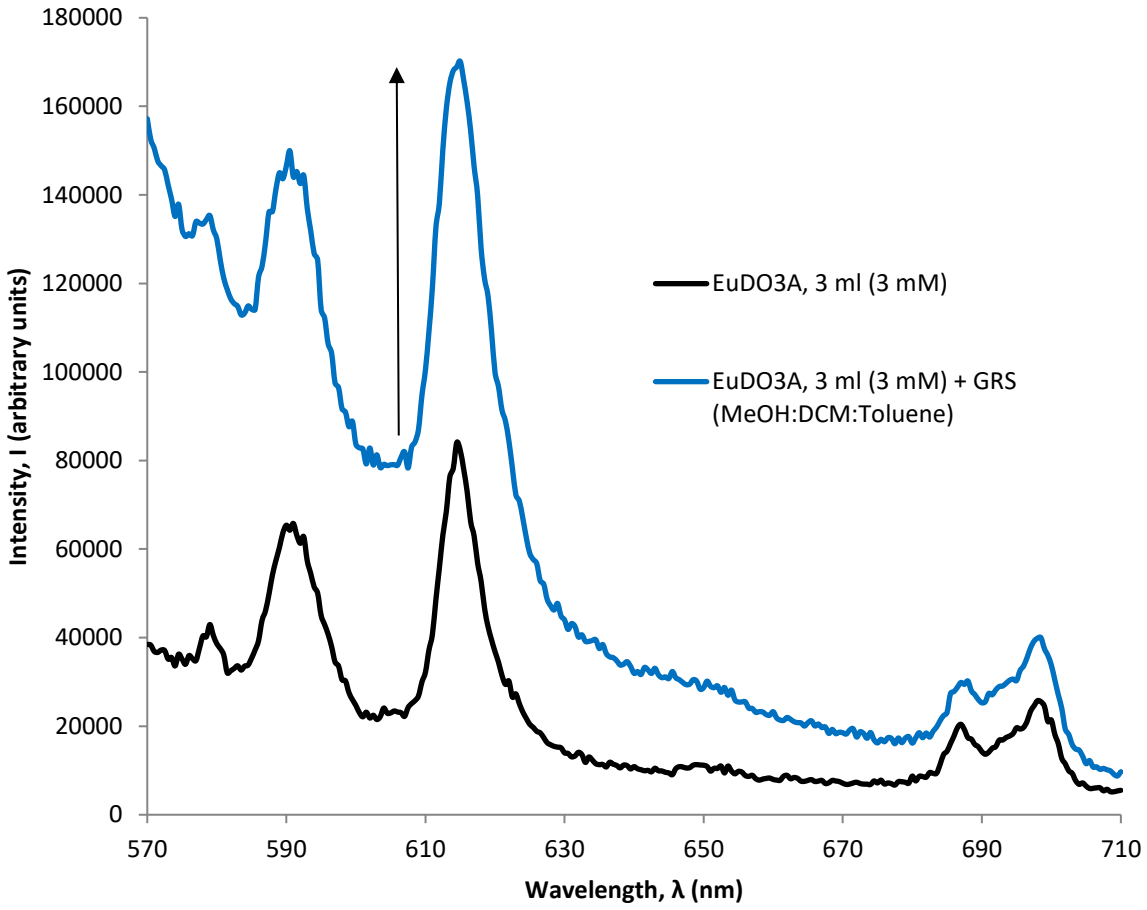

Figure 5.37 Sensor-only [EuDO3A] (3 ml, 3mM) fluorescence spectrum (black) compared with the [EuDO3A] (3 ml, 3mM) fluorescence spectrum in the presence of the GRS hot-solvent extract (blue) (λ_{Ex}=280 nm, acquisition time=0.5 sec, acquisition increment=0.5 nm, excitation and emission slit width=3 nm, pH=5)

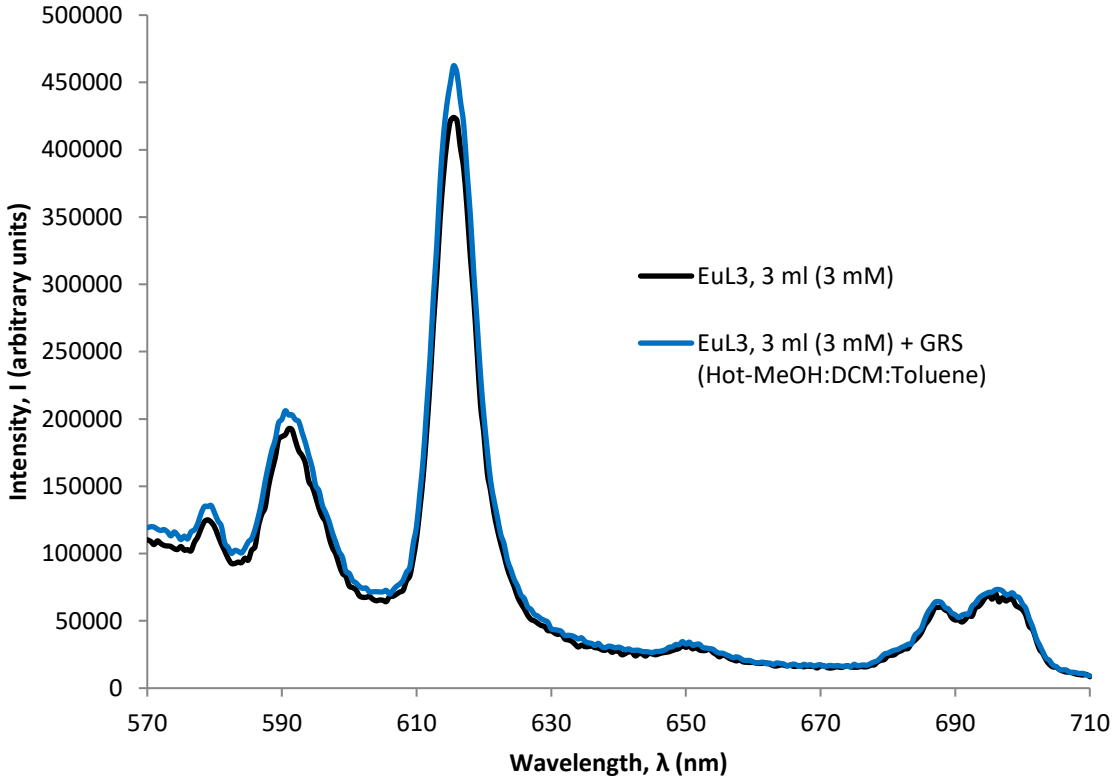

Figure 5.38 Sensor-only $[EuL3]^{3+}$ (3 ml, 3mM) fluorescence spectrum (black) compared with the $[EuL3]^{3+}$ (3 ml, 3mM) fluorescence spectrum in the presence of the GRS hot-solvent extract (blue) (λ_{Ex}=280 nm, acquisition time=0.5 sec, acquisition increment=0.5 nm, excitation and emission slit width=3 nm, pH=5)

5.4.2 Discussion of GRS extraction and fluorimetry

Hot water extract

Similar extraction protocols to those employed in this thesis, specifically involving reflux temperature extractions of GRS using organic solvents, and in the presence of water, have been carried out (McKay and Chong, 1983). The extracts obtained in that study were separated into fractions of organic acids, organic bases, neutral nitrogen compounds and hydrocarbons, which were then characterised by infrared (IR) spectroscopy. Strong IR absorbance between ~1650 cm^{-1} and 1750 cm^{-1} was ascribed to the presence of carbonyl groups of carboxylic acids, esters, and ketones or amides, and bands at ~1600 cm^{-1} were assigned to carbon-carbon absorbance indicative of aromatic carboxylic acid compound classes. Chapters 3 and 4 demonstrated that the sensors were able to detect the presence of analogue organic analytes that also possess carbonyl moieties and, hence, the results seen here indicate the presence of organic components with carbonyl moieties within the hot-water extract of the GRS.

Absorption bands at 1567 cm^{-1} and 1603 cm^{-1} were also observed by McKay and Chong (1983) and are characteristic of pyridines (a class of organic molecule not used as analogue analytes in this study) (Brandenburg and Latham, 1968, McKay et al., 1976). McKay and Chong (1983) determined that GRS contains many of these pyridine molecules, and that they are also present as pyridine carboxylic acids. Pyridine carboxylic acids are structurally analogous to benzoic acid and its derivatives, and similarly polar, so may interact with the sensors *via* a similar mechanism (Figure 5.39). It would therefore be expected that the hot-water extract obtained in this study would contain the highest concentration of these polar molecules, and thus would invoke the greatest sensor responses.

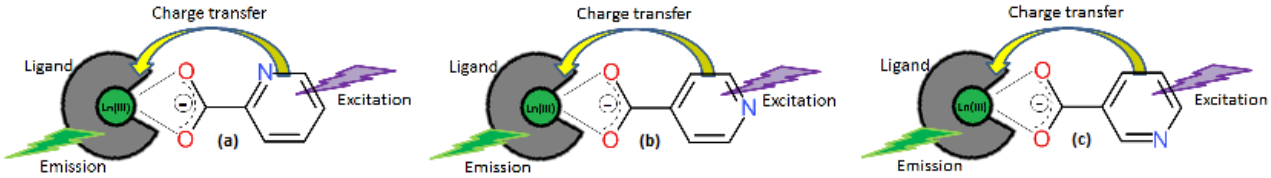

Figure 5.39 Pyridine carboxylic acid has three structures were the nitrogen atom in the aromatic ring is *ortho*- (a), *para*- (b) and *meta*- (c) to the carboxylic acid functional group. Each isomer is shown binding to the lanthanide complex facilitating indirect excitation *via* antenna effect

All europium emissions of the [EuDO3A] and $[EuL1]^{3+}$ complexes were sensitised by the presence of the GRS hot-water extracts, with a slight preferential sensitisation of the ΔJ=2 transition, though the relatively low intensity of the sensor-only $[EuL1]^{3+}$ fluorescence emissions resulted in poor spectrum resolution. However, this sensitisation of transitions was not observed when $[EuL2]^{3+}$ was applied to the GRS hot-water extracts, where desensitisation of the transitions responsible for the ΔJ=0, ΔJ=1, ΔJ=3 and ΔJ=4 emissions occur and no change in intensity for the ΔJ=2 emission. This suggests that the [EuDO3A] and $[EuL1]^{3+}$ sensors may be susceptible to interactions with aromatic carboxylic acid molecules but $[EuL2]^{3+}$ is not. This difference in sensor response may be due to steric hindrance caused by the larger pendant arms of $[EuL2]^{3+}$, thus suggesting that the aromatic structural component of the carboxylic acid molecules in the GRS hot-water extract may be larger than a single benzyl group; in the presence of benzoic acid, all sensors invoked an increase in intensity for all transitions (Chapters 3 and 4). Therefore, if this hypothesis is true, in order to detect aromatic carboxylic acid molecules where the aromatic

group is larger than a simple benzyl group, the sensor must possess short, sterically unimpeding pendant arms.

The elevated fluorescent emissions recorded below 630 nm when GRS hot-solvent extract were combined with [EuDO3A] are likely to be the result of the presence of intrinsically fluorescent components in the extract: fluorescent molecules or, possibly, fluorescent mineral particulates. This may imply that [EuDO3A] is more sensitive to the presence of such intrinsically fluorescent species than the other sensors tested in this study. Furthermore, sensitisation, but not alteration, of the relative emission intensities of each transition, caused by the presence of the GRS hot-solvent extracts, may be attributable to components that may displace water molecules from the coordination sphere but not interact electronically, e.g. carbonate anions (see below). However, it is equally possible that these analytes may coordinate but, in doing so, affect the coordination environment of the europium ion such that preferential sensitisation of the ΔJ=1 transition does not occur. Measurements of fluorescence lifetimes and q values would confirm if water molecule displacement and binding takes place.

When $[EuL3]^{3+}$ was applied to the hot-water extract of GRS, there was an approximate 35% reduction in intensity. This desensitisation of europium emissions of $[EuL3]^{3+}$ may suggest the presence of nucleobases that [EuDO3A] and $[EuL1]^{3+}$ could not detect. Nucleobases, which quench fluorescence (see Chapter 3), are smaller and may not be hindered by the steric effect of the pendant arms on $[EuL3]^{3+}$, whereas bulky aromatic carboxylic acids might. As previously discussed (*vide infra*), McKay and Chong (1983) identified aromatic carboxylic acids and their pyridine carboxylic acid analogues in the water extract of GRS. There was no specific mention regarding the detection of nucleobases, however, McKay and Chong (1983) also alluded to the presence of 'organic bases' with a high concentration of heteroatoms, especially oxygen and nitrogen. However, previous fluorescence experiments using nucleobase analytes in high concentrations, and as complex mixtures (Chapter 3), suggest that, even if there were nucleobases present, they would be unlikely to cause the responses recorded and the reduction in intensity may simply be a dilution effect. Given that these extracts sensitised emissions when

combined with DO3A, L1 and L2 europium complexes, it is more likely that $[EuL3]^{3+}$ simply does not respond as effectively as the other sensors used.

Hot-MeOH extract

When all europium complexes ([EuDO3A], $[EuL2]^{3+}$ and $[EuL3]^{3+}$) were in the presence of the GRS hot-MeOH extract, an increase in intensity was observed for all transitions, but specifically sensitisation of the ΔJ=2 transition, i.e. over and above the increase seen for all emissions. These results are comparable with those seen when [EuDO3A] was in the presence of the GRS hot-water extract, but contrary to what was observed when $[EuL2]^{3+}$ and $[EuL3]^{3+}$ were applied. It is possible that the presence of nucleobases in the hot-water extract of GRS may have had a quenching influence on the overall fluorescence emissions, but these may not be present in the hot-MeOH extract, having been fully extracted from the sample by hot water. The sensitisation of $[EuL2]^{3+}$ and $[EuL3]^{3+}$ may instead be down to the presence of sensitising aromatic carboxylic acids (including their pyridine analogues) in the hot-MeOH extract. An explanation to account for the comparable responses recorded when [EuDO3A] was applied to both the hot-water and hot-MeOH extracts is that the aromatic carboxylic acids (or their pyridine analogues) were able to coordinate in preference to the interactions of fluorescence quenching analytes e.g. nucleobases.

Hot-MeOH:DCM:Toluene (hot-solvent) extract

A sensitisation was observed when the GRS hot-solvent extract was combined with [EuDO3A], with intensity increases observed through a significant broad elevation of fluorescent emissions below 630 nm. The broad emission could be the result of intrinsically fluorescent components in this extract and, therefore, the overall increase in intensity observed may not be indicative of sensitisation of the [EuDO3A] sensor itself but that this sensor may be more susceptible to the influence of intrinsically fluorescent compounds present in the extract.

No sensor response was recorded when the $[EuL3]^{3+}$ sensor solution was applied to the hot-solvent extract of GRS. This suggests three possibilities:

1. The organic material extracted in the hot-solvent does not interact with the $[EuL3]^{3+}$ sensor and thus does not invoke a response. The lack of response is not unexpected since the sensors require polar molecule analytes for interaction; the hot-solvent extract is likely to contain a higher proportion of non-polar organic molecules.
2. The amount of material extracted is not sufficient to invoke a response; the yield of the extract was extremely low (see Table 5.10) and may, therefore, contain analytes in an abundance too low for the sensors to detect.
3. The differences in structure of the L3 ligand, compared to the other ligands, leads to greater steric hindrance. Although L3 is heptadentate, with three ethanoate pendant arms, a further pendant arm, which is not involved in chelation of the europium ion, is attached to the fourth amine of the cyclen ring. It may be that it is this fourth pendant arm that hinders organic analytes from interacting, suggesting $[EuL3]^{3+}$ is not as useful a sensor for these particular extracts.

The role of carbonate ions in an extract

Carbonate ions (CO_3^{2-}) present in an extract may contribute to an increase in intensity, but it is equally possible that organic molecules that coordinate (resulting in water displacement), but do not sensitise *via* antenna effect, may be responsible (Bruce et al., 2000).

GRS has been shown to contain a high concentration of organic acids (McKay and Chong, 1983) and carbonate minerals (Milton, 1971). Organic acids (which will be liberated during extraction) will react with carbonate compounds (i.e. minerals, such as calcite), forming dissolved organic carboxylates, cationic species (derived from the carbonate mineral) and the evolution of carbon dioxide (CO_2). It is the carboxylate ion that would coordinate with the sensor when it is applied to an extract. Since the CO_3^{2-} ions are converted to CO_2, CO_3^{2-} will not remain in solution unless liberated by the extraction process. However it known that calcite has a very low solubility in water, so the presence of CO_3^{2-} in the solutions tested here is likely to be negligible.

It is also known that methanol significantly reduces the solubility of carbonates in an aqueous solution (Kan et al., 2002) and, therefore, when the sensors were applied to the hot-MeOH and hot-solvent extracts, sensitisation due to the presence of CO_3^{2-} is not expected. Therefore, any increase in intensity recorded when the sensors are applied to GRS extracts is likely to be the result of organic interactions and not the presence of CO_3^{2-}.

5.4.3 Summary of GRS testing

The sensor responses recorded when applied to the three different solvent extracts were varied, however, there were similarities in the responses for given extracts, which suggest the sensors were able to differentiate between organic components in each.

Hot-water extracts

Application of $[EuL3]^{3+}$ to the hot-water extract resulted in a 35% decrease in intensity. This response is unlikely to be the result of dilution but may be caused by preferential detection of nucleobases or organic molecules that quench the fluorescence – possibly *via* the photo-induced electron transfer (PET) mechanisms suggested in Chapter 3 (Section 3.4.3) and because of the exclusion of sensitising organic molecules by pendant arm steric hindrance.

The response recorded when $[EuL2]^{3+}$ was applied to the hot-water extract is rather more difficult to explain. All emissions decreased in intensity with the exception of the ΔJ=2 emission. It is possible that $[EuL2]^{3+}$ may detect both quenching and sensitising organic constituents in the hot-water extract, given the decrease in intensity seen when $[EuL3]^{3+}$ was applied to the same extract, and the sensitisation of [EuDO3A] and $[EuL1]^{3+}$ ΔJ=2 transitions in its presence. This implies that $[EuL2]^{3+}$ may not be suitable for the detection of one or the other classes of molecules that have this effect, but may be used to enable a broad overview of the type of compounds present in a complex mixture (e.g. nucleobases and aromatic carboxylates).

Hot-MeOH extracts

A significant sensitisation of emissions was observed, with specific sensitisation of the transition responsible for the emission at ΔJ=2, when [EuDO3A], $[EuL2]^{3+}$ and $[EuL3]^{3+}$ were applied to the

hot-MeOH extracts of GRS. The response was comparable in magnitude for $[EuL2]^{3+}$ and $[EuL3]^{3+}$, however the increase in intensity of europium emissions (and increase in intensity of ΔJ=2 emission) appeared to be more effective for [EuDO3A] when in the presence of this extract. This suggests that the hot-MeOH contains a significant concentration of aromatic carboxylic acid-like molecules capable of coordinating to the europium metal-centre and causing sensitisation of ΔJ=2 emissions *via* the antenna effect. Furthermore, these results suggest that [EuDO3A] may be a better sensor, and this may be the result of [EuDO3A]'s less hindering pendant arms.

Hot-solvent extracts

$[EuL3]^{3+}$ was unable to detect any organic component in the hot-solvent extract, evident from a lack of sensor response. It is possible that $[EuL3]^{3+}$ cannot detect the organic molecules in this extract because they are too large to interact with the metal-centre; the $[EuL3]^{3+}$ ligand pendant arms may preclude such interactions.

The response recorded when [EuDO3A] was applied to the hot-solvent extract was reminiscent of that seen when (*L*)-tyrosine was applied to the sensors (Chapters 3 and 4). This response was attributed to the 'tail end' of the broad (*L*)-tyrosine intrinsic fluorescence, overlapping and swamping the lanthanide emissions below 630 nm. It is therefore possible that [EuDO3A] is sensitive to the presence of intrinsically fluorescent molecules, more so that any of the other sensors applied to the hot-solvent extracts. Further, this implies the hot-solvent extract is enriched with intrinsically fluorescent components (e.g. polyaromatic hydrocarbons, see Section 1.6.2), more so than any other extract, and [EuDO3A] is likely to be the most efficacious at detecting their presence in a complex mixture.

Preferential sensitisation of the ΔJ=2 transition was observed when [EuDO3A] and $[EuL1]^{3+}$ were applied to hot-water extracts, and when [EuDO3A], $[EuL2]^{3+}$ and $[EuL3]^{3+}$ were applied to hot-MeOH-extracts. This is not unexpected as it has been shown that sensitisation of specific transitions occur in the presence of benzoic acid. It would be expected that carboxylic acids would be soluble in these solvents but not in the non-polar solvents of the hot-solvent mix.

However, when europium complexes of DO3A and DO3A-like ligands were applied to benzoic acid alone (Chapter 4). This could indicate that other aromatic carboxylic acids capable of coordination and antenna effect may be present in the hot-water and hot-MeOH extracts too and that different compounds may sensitise specific transition more, or less, than others. If this is the case, these sensors may be able to differentiate between classes of aromatic, antenna-effect-inducing carboxylic acids, or even individual molecules, if separated from a complex mixture extract.

It was anticipated, therefore, that the sensors, when applied to extraterrestrial extracts, would be able to detect aromatic carboxylic acids (and derivatives or structural analogues thereof) and may also detect the presence of intrinsically fluorescent constituents and nucleobases (or classes of compounds that may quench fluorescence by a similar mechanism). To investigate this further, the sensors were applied to the extracts from carbonaceous chondrites. The results of this line of enquiry are presented in the following sections.

5.5 Carbonaceous chondrites – Murchison and ALH88045

Since it was established that the extraction protocols conceived to liberate organic material from GRS were successful, the same methodology was applied to the carbonaceous chondrites (see Chapter 2 for details of the extraction protocols). The fluorimetry protocols utilised for the analysis of GRS extracts were also employed for fluorimetric analyses of the chondritic extracts (Section 2.8.4).

5.5.1 Fluorimetry of sensors applied to Murchison extracts

The extraction protocol to which Murchison was subjected successfully liberated organic material. The mass of each Murchison extract is presented in Table 5.11 to show the disparity between each fraction and, moreover, the abundance of organic material obtainable from each geological sample. The extracts were dissolved in 200 µl of 18.2 MΩ water and the sensors applied for fluorimetric analyses (see Section 2.8.4 for the procedure).

Sensors applied to the Murchison extracts	Hot-water extract mass obtained (mg)	Hot-MeOH extract mass obtained (mg)	Hot-solvent extract mass obtained (mg)
[EuDO3A]	6.83	0.24	-
$[EuL3]^{3+}$	6.52	0.35	0.02

Table 5.11 Mass of Murchison extract obtained by each solvent extraction (in milligrams) and the sensors that were applied for fluorimetric analysis

Sensor responses to Murchison hot-water extracts

When the hot-water extract of Murchison was added to [EuDO3A], a clear increase in intensity was recorded, with the relative peak intensities remaining approximately the same as the sensor-only spectrum, i.e. the intensities of the transitions were in the order $\Delta J=2>\Delta J=1>\Delta J=4>\Delta J=0>\Delta J=3$ (Figure 5.40). The spectra obtained were similar to those recorded when [EuDO3A] was applied to the hot-water extract of GRS, with the exception of a broad overlap of fluorescence attributable to the presence of organic analytes in the Murchison hot-water extract, with intrinsic fluorescence evident below 630 nm (Figure 5.40).

The application of $[EuL3]^{3+}$ to the hot-water extract yielded an, approximately, 35% decrease in intensity, equivalent to the results from the GRS hot-water extract (Figure 5.41).

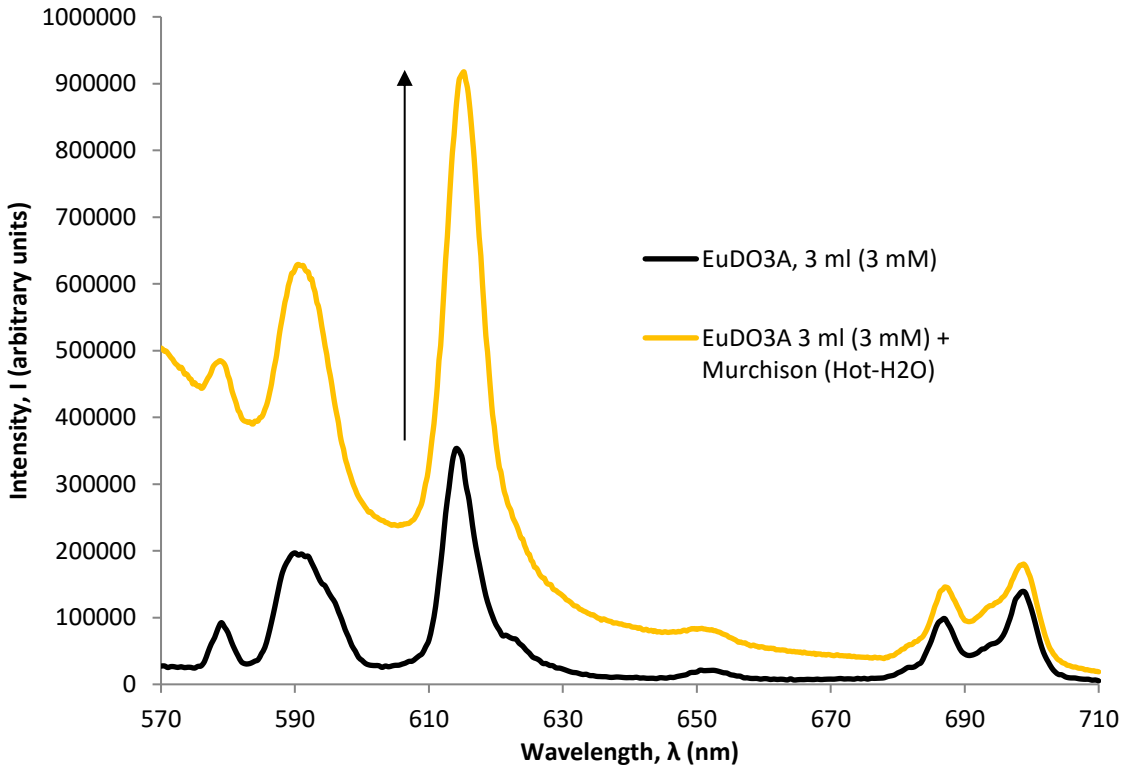

Figure 5.40 Sensor-only [EuDO3A] (3 ml, 3mM) fluorescence spectrum (black) compared with the [EuDO3A] (3 ml, 3mM) fluorescence spectrum in the presence of the Murchison hot-water extract (yellow) (λ_{Ex}=280 nm, acquisition time=0.5 sec, acquisition increment=0.5 nm, excitation and emission slit width=3 nm, pH=5)

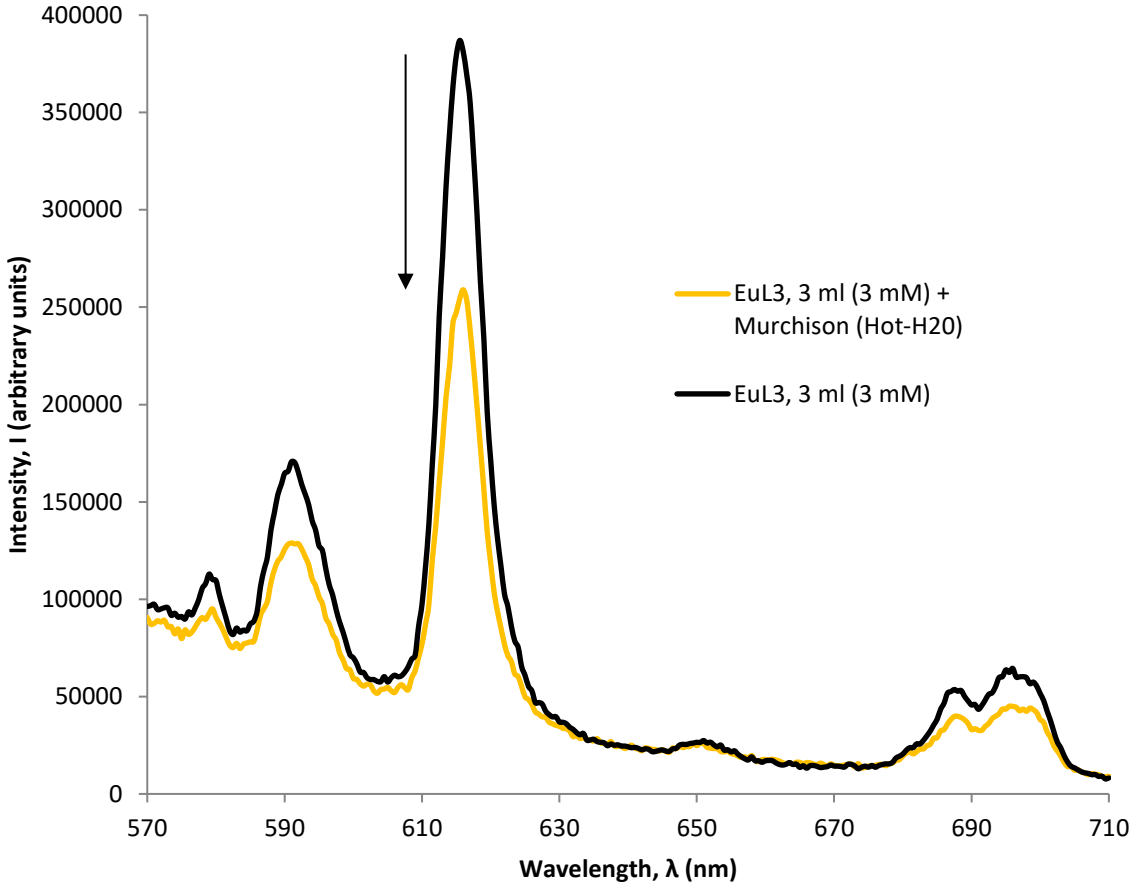

Figure 5.41 Sensor-only $[EuL3]^{3+}$ (3 ml, 3mM) fluorescence spectrum (black) compared with the $[EuL3]^{3+}$ (3 ml, 3mM) fluorescence spectrum in the presence of the Murchison hot-water extract (yellow) (λ_{Ex}=280 nm, acquisition time=0.5 sec, acquisition increment=0.5 nm, excitation and emission slit width=3 nm, pH=5)

Sensor responses to GRS hot-MeOH extracts

When [EuDO3A] was applied to the hot-MeOH Murchison extract europium fluorescence emissions were severely swamped (Figure 5.42), though it is possible some sensitisation of ΔJ=1 and ΔJ=2 may have occurred, but the resolution of these emissions are so poor that this cannot be concluded with certainty. This also suggests the presence of a significant amount of intrinsically fluorescent material within this extract. There was no change in the sensor-only europium fluorescence emission intensity when the hot-MeOH Murchison extract was combined with $[EuL3]^{3+}$ (Figure 5.43), contrary to the results recorded from the GRS hot-MeOH extract, which caused a significant sensitisation, particularly at the ΔJ=2 transition (Figure 5.36).

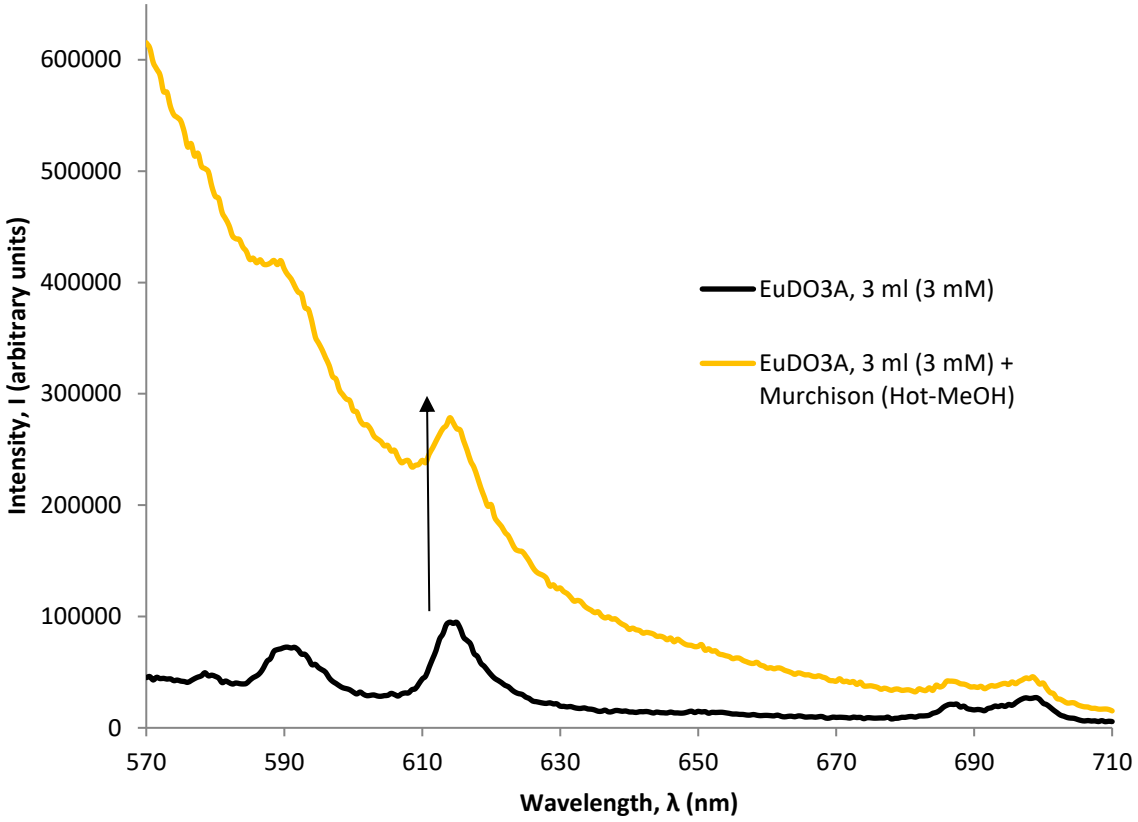

Figure 5.42 Sensor-only [EuDO3A] (3 ml, 3mM) fluorescence spectrum (black) compared with the [EuDO3A] (3 ml, 3mM) fluorescence spectrum in the presence of the Murchison hot-MeOH extract (yellow) (λ_{Ex}=280 nm, acquisition time=0.5 sec, acquisition increment=0.5 nm, excitation and emission slit width=3 nm, pH=5)

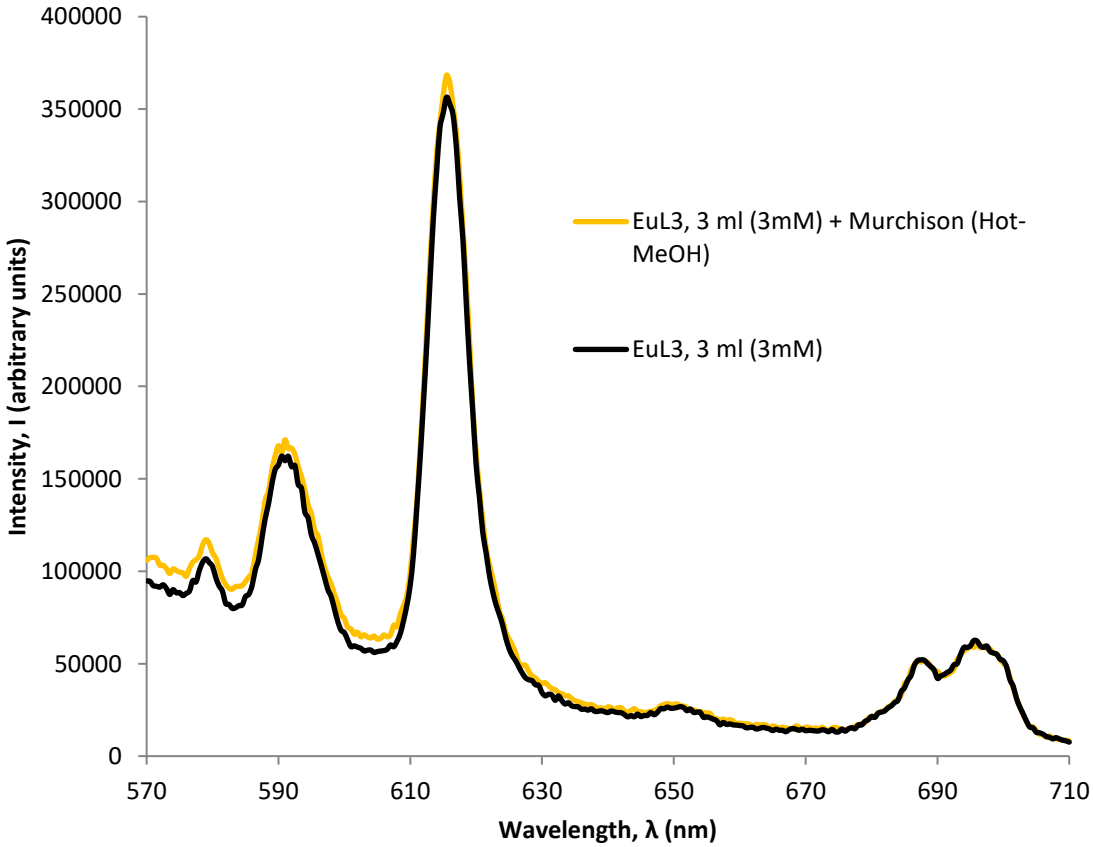

Figure 5.43 Sensor-only $[EuL3]^{3+}$ (3 ml, 3mM) fluorescence spectrum (black) compared with the $[EuL3]^{3+}$ (3 ml, 3mM) fluorescence spectrum in the presence of the Murchison hot-MeOH extract (yellow) (λ_{Ex}=280 nm, acquisition time=0.5 sec, acquisition increment=0.5 nm, excitation and emission slit width=3 nm, pH=5)

Sensor responses to GRS hot-solvent extracts

There was no change in the sensor-only europium fluorescence emission intensity when the hot-solvent Murchison extract was combined with the $[EuL3]^{3+}$ sensor solution (Figure 5.44), comparable to that observed when $[EuL3]^{3+}$ was applied to the GRS hot-solvent extract (Figure 5.38).

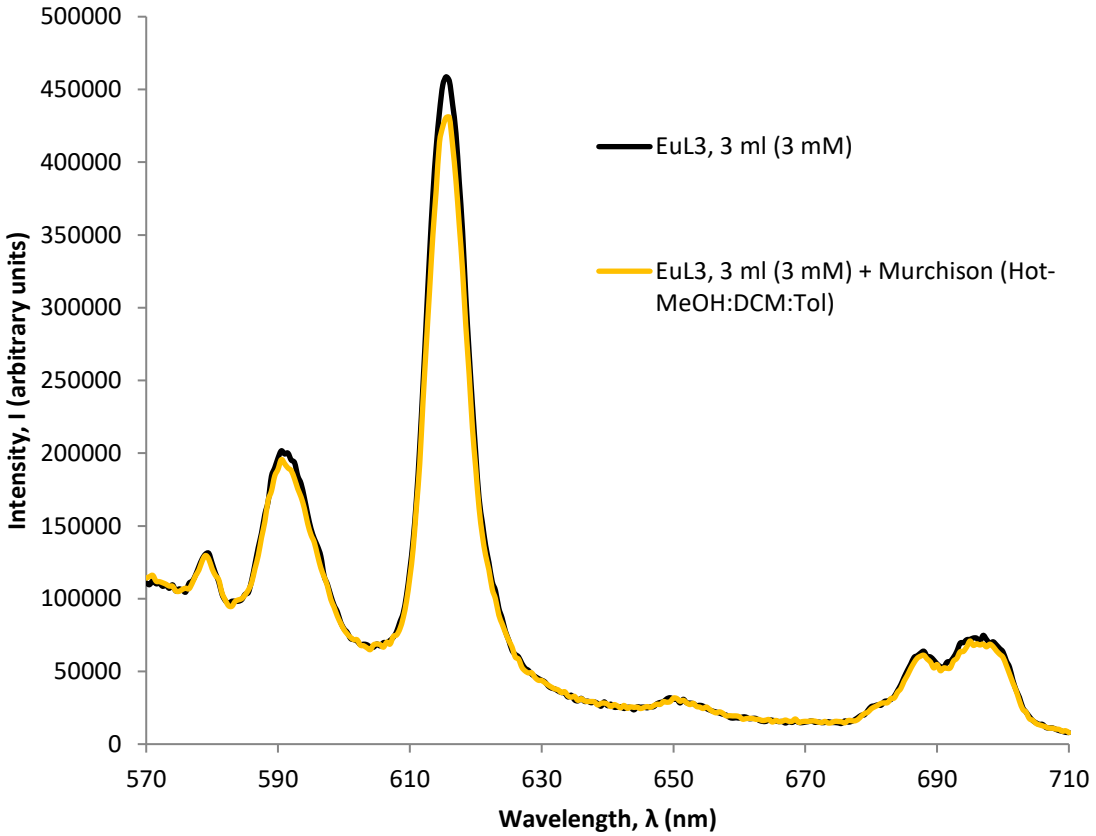

Figure 5.44 Sensor-only $[EuL3]^{3+}$ (3 ml, 3mM) fluorescence spectrum (black) compared with the $[EuL3]^{3+}$ (3 ml, 3mM) fluorescence spectrum in the presence of the Murchison hot-solvent extract (yellow) (λ_{Ex}=280 nm, acquisition time=0.5 sec, acquisition increment=0.5 nm, excitation and emission slit width=3 nm, pH=5)

5.5.2 Discussion of fluorimetry results from sensor application to Murchison

The hot-water extraction of Murchison liberated approximately three times more organic material (Table 5.10) than that liberated from the GRS sample (Table 5.3). However, the hot-MeOH extraction of Murchison liberated between seven and eleven times less than that obtained from GRS. This suggests the Murchison sample contains a higher concentration of highly-polar, water-soluble, organic material and lower concentrations of less-polar, less-water soluble organic material than the GRS sample. The MeOH-soluble component of the extract liberated by the hot-solvent extraction was approximately the same amount for both samples.

Hot-water extracts

The fluorescence responses of [EuDO3A] and $[EuL3]^{3+}$ in the presence of the hot-water extract (Figures 5.40 and 5.41, respectively) were comparable to those observed when these complexes were applied to the hot-water extract of GRS (Figures 5.30 and 5.33, respectively). This suggests that the Murchison hot-water extract may contain the same, or similar, organic components to those in the GRS hot-water extracts. The exception to this was the overlap of broad fluorescence below 630 nm, attributable to the presence of intrinsically fluorescent species (a result also recorded when $[EuL1]^{3+}$ was applied to the hot-water extract of GRS). This implies that the hot-water extract may not contain aromatic carboxylic acid-like molecules or that the presence of intrinsically fluorescent molecules at higher proportions to those in the GRS hot-water extract overlaps the ΔJ=1 transition, making the sensitisation of the ΔJ=2 transition appear less sensitised than it actually is. [EuDO3A] therefore, may not be suitable for the detection of carboxylic acid, antenna-effect-inducing aromatic molecules when they are also in the presence of intrinsically fluorescent molecules as part of a complex extract mixture.

For $[EuL3]^{3+}$, there was an approximate 35% reduction in intensity that may suggest a response to nucleobases or a dilution effect. The results were comparable with those seen with the GRS hot-water extract. It is likely, therefore that the same analytes responsible for this equivalent response is present in both extracts. As previously suggested the response is unlikely to be the result of dilution but could be caused by preferential detection of nucleobases. It was proposed, *vida supra*, the mechanism by which this may occur is PET in conjunction with exclusion of sensitising organic molecules by L3 pendant arm steric hindrance. However, as discussed in Section 5.4.2, since the hot-water extract sensitised emissions when combined with [EuDO3A], it is more likely that $[EuL3]^{3+}$ may not respond as effectively to the molecules in the hot water extract, or that it is caused by quenching, which would be confirmed by measuring the fluorescence lifetime.

Hot-MeOH extracts

Application of [EuDO3A] to the Murchison hot-MeOH extract resulted in swamping of all europium emissions (Figure 5.42), reminiscent of the response seen when (*L*)-tyrosine was applied to the sensors (Chapters 3 and 4) and when [EuDO3A] was applied to the hot-solvent GRS extract. However, the overlap and swamping of europium emissions below 630 nm was extensive with the Murchison extract, such that only the Δ*J*=2 emission was sufficiently resolved. Despite this, indicative europium emissions were observed, suggesting at least some sensitisation of transitions had taken place. This suggests that, like the hot-water extract, the hot-MeOH extract of Murchison may contain a significant amount of intrinsically fluorescent material (e.g. polyaromatic hydrocarbons, see Section 1.6.2), in much greater abundance than in the hot-solvent soluble fraction of GRS and to which [EuDO3A] may be sensitive.

Application of $[EuL3]^{3+}$ to the hot-water Murchison extract resulted in a 35% decrease in intensity and is comparable to the results obtained when $[EuL3]^{3+}$ was applied to the hot-water GRS extract. This is in contrast to the increase in intensity and sensitisation of the Δ*J*=2 transition recorded when [EuDO3A], $[EuL2]^{3+}$ and $[EuL3]^{3+}$ were applied to the GRS hot-MeOH extract. It is possible that the Murchison hot-MeOH extract does not contain the same classes of molecules that were present in the hot-MeOH extract of GRS and therefore the same response may not be recorded. It is also possible that the organic molecules in the Murchison hot-MeOH extract are not in comparable concentrations to invoke a comparable response.

Hot-solvent extract

In agreement with the GRS results (Figure 5.38), no sensor response was recorded when $[EuL3]^{3+}$ was applied to the hot-solvent extract of Murchison (Figure 5.44). Therefore, the same interpretations may be given: i) the organic material extracted in the hot-solvent does not invoke a response in the $[EuL3]^{3+}$ sensor; ii) greater steric hindrance by the pendant arms preclude analyte interaction (Section 5.4.2), or iii) the amount of material extracted is not sufficient to detect an interaction (see Table 5.11). Should interpretations i) or ii) be correct, the lack of sensor response lends credence to the suggestion that $[EuL3]^{3+}$ is not as useful a sensor for extracts that

contain a higher proportion of non-polar organic molecules which may not interact with the sensor. To test interpretation iii), a more concentrated extract solution could be used, but this would require the extraction of a larger sample of Murchison than was possible in this study.

As was the case for the application of sensors to GRS extracts, europium sensitisation in the presence of a Murchison extract may not be caused only by interaction with organic species and the antenna effect (afforded by the presence of aromatic or polyaromatic acids, their derivatives, or analogue pyridine carboxylic acids) but also by the presence of CO_3^{2-} ions. CO_3^{2-} ions may displace water molecules reducing quenching by water OH oscillations, while coordination of aromatic acids causes sensitisation of transitions (Section 5.4.2).

The role of carbonates in Murchison

Murchison is known to contain carbonate minerals (Fuchs et al., 1973) which can include dolomite ($CaMgCO_3$), calcite and aragonite ($CaCO_3$) (Barber, 1981). Calcite is dispersed throughout the matrix of CM chondrites, is readily discernible (Kerridge and Bunch, 1979) and analyses suggest a carbonate abundance in the range of 80 mg g^{-1} to 1368 mg g^{-1} (Grady et al., 1988). Analysis of the carbonate content of the Tagish Lake meteorite (CI-ungrouped) by Brown et al. (2000) revealed 3.7 wt.% carbon as carbonate, mostly as magnesite ($MgCO_3$) and siderite ($FeCO_3$), however the carbonate abundance of Tagish Lake is anomalous when compared to that of other CM and CI carbonaceous chondrites, which are typically in the 0.2 to 0.5 wt.% range (Brown et al., 2000).

The prevalence of carbonate minerals of varying compositions is a consideration in light of the role of CO_3^{2-} in displacing fluorescence quenching water molecules from the lanthanide coordination sphere. However, if CO_3^{2-} is liberated from geological samples during the extraction of organic material, the concentration in the extract is likely to be negligible, both because of the relatively low natural abundance in the sample and also because the dissolution of CO_3^{2-}, given the timescale and condition in which the extraction takes place, is unlikely. Furthermore, the limit of detection of CO_3^{2-} for [EuDO3A] has been determined to be 0.4 mM (Vaněk et al., 2013) and other studies have recorded sensor responses when CO_3^{2-} species are present at concentrations of

30 mM (Bruce et al., 2000). Therefore, it is unlikely that CO_3^{2-}, even in samples with a few wt% CO_3^{2-}, will interfere with sensor responses to organic analytes.

5.5.3 Summary of Murchison testing

The responses observed with the Murchison extracts suggest that [EuDO3A] may be able to detect analytes that invoke an increase in fluorescence. However, the lack of preferential sensitisation of transitions and the elevated broad fluorescence below 630 nm suggests water molecule displacement and intrinsic fluorescence may be responsible for the responses seen. The suggestion that [EuDO3A] is more sensitive to the presence of intrinsically fluorescent material is corroborated by its response to the Murchison hot-MeOH extract, since the broad fluorescence recorded is not observed when the same extract is applied to $[EuL3]^{3+}$.

Although the sensor responses to the solvent extracts obtained from Murchison are varied, it was anticipated that the sensors, when applied to these extracts, would be able to detect aromatic carboxylic acids (and derivatives or structural analogues thereof) and may also detect the presence of intrinsically fluorescent constituents and nucleobases (or classes of compounds that may quench fluorescence by a similar mechanism). It may be concluded that [EuDO3A] may have detected the presence of intrinsically fluorescent molecules and that $[EuL3]^{3+}$ may have detected the presence of nucleobases or similar PET mechanism quenching analytes.

In order to corroborate these results and to investigate this further, the sensors were applied to the extracts from another carbonaceous chondrite, ALH88045, to determine if these extracts may contain similar compounds or if the responses would confirm the applicability of the sensors for extraterrestrial samples. The continuing line of enquiry is presented in the following sections.

5.5.4 Fluorimetry of sensor application to ALH88045 extracts

The extraction protocol to which ALH88045 was subjected successfully liberated organic material. The mass of each ALH88045 extract applied to the sensors is presented in Table 5.12 to show the disparity between each fraction and, moreover, the abundance of organic material obtainable

from each geological sample. The extracts were dissolved in 200 µl of 18.2Ω water and the sensors were then applied to the extracts for fluorimetric analyses (see Section 2.8.4 for the procedure); the results are presented herein.

Sensors applied to the ALH88045 extracts	Hot-water extract mass obtained (mg)	Hot-MeOH extract mass obtained (mg)	Hot-solvent extract mass obtained (mg)
[EuDO3A]	1.17	0.18	0.04
$[EuL3]^{3+}$	1.24	0.23	0.05

Table 5.12 Mass of ALH88045 extract obtained by each solvent extraction (in milligrams) and the sensors that were applied for fluorimetric analysis

Sensor responses to ALH88045 hot-water extracts

Application of [EuDO3A] to the hot-water extract of ALH88045 saw a significant increase in intensity when compared to the [EuDO3A]-only fluorescence intensity, as had been the case for [EuDO3A] with both the GRS and Murchison hot water sensors; however the increase was much larger in magnitude for ALH88045. Moreover, preferential increase in intensity of the Δ*J*=1 transition was recorded, which became almost as intense as the Δ*J*=2 transition (Figure 5.45), and this was not observed with GRS or Murchison. This change in ratio of the emission intensities is indicative of species binding to the lanthanide complex.

The application of $[EuL3]^{3+}$ to the hot-water extract of ALH88045 yielded the same response as was recorded for the hot-water extracts of GRS and Murchison (Figures 5.33 and 5.41), an approximate 35% decrease in intensity (Figure 5.46).

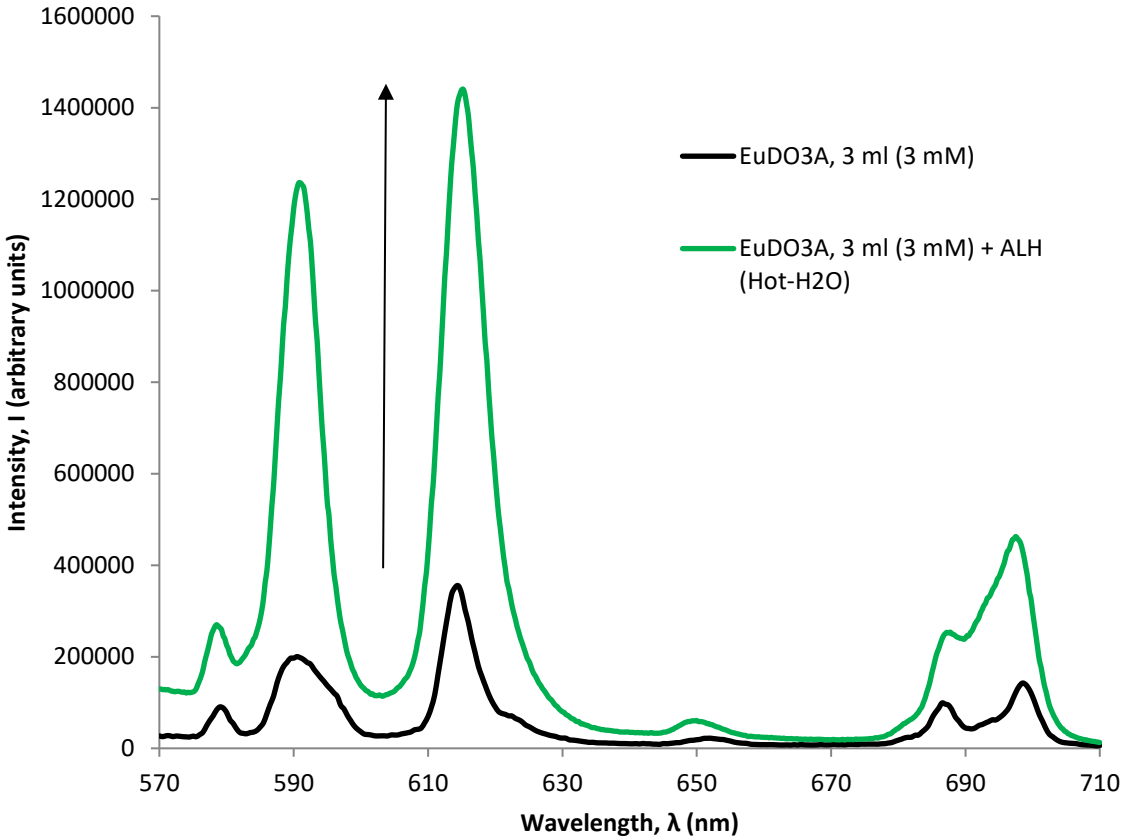

Figure 5.45 Sensor-only [EuDO3A] (3 ml, 3mM) fluorescence spectrum (black) compared with the [EuDO3A] (3 ml, 3mM) fluorescence spectrum in the presence of the ALH88045 hot-water extract (green) (λ_{Ex}=280 nm, acquisition time=0.5 sec, acquisition increment=0.5 nm, excitation and emission slit width=3 nm, pH=5)

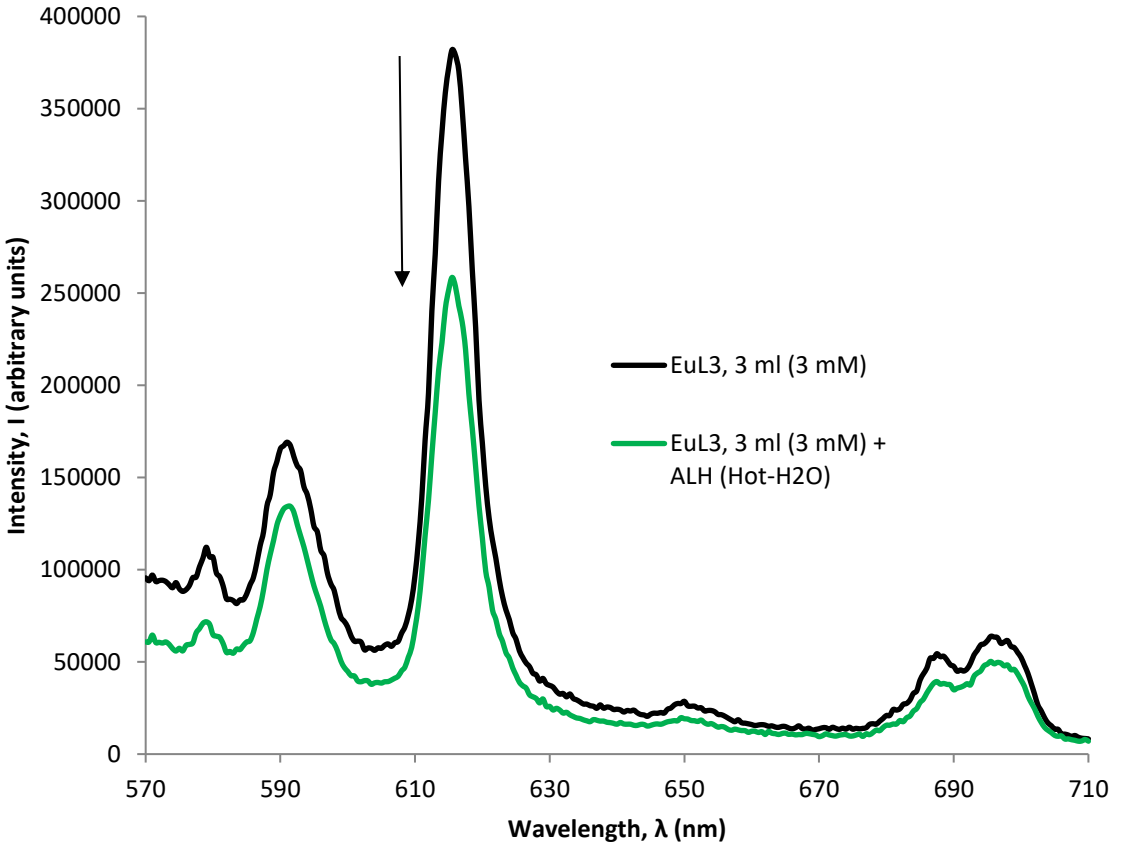

Figure 5.46 Sensor-only $[EuL3]^{3+}$ (3 ml, 3mM) fluorescence spectrum (black) compared with the $[EuL3]^{3+}$ (3 ml, 3mM) fluorescence spectrum in the presence of the ALH88045 hot-water extract (green) (λ_{Ex}=280 nm, acquisition time=0.5 sec, acquisition increment=0.5 nm, excitation and emission slit width=3 nm, pH=5)

Sensor responses to ALH88045 hot-MeOH extracts

The presence of the hot-MeOH extract of ALH88045 caused an increase in [EuDO3A]-only fluorescence emissions, exhibiting significant fluorescence swamping of europium emissions below 630 nm (Figures 5.47), so much so that the ΔJ=0 was not resolved, and the influence of the broad emission made the transition at and ΔJ=3 poorly resolved. However, the increase in intensity of the europium emissions at the ΔJ=1, ΔJ=2 and ΔJ=4 transitions suggest that the transitions responsible may have experienced some sensitisation (Figures 5.47), with no single transition appearing to have been to a greater extent than another. It is also likely that this extract contains intrinsically fluorescent organic material; a fluorescence spectrum of this extract would confirm this. This response is comparable to those recorded when [EuDO3A] was applied to the hot-solvent extract of GRS and the hot-MeOH extract of Murchison (Figures 5.37 and 5.42).

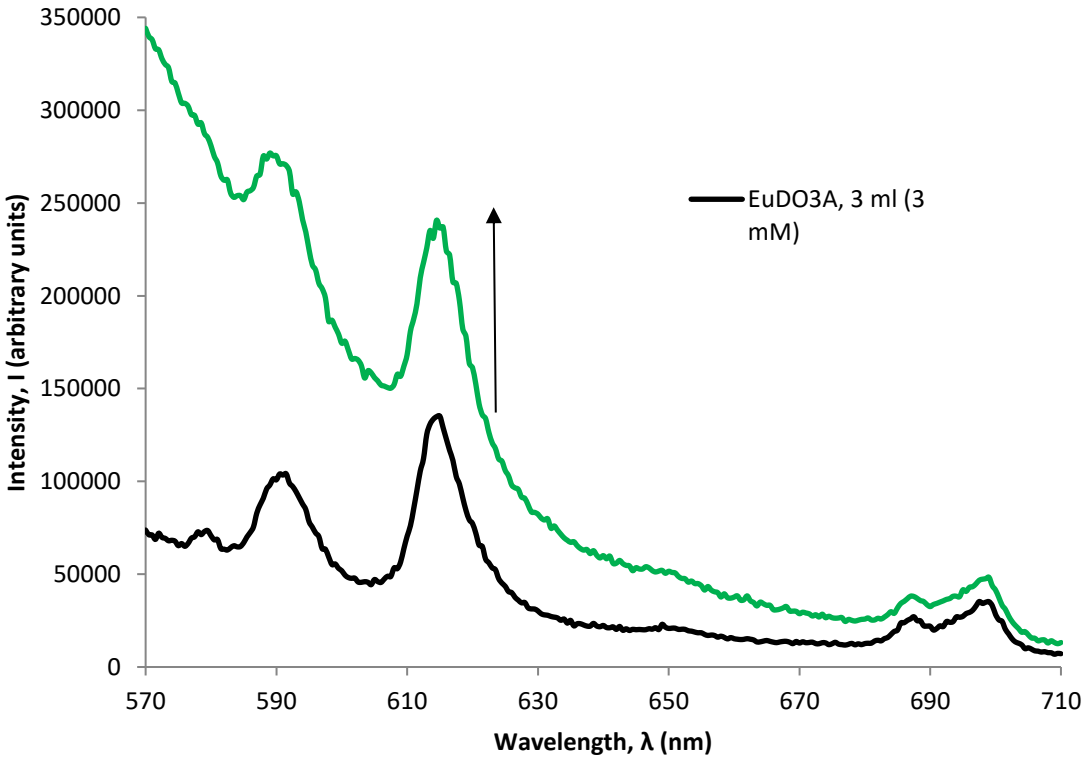

Figure 5.47 Sensor-only [EuDO3A] (3 ml, 3mM) fluorescence spectrum (black) compared with the [EuDO3A] (3 ml, 3mM) fluorescence spectrum in the presence of the ALH88045 hot-MeOH extract (green) (λ_{Ex}=280 nm, acquisition time=0.5 sec, acquisition increment=0.5 nm, excitation and emission slit width=3 nm, pH=5)

There was no change in the sensor-only europium fluorescence emission intensity when the hot-MeOH ALH88045 extract was combined with $[EuL3]^{3+}$ (Figure 5.48), consistent with the results for the hot-MeOH extract of Murchison (Figure 5.43), but contrary to those for the hot-MeOH extract of GRS, where a significant sensitisation was observed (Figure 5.36).

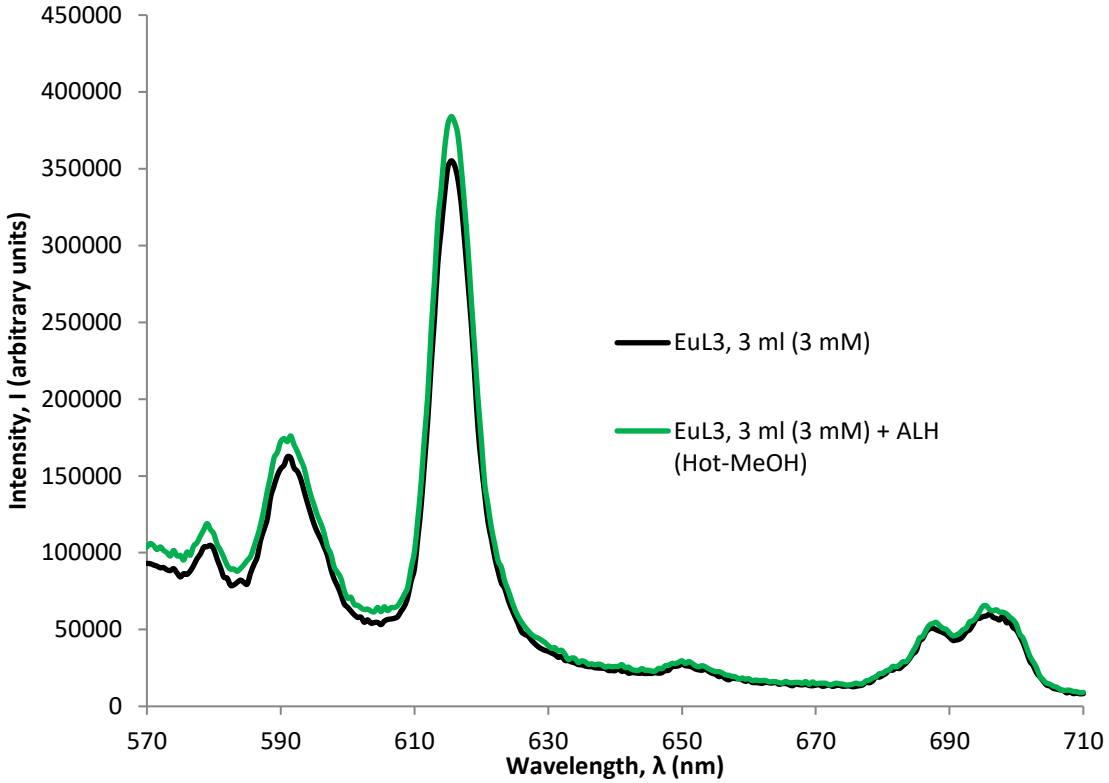

Figure 5.48 Sensor-only $[EuL3]^{3+}$ (3 ml, 3mM) fluorescence spectrum (black) compared with the $[EuL3]^{3+}$ (3 ml, 3mM) fluorescence spectrum in the presence of the ALH88045 hot-MeOH extract (green) (λ_{Ex}=280 nm, acquisition time=0.5 sec, acquisition increment=0.5 nm, excitation and emission slit width=3 nm, pH=5)

Sensor responses to ALH88045 hot-solvent extracts

The presence of the hot-solvent extract of ALH88045 caused an increase in [EuDO3A]-only fluorescence emissions, exhibiting significant fluorescence swamping of europium emissions below 630 nm (Figures 5.49). However, the increase in intensity of the europium emissions suggests that the transitions responsible may have undergone some sensitisation (Figures 5.49) or that there is intrinsically fluorescent organic material present in the extract. A fluorescence spectrum of this extract would confirm this. These responses are comparable to those recorded when [EuDO3A] was applied to the hot-MeOH extracts of GRS and Murchison (Figures 5.34 and 5.42).

There was no change in the sensor-only europium fluorescence emission intensity when the hot-solvent ALH88045 extract was combined with the $[EuL3]^{3+}$ sensor solution (Figure 5.50), comparable with the results seen when $[EuL3]^{3+}$ was applied to the hot-MeOH extract of Murchison (Figure 5.43), and both GRS and Murchison hot-solvent extracts (Figures 5.38 and 5.44).

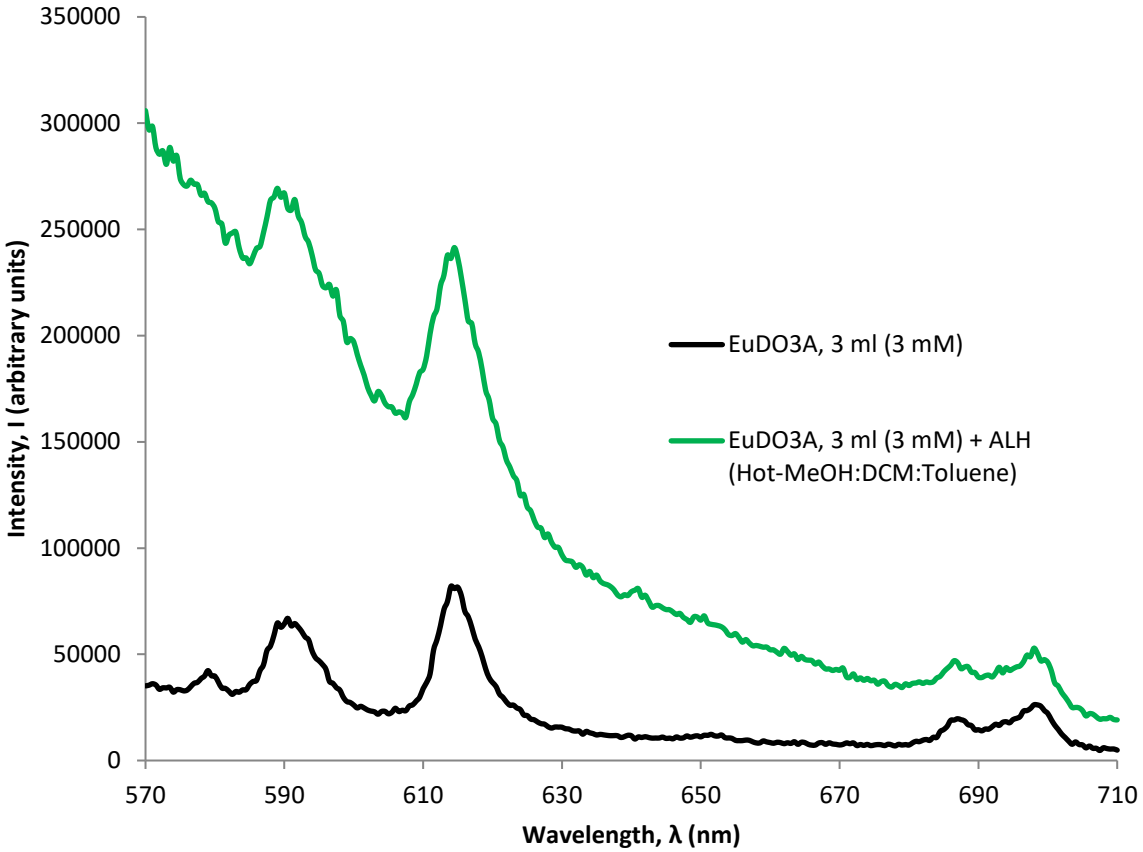

Figure 5.49 Sensor-only [EuDO3A] (3 ml, 3mM) fluorescence spectrum (black) compared with the [EuDO3A] (3 ml, 3mM) fluorescence spectrum in the presence of the ALH88045 hot-solvent extract (green) (λ_{Ex}=280 nm, acquisition time=0.5 sec, acquisition increment=0.5 nm, excitation and emission slit width=3 nm, pH=5)

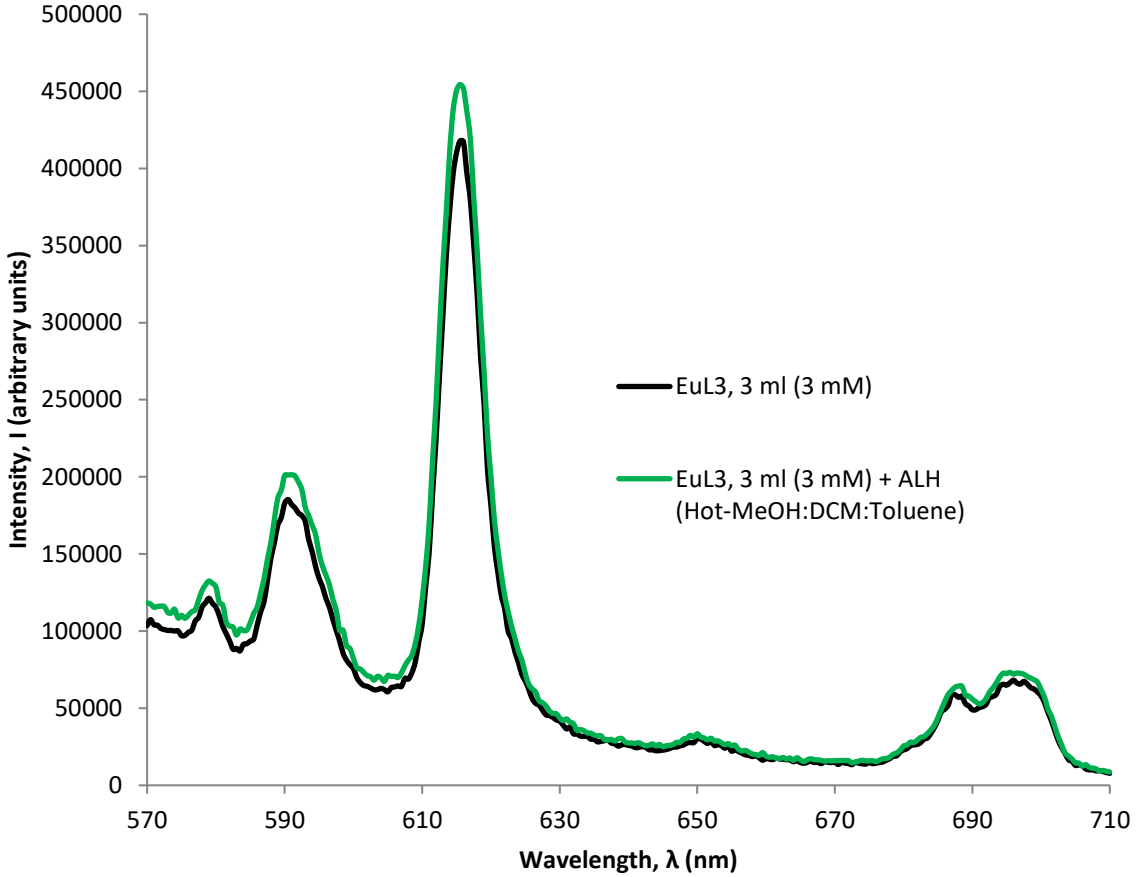

Figure 5.50 Sensor-only $[EuL3]^{3+}$ (3 ml, 3mM) fluorescence spectrum (black) compared with the $[EuL3]^{3+}$ (3 ml, 3mM) fluorescence spectrum in the presence of the ALH88045 hot-solvent extract (green) (λ_{Ex}=280 nm, acquisition time=0.5 sec, acquisition increment=0.5 nm, excitation and emission slit width=3 nm, pH=5)

5.5.5 Discussion of fluorimetry results from sensor application to ALH88045

The hot-water extraction of ALH88045 (Table 5.12) liberated approximately five times less organic material than Murchison (Table 5.11) and approximately half that obtained from the GRS sample (Table 5.10). However, the hot-MeOH extraction of ALH88045 liberated approximately the same yield as that from Murchison, but between ten and sixteen times less than that obtained from GRS. The component liberated by the hot-solvent extraction was approximately the same amount for all three samples. This suggests that ALH88045 contains a lower concentration of highly-polar, water- and MeOH-soluble, organic material and a similar quantity of non-polar organic material as Murchison and GRS; the fraction of organic material present in ALH88045 susceptible to polar solvent extraction is less than that in Murchison.

Hot-water extracts

The most significant sensor response observed with ALH88045 was when [EuDO3A] was applied to the hot-water extract; there was a significant sensitisation of emissions and an alteration to the relative intensities of the ΔJ=1 and ΔJ=2 transitions. The sensor-only fluorescence saw an unambiguous preferential sensitisation of the ΔJ=1 transition, such that the emissions of both transitions were of comparable intensity. This response can only be the result of an energy transfer to the lanthanide ion *via* antenna effect by organic analyte/metal-centre interaction, and cannot be the influence of any dissolved mineral species or mineral particulates, since this was ruled out as improbable (see Section 5.3.3). In addition, the absence of fluorescence swamping of europium emissions below 630 nm means it can be justifiably concluded that the hot-water extract of ALH88045 does not contain intrinsically fluorescent material (organic or mineral) or, if such components were present, they do not affect fluorescence emissions of [EuDO3A].

These results suggest that the ALH88045 hot-water extract may contain species that [EuDO3A] can detect by virtue of sensitisation of all transitions and preferential sensitisation of ΔJ=1. Since this transition-specific intensity was not seen with the GRS and Murchison hot water extracts (where increases in intensity for all emissions were recorded), it implies that ALH88045 may

contain more aromatic carboxylic acids and fewer water-soluble, water molecule-displacing, species (organic species capable of non-antenna effect interactions).

Comparable with the results seen for GRS and Murchison, the intensity of fluorescent emissions of $[EuL3]^{3+}$ are decreased by approximately 35% in the presence of the ALH88045 hot-water extract, suggesting $[EuL3]^{3+}$ is sensing the same components in these extracts. Those components may be nucleobases or other organic components that quench fluorescence, perhaps by a similar PET mechanism as alluded to previously for GRS and Murchison. This is a phenomenon unique to $[EuL3]^{3+}$; $[EuL3]^{3+}$ is the only sensor able to detect species that can quench fluorescence by PET mechanisms.

Hot-MeOH extract

Application of [EuDO3A] to the hot-MeOH extract of ALH88045 resulted in a swamping effect comparable to that observed when sensors were applied to (*L*)-tyrosine (Chapters 3 and 4) and attributed to the overlapping of the tail end of its broad intrinsic fluorescence. This effect was also observed when [EuDO3A] was applied to the hot-solvent extract of GRS and the hot-MeOH extract of Murchison. This result lends credence to the summation that [EuDO3A] may be susceptible to the presence of intrinsically fluorescent analytes (that would be present in the ALH88045 and Murchison hot Me-OH extracts, but not that of GRS), since this extract did not have the same influence on the fluorescence emissions of $[EuL3]^{3+}$; it did not affect the sensor-only europium emissions of $[EuL3]^{3+}$ at all. This suggests that [EuDO3A] may be utilised as a sensor for molecules with intrinsic fluorescence contained within a complex extract (e.g. (*L*)-tyrosine or polyaromatic hydrocarbons), and that $[EuL3]^{3+}$ may not.

Hot-solvent extract

The application of [EuDO3A] and $[EuL3]^{3+}$ to the hot-solvent extracts produced spectra that were comparable to the results recorded for the application of these sensors to the hot-MeOH ALH88045 extracts. Both extracts are therefore likely to contain the same (or similar) intrinsically fluorescent material to which the [EuDO3A] (but not $[EuL3]^{3+}$) sensor is sensitive. Furthermore,

just as with the hot-MeOH extracts, there was no evidence to suggest that the hot-solvent extract contained species capable of sensitising transitions.

The role of Antarctic weathering on ALH88045 minerals and organic matter

ALH88045, as explained in Section 2.2.1, is an Antarctic meteorite, which was found in 1988 (Wlotzka et al., 1989); its terrestrial age is not known. Grady et al. (1988) reported evaporite minerals such as calcium and magnesium sufates ($CaMgSO_4$), CO_3^{2-}, and bicarbonates (hydrogen carbonates, HCO_3^-) as examples of Antarctic weathering and alteration products. Comparisons between volatile element abundances of Antarctic and non-Antarctic meteorites suggests leaching of these species may occur when resident in the harsh environment of Antarctica (Dennison et al., 1986), and this process may also modify or liberate organic material. It has been suggested that Antarctic weathering of organic matter in carbonaceous chondrites follows a similar reaction pathway to that hypothesised for aqueous alteration on the meteorite parent body (Sephton et al., 2004). On exposure to the effects of liquid water (Koeberl and Cassidy, 1991) hydroxyl groups are increased and leached, alkyl side chains oxidised, and peripheral molecules on the IOM (including aromatic units) may become susceptible to liberation.

The organic matter in carbonaceous chondrites is therefore one of the most susceptible components of these Antarctic carbonaceous chondrites to terrestrial weathering (Sephton et al., 2004). It is possible, therefore, that during ALH88045's residency on Earth, the organic material may have undergone processes which may have increased the concentration of organic analytes, e.g. aromatic carboxylic acids and derivatives thereof, that may be extractable by hot water and detectable by the sensors. If this is the case, the Murchison sample (a pristine fall displaying minimal terrestrial contamination or weathering) may contain fewer indigenous aromatic carboxylates in its free fraction than ALH88045. This may explain the marked difference in the affect the hot-water extract of Murchison and the hot-water extract of ALH80045 had on the europium emissions of [EuDO3A] and $[EuL3]^{3+}$, respectively.

5.5.6 Summary of ALH88045 testing

The responses observed with the ALH88045 hot-water extract suggest that [EuDO3A], but not $[EuL3]^{3+}$, may be able to detect analytes that invoke an increase in fluorescence. The sensitisation of ΔJ=1, ΔJ=2 and ΔJ=4 transitions, and preferential spectral change of ΔJ=1 in particular, is compelling evidence of this. However, the lack of preferential sensitisation of transitions and the elevated broad fluorescence below 630 nm (when [EuDO3A] was applied to the hot-MeOH and hot-solvent extracts) suggests that water molecule displacement and intrinsic fluorescence may be responsible for these responses.

The suggestion that [EuDO3A] is more sensitive than $[EuL3]^{3+}$ to the presence of intrinsically fluorescent material is strengthened by its response to the hot-MeOH and hot-solvent extracts of ALH88045 (and was corroborated by its response to the Murchison hot-MeOH extract). This assertion is given further credence since the broad fluorescence recorded when [EuDO3A] was applied to the ALH88045 and Murchison hot-MeOH extracts was not observed when $[EuL3]^{3+}$ was applied.

The sensor responses to the solvent extracts obtained from ALH88045 were as varied as those recorded for the application of sensors to the Murchison extracts. It was anticipated that the sensors ([EuDO3A] in particular), when applied to ALH88045 extracts, would be able to detect aromatic carboxylic acids (and derivatives or structural analogues thereof) and would also detect the presence of intrinsically fluorescent constituents and nucleobases (or classes of compounds that may quench fluorescence by a similar mechanism). It may be concluded that [EuDO3A] has unequivocally detected the presence of molecules capable of coordinating and sensitising transitions *via* an antenna effect in the ALH88045 hot-water extract, and detected the presence of intrinsically fluorescent molecules in the hot-MeOH and hot-solvent extracts. Moreover, $[EuL3]^{3+}$ may have detected the presence of nucleobases or similar PET mechanism quenching analytes in the ALH88045 hot-water extract, but was unable to detect the presence of any analytes in the hot-MeOH or hot-solvent extracts, where such molecules were not expected.

5.5.7 Discussion of the application of sensors to geological samples

Although sensor responses to mineral solutions varied without a clear trend, many had the effect of decreasing the intensity detected incrementally, suggestive of an effect of dilution (LnDOTA, LnDO3A and LnL3). LnL2 increased the intensity incrementally with successive additions of some mineral solutions, and all minerals exhibited this effect when combined with TbL2. However, those responses cannot be confidently attributed to the presence of the mineral solutions or to effects of dilution; the results may also be attributed to small losses of solution from the cuvette during additions of aliquots, inconsistent aliquot volumes (both issues may exacerbated by low sample volumes) or by fluctuations in excitation light source i.e. instrument inconsistency, alone. However, in all cases, when 100 µl or 200 µl of mineral solution was combined with 1.5 ml or 3 ml, respectively, any observed deviation from the sensor-only sensor emission may also not be confidently ascribed to a sensor response to the presence of any dissolved weathered mineral sample used in this study. A summary of sensor responses to the extracts tested is provided below (Table 5.13 to 5.15).

Hot-Water Extracts	[EuDO3A]	EuL1	EuL2	EuL3
GRS	Sensitisation of all transitions, relative intensities remain constant – elevated emission intensity below 610 nm	Sensitisation of all transitions except ΔJ=0, relative intensities remain constant – no elevated emission intensity below 610 nm	Desensitisation of all transitions except ΔJ=2, which did not respond – no elevated emission intensity below 610 nm	~35% reduction in intensity of all transitions except ΔJ=3, which did not respond. relative intensities remain constant – no elevated emission intensity below 610 nm
Murchison	Sensitisation of all transitions, relative intensities remain constant – elevated emission intensity below 610 nm	Not tested	Not tested	~35% reduction in intensity of all transitions except ΔJ=3, which did not respond. Relative intensities remain constant – no elevated emission intensity below 610 nm
ALH88045	Sensitisation of all transitions, particularly the ΔJ=1 transition, almost as intense as ΔJ=2 transition	Not tested	Not tested	~35% reduction in intensity of all transitions. Relative intensities remain constant – no elevated emission intensity below 610 nm

Table 5.13 Europium complex sensor responses to hot-water extracts

Hot-MeOH extracts	[EuDO3A]	EuL1	EuL2	EuL3
GRS	Sensitisation of all transitions, particularly the ΔJ=2 transition (intensity increased x8.2, other transitions increased by ~x4) – elevated emission intensity swamping ΔJ=0 Eu emissions, not as intense as Murchison or ALH extracts.	Not tested	Sensitisation of all transitions, particularly the ΔJ=2 transition – elevated emission intensity swamping ΔJ=0 Eu emissions, effect not as not as intense as Murchison or ALH extracts with [EuDO3A].	Sensitisation of all transitions. Elevated emission intensity though effect not as intense as Murchison or ALH extracts with [EuDO3A] or EuL2.
Murchison	Increase in intensity particularly below 610 nm - elevated emission intensity swamping Eu emissions. Possibly not sensitisation of transitions.	Not tested	Not tested	No clear response
ALH88045	Increase in intensity particularly below 610 nm - elevated emission intensity swamping Eu emissions, not as intense as Murchison extract. Possibly not sensitisation of transitions.	Not tested	Not tested	No clear response

Table 5.14 Europium complex sensor responses to hot-MeOH extracts

Hot-solvent extract	[EuDO3A]	EuL1	EuL2	EuL3
GRS	Low intensity Eu emissions of extract-free [EuDO3A] resulted in poor resolution. Sensitisation of all transitions.	Not tested	Not tested	No clear response
Murchison	Not tested	Not tested	Not tested	No clear response
ALH88045	Low intensity Eu emissions of extract-free [EuDO3A] resulted in poor resolution. Increase in	Not tested	Not tested	No clear response

Hot-solvent extract	[EuDO3A]	EuL1	EuL2	EuL3
	intensity particularly below 610 nm - elevated emission intensity swamping ΔJ=0 Eu emissions.			

Table 5.15 Europium complex sensor responses to hot-solvent extracts

The hot-water extraction of Murchison (Table 5.11) liberated approximately five times more organic material than ALH88045 (Table 5.12). However, the hot-MeOH extraction of Murchison liberated approximately the same yield as that from ALH88045. The component liberated by the hot-solvent extraction was also approximately the same amount for both samples. This suggests that Murchison contains a higher concentration of highly-polar, water-soluble, organic material than ALH88045 but a similar quantity of MeOH-soluble and non-polar organic material as ALH88045, i.e. the fraction of organic material present in ALH88045 susceptible to polar-solvent extraction is less than that in Murchison.

As discussed previously (Section 5.5.5), ALH88045 has resided in the harsh oxidising, weathering terrestrial environment of the Antarctic for an undetermined period of time, so it is possible that a not inconsiderable amount of the most water-soluble organic material may have been leached out of the sample prior to location and collection, explaining less organic matter in the hot-water extract of ALH88045 when compared with Murchison. However, even if both meteorites contained the similar quantities of water-soluble organic matter, they may not necessarily contain the same relative concentrations of individual organic species or classes; ALH88045 may contain more aromatic carboxylic acids and derivatives thereof, resulting in the sensor responses seen. The elevated fluorescent emissions below 630 nm that were recorded when Murchison and GRS hot-water extracts, hot-MeOH extracts of Murchison and ALH88045, and the hot-solvent extract of ALH88045 were combined with [EuDO3A], may be the result of the intrinsic fluorescence of components in the extract. However, this same effect is not observed when GRS hot-water extracts are applied to EuL1 and EuL2 solutions, or any other extract with any other sensor

solution. This may imply that [EuDO3A] is more sensitive to the effect of intrinsically fluorescent organic molecules, or the presence of intrinsically fluorescent mineral particulates, in the mixture. The sensitisation, but not alteration, of the relative emission intensities of each transition, caused by the presence of the Murchison and GRS hot-water extracts, recorded here, may be attributable to components that may displace water molecules from the coordination sphere, but not interact electronically.

The fact that the same effect is not recorded when the ALH88045 hot-water extract is applied to [EuDO3A] supports the suggestion that the ALH88045 sample may not contain intrinsically fluorescent components or that the intrinsically fluorescent component is present in much lower concentrations. The results observed when the ALH88045 hot-water extract was applied to [EuDO3A] are reminiscent of the responses recorded when benzoic acid was added to each europium complex solution, suggesting the ALH88045 hot-water extract may contain higher concentrations of components exhibiting similar structural attributes e.g. a carboxylic acid bound to an aromatic antenna. The displacement of water would result in sensitisation of the emissions, but it is the coordination of the carboxylate and the antenna effect afforded by the, possibly aromatic, antenna which may result in the sensitisation of the ΔJ=1 and ΔJ=4 transitions, in particular. Furthermore, as previously discussed (Section 5.5.4), aqueous alteration over an undetermined period as a result of terrestrial contamination and/or weathering while residing in the Antarctic environment of its delivery to Earth, may have resulted in the depletion by leaching of some of its carbonate content, and possibly the liberation and concentration of its aromatic carboxylate content from the IOM. This may have the effect of reducing the effect of water displacement (which would only affect intensity, maintaining relative sensor-only transition intensities) and increasing the concentration of aromatic carboxylate species capable of sensitisation by antenna effect; in doing so, it would alter the coordination environment, leading to preferential transition sensitisation.

[EuDO3A] may be the most effective sensor for aromatic carboxylate species because this complex is the least hindered due to its simple ethanoate arms. This allows close approach and

facile coordination of the aromatic carboxylate antenna to the europium metal-centre facilitating sensitisation. This, does not, however, explain why the same response was not observed when [EuDO3A] was applied to other equivalent extracts. It may be reasoned, therefore, that the other extracts contained species not present in the hot-water extract of ALH88045 that could potentially hinder the ability of the antenna molecules from coordinating, therefore sensitising the transitions, or quenching any such sensitised emissions.

When the hot-water extracts of Murchison, ALH88045 and GRS were applied to the EuL3 sensor, there was an approximate 35% reduction in intensity. This desensitisation of europium emissions provides no information as to the possible composition of the extracts, other than they may contain a higher concentration of nucleobases, that have been shown to quench europium fluorescence (see Chapter 3), or that they do not contain any molecules that may coordinate and act as an antenna. Previous fluorescence experiments using nucleobase analytes in high concentrations, and as complex mixtures (Chapter 3), suggest that, even if there were nucleobases present, they would be unlikely to cause the responses recorded. The reduction in intensity may simply be the result of an effect of dilution. Given that these extracts sensitised emissions when combined with DO3A, L1 and L2 europium complexes, it is more likely that the europium complex of L3 simply does not respond as effectively as the other sensors used.

Application of all sensors, including EuL3 to the GRS hot-MeOH extract resulted in a sensitisation of all transitions. However, application of EuL3 to the hot-MeOH extracts of Murchison and ALH88045 gave no response at all – intensity of emissions remained the same as the sensor-only EuL3 solution. This suggests that the components of the hot-MeOH organic extracts of Murchison and ALH88045 may not be detectable by EuL3, but EuL3 can detect components of the GRS extract. Also, no sensor response was recorded when Murchison, ALH88045 and GRS MeOH-soluble hot-solvent extracts were combined with EuL3 solution.

This suggests three possibilities: 1) the organic material extracted in the hot-solvent solvent does not interact with the EuL3 sensor and thus does not invoke a response, 2) the amount of material

extracted is not sufficient to invoke a response, or 3) it may be due to the difference in structure of the L3 ligand, compared to the other ligands. Although L3 is heptadentate, with three ethanoate pendant arms, the fourth amine of the cyclen ring is attached to a further pendant arm, which is not involved in chelation of the europium ion. It may be that it is this fourth pendant arm that hinders organic analytes, when in a complex extract, from interacting sufficiently for efficient sensing, suggesting it is not as useful a sensor for such extracts.

5.6 Summary and conclusion

The work undertaken in this chapter first tested the europium complexes of DO3A and DO3A-like ligands with individual weathered mineral solutions in the absence of any analogue organic analytes. This was done in order to ascertain if any dissolved mineral species or mineral particulates interfere with sensor emissions. The sensors were then applied to the extracts of a terrestrial, organic-rich, terrestrial rock, Green River Shale (GRS). The purpose of selecting and using this rock was to develop an extraction procedure, and test the utility of the sensors on its extracts, before subjecting the precious carbonaceous chondrites to extraction. If the sensors had not successfully responded to the presence of the GRS extracts then they would be unlikely to respond to the presence of extraterrestrial extracts either (either because the extraction process did not liberate sufficient quantities of organic material, did not liberate organic material at all, or the sensors did not respond to the type of organic material liberated). If the former was the case then the extraction process would need to be re-assessed and further development and, perhaps a larger sample mass, required. Had the latter been the case, the inferred implication would be that the sensors would not be suitable as sensors for the detection of organic molecules in the extracts obtained from extraterrestrial samples. Fortunately, the extraction procedures, and sensor responses to these extracts, was successful and so work progressed to the extraction and application of sensors to the extracts of the carbonaceous chondrites. These extraterrestrial rock were Murchison (the reference meteorite for this study) and the Antarctic meteorite ALH88045 (chosen because it was an 'unknown' sample and, as such, would be analogous to a sample that the sensors may be subjected to in a real analytical setting.

5.6.1 Application of sensors to mineral solutions

Prior to simulated weathering, the mineral samples were analysed using SEM-EDX (Section 5.3.1), which established bulk chemistry and mineral identity while confirming homogeneity; most minerals were free of chemical anomalies with the exception of anorthite and corundum. These features, however, appeared to be isolated occurrences and, therefore, it was considered that the minerals were otherwise homogenous.

The results obtained for the addition of mineral solutions to the [LnDO3A] sensors were largely inconsistent, as were those for $[EuL2]^{3+}$, and could be the result of sensor dilution effects, contamination (exacerbated by the very small sensor volumes use, or loss of sensor solution from the cuvette during aliquots additions) (Section 5.3.2). It is, therefore, not clear if the presence of dissolved mineral species or mineral particulates (should they be present at all) have an effect upon sensor fluorescence emissions, and so any effect the mineral solutions may have had on the fluorescent emissions of the sensor could not be determined with any certainty.

All results obtained for the application of $[LnL3]^{3+}$ sensors to incrementally increasing concentrations of mineral solution indicated only decreases in sensor fluorescence intensity commensurate with that recorded for an effect of dilution (Section 5.3.2). The implication was that, if dissolved mineral species or mineral particulates are present in these mineral extracts, $[LnL3]^{3+}$ sensors were unaffected by their presence.

As explained in detail thorough this chapter, the dissolved mineral species expected in solution liberated by aqueous weathering were not expected to interact with the sensor complexes, with the exception of carbonate ions, which are known to displace fluorescence quenching water molecules, thereby increasing fluorescence emission intensity. However, the very short duration of weathering that the mineral samples were subjected to was unlikely to be sufficient to liberate any carbonate, or any dissolved mineral species and, furthermore, dissolution kinetics and solubility in the solvents used would probably preclude dissolution even over an extended period.

Hence, it could be considered with some certainty that any sensor response seen when the sensors were applied to geological extracts would be due only to the presence of organic analytes. However, the extracts were likely to contain many more dissolved inorganic species than the single mineral extracts applied in the set of tests undertaken in this study, creating additional uncertainty. A summary of the results obtained for the application of sensors to mineral solutions is presented in Table 5.16.

Mineral extract	[EuDO3A]	[TbDO3A]	EuL2	TbL2	EuL3	TbL3
18.2 MΩ water	Incremental decrease in intensity commensurate with dilution effect	Incremental decrease in intensity commensurate with dilution effect	Initial dilution runs – inconsistent. Re-run of dilutions – incremental increase in intensity	Incremental decrease in intensity commensurate with dilution effect	Incremental decrease in intensity commensurate with dilution effect	Incremental decrease in intensity commensurate with dilution effect
Anorthite ($CaAl_2Si_2O_8$)	Incremental decrease in intensity commensurate with dilution effect	Incremental decrease in intensity commensurate with dilution effect	Not tested	Not tested	Incremental decrease in intensity commensurate with dilution effect	Incremental decrease in intensity commensurate with dilution effect
Diopside ($CaMgSi_2O_6$)	Incremental decrease in intensity commensurate with dilution effect	Incremental decrease in intensity commensurate with dilution effect	Not tested	Not tested	Incremental decrease in intensity commensurate with dilution effect	Incremental decrease in intensity commensurate with dilution effect
Enstatite ($Mg_2Si_2O_6$)	Incremental decrease in intensity commensurate with dilution effect	Incremental decrease in intensity commensurate with dilution effect	Not tested	Not tested	Incremental decrease in intensity commensurate with dilution effect	Incremental decrease in intensity commensurate with dilution effect
Corundum (Al_2O_3)	Incremental decrease in intensity commensurate with dilution effect	Decrease in intensity (cannot be attributed to dilution effect alone)	Initial incremental additions – inconsistent. Re-run of incremental additions – incremental increase in intensity	Incremental decrease in intensity commensurate with dilution effect	Incremental decrease in intensity commensurate with dilution effect	Incremental decrease in intensity commensurate with dilution effect
Gypsum ($CaSO_4$ $2H_2O$)	Incremental decrease in intensity commensurate with dilution effect	Decrease in intensity (cannot be attributed to dilution effect alone)	No change in sensor-only fluorescence intensity for any transition emission	Significant increase in intensity of all emissions, no sensitisation of specific transitions	Incremental decrease in intensity commensurate with dilution effect	Incremental decrease in intensity commensurate with dilution effect
Olivine (Forsterite) ($FeMgSiO_4$)	Sensitisation of ΔJ=1 transition, no change in intensity of any other transition	Decrease in intensity (cannot be attributed to dilution effect alone)	Incremental decrease in intensity commensurate with dilution effect	Significant increase in intensity of all emissions, no sensitisation of specific transitions	Incremental decrease in intensity commensurate with dilution effect	Incremental decrease in intensity commensurate with dilution effect

Mineral extract	[EuDO3A]	[TbDO3A]	EuL2	TbL2	EuL3	TbL3
Calcite ($CaCO_3$)	Significant increase in intensity of all emissions, no sensitisation of specific transitions	Significant decrease in intensity not due to dilution effect	Initial dilution run and re-run of dilutions – all inconsistent	Significant increase in intensity of all emissions, no sensitisation of specific transitions	Incremental decrease in intensity commensurate with dilution effect	Incremental decrease in intensity commensurate with dilution effect
Magnetite (Fe_3O_4)	Incremental decrease in intensity commensurate with dilution effect	Decrease in intensity (cannot be attributed to dilution effect alone)	Significant increase in intensity of all emissions, no sensitisation of specific transitions	Significant increase in intensity of all emissions, no sensitisation of specific transitions	Incremental decrease in intensity commensurate with dilution effect	Incremental decrease in intensity commensurate with dilution effect
Nepheline ($Na_3KAl_4Si_4O_{16}$)	Incremental decrease in intensity commensurate with dilution effect	Decrease in intensity (cannot be attributed to dilution effect alone)	Significant increase in intensity of all emissions, no sensitisation of specific transitions	Small increase in intensity of all emissions, no sensitisation of specific transitions	Incremental decrease in intensity commensurate with dilution effect	Incremental decrease in intensity commensurate with dilution effect

Table 5.16 Summary of the sensor responses to incremental additions of mineral extracts

5.6.2 Application of sensors to Green River Shale extracts

The sensor responses recorded when applied to the three different solvent extracts were varied but there were similarities in the responses for given extracts suggesting the sensors were able to differentiate between organic components in each. However, there is very little published information regarding the low-molecular mass polar organic acid and base composition of GRS. Any results of the testing were, therefore, difficult to interpret. However, by comparing the responses recorded when individual analogue organic species were combined with the sensors with those recorded for addition of organic extracts, it was possible to suggest tentative explanations to account for the responses observed. Future work could attempt to characterise the organic composition of the extracts before sensor application.

[EuDO3A] may have detected the presence of antenna effect-inducing aromatic carboxylic acid molecules given the sensitisation of emissions, particularly the Δ*J*=2 transition, when applied to the hot-water extract. The same response was detected, probably caused by the presence of similar organic analytes, when [EuDO3A] was applied to the hot-MeOH extract, however, although sensitisation of emissions was observed when applied to the hot-solvent extract, a broad overlap of fluorescence emissions below 630 nm obscured europium emissions. The implication is that [EuDO3A] can detect aromatic carboxylic acids and is sensitive to the presence of intrinsically fluorescent molecules when both present in a complex mixture extract.

Sensor-only $[EuL1]^{3+}$ emissions were poorly resolved but it was clear that the presence of the hot-water extract invoked sensitisation of emissions, particularly the Δ*J*=2 transition. This suggested the presence of aromatic carboxylic acids and, therefore, $[EuL1]^{3+}$ may be a suitable sensor for these classes of compound.

An explanation to account for the response recorded when $[EuL2]^{3+}$ was applied to the hot-water extract was complex. All emissions decreased in intensity with the exception of the Δ*J*=2 emission. It was hypothesised that $[EuL2]^{3+}$ may detect both quenching and sensitising organic constituents in the hot-water extract, implying that $[EuL2]^{3+}$, although not suitable for unambiguously

determining one or the other classes of molecules that have this effect, may be able to suggest the type of compounds present in a complex mixture (e.g. nucleobases and aromatic carboxylates).

$[EuL3]^{3+}$ may have detected the presence of nucleobases or organic molecules that quench fluorescence in the GRS hot-water extract – possibly *via* the photo-induced electron transfer (PET) mechanisms suggested in Chapter 3 (Section 3.4.3). Sensitisation of emissions, particularly the ΔJ=2 transition, when applied to the hot-MeOH extract suggested that $[EuL3]^{3+}$ may have detected the presence of antenna effect-inducing aromatic carboxylic acids. However, no response was recorded upon application to the hot-solvent extract suggesting $[EuL3]^{3+}$ cannot detect intrinsically fluorescent molecules and that the hot-solvent extract may not contain aromatic carboxylic acids.

5.6.3 Application of sensors to the extracts of carbonaceous chondrites

When the europium complexes were applied to organic extracts from the extraterrestrial samples, a range of results were observed. Depleted supplies of EuL1 and EuL2 solutions, and extracts of Murchison and ALH88045, meant that these sensors could not be tested.

The application of EuL3 to the hot-water extracts of Murchison and ALH88045 caused a 35% decrease in intensity (Figures 5.39 and 5.44), however, it did not respond when it was applied to the hot-MeOH or hot-solvent extracts of Murchison or ALH88045 (Figures 5.41, 5.42, 5.46 and 5.48). Therefore, EuL3 may be useful as a sensor to detect the presence of organic molecules or nucleobases similar to those used in this study (as suggested when applied to the hot-water extract of GRS), but not for detecting non-polar molecules or those with intrinsic fluorescence. The only sensor to consistently respond with an increase in sensor-only emission intensity when applied to the organic extracts of the extraterrestrial samples was [EuDO3A]. When applied to the hot-MeOH extract of Murchison (Figure 5.40), and the hot-MeOH and hot-solvent extracts of ALH88045 (Figure 5.45 and 5.47), significant swamping of europium emissions was recorded (similar to that seen when the sensors were in the presence of (*L*)-tyrosine, Chapters 3 and 4),

which was not seen when any other sensor was in the presence of any other extract. The implication then, is that [EuDO3A] can detect the presence of intrinsically fluorescent molecules in a complex extract derived from an organic-rich geological sample.

The most significant sensitisations recorded were when [EuDO3A] was applied to the hot-water extracts of Murchison (Figure 5.38) and ALH88045, which produced a strong increase in intensity of all transitions, particularly the ΔJ=1 transition in the case of ALH88045 (Figure 5.43). This response was singularly important as it was comparable to the response observed when benzoic acid was added to [EuDO3A] (Figure 3.45). Therefore, [EuDO3A] may be used to detect the presence of similar carboxylate antenna-like molecules in a complex extract mixture derived from an organic-rich geological sample.

5.6.4 Conclusion

Previous experiments have shown that some individual analytes, e.g. nucleobases and carboxylic acid, can invoke a sensor response (Chapters 3 and 4), but complex mixtures containing these analytes do not, or the response is too ambiguous to be confidently attributed to the presence of any specific analyte within the mixture (Chapter 3). Complex abstracts from geological samples, which are expected to contain such molecules, also do not invoke a response with the europium sensors. However, some responses (e.g. [EuDO3A] when applied to the hot-water extract of ALH88045, and extracts which invoked a broad fluorescence which overlapped europium emissions) suggest that the sensors may provide an indication of the molecule classes that are present in greater concentration. This, at least, can provide information which can direct experimental procedures. For example, elucidating that an extract contains a high proportion of aromatic carboxylic acids using a quick and easy fluorescence based sensor will speed up the process of developing methodology required for their extraction, without the need for cumbersome analytical techniques and chemical derivatisation. It is this very issue (convoluted and lengthy identification procedures) that this work has been attempting to address.

The work undertaken in this thesis has shown that the sensors tested can identify the presence of some organic analytes and that the mechanisms by which they interact and invoke sensor responses are likely to be the same, or similar, for molecules of the same class. It is also likely that if these classes are in a higher abundance in a complex extract than was used in this study, compared to other analytes that do not invoke a response, then their presence may also be detected. Therefore, and given that this work has indicated that the likelihood of the presence of dissolved mineral species or mineral particulates in an extract is negligible, some of the sensors ([EuDO3A] in particular) can be applied to complex mixtures of extracts derived from organic-rich geological samples with a view to detecting specific classes of organic analytes.

Furthermore, if coupled with techniques that are able to separate these specific classes (having used the sensors to determine the classes present), and a library of responses to the presence of individual compounds within these classes created, the sensors could discriminate between individual compounds. Thus, the utility of the europium DO3A-like sensors have been shown, by the research undertaken herein, to be sound, and could, with future development, be used to identify organic molecules in extraterrestrial samples, either in the laboratory on Earth or deployed as an approach to analysing samples on other planetary bodies.

6 Thesis Summary, Suggested applications, Limitations, and Suggestions for further work

6.1 Introduction

This final chapter reviews the work presented in this thesis. Firstly, the objectives set out in Chapter 1 are reviewed. Secondly, the results, and conclusions drawn, from the work carried out in Chapter 3, 4 and 5 are summarised and interpretations presented. Thirdly, the limitations highlighted by the research are presented, along with suggestions of how the sensors and their application could be developed and tested in future. The final section of this chapter presents suggestions for future work, including potential applications beyond those that drove the work presented in this thesis.

6.1.1 Progress against objectives

The overall objective of the project was to develop one or more lanthanide-based sensors that could be used to detect extraterrestrial organic molecules.

The specific objectives were:

- To ascertain if known fluorescent complexes of europium and terbium can be used to determine the presence of organic analytes that are analogues of those molecules known to be present in carbonaceous chondrites, individually and within complex mixtures, in solution. This work was presented in Chapter 3.
- Develop new europium and terbium complexes, using structurally similar ligands, in order to determine whether sensitivity and/or selectivity of detection of these analytes may be improved. The development of new sensors was presented in Chapter 4.
- Establish whether those minerals likely to be present in carbonaceous chondrites will interfere with the organic analyte detection. These tests were presented in Chapter 5.
- To apply the fluorescent lanthanide sensors to solvent-extracted solutions of extraterrestrial and terrestrial organic material. These tests were presented in Chapter 5.

The work presented in Chapter 3, using $[LnDOTA]^-$ and [LnDO3A], demonstrated the response of these sensors to the presence of organic analyte analogues, representative of molecules found

within carbonaceous chondrites. The presence of individual nucleobases could be detected by virtue of quenching of fluorescence and, in the case of [LnDO3A], adenine could sensitise fluorescence. It was also shown that unambiguous sensitisation of all lanthanide complexes tested in Chapter 3 was caused in the presence of benzoic acid. Furthermore, although not necessarily advantageous, it was also established that the presence of intrinsically fluorescent analytes may cause swamping of emissions below 630 nm. Therefore, it was ascertained that fluorescent complexes of europium and terbium can be used to determine the presence of individual organic analytes that are analogues of those molecules known to be present in carbonaceous chondrites. It was also established that the sensors may not be able to detect specific analytes in complex mixtures, but that complexes of the less sterically hindered DO3A ligand is more sensitive to analyte interactions than the four pendant arm DOTA ligand.

With those results in mind, Chapter 4 presented the development of new and previously synthesised ligands that were structurally similar to DO3A. These were tested with organic analogue analytes representative of those known to be present in carbonaceous chondrites. When the DO3A-like lanthanide complexes were applied to these analytes, the responses confirmed the results obtained for the sensors tested in Chapter 3, however, the new sensors were not sensitised by the presence of adenine as had been seen with [LnDO3A]. Although these modifications to the ligand structure did not improve selectivity and/or sensitivity to specific analytes, the results corroborated the utility of [LnDO3A] and [LnDO3A]-like complexes as sensors for individual organic analytes analogous to those molecules known to be present in carbonaceous chondrites.

These [DO3A] and]LnDO3A]-like complexes were then tested on aqueous extracts of weathered minerals where it was ascertained that the potential for geochemical interference from mineral components intrinsic to the samples, given the timescales used for extraction and weathering here, was negligible (Section 5.3).

6.1.2 The utility of [LnDOTA]$^-$ and [LnDO3A] complexes

The fluorescence assays carried out in Chapter 3 of this thesis indicated that lanthanide complexes of DOTA and DO3A have utility as sensors for some of the selected analogue analytes chosen to represent individual classes of organic compounds in solvent extracts derived from extraterrestrial samples. This conclusion was based upon the following observations:

- Indirect excitation of all complexes at 265 nm resulted in emissions likely to be due to the antenna effect, whereby excitation of the carboxylate C=O groups of the ligand takes place, followed by a ligand to metal-centre energy transfer mechanism.
- Certain europium transitions are preferentially sensitised by modification of the europium coordination environment, such as differences in ligand denticity.
- When benzoic acid interacts by coordination to the metal-centre, preferential sensitisation of europium emissions were observed and a marked increase in intensity was recorded – presumably a resultant combination of water molecule displacement and ligand to metal-centre energy transfer *via* antenna effect, afforded by its carboxylate moiety and the phenyl group.
- All complexes were sensitive to the presence of adenine, but the presence of adenine markedly sensitised all transitions of the lanthanide complexes of DO3A.
- All sensor complexes' fluorescence was quenched by the presence of all nucleobases (except [LnDO3A] with adenine).

However, [LnDOTA]$^-$ complexes, although sensitised by the presence of benzoic acid, were not as versatile as the [LnDO3A] complexes:

- They did not respond with an increase in intensity to the presence of adenine.
- DOTA ligand consists of four pendant ethanoate arms, which increases steric hindrance around the lanthanide ion, possibly inhibiting the approach of analytes, thereby reducing the likelihood of analyte/metal-centre interactions.
- The charge on the DOTA ligand is four minus so that the overall charge on the complex when the tripositive lanthanide ion is chelated is one minus.

- The overall negative charge may further impede analyte interaction as a result of electrostatic repulsion between carboxylate moieties or molecules with dipoles.

Therefore, on the basis of the limitations of DOTA and the versatility of DO3A, the development of structurally similar ligands to DO3A were chosen in order to produce complexes that were less sterically hindered and were not electronically negatively charged.

6.1.3 The utility of [LnDO3A] and [LnDO3A]-like complexes

The fluorescence assays carried out in Chapter 4 of this study suggested that DO3A-like complexes also have utility as sensors for some of the analogue analytes selected to represent individual classes of organic compounds. This conclusion was based upon the following observations:

- Indirect excitation of all complexes at 280 nm resulted in emissions likely to be due to excitation of the carboxylate C=O groups of the ligand, *via* a ligand to metal-centre charge transfer mechanism.
- Certain europium transitions were preferentially sensitised by alterations to the europium coordination sphere.
- When benzoic acid interacted by coordination to the metal-centre, preferential sensitisation of europium emissions were observed and a marked increase in intensity was recorded. This was likely to be the result of ligand to metal-centre energy transfer *via* antenna effect, afforded by its carboxylate moiety and phenyl group, and water molecule displacement.
- The fluorescence of all sensor complexes was quenched by the presence of all nucleobases.

Therefore, on the basis that the coordination environment of europium may be determined by virtue of selective sensitisation of specific transitions (thus indicating the type of analyte interactions that may take place between the analyte and metal-centre), europium complexes of DO3A and these DO3A-like ligands show potential for great versatility. Furthermore, the reduced

steric hindrance afforded by one fewer pendant arm suggests they may have broader utility, since this suggests greater likelihood for interactions to take place.

6.2 Limitations of the lanthanide complexes as sensors

The limitations associated with the use of lanthanide complexes based upon DO3A and DO3A-like ligands are two-fold. The first involves the difficulties associated with the facile synthesis of the ligand molecules. The second is how to introduce selectivity of the sensor to the presence of analytes and the type of sensor response these analytes cause (see Parker & Williams, 1996).

6.2.1 The difficulties associated with cyclen chemistry and production of DO3A-like ligands

As eluded in Section 4.1, the synthesis and isolation of *tris*-substituted ligands based on a cyclen framework is fraught with difficulties. One issue concerns the cyclen ring molecule, which is not ridged but is constantly twisting and bending. This is further frustrated by the oscillation of the reacting Michael donor nitrogen lone pair electrons, which flip in orientation; some of the time facing outward (where they are accessible for bond formation) and some of the time facing inward, towards the centre of the ring (where they are not). The rate of flipping, however, has not been determined experimentally, and thus it is not known if one state is favoured over the other. This can be controlled, to an extent, by elevating the temperature of the reaction so that the frequency of lone pair oscillation increases thereby increasing the amount of time they are orientated outwards and therefore accessible for bond formation. The main problem associated with elevating the temperature of the reaction is the increased likelihood of undesirable side reactions occurring, e.g. possible pendant arm reagent alkene polymerisation. Therefore, carefully monitoring the reaction in order to determine the optimum duration for maximum yield of the desired *tris*-substituted cyclen is preferred over elevating the reaction temperature conditions.

Another issue with which to contend is the ease of pendant arm attachment; this is largely governed by steric considerations, and is a direct consequence of their size and structure. The

first pendant arm addition can occur at any of the four free amine nitrogen atoms of an unreacted cyclen molecule, then the second arm reagent molecule will likely bond to the amine *trans* to the first addition; this is simply because this is the least hindered reactive site. Any further additions are hindered, therefore, by the presence of the pendant arms either side of the two remaining reactive cyclen secondary amines. It is, therefore, also likely that the synthesis of the corresponding *tetra*-substituted cyclen would be increasingly more difficult to produce, if not impossible, under the reaction conditions maintained during a synthesis where the pendant arms are large and bulky. Although it may be clear that a hypothesised Michael-type reaction could take place between a pendant arm reagent and cyclen molecule, it is probable that a *tris*-substituted cyclen would not be produced at any appreciable quantity if the pendant arm was so large that the third addition could not take place. It is possible, though, that *mono*- and *bis*-analogues would be synthesised, but since it is the *tris*-substituted cyclen that is required, smaller pendant arm reagents would be needed, as well as extended work to elucidate optimisation of reaction conditions.

It is also problematic when attempting to purify and separate of the reaction products, for two reasons. Firstly, it may not possible to separate the products between aqueous and organic phases; both phases may contain all reaction products indicating they are more-or-less equally soluble in water and organic solvents. Secondly, successful separation of the *mono*-, *bis*- and *tris*-analogue products by column chromatography is difficult to achieve. This is because each of the products are very similar, the only difference being the number of free cyclen amines, and therefore will have very similar retention factors regardless of the stationary and mobile phases selected. The fewer pendant arms, the more likely a product will remain adhered to a silica column but this does not mean elution and isolation of products is assured. Furthermore, and for this reason, some of the desired *tris*- product will remain bound to the column, thus reducing the overall yield isolated.

6.2.2 Selectivity to key analytes

For all complexes, the sensor responses, in the presence of nucleobases indicated a complete quenching of fluorescence (with the exception of [LnDO3A] in the presence of adenine). Moreover, the quenching recorded was comparable for all the chosen nucleobases rendering the sensors unable to differentiate between them. The exception was for adenine, which 'switched on' when applied to europium and terbium DO3A complexes. However, when in a complex mixture of nucleobases, the sensitising effect of adenine was not discernible, suggesting that lanthanide DO3A complexes are not suitable for sensing adenine when other nucleobases are present.

It is clear that the ability of [EuDO3A] to selectively detect adenine, by virtue of the increase in emission intensity that its presence causes, indicates that [EuDO3A] has some property that the other sensors do not. Therefore, it is essential that the interactions and mechanism by which the sensitisation takes place is elucidated so that it may be replicated when designing any new sensors. However, the specific issues and difficulties associated with nucleobases and their detection in extraterrestrial samples is intrinsically linked to their very low abundance. Stoks and Schwartz (1982) reported the total concentration of purines to be 1.2 mM, and a total abundance of only 0.06 mM for the pyrimidines (Stoks and Schwartz, 1979) (Table 3.4, Section 3.4.4). As shown in Chapter 3 and 4, these concentrations would not be sufficient to allow detection by the sensors unless the nucleobases were separated and individually isolated first.

It is also important to note that, although the quenching to nucleobases (with the exception of adenine) was a recognisable response, a sensor which 'turns off' is not as useful as one which 'turns on' since the sensor is no longer detectable.

It has also been shown that none of the lanthanide complexes tested can unambiguously identify non-nucleobase molecules because the sensor responses were comparable for each analyte used. The exception to this was when the sensors were in the presence of benzoic acid. This suggests that any molecule with a carboxylate moiety, and a group capable of acting as an antenna, may

similarly invoke a sensitisation of the lanthanide fluorescence. It is known that carbonaceous chondrites contain functionalised polyaromatic hydrocarbons in high abundance (Messenger et al., 1998, Martins et al., 2006, Le Guillou et al., 2014, Huang et al., 2015) and so these sensors may be used to ascertain if a solvent extract contains these analytes. Indeed, it was shown that when the sensors were applied to some of the GRS and carbonaceous chondrite extracts, there was sensitisation of emissions and preferential sensitisation of the Δ*J*=2 transitions (and sensitisation of the Δ*J*=1 transition when [EuDO3A] was applied to the hot-water extract of ALH88045). This does suggest that the sensors had detected such molecules in these extracts.

However, when benzoic acid was mixed with other analogue analytes at equimolar concentrations within a complex mixture of the analogue analytes, the sensitisation its presence afforded when the sensors were applied to benzoic acid alone was not evident. The relative abundance of each analyte, or class of analytes, will not be equimolar in a solvent extract of a geological sample (see Tables 3.4 and 3.5, Section 3.4.4). Furthermore, the abundance of individual aromatic carboxylic acids (see Table 3.5, Section 3.4.4) and the total abundance of these aromatic acids is very low (~32 mM) when compared to, for example, amino acids (60 mM) and monocarboxylic acids (332 mM). This presents a major limitation to the utility of the sensors except for other geological samples where aromatic carboxylic acids may be present at much higher abundances than other analytes.

(*L*)-tyrosine, when added to any of the four lanthanide complexes, resulted in an increase in fluorescence. However, in these tests, the increase in intensity may only be perceived and is likely to be the result of analyte fluorescence overlapping with lanthanide fluorescence. (*L*)-tyrosine is intrinsically fluorescent, with a broad emission spectrum and intensity maxima at ~466 nm (Figure 3.9, Section 3.3.5). The longer wavelengths of this broad emission overlap the shorter wavelength lanthanide emissions, causing these emissions to be swamped and not as well resolved.

This is problematic for terbium complexes, because terbium's most intense emissions are at Δ*J*=2 (~493 nm) and Δ*J*=1 (543 nm). Also, the europium emissions at Δ*J*=0 (~578 nm), Δ*J*=1 (~590 nm)

and Δ*J*=2 (~614 nm) are overlapped. Thus, the intrinsic fluorescence from any highly fluorescent analyte, such as (*L*)-tyrosine, that fluoresces in the range in which the sensor fluoresces, could swamp the emissions, compromising the sensor's utility. Meteorite solvent extracts have been shown to contain intrinsically fluorescent compounds (Section 1.6.2) in addition to those tested here, and these fluoresce over a range of wavelengths (see Table 1.1, Section 1.6.2). These molecules may obscure the sensor emissions and render the sensor useless. However, the fluorescent lifetimes of intrinsically fluorescent organic molecules are orders of magnitude shorter than those of the lanthanides and, therefore, would not affect the utility of the sensor if time-gating were used (see Section 1.7.2).

Although the sensors tested in this work show selectivity for nucleobases and benzoic acid (two classes of compound can be detected using just one sensor), they have not shown selectivity for other molecules such as aliphatic carboxylic acids or aliphatic amino acids. This does limit the scope of application; however, future work may produce other sensors that may be able to detect the presence of these compounds.

6.3 Suggested applications for the sensors

Since this work has shown that the sensors used can detect the presence of benzoic acid *via* the mechanism described, i.e. coordination by the carboxylate resulting in displacement of water molecules in combination with the sensitisation of transitions *via* the antenna effect, it is probable that the sensors may also be able to detect any molecule with aromatic carboxylic acid structure in a sample.

Importantly, it has been suggested that benzoic acid may be a potential prebiotic molecule, involved in the synthesis of complex organic molecules *via* 'on-water' reactions (as opposed to 'in-water' reactions) (Kolb, 2012). This means that DO3A-based lanthanide sensors, such as those tested in this thesis, could be further developed for use on future life-detection missions targeting benzoic acid, and its derivatives.

Furthermore, by submitting a total extract to procedures that can separate classes of compound, and further isolating individual components from within those classes, the sensors may be able to identify the presence of specific analytes, e.g. benzoic acid (or other aromatic acids) and adenine, but only if there is no CO_3^{2-} present in the extract. This process can be achieved not just in the laboratory but could also be carried out 'in the field' as part of a 'lab-on-a-chip'-type experiment on board a life detection mission. Also, should methodology be developed to use these sensors for *in situ* sample analysis, it could be possible to locate and identify adenine and benzoic acid, or any aromatic-carboxylate molecule, using the localised sensitised lanthanide fluorescence that $[LnDOTA]^-$ and [LnDO3A] experience.

Although the sensors have been developed and tested with the express purpose of application to organic species derived from extraterrestrial samples, either in the laboratory or on a planetary surface, they may also be used to detect these molecules in terrestrial field settings. The sensors tested in this work require the analytes to be solvent soluble, specifically water soluble. For this, the molecules are required to be small and polar. Many of these kinds of molecules, above and beyond the small selection tested herein, make up living organisms; these can include everything from pigments to the components of cell membranes. This means that if the sensors may be able to detect and identify analytes derived from organisms and suggest their environment of origin, the sensors may have utility in the detection of, for example, organic contaminants in drinking water from biological or industrial sources.

Having established the utility of the lanthanide complexes based on DO3A (specifically those of europium) with a small selection of analogue organic analytes and complex mixtures derived from organic-rich terrestrial and extraterrestrial samples, the scope for further development of structurally similar fluorescent sensors is promising. Furthermore, by increasing the number of analogue analytes tested, and cataloguing their responses, the true potential for these sensors may be established and may lead to the routine use of lanthanide fluorescent sensors for fast and effective identification of compound classes in mixtures, or isolated analytes.

6.4 Suggestions for Further Work

The research undertaken for the production of this thesis has shown that lanthanide complexes based upon DO3A and DO3A-like ligands are able to detect the presence of certain analogue analytes and that their responses are the result of particular qualities of the class of analyte. That is to say, the responses may be a consequence of specific structures or properties of groups of molecules. For example, aromatic carboxylic acids able to coordinate, alter the coordination environment of the europium ion, and sensitise emissions by harvesting excitation light *via* the antenna effect.

The work was necessarily limited by the duration in which the research was carried out, the availability of reagents, the ability to synthesis and isolate the ligands (and therefore amount of sensor available to conduct the experiments), and the selection of analytes chosen. Given the success of the sensors ability to detect the presence of certain classes of compounds and the successful synthesis of ligands by using the aza-Michael reaction, the following suggestions to consider for possible future work are offered.

6.4.1 Selection of other analogue analytes to test sensors

It is clear that the sensors respond to the presence of nucleobases resulting in quenching of fluorescence. It is beyond the scope of this work to establish precisely what the mechanism is that causes this quenching. Some suggestions were made in Section 3.4.3, but in order to progress development of the sensors for the detection of nucleobases, it would first be advantageous to firmly establish the mechanism by which quenching takes place, and to understand why [EuDO3A] and [TbDO3A] experienced a sensitisation of fluorescence when in the presence of adenine, the only sensors to do so.

Moreover, understanding the quenching (and sensitising, in the case of adenine) mechanism, it may be possible to design and develop novel sensors that harness whatever mechanism is established to be the cause of the responses seen, in order to produce more effective sensors for such nucleobases, or analytes that may invoke to same effect. As previously suggested, these nucleobases (or molecules that affect the sensor via the same mechanism), could be separated

from a complex extract obtained from the regolith of a planetary surface, and identified when the sensor is applied to the various separated fractions.

The results obtained in this study have corroborated and confirmed published work detailing that benzoic acid sensitises europium emissions and that this occurs by coordination and antenna effect (e.g. Gunnlaugsson *et al*., 2003). The increase in intensity afforded by this mechanism is likely to be limited only by the ability of the light harvesting chromophore (the phenyl group, in the case of benzoic acid) to absorb and transfer excitation light to the lanthanide. It is possible that the fluorescent yield, i.e. the intensity of light emitted by the sensor, may be variable depending upon the structure and fluorescent properties of the aromatic light harvesting analyte.

Therefore, it would be advantageous to concentrate future experimentation on a large range of benzoic acid derivatives and carboxylic acids with a range of aromatic groups, and that this selection should include molecules previously detected in the organic inventory of carbonaceous chondrites. It may then be possible to produce a library of fluorescence data detailing the fluorescent yields expected for a given concentration of these analytes, as well as any specific sensitisation of transitions that may be associated with the individual analytes.

6.4.2 DO3A-like ligand syntheses

In order to provide a scope in which to undertake the research in this thesis, it was necessary to place limiting criteria on how to approach the development of the ligands to be synthesised. Aside from the chemical and physical attributes of the reagents, i.e. selection of suitable the pendant arms that would react in such a way as to maintain the DO3A-like structure, for example, it was also important to consider the ease of production and isolation of the ligands, and the cost. For this reason, if the reaction was not fast and facile, or the desired DO3A-like ligand difficult to isolate or produce in sufficient yield, then the synthesis was deemed unsuccessful under the auspices of the criteria.

One such unsuccessful synthesis was that of L4 (Table 4.2, Section 4.1.4). Although mass spectrometry analysis indicated that the aza-Michael reaction was successful and that the

reaction had produced the desired *tris*-substituted cyclen, its yield was very low when compared to the abundance of the *mono*- and *bis*-substituted analogues (see Section 4.2.5). This may have been the result of steric hindrance, the effect and result of which has been explained (Section 6.2.1). Further to this, when an attempt was made to isolate the product by aqueous washing, all products were found to be present in both the organic and aqueous phases suggesting the substituted cyclen ligands were soluble in both solvents, thus making the isolation process and loss of yield. Moreover, when an attempt was made to separate what was isolated in the organic phase by column chromatography, analysis of the eluent fractions suggested the products of the crude mixture were bound to the silica and were lost. Therefore, future work may elucidate the reason for the products being found in both phases after aqueous washing and may suggest a different organic solvent that will be able to isolate the ligand molecules. Furthermore, an eluent and alternative stationary phase may be found that can successfully separate and isolate the target molecule.

However, this still leaves the issue of low production of the desired *tris*-substituted cyclen. Given examination and experimentation with varying reaction conditions, including temperature schemes, reaction solvents and duration, it may be possible to ascertain the optimum conditions required for the successful synthesis of L4. Another option would be to simply increase the quantity of reagents; however, cyclen is a somewhat expensive compound, and so the synthesis of L4 may not be an economically viable endeavour.

Many other pendant arm reagents were suggested (Table 4.1, Section 4.1.3), but one of the criteria for selection of pendant arm reagents was that the reagent should be commercially available; most were not and were discounted. It is possible to synthesise the pendant arm reagents suggested in Table 4.1, and this should be considered in any future synthetic work to produce more novel DO3A-like ligands. Pendant arm reagents 2, 4, and 10 (Table 4.1, Section 4.1.3) should be considered in the first instance and would likely produce useful DO3A-like ligands. Of course, the yield that they would produce cannot be known without carrying out the

synthesis, but, based upon their chemistry and the strength of the electron withdrawing group, it would be anticipated that the aza-Michael reaction would take place.

6.4.3 Other experiments required

Absorbance and emission spectra should be obtained for all analyte, mineral and geological sample extracts so that they may be compared to the spectra recorded when these analytes are applied to the complexes. Intrinsic fluorescence can be identified and considered when analysis of results is undertaken. To this end, a full spectrum should be obtained from 300 nm so that any broad emissions from such species can be recorded. Geological extracts should be applied incrementally to the sensors so that fluorescence intensity *vs* concentration curves may be plotted, and binding constants calculated.

Furthermore, full ionic composition of mineral solution should be obtained using techniques such as inductively coupled plasma mass spectrometry (ICP-MS) which detects metal (and many non-metal) ions at very low concentrations (parts per quadrillion, ppq). This method ionizes the sample using inductively coupled plasma, and a mass spectrometer to separate and quantify the ions present.

In order to be sure if increases in fluorescence intensity is the result of an analyte binding to a lanthanide complex and sensitising emissions *via* antenna effect instead of displacement of water molecules alone, lifetime measurements and hydration sphere (q) values must be obtained, as detailed in Section 3.3.3, to calculate the number of bound water molecules. If the analyte-free spectrum was altered in the presence of an analyte, then the fluorescent lifetimes with and without the analyte were measured in D_2O and H_2O solvents, and it was shown that water molecules had not been displaced, but a change in intensity remained, then this would confirm the antenna effect – the increase in intensity cannot be the result of displaced water.

6.5 Concluding remarks

The research described in this thesis set out to establish if known fluorescent lanthanide sensors, based on DOTA and DO3A, could be used to detect organic molecules in extracts of solvent

soluble organic material from carbonaceous chondrites. In order to do this is was necessary to establish if the sensors would respond to the presence of a selection of individual analogue organic analytes representative of those detected in such organic-rich meteorite samples, in particular those molecules of biological importance. The sensors responses proved this to be the case for nucleobases and benzoic acid.

During the course of these experiments, it was discovered that [LnDO3A] complexes were more versatile than those of $[LnDOTA]^-$ so DO3A-like ligands were synthesised with which to produce [LnDO3A]-like complexes for further testing. Sensor responses confirmed that these sensors could also detect nucleobases and benzoic acid. However, before application to more complex extracts of geological samples, it was important to determine if dissolved mineral species or mineral particulates in suspension might be liberated during the extraction process and would interfere with the sensors fluorescence emissions. Application of the sensors to mineral solutions produced by artificial weathering suggested that ionic species or mineral particulates would not compromise the sensors' utility for detecting organic analytes.

An analogue terrestrial organic-rich rock was selected and subjected to solvent extractions in order to develop an extraction protocol and test the sensors before application to the meteorite extracts. This work proved that the sensors could detect the presence of organic material since the responses were comparable to those recorded when the sensors were applied to individual organic analytes, and furthermore, that the extraction process developed could successfully liberate organic material. Subsequently, the sensors were applied to meteorite extracts prepared in the same way, with responses recorded as seen with the organic analytes and terrestrial rock extract.

Therefore, this work has shown that fluorescent lanthanide sensors, based on DO3A, can be used to detect organic molecules in geological extracts, and that luminescence is potentially useful as an analytical technique for the detection of solvent soluble organic material contained within such extracts.

Appendices

Appendix A

The proceeding sections describe the rationale, reagents and reaction conditions used in the attempted syntheses of ligands L4, L5 and L6. The syntheses were ultimately unsuccessful, however, what follows details the methodology of the attempts and provides explanations as to the possible reasons why the reactions did not occur. Also outlined are the analyses undertaken which suggested unsuccessful production of the target molecules.

A.1 Synthesis of methyl 2-[4,7-bis(2-acetamido-1-methoxy-1-oxopropan-2-yl)-1,4,7,10-tetraazacyclododecan-1-yl]-2-acetamidopropanoate (L4)

The synthesis of methyl 2-[4,7-bis(2-acetamido-1-methoxy-1-oxopropan-2-yl)-1,4,7,10-tetraazacyclododecan-1-yl]-2-acetamidopropanoate, L4, (Figure A.1) has not been previously reported.

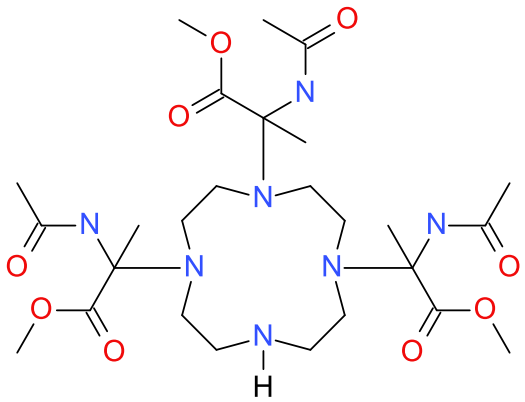

Figure A.1 Methyl 2-[4,7-bis(2-acetamido-1-methoxy-1-oxopropan-2-yl)-1,4,7,10-tetraazacyclododecan-1-yl]-2-acetamidopropanoate, L4

A.1.1 Methyl 2-acetamidoprop-2-enoate (methyl 2-acetamidoacrylate)

Unlike the other reagents used in the syntheses of the ligand molecules, the β-carbon of pendant arm reagent does not have an electron withdrawing group attached, rather two protons. The second electron withdrawing group is bonded directly to the α-carbon of the alkene to which the ester moiety is also attached. As with all ligands, the required C-N bond must be formed at the α-carbon of the alkene to maintain the required DO3A-like ester moiety stereochemical conformation.

Although the electron withdrawing groups are both adjacent to the same alkene carbon atom of methyl 2-acetamidoprop-2-enoate (methyl 2-acetamidoacrylate) (Figure A.3), they will still have the desired α-carbon activating effect.

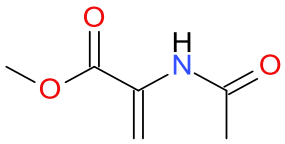

Figure A.2 Methyl 2-acetamidoprop-2-enoate (methyl 2-acetamidoacrylate)

The electron withdrawing functional group attached to the α-carbon is an amide; a carbonyl moiety attached to the α-carbon *via* a nitrogen atom. The electrons of the lone pair of the nitrogen atom, the lone pairs of electrons associated with the carbonyl oxygen and the electrons occupying the 'p' orbitals of the carbonyl carbon-oxygen pi double bond, are delocalised across the entire conjugated structure making for an effective electron withdrawing functionality.

A.1.2 Methodology of L4 synthesis

The cyclen nitrogen nucleophile should attack at the α-carbon (Scheme A.1).

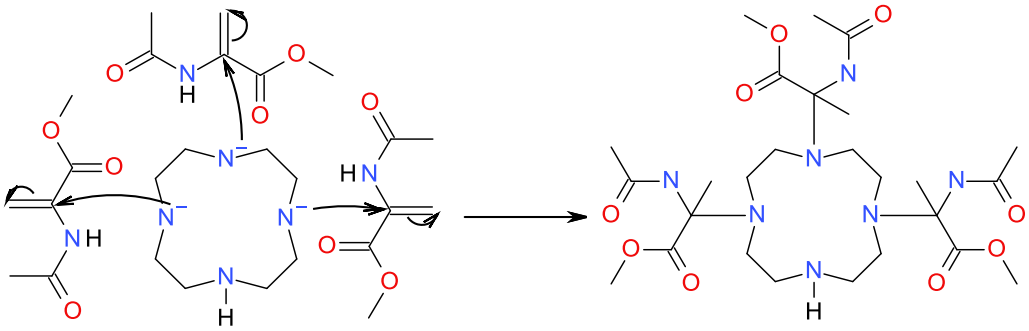

Scheme A.1 Addition of methyl 2-acetamidoacrylate to cyclen

Upon addition of the lanthanide ion, the carbonyl oxygen of the ester is expected to chelate in the same DO3A-like manner, however, the carbonyl oxygen of the amide would not provide an extra point of coordination to any lanthanide complexes produced. This is because if the carbonyl oxygen of the ester is bound, the carbonyl oxygen of the amide would be unable to reach the lanthanide metal centre.

Table A.1 shows mass peaks for reagents and all substituted cyclen products expected to be identified if the desired reaction takes place.

Expected mass peak, Da	Compound responsible	Actual mass, Da
39	Potassium ion	39.10
60	Carbonate ion	60.01
144	methyl 2-acetamidoprop-2-enoate	143.14
173	Cyclen	172.27
316	Mono-substituted cyclen	315.23
459	Bis-substituted cyclen	458.28
602	Tris-substituted cyclen	601.34
745	Tetra-substituted cyclen	744.40

Table A.1 L4: Mass peaks expected in reaction mixture

Synthesis 1

Cyclen was dissolved in dry MeCN and 3.3 equivalents of anhydrous K_2CO_3(s) was added to the solution. 5 equivalents of methyl 2-acetamidoacrylate was dissolved dry MeCN and added directly to the reaction mixture over 1 hour. The reaction was monitored using TLC and MS. At 72 hours the reaction solvent was removed yielding honey-coloured runny oil. The oil was separated into organic and aqueous fractions. The solvent was removed from the organic fraction yielding dark yellow oil but when cooled to room temperature, the oil formed a granular orange mass and colourless needle-like crystals had formed around the neck of the round bottomed flask and feather-like crystals on the glass. Both crystalline substance and orange residue were characterised using ^{1}HNMR and ^{13}CNMR and MS. The aqueous phase was collected and freeze dried yielding a light brown vitreous residue which was analysed using ^{1}HNMR, ^{13}CNMR and MS. White crystals, organic phase: ^{1}H NMR (400 MHz, $CDCl_3$); 1.91-2.02 (CH_3), 3.67 (CH_3), 4.65 (CH_2), 5.83-5.96 (NH). ^{13}C NMR (75 MHz, $CDCl_3$): 23 (CH_3), 53.06 (CH_3), 65 (CN), 116.54 (C=**C**H_2), 132.53 (**C**=C), 166.39 (C=O), 170.18 (C=O). The mass spectrometer, in positive mode (+ES), detected an ion at a mass of 166 Da ($[M+H]^+$); the theoretical mass was calculated to be 143 Da. Orange residue, organic phase: ^{1}H NMR (400 MHz, $CDCl_3$); 1.75 (NH), 2.06 (CH_3), 2.43-2.73 (CH_2), 3.78 (CH_3), 5.82 (C=C**H**), 6.35 (C=C**H**), 7.66 (NH). ^{13}C NMR (75 MHz, $CDCl_3$): 23 (CH_3), 53.06 (CH_3), 65 (CN), 108.78 (CH_2), 130 (C=C), 164 (C=O), 169 (C=O). The mass spectrometer, in positive mode (+ES), detected the target ion (very low intensity) at a mass of 602 Da ($[M+H]^+$); the theoretical mass was calculated to be 601 Da. Aqueous phase: ^{1}H NMR (400 MHz, D_2O); 1.96 (CH_3), 2.22 (NH), 2.60-2.95 (CH_2), 3.19-3.37 (NH), 3.68 (CH_3), 5.70 (CH). ^{13}C NMR (75 MHz, $CDCl_3$): 23 (CH_3),

43.57 (CH_2), 49-55 (CH_2), 108 (CH_2), 162 (C=O), 172-175 (C=O), 179 (C=O). The mass spectrometer, in positive mode (+ES), did not detect the target ion.

Synthesis 2

The reaction was carried out following the same methodology as described previously this time with 3.1 equivalents of K_2CO_3 rather than 3.3. At 48 hours 3 more equivalents of arm reagent were added. The K_2CO_3 was removed, the filtrate washed with water, the organic phase dried and the solvent removed to yield the orange organic residue and white crystals around the neck of the round bottomed flask as was previously seen in synthesis 1. The white crystalline substance and orange residue were analysed by ^{1}HNMR, ^{13}CNMR and MS. White crystals, organic phase: ^{1}H NMR (400 MHz, $CDCl_3$); 1.91-2.02 (CH_3), 3.67 (CH_3), 4.65 (CH_2), 5.83-5.96 (NH). ^{13}C NMR (75 MHz, $CDCl_3$): 23 (CH_3), 53.06 (CH_3), 65 (CN), 116.54 (C=**C**H_2), 132.53 (**C**=C), 166.39 (C=O), 170.18 (C=O). The mass spectrometer, in positive mode (+ES), detected an ion at a mass of 166 Da ($[M+H]^+$); the theoretical mass was calculated to be 143 Da. Orange residue, organic phase: ^{1}H NMR (400 MHz, $CDCl_3$); 1.75 (NH), 2.06 (CH_3), 2.43-2.73 (CH_2), 3.78 (CH_3), 5.82 (C=C**H**), 6.35 (C=C**H**), 7.66 (NH). ^{13}C NMR (75 MHz, $CDCl_3$): 23 (CH_3), 53.06 (CH_3), 65 (CN), 108.78 (CH_2), 130 (C=C), 164 (C=O), 169 (C=O). The mass spectrometer, in positive mode (+ES), detected the target ion (very low intensity) at a mass of 602 Da ($[M+H]^+$); the theoretical mass was calculated to be 601 Da.

The organic residues of synthesis 1 and 2 were combined and an attempt was made to separate the components of the organic fraction using a silica column with a 2.5% to 10% gradient ethanol/DCM.

Unlike the other reagents used in the syntheses of the ligand molecules, the β-carbon of pendant arm reagent does not have an electron withdrawing group attached, rather two protons. The second electron withdrawing group is bonded directly to the α-carbon of the alkene to which the ester moiety is also attached. As with all ligands, the required C-N bond must be formed at the α-carbon of the alkene to maintain the required DO3A-like ester moiety stereochemical conformation.

A.1.3 Results and Discussion

Synthesis 1

According to mass spectrum data, within 17 hours of the start of the first synthesis, the *mono*- and *bis*-substituted cyclen products were present in the reaction mixture (316 and 459 Da, respectively). Further, there were peaks registered with masses expected for both *mono*- and *bis*-products +38 Da, respectively. A possible explanation for this observation is the removal of a proton form the parent ion followed by its replacement with a potassium ion, the source of which was the potassium carbonate utilised as the base for the abstraction of cyclen secondary amine protons. There were no peaks indicating the presence of cyclen or methyl 2-acetamidoprop-2-enoate regents or tris- or *tetra*-substituted cyclen product (Table A.2).

Mass peak detected, Da	Compound responsible, likely	Notes/comments
316	Mono-substituted cyclen	3rd largest peak
354	Mono-substituted cyclen+38 Da	4th largest peak
459	Bis-substituted cyclen	2nd largest peak
497	Bis-substituted cyclen+38 Da	Largest peak

Table A.2 L4 (1): Mass spectrum peaks at T+17 hours

Tris- substituted cyclen was not detected at 17 hours in the crude reaction mixture. The reaction was allowed to continue to 72 hours with regular MS monitoring. MS peaks of the crude mixture at 72 hours were predominantly representative of *mono*- and *bis*- substituted cyclen with an indication of *tris*- at negligible abundance.

After cessation of reaction at 72 hours, separation of aqueous and organic phases and removal of solvents, mass spectra were obtained as well as ^{1}H and ^{13}CNMR data. MS indicated the aqueous fraction contained only *mono*- and *bis*- substituted cyclen (Table A.3).

Mass peak detected, Da	Compound responsible, likely	Notes/comments
207	?	3rd largest peak
316	*Mono*- substituted cyclen	4th largest peak
330	*Mono*- substituted cyclen + 14 Da	2nd largest peak
459	*Bis*- substituted cyclen	Largest peak

Table A.3 L4 (1): Mass spectrum peaks, aqueous phase

Proton NMR indicated substituted cyclen products consistent with MS data (Table A.4).

Peak(s), δ in ppm	Possible cause of resonance	Notes/comments
1.8428	Methyl, **C**H3 – possibly MeCN	Likely residual reaction solvent
1.9649	Methyl, **C**H3 - amide	
2.2212	N-H - cyclen	Possible only
2.6063-2.9529	Methylene, **C**H2 – cyclen or arm	
3.1958/3.3740	N-H - cyclen	Possible only
3.6760	Methyl, **C**H3 - ester	
4.6500	D2O	Solvent
5.7027	α-C proton of pendant arm	Proton added to α-C

Table A.4 L4 (1) (aqueous phase): ^{1}HNMR (Solvent: D_2O)

Carbon NMR also corroborated the presence of *mono*- and *bis*- substituted cyclen with no indication of carbon resonances associated with the target *tris*- molecule (Table A.5).

Peak(s), δ in ppm	Possible cause of resonance	Notes/comments
23	Methyl, **C**H3 - amide	
43.573	Methylene, **C**H2 – cyclen or arm	possible ring rupture/side product of arm
49-55	Methylene, **C**H2 - cyclen	
108	Methylene, β-**C**H2 - alkene	
162	Carbonyl carbon, **C**=O - amide	
172-175	Carbonyl carbon, **C**=O - ester	
179	Carbonyl carbon, **C**=O - carboxylic acid	Ester probably hydrolysed to the acid (peak shifted upscale)

Table A.5 L4 (1) (aqueous phase): ^{13}C NMR (Solvent: D_2O)

Cyclen methylene CH_2 was present as was the methine CH associated with the protonated α-carbon resultant of the formation of the nitrogen-carbon bond indicating that the reaction was successful, at least at one cyclen secondary amine and that product was present in the aqueous phase. Resonances for moieties associated with the pendant arm were also present as expected.

By comparing the intensity of MS peaks, it is clear that mostly *bis*- substituted cyclen had been produced and isolated in the aqueous phase, along with some *mono*-.

Removal of the solvent from the organic phase yielded an orange oil and colourless crystals; the latter formed around the neck of the round bottomed flask. Both were analysed, separately. The crystals were pure unreacted pendant arm reagent, as indicated by the ^{1}H and ^{13}CNMR spectra (Tables A.6 and A.7, respectively).

Peak(s), δ in ppm	Possible cause of resonance	Notes/comments
1.9148-2.0241	CH3, singlet - amide	
3.6699-3.6779	CH3, singlet - ester	
4.6500-4.6531	CH2, singlet - alkene	
5.8290-5.9620	NH, singlet - amide	Peak split to a doublet?

Table A.6 L4 (1) (organic phase, crystals): ^{1}HNMR (Solvent: D_2O)

Peak(s), δ in ppm	Possible cause of resonance	Notes/comments
23.199	Methyl, **C**H3 - amide	
53.747/53.763	Methyl, **C**H3 - ester	
116.535	Methylene, C=**C**H2 - alkene	
132.533	Methine H_2C=**C** - alkene	Adjacent to ester and amide
166.395	Carbonyl carbon, **C**=O - amide	
170.180	Carbonyl carbon, **C**=O - ester	

Table A.7 L4 (1) (organic phase, crystals): ^{13}CNMR (Solvent: D_2O)

These NMR spectra were compared to NMR spectra obtained from the stock reagent and were identical. MS analysis produced an ion mass peak of 166 Da, 23 Da more than the relative molecular mass expected for the parent reagent molecule (143 Da). It is possible that sodium ions had chelated to the molecule in the mass spectrometer to give the mass spectrum observed. The single positive charge on the sodium ion could cause it to become electrostatically bound by the lone pair electrons associated with the two oxygen atoms of the ester group, or the lone pairs associated with the nitrogen atom and oxygen atom of the amide moiety, respectively (Figure A.3).

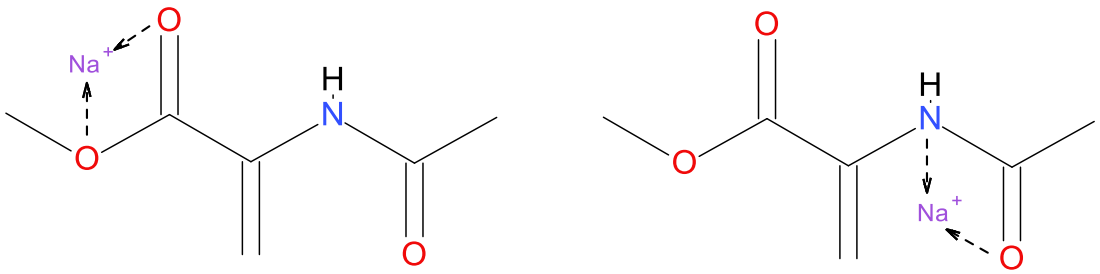

Figure A.3 Sodium adducts of methyl 2-acetamidoacrylate: mass spectrum peaks at 165 Da

Only one of these adducts forms; if both were likely, a peak at 188 Da would also be expected, which is not the case.

According to MS analysis of the orange oil, there are peaks corresponding to *mono*- (predominant component) and *bis*- with multiples of 14 Da added to their masses suggesting adducts formed during ionisation within the mass spectrometer. *Tris*- product was detected in the organic phase, at a very low intensity, along with its analogue + 14 Da adduct (Table A.8).

Mass peak detected, Da	Compound responsible	Notes/comments
344	*Mono*- substituted cyclen +2x 14 Da	Largest peak
358	*Mono*- substituted cyclen +3x 14 Da	
473	*Bis*- substituted cyclen +14 Da	
487	*Bis*- substituted cyclen +2x 14 Da	
602	Tris- substituted cyclen	Very low intensity

Table A.8 L4 (1): Mass peaks, orange fraction in organic phase

^{1}HNMR indicates substituted cyclen products (Table A.9) though resonances associated with cyclen CH_2 resonances between 2.4 and 2.8 are very weak.

Peak(s), δ in ppm	Possible cause of resonance	Notes/comments
1.7520	N-H - cyclen or amide	Most likely cyclen
2.0639	Methyl, CH3 – amide	
2.4361-2.7376	Cyclen, CH2	Weak
3.6511-3.754	?	
3.7805	Methyl, CH3 – ester	
5.8163	Conjugated vinyl proton	
6.5315	Conjugated vinyl proton	
7.1979	$DCCl_3$	Solvent
7.6587	N-H – cyclen or amide	Most likely amide

Table A.9 L4 (1) (organic phase, oil): ^{1}HNMR (Solvent: $DCCl_3$)

The ^{13}CNMR spectrum provides evidence of carbon resonances associated with the pendant arm, however, indication of the presence of cyclen carbon atoms, which would be expected at ~45 ppm, are not evident. Resonances associated with the pendant arm carbon atom forming the C-N bond at ~70 ppm are present, albeit weakly (Table A.10).

Peak(s), δ in ppm	Possible cause of resonance	Notes/comments
23	Methyl, **C**H3 - amide	
53.066	Methyl, **C**H3 - ester	
65	**C**-N	Pendant arm/cyclen bond
76.671/77.099/77.518	D**C**Cl3	Solvent
108.781	Methylene, β-**C**H2 - alkene	
130	α-**C** - alkene	Adjacent to ester and amide
164	Carbonyl carbon, **C**=O - amide	
169	Carbonyl carbon, **C**=O - ester	

Table A.10 L4 (1) (organic phase, oil): ^{13}C NMR (Solvent: $DCCl_3$)

Evidently the Michael type addition reaction does take place and, according to analyses of both the organic and aqueous fractions, all products are soluble in both polar and non-polar solvents. The orange oil in the organic phase isolated from the crude mixture appeared to be the only fraction in which *tris*-substituted cyclen is isolated. MS analysis suggests the yield of *tris*-substituted cyclen is extremely low in comparison with *mono*- and *bis*- products, by virtue of the intensity of the peaks, with the latter two in far greater abundance. It has also been shown that it

is possible to salvage pure unreacted pendant arm reagent from the organic phase. It should be possible, therefore, to isolate the *bis*- product from the crude mixture using flash column chromatography. With this isolated and prepared in a reaction vessel, further equivalents of recovered pendant arm reagent could be added in order to increase the yield of the target *tris*-substituted cyclen.

Synthesis 2

MS analysis of the reaction mixture shortly after the reaction commenced indicated *mono*-substituted cyclen had been produced (316 Da), along with a small amount of *bis*- (459 Da). By 24 hours, *bis*- was the predominant component followed by *mono*-. The presence of *tris*- was also indicated but at a low abundance (602 Da) along with peaks representative of the starting materials. The reaction mixture composition had not changed significantly by 48 hours, with the exception of the loss of the peak at 173 Da (which occurred at 30 hours), indicative of cyclen, so a further 3 equivalents of pendant arm reagent was added in order to ascertain if an increase in concentration would facilitate the production of *tris*- substituted cyclen. After 4 hours, MS analysis showed no increase in *tris*- but did indicate a large increase in abundance of a component at 182 Da. This peak is 38 Da heavier than the pendant arm reagent and is possibly an adduct in which potassium is bound. The reaction was allowed to continue for 168 hours (112 hours after the addition of extra pendant arm reagent). Only *mono*-, *bis*- and pendant arm and their adducts were seen (Table A.11).

Mass peak detected, Da	Compound responsible	Notes/comments
182	Pendant arm +38 Da	Largest peak
214	?	
330	*Mono*- substituted cyclen +14 Da	
344	*Mono*- substituted cyclen +2x 14 Da	
459	*Bis*- substituted cyclen	

Table A.11 L4 (2): Mass peaks at T+168 hours (112 hours after addition of extra pendant arm)

The reaction was stopped, the solvent removed and the crude reaction mixture separated into organic and aqueous phases. As previously described in the first attempt at synthesis, the organic fraction yielded an orange oil, and unreacted pendant arm reagent crystallised around the neck of the round bottom flask (MS peak at 182 Da; pendant arm potassium adduct). As was the case for

the first synthesis attempt, MS analysis of the crude organic mixture revealed mass peaks indicating the presence of mostly *mono*- (the predominant species) and *bis*- substituted cyclen products and their adducts, as well as a low abundance of tris-. Some pendant arm reagent adduct was also identified (Table A.12).

Mass peak detected, Da	Compound responsible	Notes/comments
182	Pendant arm +38 Da	
229	?	
330	*Mono*- substituted cyclen +14 Da	
344	*Mono*- substituted cyclen +2x 14 Da	Largest peak
358	*Mono*- substituted cyclen +3x 14 Da	
459	*Bis*- substituted cyclen	
473	*Bis*- substituted cyclen +14 Da	
487	*Bis*- substituted cyclen +2x 14 Da	
602	Tris- substituted cyclen	Very low intensity

Table A.12 L4 (2): Mass peaks, orange fraction in organic phase

The ^{1}HNMR spectrum was comparable to that of the organic oil produced in synthesis 1, as was the ^{13}CNMR spectrum, however resolution was improved such that resonances commensurate with cyclen CH_2 carbons were considerably clearer (Table A.13).

Peak(s), δ in ppm	Possible cause of resonance	Notes/comments
24.624	Methyl, **C**H3 - amide	
45	Methylene, **C**H2 - cyclen	
52.942/52.967	Methyl, **C**H3 - ester	
65	**C**-N	Pendant arm/cyclen bond
76.581/77.000/77.428	D**C**Cl3	Solvent
108.682	Methylene, β-**C**H2 - alkene	
130.791	α-**C** - alkene	Adjacent to ester and amide
164.570	Carbonyl carbon, **C**=O - amide	
169839	Carbonyl carbon, **C**=O - ester	

Table A.13 L4 (2) (organic phase, oil): ^{13}C NMR (Solvent: $DCCl_3$)

Although ^{1}HNMR analysis of the second synthesis aqueous phase was directly comparable to that of the first attempt, the MS analysis was not. Many peaks were observed clustered around the main expected peaks; these were not evident in the aqueous phase of the first synthesis. The presence of unreacted pendant arm (largest peak) and *tris*- substituted cyclen (low abundance) were also identified, which was not the case for the aqueous phase of the previous synthesis (Table A.14).

Mass peak detected, Da	Compound responsible	Notes/comments
182	Pendant arm +38 Da	Largest peak
229	?	
298		Probable *mono*- fragment
312		*Mono*- fragment
316	*Mono*- substituted cyclen	
325		*Mono*- fragment
330	*Mono*- substituted cyclen +14 Da	
344	*Mono*- substituted cyclen +2x 14 Da	Largest peak
358	*Mono*- substituted cyclen +3x 14 Da	
427		*Bis*- fragment
459	*Bis*- substituted cyclen	
473	*Bis*- substituted cyclen +14 Da	
487	*Bis*- substituted cyclen +2x 14 Da	
602	*Tris*- substituted cyclen	Very low intensity
611		*Tris*- adduct

Table A.14 L4 (2): Mass peaks, aqueous phase

Although both the organic and aqueous phases contained *mono*- and *bis*- products, only the organic phase contained the *tris*- product in both synthesis attempts. For this reason, the organic oils isolated from both synthesis attempts were combined (0.7991 g) and loaded onto a silica column in order to separate the substituted cyclen components. The eluent used was a 2.5% to 10% gradient ethanol/DCM and the eluted fractions were analysed using TLC. Only fractions 8 to 10 indicated the presence of an eluted compound, which was unreacted pendant arm. According to TLC analysis, no other compounds were eluted. After a total 130 fractions were collected it was clear that any products in the organic mixture had bound to the silica column and were not eluting. At this point the column chromatography was abandoned. MS analysis suggests the production of *tris*-substituted cyclen was minimal with the majority of the product as the *mono*- and *bis*- analogues. It was not possible to separate the products using column chromatography. That being the case, the synthesis of L4 was abandoned at this time.

Evidently a reaction does take place between methyl 2-acetamidoacrylate and cyclen. Unfortunately, according to MS analysis, the products of the reaction are predominantly *mono*- and *bis*-substituted cyclen with only a low relative abundance of *tris*-. Analyses of the organic and aqueous phases indicate separation of products cannot be achieved by washing with the water and DCM as all products were present in both the water and DCM solvent fractions. Furthermore,

separation by column chromatography proved unsuccessful as only pendant arm reagent was recovered, suggesting the products had become irretrievably bound to the silica.

It is likely the reaction yielding *mono*- and *bis*-substituted cyclen was rapid given the identification, by MS, of a significant abundance of *mono*- shortly after the reaction had commenced, and *bis*-substituted cyclen by 24 hours. This suggests the reaction is facile and needs little encouragement. The fact there was no indication of *tris*- until 24 hours, and that the relative abundance was extremely low, suggests the addition of the third pendant arm is hindered. It is likely this hindrance is caused by steric effect of the previous additions at two of the other reactive cyclen secondary amine sites. The first pendant arm reacts at a free amine of an unreacted cyclen molecule then the second arm reagent molecule bonds to the amine *trans* to the first addition. Any further additions are hindered, therefore, by the presence of the pendant arms either side of the two remaining reactive cyclen secondary amines. It is, therefore, also likely that the synthesis of the corresponding *tetra*-substituted cyclen would be increasingly more difficult to produce, if not impossible, under the reaction conditions maintained during this synthesis.

When choosing methyl 2-acetamidoacrylate as the pendant arm reagent careful consideration was given to the structure, with particular concern with regards to the stereochemistry of the alkene moiety. Since both groups adjacent to the α-carbon exhibit powerful electron withdrawing nature, and the fact that the β-carbon is conjugated to both via the alkene pi bond, it was entirely possible that it too could be sufficiently activated and thus be susceptible to nucleophilic attack. The ligand produced in this case would not maintain the requisite ester stereochemistry instead increasing the arm size by one carbon (Scheme A.2).

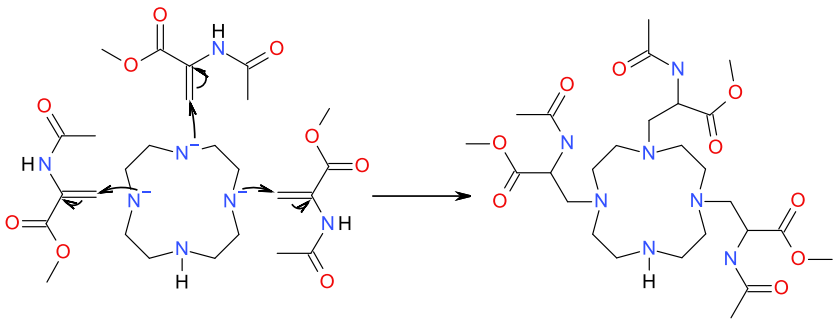

Scheme A.2 Addition at activated β-carbon of methyl 2-acetamidoacrylate

Had that have been the case then reaction at both alkene carbon atoms could have been expected. Six possible isomers would have been possible and those isomers would be indistinguishable my MS analysis, very difficult to identify by NMR spectroscopy and almost impossible to separate from a crude product mixture. However, this was not likely to be the case as ^{13}CNMR analysis did not indicate carbon resonances likely to be associated with this number of related molecules. Analysis suggests the reaction did take place at the β-carbon, as hypothesised, thus confirming the electron withdrawing groups had successful activated it for the Michaels'-type addition to take place.

A.1.4 Conclusion

As previously explained (Section 4.1), the prerequisites governing the criteria for a successful synthesis is threefold. 1) The reaction must not require catalysts; they would need to be isolated and removed from the reaction mixture post-synthesis adding extra steps, and therefore additional time, to the work-up. 2) Reactions should not require extreme conditions, e.g. high temperatures or pressures. 3) Reactions must be fast and facile, easy to achieve with good yields and uncomplicated isolation with a minimum of work-up, i.e. separation and purification.

Although it is clear that the hypothesised Michael's-type reaction does take place between the pendant arm reagent and cyclen, *tris*-substituted cyclen was not seen at any appreciable quantity. It is possible this was as a result of stearic hindrance when the addition of the second pendant arm, probably *trans* to the first, took place. The abundance of *mono*- and *bis*- analogues would suggest this is highly likely. It is also clear that separation of reaction products is problematic, for two reasons. 1) It was not possible to separate the products between aqueous and organic

phases; both phases contained all reaction products indicating they are more-or-less equally soluble in water and organic solvents. 2) The analysis of fractions eluted during the attempt at separation of products by column chromatography suggests the compounds remained adhered to the column. For these reasons, contrary to the prerequisite criteria outlined above, the overall synthesis of L4 was unsuccessful.

Methyl 2-acetamidoacrylate is an excellent pendant arm candidate for the synthesis of a *bis*-substituted cyclen ligand as the synthesis is fast and facile. However, much work must be done to develop a suitable methodology for efficient separation and purification of products. It is also likely that, given further careful research and development of reaction protocols, the target *tris*-substituted cyclen could be produced in sufficient yields given favourable reaction conditions.

A.2 Synthesis of ethyl 2-{4,7-bis[1-ethoxy-1-oxo-3-(phenylamino)butan-2-yl]-1,4,7,10-tetraazacyclododecan-1-yl}-3-(phenylamino)butanoate (L5)

The ligand ethyl 2-{4,7-bis[1-ethoxy-1-oxo-3-(phenylamino)butan-2-yl]-1,4,7,10-tetraazacyclododecan-1-yl}-3-(phenylamino)butanoate, L5 (Figure A.4), is discussed in this section and has not been previously synthesised.

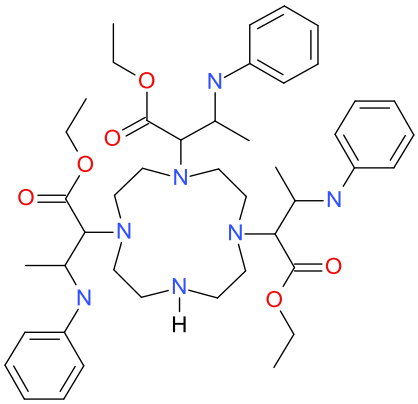

Figure A.4 ethyl 2-{4,7-bis[1-ethoxy-1-oxo-3-(phenylamino)butan-2-yl]-1,4,7,10-tetraazacyclododecan-1-yl}-3-(phenylamino)butanoate, L5

It was, therefore, not possible to know if reaction conditions previously used would be sufficient for successful synthesis, or, indeed, if the pendant arm reagent would react to produce the required *tris*-substituted cyclen. The choice of pendant arm reagent was based entirely on; i) the presence of a reactive alkene moiety, ii) groups which provide a sufficient electron-withdrawing

effect, in the correct position, to activate the alkene α-carbon and iii) carbonyl groups in the correct position which, when bonded to the cyclen molecule, produce a DO3A-like conformation.

A.2.1 Ethyl (2*E*)-3-(phenyl amino)but-2-enoate (ethyl 3-anilinocrotonate)

(2*E*)-3-(phenyl amino)but-2-enoate (or ethyl 3-anilinocrotonate) (Figure A.5) was chosen as the reagent for the pendant arm to produce the *tris*-substituted cyclen, L5.

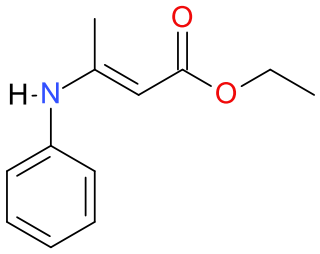

Figure A.5 (2E)-3-(phenyl amino)but-2-enoate (ethyl 3-anilinocrotonate)

Ethyl 3-anilinocrotonate exhibits the alkene required for Michaels-type addition reaction. The carbonyl carbon of the ester moiety is bonded directly to the α-carbon of the alkene maintaining the necessary DO3A-like stereochemistry. The functional groups attached to the alkene β-carbon are a methyl group and a secondary phenyl amine, the phenyl group is bonded via the amine nitrogen.

It is the phenyl amine which is expected to provide the electron-withdrawing function to facilitate sufficient activation of the α-carbon for successful nucleophilic addition. The alkene is conjugated to the phenyl ring delocalised pi electrons via the lone pair of electrons associated with the secondary amine nitrogen atom, this should result in electron withdrawal from the α-carbon.

A.2.2 Methodology of L5 synthesis

The formation of a C-N bond between a cyclen secondary amine and the activated α-carbon of the alkene will take place if the electron withdrawal is sufficient to create a slight positive charge on the α-carbon and if steric factors do not hinder the reaction (Scheme A.3).

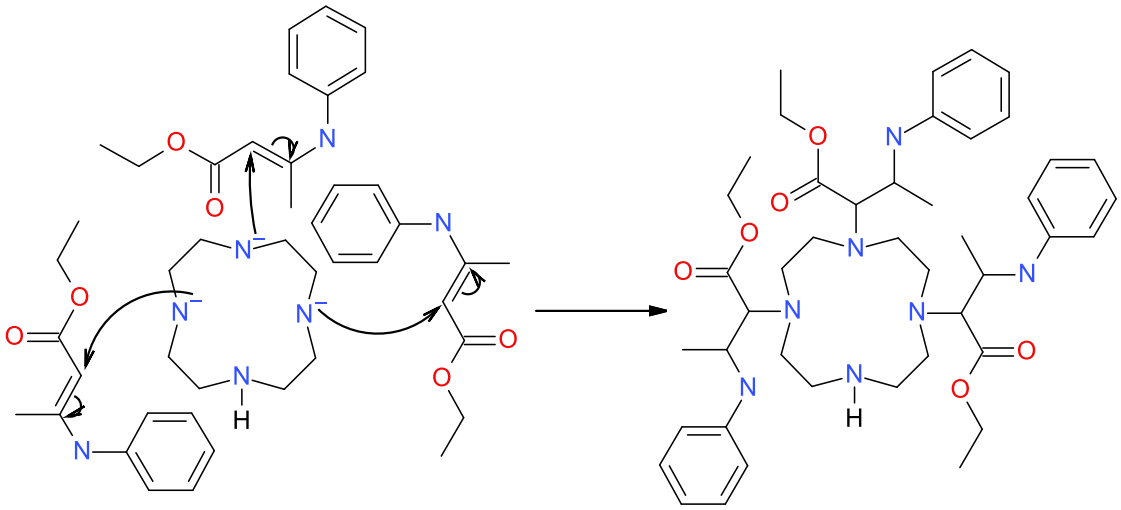

Scheme A.3 Addition of ethyl 3-anilinocrotonate to cyclen

The large bulk of the phenyl group could inhibit satisfactory proximity between the α-carbon and the cyclen nitrogen, in which case, the C-N bond will not form.

Expected mass spectrum mass peaks for reagents and all substituted cyclen products for the synthesis of MTA#3, since it is likely there will be a mixture of by-products present, assuming the desired addition reaction takes place, are shown in Table A.15.

Expected mass peak, Da	Compound responsible	Actual mass, Da
39	Potassium ion	39.10
60	Carbonate ion	60.01
206	(2*E*)-3-(phenyl amino)but-2-enoate	205.26
173	Cyclen	172.27
378	Mono-substituted cyclen	377.53
583	Bis-substituted cyclen	582.79
789	Tris-substituted cyclen (L3)	788.05
993	Tetra-substituted cyclen	992.61

Table A.15 L5: Mass expected in reaction mixture

It is expected that the reaction will occur under the same reaction conditions used for the synthesis of L2. The cyclen secondary amines will be deprotonated, using K_2CO_3 as the base, and subsequently nucleophilically attack at the sufficiently activated α-carbon, forming the C-N bond.

The first attempt at synthesis used 3.1 equivalents of the pendant arm reagent and 3.3 equivalents of K_2CO_3 to 1 equivalent of cyclen, all of which were combined in dry acetonitrile. The reaction was maintained at 80°C reflux for 68 hours after which time the aqueous and organic fractions were separated and analysed using MS and ^{1}HNMR and ^{13}CNMR.

The second attempt employed 3.3 equivalents of triethylamine (TEA) as the base in order to ascertain if the reaction would be successful utilising a different base reagent for deprotonation of the cyclen secondary amines. All other reagent equivalents were as described above. The reaction was monitored using MS and NMR throughout the 120 hour reaction time.

A.2.3 Results and Discussion

Synthesis 1

Results of MS showed no reaction had taken place; the organic fraction contained pendant arm reagent (peak at 206 Da), with no evidence for any substituted cyclen products. The presence of only pendant arm reagent in the organic fraction after separation was confirmed by ^{1}HNMR and ^{13}CNMR analysis (Tables A.16 and A.17).

Peak(s), δ in ppm	Assignment	
1.2176	CH3, alkene side group	
1.8903-1.9613	CH3, ester	
2.0845/2.1087	Residual cyclen CH2	
3.3758	CH, alkene	
4.0549-4.0902	CH2, Ester	
4.6181	NH, phenyl amine proton	
6.6096-6.6870	Benzyl proton (ortho)	
7.0025-7.0218	Benzyl proton (para)	
7.2310-7.2498	Benzyl protons (meta)	
10.3083	NH, residual cyclen	

Table A.16 L5 (1) (organic phase): ^{1}HNMR (Solvent: $DCCl_3$)

Peak(s), δ in ppm	Assignment	
14.565	Methyl, **C**H3 - ester	
20	Methyl, **C**H3	Adjacent to NH2
58	Methylene, **C**H2 - ester	
76.581/77.000/77.428	D**C**Cl3	Solvent
83.983/84.008	Methine C=**C**H - alkene	Adjacent to ester
115.081	Phenyl carbon	para
124.392/124.893	Phenyl carbon	meta
129.022/129.261	Phenyl carbon	ortho
170	Carbonyl carbon, C=O - ester	

Table A.17 L5 (1) (organic phase): ^{13}CNMR (Solvent: $DCCl_3$)

Only resonances associated with cyclen methylene (CH_2) and secondary amine (NH) were observed when ^{1}HNMR and ^{13}CNMR analyses were performed upon the aqueous phase, and MS indicated only the cyclen parent ion peak at 173 Da.

Synthesis 2

The second attempt, using TEA as the cyclen deprotonating reagent produced the same results as the previous attempt at synthesis which were confirmed by MS, ^{1}HNMR and ^{13}CNMR; isolation of the pendant arm reagent in the organic fraction with no expected substituted cyclen products present. Analysis of the aqueous phase also indicated only cyclen with a peak at 173 Da by MS and commensurate resonances for cyclen by ^{1}HNMR and ^{13}CNMR (Tables A.18 and A.19).

Peak(s), δ in ppm	Assignment	
1.8325	N-H	Secondary amine protons
2.8	Methylene, CH2	Cyclen

Table A.18 L5 (2) (aqueous phase): ^{1}HNMR (Solvent: D_2O)

Peak(s), δ in ppm	Assignment	
44.732	Methylene, CH2	cyclen
77.023	DCCl3	Solvent impurity

Table A.19 L5 (2) (aqueous phase): ^{13}CNMR (Solvent: D_2O)

A.2.4 Conclusion

Mass spectrum and NMR analysis suggest the Michael's-type addition reaction did not take place. The formation of the C-N bond was unsuccessful; no substituted cyclen products were detected and only starting reagents were observed. By comparing the pendant arm reagent characteristics with those used for the successful production of L1 and L2, the fact that L5 was not produced suggests either, i) the α-carbon was insufficiently activated, ii) steric hindrance caused by the large phenyl amine precluded sufficient proximity, or iii) both factors played a part.

It is possible the electron-withdrawing effect of the phenyl amine was not strong enough to sufficiently activate the α-carbon. The single pi electron orbital associated with the amine does not provide full conjugation of the alkene with the phenyl group. The methyl group bonded to the α-carbon is electron donating so this would have further hindered sufficient activation. If the α-carbon was sufficiently activated, then it is likely steric hindrance caused by the large size of the phenyl group may have been the dominant factor, enough to inhibit the reaction entirely.
Given that the reaction had not fulfilled the given criteria; fast and facile; when using ethyl 3-anilinocrotonate as the pendant arm, and that analysis had provided evidence to suggest the expected reaction had taken not place, attempts at further reactions were retired.

A.3 Synthesis of ethyl 3-amino-2-[4,10-bis(3-amino-1-ethoxy-1-oxobutan-2-yl) 1,4,7,10-tetraazacyclododecan-1-yl]butanoate (L6)

The pendant arm reagent was chosen for the synthesis of ethyl 3-amino-2-[4,10-bis(3-amino-1-ethoxy-1-oxobutan-2-yl)-1,4,7,10-tetraazacyclododecan-1-yl]butanoate, L6, (Figure A.6) first, based upon its ability to provide the required functional groups needed for DO3A-like stereochemistry and to facilitate the desired reaction.

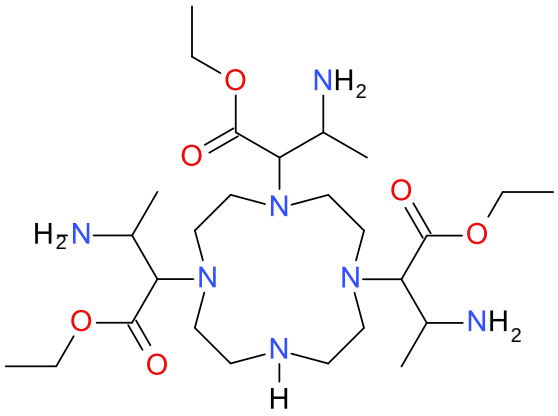

Figure A.6 ethyl 3-amino-2-[4,10-bis(3-amino-1-ethoxy-1-oxobutan-2-yl)-1,4,7,10-tetraazacyclododecan-1-yl]butanoate, L6

That is to say, the ligand structure was not conceived first, followed by retrosynthetic analysis to identify a pendant arm reagent. The nature of the electron-withdrawing group was the only other consideration. Ideally this group should have some synthetic utility which could be taken advantage of at a later time if desired. The pendant arm reagent used in the attempted synthesis of L6 is similar to that used for L5 in that the β-carbon of the alkene is bound directly to an electron-withdrawing amine nitrogen and an electron donating methyl, CH_3, group.

A.3.1 Ethyl (2*Z*)-3-aminobut-2-enoate (ethyl 2-aminocrotonate)

Ethyl (2*Z*)-3-aminobut-2-enoate (ethyl 2-aminocrotonate) (Figure A.7) comprises the requisite functional groups necessary for the Michael's-type addition and maintains the stereochemistry of the carbonyl carbon of the ester moiety. These are, i) an alkene, ii) an electron withdrawing primary amine group adjacent to the β-carbon the alkene to activate the α-carbon (which acts as a Michael's acceptor to the Michael's donor lone pair of a cyclen secondary amine, forming the C-

N bond), and iii) an ethyl ester carbonyl group adjacent to alkene α-carbon. Also attached to the alkene β-carbon is a methyl group.

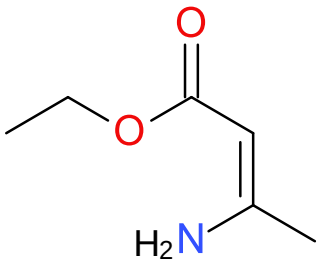

Figure A.7 ethyl 2-aminocrotonate

Although the methyl group is an electron donating group, it is hoped the amine nitrogen should be sufficiently electron withdrawing to induce a slight positive charge on the alkene α-carbon required to facilitate N-C bond formation. Even though the amine is the least electron withdrawing of the pendant arm reagents chosen, it was hypothesised that the reaction would take place at the α-carbon due to reduced steric hindrance because of the much smaller size of the side groups; the *tris*-substituted cyclen should be produced.

A.3.2 Methodology of L6 synthesis

As with all previously described ligand synthesis reactions, after deprotonation of three cyclen secondary amines, nucleophilic attack should occur at α-carbon of the alkene moiety of the chosen pendant arm reagent, if the α-carbon is sufficiently activated, thus forming the C-N bond (Scheme A.4).

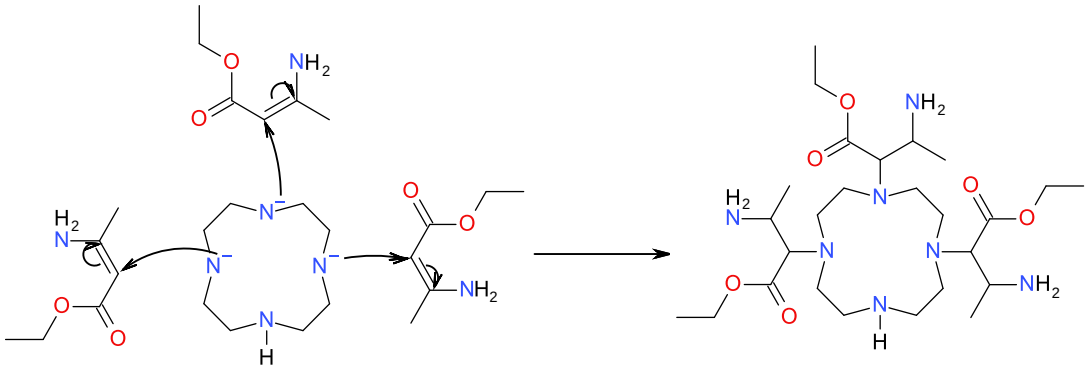

Scheme A.4 Addition of ethyl 2-aminocrotonate to cyclen

The reaction is complete when the β-carbanions (formed when the alkene double bond cleaves) are protonated by the HCO_3^- ions.

Table A.20 shows expected mass peaks for reagents and all substituted cyclen products for the synthesis of MTA#5, assuming the desired addition reaction takes place, since it is likely there will be a mixture of by-products present.

Expected mass peak, Da	Compound responsible	Actual mass, Da
39	Potassium ion	39.10
60	Carbonate ion	60.01
130	ethyl (2Z)-3-aminobut-2-enoate	129.16
173	Cyclen	172.27
302	Mono-substituted cyclen	301.25
431	Bis-substituted cyclen	430.33
660	Tris-substituted cyclen	559.41
689	Tetra-substituted cyclen	688.48

Table A.20 L6: Mass peaks expected in reaction mixture

The reaction must occur at three cyclen secondary amine nitrogen atoms to produce the *tris*-substituted cyclen target molecule. The product must also be easily isolated, in sufficient yield, for the synthesis to be considered a success.

The first attempt at the synthesis of L6 used 5 equivalents of ethyl 2-aminocrotonate and 3.3 equivalents of anhydrous K_2CO_3(s) to 1 equivalent of cyclen, all of which is directly combined in 35 ml of dry acetonitrile and heated, with stirring, to a reflux temperature of 80°C for 94 hours. 5 equivalents of pendant arm reagent were used because a stoichiometry of 3.1 equivalents did not yield product when an attempt at the production of L3 was made. It was reasoned that since this reaction uses a similar pendant arm reagent to that used for L3, in that the electron-withdrawing group is an amine and is lower than that of other pendant arm reagents, then increasing the concentration might improve probability of successful reaction. If the reaction takes place, a slight excess of this reagent was not anticipated to yield more *tetra*-substituted cyclen since the base reagent was maintained at 3.3 equivalents thus limiting the deprotonated amine stoichiometry, only increasing the availability of pendant arm for reaction. The reaction was monitored using MS and TLC analysis.

A second attempt at the synthesis followed the protocol which proved successful for L2 (Section 4.3) and L4 (Section 4.5). In this attempt, 5 equivalents of the pendant arm reagent was dissolved in 17.5 ml of dry MeCN and 1 equivalent of cyclen was combined with 3.3 equivalents of K_2CO_3 in a separate 17.5 ml of dry MeCN. The addition of the pendant arm was then carried out over a duration of half an hour after which the mixture was refluxed for a further 72 hours at 80°C, with stirring. The reaction was monitored using TLC and MS.

After 94 hours the K_2CO_3 was filtered out under vacuum and the solvent removed to yield orange oil (1.58 g). Upon separation, the oil yielded an aqueous phase of dark brown viscous oil (1.00 g) and an organic phase of orange oil (0.46 g). Both residues were characterised using MS and ^{1}HNMR and ^{13}CNMR; all showed the desired reaction had not taken place. ^{1}HNMR and ^{13}CNMR identify pendant arm in the organic phase (Tables A.22 and A.23).

A.3.3 Results and Discussion

Synthesis 1

During the course of the reaction, TLC showed no changes in separation or position of spots indicating only the presence of cyclen, which did not move from the baseline, and the pendant arm reagent.

MS analysis provided no evidence for the presence of any substituted cyclen products. Table A.21 shows only the presence of cyclen (~173) and pendant arm reagent (~130) at 67 hours.

Mass peak, Da	Compound responsible	
130.07	ethyl (2Z)-3-aminobut-2-enoate	Low intensity
173.10	Cyclen	Largest peak

Table A.21 L6 (1): Mass peaks at T+67 hours

Peak(s), δ in ppm	Possible cause of resonance	
1.0698-1.2907	CH3, triplet - ester	
1.8289	CH3, singlet – methyl group	Adjacent to NH2
3.9319-4.1668	CH2, quartet - ester	
4.4432	CH, singlet - alkene	Adjacent to ester
7.2150	DCCl3	Solvent

Table A.22 L5 (1) (organic phase): ^{1}HNMR (Solvent: $DCCl_3$)

Peak(s), δ in ppm	Possible cause of resonance	
14.491	Methyl, **C**H3 - ester	
22.222/22.239	Methyl, **C**H3	Adjacent to NH2
58.420	Methylene, **C**H2 - ester	
76.572/77.000/77.419	D**C**Cl3	Solvent
83.983/84.008	Methine C=**C**H - alkene	Adjacent to ester
159.644	**C**=C - alkene	Adjacent to CH3 and NH2
170.180	Carbonyl carbon, C=O - ester	

Table A.23 L6 (1) (organic phase): ^{13}CNMR (Solvent: $DCCl_3$)

^{1}HNMR and ^{13}CNMR clearly identifies cyclen in the aqueous phase (Tables A.24 and A.25).

Peak(s), δ in ppm	Possible cause of resonance	
1.8386-1.8416	Methyl, **C**H3 – possibly MeCN	Likely residual reaction solvent
1.8868-2.0204	N-H - cyclen	
2.23963-3.7023	Methylene, **C**H2 – cyclen or arm	Broad humps – possible ring rupture
4.6500-4.6659	D2O	Solvent

Table A.24 L6 (1) (aqueous phase): ^{1}HNMR (Solvent: D_2O)

Peak(s), δ in ppm	Possible cause of resonance	
22.015/22.048	Methyl, **C**H3	Adjacent to NH2
42	Methylene, **C**H2 – cyclen or arm	
44.502	Methylene, **C**H2 - cyclen or arm	
49	Methylene, **C**H2 - cyclen or arm	
51.016	Methylene, **C**H2 - cyclen or arm	
77.023	DCM	From phase separation
179	Carbonyl carbon, C=O – carboxylic acid	Ester probably hydrolysed to the acid (peak shifted up-scale)

Table A.25 L6 (1) (aqueous phase): ^{13}C NMR (Solvent: D_2O)

Analyses unequivocally indicated that the desired reaction had not taken place under these reaction conditions.

Synthesis 2

Based upon successes seen in producing L2 and L4, a second attempt was made, this time adding the pendant arm separately as a solution to make up the final reaction solvent volume.

NMR analysis obtained during the course of the second synthesis indicated no change in the composition of the reaction mixture and no substituted cyclen resonances (Tables A.26 and A.27) suggesting the reaction had not taken place even after 72 hours.

Peak(s), δ in ppm	Possible cause of resonance	Notes/comments
1-1.3	CH3, triplet - ester	
1.8	CH3, singlet – methyl group	Adjacent to NH2
2.6	Methylene, **C**H2 – cyclen	
3.9-4.1	CH2, quartet - ester	
4.4	CH, singlet - alkene	Adjacent to ester
7.2	DCCl3	Solvent

Table A.26 L6 (2) (crude reaction mixture, T=0, 5, 26, 48 and 72): ^{1}HNMR (Solvent: $DCCl_3$)

Peak(s), δ in ppm	Possible cause of resonance	Notes/comments
14.5	Methyl, **C**H3 - ester	
22.4	Methyl, **C**H3	Adjacent to NH2
31.0		
46.0	Methylene, **C**H2 – cyclen	
58.5	Methylene, **C**H2 - ester	
76-77	D**C**Cl3	Solvent
84.2	Methine C=**C**H - alkene	Adjacent to ester
159.6	**C**=C - alkene	Adjacent to CH3 and NH2
170.2	Carbonyl carbon, C=O - ester	

Table A.27 L6 (2) (crude reaction mixture, T=0, 5, 26, 48 and 72): ^{13}CNMR (Solvent: $DCCl_3$)

Once separated into aqueous and organic phases, mass spectra were obtained (Tables A.28 and A.29) the results of which further confirmed that the reaction had not taken place at all – there was no evidence to suggest even the presence of *mono*- or *bis*- products.

Mass peak, Da	Compound responsible	
130.15	ethyl (2Z)-3-aminobut-2-enoate	Largest peak
173.21	Cyclen	Low intensity
259.15	ethyl (2Z)-3-aminobut-2-enoate	Dimer

Table A.28 L6 (2): Mass peaks (organic phase)

Mass peak, Da	Compound responsible	Notes/comments
173.21	Cyclen	Largest peak
345.26	Cyclen dimer	Low intensity

Table A.29 L6 (2): Mass peaks (aqueous phase)

Final ^{1}HNMR and ^{13}CNMR analyses of the aqueous and organic extracts indicated only the presence of starting materials.

A.3.4 Conclusion

Both attempts at synthesising the desired *tris*-substituted cyclen L6 target molecule were unsuccessful. Analysis using NMR and MS indicated that no addition reaction took place; *mono*- or *bis*- substituted cyclen was not produced under these conditions either. These results suggest the α-carbon was insufficiently activated. It was argued that, even taking into account the lesser electron-withdrawing ability of the amine, activation of the α-carbon would be sufficient and that

the small size of the amine/methyl side groups would not result in steric hindrance such that the reaction should take place. This has proved not to be the case. It is probable that the amine group electron-withdrawing nature was not effective enough and it is likely the electron-donating methyl group detracted from this further.

Given that on both occasions no reaction was observed to have taken place and, upon separation into aqueous and organic phases, final analysis indicated only the presence of starting materials, it was conceded that further syntheses of L6 would not be attempted at this time.

Appendix B

In order to select analogue minerals to subject to weathering, a literature review of fluorescent minerals found in carbonaceous chondrites was undertaken. The fluorescent minerals found in Murchison (the reference meteorite chosen for this study) were then shortlisted (see Table 2.1, Section 2.2.3). Table A.1 provides information regarding the chemical alterations and fluorescence activators as well as the main emission wavelengths. It also comments on the colour, intensity and any specific peculiarities, for completeness.

Mineral	Formula	Family	Chemical alterations	Emmittance lines (nm) (major lines in bold)	Main emmitting colour	Intensity	Activators	Comments
Montecellite	$CaMgSiO_4$	Silicates	-	460, 560, 600, 688, 525	Pink/Orange	-	Sm^{3+}	-
Sodalite	$Na_8(Al_6Si_6O_{24})Cl_2$	Silicates	-	587, 608, 628, 633, 653, 655, 678	Orange/yellowish -white	V. strong/medium	S_2^-, Fe^{3+}, Mn^{2+}, $(UO_2)^{2+}$	can also exihibit Y-Wt, R O and Gr hues
			Fe^{3+} replaces Al^{3+}	687-720	-	-	-	-
			Mn^{2+} replaces Na^+	650	-	-		1 Mn^{2+} ion replaces 2 Na^+ ions
			$(UO_2)^{2+}$	495, 515, 537	-	-	-	uranyl ion present as an impurity
Grossular	$Ca_3Al_2(SiO_4)_3$	Silicates	-	-	Red	Weak	Cr^{3+}, Mn^{2+}, V^{2+}	can also exihibit V R, Pk, Sal, O hues
			Cr^{3+}	690, 694, 698, 707	-	-	-	Grossular is also known as Garnet or Hessonite
			V^{2+}	717	-	-	-	-
			Nd^{3+}	462, 476, 482, 501	-	-	-	-
			Mn^{2+} replaces Ca^{2+}	590, (605-610)	-	-	-	-
Anorthite	$CaAl_2Si_2O_8$	Silicates	-	-	Yellow/white	-	Fe^{3+}, Mn^{2+}, Sm^{3+}, Ce^{3+}, Eu^{2+}	-
			Fe^{3+}	700	-	-	-	-
			Mn^{2+}	323, 339, 352, 403, 417, 476, 550-565, 570,	-	-	-	-
			Sm^{3+}	598, 643	-	-	-	-
			Ce^{3+}	490	-	-	-	-

Mineral	Formula	Family	Chemical alterations	Emmittance lines (nm) (major lines in bold)	Main emmitting colour	Intensity	Activators	Comments
			Eu^{2+}	**420**, 470	-	-	-	-
Albite	$NaAlSi_3O_8$	Silicates	-	-	Red	Very weak	Fe^{3+}, Dy^{3+}, Sm^{3+}, Tb^{3+}, Yb^{3+}	can also exihibit Wt , Y-Wt , O , V R , V Pk and Pk hues
			Dy^{3+}	480, 560, 660	-	-	-	-
			Sm^{3+}	600, 645, 650, 700	-	-	-	-
			Tb^{3+}	415, 420, 470, 490, 500	-	-	-	-
Oldhamite	(Ca,Mg,Fe)S	Sulfides	-	(Phosphorescence)	Orange	-	-	-
			Ce^{3+}	532	-	-	-	-
			Mn^{2+}	584	-	-	-	-
Cristobalite	SiO_2	Oxides	-	445[£], 450	-	-	Intrinsic	[£]at 173 K (-100˚C)
Tridymite-α	SiO_2	Oxides	-	-	Red	Weak	Intrinsic	
Diopside	$CaMgSi_2O_6$	Silicates	-	-	Blue	Strong	$_n[TiO_6]$ clusters, Cr^{3+}, Mn^{2+}	can also exhibit weak Y hues
			$[TiO_n]^{m-}$	415/520	-	-	-	-
			Mn	585, 670	-	-	-	-
			Mn^{2+} replaces Mg^{2+}	690	-	-	-	-
			Mn^{2+} replaces Ca^{2+}	580	-	-	-	-
			Cr^{2+} replaces Mg^{2+}	684, 705	-	-	-	-
Spinel	$MgAl_2O_4$	Oxides and hydroxides	-	-	Red		Cr^{3+}, Mn^{2+}	

Mineral	Formula	Family	Chemical alterations	Emmittance lines (nm) (major lines in bold)	Main emmitting colour	Intensity	Activators	Comments
			Cr^{3+}	676, 686, 698, 690, 708, 718				
			Mn^{2+}	521.6, 525, 550-612				
Enstatite	MgSiO3 or $Mg_2Si_2O_6$	Silicates	-	-	Bluish white	Weak	TiO_6^{8-}, $_n[TiO_6]$ clusters, Mn^{2+}, O*	
			TiO_6^{8-} (Ti^{4+} - Si^{4+})	520				Where Ti4+ replaces Si4+
			$_n[TiO_6]$ cluster	550				
			Mn^{2+}	400, 674, 670				
			Mn^{2+} replaces Mg^{2+}	630				
Pyrochlore	$(Na,Ca)_2Nb_2O_6(OH,F)$		-	-	Yellowish green	-	$(UO_2)^{2+}$, Dy^{3+}, Sm^{3+}, Tb^{3+}, Eu^{3+}	
			$(UO_2)^{2+}$					uranyl ion present as an impurity
			Dy^{3+}	479, 577				
			Sm^{3+}	601				
			Tb^{3+}	546				
			Eu^{3+}	552, 618				
Baddeleyite	ZnO_2	Oxides	-	-	Green	Strong	$_n[TiO_6]$ cluster, $(UO_2)^{2+}$, Dy^{3+}, Sm^{3+}, Tb^{3+}, Eu^{3+}	

Mineral	Formula	Family	Chemical alterations	Emmittance lines (nm) (major lines in bold)	Main emmitting colour	Intensity	Activators	Comments
			Anion vacancy	500				
			$(UO_2)^{2+}$				Uranyl ion as impurities	
			TiO_6^{8-}	520-550				
			Dy^{3+}	490, 579				
			Sm^{3+}	549				
			Tb^{3+}	546				
			Eu^{3+}	617				
Titanite	$CaTiSiO_5$	Silicates	-		Dark Orange		Cr^{3+}, Ti^{3+}, Sm^{3+}, Eu^{3+}, Er^{3+}, Pr^{3+}, Tm^{3+}	Possible activators; TiO_6, REE^{2+}, REE^{3+}, Pb^{2+}/Mn^{2+} replacing Ca^{2+}, Cr^{3+}/Mn^{4+} replacing $Ti^{4+}/Cr^{4+}/Cr^{5+}$ and Fe^{3+} replacing Si^{4+}
			Cr^{3+}	686				U impurities could induce luminescence due to radiation
			Eu^{3+}	563, 620, 703				
			Pr^{3+}	487				
			Sm^{3+}	562, 600				
			Tm^{3+}	805				
Wollastonite	$CaSiO_3$	Silicates	-	-	Orange/yellow	Strong	Mn^{2+}, Cr^{3+}, Fe^{3+}	can also exihibit B-Wt and Y-Wt hues
			Fe^{3+}	700				

Mineral	Formula	Family	Chemical alterations	Emmittance lines (nm) (major lines in bold)	Main emmitting colour	Intensity	Activators	Comments
			Mn^{2+}	550, 560, 565,				
			Mn^{2+} replaces Ca^{2+}	555-560, 580, 603, 640				
			Fe^{3+} replaces Si^{4+}	690-700				
Corundum	Al_2O_3	Oxides	-	-	Red	Very strong	Cr^{3+}, Fe^{3+}	Can also exihibit O hues
			Intrinsic	400-450, 500-550, 525-550				
			Cr^{3+} replaces Al^{3+}	693, 694				
Muscovite	$KAl_2(AlSi_3O_{10}(OH)_2$	Silicates	-	680	Yellowish-white	-		
Saponite	$(Ca_{0,5},Na)_{0,3}(Mg,Fe^{+2})_3(Si,Al)_4O_{10}(OH)_2 \cdot 4H_2O$	Silicates	-	-	Yellow/White	-	-	-
Phlogopite	$KMg_3AlSi_3O_{10}(OH)_2$	Silicates	-	-	Yellow	Strong	$_n[TiO_6]$ clusters, Mn^{2+}, O*	can also exihibit Y-Wt , O-Wt and Gr-Wt hues
			Mn^{2+} replaces Mg^{2+}	580, 630				
			TiO_6^{8-}	610				
			$_n[TiO_6]$	500				
Powellite	$CaMoO_4$	Tungstates, Molybdates		530-550 (broad), 526, 564, 601, 646	Yellow	Very strong	MoO_4^{2-}	The very strong Y fluorescence is due to MoO42- tetrahera distortions

Mineral	Formula	Family	Chemical alterations	Emmittance lines (nm) (major lines in bold)	Main emmitting colour	Intensity	Activators	Comments
Periclase	MgO	Oxides	-	-	Pale yellow		Cr^{3+}, Fe^{3+}, Mn^{2+}, V^{2+}, Intrinsic, Lattice defect, Phonon	
			Fe^{3+}	**704**, **685**				
			Mn^{2+}	610, 615				
			F/F+ centres	520/390				
			Lattice defect	400-500				
			Zero phonon	588				
			Intrinsic	450, 526, 535				
Amesite	$Mg_2Al(SiAl)O_5(OH)_4$	Silicates	-	-	Red		Cr^{3+}	
			Cr^{3+} replaces Al^{3+}	678, 684				
Gypsum	$CaSO_4$ $2H_2O$	Sulfates		-	Orange/yellow	medium	Organic impurities, Uranyl ion as impurities	Y-Wt and B-Wt
			$(UO_2)^{2+}$	469, 486, 507, 530, 554				Gr luminescence caused by uranyl
			Organics	440-630				Gr-Wt and B fluorescence most probably due to organic impurities.

Mineral	Formula	Family	Chemical alterations	Emmittance lines (nm) (major lines in bold)	Main emmitting colour	Intensity	Activators	Comments
Whewellite	$Ca(C_2O_4)\cdot H_2O$	Organic	Organics	410, 480, 512, 546, 604, 708	Bluish white	Strong	Intrinsic organic impurities	ethandioate anion (Oxalate anion) strong fluorescence could be due to inclusion of humic acid
Moissanite	SiC	Native elements	-	-	Orange/yellow	-	-	Can also show Gr fluorescent hues
Chlorapatite	$Ca_5(PO_4)_3Cl$	Phosphates, Arseniates, Vanadates	Yb^{2+}	435	Orange/yellow	-	Yb^{2+}	-
Sphalerite	(Zn,Fe)S	Sulfides			Orange	Strong/medium	Mn^{2+}, Cu^{+}	also fluoresceces O-Y, V Pk and B hues
			Mn^{2+} replaces Zn^{2+}	595				Large band, peaks at 595
			Cu^{+}-Ga^{3+}replaces Zn^{2+}	640, 670, 675				Cu+ combined with tricationic Ga3+ combine to give 4+ to replace 2 dipositive Zn2+ ions
			Cu^{+}-In^{3+}replaces Zn^{2+}	640, 670, 675				Cu+ combined with tricationic In3+ combine to give 4+ to replace 2 dipositive Zn2+ ions
			V_{Zn}-Cl^{-}	450, 460, 470				?????
Blödite	$Na_2Mg(SO_4)_2\ 4H_2O$	Sulfates			Greenish	weak		
Forsterite	Mg_2SiO_4	Silicates	-	-	Yellowish-white	-	Mn^{2+}, Cr^{3+}, Fe^{3+}, O*, lattice defect	Ni2+ doping exhibits flourescence at 410, 420 and 790 at 23˚C. At -196˚C it fluoresces at

Mineral	Formula	Family	Chemical alterations	Emmittance lines (nm) (major lines in bold)	Main emmitting colour	Intensity	Activators	Comments
								693 698, 708, 717, 721, 739, 790 and 800 nm
			lattice defect	428, 432, 452, 460				
			Cr^{3+}	698				
			Mn^{2+} replaces Mg^{2+}	600-660, 683, 693				
			Mn^{2+}	630				
			O*Si around SiO_4	420, 440				
			O*Al (Al^{3+} - Si^{4+}	470				
Calcite	$CaCO_3$	Carbonates	-	-	Pink/Red/Blue	All strong	Mn^{2+}, Pb^{2+}, Fe3+, Ce^{3+}, Sm^{3+}, Eu^{3+}, Dy^{3+}, Tb^{3+}, PO_2^{*}, CO_3^{-*}	Wt, B-Wt, Y-Wt, Pk-Wt, Y, O-Y, O, O R, V R, V Pk, Sal Pk, Gr-Y, V, Gr-Wt, V B, Y-Gr, Gr-B, Pale Y, Gr
			Ce^{3+}	400, **545**, **700**				$^{\#}$ emmitance at -196˚C
			Dy^{3+}	483, 485, **500**, 576-577, **580**, **680**				
			Eu^{3+}	592, 619				
			Sm^{3+}	565, 570, 600, 610, 614, 615, 626, **650**, 710				
			Tb^{3+}	488, 544, 545				

Mineral	Formula	Family	Chemical alterations	Emmittance lines (nm) (major lines in bold)	Main emmitting colour	Intensity	Activators	Comments
			Tm^{3+}	452				
			Mn^{2+}	588, **605**, **610**, 615, 620, 667, 560-630				
			Fe^{3+}	695				
			Pb^{2+} replaces Ca^{2+}	320-325				
			Mn^{2+} replaces Ca^{2+}	580-620, 610-630				
			$[PO_2]^*$ replaces $[CO_3]$	570				
			$[CO_3\text{-}]$*	420				
			CO_3^{2-}	450				
			Defect centre	520, 560				
			Eu^{3+} replaces Ca^{2+}	575, 591, 618, 696, 709				
			Intrinsic	400, 420, 545, 560, 578, 580#, 605, 648, 670, 695				# emmitance at -196˚C as well as room temperature
Antigorite	$(Mg,Fe^{+2})_3Si_2O_5(OH)_4$	Silicates	-	-	Blue			A.k.a. Serpentine and Lizardite
Apatite	$Ca_5(PO_4)_3(F,Cl,OH)$	Phosphates, Arseniates, Vanadates	-	-	Pale yellow/Violet/Orangy yellow	weak/medium strong	O_2, $(UO_2)^{2+}$, Mn^{2+}, Mn^{3+}, Eu^{2+}, Eu^{3+}, Ce^{3+}, Sm^{2+}, Sm^{3+}, Eu^{3+}, Dy^{3+}, Er^{3+}, Tb^{3+},	Includes Fluorapatite, chloapatite and hydroxyapatite

Mineral	Formula	Family	Chemical alterations	Emmittance lines (nm) (major lines in bold)	Main emmitting colour	Intensity	Activators	Comments
							Gd^{3+}, Yb^{2+}, Pr^{3+}, Tm^{3+}	
			Ce^{3+}	390-400, 458, 543				
			Dy^{3+}	470, 475, 478, **480**, **481**, **482**, 488, **485**, **568**, **570**, **575**, 577-579, 580, 586, 579, 651, 656, 661, **663**, 664, 667				
			Eu^{2+}	410, 410-445, 430-450, 450, 450-460, **451**,				
			Eu^{3+}	573, 578, **579**, 585, **590**, 608, **615**, 616, **618**, 627, 631, 645, **653**, 690, **695**, **700**				
			Er^{3+}	**403**, 544, **545**				
			Sm^{2+}	689, 691, 695, 704, 708				
			Sm^{3+}	420, 560, 563, **565**, 566, 593, 595, **599**, 600, 603, 604, 637, 639, 640, 641, **645**, 646, 648, **649**, 651,				

Mineral	Formula	Family	Chemical alterations	Emmittance lines (nm) (major lines in bold)	Main emmitting colour	Intensity	Activators	Comments
				652, **654**, 690, 695, 598, 704				
			Tb^{3+}	411, **414**, **415**, 416, 420, 436, 437, 438, 439, 443, 446, 490, 540, 545, 546				
			Pr^{3+}	485, **600**, 607, **650**				
			Tm^{3+}	**364**, **452**, 453, **700**				
			Mn^{2+}	**560**, 562, **565**, 570, 576, **577**, 590, 595, 600				
			Mn^{3+}	583				
			$(UO_2)^{2+}$	467, 486, 505, 508#, 524#, 526, 546#, 550				# emmitance at -196˚C
			Intrinsic	432				
			Mn^{2+} replaces Ca^{2+}	569, 583				
			Ce^{3+} replaces Ca^{2+}	430				
			Eu^{3+} replaces Ca^{2+}	574#, 589, 601#, 617, 623#, 630#, 651, 695, 696#				# emmitance at -196˚C
			Sm^{3+} replaces Ca^{2+}	**565**, **599**, **607**, **645**, **654**				

Mineral	Formula	Family	Chemical alterations	Emmittance lines (nm) (major lines in bold)	Main emmitting colour	Intensity	Activators	Comments
			Tb^{3+} replaces Ca^{2+}	487				In combination with Dysoprosium
			Tb^{3+} replaces Ca^{2+}	545				
Magnetite	Fe_3O_4	Oxides	Intrinsic	477				
Plagioclase	$(Na,Ca)AlSi_3O_8$	Silicates	-	-	Red		Pb^{2+}, Cr^{3+}, Eu^{2+}, Ce^{3+}, Sm^{3+}, Eu^{3+}, Tb^{3+}, Tl^{+}, Fe^{2+}, Fe^{3+}, Cu^{2+}, Mn^{2+}, Ti^{4+}	
			Eu^{2+}	420, 405-412				
			Eu^{3+}	600-615				
			Sm^{3+}	560, 600, 645				
			Tb^{3+}	580, 620				
			Cu^{2+}	420				
			Fe^{2+}	550				
			Mn^{2+}	**404**, 421, 487, 559, 560, 570, 580				
			Ti^{4+}	400-550				
			Fe^{3+}	700				
			Fe^{3+} replaces Al^{3+}	700-750-780 (broad band)				
			Tl^{+} replaces Na^{+}	287				

Mineral	Formula	Family	Chemical alterations	Emmittance lines (nm) (major lines in bold)	Main emmitting colour	Intensity	Activators	Comments
			Mn^{2+} replaces Ca^{2+}	555-570 (broad bands)				
			Cr^{3+} replaces Al^{3+}	680, 683				
			Pb^{+} replaces Na^{+}	850				
Feldspar	$(K,Na)AlSi_3O_8$	Silicates	-	-	Red		Al-[O^{-}]-Al, Co, Cr^{3+}, Dy^{3+}, Er^{3+}, Eu^{2+}, Eu^{3+}, Sm^{3+}, Tb^{3+}, Fe^{2+}, Mn^{2+}, Fe^{3+}	can also exihibit B hues
			Eu^{2+}	404, 420				
			Eu^{3+}	614, 624				
			Dy^{3+}	479, 472, 576, 653				
			Er^{3+}	404, 472, 504, 526, 532, 540, 549, 559, 668				
			Sm^{3+}	603, 640				
			Tb^{3+}	413, 437, 450, 546, 559, 560				
			Fe^{3+}	700				
			Co	430`				
			Cr^{3+}	405				
			Mn^{2+}	**560, 570**				

Mineral	Formula	Family	Chemical alterations	Emmittance lines (nm) (major lines in bold)	Main emmitting colour	Intensity	Activators	Comments
			Al-[O^-]-Al	380-500				caused by absorbtion by the Al to O- to Al bonding electrons
			Intrinsic	430, **470-620**				
Nepheline	$Na_3KAl_4Si_4O_{16}$	Silicates	-	-	Orange			
Magnesiohornblende	$XCa_2[Mg_4(Al,Fe^{+3})]Si_7AlO_{22}(OH)_2$	Silicates	-	-	Greenish-blue	very weak		
Anthophyllite	$XMg_7Si_8O_{22}(OH)_2$	Silicates	-		Violet pink	Strong	Mn^{2+}	
			Mn^{2+}	398, 513, 585				
			Mn^{2+} replaces Mg^{2+}	651-655				
Talc	$Mg_3Si_4O_{10}(OH)_2$	Silicates	-	-	Yellowish-white	-	$_n[TiO_6]$ clusters, Mn^{2+}, O*	
			TiO_n (Ti^{4+} - Si^{4+})	520				
			$n.TiO_n$	550				
			Mn^{2+} replaces Mg^{2+}	600				
Cordierite	$(Mg,Fe)_2Al(Al_3Si_5O_{18})x(H_2O,CO_2)$	Silicates	-	-	Red	-	Cr^{3+}, Mn^{2+}	Doubtful fluorescence but it is cited
			Mn^{2+} replaces Mg^{2+}	640				
			Cr^{3+} replaces Al^{3+}	693				

Mineral	Formula	Family	Chemical alterations	Emmittance lines (nm) (major lines in bold)	Main emmitting colour	Intensity	Activators	Comments
Margarite	$CaAl_2XAl_2Si_2O_{10}(OH)_2$	Silicates	-	-	Blue	weak/strong		Some cite weak, some strong fluorescence
Sheelite	$CaWO_4$	Tungstates, Molybdates	-	-	Violet pink, Yellow, Bluish-white	v. weak/v.strong/v .strong	WO_4^{2-}, Sm^{3+} , Eu^{3+} , Dy^{3+} , Er^{3+} , Tb^{3+} , Pr^{3+}, MoO_4^{2-} , Nd^{3+} , Gd^{3+} , Yb^{3+}	can also exihibit Y-W and R hues
			Nd^{3+}	417				
			Tb^{3+}	414, 415, 436, 439, 458, 475, 488, **490**, **544**, 545, 590, **625**, 655, 675				
			Dy^{3+}	480, 488, 490, 575, 576, 663				
			Sm^{3+}	609, 647				
			Pr^{3+}	600, 607, 647, 649				
			Tm^{3+}	364, 452, 453, 700				
			Cr^{3+}	420-470				
			Er^{2+}	442				
			Er^{3+}	527, 545, 553, 615, 616				
			Ho^{3+}	543				
			WO_4^{2-}	425 - **435** (broad band), **460**, **465**, **480**, **505**				attributed to an intrinsic slight distortion of the $[WO_4]$ tetrahedra

Mineral	Formula	Family	Chemical alterations	Emmittance lines (nm) (major lines in bold)	Main emmitting colour	Intensity	Activators	Comments
			MoO_4^{2-}	560				Green emission due to $(MoO_4)^{2-}$(Tarashchan) or possibly Pb (Blasse).
Diamond	C	Native elements	-	-	Blue	Strong	N (nitrogen), B (boron)	Strong, B-W phosphorescence after exposure to sunlight
			A-band center	443-517, 452				A-band centre - neutral nearest-neighbour pair of nitrogen atoms substituting for the carbon atoms
			N3 centre	415, 428, 439, 442, 452, 507				N3 center - 3 nitrogen atoms surrounding a vacancy; defect produces characteristic absorption and luminescence line at 415 nm
			H3 centre	520				
			N	388.9				
			Dislocation	425, 439.7				
			S3 centre	519				
			Intrinsic	380-600, 507				
Sepiolite	$Mg_4Si_6O_{15}(OH)_2\ 6H_2O$	Silicates	-	-	Yellowish-white			
Palygorskite	$(Mg,Al)_4Si_8(O,OH,H_2O)_{26}\ 5H_2O$	Silicates	-	-	Yellowish-white			

Mineral	Formula	Family	Chemical alterations	Emmittance lines (nm) (major lines in bold)	Main emmitting colour	Intensity	Activators	Comments
Dolomite	$CaMg(CO_3)$	Carbonates	-	-	Yellowish-white		Organic impurities , Ce^{3+}, Sm^{3+}, Dy^{3+}, Tb^{3+}, Gd^{3+}, Mn^{2+}	B-W, P-W, O R, R , V P, P, G W, W, P-W, G-W, Y
			Mn^{2+}	650				
			Fe^{3+}	630-720				
			Ce^{3+}	370				
			Gd^{3+}	312				
			Tb^{3+}	480, 545				
			Dy^{3+}	500, 585				
			Sm^{3+}	560, 602, 645				
			$[CO]_n^*$ Intrinsic	410				
			?	475, 640, 670				
			Mn^{2+} replaces Ca^{2+}	**575**, 582, 660				
			Mn^{2+} replaces Mg^{2+}	**661**				
Magnesite	$MgCO_3$	Carbonates	-	-	Yellowish-white/Bluish-white		O*, Organic impurities , Mn^{2+}	
				660				
			O^*around $[CO_3]^*$	430				
			?	520				

Mineral	Formula	Family	Chemical alterations	Emmittance lines (nm) (major lines in bold)	Main emmitting colour	Intensity	Activators	Comments
Epsomite	$MgSO_4$ $7H_2O$	Sulfates	-	-	Yellowish-white/Blue	/weak		
Sulfur	S	Native elements	-	-	Greenish			DOUBTFULL FLUORESCENCE but cited by some authors
Brucite	$Mg(OH)_2$	Oxides and hydroxides	-	-	Bluish-white	weak		

Table A.1 Fluorescent minerals found in carbonaceous chondrites

Appendix C

The purpose of mineral analysis using the scanning electron microscope (SEM) was to establish the homogeneity of the mineral samples and to confirm their chemical composition.

The samples were imaged using backscatter and secondary electron imaging. Heavier atoms cause the angle of this backscatter to be higher, resulting in an increase in the intensity of these electrons detected. So, the intensity of the image will be related to the atomic mass of the atoms thus elucidating chemical composition and, therefore, heterogeneity in the sample. The bulk chemical composition, and any anomalies identified, were characterised using these electron backscatter electron diffraction patterns (Dijkstra, 2016).

Anorthite

Secondary electron (SE) images revealed a range of grain sizes from ~0.5 mm to tens of µm (Figure B.1, left) while electron backscatter electron diffraction (EBSD) bulk chemical composition analysis identified a single grain with an anomalous chemistry (Figure B.1, right, circled in yellow). A grain representative of the bulk sample (Figure B.2, left) was analysed and indicated the elemental composition expected for a sample of anorthite, as shown in the accompanying spectrum (Figure B.2, right). The single anomalous grain (Figure B.3, top) was analysed using EBSD and the spectrum generated revealed a higher concentration of iron and titanium (Figure B.3, bottom). Careful inspection of the images suggests the bright iron/titanium enriched band is likely a natural inclusion, vein or growth on the mineral grain. No other inclusions were observed so it was concluded that this was an isolated anomaly.

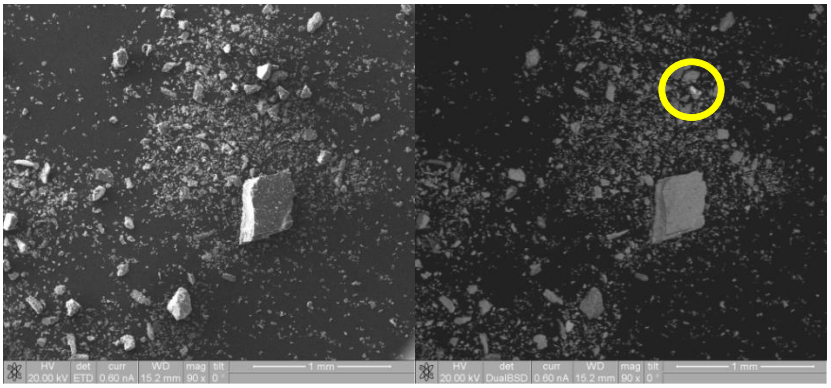

Figure C.1 Secondary electron (left) and EBSD (right) images representitive of the bulk sample of anorthite. Anomaly circled in yellow

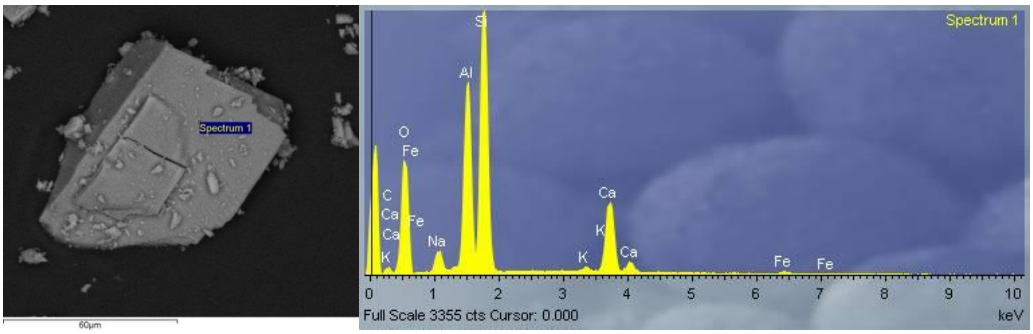

Figure C.2 Representative grain of the bulk sample (left) with spectrum indicating elemental composition expected for Anorthite

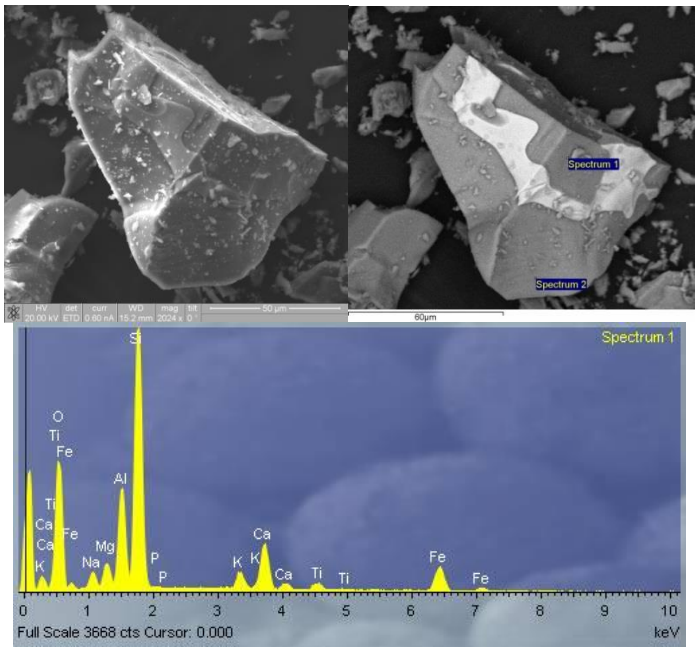

Figure C.3 Anomalous Anorthite grain (SE image, top left and EBSD image, top right) was analysed. The spectrum generated revealed a higher concentration of iron and titanium (bottom)

Calcite

Grain size of the pulverised calcite was more uniform, typically 0.1 mm or less as shown by the SE image (Figure B.4, top left) and EBSD did not reveal any anomalous chemical composition amongst the bulk sample (Figure B.4, top right). Analysis of a typical grain (Figure B.4, bottom left)

was shown to consist of only calcium carbonate with traces of iron and manganese present at concentrations less than 0.5% (Figure B.4, bottom right).

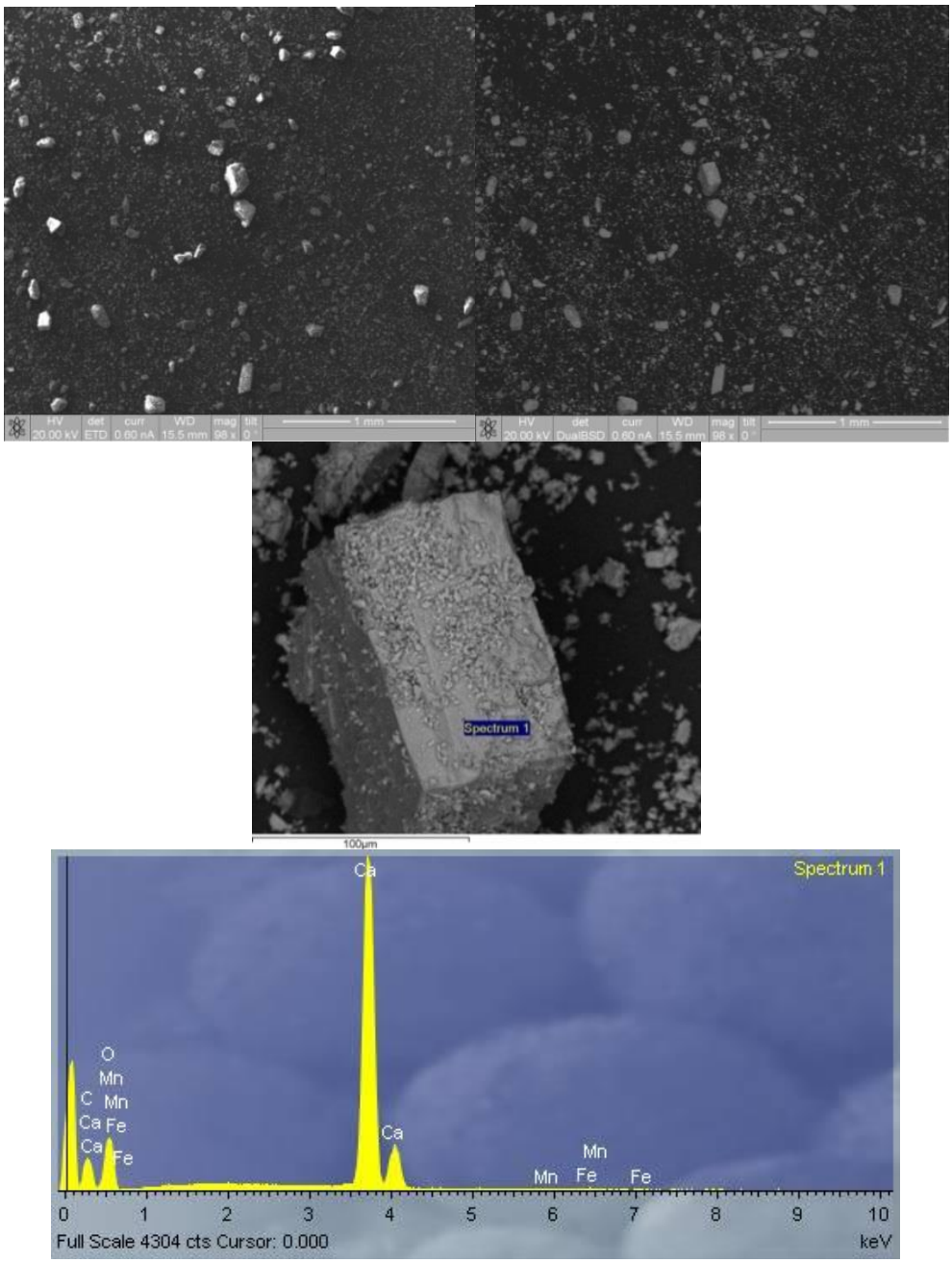

Figure C.4 SE image (top left) and EBSD image (top right) of calcite bulk sample, with no anomalous chemical composition. A typical grain (middle) spectrum (bottom) shows only calcium carbonate and traces of iron and manganese at less than 0.5%

Since calcite did appear to invoke a response when applied to the lanthanide sensors, the weathered solid sample was also analysed to determine if chemical composition had been altered. SE and EBSD images of the bulk composition (Figure B.5, top left and right, respectively) and analysis of individual grains revealed it had not been (Figure B.5, bottom left and right).

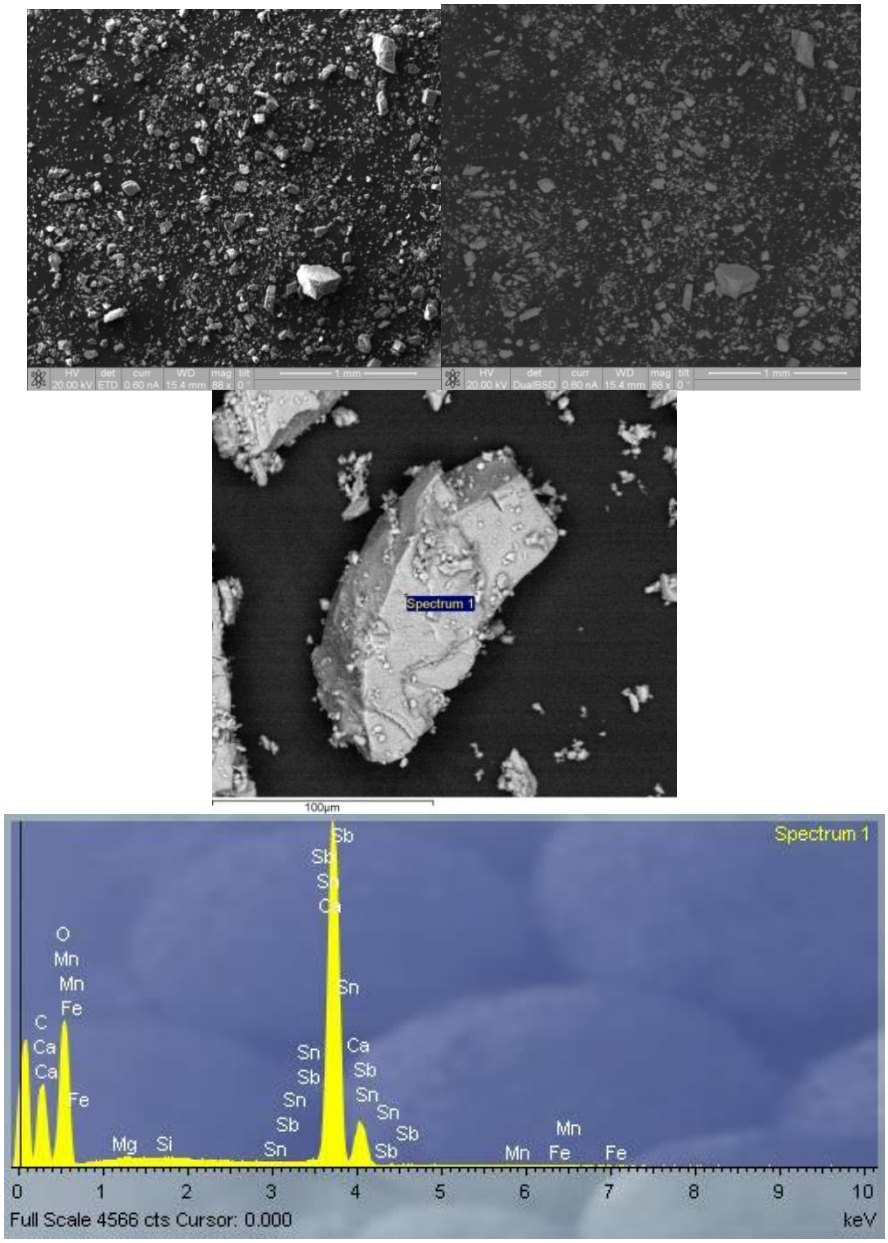

Figure C.5 SE image (top left) and EBSD image (top right) of weathered calcite bulk sample. Analysis of a typical grain (middle) shows no change in chemistry (spectrum, bottom)

Corundum

EBSD images of the bulk composition of corundum revealed some anomalies (Figure B.6, top right, circled in yellow). When individual grains were analysed, the bulk of the sample was shown to be pure aluminium oxide and traces of iron (the latter trace element imbues the corundum with its blue hue) (Figure B.6, middle left, and spectrum, middle right). The bright grains (e.g. Figure B.6, middle left) were revealed to be metal flakes rich in iron, chromium, nickel, and manganese (Figure B.6, spectrum, bottom); however, these grains were few and are likely extraneous contaminants rather than intrinsic to the mineral.

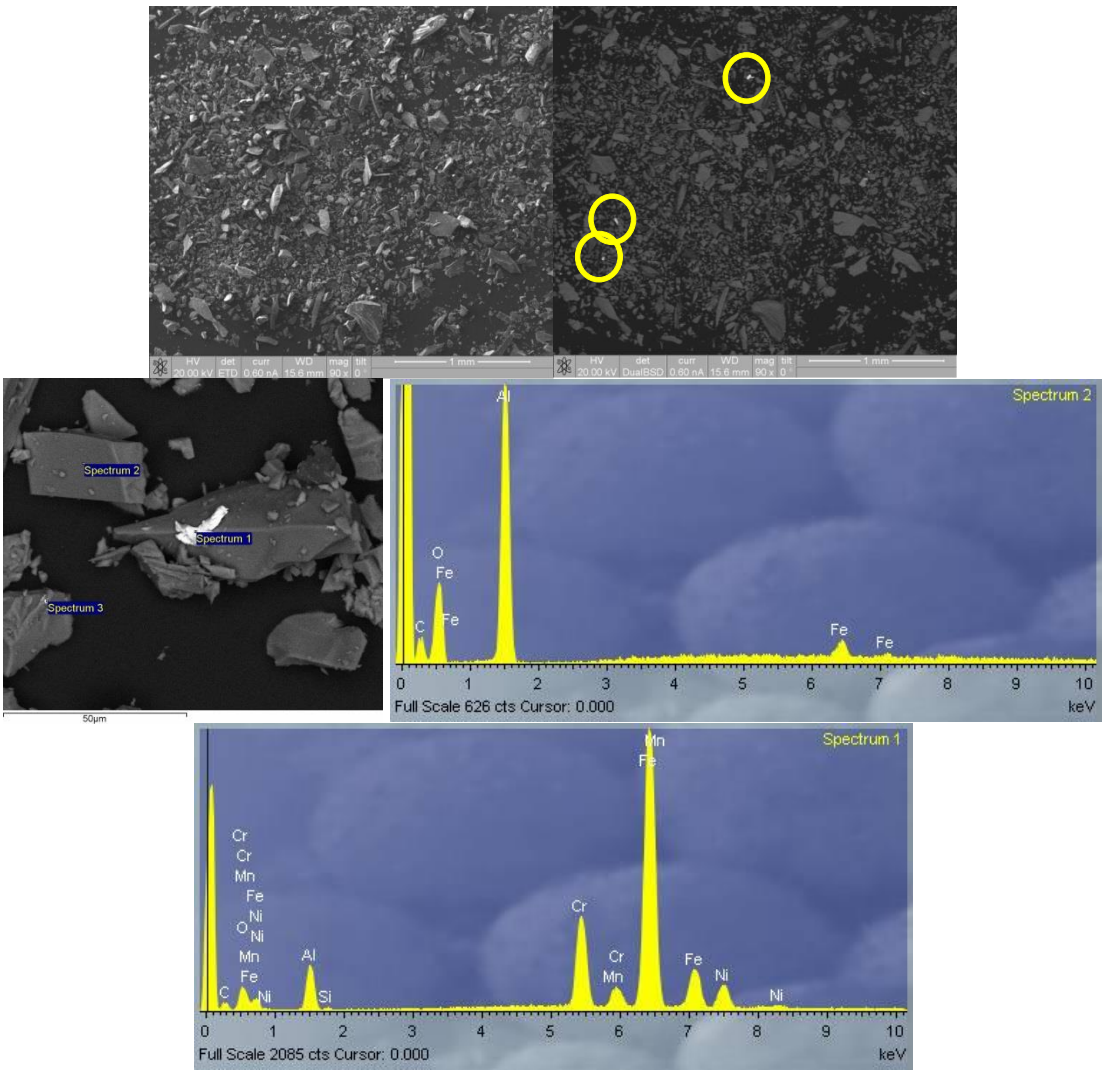

Figure C.6 An ES image (top left), and EBSD image, of the bulk composition of corundum revealing anomalies (top right, circled in yellow). Individual grain (middle left) analysis shows elemental composition (spectrum, middle right and bottom)

Diopside

Diopside is a magnesium calcium silicate mineral and is often found with some trace iron impurities. SE and EBSD analyses revealed that the Diopside sample was pure with no anomalies or contamination indicated (Figure B.7, top left and right, respectively), and individual grain analysis trace iron was indeed present and intrinsic to the chemical composition of the mineral (Figure B.7, bottom left and right, respectively).

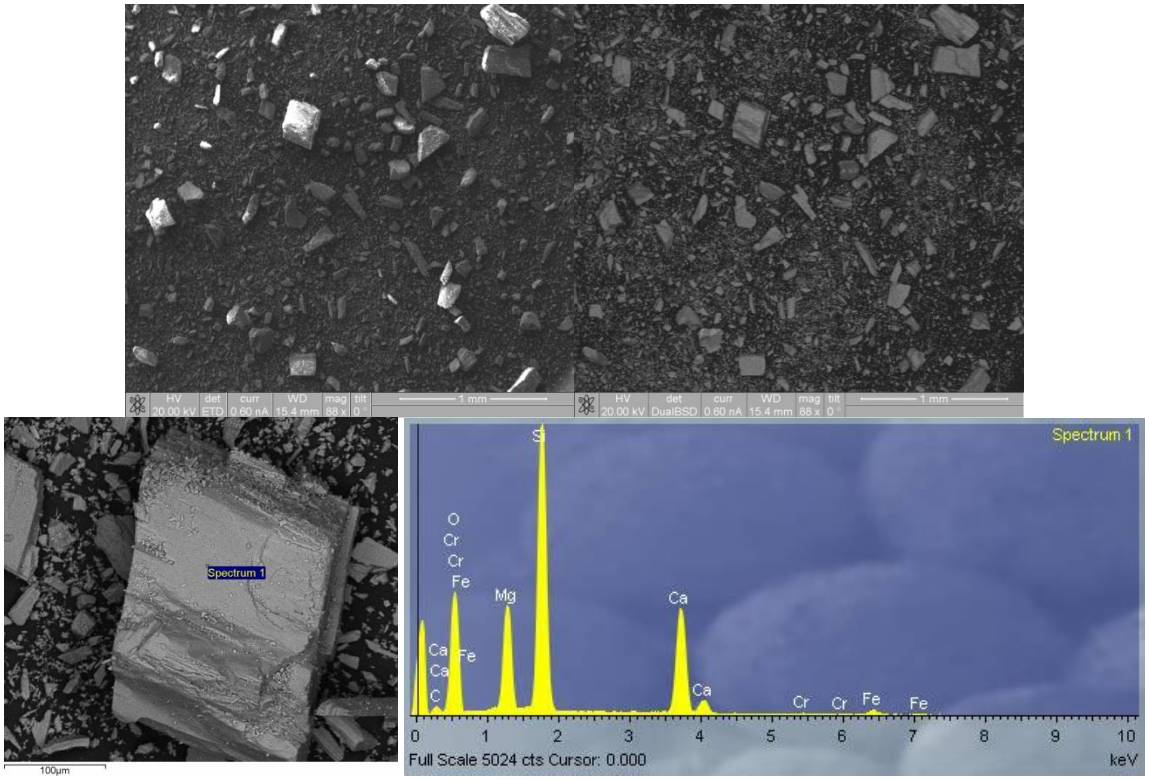

Figure C.7 ES (top left) and EBSD (top right) images of the bulk composition of diopside revealing no anomalies. Individual grain (bottom left) analysis shows elemental composition (spectrum, bottom right)

Enstatite

Images of the bulk sample produced by EBSD indicated a large amount of bright anomalies throughout the sample (Figure B.8, top right). Analysis of a typical selection of grains (Figure B.8, middle left) indicated that the cause of the bright grains are titanium and iron enriched estatite particles (Figure B.8, middle left) and, furthermore, individual grains are shown to consist of both iron enriched and iron depleted enstatite (Figure B.8, bottom left and right). This is not unexpected as estatite is often found with ‘significant iron impurities’.

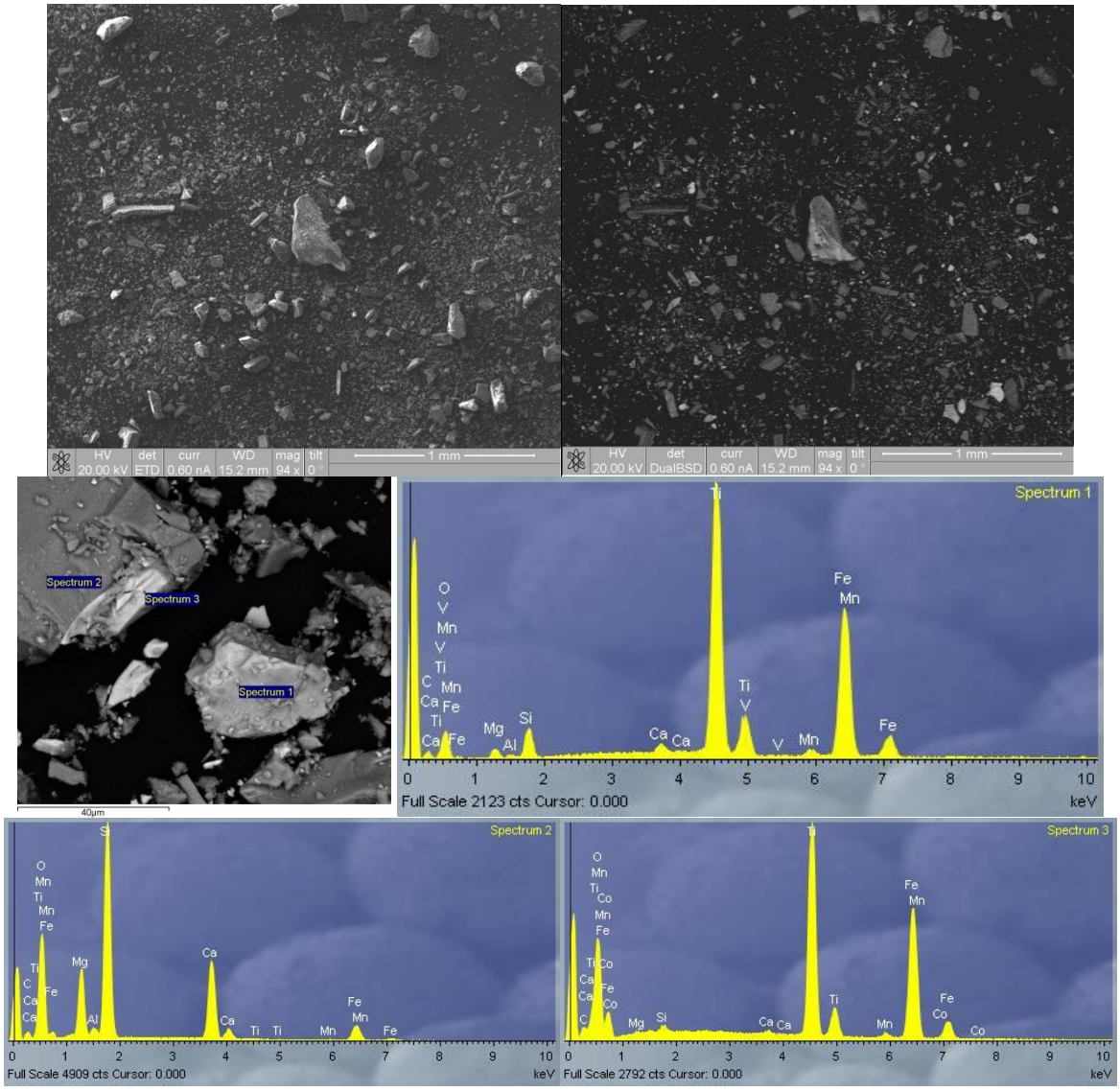

Figure C.8 Bulk Enstatite sample composition SE and EBSD images (top left and right) with individual grain point analyses (middle left) and associated spectra of chemical composition (middle right and bottom left and right)

Gypsum

The ES image revealed grain sizes of no more than ~0.1 mm (Figure B.9, top left) and the EBSD image indicated no anomalous chemical composition in the bulk sample (Figure B.9, top right). Gypsum is pure calcium sulfate, and upon individual grain analysis, this was confirmed to be the case for the entire bulk sample (Figure B.9, middle left and right). Since the appearance of the dried weathered sample had altered during the weathering process and some mass had been lost, the weathered sample was re-analysed. Although the appearance of the grains had become 'flakey', the bulk chemical composition had not been altered (Figure B.9, bottom left and right).

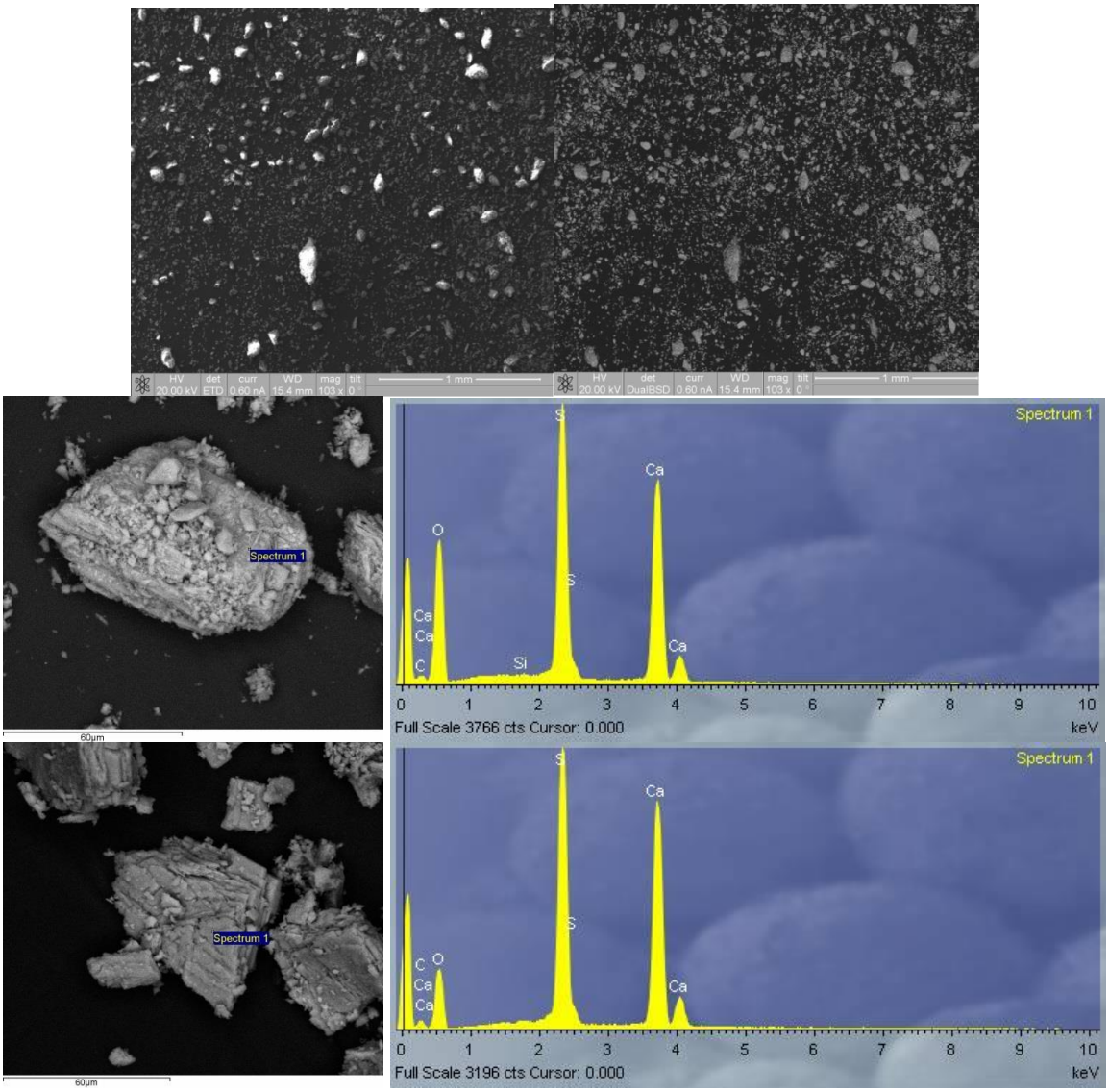

Figure C.9 ES (top left), and EBSD (top right) images, of the bulk composition of gypsum revealing no anomalies. Individual grain (middle left) analysis shows elemental composition (spectrum, middle right). Analysis of the weathered mineral indicates no change in composition (bottom left and right)

Olivine

The olivine sample used in this study is the San Carlos olivine standard which is magnesium rich ($Mg_{0.92}$, $Fe_{0.08}$); EBSD analysis confirms this homogenous bulk chemistry (Figure B.10, bottom left and right) and no anomalous signatures were detected throughout the sample (Figure B.10, top right). Addition of the weathered olivine solution to some lanthanide complex solutions did result in a sensor response; furthermore, although olivine itself is insoluble, it does react with water (see Section 5.3.3). It was therefore of interest to ascertain if weathering had altered the chemical composition of the mineral sample, and if this was the case, what ions may be present in the weathered mineral solution. EBSD analysis of the bulk weathered olivine sample revealed no

anomalies (Figure B.11, top right) and that the individual grain chemical composition had not been altered (Figure B.11 bottom left and right).

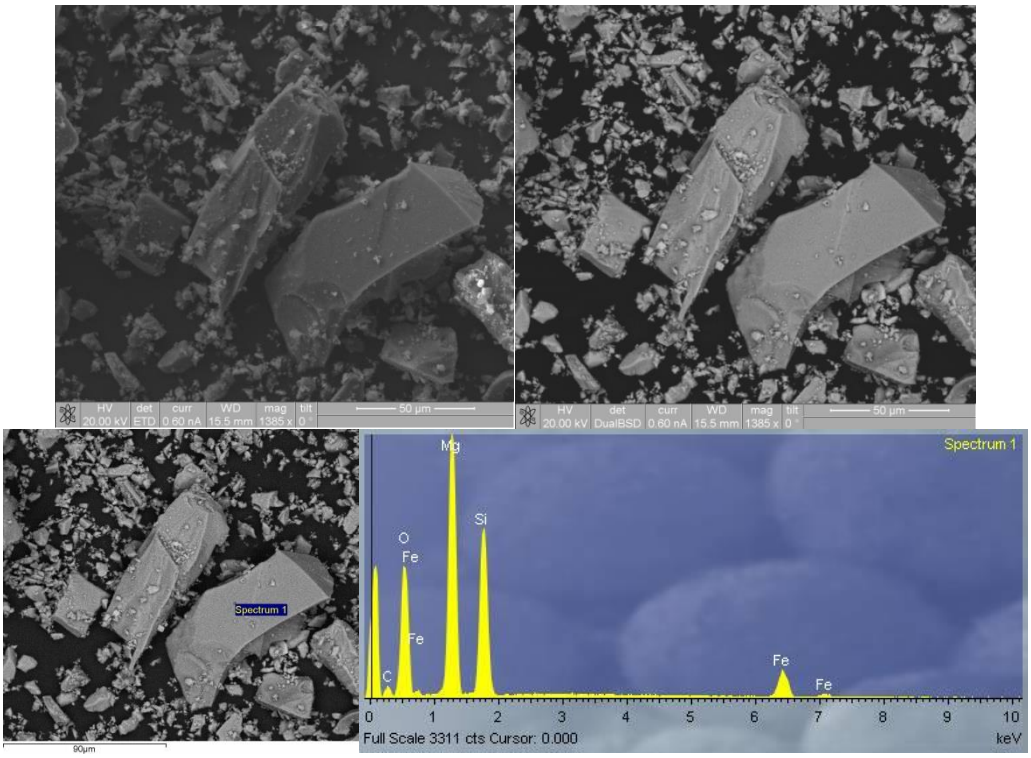

Figure C.10 EBSD of image of bulk sample (top left) indicates no anomalous signatures. EBSD grain analysis confirms expected San Carlos olivine chemical composition (bottom left and right)

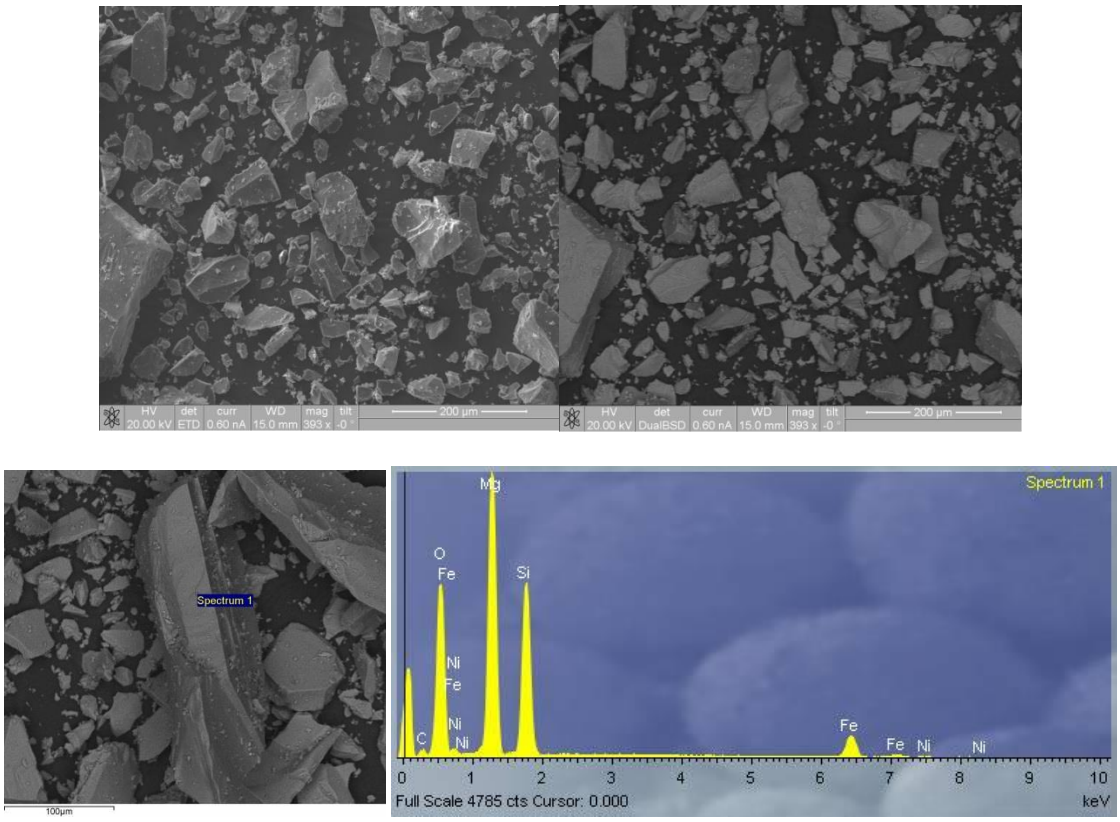

Figure C.11 EBSD analysis of the bulk weathered olivine sample reveals no anomalies (top right) and individual grain chemical composition has not been altered (bottom left and right)

Magnetite

Grain size was revealed to be no larger than ~0.2 mm by ES imaging (Figure B.12, top left) and EBSD images of the bulk sample revealed no anomalies, indicating a homogenous pure mineral sample (Figure 5. B.12, bottom left). EBSD analysis of a typical grain (Figure B.12, top left) confirmed the sample consisted of iron oxide, as is expected for magnetite (Figure B.12, bottom left).

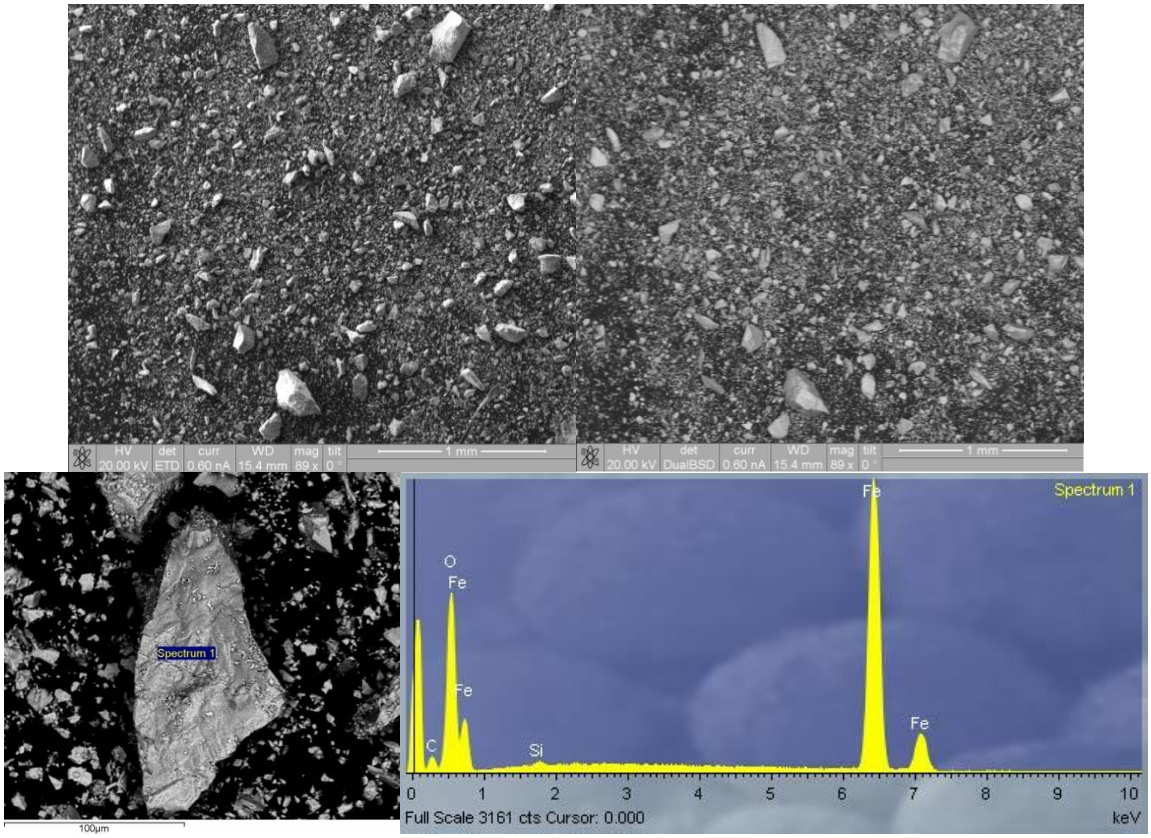

Figure C.12 ES and EBSD images of magnetite (top left and right). Point analysis of an individual grain (bottom left) and spectrum of chemical composition (bottom right)

Nepheline

Nepheline is a sodium potassium aluminium silicate. EBSD imaging of the bulk sample did not indicate any anomalies (Figure B.13, top right) and analysis of a typical grain (Figure B.13, bottom left) confirmed this, as indicated by the elemental spectrum of its composition (Figure B.13, bottom right). SE images of the bulk sample (Figure B.13, top left) indicate the largest grain sizes to be ~0.3 mm. It is reasonable, therefore to suggest that the mineral sample was homogenous.

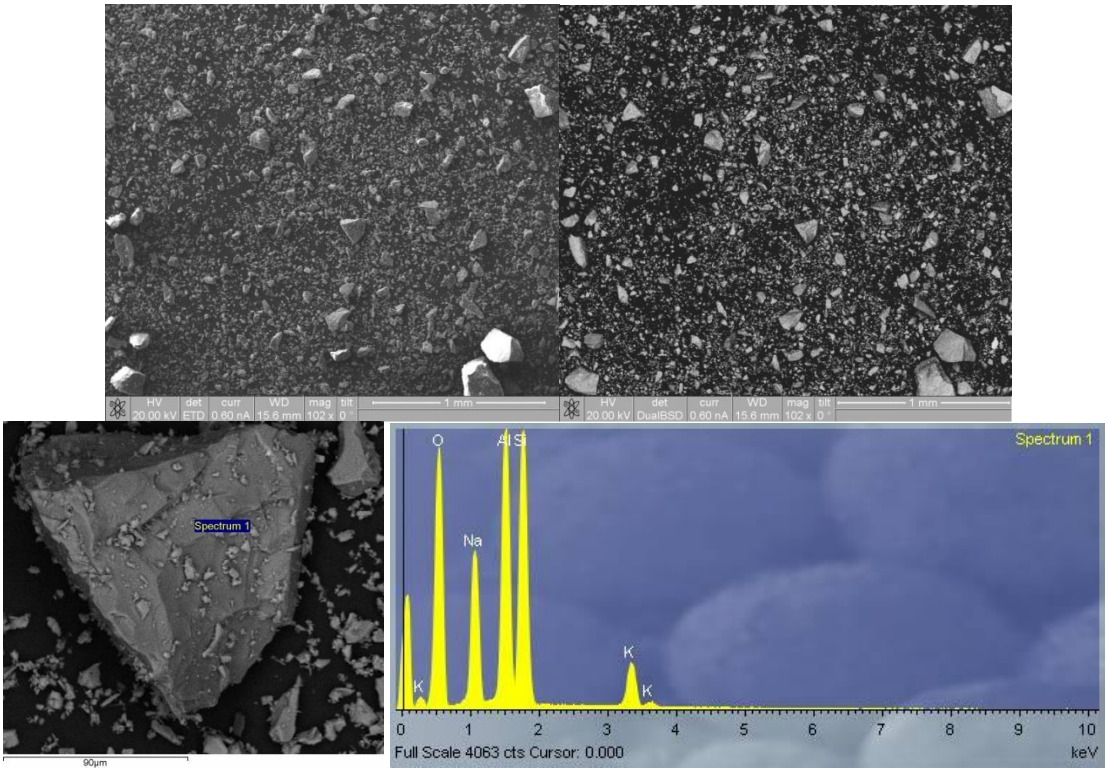

Figure C.13 EBSD of image of bulk sample (top left) indicates no anomalous signatures. EBSD grain analysis confirms homogeneity in the chemical composition of the nepheline sample (Figure 5.34, bottom left and right)

Appendix D

GCMS chromatograms showed substantial column bleed (e.g. Figures D.1, D.2 and D.3) and ion peaks for oganic material not expected to be components of extracts liberated from samples (e.g. ALH88045, Figure D.2). Figure D.3 is a chromatogram obtained from the quartz/feldspar blank (which does not contain organic material), which shows ion peaks indicating the presence of organics, suggesting these are originating from the column. These chromatograms are examples of those which lead to the conclusion that the data obtained are unreliable, inconclusive and of no qualitative value, and could not be used to identify with any certainty the constituents of the extracts. Therefore, literature references were used to suggest what an extract from GRS, ALH88045 and Murchison would contain.

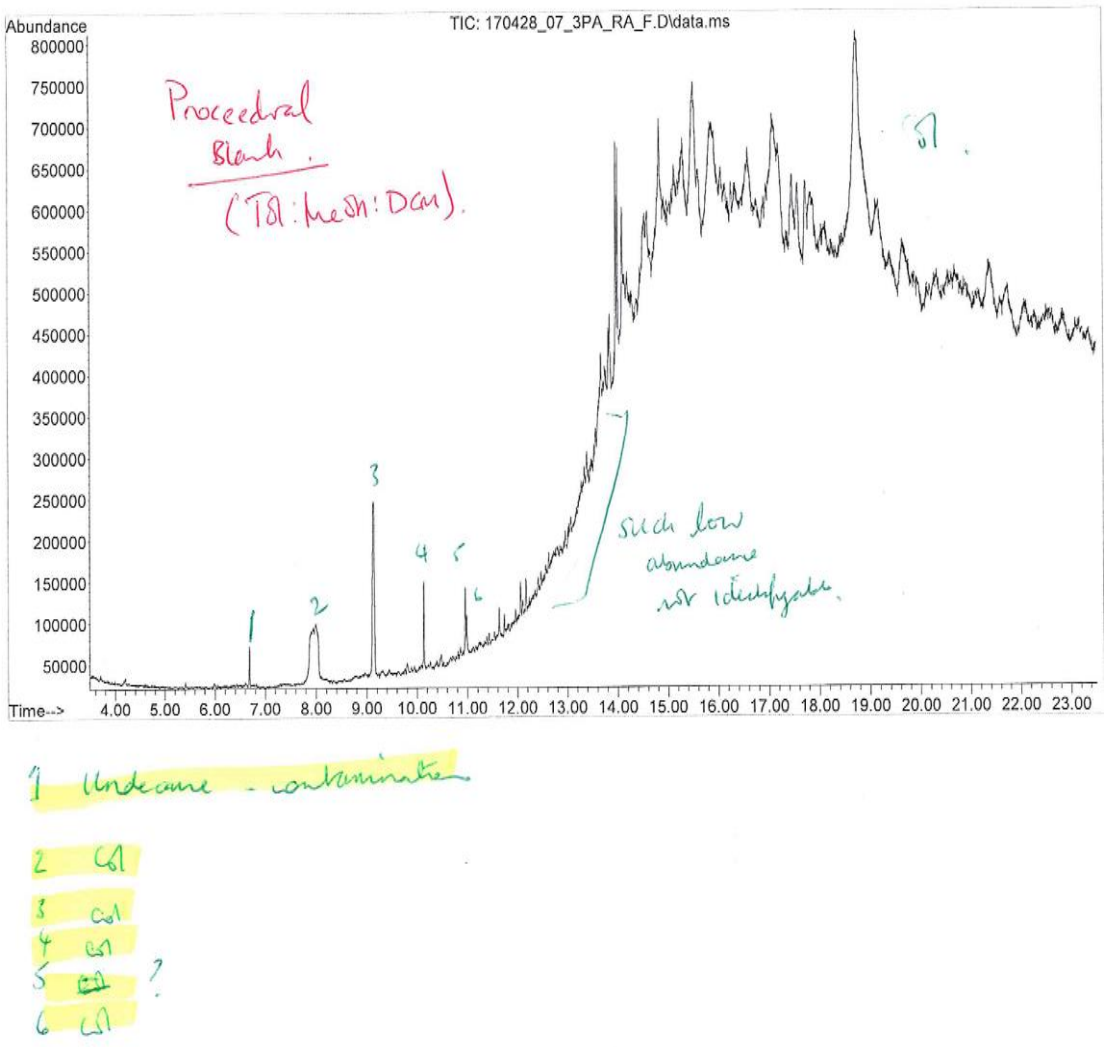

Figure D.1 GCMS chromatogram of the procedural blank indicating substantial column bleed of the siloxane stationary phase and indication of organic contamination from the column

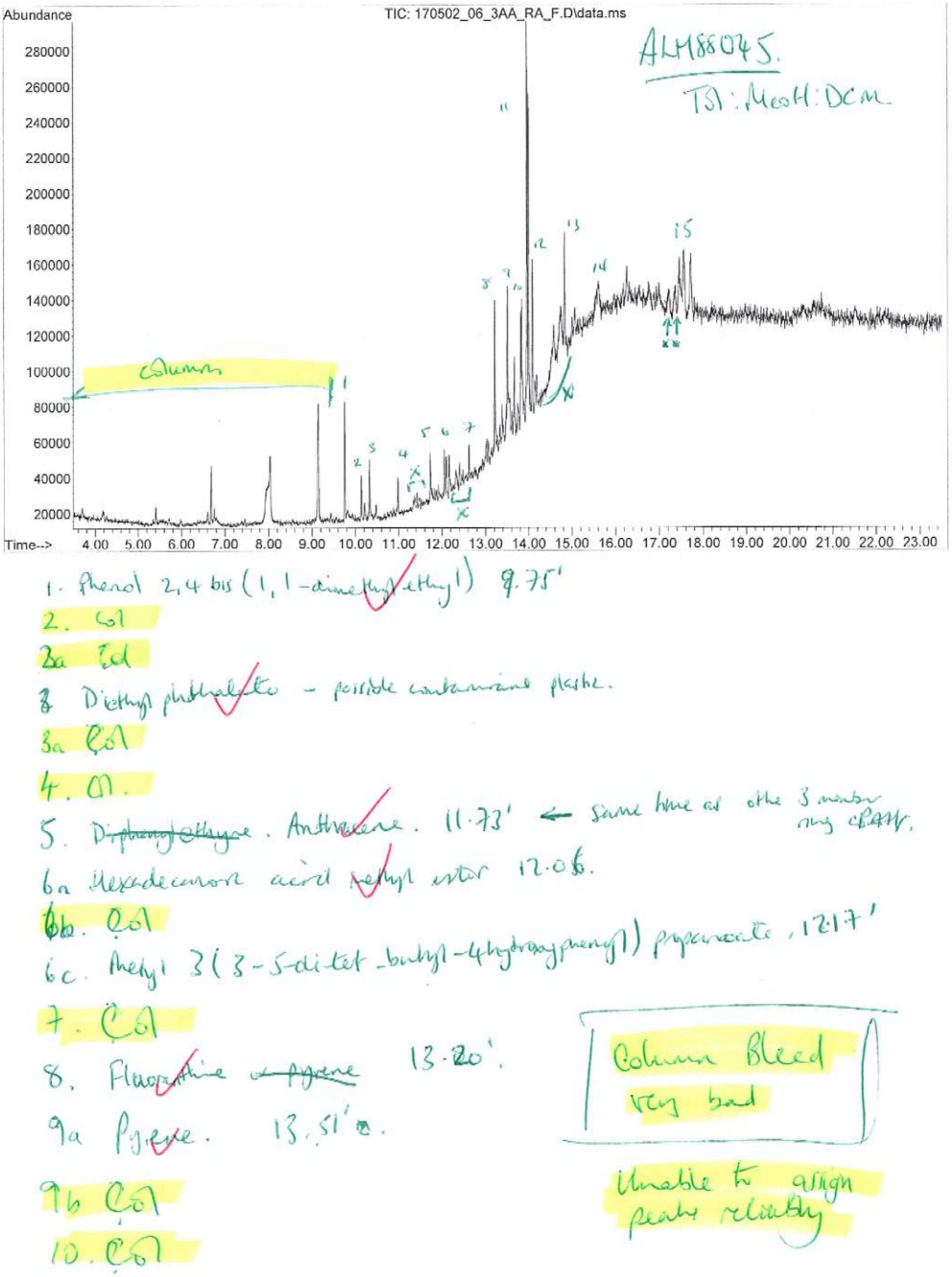

D.2 GCMS chromatogram indicating substantial column bleed and ion peaks representative of organic molecules not expected to be part of the expected organic inventory, which is suggestive of contamination from the column

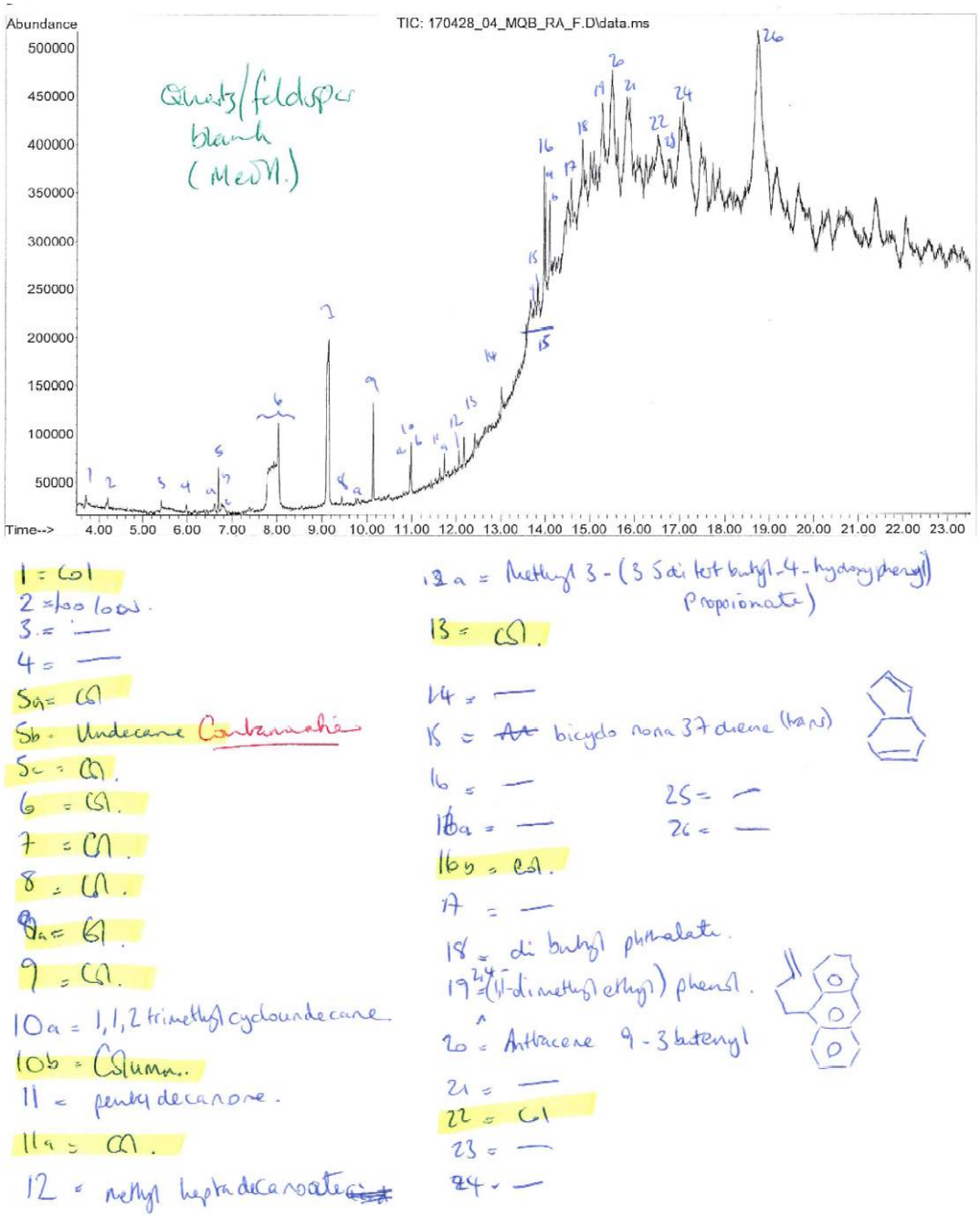

Figure D.3 GCMS chromatogram obtained from the quartz/feldspar blank (which does not contain organic material), ion peaks indicate the presence of organics, suggesting these are contaminants originating from the column, phthalates (likely from plastisiser contamination) and further substantial column bleed of siloxane stationary phase

References

Fluorescence and Phosphorescence [Online]. Available: http://www.physik.unibas.ch/Praktikum/VPII/Fluoreszenz/Fluorescence_and_Phosphorescence.pdf 2013].

ACHILLES, C., DOWNS, R., MING, D., RAMPE, E., MORRIS, R., TREIMAN, A., MORRISON, S., BLAKE, D., VANIMAN, D. & EWING, R. 2017. Mineralogy of an active eolian sediment from the Namib Dune, Gale Crater, Mars. Journal of Geophysical Research: Planets.

AERTS, J. W., RÖLING, W. F., ELSAESSER, A. & EHRENFREUND, P. 2014. Biota and biomolecules in extreme environments on earth: implications for life detection on Mars. Life, 4, 535-565.

AIME, S., BOTTA, M., FASANO, M. & TERRENO, E. 1998. Lanthanide (III) chelates for NMR biomedical applications. Chemical Society Reviews, 27, 19-29.

ALÉON, J. 2010. Multiple Origins of Nitrogen Isotopic Anomalies in Meteorites and Comets. The Astrophysical Journal, 722, 1342.

ALEXANDER, C. O. D., FOGEL, M., YABUTA, H. & CODY, G. 2007. The origin and evolution of chondrites recorded in the elemental and isotopic compositions of their macromolecular organic matter. Geochimica et Cosmochimica Acta, 71, 4380-4403.

ALEXANDER, C. O. D., CODY, G., DE GREGORIO, B., NITTLER, L. & STROUD, R. 2017. The nature, origin and modification of insoluble organic matter in chondrites, the major source of Earth's C and N. Chemie der Erde-Geochemistry.

ALLAMANDOLA, L. J., BERNSTEIN, M. P., SANDFORD, S. A. & WALKER, R. L. 1999. Evolution of interstellar ices. Space Science Reviews, 90, 219-232.

AMARI, S., LEWIS, R. S. & ANDERS, E. 1994. Interstellar grains in meteorites: I. Isolation of SiC, graphite and diamond; size distributions of SiC and graphite. Geochimica et Cosmochimica Acta, 58, 459-470.

ANDERS, D. & ROBINSON, W. 1971. Cycloalkane constituents of the bitumen from Green River Shale. Geochimica et Cosmochimica Acta, 35, 661-678.

ANDERS, E., HAYATSU, R. & STUDIER, M. H. 1973. Organic Compounds in Meteorites. Science, 182, 781-790.

ANDRE, P., WARD-THOMPSON, D. & BARSONY, M. 2000. From prestellar cores to protostars: the initial conditions of star formation. Protostars and Planets IV, 1, 59.

ANEESH, P. & JAYARAJ, M. 2010. Red luminescence from hydrothermally synthesized Eu-doped ZnO nanoparticles under visible excitation. Bulletin of Materials Science, 33, 227-231.

APONTE, J. C., DWORKIN, J. P. & ELSILA, J. E. 2014. Assessing the origins of aliphatic amines in the Murchison meteorite from their compound-specific carbon isotopic ratios and enantiomeric composition. Geochimica et Cosmochimica Acta, 141, 331-345.

ARMELAO, L., QUICI, S., BARIGELLETTI, F., ACCORSI, G., BOTTARO, G., CAVAZZINI, M. & TONDELLO, E. 2010. Design of luminescent lanthanide complexes: From molecules to highly efficient photo-emitting materials. Coordination Chemistry Reviews, 254, 487-505.

BANDURSKI, E. L. & NAGY, B. 1976. The polymer-like organic material in the Orgueil meteorite. Geochimica et Cosmochimica Acta, 40, 1397-1406.

BARBER, D. 1981. Matrix phyllosilicates and associated minerals in C2M carbonaceous chondrites. Geochimica et Cosmochimica Acta, 45, 945-970.

BARMARIN, G. 2009. Complete List of Luminescent Minerals [Online]. Available: http://www.fluomin.org/uk/list.php?liste=1 [Accessed October 2013 2013].

BARTHELMY, D. 1996. Mineralogy Database [Online]. Available: http://www.webmineral.com/ [Accessed October 2013 2013].

BARUCCI, M. & FULCHIGNONI, M. 2017. Major achievements of the Rosetta mission in connection with the origin of the solar system. The Astronomy and Astrophysics Review, 25, 3.

BECKER, R. H. & EPSTEIN, S. 1982. Carbon, hydrogen and nitrogen isotopes in solvent-extractable organic matter from carbonaceous chondrites. Geochimica et Cosmochimica Acta, 46, 97-103.

BEEBY, A., CLARKSON, I. M., DICKINS, R. S., FAULKNER, S., PARKER, D., ROYLE, L., DE SOUSA, A. S., WILLIAMS, J. G. & WOODS, M. 1999. Non-radiative deactivation of the excited states of europium, terbium and ytterbium complexes by proximate energy-matched OH, NH and CH oscillators: an improved luminescence method for establishing solution hydration states. Journal of the Chemical Society, Perkin Transactions 2, 493-504.

BELLOCHE, A., GARROD, R., MÜLLER, H., MENTEN, K., COMITO, C. & SCHILKE, P. 2009. Increased complexity in interstellar chemistry: detection and chemical modeling of ethyl formate and n-propyl cyanide in sagittarius B2 (N). Astronomy & Astrophysics, 499, 215-232.

BEREZIN, M. Y. & ACHILEFU, S. 2010. Fluorescence Lifetime Measurements and Biological Imaging. Chemical Reviews, 110, 2641-2684.

BERNSTEIN, M. P., SANDFORD, S. A., ALLAMANDOLA, L. J., CHANG, S. & SCHARBERG, M. A. 1995. Organic compounds produced by photolysis of realistic interstellar and cometary ice analogs containing methanol. The Astrophysical Journal, 454, 327.

BIRKS, J., CONTE, J. & WALKER, G. 1968. The fluorescence excitation spectra of aromatic liquids and solutions. Journal of Physics B: Atomic and Molecular Physics, 1, 934.

BIVER, N., BOCKELÉE-MORVAN, D., DEBOUT, V., CROVISIER, J., BOISSIER, J., LIS, D., RUSSO, N. D., MORENO, R., COLOM, P. & PAUBERT, G. 2014. Complex organic molecules in comets C/2012 F6 (Lemmon) and C/2013 R1 (Lovejoy): Detection of ethylene glycol and formamide. Astronomy & Astrophysics, 566, L5.

BLAKE, D., VANIMAN, D., ANDERSON, R., BISH, D., CHIPERA, S., CHEMTOB, S., CRISP, J., DESMARAIS, D., DOWNS, R. & FARMER, J. The CheMin mineralogical instrument on the Mars Science Laboratory mission. Lunar and Planetary Science Conference, 2009.

BLAND, P. A., CRESSEY,G., ALARD, O., ROGERS, N. W., FORDER, S. D., GOUNELLE, M. 2002. Modal Mineralogy of Carbonaceous Chondrites and chemical variations in Chondrite Matrix. Lunar and Planetary Science XXXIII.

BLAND, P. A., JACKSON, M. D., COKER, R. F., COHEN, B. A., WEBBER, J. B. W., LEE, M. R., DUFFY, C. M., CHATER, R. J., ARDAKANI, M. G. & MCPHAIL, D. S. 2009. Why aqueous alteration in asteroids was isochemical: High porosity≠ high permeability. Earth and Planetary Science Letters, 287, 559-568.

BOCK, E. 1961. ON THE SOLUBILITY OF ANHYDROUS CALCIUM SULPHATE AND OF GYPSUM IN CONCENTRATED SOLUTIONS OF SODIUM CHLORIDE AT 25 °C, 30 °C, 40 °C, AND 50 °C. Canadian Journal of Chemistry, 39, 1746-1751.

BOSS, A. P. 1998. Temperatures in protoplanetary disks. Annual Review of Earth and Planetary Sciences, 26, 53-80.

BOSS, A. P. & GOSWAMI, J. N. 2006. Presolar cloud collapse and the formation and early evolution of the solar nebula. Meteorites and the early solar system II, 171-186.

BOTTA, O. & BADA, J. 2002. Extraterrestrial Organic Compounds in Meteorites. Surveys in Geophysics, 23, 411-467.

BOTTA, O., GLAVIN, D. P., KMINEK, G. & BADA, J. L. 2002. Relative amino acid concentrations as a signature for parent body processes of carbonaceous chondrites. Origins of Life and Evolution of Biospheres, 32, 143-163.

BOTTA, O., MARTINS, Z. & EHRENFREUND, P. 2007. Amino acids in Antarctic CM1 meteorites and their relationship to other carbonaceous chondrites. Meteoritics & Planetary Science, 42, 81-92.

BRAMALL, N. & ALLAMANDOLA, L. 2012. Native Fluorescence for the Detection of Organics. LPI Contributions, 1679, 4299.

BRANDENBURG, C. & LATHAM, D. 1968. Spectroscopic identification of basic nitrogen compounds in Wilmington petroleum. Journal of Chemical & Engineering Data, 13, 391-394.

BRASLAVSKY, S. E. 2007. Glossary of terms used in photochemistry, (IUPAC Recommendations 2006). Pure and Applied Chemistry, 79, 293-465.

BREARLEY, A. J. & JONES, R. H. 1998. Chondritic meteorites. Reviews in mineralogy and geochemistry, 36, 3.1-3.398.

BREARLEY, A. J. Heterogeneous distribution of carbonaceous material in Murchison matrix: In situ observations using energy filtered transmission electron microscopy. Lunar and Planetary Science Conference, 2002. 1388.

BREARLEY, A. J. 2006. The action of water. Meteorites and the early solar system II, 943, 587-624.

BRIGGS, M. H. 1961. Organic constituents of meteorites. Nature, 191, 1137-1140.

BROWN, P. D. & MILLAR, T. 1989. Models of the gas–grain interaction–deuterium chemistry. Monthly Notices of the Royal Astronomical Society, 237, 661-671.

BROWN, P. G., HILDEBRAND, A. R., ZOLENSKY, M. E., GRADY, M., CLAYTON, R. N., MAYEDA, T. K., TAGLIAFERRI, E., SPALDING, R., MACRAE, N. D., HOFFMAN, E. L., MITTLEFEHLDT, D. W., WACKER, J. F., BIRD, J. A., CAMPBELL, M. D., CARPENTER, R., GINGERICH, H., GLATIOTIS, M., GREINER, E., MAZUR, M. J., PHIL, J. A. M., PLOTKIN, H. & MAZUR, T. R. 2000. The Fall, Recovery, Orbit, and Composition of the Tagish Lake Meteorite: A New Type of Carbonaceous Chondrite. Science, 290, 320-325.

BRUCE, J. I., DICKINS, R. S., GOVENLOCK, L. J., GUNNLAUGSSON, T., LOPINSKI, S., LOWE, M. P., PARKER, D., PEACOCK, R. D., PERRY, J. J. B., AIME, S. & BOTTA, M. 2000. The Selectivity of Reversible Oxy-Anion Binding in Aqueous Solution at a Chiral Europium and Terbium Center: Signaling of Carbonate Chelation by Changes in the Form and Circular Polarization of Luminescence Emission. Journal of the American Chemical Society, 122, 9674-9684.

BRUCE, J. I., LOWE, M. P., PARKER, D. 2001. Photophysical aspects of lanthanide (III) complexes.

BÜNZLI, J.-C. G. & ELISEEVA, S. V. 2011. Basics of lanthanide photophysics. Lanthanide Luminescence. Springer.

BURLINGAME, A., HAUG, P., BELSKY, T. & CALVIN, M. 1965. Occurrence of biogenic steranes and pentacyclic triterpanes in an Eocene shale (52 million years) and in an early Precambrian shale (2.7 billion years): A preliminary report. Proceedings of the National Academy of Sciences, 54, 1406-1412.

BURTON, A. S., STERN, J. C., ELSILA, J. E., GLAVIN, D. P. & DWORKIN, J. P. 2012. Understanding prebiotic chemistry through the analysis of extraterrestrial amino acids and nucleobases in meteorites. Chemical Society Reviews, 41, 5459-5472.

BURTON, A. S., GLAVIN, D. P., ELSILA, J. E., DWORKIN, J. P., JENNISKENS, P. & YIN, Q.-Z. 2014. The amino acid composition of the Sutter's Mill CM2 carbonaceous chondrite. Meteoritics & Planetary Science, 49, 2074-2086.

BUSEMANN, H., YOUNG, A. F., CONEL, M. O. D. A., HOPPE, P., MUKHOPADHYAY, S. & NITTLER, L. R. 2006. Interstellar Chemistry Recorded in Organic Matter from Primitive Meteorites. Science, 312, 727-730.

BUTLER, S. J. & PARKER, D. 2013. Anion binding in water at lanthanide centres: from structure and selectivity to signalling and sensing. Chemical Society Reviews, 42, 1652-1666.

BUTTERWORTH, A. L., ABALLAIN, O., CHAPPELLAZ, J. & SEPHTON, M. A. 2004. Combined element (H and C) stable isotope ratios of methane in carbonaceous chondrites. Monthly Notices of the Royal Astronomical Society, 347, 807-812.

CAFFERTY, B. J., FIALHO, D. M., KHANAM, J., KRISHNAMURTHY, R. & HUD, N. V. 2016. Spontaneous formation and base pairing of plausible prebiotic nucleotides in water. Nature communications, 7.

CALLAHAN, M. P., SMITH, K. E., CLEAVES, H. J., RUZICKA, J., STERN, J. C., GLAVIN, D. P., HOUSE, C. H. & DWORKIN, J. P. 2011. Carbonaceous meteorites contain a wide range of extraterrestrial nucleobases. Proceedings of the National Academy of Sciences, 108, 13995-13998.

CALLAHAN, M. P., MARTIN, M. G., BURTON, A. S., GLAVIN, D. P. & DWORKIN, J. P. 2014. Amino acid analysis in micrograms of meteorite sample by nanoliquid chromatography–high-resolution mass spectrometry. Journal of Chromatography A, 1332, 30-34.

CAMERON, A., G. W. 1955. Origin of anomalous abundances of the elements in giant stars. The Astrophysical Journal, 121, 144.

CAMI, J., BERNARD-SALAS, J., PEETERS, E. & MALEK, S. E. 2010. Detection of C_{60} and C_{70} in a Young Planetary Nebula. Science, 1180-1182.

CARAVAN, P., ELLISON, J. J., MCMURRY, T. J. & LAUFFER, R. B. 1999. Gadolinium(III) Chelates as MRI Contrast Agents: Structure, Dynamics, and Applications. Chemical Reviews, 99, 2293-2352.

CHAN, H. S., MARTINS, Z. & SEPHTON, M. A. 2012. Amino acid analyses of type 3 chondrites Colony, Ornans, Chainpur, and Bishunpur. Meteoritics & Planetary Science, 47, 1502-1516.

CHAN, Q. H. S., CHIKARAISHI, Y., TAKANO, Y., OGAWA, N. O. & OHKOUCHI, N. 2016. Amino acid compositions in heated carbonaceous chondrites and their compound-specific nitrogen isotopic ratios. Earth, Planets and Space, 68, 7.

CHAN, Q., ZOLENSKY, M., KEBUKWA, Y., FRIES, M. & STEELE, A. 2017. Organic Matter in Extraterrestrial Water-Bearing Salt Crystals.

CHANG, Y.-S., LIN, H.-J., LI, Y.-C., CHAI, Y.-L. & TSAI, Y.-Y. 2007. Synthesis and luminescent properties of Tb3+-activated yttrium indium germanate phosphor. Journal of Solid State Chemistry, 180, 3076-3081.

CIESLA, F. J. 2007. Outward transport of high-temperature materials around the midplane of the solar nebula. science, 318, 613-615.

CIESLA, F. J. & SANDFORD, S. A. 2012. Organic synthesis via irradiation and warming of ice grains in the solar nebula. Science, 1217291.

CLEAVES, H. J. I., SCOTT, A. M., HILL, F. C., LESZCZYNSKI, J., SAHAI, N. & HAZEN, R. 2012. Mineral-organic interfacial processes: potential roles in the origins of life. Chemical Society Reviews, 41, 5502-5525.

CLEMETT, S., MESSENGER, S., THOMAS-KEPRTA, K., WENTWORTH, S., ROBINSON, G. & MCKAY, D. Spatially resolved analysis of amines using a fluorescence molecular probe: molecular analysis of IDPs. Lunar and Planetary Institute Science Conference Abstracts, 2002. 1898.

CLOUTIS, E. A., HUDON, P., HIROI, T., GAFFEY, M. J. & MANN, P. 2011. Spectral reflectance properties of carbonaceous chondrites: 2. CM chondrites. Icarus, 216, 309-346.

CODY, G. D., ALEXANDER, C. M. O. D. & TERA, F. 2002. Solid-state (1H and 13C) nuclear magnetic resonance spectroscopy of insoluble organic residue in the Murchison meteorite: a self-consistent quantitative analysis. Geochimica et Cosmochimica Acta, 66, 1851-1865.

COLLINS, M. J., BISHOP, A. N. & FARRIMOND, P. 1995. Sorption by mineral surfaces: Rebirth of the classical condensation pathway for kerogen formation? Geochimica et Cosmochimica Acta, 59, 2387-2391.

CONNALLY, R.E., VEAL, D. & PIPER, J.A., 2004. Flash lamp-excited time-resolved fluorescence microscope suppresses autofluorescence in water concentrates to deliver an 11-fold increase in signal-to-noise ratio. *Journal of biomedical optics*, *9*(4), pp.725-735.

COOPER, G. W. & CRONIN, J. R. 1995. Linear and cyclic aliphatic carboxamides of the Murchison meteorite: Hydrolyzable derivatives of amino acids and other carboxylic acids. Geochimica et Cosmochimica Acta, 59, 1003-1015.

COOPER, G., KIMMICH, N., BELISLE, W., SARINANA, J., BRABHAM, K. & GARREL, L. 2001. Carbonaceous meteorites as a source of sugar-related organic compounds for the early Earth. Nature, 414, 879-883.

COOPER, G., REED, C., NGUYEN, D., CARTER, M. & WANG, Y. 2011. Detection and formation scenario of citric acid, pyruvic acid, and other possible metabolism precursors in carbonaceous meteorites. Proceedings of the National Academy of Sciences, 108, 14015-14020.

COTTON, A. F., WILKINSON, G., BOCHMANN, M. & MURILLO, C. A. 1999. Advanced inorganic chemistry, Wiley.

CRONIN, J. 1976. Acid-labile amino acid precursors in the Murchison meteorite. Origins of life, 7, 337-342.

CRONIN, J. R. & HARE, P. E. 1977. Chromatographic analysis of amino acids and primary amines with o-phthalaldehyde detection. Analytical Biochemistry, 81, 151-156.

CRONIN, J. R., GANDY, W. E. & PIZZARELLO, S. 1981. Amino acids of the murchison meteorite. Journal of Molecular Evolution, 17, 265-272.

CRONIN, J. R. & PIZZARELLO, S. 1983. Amino acids in meteorites. Advances in Space Research, 3, 5-18.

CRONIN, J. R., PIZZARELLO, S. & YUEN, G. U. 1985. Amino acids of the Murchison meteorite: II. Five carbon acyclic primary β-, γ-, and δ-amino alkanoic acids. Geochimica et Cosmochimica Acta, 49, 2259-2265.

CRONIN, J. R. & PIZZARELLO, S. 1986. Amino acids of the Murchison meteorite. III. Seven carbon acyclic primary α-amino alkanoic acids1. Geochimica et Cosmochimica Acta, 50, 2419-2427.

CRONIN, J. R., PIZZARELLO, S. & CRUIKSHANK, D. P. 1988. Organic matter in carbonaceous chondrites, planetary satellites, asteroids and comets. Meteorites and the early solar system, 819-857.

CRONIN, J. & CHANG, S. 1993. Organic Matter in Meteorites: Molecular and Isotopic Analyses of the Murchison Meteorite. In: GREENBERG, J. M., MENDOZA-GÓMEZ, C. X. & PIRRONELLO, V. (eds.) The Chemistry of Life's Origins. Springer Netherlands.

CRONIN, J. R., PIZZARELLO, S., EPSTEIN, S. & KRISHNAMURTHY, R. V. 1993. Molecular and isotopic analyses of the hydroxy acids, dicarboxylic acids, and hydroxydicarboxylic acids of the Murchison meteorite. Geochimica et Cosmochimica Acta, 57, 4745-4752.

CRONIN, J. R. & PIZZARELLO, S. 1997. Enantiomeric Excesses in Meteoritic Amino Acids. Science, 275, 951-955.

DARTNELL, L. R., STORRIE-LOMBARDI, M. C. & WARD, J. M. 2010. Complete fluorescent fingerprints of extremophilic and photosynthetic microbes. International Journal of Astrobiology, 9, 245-257.

DARTNELL, L. R., PATEL, M. R., STORRIE-LOMBARDI, M. C., WARD, J. M. & MULLER, J.-P. 2012. Experimental determination of photostability and fluorescence-based detection of PAHs on the Martian surface. Meteoritics & Planetary Science, 47, 806-819.

DE MESQUITA, M. E., DE SÁ, G. F. & MALTA, O. L. 1997. Spectroscopic studies of the Eu(III) and Gd(III) tris(3-aminopyridine-2-carboxylic acid) complexes. Journal of Alloys and Compounds, 250, 417-421.

DE SANCTIS, M., AMMANNITO, E., MCSWEEN, H., RAPONI, A., MARCHI, S., CAPACCIONI, F., CAPRIA, M., CARROZZO, F., CIARNIELLO, M. & FONTE, S. 2017. Localized aliphatic organic material on the surface of Ceres. Science, 355, 719-722.

DEAMER, D. W. & PASHLEY, R. 1989. Amphiphilic components of the Murchison carbonaceous chondrite: surface properties and membrane formation. Origins of Life and Evolution of the Biosphere, 19, 21-38.

DELGADO, R., FELIX, V., LIMA, L. M. P. & PRICE, D. W. 2007. Metal complexes of cyclen and cyclam derivatives useful for medical applications: a discussion based on thermodynamic stability constants and structural data. Dalton Transactions, 2734-2745.

DENNISON, J. E., LINGNER, D. W. & LIPSCHUTZ, M. E. 1986. Antarctic and non-Antarctic meteorites form different populations. Nature, 319, 390.

DERENNE, S. & ROBERT, F. 2010. Model of molecular structure of the insoluble organic matter isolated from Murchison meteorite. Meteoritics & Planetary Science, 45, 1461-1475.

DESAI, R., COATES, A., WELLBROCK, A., VUITTON, V., CRARY, F., GONZÁLEZ-CANIULEF, D., SHEBANITS, O., JONES, G., LEWIS, G. & WAITE, J. 2017. Carbon Chain Anions and the Growth of Complex Organic Molecules in Titan's Ionosphere. The Astrophysical Journal Letters, 844, L18.

DICKINS, R. S., PARKER, D., I. BRUCE, J. & J. TOZER, D. 2003. Correlation of optical and NMR spectral information with coordination variation for axially symmetric macrocyclic Eu(iii) and Yb(iii) complexes: axial donor polarisability determines ligand field and cation donor preference. Dalton Transactions, 1264-1271.

DOOSE, S., NEUWEILER, H. & SAUER, M. 2009. Fluorescence quenching by photoinduced electron transfer: a reporter for conformational dynamics of macromolecules. ChemPhysChem, 10, 1389-1398.

DYNI, J. R. 2003. Geology and resources of some world oil-shale deposits. Oil shale, 20, 193-253.

EHRENFREUND, P. & CHARNLEY, S. B. 2000. Organic molecules in the interstellar medium, comets, and meteorites: a voyage from dark clouds to the early Earth. Annual Review of Astronomy and Astrophysics, 38, 427-483.

ENGEL, M. H. & NAGY, B. 1982. Distribution and enantiomeric composition of amino acids in the Murchison meteorite. Nature, 296, 837-840.

ENGEL, M. H. & MACKO, S. 1997. Isotopic evidence for extraterrestrial non-racemic amino acids in the Murchison meteorite. Nature, 389, 265-268.

FAULKNER, S., POPE, S. J. & BURTON-PYE, B. P. 2005. Lanthanide complexes for luminescence imaging applications. Applied Spectroscopy Reviews, 40, 1-31.

FERRO, S. & DE BATTISTI, A. 2002. Electrochemistry of the aqueous europium(III)/europium(II) redox couple at conductive diamond electrodes. Journal of Electroanalytical Chemistry, 533, 177-180.

FITCH, F., SCHWARCZ, H. P. & ANDERS, E. 1962. 'Organized elements' in carbonaceous chondrites.

FLYNN, G. J., WIRICK, S. & KELLER, L. P. 2013. Organic grain coatings in primitive interplanetary dust particles: Implications for grain sticking in the Solar Nebula. Earth, Planets and Space, 65, 13.

FOLSOME, C. E., LAWLESS, J., ROMIEZ, M. & PONNAMPERUMA, C. 1971. Heterocyclic Compounds indigenous to the Murchison Meteorite. Nature, 232, 108-109.

FOLSOME, C. E., LAWLESS, J. G., ROMIEZ, M. & PONNAAMPERUMA, C. 1973. Heterocyclic compounds recovered from carbonaceous chondrites. Geochimica et Cosmochimica Acta, 37, 455-465.

FOOTE, K. G. & MACLENNAN, D. N. 1984. Comparison of copper and tungsten carbide calibration spheres. The Journal of the Acoustical Society of America, 75, 612-616.

FU, J., WANG, L., CHEN, H., BO, L., ZHOU, C. & CHEN, J. 2010. A selective fluorescence probe for mercury ion based on the fluorescence quenching of terbium(III)-doped cadmium sulfide composite nanoparticles. Spectrochimica Acta Part A: Molecular and Biomolecular Spectroscopy, 77, 625-629.

FUCHS, L. H., OLSEN, E. & JENSEN, K. J. 1973. Mineralogy, mineral-chemistry, and composition of the Murchison (C2) meteorite.

GARROD, R. & HERBST, E. 2006. Formation of methyl formate and other organic species in the warm-up phase of hot molecular cores. Astronomy & Astrophysics, 457, 927-936.

GIELEN, C., CAMI, J., BOUWMAN, J., PEETERS, E. & MIN, M. 2011. Carbonaceous molecules in the oxygen-rich circumstellar environment of binary post-AGB stars-C60 fullerenes and polycyclic aromatic hydrocarbons. Astronomy & Astrophysics, 536, A54.

GLAVIN, D. P. & DWORKIN, J. P. 2009. Enrichment of the amino acid l-isovaline by aqueous alteration on CI and CM meteorite parent bodies. Proceedings of the National Academy of Sciences, 106, 5487-5492.

GLAVIN, D. P., ELSILA, J. E., BURTON, A. S., CALLAHAN, M. P., DWORKIN, J. P., HILTS, R. W. & HERD, C. D. K. 2012. Unusual nonterrestrial l-proteinogenic amino acid excesses in the Tagish Lake meteorite. Meteoritics & Planetary Science, 47, 1347-1364.

GOESMANN, F., ROSENBAUER, H., BREDEHÖFT, J. H., CABANE, M., EHRENFREUND, P., GAUTIER, T., GIRI, C., KRÜGER, H., LE ROY, L. & MACDERMOTT, A. J. 2015. Organic compounds on comet 67P/Churyumov-Gerasimenko revealed by COSAC mass spectrometry. Science, 349, aab0689.

GOODYEAR, M., GILMOUR, I. & PEARSON, V. 2011. Development of visualisation methodology for organic materials contained within carbonaceous chondrites.

GOODYEAR, M. C. 2013. Organic chemistry and mineral interactions in the solar system. Open University.

GÖRLLER-WALRAND, C., BINNEMANS, K., GSCHNEIDNER JR, K. & EYRING, L. 1996. Handbook on the Physics and Chemistry of Rare Earths, vol. 25. Elsevier, Amsterdam, 121.

GRADY, M. M., WRIGHT, I. P., SWART, P. K. & PILLINGER, C. T. 1988. The carbon and oxygen isotopic composition of meteoritic carbonates. Geochimica et Cosmochimica Acta, 52, 2855-2866.

GRADY, M.M., WRIGHT, I.P. & PILLINGER, C.T., 1989. A preliminary investigation into the nature of carbonaceous material in ordinary chondrites. Meteoritics, 24(3), pp.147-154.

GUNNLAUGSSON, T., HARTE, A. J., LEONARD, J. P. & NIEUWENHUYZEN, M. 2003. The formation of luminescent supramolecular ternary complexes in water: delayed luminescence sensing of aromatic carboxylates using coordinated unsaturated cationic heptadentate lanthanide ion complexes. Supramolecular Chemistry, 15, 505-519.

HÄNNINEN, P. & HÄRMÄ, H. 2011. Lanthanide luminescence: photophysical, analytical and biological aspects, Springer.

HASEGAWA, T. I., HERBST, E. & LEUNG, C. M. 1992. Models of gas-grain chemistry in dense interstellar clouds with complex organic molecules. the Astrophysical Journal Supplement Series, 82, 167-195.

HAAS, K. L. & FRANZ, K. J. 2009. Application of Metal Coordination Chemistry to Explore and Manipulate Cell Biology. Chemical reviews, 109, 4921-4960.

HAUG, P., SCHNOES, H. K. & BURLINGAME, A. L. 1967. Isoprenoid and Dicarboxylic Acids Isolated from Colorado Green River Shale (Eocene). Science, 158, 772-773.

HAUSRATH, E. M. & BRANTLEY, S. L. 2010. Basalt and olivine dissolution under cold, salty, and acidic conditions: What can we learn about recent aqueous weathering on Mars? Journal of Geophysical Research: Planets, 115, n/a-n/a.

HAYATSU, R., STUDIER, M. H., MOORE, L. P. & ANDERS, E. 1975. Purines and triazines in the Murchison meteorite. Geochimica et Cosmochimica Acta, 39, 471-488.

HAYATSU, R., MATSUOKA, S., SCOTT, R. G., STUDIER, M. H. & ANDERS, E. 1977. Origin of organic matter in the early solar system—VII. The organic polymer in carbonaceous chondrites. Geochimica et Cosmochimica Acta, 41, 1325-1339.

HAYES, J. M. 1967. Organic constituents of meteorites—a review. Geochimica et Cosmochimica Acta, 31, 1395-1440.

HAYES, J. M. & BIEMANN, K. 1968. High resolution mass spectrometric investigations of the organic constituents of the Murray and Holbrook chondrites. Geochimica et Cosmochimica Acta, 32, 239-267.

HEGER, A., FRYER, C. L., WOOSLEY, S. E., LANGER, N. & HARTMANN, D. H. 2003. How massive single stars end their life. The Astrophysical Journal, 591, 288.

HELLING, C., JORGENSEN, U., PLEZ, B. & JOHNSON, H. R. 1996. Formation of PAHs, polyynes, and other macromolecules in the photosphere of carbon stars. Astronomy and Astrophysics, 315, 194-203.

HENDERSON, W., WOLLRAB, V. & EGLINTON, G. Identification of steranes and triterpanes from a geological source by capillary gas liquid chromatography and mass spectrometry. Advances in Organic Geochemistry 1968: Proceedings of the 4th International Meeting on Organic Geochemistry, Held in Amsterdam, September 16-18, 1968, 2013. Elsevier, 181.

HENKEL, G. 1989. The Henkel glossary of fluorescent minerals, Fluorescent Mineral Society.

HERBST, E. & DISHOECK, E. F. V. 2009. Complex Organic Interstellar Molecules. Annual Review of Astronomy and Astrophysics, 47, 427-480.

HEZEL, D. C. & PALME, H. 2010. The chemical relationship between chondrules and matrix and the chondrule matrix complementarity. Earth and Planetary Science Letters, 294, 85-93.

HILL, H. G. & NUTH, J. A. 2003. The catalytic potential of cosmic dust: implications for prebiotic chemistry in the solar nebula and other protoplanetary systems. Astrobiology, 3, 291-304.

HILL, I. & GRAY, T. 1967. Application of the fluorescent-antibody technique to an ecological study of bacteria in soil. Journal of bacteriology, 93, 1888-1896.

HILTS, R. W., HERD, C. D., SIMKUS, D. N. & SLATER, G. F. 2014. Soluble organic compounds in the Tagish Lake meteorite. Meteoritics & Planetary Science, 49, 526-549.

HIROI, T., ZOLENSKY, M. E. & PIETERS, C. M. 2001. The Tagish Lake meteorite: A possible sample from a D-type asteroid. Science, 293, 2234-2236.

HORROCKS, W. D. & ALBIN, M. 1984. Lanthanide ion luminescence in coordination chemistry and biochemistry. Prog. Inorg. Chem, 31, 1-104.

HOWERTON, S. B., GOODPASTER, J. V. & MCGUFFIN, V. L. 2002. Characterization of polycyclic aromatic hydrocarbons in environmental samples by selective fluorescence quenching. Analytica Chimica Acta, 459, 61-73.

HUANG, W., H. 1974. Stabilities of Kaolinite and Halloysite in Relation to Weathering Feldspars and Nepheline in Aqueous Solution. American Mineralogist, 59, 365-371.

HUANG, Y., WANG, Y., ALEXANDRE, M. R., LEE, T., ROSE-PETRUCK, C., FULLER, M. & PIZZARELLO, S. 2005. Molecular and compound-specific isotopic characterization of monocarboxylic acids in carbonaceous meteorites. Geochimica et Cosmochimica Acta, 69, 1073-1084.

HUANG, Y., APONTE, J. C., ZHAO, J., TAROZO, R. & HALLMANN, C. 2015. Hydrogen and carbon isotopic ratios of polycyclic aromatic compounds in two CM2 carbonaceous chondrites and implications for prebiotic organic synthesis. Earth and Planetary Science Letters, 426, 101-108.

IZAWA, M., CRAIG, M., APPLIN, D., SANCHEZ, J., REDDY, V., LE CORRE, L., MANN, P. & CLOUTIS, E. 2015. Variability, absorption features, and parent body searches in “spectrally featureless” meteorite reflectance spectra: Case study–Tagish Lake. Icarus, 254, 324-332.

JENNINGS, J. & WARD, S. 1989. Ammonia synthesis. Wolfe Publishing Ltd.

JOHANNA, V. & TERO, S. 2014. Luminescent lanthanide reporters: new concepts for use in bioanalytical applications. Methods and Applications in Fluorescence, 2, 012001.

JOHANSEN, A., LOW, M.-M. M., LACERDA, P. & BIZZARRO, M. 2015. Growth of asteroids, planetary embryos, and Kuiper belt objects by chondrule accretion. Science Advances, 1.

JOHNSON, N., STEINER M. E. NUTH J. A. 2007. Lunar and Planetary Science XXXVIII (2007) full203. pdf.

JOVANOVIC, S. V. & SIMIC, M. G. 1986. One-electron redox potentials of purines and pyrimidines. The Journal of Physical Chemistry, 90, 974-978.

JUNGCLAUS, G., YUEN, G., MOORE, C. & LAWLESS, J. 1976. Evidence for the presence of low molecular weight alcohols and carbonyl compounds in the Murchison meteorite. Meteoritics & Planetary Science, 11, 231-237.

KATHERINE, L. 1987. Weathering of basalt: formation of iddingsite. Clays and Clay Minerals, 35, 418-428.

KEBUKAWA, Y., ZOLENSKY, M. E., CHAN, Q. H. S., NAGAO, K., KILCOYNE, A. L. D., BODNAR, R. J., FARLEY, C., RAHMAN, Z., LE, L. & CODY, G. D. 2017. Characterization of carbonaceous matter in xenolithic clasts from the Sharps (H3.4) meteorite: Constraints on the origin and thermal processing. Geochimica et Cosmochimica Acta, 196, 74-101.

KERRIDGE, J. & BUNCH, T. 1979. Aqueous activity on asteroids-Evidence from carbonaceous meteorites. Asteroids, 745-764.

KERRIDGE, J. 1999. Formation and Processing of Organics in the Early Solar System. Space Science Reviews, 90, 275-288.

KING, A., SCHOFIELD, P. & RUSSELL, S. 2017. Type 1 aqueous alteration in CM carbonaceous chondrites: Implications for the evolution of water-rich asteroids. Meteoritics & Planetary Science.

KLEIN, H. P. 1979. The Viking mission and the search for life on Mars. Reviews of Geophysics, 17, 1655-1662.

KOEBERL, C. & CASSIDY, W. A. 1991. Differences between Antarctic and non-Antarctic meteorites: An assessment. Geochimica et Cosmochimica Acta, 55, 3-18.

KOLB, V. M. Application of the organic "on water" reactions to prebiotic chemistry. Proc. of SPIE Vol, 2012. 85210D-1.

KRAEMER, S. M. 2004. Iron oxide dissolution and solubility in the presence of siderophores. Aquatic sciences, 66, 3-18.

KRESS, M. E. & TIELENS, A. G. G. M. 2001. The role of Fischer-Tropsch catalysis in solar nebula chemistry. Meteoritics & Planetary Science, 36, 75-91.

KRISHNAMURTHY, R. V., EPSTEIN, S., CRONIN, J. R., PIZZARELLO, S. & YUEN, G. U. 1992. Isotopic and molecular analyses of hydrocarbons and monocarboxylic acids of the Murchison meteorite. Geochimica et Cosmochimica Acta, 56, 4045-4058.

KUGA, M., MARTY, B., MARROCCHI, Y. & TISSANDIER, L. 2015. Synthesis of refractory organic matter in the ionized gas phase of the solar nebula. Proceedings of the National Academy of Sciences, 112, 7129-7134.

KUMAR, R., CHAUDHARY, P., NIMESH, S. & CHANDRA, R. 2006. Polyethylene glycol as a non-ionic liquid solvent for Michael addition reaction of amines to conjugated alkenes. Green Chemistry, 8, 356-358.

KVENVOLDEN, K., LAWLESS, J., PERING, K., PETERSON, E., FLORES, J., PONNAMPERUMA, C., KAPLAN, I. R. & MOORE, C. 1970. Evidence for Extraterrestrial Amino-acids and Hydrocarbons in the Murchison Meteorite. Nature, 228, 923-926.

KVENVOLDEN, K. A., LAWLESS, J. G. & PONNAMPERUMA, C. 1971. Nonprotein Amino Acids in the Murchison Meteorite. Proceedings of the National Academy of Sciences, 68, 486-490.

KWOK, S. 2009. Delivery of Complex Organic Compounds from Planetary Nebulae to the Solar System. International Journal of Astrobiology, 8, 161-167.

KWOK, S. 2016. Complex organics in space from Solar System to distant galaxies. The Astronomy and Astrophysics Review, 24, 8.

LAKOWICZ, J. R. 1983. Principals of Fluorescence Spectroscopy. Springer, Boston, MA.

LANGER, W. D., VANDISHOECK, E. F., BERGIN, E. A., BLAKE, G. A., TIELENS, A. G., VELUSAMY, T. & WHITTET, D. C. 2000. Chemical evolution of protostellar matter.

LAWLESS, J. G. 1973. Amino acids in the Murchison meteorite. Geochimica et Cosmochimica Acta, 37, 2207-2212.

LAWLESS, J. G., ZEITMAN, B., PEREIRA, W. E., SUMMONS, R. E. & DUFFIELD, A. M. 1974. Dicarboxylic acids in the Murchison meteorite. Nature, 251, 40-42.

LAWLESS, J. G. & YUEN, G. U. 1979. Quantification of monocarboxylic acids in the Murchison carbonaceous meteorite. Nature, 282, 396-398.

LE GUILLOU, C., BERNARD, S., BREARLEY, A. J. & REMUSAT, L. 2014. Evolution of organic matter in Orgueil, Murchison and Renazzo during parent body aqueous alteration: In situ investigations. Geochimica et Cosmochimica Acta, 131, 368-392.

LE GUILLOU, C. & BREARLEY, A. 2014. Relationships between organics, water and early stages of aqueous alteration in the pristine CR3.0 chondrite MET 00426. Geochimica et Cosmochimica Acta, 131, 344-367.

LERNER, N. R. & COOPER, G. W. 2005. Iminodicarboxylic acids in the Murchison meteorite: Evidence of Strecker reactions. Geochimica et Cosmochimica Acta, 69, 2901-2906.

LEVY, R. L., GRAYSON, M. A. & WOLF, C. J. 1973. The organic analysis of the murchison meteorite. Geochimica et Cosmochimica Acta, 37, 467-483.

LI, C. & WONG, W.-T. 2002. A convenient method for the preparation of mono< i> N</i>-alkylated cyclams and cyclens in high yields. Tetrahedron letters, 43, 3217-3220.

LI, L., TIAN, L., WANG, Y., ZHAO, W., CHENG, F., LI, Y. & YANG, B., 2016. Smart pH-responsive and high doxorubicin loading nanodiamond for in vivo selective targeting, imaging, and enhancement of anticancer therapy. Journal of Materials Chemistry B, 4(29), pp.5046-5058.

LIS, S., ELBANOWSKI, M., MĄKOWSKA, B. & HNATEJKO, Z. 2002. Energy transfer in solution of lanthanide complexes. Journal of Photochemistry and Photobiology A: Chemistry, 150, 233-247.

LORD, H. & PAWLISZYN, J. 2000. Evolution of solid-phase microextraction technology. Journal of Chromatography A, 885, 153-193.

LOWE, M. P. & PARKER, D. 2000. Controllable pH modulation of lanthanide luminescence by intramolecular switching of the hydration state. Chemical Communications, 707-708.

LOWE, M. P., PARKER, D., REANY, O., AIME, S., BOTTA, M., CASTELLANO, G., GIANOLIO, E. & PAGLIARIN, R. 2001. pH-Dependent Modulation of Relaxivity and Luminescence in Macrocyclic Gadolinium and Europium Complexes Based on Reversible Intramolecular Sulfonamide Ligation. Journal of the American Chemical Society, 123, 7601-7609.

MACPHERSON, G. J., BAR-MATTHEWS, M., TANAKA, T., OLSEN, E. & LAWRENCE, G. 1983. Refractory inclusions in the Murchison meteorite. Geochimica et Cosmochimica Acta, 47, 823-839.

MACPHERSON, G. J. 2003. Calcium-aluminum-rich inclusions in chondritic meteorites. Treatise on Geochemistry, 1, 711.

MACPHERSON, G. J. 2007. 1.08 - Calcium–Aluminum-Rich Inclusions in Chondritic Meteorites A2 - Holland, Heinrich D. In: TUREKIAN, K. K. (ed.) Treatise on Geochemistry. Oxford: Pergamon.

MACRAE, C. M. & WILSON, N. C. 2008. Luminescence database I—minerals and materials. Microscopy and Microanalysis, 14, 184-204.

MARQUEZ, C., PISCHEL, U. & NAU, W. M. 2003. Selective fluorescence quenching of 2, 3-diazabicyclo [2.2. 2] oct-2-ene by nucleotides. Organic letters, 5, 3911-3914.

MARSHALL, A. G., HENDRICKSON, C. L. & JACKSON, G. S. 1998. Fourier transform ion cyclotron resonance mass spectrometry: a primer. Mass spectrometry reviews, 17, 1-35.

MARTINS, Z., WATSON, J., SEPHTON, M., BOTTA, O., EHRENFREUND, P. & GILMOUR, I. 2006. Free dicarboxylic and aromatic acids in the carbonaceous chondrites Murchison and Orgueil. Meteoritics and Planetary Science, 41, 1073-1080.

MARTINS, Z., ALEXANDER, C. O. D., ORZECHOWSKA, G., FOGEL, M. & EHRENFREUND, P. 2007. Indigenous amino acids in primitive CR meteorites. Meteoritics & Planetary Science, 42, 2125-2136.

MARTINS, Z., BOTTA, O., FOGEL, M. L., SEPHTON, M. A., GLAVIN, D. P., WATSON, J. S., DWORKIN, J. P., SCHWARTZ, A. W. & EHRENFREUND, P. 2008. Extraterrestrial nucleobases in the Murchison meteorite. Earth and Planetary Science Letters, 270, 130-136.

MARTINS, Z. 2015. Organic molecules in meteorites. Proceedings of the International Astronomical Union, 11, 411-415.

MARTINS, Z., MODICA, P., ZANDA, B. & D'HENDECOURT, L. L. S. 2015. The amino acid and hydrocarbon contents of the Paris meteorite: Insights into the most primitive CM chondrite. Meteoritics & Planetary Science, 50, 926-943.

MATSUDA, Y., MAKISHIMA, S. & SHIONOYA, S. 1969. Mechanism of Intramolecular Energy Transfer in Rare Earth Chelates as Revealed by Infrared Absorption Measurements. Bulletin of the Chemical Society of Japan, 42, 356-&.

MATSUOKA, M., NAKAMURA, T., KIMURA, Y., HIROI, T., NAKAMURA, R., OKUMURA, S. & SASAKI, S. 2015. Pulse-laser irradiation experiments of Murchison CM2 chondrite for reproducing space weathering on C-type asteroids. Icarus, 254, 135-143.

McADAM, M. M., SUNSHINE, J. M., HOWARD, K. T. & MCCOY, T. M. 2015. Aqueous alteration on asteroids: Linking the mineralogy and spectroscopy of CM and CI chondrites. Icarus, 245, 320-332.

McGEOCH, J. E. M. & MCGEOCH, M. W. 2015. Polymer amide in the Allende and Murchison meteorites. Meteoritics & Planetary Science, 50, 1971-1983.

McMURRY, J. 2000. Organic Chemistry, Brooks Cole.

McKAY, J., WEBER, J. & LATHAM, D. 1976. Characterization of nitrogen bases in high-boiling petroleum distillates. Analytical Chemistry, 48, 891-898.

McKAY, J. F. & CHONG, S.-L. 1983. Characterization of organic matter recovered from Green River oil shale at temperatures of 400 C and below. Liquid Fuels Technology, 1, 289-324.

McSWEEN, H. Y. 1979. Alteration in CM carbonaceous chondrites inferred from modal and chemical variations in matrix. Geochimica et Cosmochimica Acta, 43, 17611767-17651770.

McSWEEN, H. Y. 1999. Meteorites and their parent planets, Cambridge University Press.

MEIERHENRICH, U. J., MUÑOZ CARO, G. M., BREDEHÖFT, J. H., JESSBERGER, E. K. & THIEMANN, W. H.-P. 2004. Identification of diamino acids in the Murchison meteorite. Proceedings of the National Academy of Sciences of the United States of America, 101, 9182-9186.

MESSENGER, S., AMARI, S., GAO, X., WALKER, R. M., CLEMETT, S. J., CHILLIER, X. D. F., ZARE, R. N. & LEWIS, R. S. 1998. Indigenous Polycyclic Aromatic Hydrocarbons in Circumstellar Graphite Grains from Primitive Meteorites. The Astrophysical Journal, 502, 284.

MESSENGER, S., KELLER, L., CLEMETT, S., NGUYEN, A. & GIBSON, E. 2013. Coordinated In Situ Analyses of Organic Nanoglobules in the Sutter's Mill Meteorite.

MILLER, S. L. 1953. A production of amino acids under possible primitive earth conditions. Science, 117, 528-529.

MILTON, C. 1971. Authigenic minerals of the Green River Formation. Rocky Mountain Geology, 10, 57-63.

MINERALS.NET. n. d. The Mineral Enstatite [Online]. Available: http://www.minerals.net/mineral/enstatite.aspx.

MONTGOMERY, C. P., MURRAY, B. S., NEW, E. J., PAL, R. & PARKER, D. 2009. Cell-Penetrating Metal Complex Optical Probes: Targeted and Responsive Systems Based on Lanthanide Luminescence. Accounts of Chemical Research, 42, 925-937.

MOORE, C. B. & LEWIS, C. F. 1967. Total carbon content of ordinary chondrites. Journal of Geophysical Research, 72, 6289-6292.

MORSS, L. R. 1976. Thermochemical properties of yttrium, lanthanum, and the lanthanide elements and ions. Chemical Reviews, 76, 827-841.

MOSKOVITZ, N. & GAIDOS, E. 2011. Differentiation of planetesimals and the thermal consequences of melt migration. Meteoritics & Planetary Science, 46, 903-918.

MURAE, T. 1999. Fluorescent organic matter in carbonaceous chondrites. Advances in Space Research, 24, 469-476.

NADEAU, J. L., PERREAULT, N., NIEDERBERGER, T., WHYTE, L., SUN, H. & LEON, R. 2008. Fluorescence microscopy as a tool for in situ life detection. Astrobiology, 8, 859-874.

NAKAMURA, K., ZOLENSKY, M. E., TOMITA, S., NAKASHIMA, S. & TOMEOKA, K. 2002. Hollow organic globules in the Tagish Lake meteorite as possible products of primitive organic reactions. International Journal of Astrobiology, 1, 179-189.

NARAOKA, H., SHIMOYAMA, A. & HARADA, K. 1999. Molecular distribution of monocarboxylic acids in Asuka carbonaceous chondrites from Antarctica. Origins of Life and Evolution of the Biosphere, 29, 187-201.

NASSO, I., GEUM, N., BECHARA, G., MESTRE-VOEGTLÉ, B., GALAUP, C. & PICARD, C. 2014. Highly luminescent Tb(III) macrocyclic complex based on a DO3A hosting unit and an appended carboxylated N,C-pyrazolylpyridine antenna. Journal of Photochemistry and Photobiology A: Chemistry, 274, 124-132.

NICHOLS, R. 2006. Chronological constraints on planetesimal accretion. Meteorites and the early solar system II, 463-472.

NORMAN, R. O. & COXON, J. M. 1993. Principles of organic synthesis, CRC Press.

NUTH, J. A. I., CHARNLEY, S. B. & JOHNSON, N. M. 2006. Chemical processes in the interstellar medium: Source of the gas and dust in the primitive solar nebula. Meteorites and the early solar system II, 2, 147-167.

O'CONNELL, P. J. 2009. Synthesis and Characterisation of Bifunctional MRI Contrast Agents. The Open University.

ORTHOUS-DAUNAY, F. R., QUIRICO, E., LEMELLE, L., BECK, P., DEANDRADE, V., SIMIONOVICI, A. & DERENNE, S. 2010. Speciation of sulfur in the insoluble organic matter from carbonaceous chondrites by XANES spectroscopy. Earth and Planetary Science Letters, 300, 321-328.

PALME, H., SPETTEL, B. & IKEDA, Y. 1993. Origin of chondrules and matrix in carbonaceous chondrites. Meteoritics, 28.

PAPIKE, J. J. 1998. Planetary materials, Mineralogical Society of America Chantilly, VA.

PARKER, D. & WILLIAMS, J. G. 1996. Getting excited about lanthanide complexation chemistry. Journal of the Chemical Society, Dalton Transactions, 3613-3628.

PARKER, D. 2000. Luminescent lanthanide sensors for pH, pO 2 and selected anions. Coordination Chemistry Reviews, 205, 109-130.

PASHITSKII, E. A. 2017. On fast solid-body rotation of the solar core and differential (liquid-like) rotation of the solar surface. Plasma Physics Reports, 43, 733-740.

PEARSON, V. K., SEPHTON, M. A., KEARSLEY, A. T., BLAND, P. A., FRANCHI, I. A. & GILMOUR, I. 2002. Clay mineral-organic matter relationships in the early solar system. Meteoritics & Planetary Science, 37, 1829-1833.

PEARSON, V. K., SEPHTON, M. A. & GILMOUR, I. 2006. Molecular and isotopic indicators of alteration in CR chondrites. Meteoritics & Planetary Science, 41, 1291-1303.

PEARSON, V., KEARSLEY, A., SEPHTON, M. & GILMOUR, I. 2007. The labelling of meteoritic organic material using osmium tetroxide vapour impregnation. Planetary and Space Science, 55, 1310-1318.

PEARSON, V. K., WILSON, R. C., GILMOUR I. 2010. Extraterrestrial Organic Matter as Recorded in Meteorites. In: BASIUK, V. A. (ed.) Astrobiology: Emergence, Search and Detection of Life. American Scientific Publishers.

PELTZER, E., BADA, J., SCHLESINGER, G. & MILLER, S. 1984. The chemical conditions on the parent body of the Murchison meteorite: some conclusions based on amino, hydroxy and dicarboxylic acids. Advances in Space Research, 4, 69-74.

PIKRAMENOU, Z., YU, J.-A., LESSARD, R. B., PONCE, A., WONG, P. A. & NOCERA, D. G. 1994. Luminescence from supramolecules triggered by the molecular recognition of substrates. Coordination Chemistry Reviews, 132, 181-194.

PIZZARELLO, S., FENG, X., EPSTEIN, S. & CRONIN, J. R. 1994. Isotopic analyses of nitrogenous compounds from the Murchison meteorite: ammonia, amines, amino acids, and polar hydrocarbons. Geochimica et Cosmochimica Acta, 58, 5579-5587.

PIZZARELLO, S. & CRONIN, J. R. 2000. Non-racemic amino acids in the Murray and Murchison meteorites. Geochimica et Cosmochimica Acta, 64, 329-338.

PIZZARELLO, S., HUANG, Y., BECKER, L., POREDA, R. J., NIEMAN, R. A., COOPER, G. & WILLIAMS, M. 2001. The organic content of the Tagish Lake meteorite. Science, 293, 2236-2239.

PIZZARELLO, S. & HUANG, Y. 2002. Molecular and isotopic analyses of Tagish Lake alkyl dicarboxylic acids. Meteoritics & Planetary Science, 37, 687-696.

PIZZARELLO, S., COOPER, G. & FLYNN, G. 2006. The nature and distribution of the organic material in carbonaceous chondrites and interplanetary dust particles. Meteorites and the early solar system II, 1, 625-651.

PIZZARELLO, S. & HOLMES, W. 2009. Nitrogen-containing compounds in two CR2 meteorites: 15 N composition, molecular distribution and precursor molecules. Geochimica et Cosmochimica Acta, 73, 2150-2162.

PODHORODECKI, A., GAPONENKO, N., BAŃSKI, M., KIM, T. & MISIEWICZ, J. 2010. Excitation Mechanisms of Green Emission from Terbium Ions Embedded Inside the Sol-Gel Films Deposited onto Nanoporous Substrates. ECS Transactions, 28, 81-88.

POOLE, R. A., BOBBA, G., CANN, M. J., FRIAS, J.-C., PARKER, D. & PEACOCK, R. D. 2005. Synthesis and characterisation of highly emissive and kinetically stable lanthanide complexes suitable for usage 'in cellulo'. Organic & biomolecular chemistry, 3, 1013-1024.

RADKE, M., WILLSCH, H., LEYTHAEUSER, D. & TEICHMÜLLER, M. 1982. Aromatic components of coal: relation of distribution pattern to rank. Geochimica et Cosmochimica Acta, 46, 1831-1848.

RAGHUNAND, N., GUNTLE, G. P., GOKHALE, V., NICHOL, G. S., MASH, E. A. & JAGADISH, B. 2010. Design, Synthesis, and Evaluation of 1,4,7,10-Tetraazacyclododecane-1,4,7-triacetic Acid-Derived, Redox-Sensitive Contrast Agents for Magnetic Resonance Imaging. Journal of medicinal chemistry, 53, 6747-6757.

RALPH, J. n. d. Iddingsite [Online]. Available: https://www.mindat.org/min-7006.html [Accessed 08/08/17.

RALPH, J. 2001. mindat.org - the mineral and locality database [Online]. Available: http://www.mindat.org/ [Accessed October 2013 2013].

REED, W. E. 1977. Molecular compositions of weathered petroleum and comparison with its possible source. Geochimica et Cosmochimica Acta, 41, 237-247.

REMUSAT, L. Organic material in meteorites and the link to the origin of life. BIO Web of Conferences, 2014. EDP Sciences, 03001.

RICHARDSON, F. S. 1982. Terbium(III) and europium(III) ions as luminescent probes and stains for biomolecular systems. Chemical Reviews, 82, 541-552.

RING, D., WOLMAN, Y., FRIEDMANN, N. & MILLER, S. L. 1972. Prebiotic Synthesis of Hydrophobic and Protein Amino Acids. Proceedings of the National Academy of Sciences, 69, 765-768.

RINGE, D. & PETSKO, G. A. 2008. How enzymes work. SCIENCE-NEW YORK THEN WASHINGTON-, 320, 1428.

RIVERA-FIGUEROA, A. M., RAMAZAN, K. A. & FINLAYSON-PITTS, B. J. 2004. Fluorescence, Absorption, and Excitation Spectra of Polycyclic Aromatic Hydrocarbons as a Tool for Quantitative Analysis. Journal of Chemical Education, 81, 242.

RIZZO, F., MEINARDI, F., TUBINO, R., PAGLIARIN, R., DELLEPIANE, G. & PAPAGNI, A. 2009. Synthesis of 8-hydroxyquinoline functionalised DO3A ligand and Eu(III) and Er(III) complexes: Luminescence properties. Synthetic Metals, 159, 356-360.

RODRÍGUEZ-RODRÍGUEZ, A., ESTEBAN-GÓMEZ, D., DE BLAS, A., RODRÍGUEZ-BLAS, T., FEKETE, M., BOTTA, M., TRIPIER, R. & PLATAS-IGLESIAS, C. 2012. Lanthanide(III) Complexes with Ligands Derived from a Cyclen Framework Containing Pyridinecarboxylate Pendants. The Effect of Steric Hindrance on the Hydration Number. Inorganic Chemistry, 51, 2509-2521.

ROY, D., NAJAFIAN, K. & VON RAGUÉ SCHLEYER, P. 2007. Chemical evolution: The mechanism of the formation of adenine under prebiotic conditions. Proceedings of the National Academy of Sciences, 104, 17272-17277.

RUBIN, A. E. 2007. Petrogenesis of acapulcoites and lodranites: A shock-melting model. Geochimica et Cosmochimica Acta, 71, 2383-2401.

RUSTON, L. L., ROBERTSON, G. M. & PIKRAMENOU, Z. 2010. Luminescence Screening Assays for the Identification of Sensitizers for Lanthanides Based on the Controlled Formation of Ternary Lanthanide Complexes with DTPA–Bisamide Ligands. Chemistry – An Asian Journal, 5, 571-580.

SABBATINI, N., GUARDIGLI, M. & LEHN, J.-M. 1993. Luminescent lanthanide complexes as photochemical supramolecular devices. Coordination Chemistry Reviews, 123, 201-228.

SALADINO, R., CRESTINI, C., COSTANZO, G. & DIMAURO, E. 2005. On the prebiotic synthesis of nucleobases, nucleotides, oligonucleotides, pre-RNA and pre-DNA molecules. Prebiotic chemistry. Springer.

SALMON, V., DERENNE, S., LALLIER-VERGES, E., LARGEAU, C. & BEAUDOIN, B. 2000. Protection of organic matter by mineral matrix in a Cenomanian black shale. Organic Geochemistry, 31, 463-474.

SANDFORD, S. A., ALÉON, J., ALEXANDER, C. M. D., ARAKI, T., BAJT, S. A., BARATTA, G. A., BORG, J., BRADLEY, J. P., BROWNLEE, D. E. & BRUCATO, J. R. 2006. Organics captured from comet 81P/Wild 2 by the Stardust spacecraft. Science, 314, 1720-1724.

SARADHI, M. P. & VARADARAJU, U. V. 2006. Photoluminescence Studies on Eu2+-Activated Li2SrSiO4a Potential Orange-Yellow Phosphor for Solid-State Lighting. Chemistry of Materials, 18, 5267-5272.

SCHÄFERLING, M. 2012. The art of fluorescence imaging with chemical sensors. Angewandte Chemie International Edition, 51, 3532-3554.

SCHÖLER, H. F., NKUSI, G., NIEDAN, V. W., MÜLLER, G. & SPITTHOFF, B. 2005. Screening of organic halogens and identification of chlorinated benzoic acids in carbonaceous meteorites. Chemosphere, 60, 1505-1512.

SCHMITT-KOPPLIN, P., GABELICA, Z., GOUGEON, R. D., FEKETE, A., KANAWATI, B., HARIR, M., GEBEFUEGI, I., ECKEL, G. & HERTKORN, N. 2010. High molecular diversity of extraterrestrial organic matter in Murchison meteorite revealed 40 years after its fall. Proceedings of the National Academy of Sciences, 107, 2763-2768.

SCHMITT, B., PHILIPPE, S., GRUNDY, W., REUTER, D., CÔTE, R., QUIRICO, E., PROTOPAPA, S., YOUNG, L., BINZEL, R. & COOK, J. 2017. Physical state and distribution of materials at the surface of Pluto from New Horizons LEISA imaging spectrometer. Icarus, 287, 229-260.

SEIDEL, C. A. M., SCHULZ, A. & SAUER, M. H. M. 1996. Nucleobase-Specific Quenching of Fluorescent Dyes. 1. Nucleobase One-Electron Redox Potentials and Their Correlation with Static and Dynamic Quenching Efficiencies. The Journal of Physical Chemistry, 100, 5541-5553.

SEPHTON, M. A. & GILMOUR, I. 2001. Pyrolysis–gas chromatography–isotope ratio mass spectrometry of macromolecular material in meteorites. Planetary and Space Science, 49, 465-471.

SEPHTON, M. A. 2002. Organic compounds in carbonaceous meteorites. Natural Product Reports, 19, 292-311.

SEPHTON, M., BLAND, P., PILLINGER, C. & GILMOUR, I. 2004. The preservation state of organic matter in meteorites from Antarctica. Meteoritics & Planetary Science, 39, 747-754.

SHIBASAKI, M., KANAI, M. & MITA, T. 2004. The Catalytic Asymmetric Strecker Reaction. Organic Reactions. John Wiley & Sons, Inc.

SHIMOYAMA, A., NARAOKA, H., KOMIYA, M. & HARADA, K. 1989. Analyses of carboxylic acids and hydrocarbons in Antarctic carbonaceous chondrites, Yamato-74662 and Yamato-793321. Geochemical Journal, 23, 181-193.

SHIMOYAMA, A., HAGISHITA, S. & HARADA, K. 1990. Search for nucleic acid bases in carbonaceous chondrites from Antarctica. GEOCHEMICAL JOURNAL, 24, 343-348.

SHIMOYAMA, A. & SHIGEMATSU, R. 1994. Dicarboxylic acids in the Murchison and Yamato-791198 carbonaceous chondrites. Chemistry letters, 23, 523-526.

SIEBENMORGEN, R. & KRÜGEL, E. 2010. The destruction and survival of polycyclic aromatic hydrocarbons in the disks of T Tauri stars. A&A, 511, A6.

SIMS, M., CULLEN, D., BANNISTER, N., GRANT, W. & JONES, R. A life marker chip for the specific molecular identification of life experiment. Tools and Technologies for Future Planetary Exploration, 2004. 139-146.

SKELLEY, A. M. & MATHIES, R. A. 2003. Chiral separation of fluorescamine-labeled amino acids using microfabricated capillary electrophoresis devices for extraterrestrial exploration. Journal of Chromatography A, 1021, 191-199.

SMITH, D. P. T. 2008. High-Intensity Contrast Agents in Medical Imaging. The Open University.

SMITH, K. E., CALLAHAN, M. P., GERAKINES, P. A., DWORKIN, J. P. & HOUSE, C. H. 2014. Investigation of pyridine carboxylic acids in CM2 carbonaceous chondrites: Potential precursor molecules for ancient coenzymes. Geochimica et Cosmochimica Acta, 136, 1-12.

SNOWDEN, T. S. & ANSLYN, E. V. 1999. Anion recognition: synthetic receptors for anions and their application in sensors. Current opinion in chemical biology, 3, 740-746.

SOBRON, P., WANG, A. & SOBRON, F. 2012. Extraction of compositional and hydration information of sulfates from laser-induced plasma spectra recorded under Mars atmospheric conditions — Implications for ChemCam investigations on Curiosity rover. Spectrochimica Acta Part B: Atomic Spectroscopy, 68, 1-16.

STASIUK, G. J. & LONG, N. J. 2013. The ubiquitous DOTA and its derivatives: the impact of 1,4,7,10-tetraazacyclododecane-1,4,7,10-tetraacetic acid on biomedical imaging. Chemical Communications, 49, 2732-2746.

STOKS, P. G. & SCHWARTZ, A. W. 1979. Uracil in carbonaceous meteorites. Nature, 282, 709-710.

STOKS, P. G. & SCHWARTZ, A. W. 1981. Nitrogen-heterocyclic compounds in meteorites: significance and mechanisms of formation. Geochimica et Cosmochimica Acta, 45, 563-569.

STOKS, P. G. & SCHWARTZ, A. W. 1982. Basic nitrogen-heterocyclic compounds in the Murchison meteorite. Geochimica et Cosmochimica Acta, 46, 309-315.

STORRIE-LOMBARDI, M. C., MULLER, J.-P., FISK, M. R., COUSINS, C., SATTLER, B., GRIFFITHS, A. D. & COATES, A. J. 2009. Laser-Induced Fluorescence Emission (LIFE): searching for Mars organics with a UV-enhanced PanCam. Astrobiology, 9, 953-964.

STUDIER, M. H., HAYATSU, R. & ANDERS, E. 1965. Organic Compounds in Carbonaceous Chondrites. Science, 149, 1455-1459.

TAMAURA, Y., TODOKORO, K., IKEBE, M., MAKINO, H., HIROSE, S. & INADA, Y. 1975. Fluorometric assay for discriminating the states of amino groups in insulin, lysozyme and asparaginase with fluorescamine. FEBS Letters, 50, 70-73.

TELGMANN, L., WEHE, C.A., KÜNNEMEYER, J., BÜLTER, A.C., SPERLING, M. AND KARST, U., 2012. Speciation of Gd-based MRI contrast agents and potential products of transmetalation with iron ions or parenteral iron supplements. Analytical and bioanalytical chemistry, 404(8), pp.2133-2141.

TERAI, T., KIKUCHI, K., IWASAWA, S.-Y., KAWABE, T., HIRATA, Y., URANO, Y. & NAGANO, T. 2006. Modulation of Luminescence Intensity of Lanthanide Complexes by Photoinduced Electron Transfer and Its Application to a Long-Lived Protease Probe. Journal of the American Chemical Society, 128, 6938-6946.

THIBON, A. & PIERRE, V. C. 2009. Principles of responsive lanthanide-based luminescent probes for cellular imaging. Analytical and Bioanalytical Chemistry, 394, 107-120.

TONUI, E., ZOLENSKY, M., HIROI, T., NAKAMURA, T., LIPSCHUTZ, M. E., WANG, M.-S. & OKUDAIRA, K. 2014. Petrographic, chemical and spectroscopic evidence for thermal metamorphism in carbonaceous chondrites I: CI and CM chondrites. Geochimica et Cosmochimica Acta, 126, 284-306.

TORIMURA, M., KURATA, S., YAMADA, K., YOKOMAKU, T., KAMAGATA, Y., KANAGAWA, T. & KURANE, R. 2001. Fluorescence-Quenching Phenomenon by Photoinduced Electron Transfer between a Fluorescent Dye and a Nucleotide Base. Analytical Sciences, 17, 155-160.

TREIMAN, A. H., BISH, D. L., VANIMAN, D. T., CHIPERA, S. J., BLAKE, D. F., MING, D. W., MORRIS, R. V., BRISTOW, T. F., MORRISON, S. M. & BAKER, M. B. 2016. Mineralogy, provenance, and diagenesis of a potassic basaltic sandstone on Mars: CheMin X-ray diffraction of the Windjana sample (Kimberley area, Gale Crater). Journal of Geophysical Research: Planets, 121, 75-106.

TSUBOI, H., SOGA, K., INOUE, H. & MAKISHIMA, A. 1998. Synthesis and Fluorescence Properties of Eu2+-Complex-Doped SiO2 Gels. Journal of the American Ceramic Society, 81, 1197-1202.

UDENFRIEND, S., STEIN, S., BÖHLEN, P., DAIRMAN, W., LEIMGRUBER, W. & WEIGELE, M. 1972. Fluorescamine: A Reagent for Assay of Amino Acids, Peptides, Proteins, and Primary Amines in the Picomole Range. Science, 178, 871-872.

VALEUR, B. & BERBERAN-SANTOS, M. N. 2013. Molecular fluorescence: principles and applications, John Wiley & Sons.

VANĚK, J., LUBAL, P., HERMANN, P. & ANZENBACHER, P. 2013. Luminescent sensor for carbonate ion based on lanthanide (III) complexes of 1, 4, 7, 10-tetraazacyclododecane-1, 4, 7-triacetic acid (DO3A). Journal of fluorescence, 23, 57-69.

VAN DER VELDEN, W. & SCHWARTZ, A. W. 1977. Search for purines and pyrimidines in the Murchison meteorite. Geochimica et Cosmochimica Acta, 41, 961-968.

VAN DISHOECK, E. F., BLAKE, G. A., DRAINE, B. T. & LUNINE, J. The chemical evolution of protostellar and protoplanetary matter. Protostars and Planets III, 1993. 163-241.

VARELA, M.E. & METRICH, N., 2000. Carbon in olivines of chondritic meteorites. Geochimica et Cosmochimica Acta, 64(19), pp.3433-3438.

VASTEL, C., CECCARELLI, C., LEFLOCH, B. & BACHILLER, R. 2014. The origin of complex organic molecules in prestellar cores. The Astrophysical Journal Letters, 795, L2.

VITIELLO, B. 2018. PhD, The Open University.

VOLLMER, C., KEPAPTSOGLOU, D., LEITNER, J., BUSEMANN, H., SPRING, N. H., RAMASSE, Q. M., HOPPE, P. & NITTLER, L. R. 2014. Fluid-induced organic synthesis in the solar nebula recorded in extraterrestrial dust from meteorites. Proceedings of the National Academy of Sciences, 111, 15338-15343.

WANG, X., CHANG, H., XIE, J., ZHAO, B., LIU, B., XU, S., PEI, W., REN, N., HUANG, L. & HUANG, W. 2014. Recent developments in lanthanide-based luminescent probes. Coordination Chemistry Reviews, 273–274, 201-212.

WATSON, J. D. & CRICK, F. H. 1953. Molecular structure of nucleic acids. Nature, 171, 737-738.

WATSON, W. D. 1976. Interstellar molecule reactions. Reviews of Modern Physics, 48, 513-552.

WATSON, J., SEPHTON, M. & GILMOUR, I. Macromolecular Organic Acids in the Murchison Meteorite. 36th Annual Lunar and Planetary Science Conference, 2005. 1829.

WATSON, J. S., SEPHTON, M. A. & GILMOUR, I. 2010. Thermochemolysis of the Murchison meteorite: identification of oxygen bound and occluded units in the organic macromolecule. International Journal of Astrobiology, 9, 201-208.

WEISS, F. T. 1970. Determination of organic compounds: methods and procedures.

WEISS, J. 1943. Fluorescence of Organic Molecules. Nature, 152, 176-178.

WEN, G.-X., WU, Y.-P., DONG, W.-W., ZHAO, J., LI, D.-S. & ZHANG, J. 2016. An Ultrastable Europium(III)–Organic Framework with the Capacity of Discriminating Fe2+/Fe3+ Ions in Various Solutions. Inorganic Chemistry, 55, 10114-10117.

WHEATLEY, A. D. & SADHRA, S. 1998. Use of Fluorescence Emission Spectra for the Routine Identification of Polycyclic Aromatic Hydrocarbons in Liquid Chromatography. Journal of Liquid Chromatography & Related Technologies, 21, 2509-2521.

WLOTZKA, F., SPETTEL, B., PALME, H. & SCHULTZ, L. 1989. Two new CM chondrites from Antarctica: Different mineralogy, but same chemistry. Meteoritics, 24, 341.

WLOTZKA, F. 1991. The Meteoritical Bulletin, No. 71. Meteoritics & Planetary Science, 26, 255-262.

WÜNSCH, U. J., MURPHY, K. R. & STEDMON, C. A. 2015. Fluorescence Quantum Yields of Natural Organic Matter and Organic Compounds: Implications for the Fluorescence-based Interpretation of Organic Matter Composition. Frontiers in Marine Science, 2.

YUEN, G. U. & KVENVOLDEN, K. A. 1973. Monocarboxylic Acids in Murray and Murchison Carbonaceous Meteorites. Nature, 246, 301-303.

YUEN, G., BLAIR, N., DES MARAIS, D. J. & CHANG, S. 1984. Carbon isotope composition of low molecular weight hydrocarbons and monocarboxylic acids from Murchison meteorite. Nature, 307, 252-254.

ZHANG, X. & JIANG, J. 2010. N-Based Rare Earth Complexes. Rare Earth Coordination Chemistry. John Wiley & Sons, Ltd.

Zhengming, Q. & Shaoping, L. 2016. Analysis of Cordyceps by multi-column liquid chromatography. Acta Pharmaceutica Sinica B, 7, 202-207.

ZOLENSKY, M., BARRETT, R. & BROWNING, L. 1993. Mineralogy and composition of matrix and chondrule rims in carbonaceous chondrites. Geochimica et Cosmochimica Acta, 57, 3123-3148.

ZOLENSKY, M. E., MITTLEFEHLDT, D. W., LIPSCHUTZ, M. E., WANG, M.-S., CLAYTON, R. N., MAYEDA, T. K., GRADY, M. M., PILLINGER, C. & B, D. 1997. CM chondrites exhibit the complete petrologic range from type 2 to 1. Geochimica et Cosmochimica Acta, 61, 5099-5115.